Mechanisms of Antifatigue Agents Used in Natural Rubber

Kenichi Sugimoto

Doctor of Philosophy

University of Aston in Birmingham

May 1995

Summary

Large number of compounds containing quinonoid or hindered phenol functions were examined for their roles as antifatigue agents. Among the evaluated quinones and phenols expected to have macroalkyl radical scavenging ability, BQ, αTOC, γTOC and GM showed relatively good performance for fatigue resistance (although their performance was slightly less effective than the comercial aromatic amine antioxidants, IPPD and 6PPD). The compounds which were shown to have higher reactivity with alkyl radicals (via calculated reactivity indices) showed better fatigue resistance. This fact supports the suggestion that strong alkyl radical scavengers should be also effective antifatigue agents. Evidence produced based on calculation of reactivity indices suggests that the quinones examined react with alkyl radicals on the meta position of the quinone rings producing phenoxyl radicals. The phenoxyl radicals are expected either to disproportionate, to recombine with a further alkyl radical, or to abstract a hydrogen from another alkyl radical producing an olefine. The regeneration of quinones and formation of the corresponding phenols is expected to occur during the antifatigue activity. The phenol antioxidant, HBA is expected to produce a quinonoid compound and this is also expected to function in a similar way to other quinones. Another phenol, GM, which is also known to scavenge alkyl radicals showed good antifatigue performance. Tocopherols had effective antifatigue activity and are expected to have different antifatigue mechanisms from that of other quinones, hence αTOC was examined for its mechanisms during rubber fatiguing using HPLC analysis. Trimers of αTOC which were produced during vulcanisation are suggested to contribute to the fatigue activity observed. The evidence suggests that the trimers reproduce αTOC and a mechanism was proposed.

Although antifatigue agents evaluated showed antifatigue activity, most of them had poor thermoxidative resistance, hence it was necessary to compensate for this by using a combination of antioxidants with the antifatigue agents. Reactive antioxidants which have the potential to graft on the polymer chains during reactive processing were used for this purpose. APMA was the most effective antioxidant among other evaluated reactive antioxidants. Although high ratio of grafting was achieved after optimisation of grafting conditions, it is suggested that this was achieved by long branches of APMA due to large extent of polymerisation. This is expected to cause maldistribution of APMA leading to reducing the effect of CB-D activity (while CB-A activity showed clear advantages for grafting). Further optimisation of grafting conditions is required in order to use APMA more effectively. Moreover, although synergistic effects between APMA and antifatigue agents were expected, none of the evaluated antifatigue agents, BQ, αTOC, γTOC and TMQ, showed significant synergism both in fatigue and thermoxidative resistance. They performed just as additives.

Key Words: Antifatigue agents, Antioxidants, Natural Rubber, Fatigue, Mechano degradation, Thermoxidative degradation

Acknowledgements

I would like to acknowledge with gratitude the guidance, advice and continuous encouragement given by my supervisor, Dr. Sahar Al-Malaika, during the course of this work. I am thankful to Professor Gerald Scott for the many valuable suggestions and discussions.

I am also grateful to Bridgestone Corporation for the provision of a research grant to carry out this work.

I acknowledge with thanks the co-operation of all the members of the Polymer Processing and Performance Research Group for their numerous suggestions and discussions. I am grateful to Dr. M. C. Perry for NMR analysis and to the Departmental Technical Staff for practical help given.

My thanks are also due to Dr. K. B. Chakraborty and other members of Robinson Brothers Ltd. for their technical assistance.

Last but by no means least, my special thanks go to my family for their love and encouragement during all these years.

List of Contents

List of Figures

List of Schemes

List of Tables

Chapter 1 Introduction

1.1 Background

Natural rubber (NR) was first discovered by C. Columbus in the Haiti island in 1493. Initially its usage was very limited e.g. in rubber erasers, but after the discovery of the curing process by C. Goodyear in 1839, the applications diversified rapidly. In 1888, J. B. Dunlop invented the pneumatic tire and tire manufactures became the biggest consumers of rubbers. Nowadays NR is used in large number of applications, e.g. conveyer belts, hose tubes, shoe soles, balls, medical supplies.

Ecological and energy saving issues are of major concerns today. In the case of the tire industry, many approaches to the recycling and re-use of tires at the end of their first useful lifecycle have been employed. For example, after the tire tread wears out, the tire may either be retreaded or recycled into fuel or may be blended with asphalt.

The problems associated with the deterioration of rubber products are caused by different parameters: heat (oxidation), uv-light (photoxidation), chemicals (e.g. acids, bases, oils, and organic solvents) and stress (fatigue). Because of their elastic property, many rubber products are often used under severe fatiguing conditions and therefore, studies on the role and action of effective stabilisers which can prevent rubber deterioration under the action of fatigue is very important since this can lead to enhanced service life and reliability of the rubber products. Hence the research work in this thesis focuses on an investigation of the role of antioxidant action of new types of stabilisers for rubbers with the aim of preventing deterioration by fatigue.

1.2 General Properties and Structure of Natural Rubber

Rubber is a very high molecular weight polymer containing highly entangled molecular chains. When a stress is applied on the rubber, the molecular chains stretch and undergo disentanglement and deformation. If the rubber is stretched for a long time, it may not return to its original shape, with a simultaneous loss of elasticity; this is defined as 'plastic deformation, i.e. unrecoverable deformation'. However, vulcanisation (crosslinking) of the rubber limits the freedom of molecular slippage, and when the stress is removed the rubber will then recover to its original shape hence retaining its elasticity (elastic deformation), see Fig. 1.1 [1]. Vulcanisation, therefore, is a process which transforms the predominantly thermoplastic raw rubber into an elastic rubbery material by association of macromolecules through reactive sites; this process is also called crosslinking or curing.

Fig.1.1 Schematic representation of plastic and elastic deformation of rubber [1].

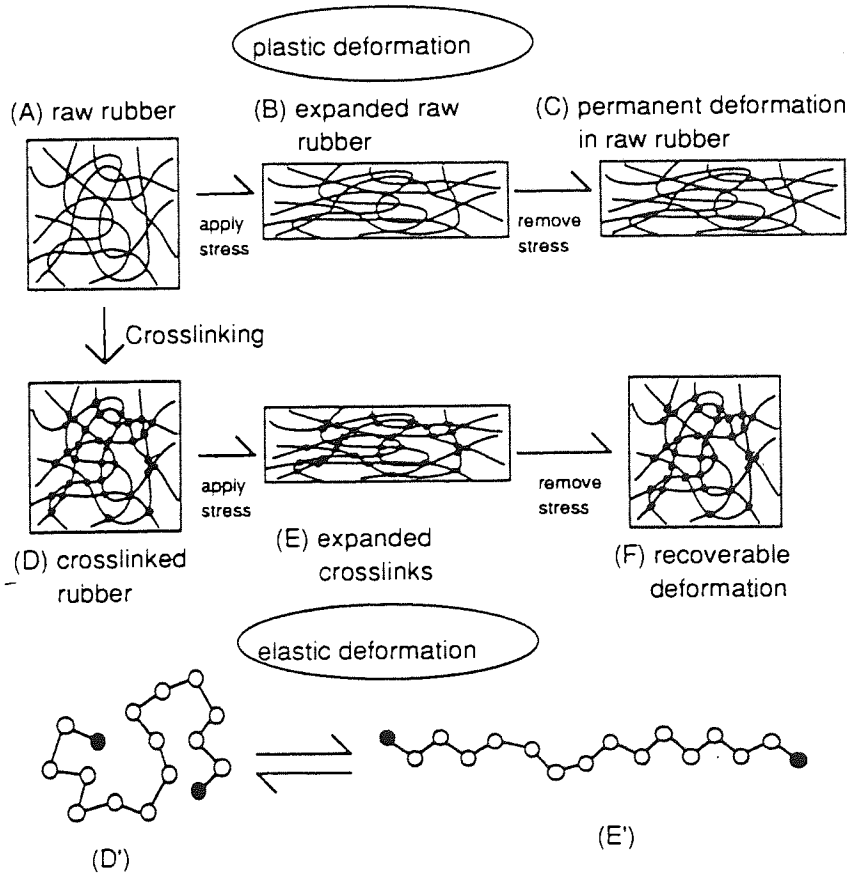

There is a close relationship between structure and properties (mechanical and chemical) of rubber. For example, natural rubber (NR) which has an isoprene (IR) repeat unit , see fig. 1.2, has good elastic properties but has poor thermoxidative and UV stability and is highly susceptible to attack by ozone due to the presence of the double bonds in the main chain.

Fig. 1.2 Structure of isoprene repeate unit of NR.

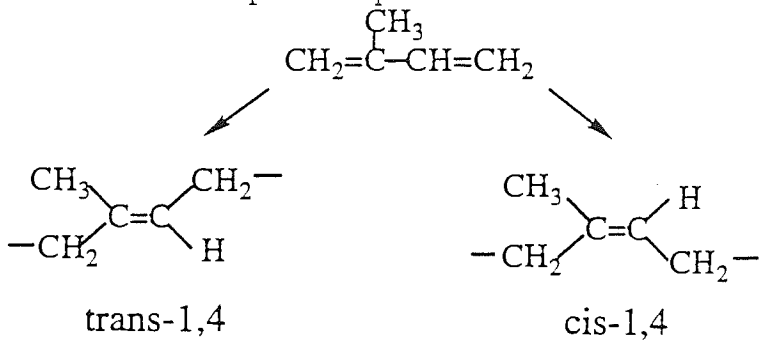

1.3 Crosslinking of Rubber (Vulcanisation)

During curing, the chain-like molecules become joined by chemical crosslinks and one out of every hundred isoprene units in natural rubber become crosslinked in any practical cure. There are mainly two types of crosslinks; the bridge-type bonds and the C-C crosslinks [2]. The bridge-type bonds are formed by curing agents which are bivalent (e.g. sulphur and its analogues) or bifunctional organic compounds. Carbon-carbon crosslinks are effected by high energy radiation or substances which form monovalent free radicals under curing condition. In this research sulphur curing system was used throughout the work.

1.3.1. Accelerated Sulphur Curing.

Sulphur is the most common crosslinking agents for NR; however, it is generally used with other components such as accelerators and activators (e.g. zinc oxide and stearic acid) due to the slow crosslinking rate. The reaction mechanism of curing process is very complicated and depends on the type of the accelerator used;. thiazoles are one of the most widely used accelerators in the industry. The mechanisms of their action can be divided into three steps [3, 4], first of all, formation of sulfurating reagents from vulcanising ingredients, scheme 1.1 (1), this is followed by initial crosslinking of the rubber molecules, scheme 1.1 (2), and finally the full formation of a networks step, scheme 1.1 (3). Although thiazoles themselves have strong S-nucleophilicity, they become stronger when zinc oxide and stearic acid form intermediates with the accelerators [5-7], see Fig.1.3.

Scheme 1.1. Vulcanisation mechanisms of NR in the presence of thiazoles-sulphur system.

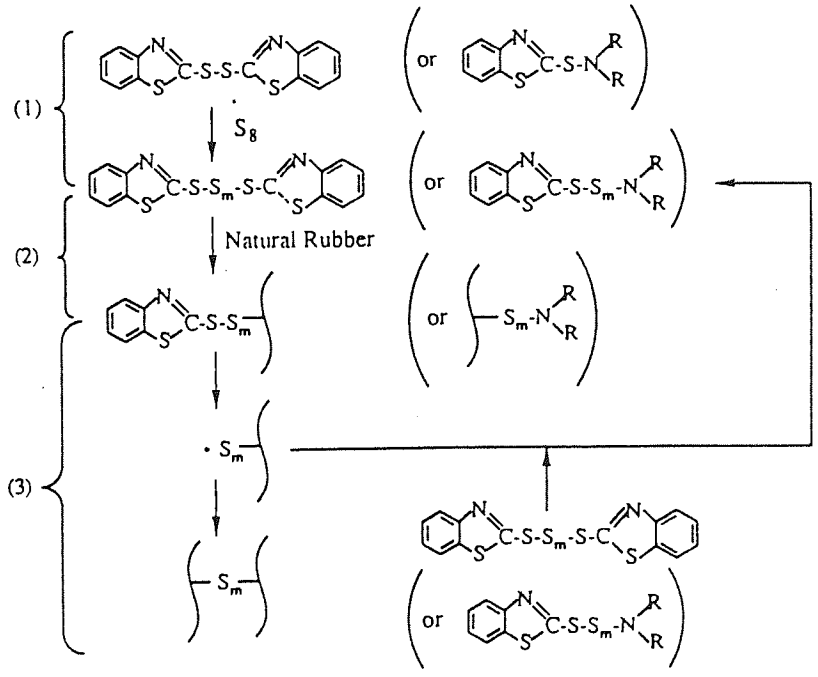

Fig. 1.3. Intermediate materials from thiazoles, zinc oxide and stearic acid [5, 8].

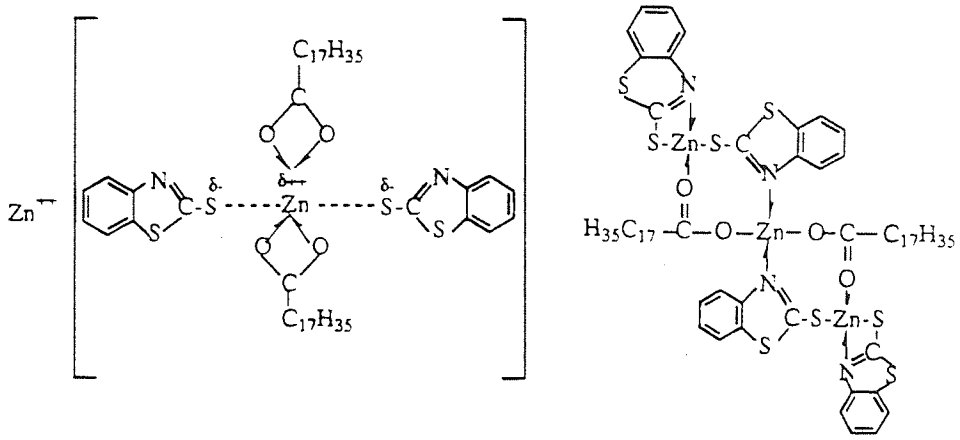

A model for the different sulphur crosslink structures produced from the above reactions is shown in fig. 1.4 and consist of cyclic sulphur structure, monosulfide crosslinks, disulphide crosslinks, polysulphide crosslinks, and pendant sulphide groups [9].

Fig. 1.4. Model of different structures of crosslinks in NR [9].

A : Unmodified Polymer

B : Crosslinks: (a) monosulphide, (b) disulphide, (c) polysulphide

C : (d) cyclic, and (e) pendant

E.N.M. : Extranetwork materials

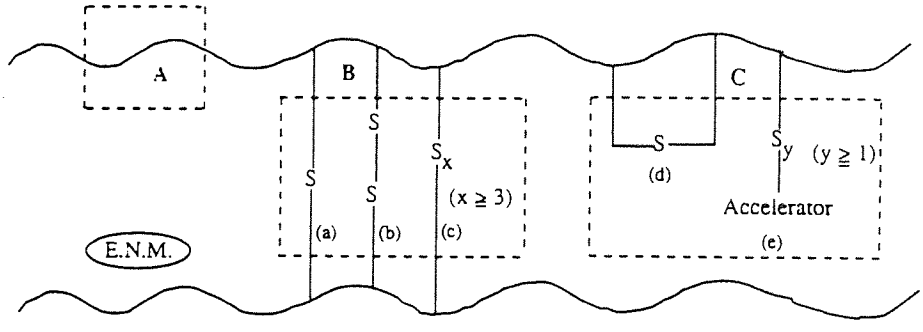

When CBS is used as an accelerator, the distribution of the crosslink structure changes with curing time as shown in fig. 1.5 [10]. The density of the polysulphide crosslinks decrease, while that of monosulphide crosslinks increase with increasing curing time.

Fig. 1.5. Distribution of crosslink types and pendant groups as a function of cure time at 140°C for NR vulcanised with sulphur and CBS (S 1.5, CBS 2.37, ZnO 5, Lauric Acid 1 phr) [10].

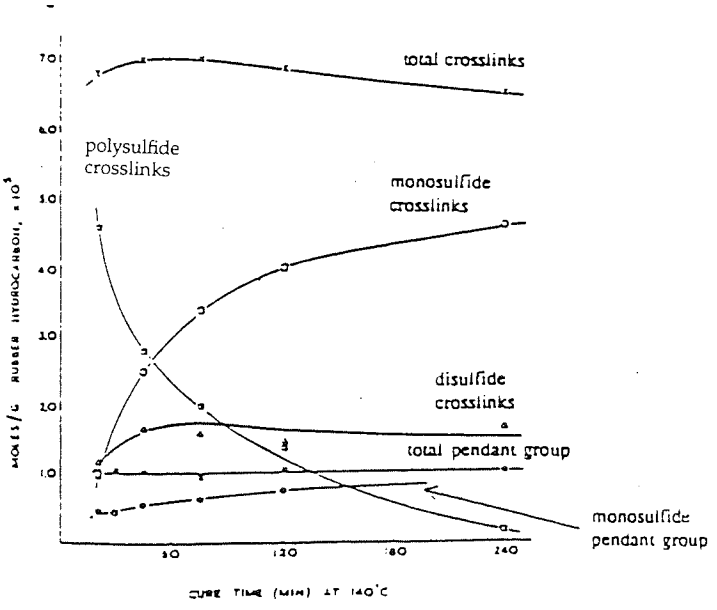

1.3.2. Effects of Crosslinkings on Properties of Rubber

The physical properties of vulcanisates are influenced by the crosslink densities and crosslink structures. The major effects of crosslink densities are summarised in table 1.1 [11] and are illustrated in fig. 1.6 [12]. In general, the properties derived from nondestructive tests, such as modulous, hardness, and permanent set either increase or decrease in a simple manner, whereas the properties derived from destructive tests such as tear strength and tensile strength show typically a peak.

Table 1.1. Influence of degree of crosslinkings on physical properties of vulcanisates [11].

Property	Change with increase in degree of crosslinking
Properties dependent only on degree of crosslinking	
stiffness	increase
hardness	increase
Properties partly dependent on degree of crosslinking	
elongation to break	decrease
resilience	increase
heat build-up	decrease
solvent swelling	decrease
creep, stress relaxation	decrease
set	decrease
abrasion resistance	increase
fatigue cracking	increase
low temperature crystallisation	decrease in rate
tensile strength, tear strength	increase, then decrease

Fig. 1.6. Effects of crosslink density on properties [12].

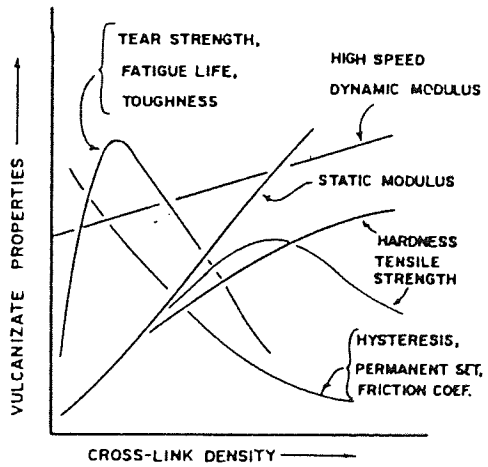

The relationship between the structure of the crosslink and properties of the vulcanised rubber is shown in table 1.2. and fig. 1.7 [5].

Table 1.2. Influence of di- and polysulphide crosslinkings on properties [11].

Property	Change with increase in proportion of di- and polysulphides
creep, stress relaxation	increase
set	increase
incremental swelling	increase
tensile strength, tear strength	increase
resilience	increase
fatigue failure	decrease
heat resilience	decrease
thermal ageing resistance	decrease

Fig. 1.7. Tensile strength of pure gum NR vulcanisates plotted against 1/Mc for various vulcanisation system [5].

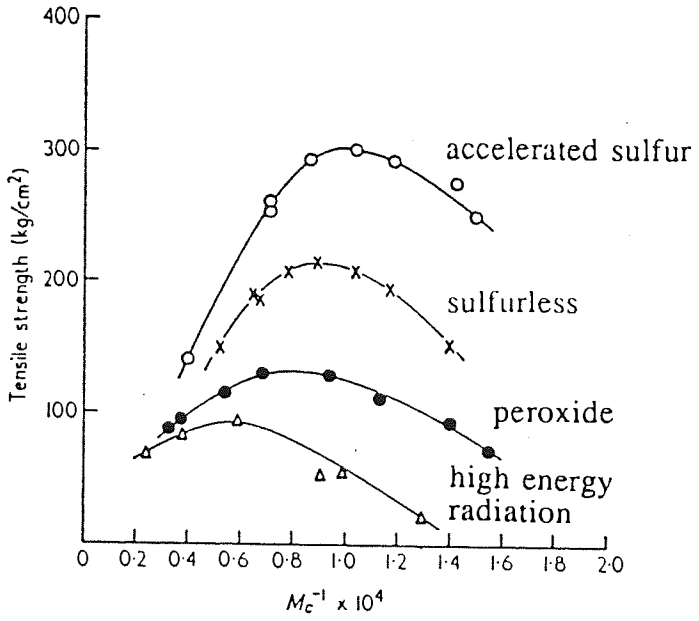

1.4. Thermal Oxidative Degradation of NR.

The word "degradation" has been used in connection with the deterioration of properties of both raw rubber and final fabricated products caused by physical or chemical changes during storage and in service. It is important to define clearly the differences in the degradation modes. In this work, the terms "thermal degradation", and "thermal oxidation" are used to describe the deterioration of properties caused by chemical changes under the effect of high temperature and air. (This does not include anaerobic thermal ageing such under nitrogen, argon or vacuum atmosphere.) The terms "fatiguing", "physical ageing" and "mechano degradation" are used to describe the deterioration of properties caused by both physical and chemical changes which are initiated mechanically (by stress) during service or during processing.

Thermal oxidation of vulcanised rubber involves oxidation of the main chain as well as that of the crosslinks. A simplified picture of a rubber vulcanisate (see fig. 1.4) includes a network and extra network materials, the latter consists of uncured vulcanisation ingredients and products of the vulcanisation reaction without combining with the networks. The network consists of; (A) the main chains of the original rubber molecules; (B) the crosslinks which may be mono, di, or polysulphides, including structural features of the main chain in the immediate vicinity of crosslinks; and (C) modification at sites away from the crosslinks [9].

1.4.1. Thermal Degradation along the Main Chain (Part A).

Polymer oxidation occures via a complex set of elementary reaction steps during the stages of initiation, propagation, and termination, see scheme 1.2 [13-15].

Scheme 1.2 Radical chain mechanisms of hydrocarbon autoxidation [13-15].

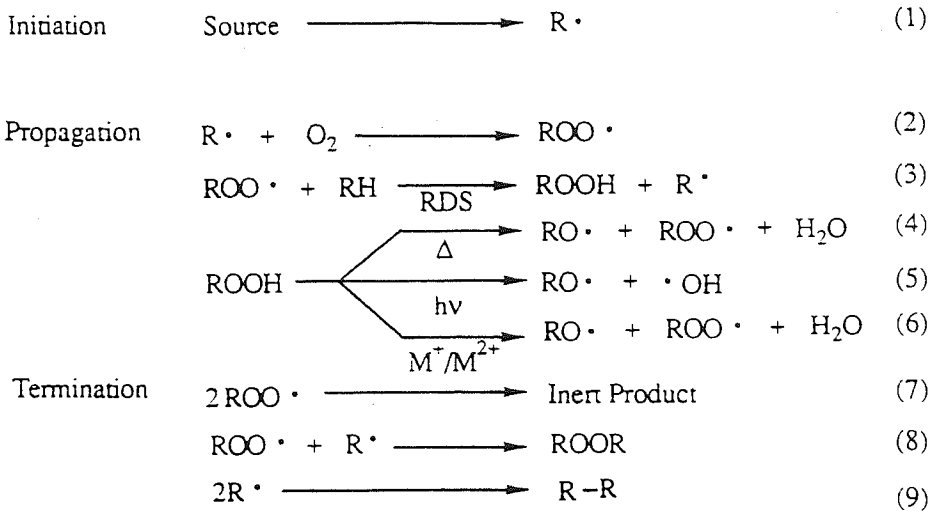

The rate determining step is the reaction of alkylperoxyl radicals with hydrogen and the ease of H-abstraction depends on the structure of the polymer [16-18], α-H in NR chain is easily abstracted due to resonance stabilisation of the radical produced and the main oxidation mechanisms of NR are shown in scheme 1.3 [9, 19].

Scheme 1.3. Oxidation mechanisms of NR [9, 19].

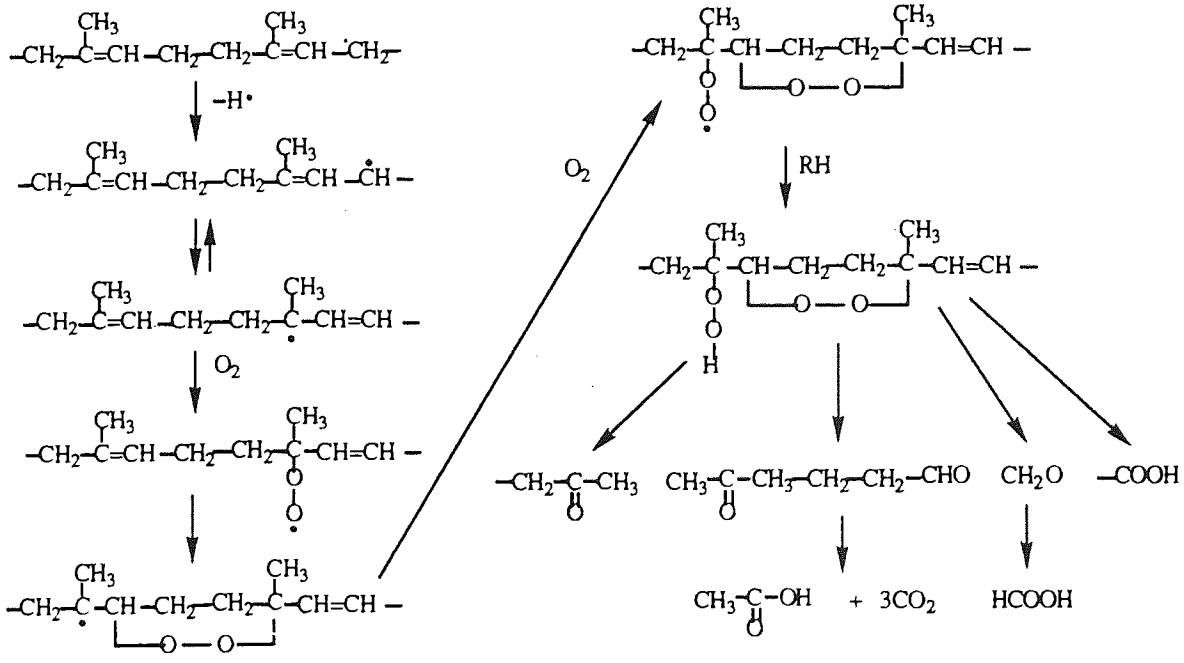

1.4.2. Thermal Oxidation at Crosslinks (Part B and C).

Although the number of crosslinks in a typical vulcanised NR is much lower than that of the main chain units, oxidation of crosslinks is quite important. Further, the degradation rates of the same rubber vary depending on the nature of the curing system used. Polysulphide crosslinks for example are easily cleaved hence they can act as initiators for the radical chain reaction, see scheme 1.4 [1]. The bond dissociation energy of polysulphide closslinks is lower than that of monosulphide or carbon to carbon crosslink, see table 1.3 [20, 21].

Scheme 1.4. Oxidation at polysulphide crosslink [1].

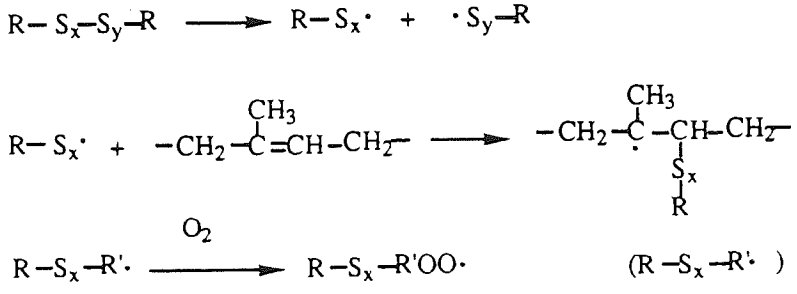

Table 1.3. Dissociation energy for variety types of crosslink structures [20, 21].

Crosslink Structure	Curing System	Dissociation Energy (kcal/mol)
C-Sx-C	S + CBS	27.5
C-S-S-C	TT	27.5
C-S-C	TT	54.5
C-C	DCP	62.3

Oxidation of rubber containing monosulphidic crosslinks is shown in scheme 1.5 [9].

Scheme 1.5. Oxidation at monosulphide crosslink [9].

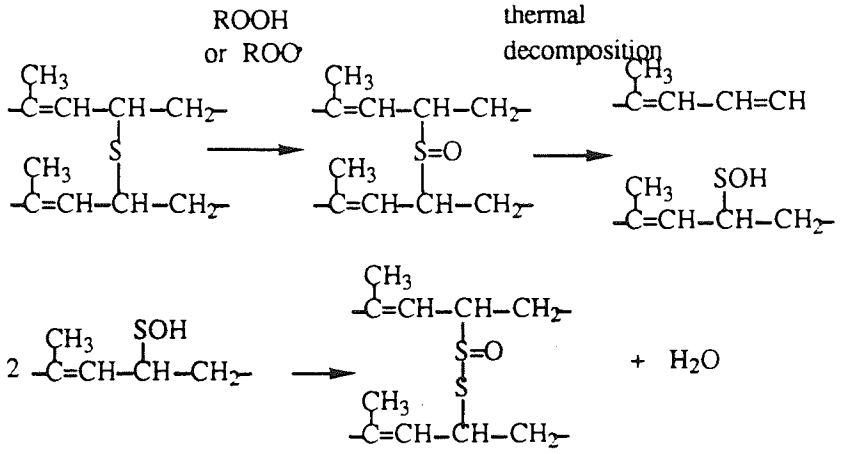

Furthermore, oxidation can take place on the carbon next to a crosslinking site as shown in scheme 1.6 [9].

Scheme 1.6. Oxidation near the crosslink [9].

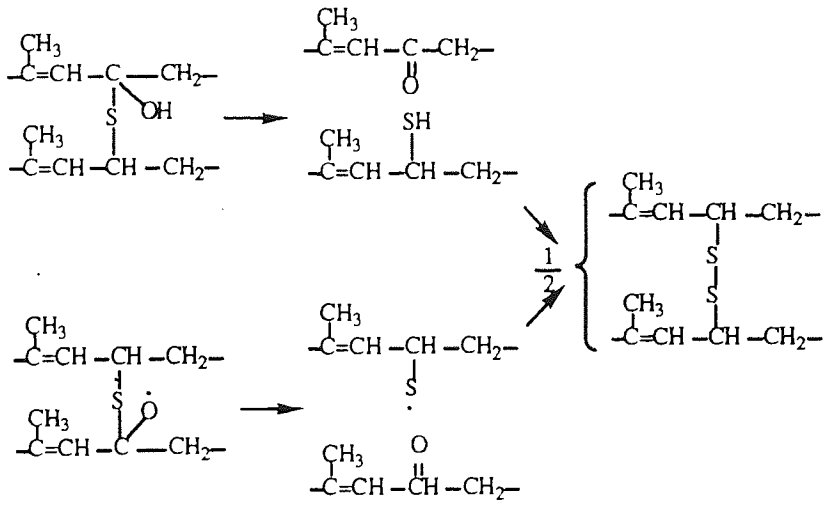

1.5. Mechano Degradation (Fatigue)

Mechano degradation can be divided into three categories; degradation of unvulcanised rubber by milling and processing , degradation of vulcanised rubber caused by intermittent stress (fatigue), and degradation caused by ultrasound. In this chapter fatigue will be discussed mainly.

As mentioned before, fatigue can be defined as the deterioration of properties caused by both physical and chemical changes which are initiated by repeated stress or strain. Repeated mechanical inputs are normally applied onto the rubber, via one of a number of modes; viz. (1) regular or irregular input, (2) constant stress or strain, (3) continuous or intermittent application of force and different magnitude of frequency, (4) force applied in extension, compression, shear or any combination of these, (5) monoaxial, biaxial or triaxial, (6) for a given constant stress (or strain, shear), either upper, lower or both limits are kept constant, etc.

1.5.1. Basic Theory of Fatigue

There are two theories which explain the process of failure of rubber exposed to intermittent stress. Radical transformation theory has been proposed [22]. When rubber is deformed, one of rubber chains can not stand the stress and will eventually rupture. Radicals will be generated at the end of the ruptured chains, which will propagate involving the other chains close by and resulting in the failure of rubber, see fig. 1.8.

Fig. 1.8. Rubber failure by propagation of radical reaction: (a) stress induced chain scission, (b) formation of chain-end radicals, (c) radical reaction leading to main-chain radicals, (d) scission of radicalised chains, (e) formation of a submicrocrack by repetition of the steps (c) and (d); ⊗ chain-end radical e.g. $-CH_2-\dot{C}H_2$, ⊗ main-chain radical e.g. $-CH_2-\dot{C}H-CH_2-$, • stable end groups e.g. $-CH_2-CH_3$. (Zhurkov's theory in ref. 22)

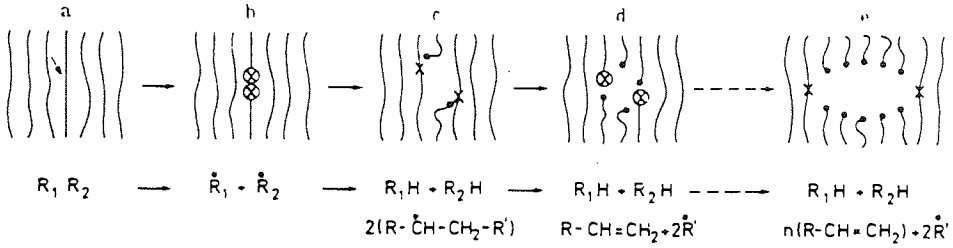

Another theory is based on the failure of rubber caused by the stress concentration of flaw. The theory of cut growth and fatigue was presented by Lake et. al. [23]. The basic process of cut growth was studied under static and dynamic conditions. A cut was shown to grow if the energy stored elastically at the tip of the cut by the imposed deformation exceeded the characteristic energy for tearing. If the rubber strip has a cut of length C which is under tension, the tearing energy T will be given by equation (1).

$$T=2KWC \qquad (1)$$

where K is a function of the extension ratio and W is the strain energy / unit volume. For a number of polymers, the rate of cut growth has been shown as described in equation (2).

$$\frac{dC}{dN} = \frac{T^n}{G} \qquad (2)$$

where G is a cut growth constant and n is constant. combining equations (1) and (2),

$$\frac{dC}{dN} = \frac{(2KWC)^n}{G} \qquad (3)$$

Integrating (3)

$$N = \frac{G}{(n-1)(2KW)^n}\left[\frac{1}{C_0^{n-1}} - \frac{1}{C^{n-1}}\right] \qquad (4)$$

where N is the number of cycles for cut growth from length C_o to length C. If $C >> C_o$, then equation (4) becomes

$$N = \frac{G}{(n-1)(2KW)^n} \cdot \frac{1}{C_0^{n-1}} = \frac{G'}{(n-1)w^n} \cdot \frac{1}{C_0^{n-1}} \qquad (5)$$

where G′ is modified cut growth constant. In the absence of an imposed cut, equation (5) will be obeyed and C_o becomes the effective initial flaw size. Plotting log(fatigue life, N) against log(strain energy, W), the gradient of a fatigue curve gives a constant n; typical fatigue curve is shown in fig. 1.9. It consist of three regions; in the small strain region, cut growth was shown to be ozone controlled, while in the higher strain region, catastrophic tear occurs [23]. Usually equations (4) and (5) are applicable in the middle region.

Fig. 1.9 Typical full fatigue curve.

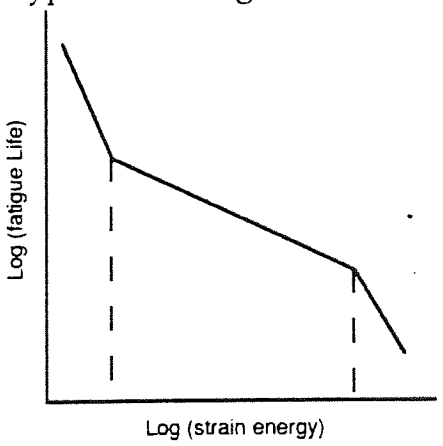

1.5.2. Mechano-Chemical Analysis of Fatigue Phenomena

When stress is applied to a rubber test piece, the mechanical energy applied will either disperse through the relaxation process or used for chain scission. Both of these processes occur competitively [24]. If all energy is released by relaxation, there will be no chemical reaction. In the case of NR, the following chain scission process were presented, see scheme 1.7 [25]. The weakest carbon-carbon bonds are cleaved and form free radicals which subsequently react with oxygen to give rise to alkylperoxyl radicals.

Scheme 1.7 Radical formation by stress [25].

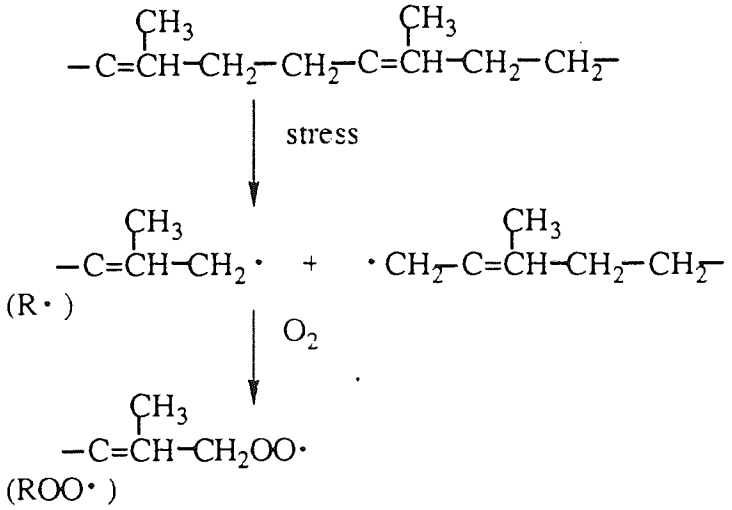

Obviously the radical formation will increase when the relaxation process is disturbed. Hence the polarity of the polymer, any hydrogen bonding, crystallinity, and mobility of the chains will affect the radical formation process. From this point of view, it is possible to classify polymers into three categories, see table 1.4.

Table 1.4 Concentration of free radicals formed under tension [26, 27].

Polymer		[R·] (spins / cm^3)
1. Amorphous Polymer		
PS		$10^{13} \sim 10^{14}$
PMMA		
PVC		
2. Crystalline Fibbers		
nonpolar :	PE, PP	$10^{13} \sim 5 \times 10^{16}$
polar :	PC	2×10^{16}
	PET	5×10^{16}
	Nylon, Nylon-6.6	$5 \times 10^{16} \sim 5 \times 10^{18}$
	Silk	$10^{17} \sim 10^{18}$
3. Rubbers		
NR		$4 \times 10^{17} \sim 11 \times 10^{18}$
Silicone Rubber		$2 \times 10^{16} \sim 5 \times 10^{16}$
Acrylonitlile-Butadiene Rubber		$10^{17} \sim 10^{18}$

Compared with other polymers, the concentration of radicals generated in rubbers were shown to be much higher than in other polymers. It was explained that rubbers have large number of entanglements of chains due to their low Tg leads to higher mobility of the chains [26]. This causes more local stress between entanglement points and will have more possibilities of chain scission.

Natarajan et. al. studied the relationship between yield stress, sulphur concentration, and spin concentration formed, see fig. 1.10 [28]. Andrews presented the quantitative discussion of the relationship between radical formation and sulphur concentration, and presented the linear relation between **log [R·]** and **1/3 log [S%]** [29].

Fig. 1.10 Yield, crazing, and fracture behaviour of cis-polyisoprene (cross-linked by sulphur) below Tg. pre-orientation 100% [28].

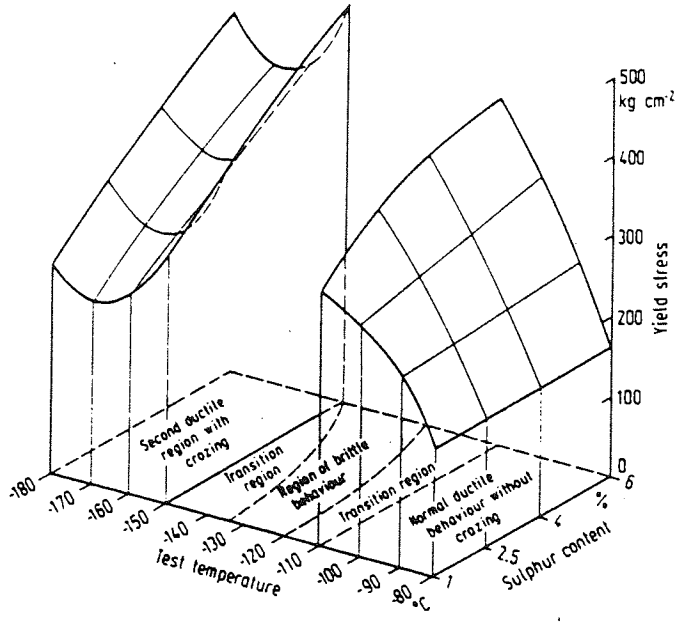

1.5.3. Effect of Polymer Structure, Closslink Structure.

As mentioned in the previous section, radical formation by chain scission occurs competitively with the relaxation process. Hence fatigue resistance will be affected by polymer structure, crosslink structure and its density.

(1) Polymer Structure and Molecular Weight

Higher mobility chains will have more resistance to stress. The mobility of a chain will depend on the free volume, interaction by polar functional groups, and condition of packing of molecular segments [30]. For example, in the case of styrene-butadiene rubber (SBR) which has large functional group lead to higher radical concentration [31], see fig. 1.11, and is well known to be less fatigue resistant.

Fig. 1.11 Spin density of fatigued vulcanised rubbers [31].

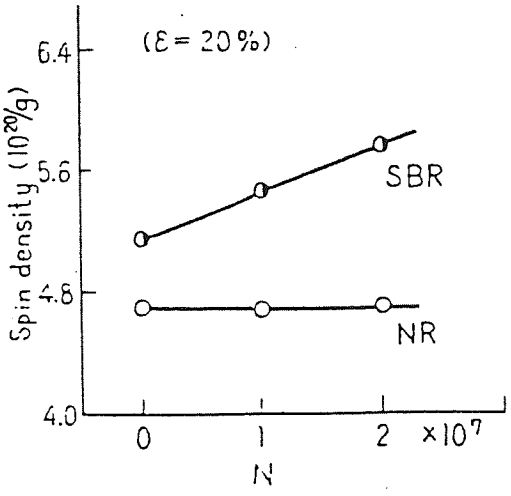

Generally in other polymer materials, the higher the molecular weight of polymers, the higher is the fatigue resistance [32], see fig. 1.12. (The molecular weight involved in this relationship is not weight-average molecular weight but number-average molecular weight.) Hence molecular weight will also affect the fatigue resistance.

Fig. 1.12 Effect of molecular weight on fatigue behavior of PS [33].

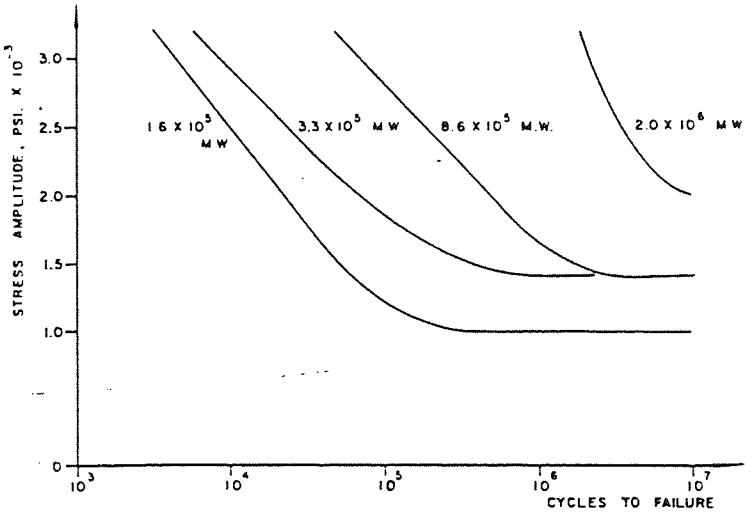

(2) Crosslink Structure and its Density.

Generally, under constant strain stretching condition, rubbers which have higher polysulphide ratios show better fatigue resistance [30, 34], see fig. 1.13. It has been explained that the restructuring (rupture and rebinding) of crosslinks will increase relaxation. Although polysulphides are effective in enhancing fatigue life, they cause changes of properties during fatigue, see table 1.5. The crosslink density and the uniformity of crosslinking are expected to affect the fatigue resistance as well.

Fig. 1.13 Effect of crosslink structure on fatigue life of different rubbers [34].
(DPG : diphenyl guanidine, TT : tetramethylthiuramdisulfide)

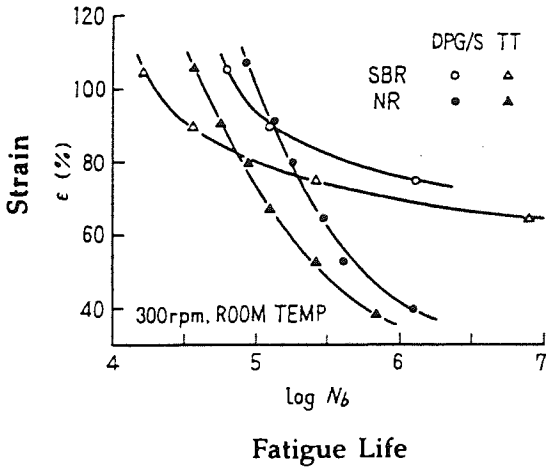

Table 1.5 Effect of crosslink structure on properties changes during fatigue [30].
(DPG : diphenyl guanidine, MBT : mercaptobenzothiazole
TT : tetramethylthiuramdisulfide)

	Retention of Properties (%)		
	Guanidines (DPG + S)	Thiazoles (MBT + S)	Thiurams (TT)
tan δ	-31	-25	+2.0
Eb	-8.9	-9.0	-7.0
Tb	-6.0	-2.6	+1.5
Tear	-30	-22	0

1.5.4 Effect of Fatigue Variables.

There are large numbers of factors which affect fatigue resistance, see table 1.6. Typical examples of fatigue variables are shown in figures 1.14 - 19 [23, 35-38].

Table 1.6 Factors which affect fatigue resistance of rubbers.

Energy Input Modes
Constant stress or Constant Strain
Compression, extension, torsion bending, or shear
Monoaxial or biaxial
Lower Limit Strain (or Stress) is Zero or not
Testing Conditions
Frequency
Temperature
Humidity
Atmosphere
Test Pieces
Shape of Test pieces
Initial Cut or not

Fig. 1.14 Effect of Strain on fatigue life [35].

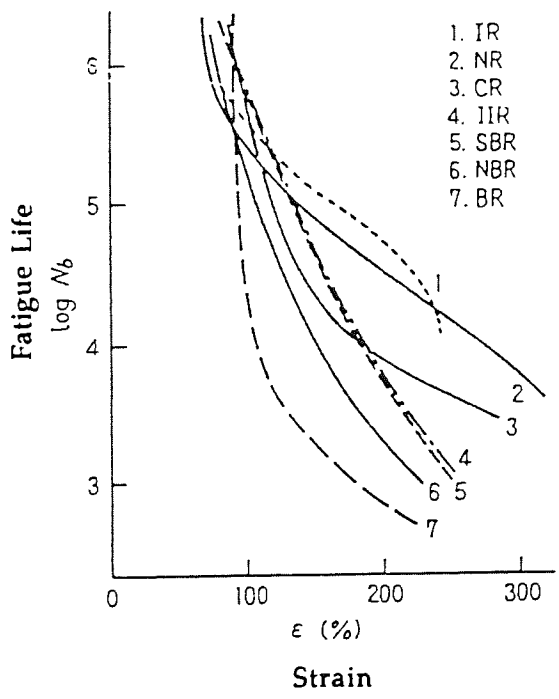

Fig. 1.15 Effect of non-zero strain cycles on fatigue. (fatigue life as function of minimum strain of cycle, maximum 250%, for vulcanisates of NR and SBR) [23].

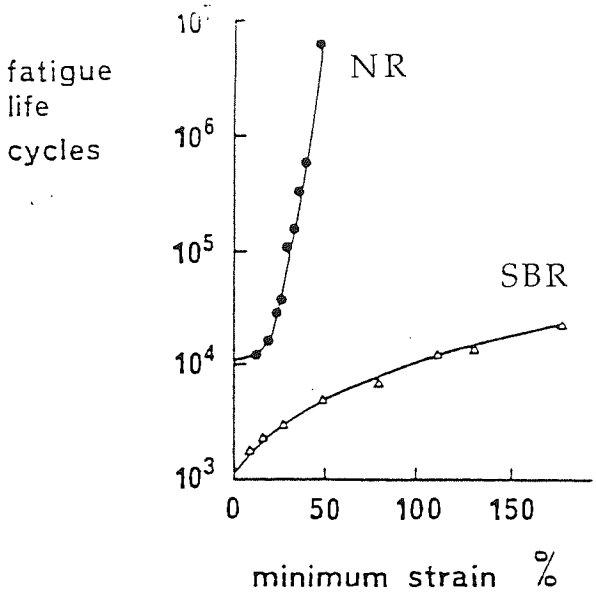

Fig. 1.16 Fatigue life versus temperature for test pieces of NR and SBR stretched repeatedly to 175% tension [38].

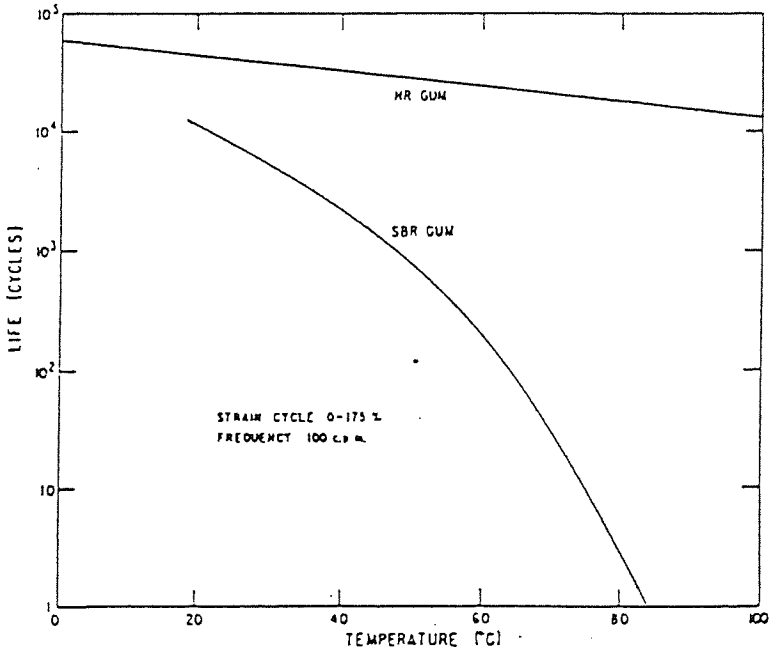

Fig. 1.17 Oxidative effects on fatigue life for a NR vulcanisate [23].

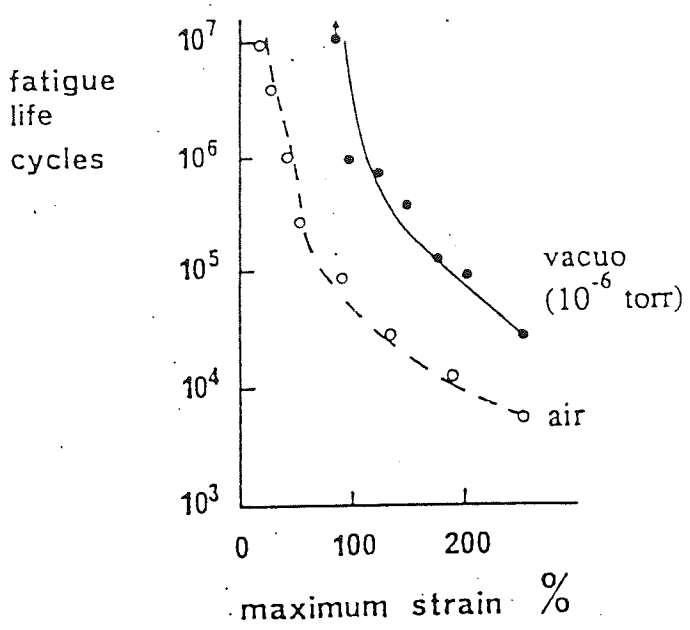

Fig. 1.18 Effects of ozone concentration on fatigue life for a NR vulcanisate [23]. (fatigue strain cycle 0 - 150 %, 100 cycles / min)

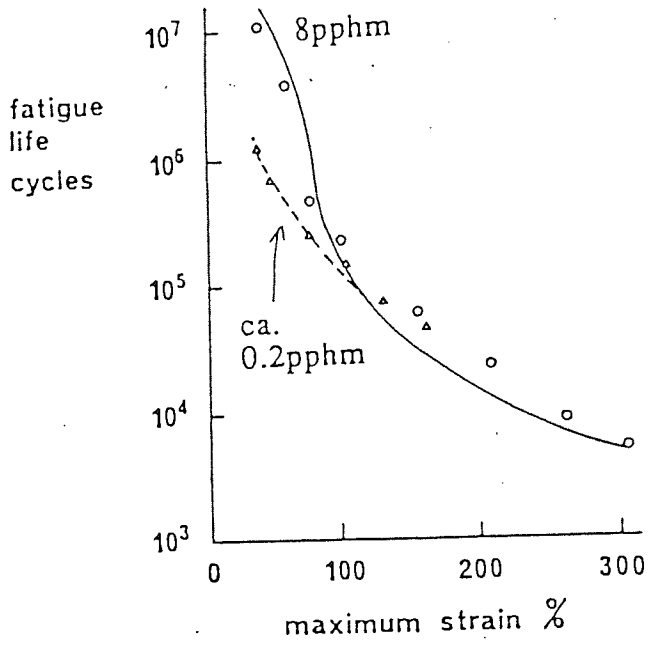

Fig. 1.19 Fatigue life versus depth of initial cut for test pieces of NR and SBR stretches repeatedly to 50% extension [36, 37].

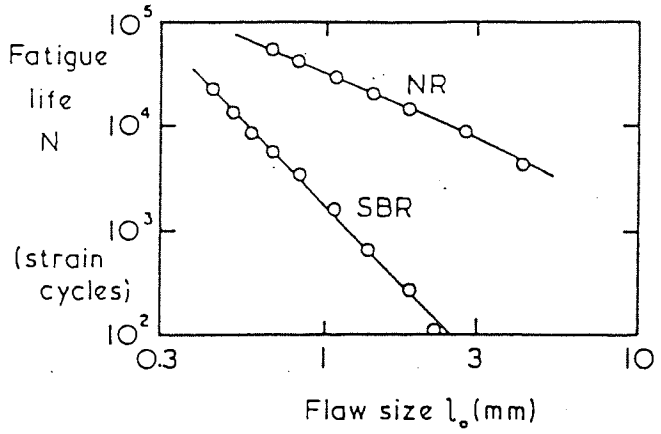

1.5.5 Statistical Approach to Fatigue.

(1) The Pattern of Fatigue Failures with Time.

There are three basic ways which characteristic in fatigue failures; decreasing, constant, and increasing failure rate, see fig. 1.20 [39-41]. The decreasing failure rate curve is observed when materials contain weak points, for example in case of rubbers flaws, heterogeneties, cuts, dirt particles, gel, moulding defects all of which may cause failures in the early stages of fatigue. The constant failure rate curve, on the other hand, is caused by the externally induced failure and it is random. For example, products in service may have extraordinary overload and failure compared with the average application load. Finally, the increasing failure rate curve is brought about by material deterioration due to fatigue. The combination of these three curves are called as bathtub curve [39-41].

Fig. 1.20 The bathtub curve [39-41].

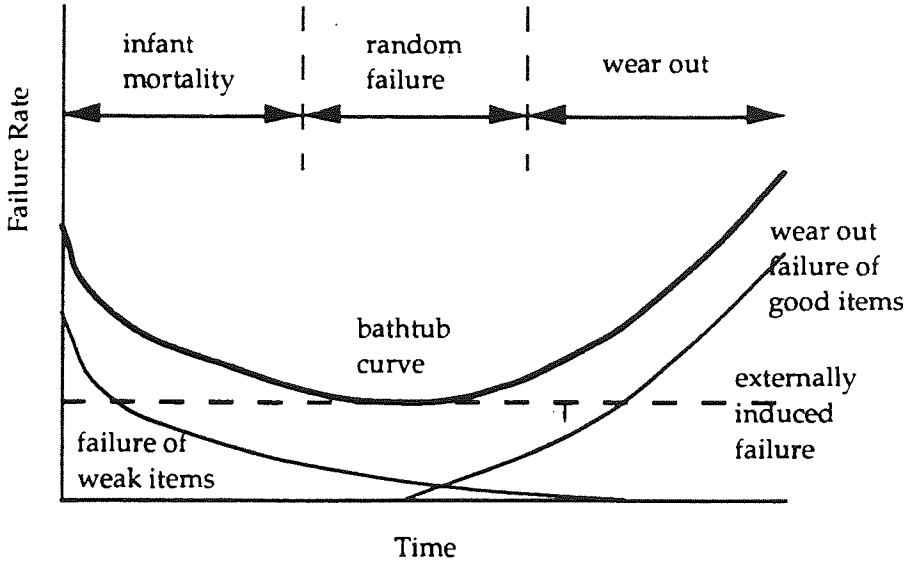

(2) Distribution of Failure

For the analysis of "wear out" failure, several mathematical models have been constructed; Weibull, normal, lognormal, gamma, binormal exponential distribution etc [40, 42]. The model can be applied case by case according to the type of materials and ways of fatiguing. The definition of technical terms often used are as follows [40, 41, 43];

f(t) = probability density function of occurrence of failure

F(t) = cumulative probability function of occurrence of failure

R(t) = cumulative probability function of occurrence of survival

$$f(t) = \frac{d}{dt}[F(t)] = -\frac{d}{dt}[R(t)]$$

$$F(t) = 1 - R(t)$$

$\lambda(t)$ = failure rate or hazard

$$\lambda(t) = \frac{f(t)}{R(t)} = -\frac{\frac{d}{dt}[R(t)]}{R(t)}$$

Fig. 1.21 Graphical representation of failure's terms.

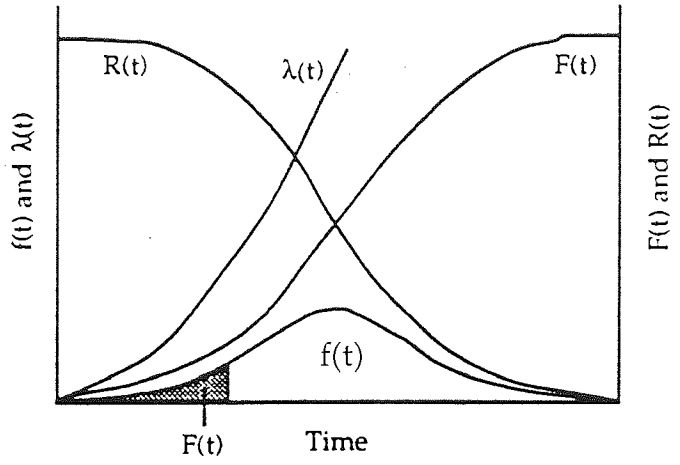

(3) Load - Strength Model

The basic idea of fatigue failure can be explained by the relationship of load and strength distributions. The failure occurs when these distribution start interfering, even though the nominal strength of material is higher than the mean load applied [40, 44, 45]. Initially products are designed not to have these curves interfering; however, the material strength decays during the service due to deterioration resulting in an overlap of these curves.

Fig. 1.22 Load - strength interfering distribution [40, 44, 45].

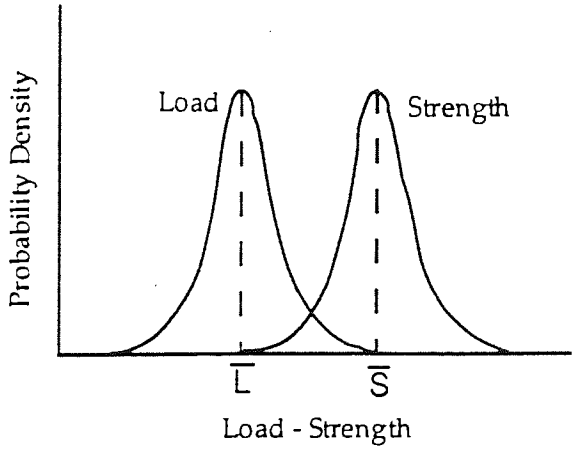

1.5.6 Fatigue Fractography

The morphology of fracture surface represents well the process involved in the fracture. It provides important information on deformation, tearing, crack initiation, crack propagation, crack deviation etc [46]. Compared with other materials such as metal, the fractography of rubber has been less studied. There are many ways to express the surface condition. Deuri et. al. defined the terms, see fig. 1.23 [47].

Fig. 1.23 Nomenclature of different terms used in morphology of fracture surface [47].

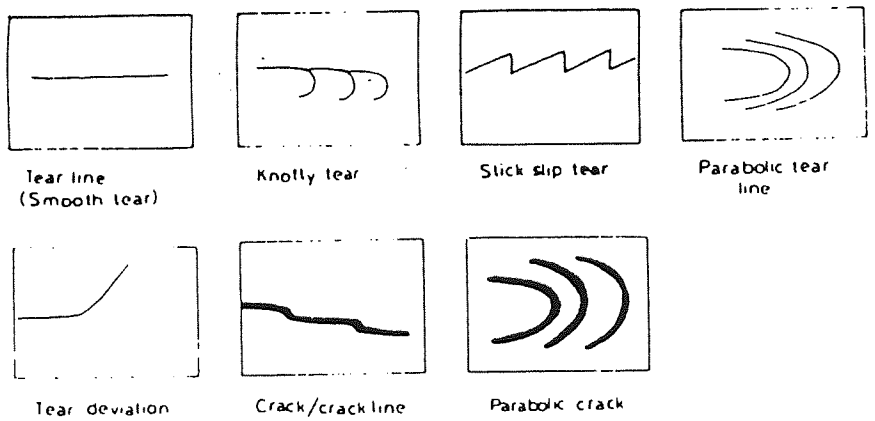

Kawamura et. al. also classified the surface morphology of rubber fracture in terms of macroscopic and microscopic observation [48]. They defined mirror region, rough region, tear-line pattern, crack pattern, lumpy pattern, and beach mark as macroscopic fracture pattern and also defined parabola pattern, pin-hole pattern, mirror pattern, tear line pattern, river pattern, striation pattern, cross pattern, cast iron-like pattern, flake pattern, cedar pattern, and tire truck pattern as microscopic fracture surface.

1.6 Protection of Degradation Process

Stabilisers for rubber can be classified into three categories; antioxidants, antiozonants, and antifatigue agents, according to the causes of deterioration.

1.6.1 Antioxidants

Antioxidants are chemical agents which can effectively interfere with the autoxidation cycles [15] (see scheme 1.8) and hence protect the polymer during fabrication and in service. Antioxidants can therefore be classified according to the mechanism by which they interfere with the oxidation cycles. There are two types of antioxidants. They are referred to as chain breaking (CB) antioxidants and peroxide decomposers (PD), see scheme 1.8.

Scheme 1.8 Oxidative degradation process and antioxidant mechanisms [15].

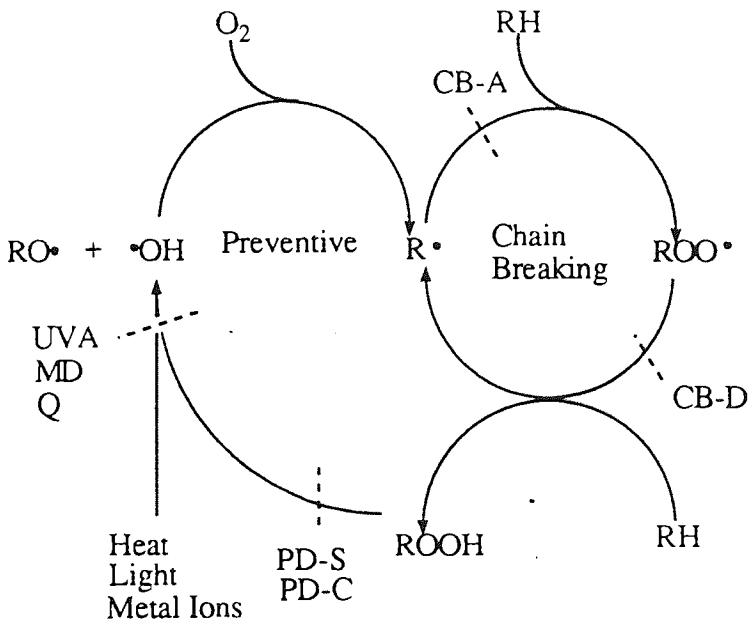

1.6.1.1 Chain Breaking Antioxidants (CB) [15]

Chain breaking antioxidants interfere with the main oxidative cycle by deactivating the propagating radicals before their reaction with other molecules. They can be subdivided into electron acceptors (CB-A) and electron donors (CB-D) according to the way they inactivate the different propagating radicals. CB-A antioxidants oxidise or spin trap alkylradicals in absence of oxygen and may ultimately form unsaturation, while CB-D antioxidants reduce peroxyl radicals to hydroperoxides.

Usually under normal oxygen pressure, the formation of alkylperoxyl radical ($R\bullet + O_2 \rightarrow ROO\bullet$) is much faster than the formation of alkyl radical ($RH \rightarrow R\cdot$), so ROO · plays more important roll in termination process. Hence CB-D antioxidants are widely used, while CB-A antioxidants normally operate only under low oxygen concentration (or high alkyl radical concentration) condition.

CB-D (AH) antioxidants react with peroxyl radical ($ROO\bullet$) and provide a proton to terminate the chain reaction; the stable radical produced lead to further products which may be antioxidants' themselves or pro-oxides.

$$ROO\bullet + AH \rightarrow ROOH + A\bullet$$

Hindered phenols and arylamines are well known to work by this mechanisms. Generally amines show better stabilising performance but most of them have staining properties. Phenols are mainly used for products in which is not acceptable staining. Scheme 1.9 an 1.10 show the chemistry of oxidation of N-phenyl-N'-isopropyl-p-phenylenediamine (IPPD) and 2,6-di-t-butyl-4-methylphenol (BHT).

Scheme 1.9 Alternative transformation products of IPPD in the presence of alkylperoxyl radicals [49].

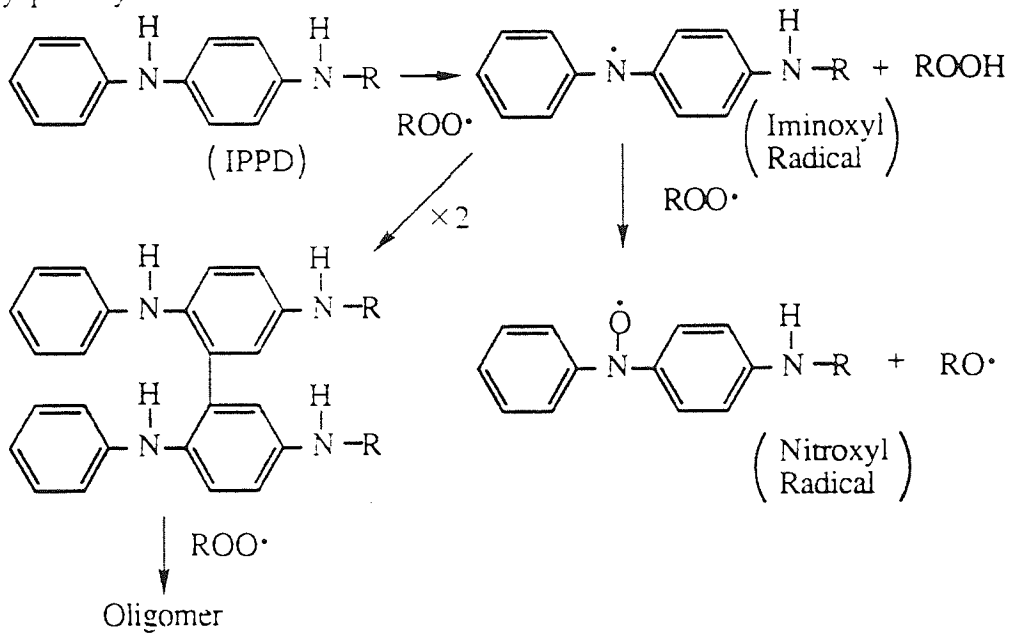

Scheme 1.10 Chemistry of oxidation of BHT [15].

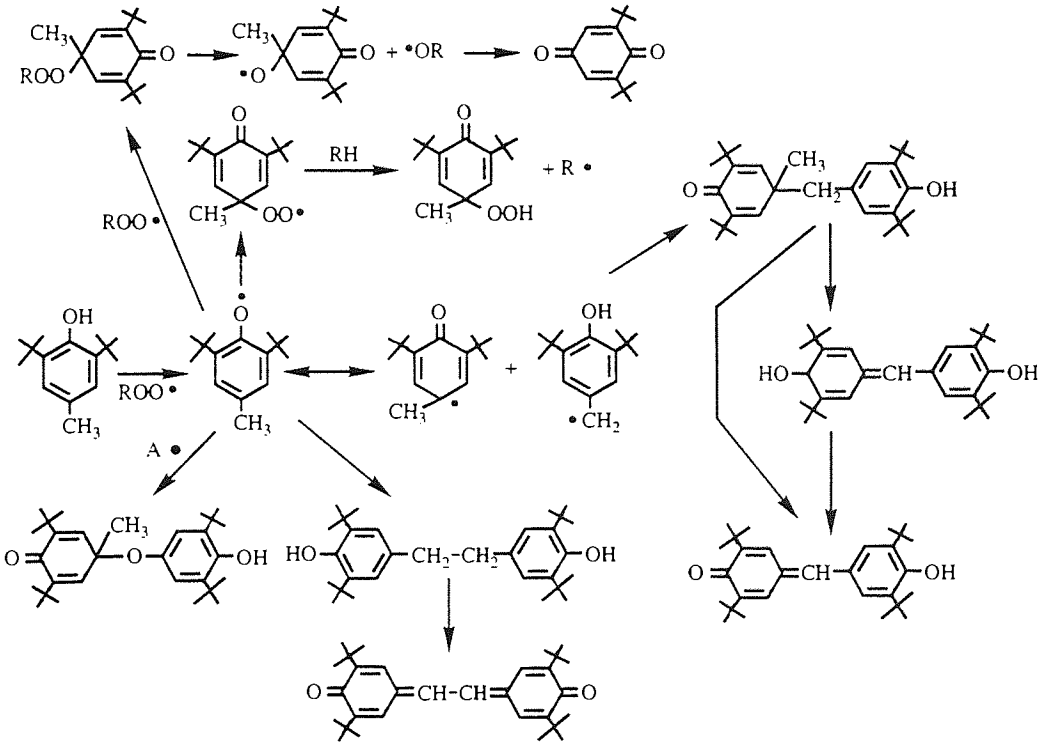

1.6.1.2 Preventive Antioxidants [15)]

One way of reducing the effects of initiating radicals is to remove substances which may produce these radicals and hence preventing the process of the chain reaction hence the class of preventive antioxidants. Peroxide decomposers (PD) are the most important antioxidants in this class, because the major source of radicals is the hydrperoxides. A variety of organic sulphur and phosphorous containing compounds belong to this class since they can help the decomposition of hydroperoxides without the production of free radicals.

Scheme 1.11 Mechanisms of peroxide decomposition [50)].

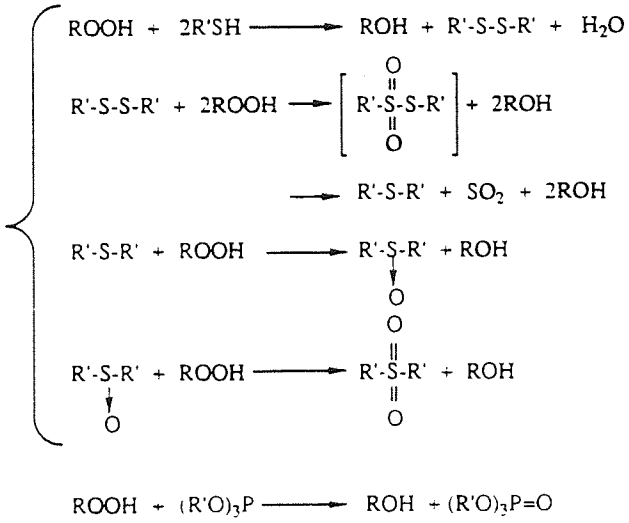

1.6.1.3 Reactive Antioxidants

Nowadays rubber products are used under wide range of environments. In order to increase the reliability of products, the loss of antioxidants is a major problem. There are mainly three causes of antioxidants loss; leaching, volatilisation, and migration.

The rubbers used for sealants or for hoses are normally in direct contact with oils and solvents in which antioxidants are generally soluble. Although most of the antioxidants are insoluble or less soluble in distilled water, amines may be soluble into acid rain, see fig. 1.24 [51]. and rubber products which are designed for uses outdoor have to have the antioxidants which are resistant to loss by rain water.

Fig. 1.24 Solubility of antioxidants into water as a function of pH [51]. (IPPD, SBPPD, MBPPD, DEMP, DMP-SPD are amine antioxidants).

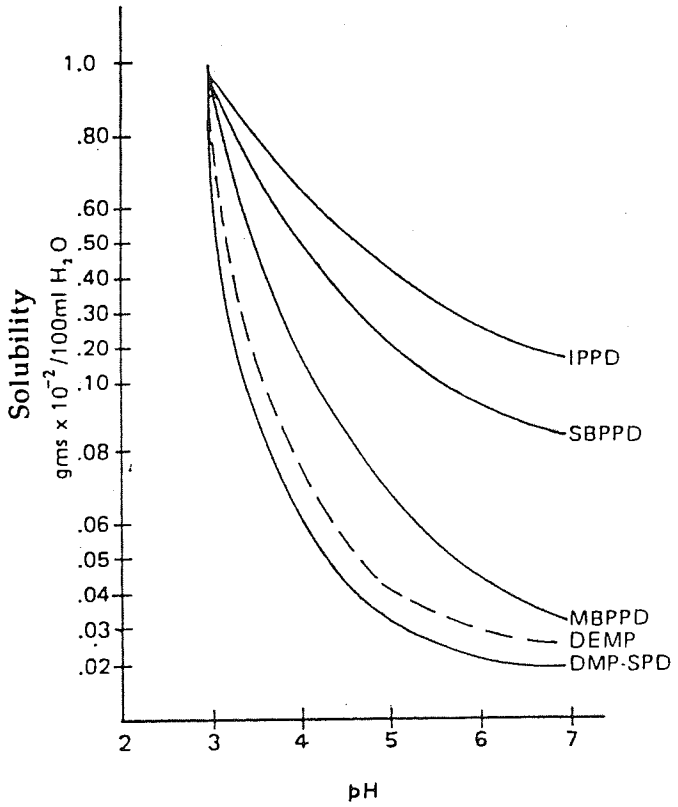

Some antioxidants, for example BHT, have a problem when it is used under high temperature. Although BHT is widely used as a phenol antioxidant, it can volatilise very easily; therefore, it is not suitable for products which have to be exposed to high temperature in service, see fig. 1.25 [52].

Fig. 1.25 Volatility of antioxidants [52].
1010 : tetrakis [methylene-3-(3,5-di-t.-butyl-4-hydroxyphenyl) propyonate] methane
1076 : n-octadecyl-3-(4-hydroxy-3',5'-di-t.-butylphenyl) propyonate
DPPD : N,N'-diphenyl-p-phenylen-diamine
TMDQ : polymerised 2,2,4-trimethyl-1,2-dihydroquinoline
MBMTB : 2,2'-methylenbis-(4-methyl-6-t.-butylphenol)
BPP : 2,6-di-t.-butyl-4-phenylphenol
HPPD : N-(1,3-dimethyl-butyl)-N'-phenyl-p-phenylendiamine
IPPD : N-phenyl-N'-isopropyl-p-phenylendiamine
DTBMP : 2,6-di-t.-butyl-p-cresol
ETMDQ : 6-ethoxy-2,2,4-trimethyl-1,2-dihydroquinoline

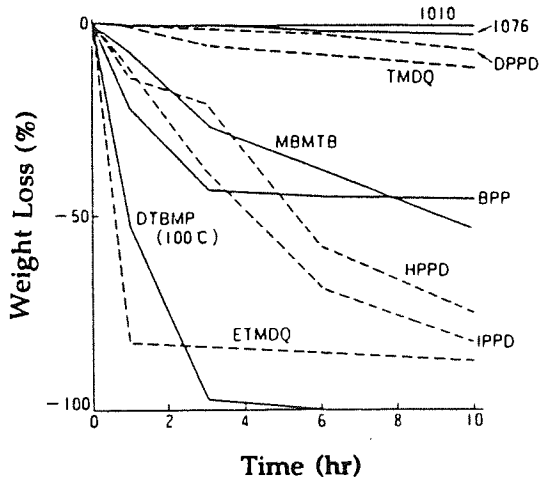

When rubber blocks which have different formula are pasted together, part of antioxidants will migrate into another rubber block which does not have that antioxidant, then those rubber blocks become completely different formula from ofiginal formula. John et. al. had a investigation about antioxidants migration in rubbers, see fig. 1.26 [53].

Fig. 1.26 Migration of antioxidants in rubber bloks which have different formula [53].

6PPD : N-(1,3-dimethylbutyl)-N'-phenyl-p-phenylenediamine
DTPD : a mixture of diphenyl-ditoluyl, toluylphenyl-p-phenylenediamine
TMQ : 2,2,4-trimethl-1,2-dihydroquinoline polimerised
ADPA-HV : acetone diphenylamine condensate high viscosity liquid

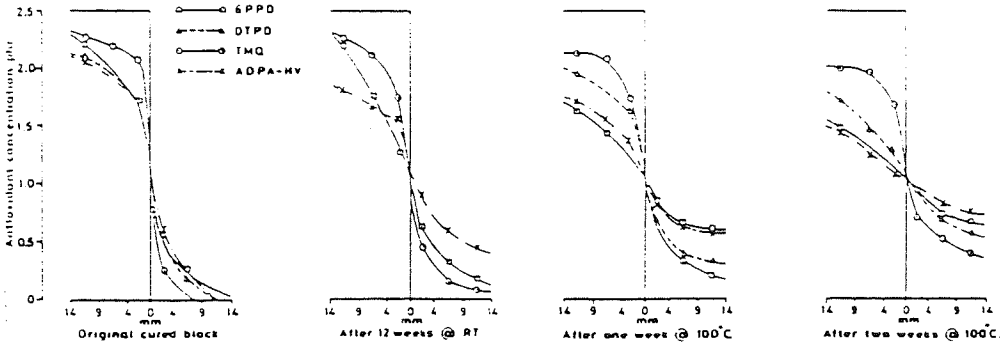

There are mainly two trends to prevent antioxidant loss by leaching, volatilisation and migration [54]. Firstly to increase the molecular weight of antioxidants. Generally the higher molecular weight antioxidants show less volatility and lower diffusion coefficient; however, at the same time, they often show high melting points and are badly dispersed into rubbers. Furthermore, of higher molecular weight antioxidants tend to be lower compatibility. A second approach is to react antioxidants onto the polymer chain. These are called reactive antioxidants and have polymer-reactive functional groups in addition to their antioxidant function. Examples of polymer-reactive functional groups are: nitroso group, allyl group, thiol group, and unsaturated acryl group such as acryloyl and methacryloyl groups, may be introduced into hindered phenols' and arylamines' basic structures.

Cain et. al. studied nitroso group containing antioxidants [55]. They reacted these antioxidants onto the rubber chains during curing, and had shown that this had led to high retention of the thermal stability of the the rubbers even after extraction, see table 1.7. The nitroso group was considered to graft onto NR chain by the mechanism shown in scheme 1.12.

Table 1.7 Comparison between nitroso group containing antioxidants and commercial antioxidants [55].

Antioxidants	Time required to absorb 1wt% of O_2	
	before extraction	after extraction
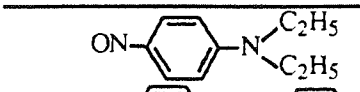	39	30
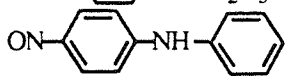	60	53
	31	30
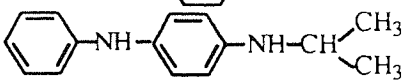	47	4
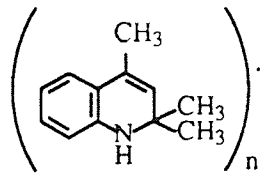	53	5
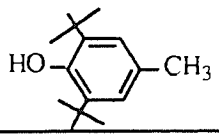	47	4

Scheme 1.12 Reaction mechanism between p-nitrosodiphenylamine and NR 55).

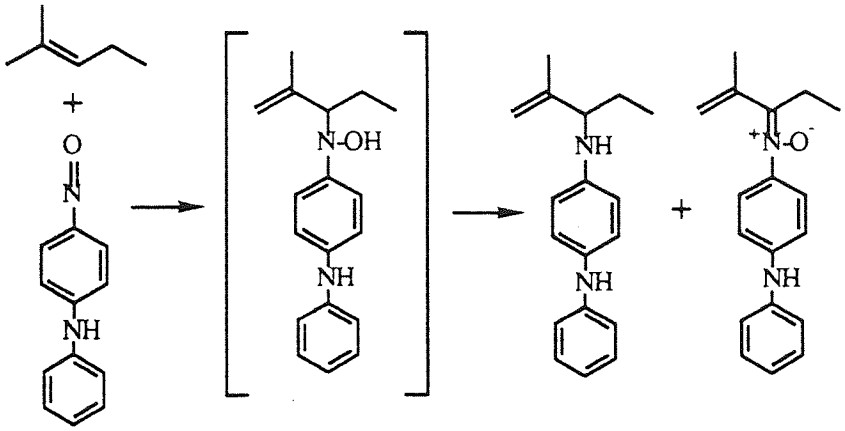

Yamamoto et. al. studied allylphenols as reactive antioxidants, see table 1.8 56). The antioxidants which have more allyl group in their structure showed better reactivity onto the rubber chain and also showed better thermal resistance after extraction, see fig. 1.27 56).

Table 1.8 Evaluated allylphenols 56).

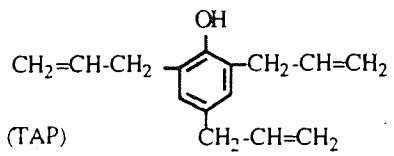 (TAP)	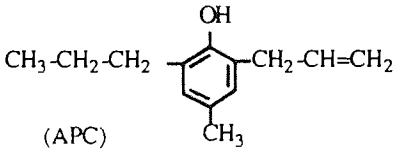 (APC)
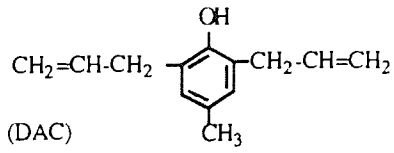 (DAC)	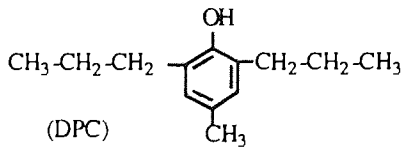 (DPC)

Fig. 1.27 Stress relaxation of NR vulcanisates (after extraction) which are including allylphenols [56].

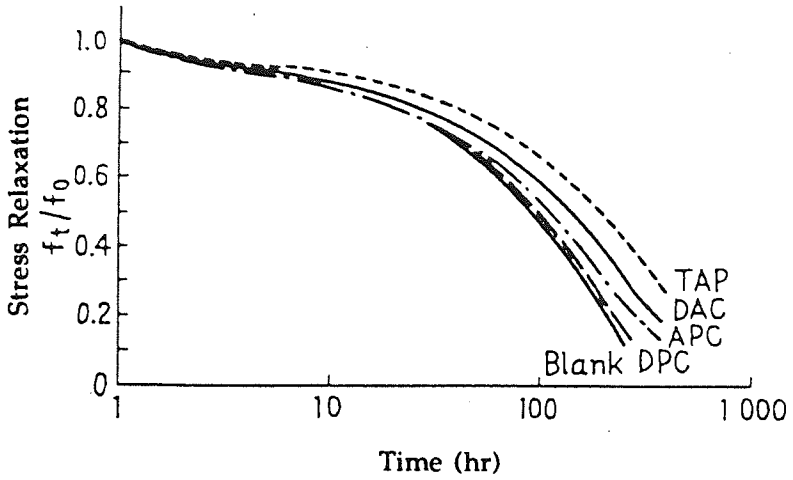

Scott et. al. found that thiolic radical can mechanically react with NR and SBR, see table 1.9 and scheme 1.13 shows the mechanism proposed [57, 58].

Table 1.9 Antioxidants which produce thiolic radicals [58].

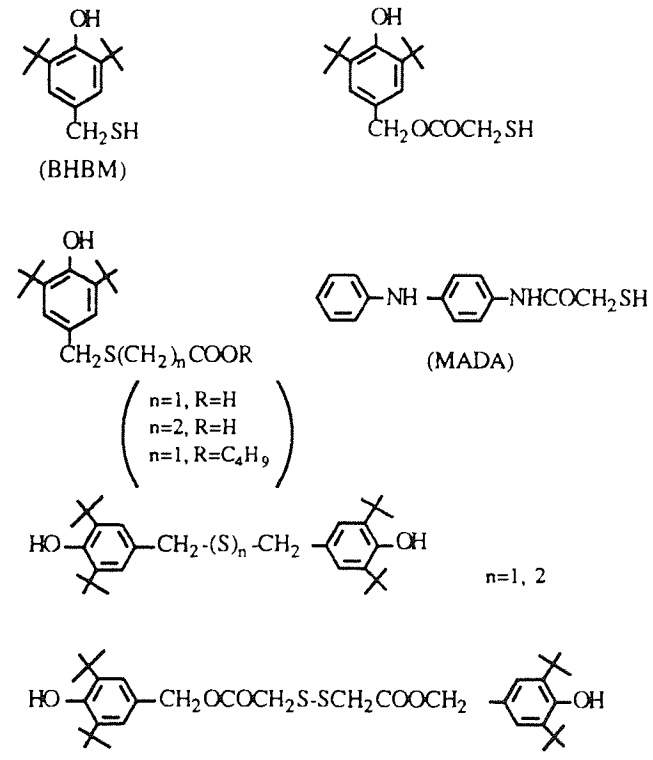

Scheme 1.13 Reaction mechanism of BHBM with NR [57].

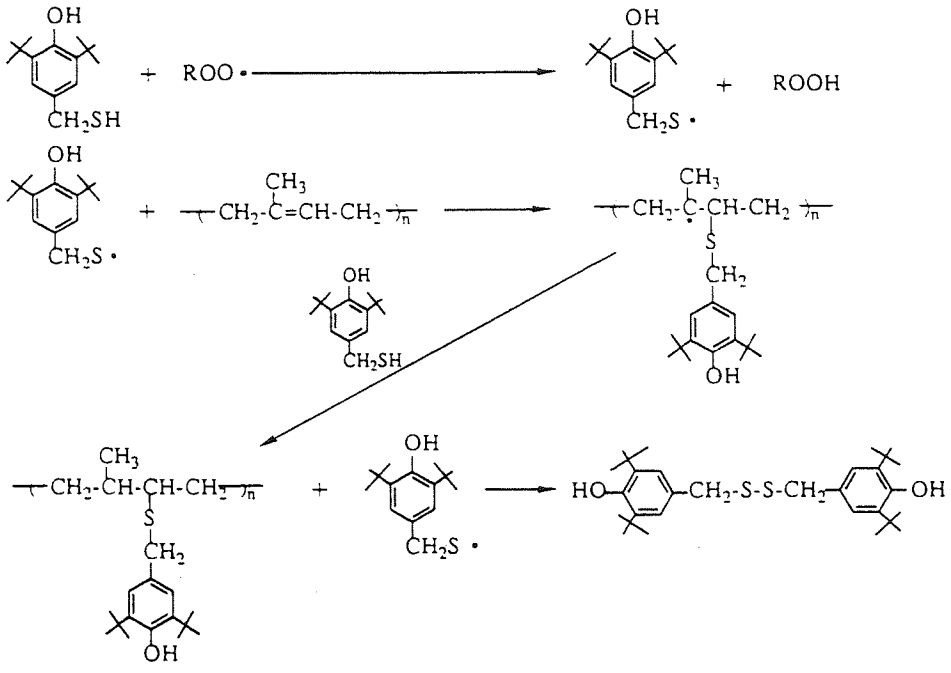

Kline et. al. studied polymerisable antioxidants for emulsion rubber [59]. They used 4-anilinophenyl group and 3,5-di-t-butyl group as antioxidant functions and introduced acryloyl and methacryloyl group as polimerizable groups, see table 1.10.

Table 1.10 Required time (hr) to absorb 1% oxygen by the sample (at 100°C) [59].

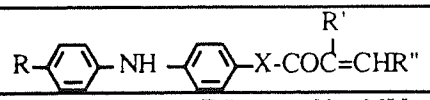

R	R'	R''	X = NH	X = O
H	H	H	200	180
H	CH_3	H	168	230
H	H	CH_3	212	300
H	H	Ph	185	253
CH_3	H	H	282	
CH_3	CH_3	H	336	
CH_3O	H	H	269	
CH_3O	CH_3	H	248	

(continue)

Table 1.10 Required time (hr) to absorb 1% oxygen by the sample (at 100°C) [59].

(continue)

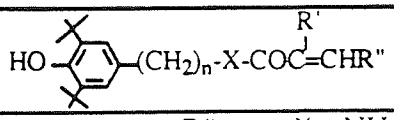

n	R'	R"	X = NH	X = O
0	H	H	178	102
0	CH_3	H	135	104
0	H	CH_3	151	97
0	H	Ph	183	108
1	H	H	125	61
1	CH_3	H	86	65
2	CH_3	H	147	142
3	CH_3	H	134	114
4	CH_3	H		155

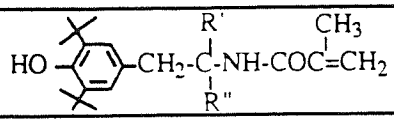

R'	R"	
CH_3	H	141
C_2H_5	H	124
CH_3	CH_3	116

1.6.1.4 Synergism and Antagonism

It is very rare that the case of two antioxidants lead simply to an additive effect. In most cases, they show either synergistic or antagonistic effects. Because the words "synergism" and "antagonism" have been used in a number of different ways; therefore, in this work, they are defined according to Scott [60]. Concerning the general case where a powerful antioxidant **A** at concentration c_1 has a effect a_1, and at twice the concentration c_2 an effect a_2, and a weaker antioxidant **B** at concentration c_1 has an effect b_1 and at twice its concentration c_2 an effect b_2 then the possible effects of the antioxidants, alone and in combination are summarised in table 1.11 and fig. 1.28.

Table 1.11 Combination effects of antioxidants [60].

Description	AO Concentration [A]	AO Concentration [B]	Effect
Additive	c_1		a_1
		c_1	b_1
	c_2		$a_2 (=2a_1)$
		c_2	$b_2 (=2b_1)$
	c_1	c_1	$= (a_1+b_1)$
Antagonism	c_1	c_1	$< (a_1+b_1)$
Synergism	c_1	c_1	$> (a_1+b_1)$

Fig. 1.28 Synergism and antagonism [61].

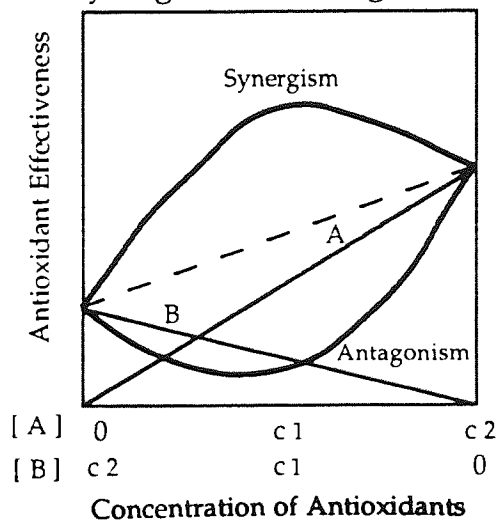

Generally three types of synergistic combinations can be distinguished homosynergism, heterosynergism and autosynergism. In any case, the largest reason for synergism is regeneration of the antioxidant.

In homosynergism, two antioxidants act by the same mechanism. Typical example can be seen when two different phenols are used in the same compound. Figure 1.29 shows the homosynergism of NR containing BHT and 4,4'-dihydroxydiphenyl (DOD) [62].

Fig. 1.29 Homosynergism beteen DOD and BHT in NR [62]. (at 100°C after 3 days ageing)

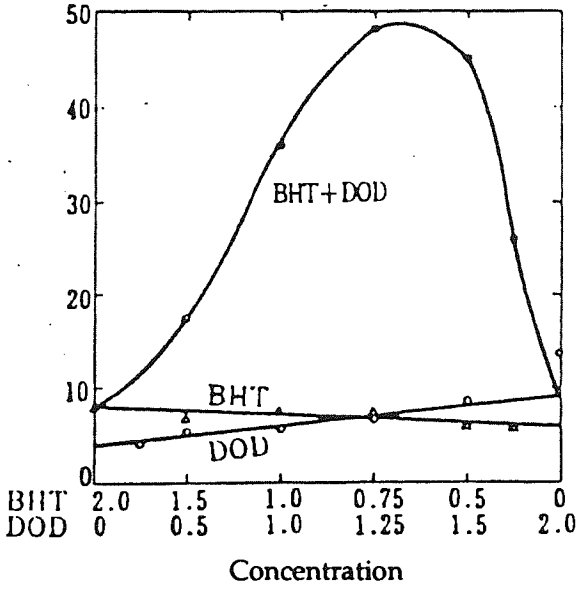

Peroxyl radical is easy to react with DOD because of lower steric hindrance and hence higher reactivity. Although DOD becomes a phenoxyl radical, it can be regenerated by BHT, see scheme 1.14 [62].

Scheme 1.14 Regeneration of DOD by BHT [62].

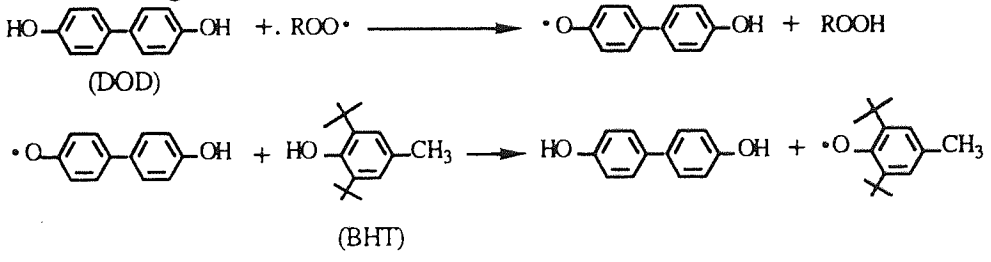

In heterosynergism, antioxidants act by a different mechanism and hence complement one another. Most popular combination for this kind of synergism is the combination of a CB-D such as phenols or amines and a PD such as sulphur or phosphorous compounds. Figure 1.30 and scheme 1.15 show the examples of this synergism [62].

Fig. 1.30 Heterosynergism between DPPD and MBZ in NR [62].
DPPD : N,N'-diphenyl-p-phenylenediamine
MBZ : zinc salt of 2-mercaptobenzoimidazole

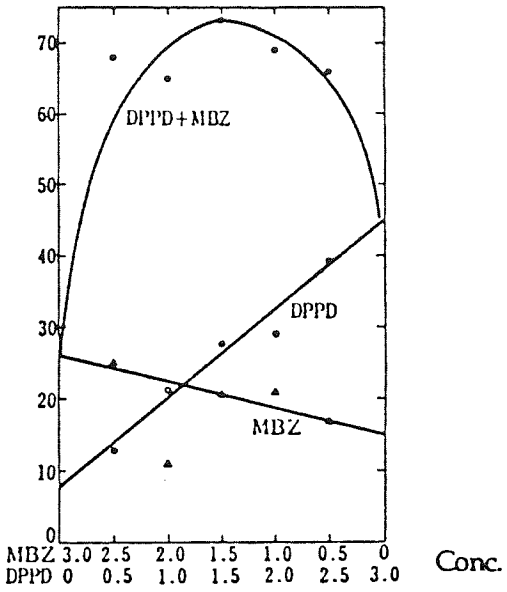

Scheme 1.15 Heterosynergism between phenols and thiopropionate esters [61].

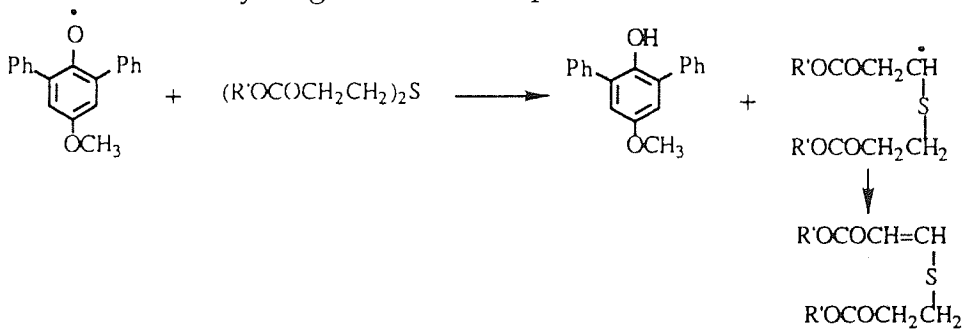

Autosynergism can be seen when antioxidants have two different types of functions in the same molecule. 3,5- Di-t-butyl-4-hydroxybenzyl mercaptan (BHBM) and 4-mercaptoacetamidodiphenylamine (MADA) are typical examples for autosynergism, see scheme 1.13 [57].

1.6.2. Antifatigue Agents

Antifatigue agents are chemical agents which can effectively deactivate free radicals (usually alkyl radicals) which are produced by cyclical mechanical stress in vulcanised rubbers during service.

The autoxidation mechanisms have been already described in a previous section (see scheme 1.2). In this mechanism, reaction (7) is important at ambient oxygen pressure, however, at low oxygen pressure, reactions (8) and (9) become more important especially when the alkyl radicals, R· , are tertiary or stabilised by electron delocalizing groups e.g. in alkyl radical (I) below [14],

Scheme 1.16 Stabilisation of radical by electron delocalisation [15]

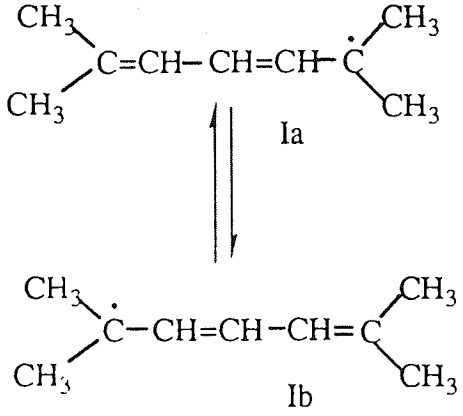

Under fatiguing conditions, concentration of R· is high and agents which can deactivate R· may act as good antifatigue agents. As alkyl radical scavengers nitroxyl radicals, nitrones, sulphur compounds, and quinonoid compounds have been studied previously [63-71].

1.6.2.1 Aromatic Amines and Nitroxyl Radicals

Aromatic p-phenylene diamines such as IPPD are one of the most widely used antioxidants in vulcanised rubbers. Normally they are also effective antifatigue agents, because nitroxyl radicals which will be produced during CB-D activity will be expected to trap alkyl radicals. Based on the ESR study, Dweik et. al. presented the following cyclic mechanisms, see scheme 1.17 [63, 64].

Scheme 1.17 Antifatigue mechanism of diarylamines [63, 64].

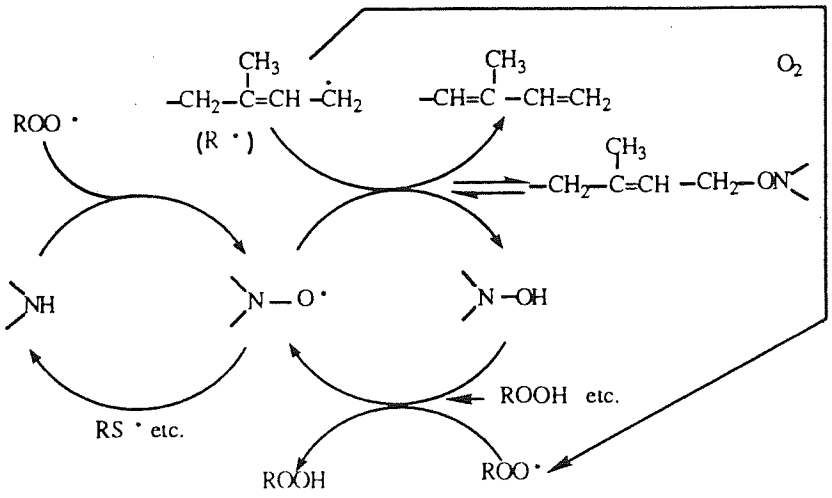

Nitroxyl radicals and alkyl peroxyl radicals were rapidly produced during fatigue, see fig 1.31 [65]. Alkylperoxyl radicals concentration peak came before nitroxyl radicals concentration peak. Both of them decayed and finally became constant. This suggests that nitroxyl radicals were transformed during the peroxyl radical trapping process.

Fig. 1.31 Change in alkylperoxyl (A) and nitroxyl (B) concentration during fatiguing of NR vulcanisate containing IPPD [65].

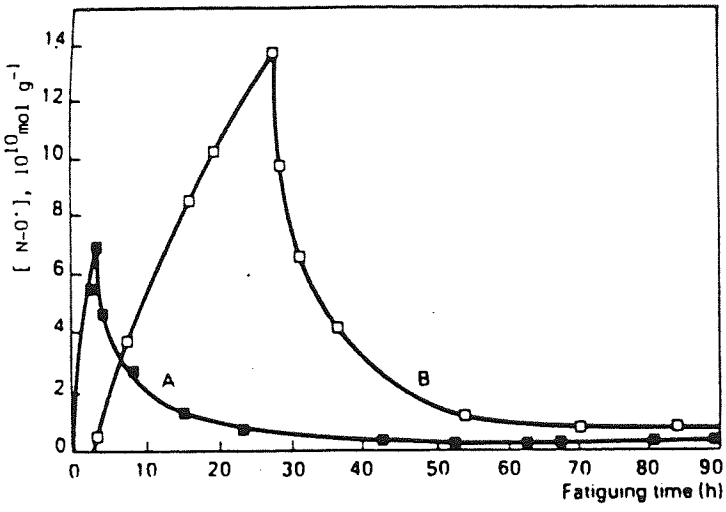

The concentration of nitroxyl radical was constant during the early stage of fatigue when it increased the concentration of amine and hydroxylamine decreased, see fig. 1.32 [63]. Although the regenerative system will not continue indefinitely, evidence for the cyclical mechanism is clearly obtained from these studies.

Fig. 1.32 Change in concentration of nitroxyl (DMDP-O, by ESR) and amine + hydoxylamine (DMDP-H + DMDP-OH, by UV absorbance at 280nm) during fatiguing of rubber containing nitroxyl derived from 4,4'-dimethoxydiphenylamine (DMDP-H) [63].

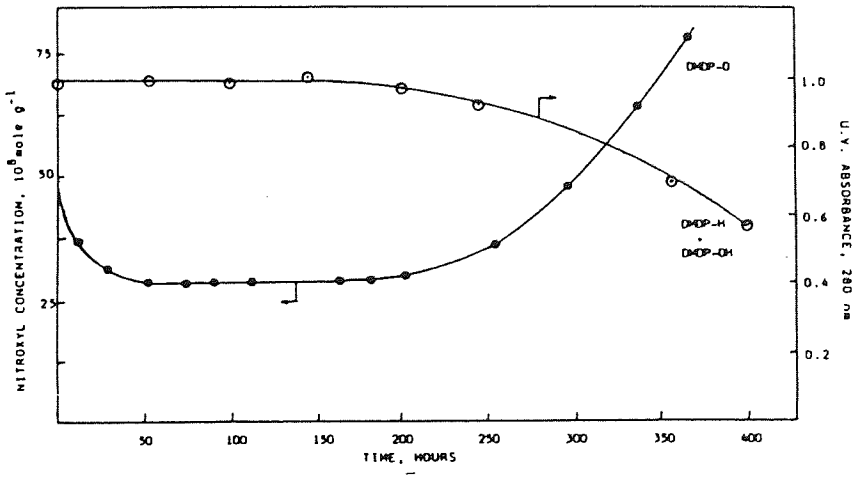

Table 1.12 shows that nitroxyl radicals and hydroxylamines are effective antifatigue agents as well as their parent amines. Although nitroxyl radicals have strong antifatigue activity, side reaction accompanied with the reduction process to their corresponding amines may also play an important role, because the nitroxyl radicals derived from the amines without antioxidant activity, such as HALS, did not show antifatigue activity, see table 1.12 [66].

Table 1.12 Fatigue lives of NR vulcanisates containing amines and their derived oxidation products [66].

Additives	Time to Fatigue Failure (hr)		
	R = H	O	OH
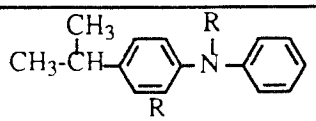	273	337	
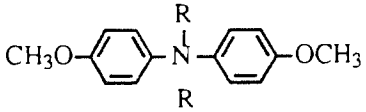	207	411	55
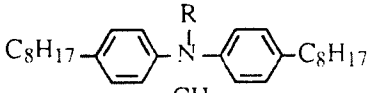	83	88	107
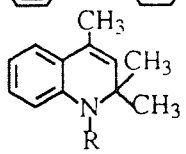	53	56	55
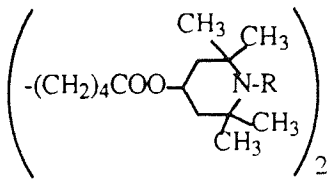	25	30	
no additive		21	

The reductive actions of thiols and their derived thiyl radical on nitroxyl radicals has been reported. Hence it was considered that the reduction to corresponding amines from nitroxyl radical is likely to involve the sulfoxide, see scheme 1.18 [63].

Scheme 1.18 Reduction of nitroxyl radicals by thiyl radicals [63].

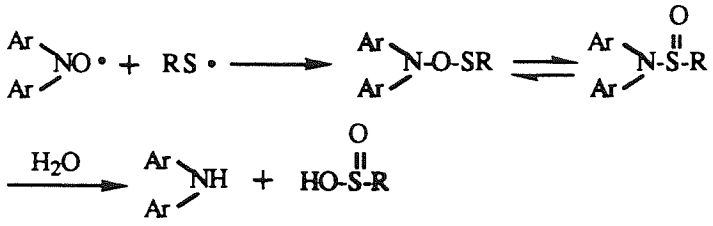

where R is either part of the rubber vulcanisate or is derived from an accelerator residue.

1.6.2.2 Nitrones

Nitrones have been reported to give nitroxyl radicals in the presence of alkyl radical, see scheme 1.19 [67, 68].

Scheme 1.19 Expected reaction of nitroxyk radical formation from nitrones [69].

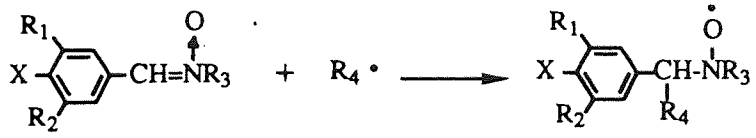

Nethsinghe et. al. studied variety types of nitrones on their antifatigue activity [69]. Although the one with X = H did not show significant fatigue resistance, the one with X = OH showed antifatigue activity, see table 1.13.

Table 1.13 Fatigue lives of NR vulcanisates containing benzalnitrones [69].

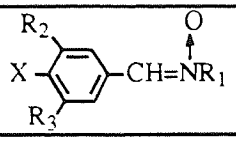

X	R1	R2	R3	Time to Fatigue Failure (hr)
H	tBu	H	H	26
OH	tBu	H	H	30
Cl	iPr	H	H	37
OMe	iPr	H	H	33
OH	tBu	Me	Me	110
OH	iPr	Me	Me	130
OH	Et	Me	Me	93
OH	Me	Me	Me	80
H	Me	H	H	29
	IPPD			270
	no additive			20

Considering the fact that nitrones without hydroxyl group did not show antifatigue activity, the mechanisms of nitroxyl formation was expected not to be via the reduction by alkyl radical but to be via the oxidation by alkylperoxyl radical, see scheme 1.20. However no phnoxyl radicals were detected by ESR. Hence transformed material by oxidation seemed to be more correctly represented by quinonoid compound rather than phenoxyl radicals, see scheme 1.20.

Scheme 1.20 Proposed antifatigue mechanism for 4-hydroxyl benzalnitrones in NR [69].

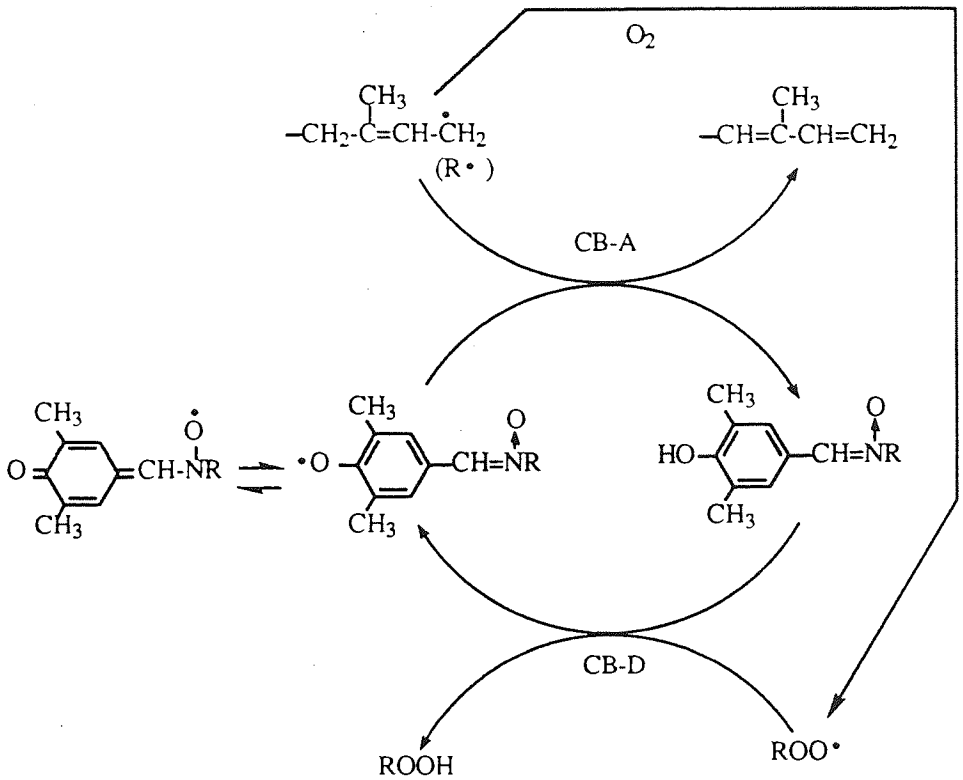

1.6.2.3 Sulphur Compounds

It is well known that sulphur vulcanised rubber shows good fatigue resistance. It has been explained that sulphur crosslinks continue to rupture, recombine and release the local stress [72, 73]. However some of sulphur compounds, see table 1.14, also improve the fatigue resistance of peroxide crosslinking rubber [65, 66]. It can not be explained by the restructuring the crosslinkings. Coker et. al. presented the following mechanisms for the sulphur compounds as antifatigue agents, see scheme 1.21 [70].

Table 1.14 Fatigue lives of peroxide cured NR with added sulphur compounds.

		Improvement in Fatigue Life relative to control (%)		
Additive Concentration	(phr)	0.5	1.0	2.0
$(C_{12}H_{25}OCOCH_2CH_2)_2S$	(DLTP)	95	127	166
$(C_{12}H_{25}OCOCH_2CH_2)_2S$-O	(DLSP)	105	157	209
$(CH_{12}H_{25}OCOCH_2CH_2S)_2$	(DLPDS)	133	293	380

Scheme 1.21 Proposed mechanism for fatigue inhibitation by sulphur compounds [70].

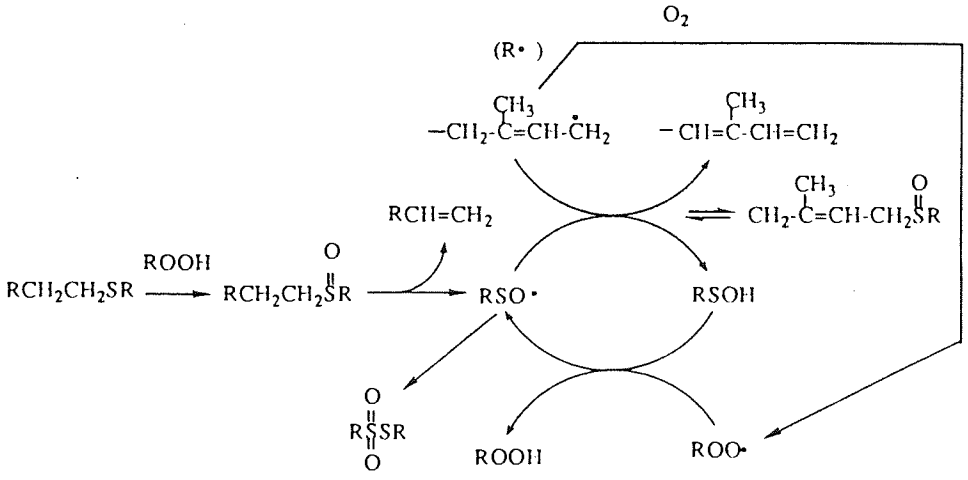

1.6.2.4 Quinonoid Compounds and Phenols

Because of analogy, melt stabilisers for polyolefines can be expected to have antifatigue activity. Both antifatigue agents and melt stabilisers should have strong alkyl radical trapping ability. Henman studied many types of melt stabilisers and summarised the species which will be scavenged, see table 1.15 [71].

Table 1.15 Tentative classification of stabiliser types according to their scavenging behavior [71].

Type	*Species scavenged*				
	$R\cdot$	O_2	$RO_2\cdot$	RO_2H	$RO\cdot$
para cresol derivatives	(√)	?	√	(√)	?
other monophenols		?	√		?
quinone methides	√		(√)	√	
quinones	√				
sulphides	(√)			(√)	(?)
sulphoxides	(√)			√	?
phosphites				√	
phosphonites				√	
phosphines		?		√	?
Free radicals	√				?
Radical acceptors	√				?
Iodo-compounds	√			(√)	
Ammonium compounds etc.	?	√			
Phosphonium salts		√		(√)	
Reducing agents				√	
Metal stearates	√		?		
Inorganic salts				√	

() = deactivation by an artefact.

Phenols and quinones which have good melt stabilisation activity in polyolefines, represented by melt flow index, will be interesting to study as antifatigue agents for rubber as well, see Table 1.16 [71].

Table 1.16 Evaluation of phenols and quinones for melt stabilising performance [71].

Type			R	ΔMFI	
				4.5	0.5
Phenols	BHT (reference)	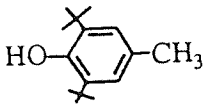		100	270
	2,6-Di-t-butyl-phenols containing polar 4-substitutes	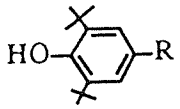	-CN	55	65
			-CHO	85	230
			-OH	65	125
			$-NO_2$	70	
	2,6-Di-t-butyl-phenols containing electron-withdrawing substitutes	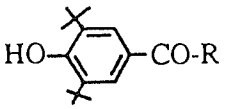	-CH=CHCOOH	60	
		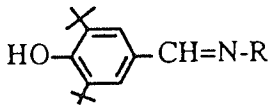	-Ph	70	
			$-NMe_2$	70	
			$-N^+Me_3I^-$	55	
Quinones	Quinone-disubstituted	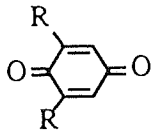	-H	40	60
			-Me	65	110
			-tBu	55	65
			-Ph	50	65
	Quinone-tetrasubstituted	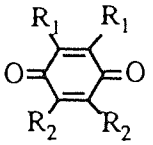	R_1=Me, R_2=Me	80	165
			R_1=Cl, R_2=CN	70	125
		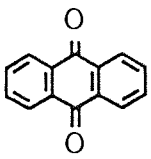		125	280
	Diphenoquinone	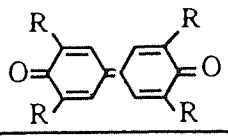	-H	40	65
			-tBu	125	220
	Stilbenequinone	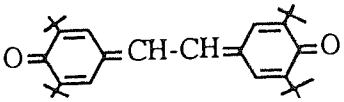		50	60

Chapter 2 General Experimental Techniques

2.1. Materials

2.1.1. Natural Rubber (NR)

The rubber industry uses widely two different types of dry rubbers which are classified according to the process used for their production; sheet rubber and block rubber [74]. The ribbed smoked sheet rubber (RSS) is the most typical sheet rubber. Its grades are classified by visual examination and based on the presence or absence of extraneous foreign matter (dirt), bubbles, uniformity and intensity of colour, mold und rust spot. On the other hand the block rubber products are graded based on technical specification, such as dirt content (retained on 44mm aperture sieve), ash content, nitrogen content, volatile matter, Wallace rapid plasticity (minimum initial value), plasticity retention index (PRI), colour, (Lovibond Scale), Mooney viscosity, and cure, hence they are called technically specified rubber (TSR) [75]. In this work, the block rubber produced in Malaysia which is called SMR (Standard Malaysian Rubber) grade L was used. The specification of SMR-L are shown in Table 2.1. FT-IR spectrum of SMR-L is also shown in fig. 2.1 which are at the end of this chapter.

Table 2.1 Standard of SMR-L [75].

Parameter	SMR-L
Dirt retained on 44μ aperture (max., %wt)	0.03
Ash content (max., %wt)	0.50
Nitrogen content (max. wt)	0.60
Volatile matter (max., %wt)	0.80
Wallace Rapid Plasticity-minimum initial value (P_0)	30
Plasiticity Retention Index, PRI (min., %)	60
Colour limit (Lovibond Scale, max.)	6.0

2.1.2. Compounding Ingredients and Other Chemicals

Table 2.2. gives the main compounding ingredients used in formulating the rubber mixture and other chemicals used for other experiments. The curing agent was sulfur, the activators were zinc oxide and stearic acid, and the accelerator for sulfur curing was N-cyclohexyl-2-benzothiazolesulphenamide (CBS). Azobisisobutyronitrile (AIBN) was used as a radical initiator for grafting of reactive antioxidants on to the rubber main chain. Squalene was used as a model compound for investigation of mechanisms of a reactive antioxidant.

Table 2.2. Compounding ingredients and other chemicals

Name	Formula (M.w.)	Manufacture	Purity (%)	Colour & Form
Zinc oxide	ZnO (81)	Robinson Brother Ltd.	85	White pellets
Stearic acid	$CH_3(CH_2)_{16}COOH$ (284)	BDH Chemicals Ltd.	99	White powder
N-Cyclohexyl-2-benzotiazole-sulphenamide (CBS)	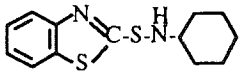 (264)	Robinson Brother Ltd.	75	Green blue pellets
Sulfur	S_8 (256)	Robinson Brother Ltd.	80	Yellow pellets
Azobis-isobutyro-nitrile (AIBN)	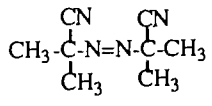 (164)	Fluka chemika	>98	White powder
Squalene	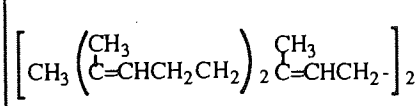 (411)	Aldrich Chemical Company Inc.	99	Transparent liquid

All characterisation results of these compounds, i.e. tables 2.3 - 2.5 and figures 2.2 - 2.7, are shown at the end of this chapter. Table 2.3 lists the characteristic IR absorption bands of these compounds, and their IR spectra are shown in figures 2.3 - 2.5. Tables 2.4 and 2.5 show the summary of ^{1}H-NMR and ^{13}C-NMR of squalene, and these specra are shown in fig. 2.6 and 2.7, respectively.

2.1.3 Antifatigue Agents and Antioxidants

Table 2.6 gives all antifatigue agents and antioxidants which were compounded into natural rubber and examined various mechanical performances and mechanisms of antifatigue activites in the following three chapters.

Table 2.6 Antifatigue agents and antioxidants

Type		Code	Name and Formula (M.w.)	Manufacture	Colour & Form
Antifatigue Agents	Quinones	BQ	2,6-di-t-butyl-1,4-benzoquinone 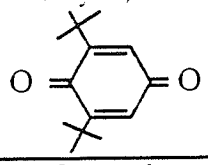 (220)	Lancaster Synthesis Ltd.	orange powder
		DPQ	3,3',5,5'-Tetra-t-butyl-4,4'-diphenoquinone 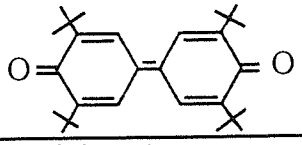 (409)	Lancaster Synthesis Ltd.	violet needles
		NQ	1,4-Naphthoquinone 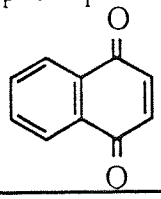 (158)	Hopkins & Wiliams	green powder
		PDO	4-Pyridone 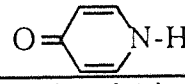 (95)	Tokyo Kasei Organic Chemicala	brown powder
	Phenols	HBA	3,5- Di-t-butyl-4-hydrobenzaldehyde 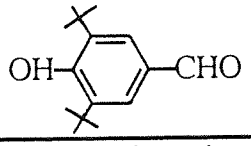 (234)	Aldrich Chemical Company Inc.	light golden brow flales
		αTOC	5,7,8-Trimethyl-tocol (α-Tocopherol) 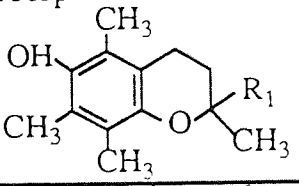 (431)	F. Hoffmann La Roche & Co.	dark yellow oily liquid

$-R_1 = -(CH_2)_3-CH(CH_3)-(CH_2)_3-CH(CH_3)-(CH_2)_3-CH(CH_3)-CH_3$

(continue)

Table 2.6 Antifatigue agents and antioxidants (continue)

Type		Code	Name and Formula (M.w.)	Manufacture	Colour & Form
Antifatigue Agents	Phenols	γTOC	7,8-Dimethyl-tocol (γ-Tocopherol) 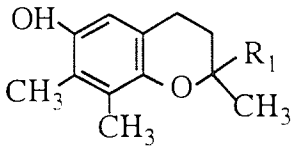 (417)	F. Hoffmann La Roche & Co.	dark yellow oily liquid
		GM	2-t-Butyl-6-(3-t-butyl-2-hydroxy-5-butylbenzyl)-4-methylphenyl acrylate 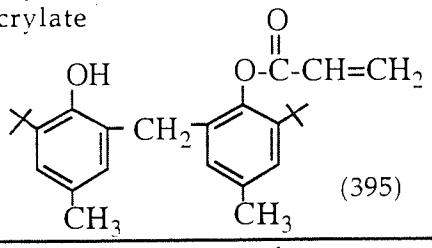 (395)	Sumitomo Chemical Co.,Ltd.	white powder
	Amines	IPPD	N-Phenyl-N'-isopropyl-p-phenylenediamine (226) 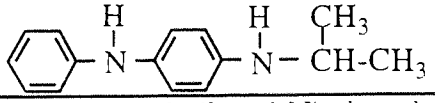	Monsant Chemicals Ltd.	dark brown violet flakes
		6PPD	N-1,3-Dimethylbutyl-N'-phenyl-p-phenylenediamine 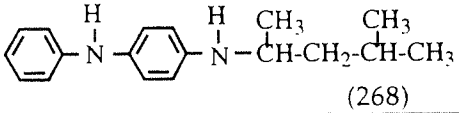 (268)	Monsant Chemicals Ltd.	violey pelets
		TMQ	Polymerised 2,2,4-trimethyl-1,2-dihydroquinoline 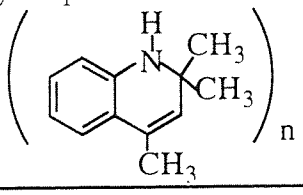	Monsant Chemicals Ltd.	orange pastilles
Antioxidants	Reactive Antioxidants	PM	N-(4-anilinophenyl) maleimide 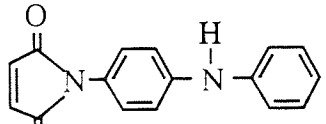 (264)	Synthesised	scarlet powder

(continue)

Table 2.6 Antifatigue agents and antioxidants (continue)

Type		Code	Name and Formula (M.w.)	Manufacture	Colour & Form
Antioxidants	Reactive Antioxidants	BTMI	Tetrahydro-N-(1-methyl-1-[3-(1-methylethenyl)phenyl] 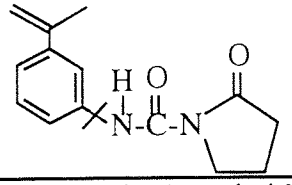 (224)	Goodyear Tire & Rubber Company	white powder
		APMA	2-Propenamide, 2-methyl-N-[4-phenylaminophenyl] (252) 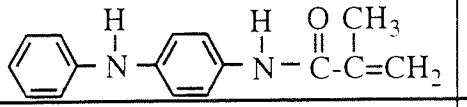	Goodyear Tire & Rubber Company	light green powder
		MADA	4-Mercaptoacetoamido-diphenylamine (258) 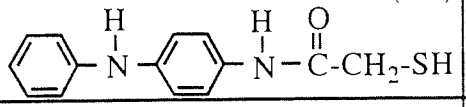	Synthesised	gray powder
	Peroxide Decomposers	P168	Tri (2,4-di-t-butylphenyl) phosphite 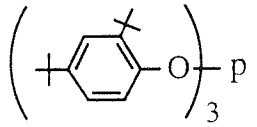 (647)	CIBA-GEIGY	white powder
		P626	Bis (2,4-di-t-butylphenyl) pentaerythritol diphosphite (605) 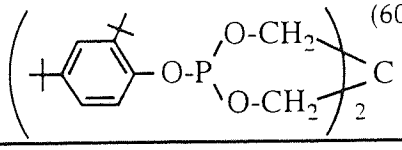	Borg-Warner	white powder

2.1.3.1 Synthesis of Antioxidants

(1) Synthesis of N-(4-Anilinophenyl)maleimide (PM).

N-(4-anilinophenyl)maleimide (PM) was prepared by a two-stage process; firstly maleic anhydride was reacted with 4-anilinodiphenylamine to yield N-(4-anilinophenyl)maleic acid, secondly it was converted into PM by sodium acetate and acetic anhydride, see scheme 2.1.

Scheme 2.1 Synthetic reaction for PM.

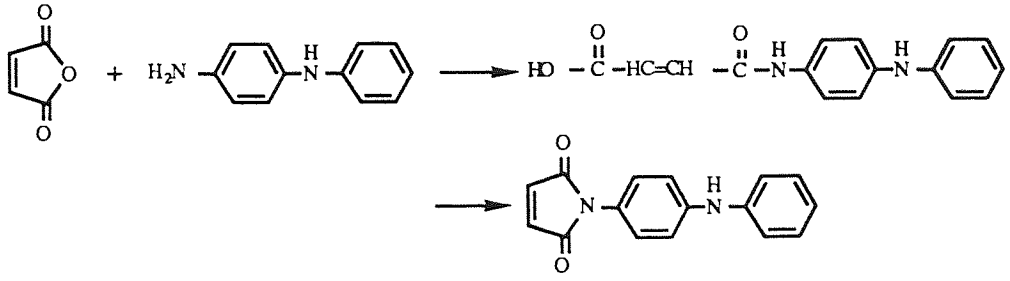

19.6 g (0.2 moles) of maleic anhydride and 36.8 g (0.2 moles) of 4-anilinodiphenylamine were dissolved in 250 ml chloroform. The resultant orange precipitate was filtered off after 30 minutes, then washed with chloroform and dried at room temperature under vacuum to give a yield of 90 % with a melting point 183°C.

50.0 g (0.177 moles) of N-(4-anilinophenyl)maleimic acid was dissolved in 200 ml of acetic anhydride at 70°C with 11.0 g (0.14 moles) of sodium acetate. After 10 minutes the solution was poured into cold water. The resultant scarlet precipitate was filtered off, washed with cold methanol and dried at room temperature under vacuum to give a yield of 70% with 154 - 156°C (Lit. 161 - 163°C) [76].

(2) Synthesis of 4-Mercaptoacetoamidodiphenylamine (MADA).

18.4 g (0.1 moles) of 4-anilinodiphenylamine was dissolved in 300 ml of xylene in a 500 ml round bottom three neck flask. 13.8 g (0.15 moles) of thioglycollic acid was then added to this solution. Excess thioglycolic acid was used in order to shift the reaction to the right, see in scheme 2.2.

Scheme 2.2 Synthetic reaction of MADA.

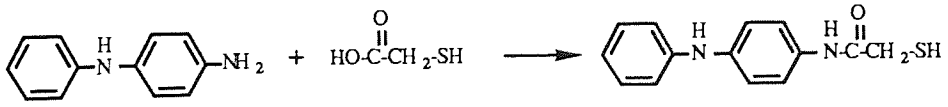

The flask was then fitted with a Dean and Stark trap and a water condencer, see fig. 2.8. A stream of nitrogen was bubbled through during the reaction. The mixture was refluxed for 15 hours. At the end of the reaction, the flask was allowed to cool and mixture was diluted with n-hexane and left to crystallise in an ice bath. The product obtained was filtered off and recrystallised with isopropanol to give a yield of 66% with melting point 122 - 147°C (Lit. 135.5 - 137.0°C) [77].

Fig. 2.8 Experimental apparatus of synthesis of MADA

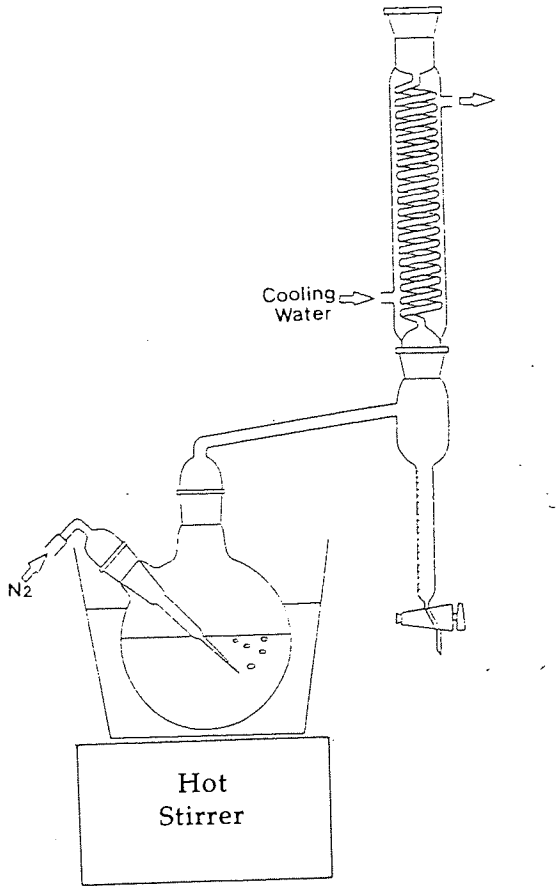

2.1.3.2 Characterisation of Antifatigue Agents and Antioxidants

All antifatigue agents and antioxidants listed in table 2.6 were characterised with FT-IR, UV, ^{1}H-NMR, ^{13}C-NMR and melting point. These characterisation results are shown in tables 2.8 - 2.41 and figures 2.9 - 2.76 and are placed at the end of this chapter.

2.2. Preparation of Vulcanised Rubber

2.2.1. Mastication

Mastication is the break down of the high molecular weight rubber by chemical effect or mechanical shear in order to make compounding easier. Due to chemical bond scission and disentanglement of molecular chains, rubber elasticity decreases whereas its plasticity increases during mastication.

Mastication can be carried out either at low temperature on a two-roll mill where mechanical stress causes the breakdown of the chains, or at high temperature in an internal mixer (temperature of rubber may reach to above 120°C) where thermal oxidation rather than mechanical stress predominates, leading to the break down of the rubber molecules [78].

In this work, low temperature mastication was applied. Natural rubber was masticated on a 12 inch two roll mill. Generally, the smaller the nip size, the lower the roll mill temperature, and the bigger the roll friction rate, the more efficient is the mastication [78]. Therefore, a nip size of 0.5mm, a friction rtio of 1:1.25, and a slower roll rotation speed of 20rpm were employed. The rubber was allowed to go through the roll three times for any typical mastication.

2.2.2. Compounding by Two Roll Mill

General procedure for mixing standard compounds is described in BS 1674 [79] and ASTM D3182-87 [80]. Rubber and most of the ingredients were mixed on the roll mill, see fig. 2.77. However, in the case of α- and γ-tocopherol, these were first dissolved in about 20ml of n-hexane and the solution was dropped on the compounding rubber sheet which was then left on a bench at room temperature about twenty minutes in order to dry the solvent. Rubber compounds were prepared according to the following formulations, see table 2.42.

Fig. 2.77 Schematic diagram of two roll mill [78].
(1) Slower Roll (20 rpm) (2) Faster Roll (25,20 rpm) (3) Nip Size
(4) Band Rubber (5) Bank Rubber (6) Shrinkage (7) Elongation
(8) Ingredients

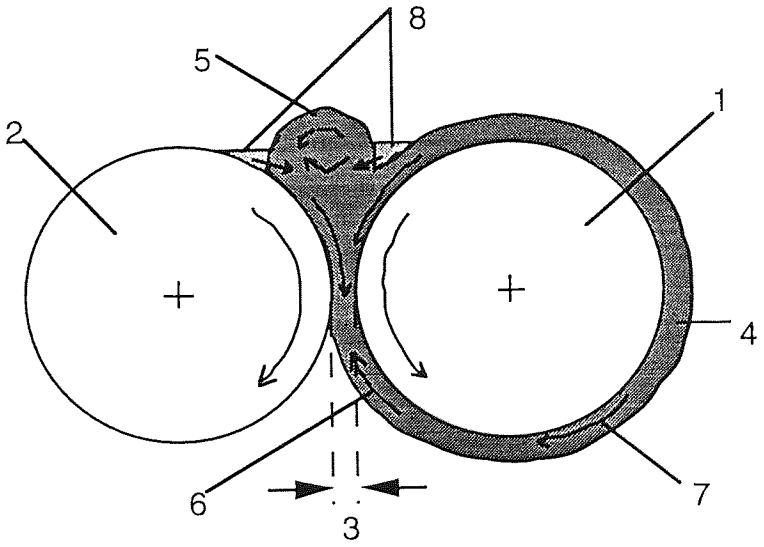

Table 2.42. Formulations of typical compounding

Ingredients	Sulfur Cure (phr)	DCP Cure (phr)
Natural Rubber	100	100
Zinc Oxide (85%)	3.53 (3.00)	3.53 (3.00)
Stearic Acid	2.50	2.50
Antifatigue Agents or Antioxidants	1.50	1.50
CBS (75%)	0.67 (0.50)	——
Sulfur (80%)	3.13 (2.50)	——
DCP	——	2.50

† ( ) is net value
* small number of DCP cure samples were compounded for reactivity index test

A friction ratio of 1:1 was employed for compounding. In order to distribute the ingredients thoroughly, the amount of bank rubber, see fig. 2.77, should be appropriate and should be rotated on the mill. If there is too much band rubber, some part will not go into the rolls and will cool down resulting in non-uniform distribution of ingredients, as they tend to go into the softer and higher temperature part of rubber. The ammount of band rubber was adjusted by the roll width and the nip size. In addition, the rubber band on the roll should be cut from right and left alternatively then turned over six times respectively at each stage in order to distribute the ingredients equally in the rubber, see fig. 2.78. The interval of the cut should be less than thirty seconds.

Fig. 2.78 Cross section view of compounding on two roll mill
(1) roll guide, (2) bank rubber, (3) band rubber, 4) direction of cutting (around 3/4 of roll width) (5) direction of roll rotation, (6) roll width.

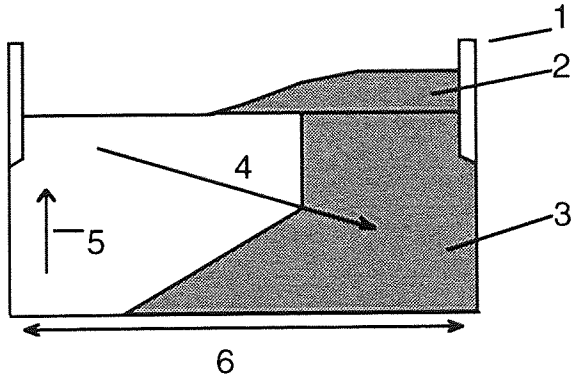

Zinc oxide was mixed first due to difficulty of its dispersion, while sulfur was mixed last in order to prevent any curing reaction during processing. Liquids were not mixed in the early stages because they affect the shear stress and lead to bad dispersion of ingredients. The details of the compounding schedule are presented in table 2.43.

Table 2.43 Compounding schedule on two roll mill.

materials to add	without any antifatigue agents		with α- or γ-tocopherol		with other antifatigue agents	
	time (min)	nip size (mm)	time (min)	nip size (mm)	time (min)	nip size (mm)
NR	2	0.51	2	0.51	2	0.51
zinc oxide	2	0.51	2	0.51	2	0.51
stearic acid	2	0.76	2	0.76	2	0.76
α- or γ-tocopherol			20 drying			
antifatigue agent					2	0.76
CBS	2 [0]	1.01	2 [0]	1.01	2 [0]	1.01
sulfur [DCP]	2 [2]	1.01	2 [2]	1.01	2 [2]	1.01
concluding	1	2.03	1	2.03	1	2.03

† [ ] is DCP curing for reactivity index test

2.2.3 Curing

The compounded rubber was sheeted out on a two roll mill and the shape and thickness of each sheet was adjusted as required for different tests. Rubber sheets were cut out and placed on a vulcaization mould which was pre-heated at 150°C. Then samples were vulcanized for about 20 minutes at 150°C. The accurate curing time of each sample was calculated from the results of rheometer, $t_{0.9}$, see section 2.3.3. The best cure time of the sample was 1.5 times the $t_{0.9}$ value.

Figure 2.79 shows the effects of temperature on curing time. Most samples which were cured with sulfur and CBS showed similar results.

Fig. 2.79 The effects of temperature on curing time.
(DCP 2.5 phr ; Sulfur 2.5 phr + CBS 0.5 phr)

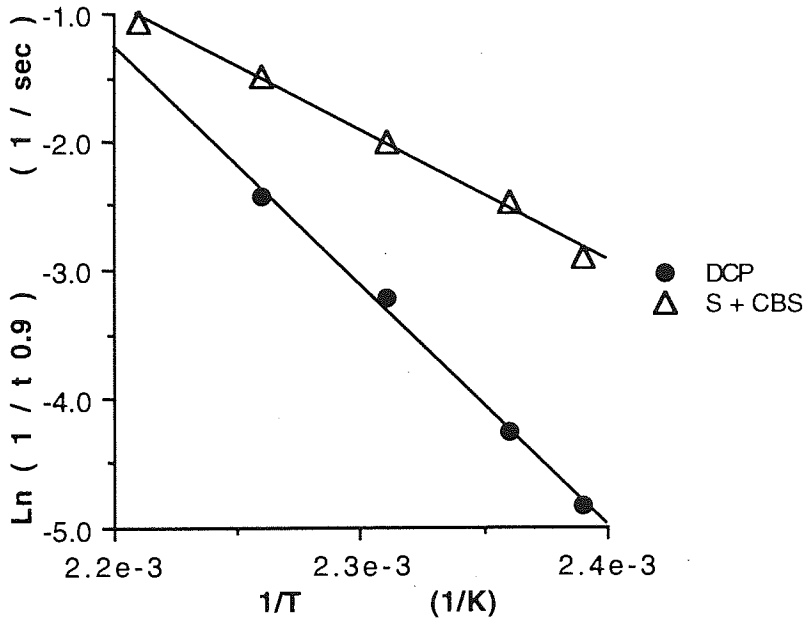

2.3. Physical Tests for Unvulcanized Rubber

2.3.1. Mooney Viscosity

Mooney viscosity is measured in order to assess the effect of mastication and compounding on the rubber. Viscosity reflects the size and length of molecules (molecular weight), their degree of entanglements, and their interaction via Van der Waals force, hence it is used as an index for mixing of the rubber.

The details of Mooney test are described in BS903: part A58 [81] and ASTM D1646-87 [82] which are nearly equivalent. The test specimen consists of two pieces of rubber of total mass of 27±3g. The rotor and die were pre-heated at the test temperature of 100°C. Then the rotor was sandwiched between the two rubber pieces and they were placed in the dies. After closing the dies, the test specimen was pre-heated in the die for one minute before starting the rotor. After four minutes running, the value in Mooney units was read and used as a Mooney viscosity. The test results are usually expressed in the following format:

$$\left[\begin{matrix}\text{Test Reading}\\ \text{(Mooney units)}\end{matrix}\right] \text{M} \left[\begin{matrix}\text{Rotor Size}\\ \text{(L orS)}\end{matrix}\right] \left(\begin{matrix}\text{Pre-heahing}\\ \text{time (min)}\end{matrix} + \begin{matrix}\text{Running time}\\ \text{(min)}\end{matrix}\right) \left[\begin{matrix}\text{Test temp.}\\ (^{\circ}\text{C})\end{matrix}\right]$$

For example, the Mooney viscosity results of 30 Mooney units tested at 100°C with a preheating time of 1 min, a running time of 4 min, and using a large (38.1 mm) rotor would be expressed as 30 ML (1+4) 100°C. In this work, ML(1+4)100°C was used as the most commonly specified value. Figure 2.80 shows a typical plot obtained from Mooney viscosity values against time.

Fig. 2.80. Typical plot for determination of Mooney viscosity

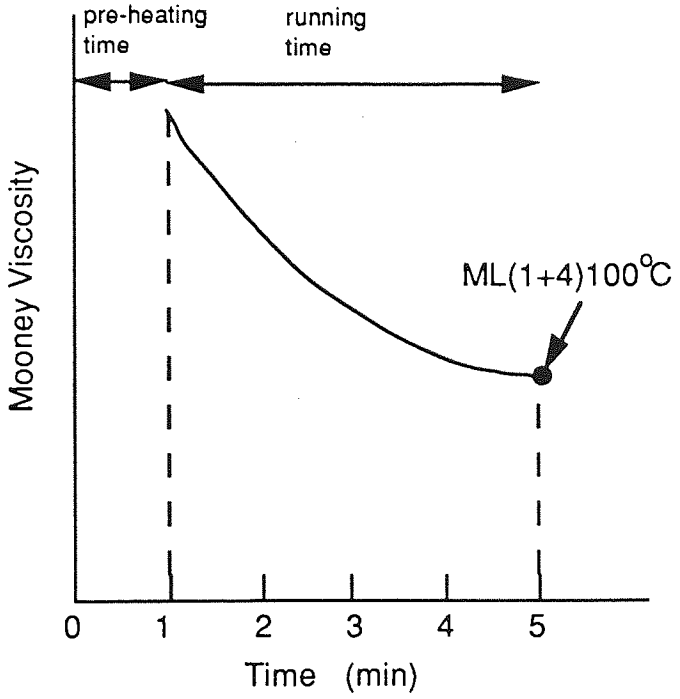

2.3.2. Monsanto Oscillating Disc Rheometry

This test method is used to determine the vulcanization characteristics of rubbers. The Monsanto oscillating disc rheometer (model 100) was used for this purpose.

The test method is described in BS 1673: Part 10 [83] and ASTM D2084-87 [84]. A sample which was approximately 15g , 30 mm diameter and 12.5 mm in thickness was inserted into the cavity of the rheometer. It was held under pressure and heated up to the vulcanization temperature. Then the disc started to oscillate and the shear strain was measured.

Three typical torque-time curves are presented in fig. 2.81 [85]. Sulfur cured natural rubber with CBS gives rise to a reversion-type curve, see curve (c) in fig. 2.81.

The test temperature, rotational amplitude (±1°, ±3°, or ±5°), minimum torque, maximum torque, scorch time, and cure time reported. In this work, test was carried out with ±3° of rotational amplitude at 150°C.

Fig. 2.81 Different type of cure curves [85].

f_{min} = minimum torque
f_{max} = maximum torque
F_{HM} = maximum torque at specified time of marching modulus cure
F_{HP} = maximum torque of plateau cure
F_{HR} = maximum torque of reversion cure
$t_{0.1}$ = time to 10% of maximum torque ,$(f_{max}-f_{min})\times 0.1+f_{min}$
$t_{0.9}$ = time to 90% of maximum torque ,$(f_{max}-f_{min})\times 0.9+f_{min}$

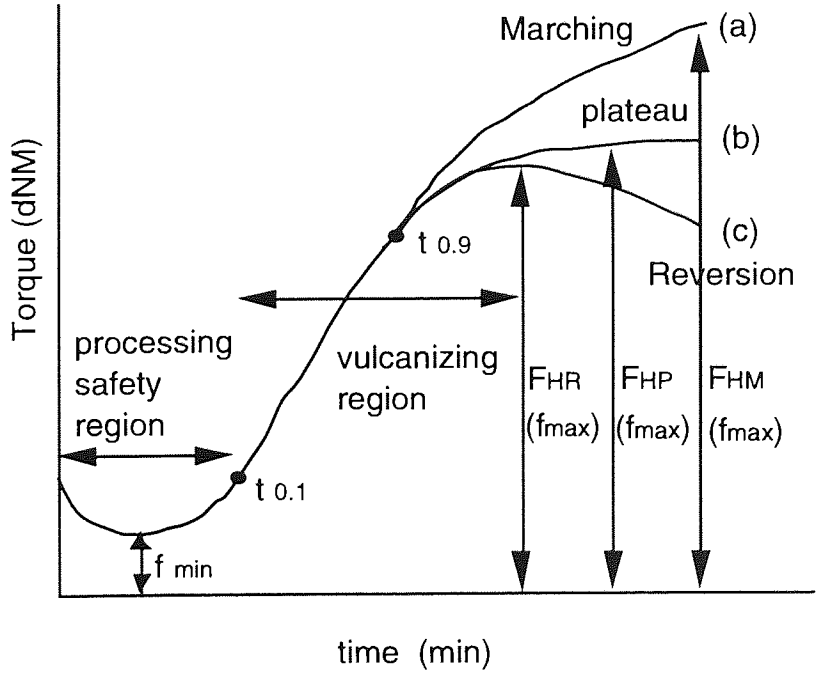

2.4. Physical Tests for Vulcanized Rubber

2.4.1. Tensile Tests

2.4.1.1. Test Pieces

The test pieces which were used for tensile tests were dumb-bells (BS Type 2 [86]) (see fig.2.82). A Testometric Micro 500 (TCS Laboratory) testometer was used for this test.

Fig. 2.82. Shapes of Dumb-bell testpiece and die [86].

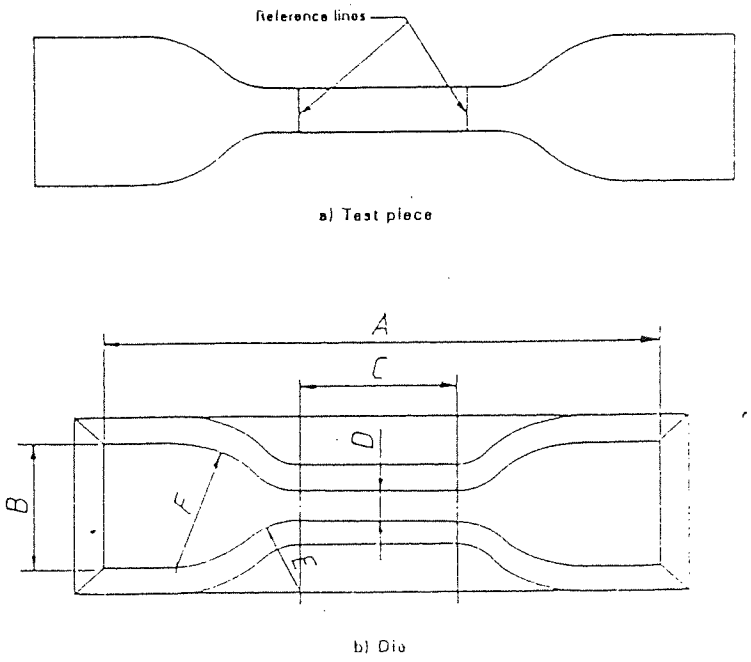

Table 2.44 Die dimension for Dumb-bell test pieces [86].

Dimension (mm)	Type 2
A Overall length	75
B Width of ends	12.5±1
C Length of narrow parallel portion	25±1
D Width of narrow parallel portion	4.0±1
E Small radius	8±0.5
F Large radius	12.5±1

2.4.1.2. Mechanical Properties after Thermal Ageing of Rubber Samples

Tensile strength and elongation at break were measured both before and after thermal ageing and were used for an evaluation of thermal resistance of natural rubber. The details of tensile test method are described in BS903: Part A2 [86] and ASTM D412-87 [87]. Dumb-bell types test pieces were extended at 500 mm/min until break. Tensile strength and elongation at break were determined from four (sometimes three) sets of results. As a mean procedure, JIS mean method was used. Generally, tensile strength and elongation at break have binominal exponential distribution which cluster to the higher part; therefore, mean procedure permits the emphasis on the higher values rather than arithmetic average and the following equations were used;

2 samples 0.9A+0.1B

3 samples 0.7A+0.2B+0.1C

4 samples 0.5A+0.3B+0.1C+0.1D

where A,B,C, and D are either tensile strength or elongation at break whereby A>B>C>D [88]. The mean values of tensile strength and elongation at break were compared between, before, and after ageing. The retention was expressed as the ratio of the mean value before ageing to the one after ageing.

Single cell ovens were used for thermal ageing. Samples were suspended in separate cells and were aged at three different temperatures;. 70°C (for 90 and 180hr), 100°C (for 24 and 48hr), and 120°C for (6 and 12hr).

2.4.1.3. Mooney-Rivlin Plots

Mooney-Rivlin plots were used for determination of crosslink density of rubber using tensile stress-strain data. The same tensile test pieces (BS type2), and the same tensometer (Testometric Micro 500) were used. However, the extention speed used here was much lower than in a normal tensile test and was 1mm/min, in order to eliminate the effect of entanglement of rubber. The crosslink density was calculated using the following equations;

$$\sigma=2C_1(\lambda-1/\lambda^2)+2C_2(1-\lambda^{-3})$$

$$2C_1=\nu_eRT$$

where σ is stress, λ is strain (l/l_0), R is Gas constant, T is absolute temperature, ν_e is crosslink density, and C_1 and C_2 are constants [89]. Fig. 2.43 shows typical Mooney-Rivlin plots. Using the linear region, the crosslink density was obtained from the intercept and this was used for the analysis of chemical stress relaxation results, see section 2.4.2.

Fig. 2.83 Mooney-Rivlin plots [90].
(○ : NR1 sulfur 0.7 phr, ● : NR2 sulfur 2.0 phr, ⊖ : NR3 sulfur 5.0 phr)

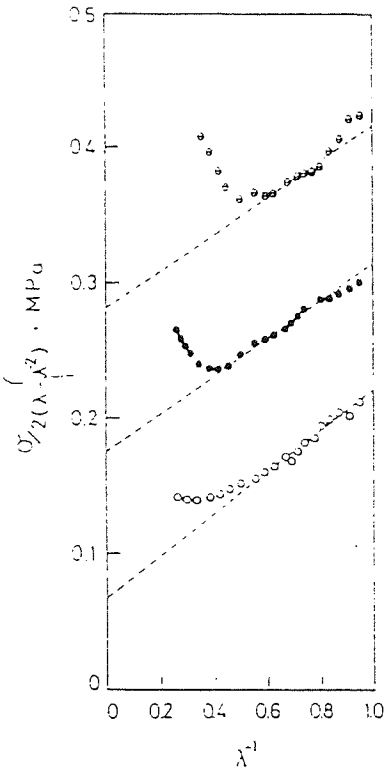

2.4.1.4. Measurement of Strain Energy

Strain energy was used for the analysis of fatigue failure tests. The test pieces were cut out from the fatigue rubber sheet, which was cured into rectangular rubber sheet with beaded edges using BS type 2 dumb-bell cutter. Those samples were subjected to more than 30 cycles at maximum extention ratio (1.60) used in determining the fatigue life. After fatiguing, the beaded edges were cut off and stress strain curve was measured using extention speed of 1 mm/min. The strain energy values were obtained from the integration of stress strain curve, see fig. 2.84.

Fig. 2.84 Measurement of strain energy

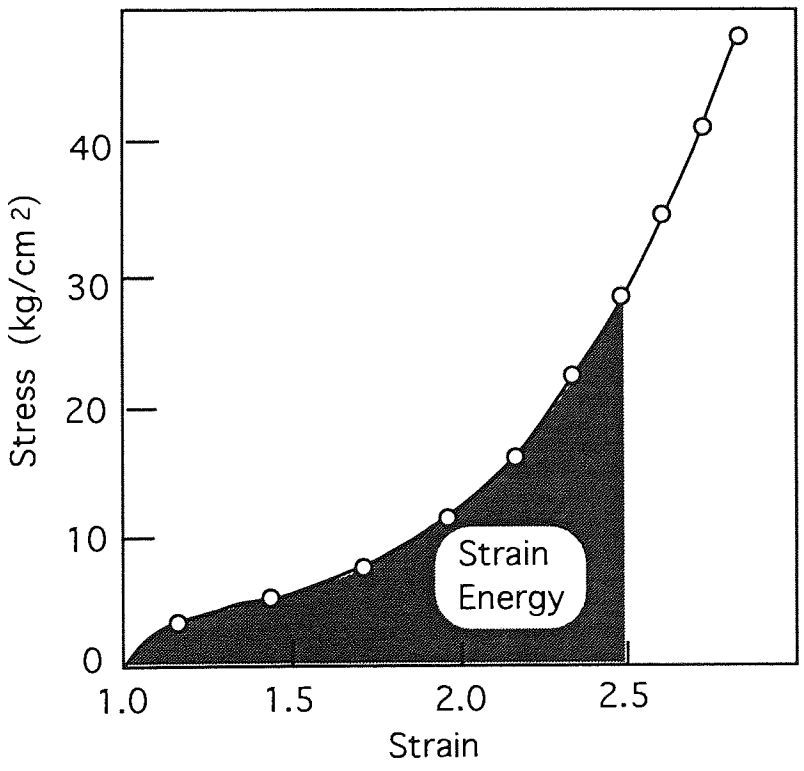

2.4.2. Chemical Stress Relaxation

This test method was used for assessment of thermal resistance. Viscoelastic changes which occur as a consequence of chemical changes were measured. The test was first developed by Tobolsky and corwerkers [91, 92] who termed the viscoelastic behavior which is induced by chemical reaction as "chemorheology", and this test was further improved by Murakami and coworkers [93, 94].

Although there are two test modes, continuous and intermittant, in a chemical stress relaxation, only the continuous mode was used in this work. This evaluates the ratio of random scission along the rubber main chain. Thin vulcanized strips, less than 0.5mm in thickness and about 4 cm in length, were set up onto the Wallace Shawbury age-tster. The age-tster consists of a balanced beam, on which tension exerted by a rubber strip is counter balanced by that of a helical spring. By means of electrical contacts at the end of the beam, and a motor, the tension in the spring is automatically adjusted to the balance of the tention in the rubber. A pen attached to the moving end of the spring records the stress in the sample on a chart. After setting the rubber strip, the zero and full scale deflection were adjusted. These stress relaxometers were placed in single cells air ageing Wallace oven which was adjusted at 100°C, and pre-heated for 15 minutes before running. At the start of measurement, the rubber strips were extended to 60% of their original length.

In the case of sulfur cured natural rubber, scission along the main chain and exchange reaction at the crosslink points occur during thermal oxidative degradation [93]. Normally the ratio of exchange scission which occures at the di- or poly-sulfide crosslinks was shown to be faster and showed a quick

relaxation. The ratio of main chain scission and exchange reaction can be expressed as follows;

$$f(t)/f(0) \approx A e^{-k_1 t} + B e^{-k_2 t}$$

$$-k_1 t = -q_m(t)/N(0) \approx -q_0 t/N(0)$$

where **t** is the ageing time, **f(t)** and **f(0)** are the tension after **t** hr and after time zero, k_1 and k_2 are rate constants of main chain scission and exchange reaction,. $q_m(t)$ is a number of chain scission during **t** hr and it is approximated to be the product of the constant number of chain scission per hr, q_0 by time **t**, and **N(0)** is a initial total number of network chains [93, 94]. In this work, the crosslink density which was determined by chemical stress relaxation was used for **N(0)**. When **ln { f(t) / f(0) }** is plotted against time, the curve can be fitted to a line, see fig.2.85. In the end of relaxation, the curve is approximated to the slowest relaxation, main chain scission. Hence the rate constant of the main chain scission was obtained from the slope of the end region of relaxation curve. The details of stress relaxation theory is described in Murakami's book [94].

Fig. 2.85. Analysis of chemical stress relaxation curve.

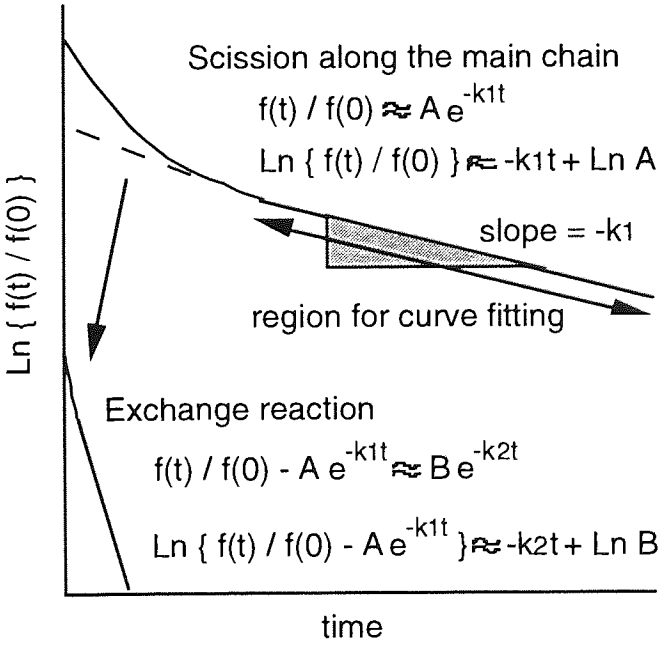

2.4.3. Fatigue Test

This test method is used for assessment of fatigue resistence. General procedure for this test is described in BS 903, part A51 [95] and ASTM D4482-85 [96]. The rubber specimen is extended intermittently from zero % to a constant maximum strain. These cycles were repeated until the rubber specimen failed. In this work, fatigue life is defined as the total number of cycles required to rupture the specimen completely.

The fatigue instrument used was the Monsanto Fatigue-to-Failure Tester. The maximum applied strain may be varied by changing the drive cam. The cured recutangular sheet with beaded edges was cut by BS type 2 dumb-bell cutter and was set onto the equipment. After 30 cycles of fatigue, the strain was measured using the reference lines which were marked on the narrow parallel portion of samples before fatiguing. The frequency of fatigue of this machine is 100 cycles per minute.

Fatigue life is determined from four sets of results for each sample. The JIS average method [97] was used for all results like that discussed under the tensile strength and elongation at break section, see section 2.4.1.2.

2.5 Evaluation of Binding Efficiency of Reactive Antioxidants

2.5.1. Grafting of Antioxidants in an Internal Mixer

Reactive antioxidants such as 2-propenamide, 2-methyl-N-[4-phenylaminophenyl] (APMA) and 4-mercaptoacetoamido-diphenylamine (MADA), see table 2.6, were mechanochemically grafted onto the rubber main chain during processing in an internal mixer (RAPRA-Hampshire torque rheometer connected to a Brabender motor which is oil heated), see fig. 2.86. After heating the oil and the torque rheometer block to the required temperature, nitrogen gas was flushed into the chamber. The masticated natural rubber and reactive antioxidant were then charged (total mass charge was 30 g) into the mixer. After closing the ram, the rotors were started. The block temperature and the torque were monitered during mixing. The mixing conditions, temperature, mixing time, and rotor speed, as well as antioxidants concentration, were varid and will be discussed in chapter 4.

Fig. 2.86. Internal mixer

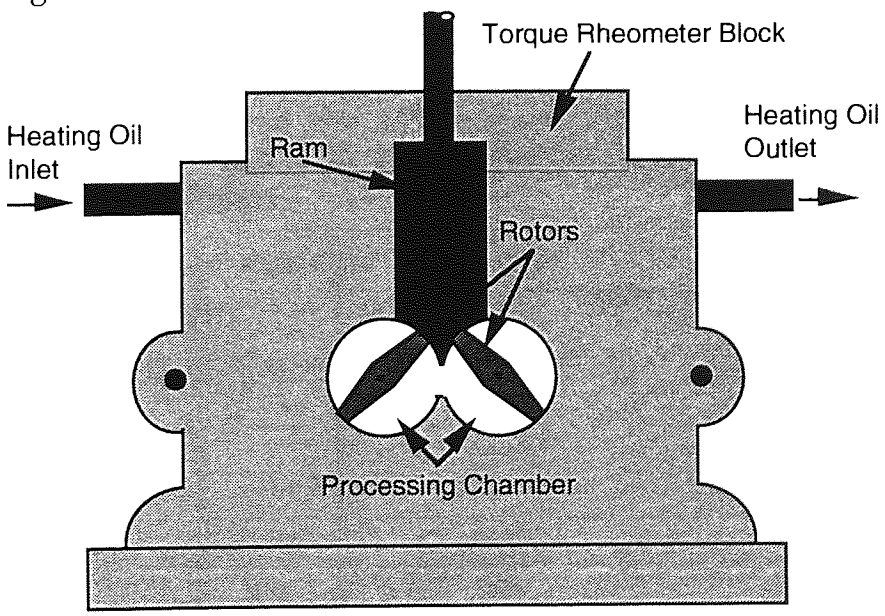

2.5.2. Measurement of Binding Efficiency

2.5.2.1 Extraction Methodology of Free (Unreacted) Reactive Antioxidants

The binding efficiency of reactive antioxidants was determined by using FT-IR spectroscopy. Before measurement, the free (unreacted) antioxidant was extracted and the antioxidant concentration after extraction was compared with initial concentration in the rubber before extraction. The extraction was carried out either before or after vulcanisation. The details of the experimental methodology will be discussed in chapter 4.

In the case of the extraction from unvulcanized rubber, acetone was used as a solvent. The natural rubber which was mixed with the antioxidant in an internal mixer (masterbatch rubber) was extracted by acetone using Soxhlet extractor for 90hr. The extraction time of 90 hr was decided from the measurement of UV absorbance of APMA at 308 nm in the extracted solvent, see fig. 2.87. The compounding ingredients were added after that on the two roll mill and the rubber was cured into a very thin film.

Fig. 2.87. Extracted free APMA from 1g of unvulcanized master batch rubber, measured APMA UV absorbance at 308 nm in the exracted solution. (reference: acetone)

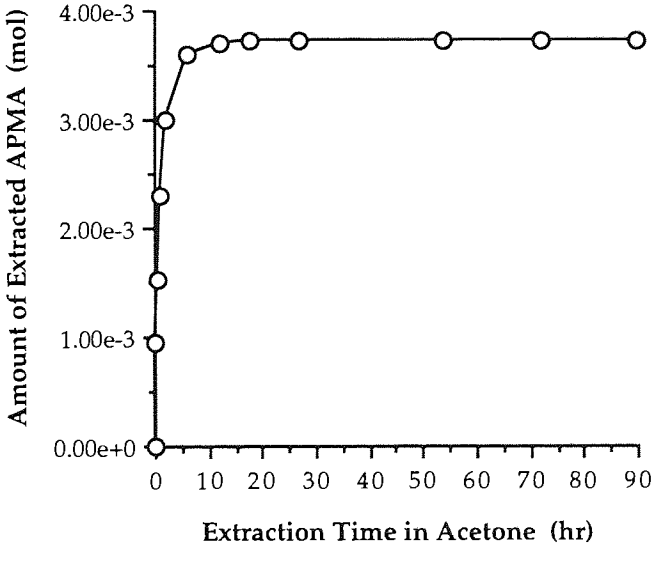

On the other hand, in the case of extraction from vulcanized rubber, azeotropic solvent was used for extraction. The compounding ingredients were added to the master batch rubber on a 2-roll mill. Then it was cured into a thin film. The vulcanized rubber was then extracted by the azeotropic solvent using a Soxhlet extractor for 90 hr. The azeotropic solvents consisted of 19.8 vol % of methanol, 51.9 vol % of acetone, and 28.3 vol % of 1,1,1-trichloroethane. The extraction time of 90 hr was decided from the measurement of UV absorbance of APMA at 308 nm in the extracted solvent, see fig. 2.88. For measurement of UV absorbance solvent was replaced from azeotropic solvent to methanol in each time. In this measurement, the rubber sheet which is around 1.5mm in thickness was used for extraction instead of thin film.

Fig 2.88. Extracted free APMA from 1g of vulcanized rubber measured APMA UV absorbance at 308 nm in extracted solvent. (reference: methanol)

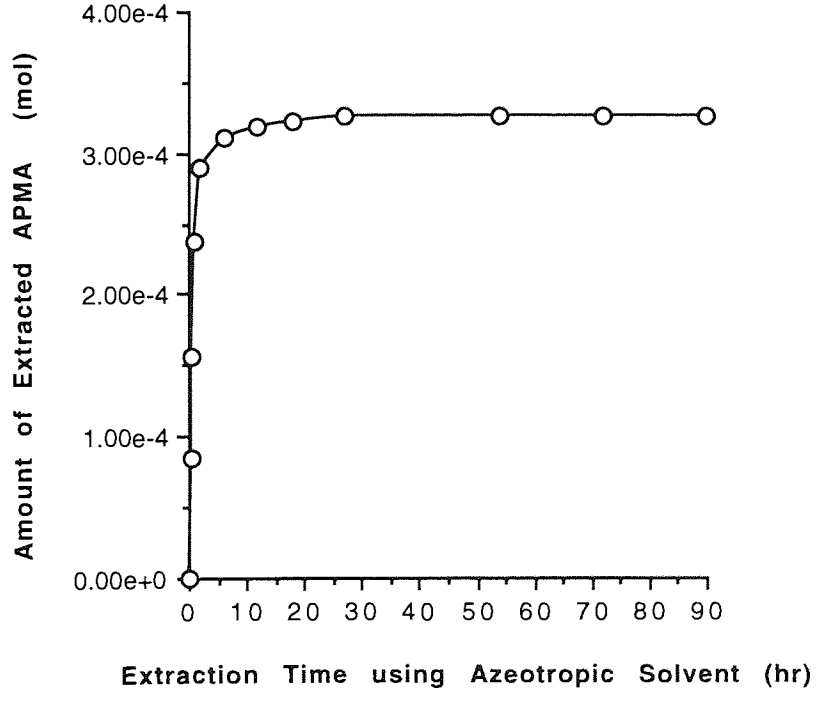

2.5.2.2 FT-IR of Rubber Films of Determination of the Extent of Binding

Infrared spectroscopy was used to determine the amount of reactive antioxidants bound to the rubber. As mentioned above, the samples were cured into thin films. Because reactive antioxidant used (APMA, see table 2.6) have secondary amide group (3355 cm^{-1}), this peak was used for determination of the level of grafting. To overcome the error due to the difference in sample thickness, an invariant peak at 2727 cm^{-1} which is a characteristic for natural rubber was used as a reference peak. The peak area ratio of the secondary amide N-H strech peak to the reference peak was compared for the samples before and after extraction.

$$\text{Sec. Amide Index} = \frac{\text{Sec. Amide Peak Area at 3355 cm}^{-1}}{\text{Reference Peak Area at 2727 cm}^{-1}}$$

$$\text{Binding Eficiency (\%)} = \frac{\text{Sec. Amide Index of Extracted Film}}{\text{Sec. Amide Index of Non-extracted Film}} \times 100$$

Fig 2.89. IR spectrum of APMA bound natural rubber in amide region.

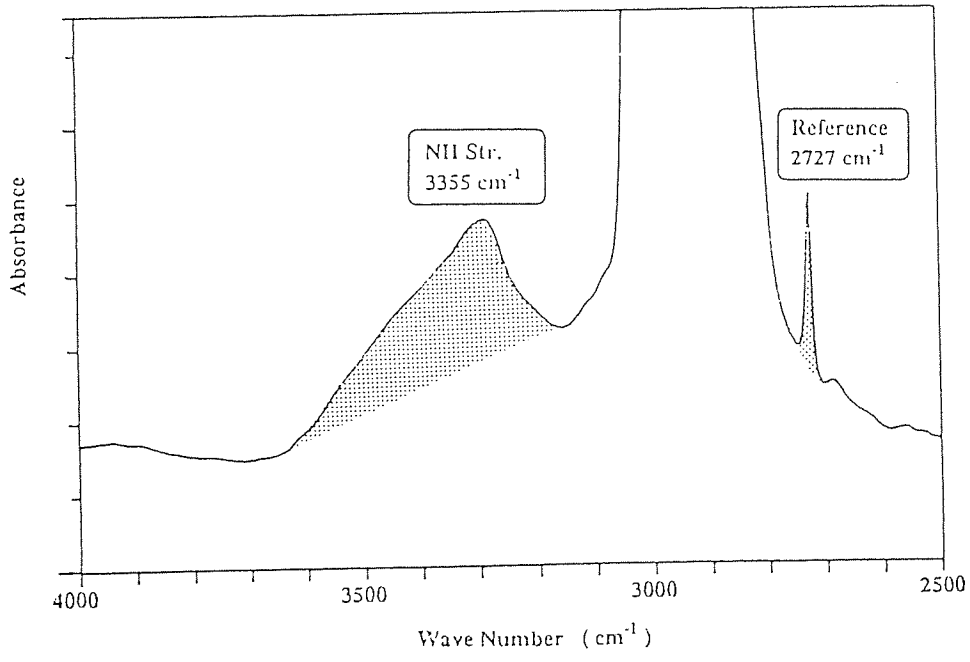

2.5.2.3 Criteria of Outliers

Amide indices measured had less repeatability in a set of results and some amide indices seemed to differ unreasonably from the others in the sets. (Such a value is called outlier [98].) In order to assess whether such suspicious values should be removed or not, two methods; Dixon's methods and Grubbs's method, were applied. Dixon's method was applied to the case when amide indices have only one suspicious value in a set of measurement, whereas the Grubbs's method was applied in cases where amide indices showed more than two suspicious values [99].

The suspected amide index is either the lowest (x_1) or the highest (x_n) value among all the data.

$$x_1 \leq x_2 \leq ..... \leq x_{n-1} \leq x_n$$

If the calculated **Q** in table 2.45 is larger than the critical value, the suspected amide index should be rejected from the calculation of grafting efficiency. Table 2.45 gives the critical values for Dixon's method at 0.05 significant level [99].

Table 2.45 Calculation of Dixon's Q and critical value [99].

Number of Data	Calculation for Criterion	Critical Value P=0.05
3	$Q_{10} = (x_2 - x_1) / (x_n - x_1)$: x_1 is suspected	0.941
4	$= (x_n - x_{n-1}) / (x_n - x_1)$: x_n is suspected	0.765
5		0.642
6		0.560
7		0.507
8	$Q_{11} = (x_2 - x_1) / (x_{n-1} - x_1)$: x_1 is suspected	0.554
9	$= (x_n - x_{n-1}) / (x_n - x_2)$: x_n is suspected	0.512
10		0.477
11	$Q_{21} = (x_3 - x_1) / (x_{n-1} - x_1)$: x_1 is suspected	0.576
12	$= (x_n - x_{n-2}) / (x_n - x_2)$: x_n is suspected	0.546
13		0.521

(continue)

Table 2.45 Calculation of Dixon's Q and critical value. (continue) [99]

Number of Data	Calculation for Criterion	Critical Value P=0.05
14	$Q_{22} = (x_3 - x_1) / (x_{n-2} - x_1)$: x_1 is suspected	0.546
15	$= (x_n - x_{n-2}) / (x_n - x_3)$: x_n is suspected	0.525
16		0.507
17		0.490
18		0.475
19		0.462
20		0.450
21		0.440
22		0.430
23		0.421
24		0.413
25		0.406

For the set of amide indices where there are more than two suspected values, Grubbs's method was used instead of the Dixon's method [99]. The calculation for this was as follows;

(x_1 is suspected) $T_1 = \dfrac{\bar{x} - x_1}{s}$

(x_n is suspected) $T_n = \dfrac{x_n - \bar{x}}{s}$

Table 2.46 gives the critical values of Grubbs's method at 0.05 significant level. If calculated T is lager than the critical value in table 2.46, the measurement include error and should be rejected.

Table 2.46 Critical values for Grubbs's method [99) 100]

Number of Data	Critical Value P=0.05	Number of Data	Critical Value P=0.05
3	1.15	15	2.41
4	1.46	16	2.44
5	1.67	17	2.48
6	1.82	18	2.50
7	1.94	19	2.53
8	2.03	20	2.56
9	2.11	21	2.58
10	2.18	22	2.60
11	2.23	23	2.62
12	2.28	24	2.64
13	2.33	25	2.66
14	2.37	30	2.74

2.6. Investigation of Reaction Mechanisms

2.6.1. Extraction Methodlogy

The antifatigue agents and any transformation products were extracted from vulcanized rubber samples at the end of their fatigue life with the aim of investigating their mechanisms. Since products of antifatigue agents can be expected to be unstable under thermal oxdative conditions, the extraction method required special care. In this work, four points of caution were considered: firstly, to prevent the thermoxidative reaction of antifatigue agents' derivatives during the extraction process. Secondly, to reduce the loss of antifatigue agents' derivatives during extraction and evaporation. Thirdly, to avoid the chemical changes during the storage time of fatigued rubber and extracted solvent. Moreover, sample cut must be avoided due to the generation of macroalkylradicals. For these reasons, the following procedures were used in this work. When the fatigue test had finished, test pieces were subjected to the extraction immediately to avoid any chemical changes during storage. Only the narrow parallel portion of the fatigued test pieces were cut off and used for the extraction, see fig. 2.82 (portion C). The test samples were not broken into small pieces in order to avoid the generation of mechano radicals and the rubber samples were finally placed in the Soxhlet extractor, see fig 2.90. Small stream of nitrogen gas was continuously flashed during the extraction to avoid any oxidation. The required solvent was poured into the extractor through the condencer but extraction was carried out at ambient temperature. The solvent was renewed several times and when the extraction finished more solvent was poured to wash the extractor. After extraction all the solvent was fulshed down into the flask and the solvent was evaporated at room temperature under nitrogen flow. The solvent used in this work was n-hexane. The extraction time was two days, this was also decided from the measurement of αTOC UV absorbance at 296 nm in extracted solvent, see fig.2.91.

Fig. 2.90 Extraction of antifatigue agents and their transformed products using Soxhlet extractor.

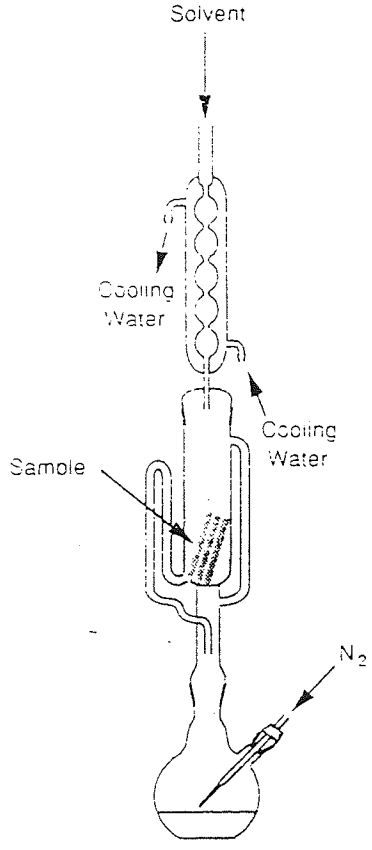

Fig. 2.91. Extracted α-tocopherol concentration using n-hexane, measured by UV absorbance at 296 nm in extracted solvent. (reference: n-hexane)

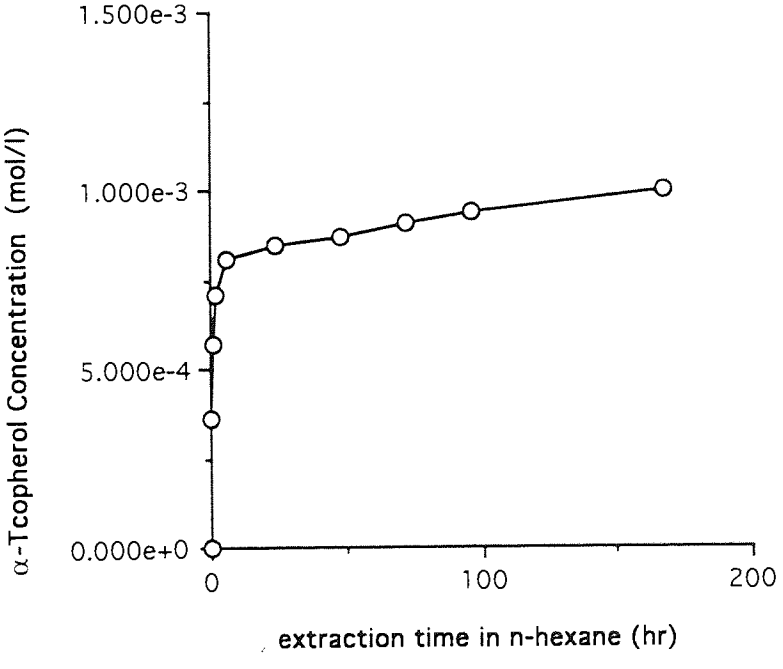

After the extracted solvent was evaporated an HPLC solvent was used to dissolve the sample ready for HPLC analysis, flasks were filled with argone gas and were tightly closed and placed in the refrigerator until ready for analysis.

2.6.2 HPLC Conditions

In order to investigate the reaction mechanisms of antifatigue agents, extracted substances from rubber samples were analysed using HPLC. The instrument used was a Philips PU4100 liquid chromatograph using a PU4120 diode array detector controlled by PU6003 software. The analysis was carried out isocratically both in reversed phase and in normal phase. The mobile phase was optimised by changing solvent strength and selectivity factor. The details of solvent optimisation are described in chapter 5. All solvents used in this work were HPLC grade, ex Fisons. All other HPLC analysis conditions were as follows;

Reversed Phase Condition	
Stationary Phase	Zorbax ODS 4.6 mm ID × 25 cm
Mobile Phase	Methanol : Isopropanol = 90 : 10 v/v †
Flow Rate	0.8 ml/min
Wave Length of UV Detector	290nm, 268 nm
Temperature	Ambient

Normal Phase Condition	
Stationary Phase	Zorbax SIL 4.6 mm ID × 25 cm
Mobile Phase	n-Hexane : 1,4-Dioxane = 100 : 0.3 v/v †
Flow Rate	0.8 ml/min
Wave Length of UV Detector	290nm, 268 nm
Temperature	Ambient

† mobile phase used as main condition of α-tocopherol transformation products analysis

Fig. 2.1 FT-IR spectrum of SMR-L casted by benzene.
A : Str. =CH (3035 cm^{-1}), B : Str. CH (2960, 2854 cm^{-1}),
C : Str. C=C (1664 cm^{-1}), D : Def. CH (1450, 1376 cm^{-1}).

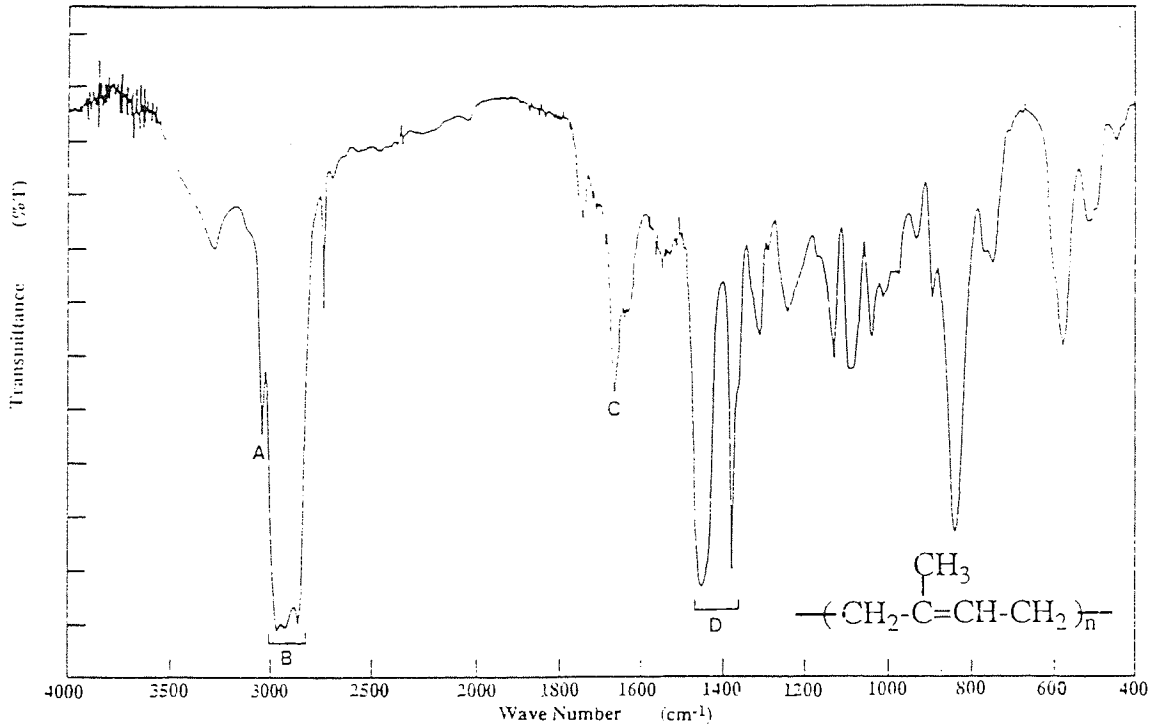

Fig. 2.2 FT-IR spectrum of stearic acid using KBr disk.
A : Str. OH (3500-2500 cm^{-1}), B : Str. CH (2955,2917, 2871, 2849 cm^{-1}),
C : Str. C=O (1703 cm^{-1}), D : str. C-O (1298 cm^{-1}), E : Def. OH (942 cm^{-1}).

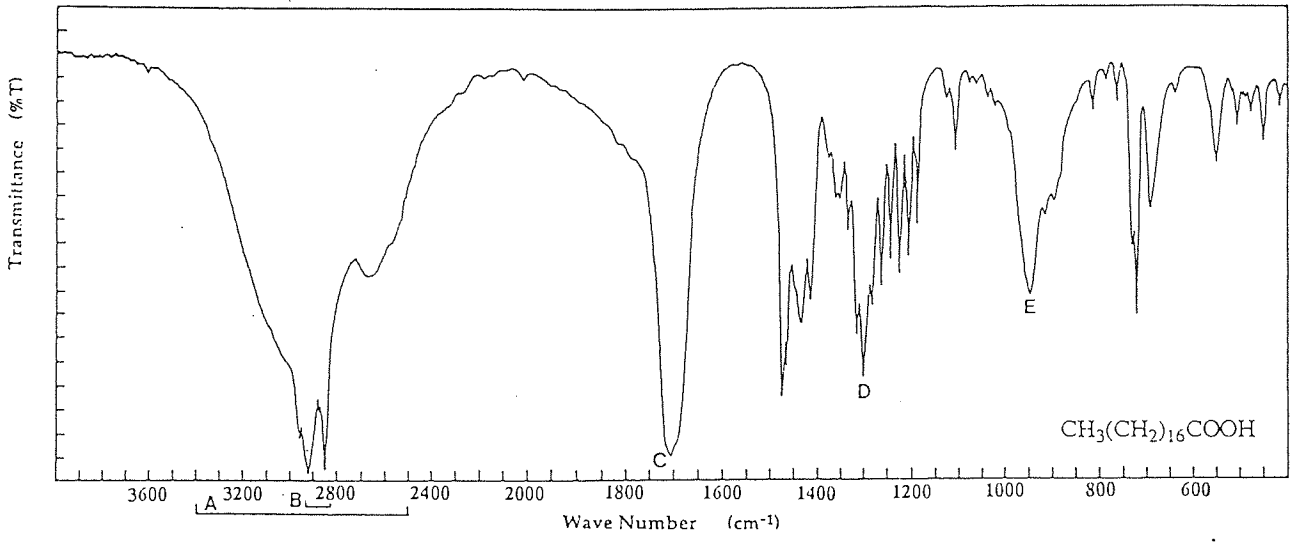

Fig. 2.3 FT-IR spectrum of CBS using KBr disk.
A : Str. NH (3221 cm^{-1}), B : Str. CH (2930, 2853 cm^{-1}),
C : Str. Ring (1561, 1463, 1429 cm^{-1}).

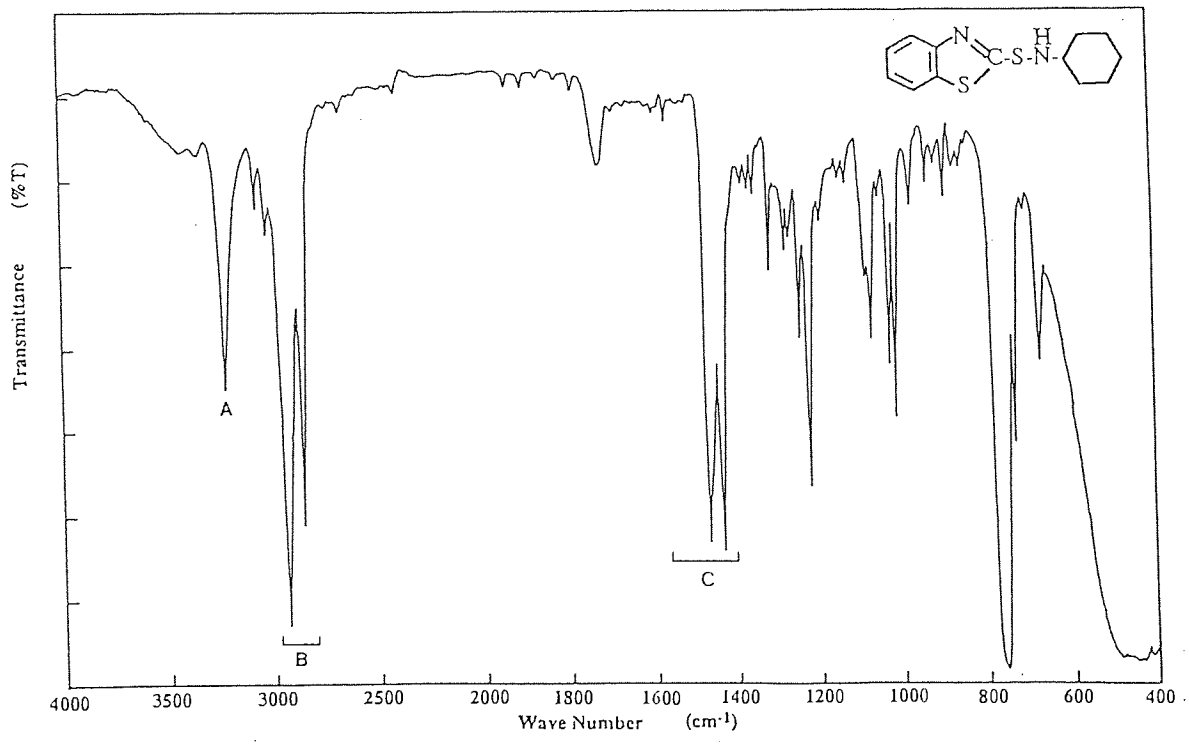

Fig. 2.4 FT-IR spectrum of AIBN using KBr disk.
A : Str. CH (2997, 2949, 2874 cm^{-1}), B : Str C N (2244 cm^{-1}), C : Def. CH (1471, 1460, 1381, 1366, 950 cm^{-1}), D : Skel $(CH_3)_2C$ (1229, 1175 cm^{-1}).

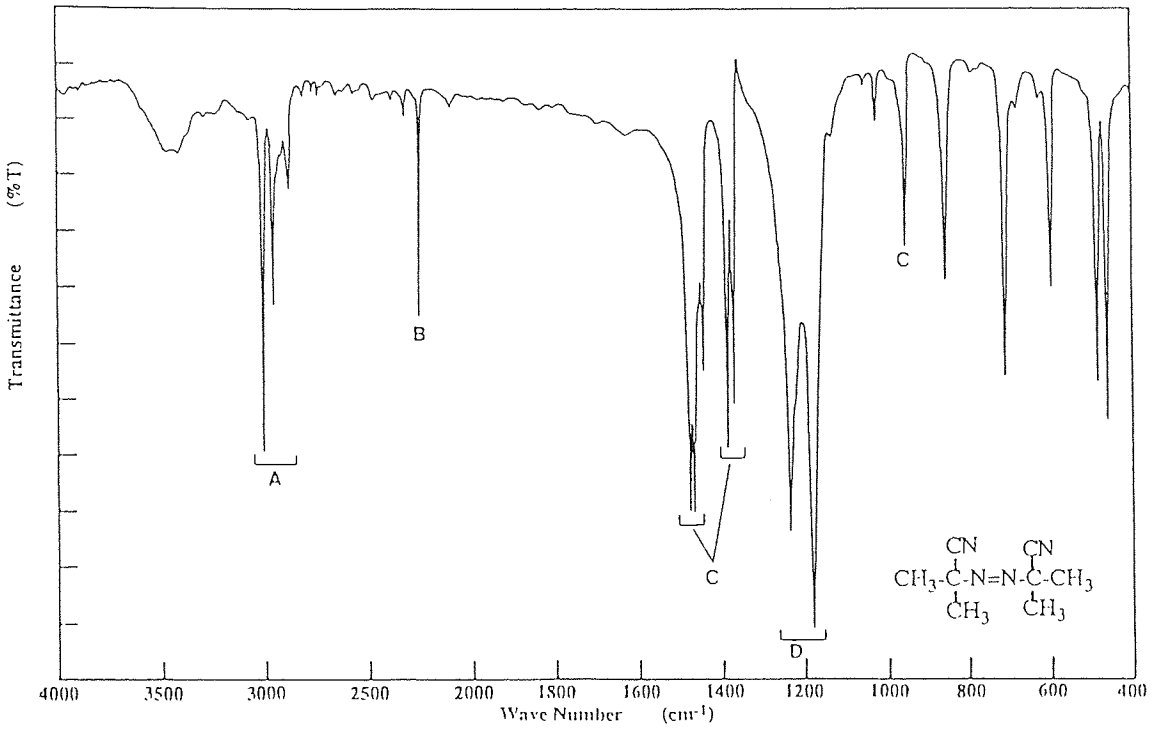

Fig. 2.5 FT-IR spectrum of squalene pasted on KBr crystal.
A : Str. =CH (3040 cm^{-1}), B : Str. CH (2964, 2910, 2851 cm^{-1}),
C : Str. C=C (1668 cm^{-1}), D : Def. CH (1446, 1382 cm^{-1}).

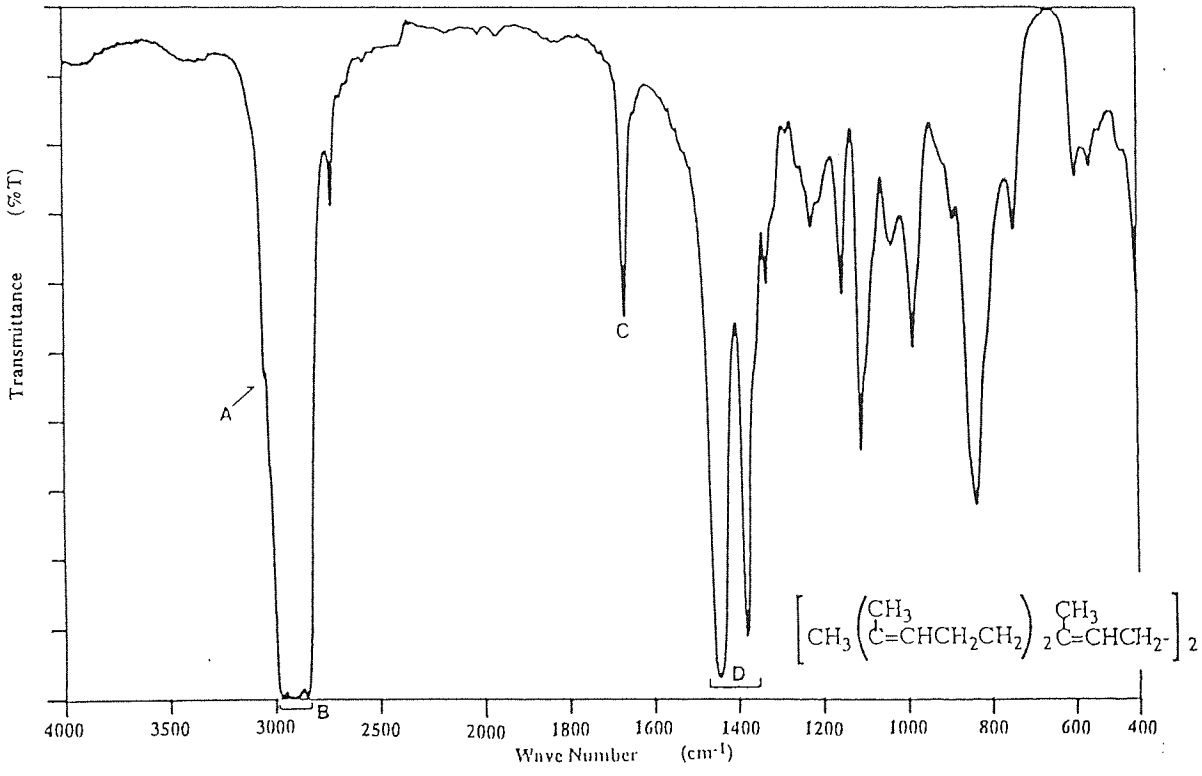

Fig. 2.6 ^{1}H-NMR spectrum of squalene. (300MHz)

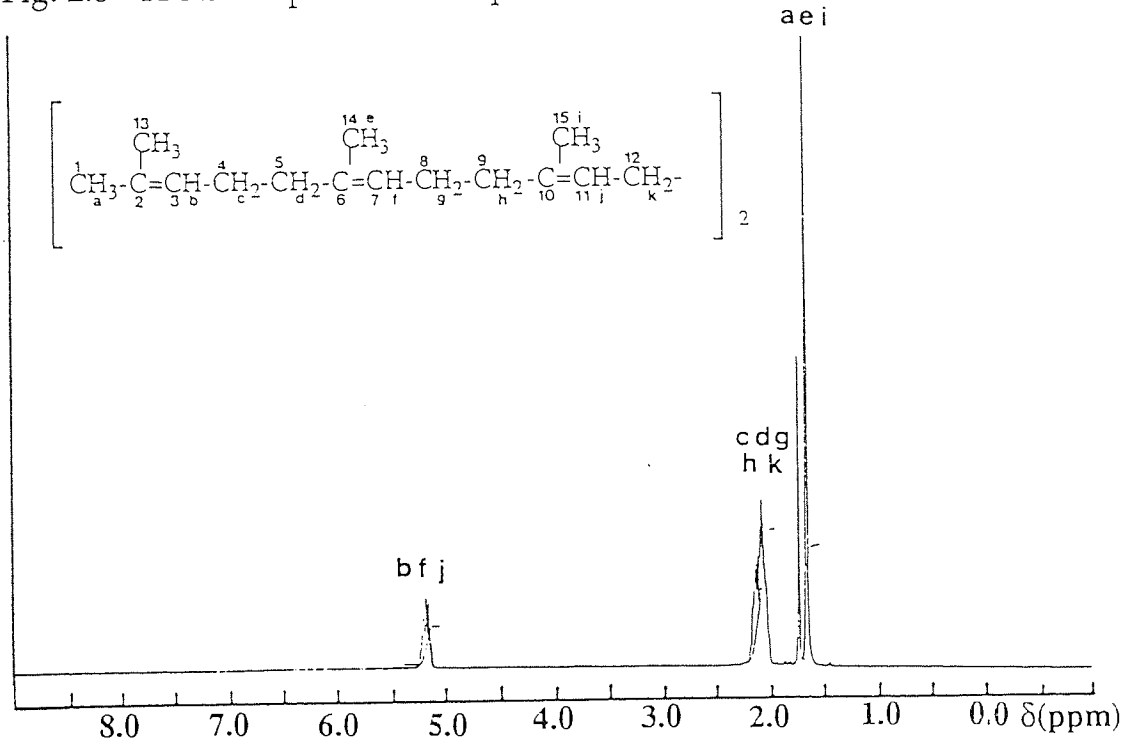

Fig. 2.7 ^{13}C-NMR spectrum of squalene. (75.5MHz)

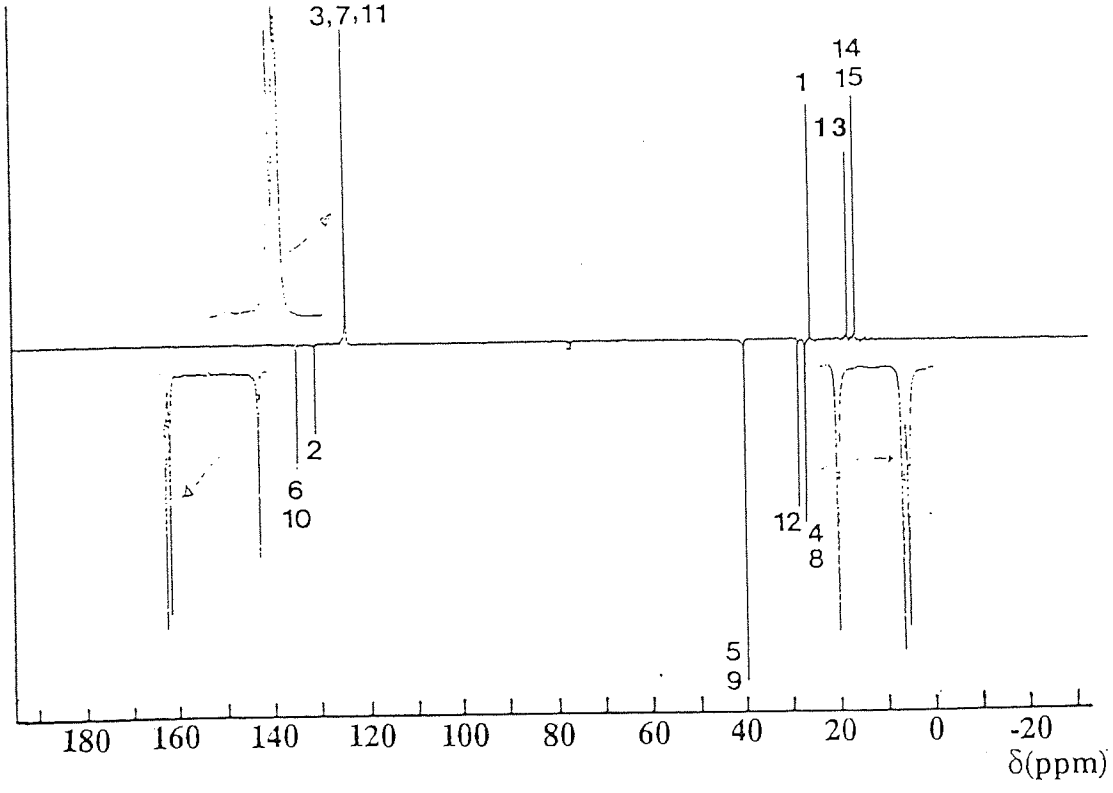

Table 2.3. Characteristic absorption bands of natural rubber, compounding ingredients and other chemicals.

	Wave Number (cm-1)	IR Bands
NR	A : 3035	Str. =CH
	B : 2960, 2854	Str. CH
	C : 1664	Str. C=C
	D : 1450, 1376	Def. CH
Stearic acid	A : 3500 - 2500	Str. OH
	B : 2955, 2917,2871, 2849	Str. CH
	C : 1703	Str. C=O
	D : 1298	Str. C-O
	E : 942	Def. OH
CBS	A : 3221	Str. NH
	B : 2930, 2853	Str. CH
	C : 1561, 1463, 1429	Str. Ring
AIBN	A : 2997, 2949, 2874	Str. CH
	B : 2244	Str. C N
	C : 1471,1460, 1381, 1366, 950	Def. CH
	D : 1229, 1175	Skel. $(CH_3)_2C$
Squalene	A : 3040	Str. =CH
	B : 2964, 2910, 2851	Str. CH
	C : 1668	Str. C=C
	D : 1446, 1382	Def. CH

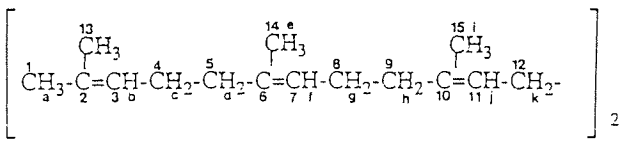

Table 2.4 ^{1}H-NMR summary of squalene.

No. of Atom	Chemical Shift δ (ppm)	Integral	H
b,f, j	5.2128, 5.1850, 5.1591, 5.1398, 5.1360	23.792	6H
c, d, g, h, k	2.1624, 2.1380, 2.1168, 2.0969, 2.0765, 2.0625, 2.0361	82.511	20H
impurities	1.7345	25.477	
a, e, i	1.6600, 1.6571	72.572	18H

Table 2.5 ^{13}C-NMR summary of squalene.

No. of Atom	Chemical Shift δ (ppm)	(+)/(-)
6, 10	134.7429, 134.5569	(-)
2	130.7742	(-)
3, 7, 11	124.4560, 124.3308, 124.2773	(+)
5, 9	39.7585	(-)
12	28.2737	(-)
4, 8	26.7660, 26.6279	(-)
1	25.5873	(+)
13	17.5203	(+)
14, 15	15.8868, 15.8606	(+)

Table 2.7 Characteristic IR absorption bands, UV absorbance, and melting points.

Code	FT-IR		UV		m.p. (°C)		
	Wave Number (cm^{-1})	Absorption Bands	λ max (nm)	log ε	exp.	lit.	ref.
BQ	A : 3005	Str. =CH	258	4.24	66.0 - 68.2	65.0 - 66.0	101
	B : 2966, 2913, 2871	Str. CH					
	C : 1665	Str. C=O					
	D : 1459, 1393, 1364 922	Def. CH					
	E : 1245	Skel. $(CH_3)_3C$					
DPQ	A : 3002	Str. =CH	424	3.85	246.0 - 249.0	246.0 - 247.5	102
	B : 2958, 2909, 2865	Str. CH					
	C : 1640	Str. C=O					
	D : 1459, 1388, 1363, 899	Def. CH					
	E : 1262	Skel. $(CH_3)_3C$					
NQ	A : 1661	Str. C=O	252	4.22	118.0- 121.0	126	103
	B : 1604, 1588	Str. Ring					
PDO	A : 3260 - 2840	Str. NH	253	4.14	136.0 - 140.0		
	B : 1635	Str. C=O					
	C : 1524	Str. C=C coupled with C-N Str.					
	D : 1385	Str. C=N coupled with C=C Str.					
	E : 847	Def. CH					
HBA	A : 3431	Str. OH	286	4.17	189.0 - 193.0	189.0 - 190.0	104
	B : 3000	Str. CH for Ar.					
	C : 2956, 2911, 2872	Str. CH					
	D : 2823, 2734	Str. CH for aldehydes					
	E : 1668	Str. C=O					
αTOC	A : 3467	Str. OH	296	3.55	-	-	
	B : 2951, 2927, 2968	Str. CH					
	C : 1584, 1461, 1422	Str. Ring					
	D : 1262	Str. CCO					
	E : 1086	Str. COC					

(continue)

Table 2.7 Characteristic IR absorption bands, UV absorbance, and melting points. (continue)

Code	FT-IR		UV		m.p.(°C)		
	Wave Number (cm^{-1})	Absorption Bands	λ max (nm)	log ε	exp.	lit.	ref.
γTOC	A : 3408	Str. OH	298	3.59	-	-	
	B : 2927, 2868	Str. CH					
	C: 1593, 1461, 1427	Str. Ring					
	D: 1225	Str. CCO					
	E : 1081	Str. COC					
GM	A : 3493	Str. OH	278	3.50	130.0 - 132.0	128.0 - 132.0	105
	B : 3106	Str. CH for Ar.					
	C: 3003	Str. =CH					
	D: 2956, 2915, 2868	Str. CH					
	E: 1729	Str. C=O					
	F: 1599, 1479, 1439	Str. Ring					
IPPD	A : 3378	Str. NH	292	4.23	75.0 - 76.5	75.0	106
	B : 3084, 3026	Str. CH for Ar.					
	C : 2978, 2964, 2931, 2868	Str. CH					
	D : 1516	Def. NH					
	E : 1314	Str. =C-N					
	F : 1299	Str. C-N					
6PPD	A : 3390, 3378	Str. NH	292	4.21	48.0 - 50.0	46.0	106
	B : 3043, 3021	Str. CH for Ar.					
	C : 2963, 2951, 2917, 2865	Str. CH					
	D : 1516	Def. NH					
	E : 1314	Str. =C-N					
	F : 1264	Str. C-N					
TMQ	A : 3372	Str. NH	240	$E^{1\%}$= 829	77.0 - 94.0	83.0 - 90.0	106
	B : 3017	Str. =CH					
	C : 2960, 2927, 2866	Str. CH					
	D : 1650	Str. C=C					
PM	A : 3363	Str. NH	282	4.23	154.0 - 156.0	160.0	76
	B : 3065	Str. =CH	440	4.22			
	C : 1757	Str. C=O					
BTMI	A : 3298	Str. NH	248	3.94	54.0 - 58.0		
	B : 3090, 3005	Str. =CH					
	C : 2982, 2963, 2917	Str. CH					
	D : 1712, 1682	Str. C=O					
	E : 1526	Def. NH					
	F : 1244	Str. CN					
APMA	A : 3350	Str. NH	308	4.23	105.0 - 108.0	106.0 - 108.0	107
	B : 1653	Str. C=O					
	C : 1522	Def. NH					

(continue)

Table 2.7 Characteristic IR absorption bands, UV ubsorbance, and melting points. (continue)

Code	FT-IR		UV		m.p. (°C)		
	Wave Number (cm^{-1})	Absorption Bands	λ max (nm)	log ε	exp.	lit.	ref.
MADA	A : 3365	Str. NH	300	4.37	122.3 - 147.3	135.5 - 137.0	77
	B : 2525	Str. SH					
	C : 1650	Str. C=O					
	D : 1539	Def. NH					
P168	A : 3031	Str. CH for Ar.	270	3.49	179.0 - 181.0	180.0 - 185.0	108
	B : 2960, 2907, 2868	Str. CH					
	C : 1602, 1490	Str. Ring					
	D : 1213	Str. POC					
	E : 906	Str. POP					
P626	A : 2957, 2885, 2868	Str. CH	272	3.35	162.0 - 174.0	160. 0 - 175.0	109
	B : 1605, 1495	Str. Ring					
	C : 1227	Str. POC					

Fig. 2.9 UV spectrum of BQ in DCM solution.

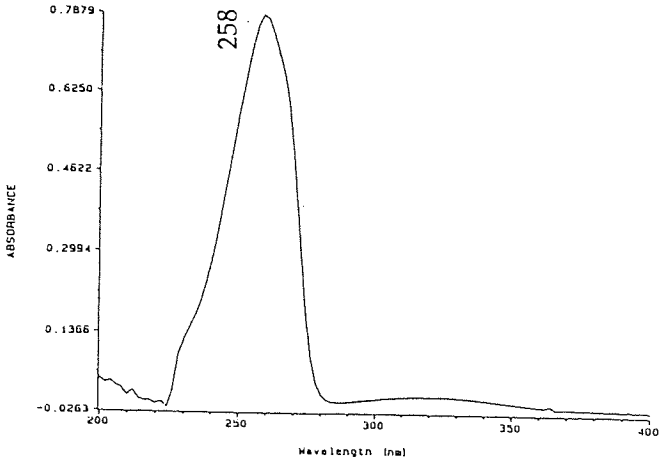

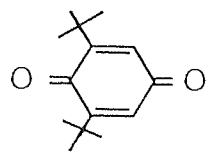

BQ

m.p. = 66.0-68.2 (°C)

λ_{max} = 258 nm

log ε_{max} = 4.24

Fig. 2.10 FT-IR spectrum of BQ using KBr disk.
A : Str. =CH (3005 cm^{-1}), B : Str. CH (2966, 2913, 2871 cm^{-1}),
C : Str. C=O (1665 cm^{-1}), D : Def. CH (1459, 1393, 1364, 922 cm^{-1}),
E : Skel. $(CH_3)_3C$- (1245 cm^{-1}).

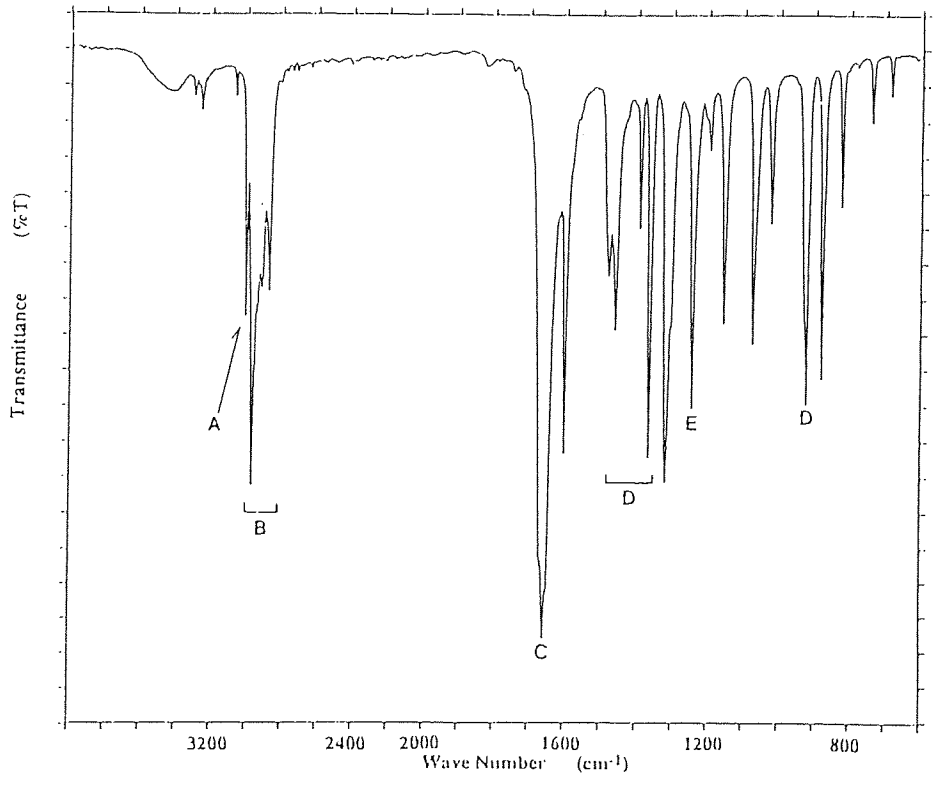

Fig. 2.11 UV spectrum of DPQ in DCM solution.

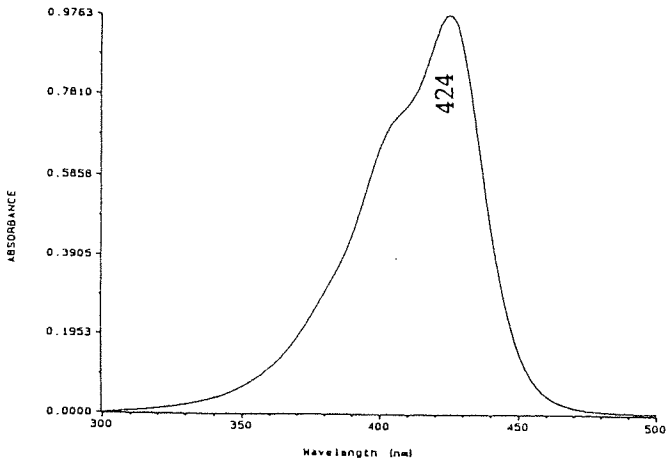

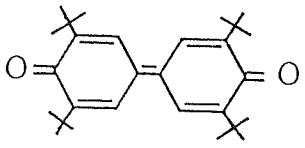

DPQ

m.p. = 246.0-249.0 (°C)

λ_{max} = 424 nm

log ε_{max} = 3.85

Fig.2.12 FT-IR spectrum of DPQ using KBr disk.
A : Str. =CH (3002 cm^{-1}), B : Str. CH (2958, 2909, 2865 cm^{-1}),
C : Str. C=O (1640 cm^{-1}), D : Def. CH (1459, 1388, 1363, 899 cm^{-1}),
E : Skel. $(CH_3)_3C$- (1262 cm^{-1}).

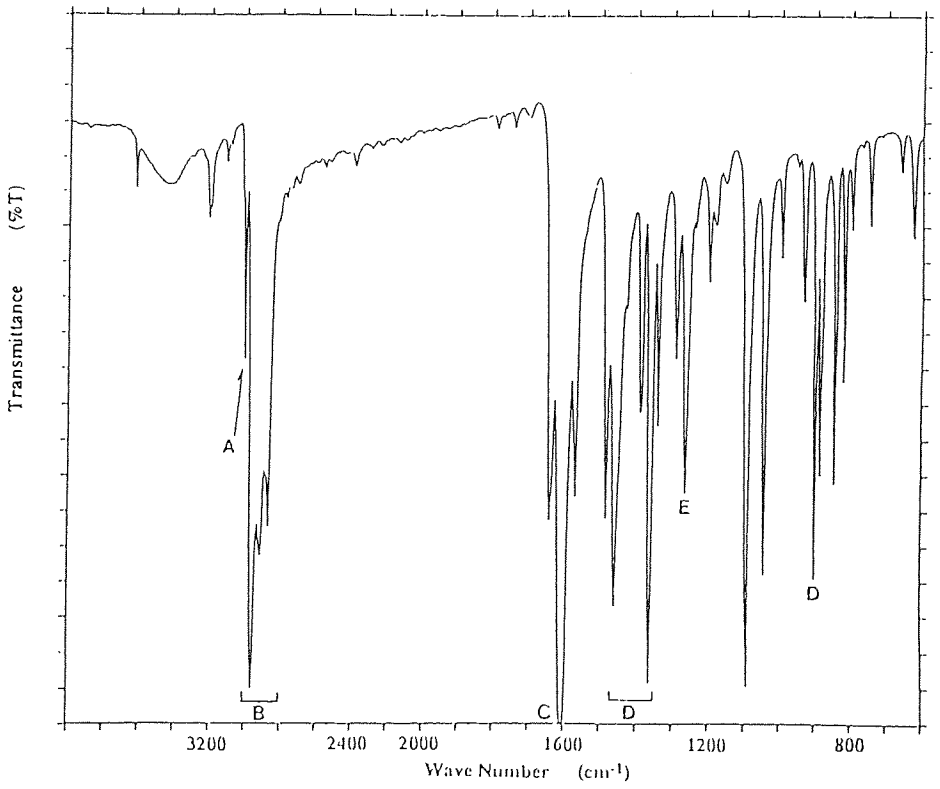

Fig. 2.13 UV spectrum of NQ in DCM solution.

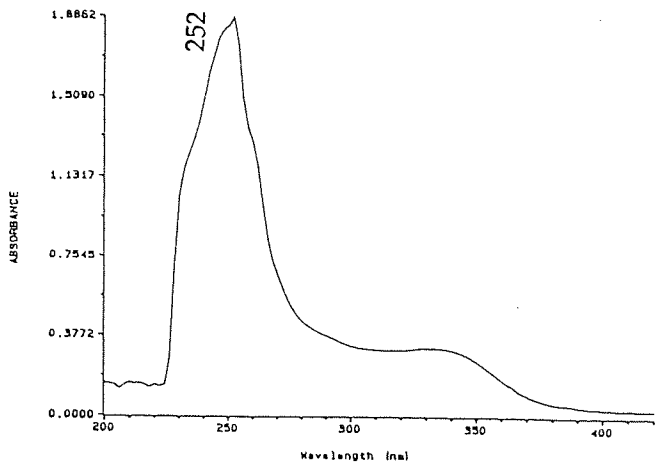

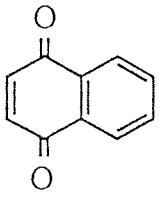

NQ

m.p. = 118.0-121.0 (°C)

λ_{max} = 252 nm

log ε_{max} = 4.22

Fig. 2.14 FT-IR spectrum of NQ using KBr disk.
A : Str. C=O (1661 cm^{-1}), B : Str. ring (1604, 1588 cm^{-1}).

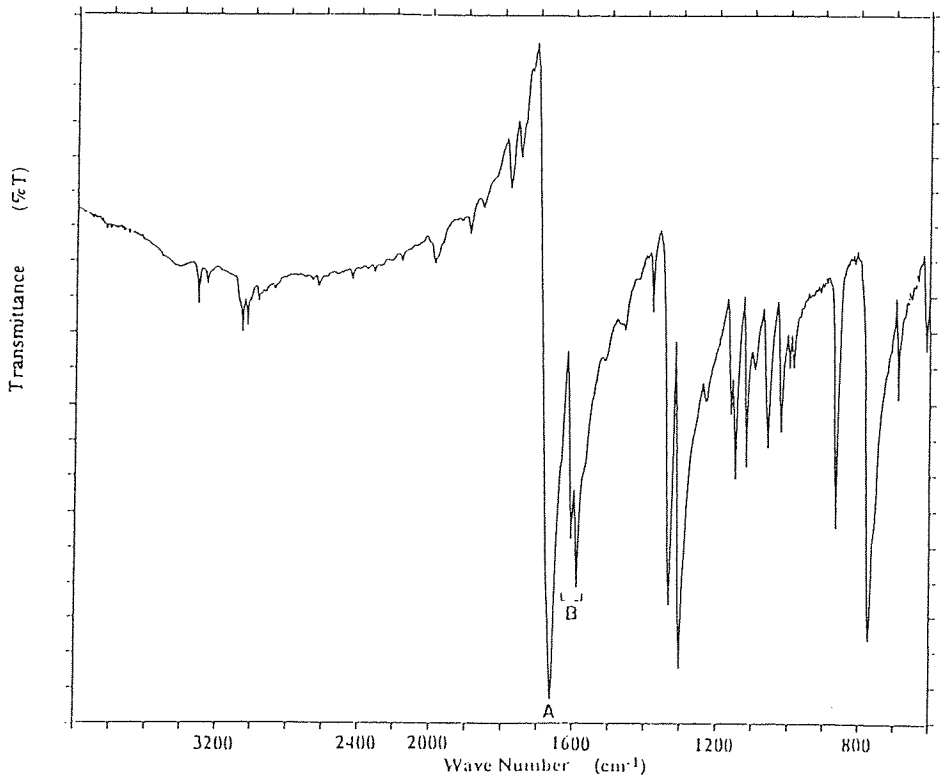

Fig. 2.15 UV spectrum of PDO in methanol solution.

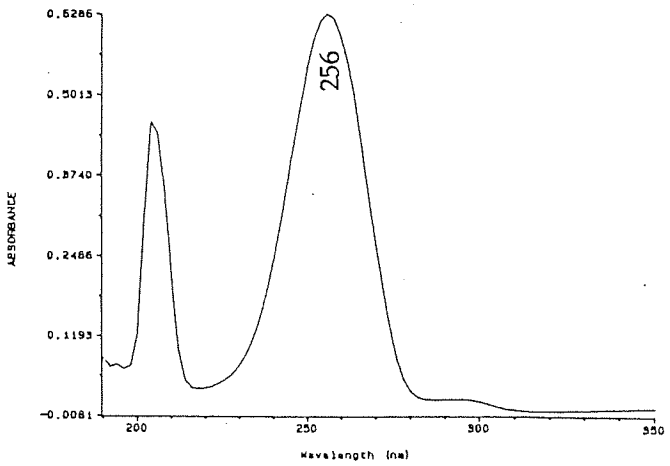

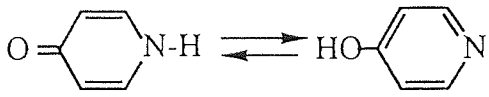

PDO
m.p. =136.0-140.0 (°C)
λ_{max} = 256 nm
log ε_{max} = 4.14
(in Methanol)

Fig. 2.16 FT-IR spectrum of PDO using KBr disk.
A : Str. NH (3260-2840 cm^{-1}), B : Str. C=O (1635 cm^{-1}), C : Str. C=C coupled with Str. CN (1524cm^{-1}), D : Str. C=N coupled with Str. C=C (1385 cm^{-1}), E : Def. CH (847 cm^{-1}).

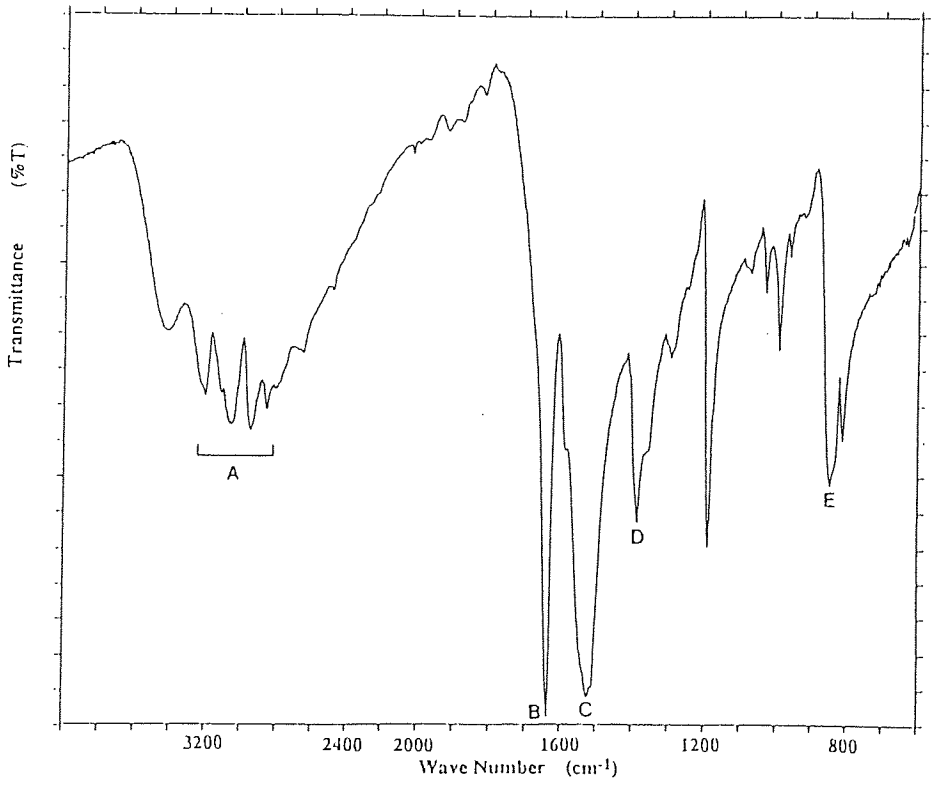

Fig. 2.17 UV spectrum of HBA in DCM solution.

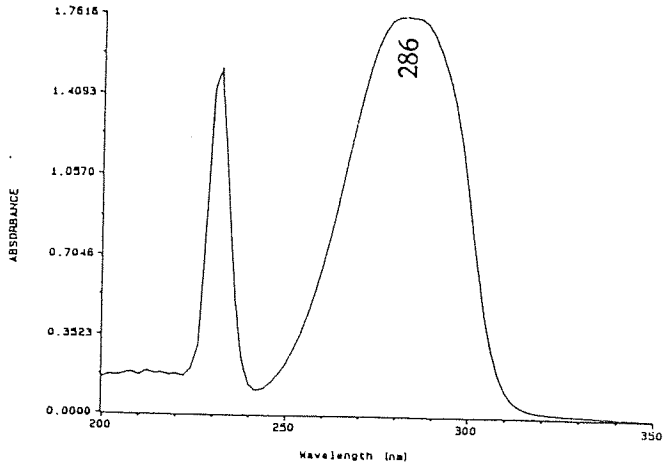

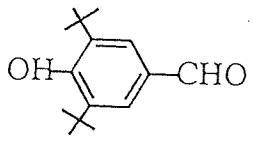

HBA
m.p. = 189.0-193.0 (°C)
λ_{max} = 286 nm
log ε_{max} = 4.17

Fig.2.18 FT-IR spectrum of HBA using KBr disk.
A : Str. OH (3431 cm^{-1}), B : Str. CH for Ar. (3000 cm^{-1}), C : Str. CH (2956, 2911, 2872 cm^{-1}), D : Str. CH for aldehydes (2823, 2734 cm^{-1}), E : Str. C=O (1668 cm^{-1}).

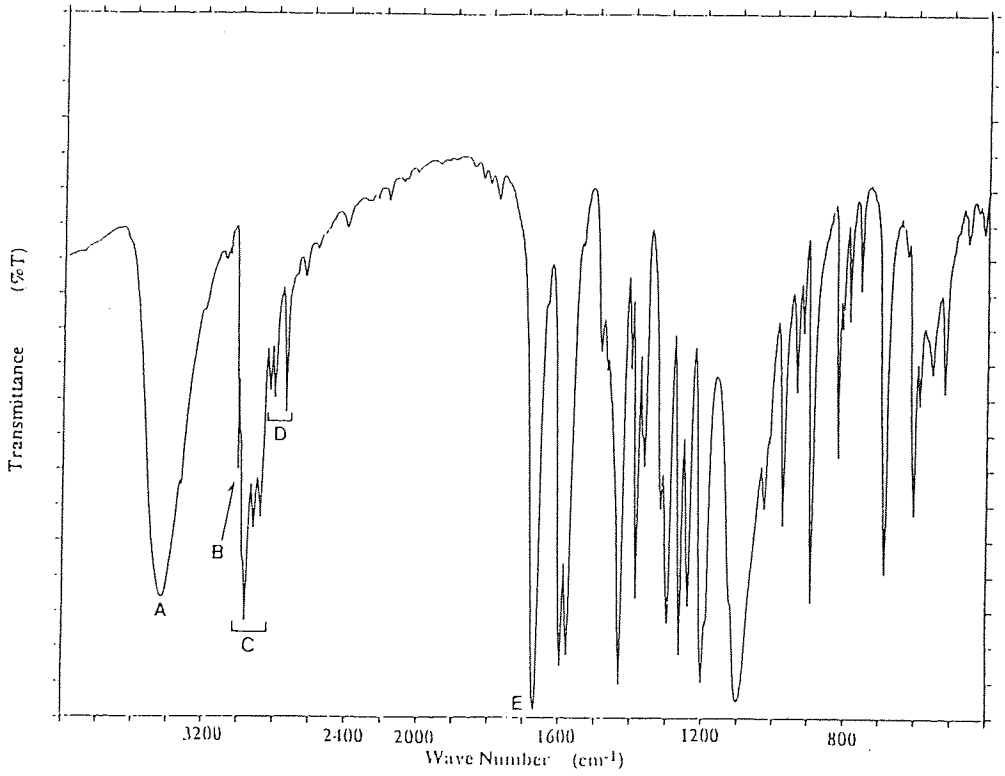

Fig. 2.19 UV spectrum of αTOC in DCM solution.

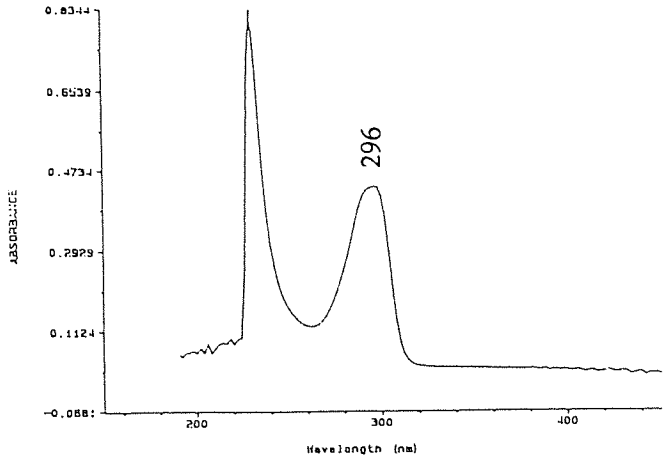

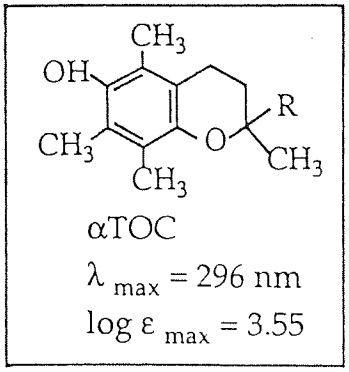

Fig. 2.20 FT-IR spectrum of αTOC pasted on KBr crystal.
A : Str. OH (3467 cm^{-1}), B : Str. CH (2952, 2927, 2868 cm^{-1}), C : Str. ring (1584, 1461, 1422 cm^{-1}), D : Str. CCO (1262 cm^{-1}), E : Str. COC (1086 cm^{-1}).

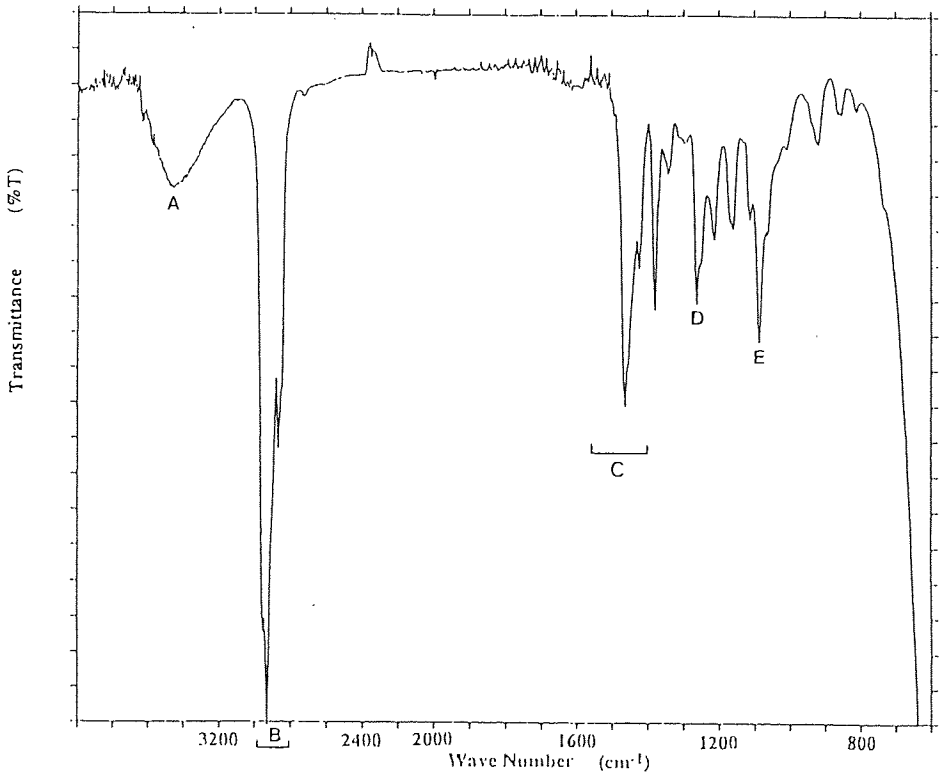

Fig. 2.21 UV spectrum of γTOC in DCM solution.

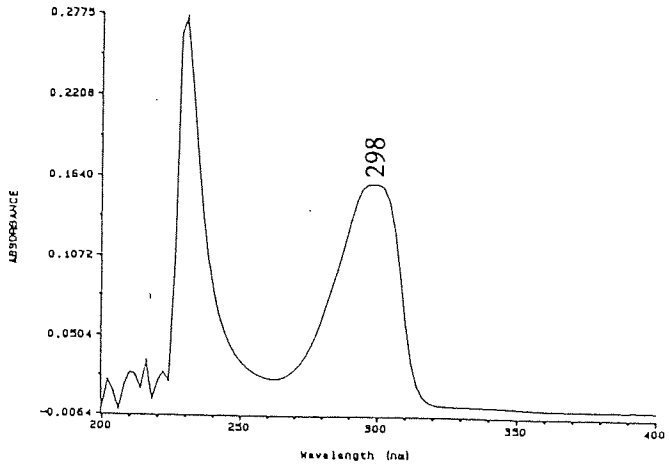

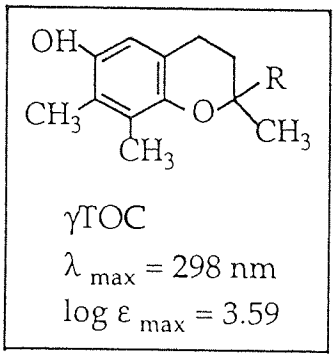

Fig. 2.22 FT-IR spectrum of γTOC pasted on KBr crystal.
A : Str. OH (3408 cm^{-1}), B : Str. CH (2927, 2868 cm^{-1}), C : Str. ring (1593, 1461, 1427 cm^{-1}), D : Str. CCO (1225 cm^{-1}),
E : Str. COC (1081 cm^{-1}).

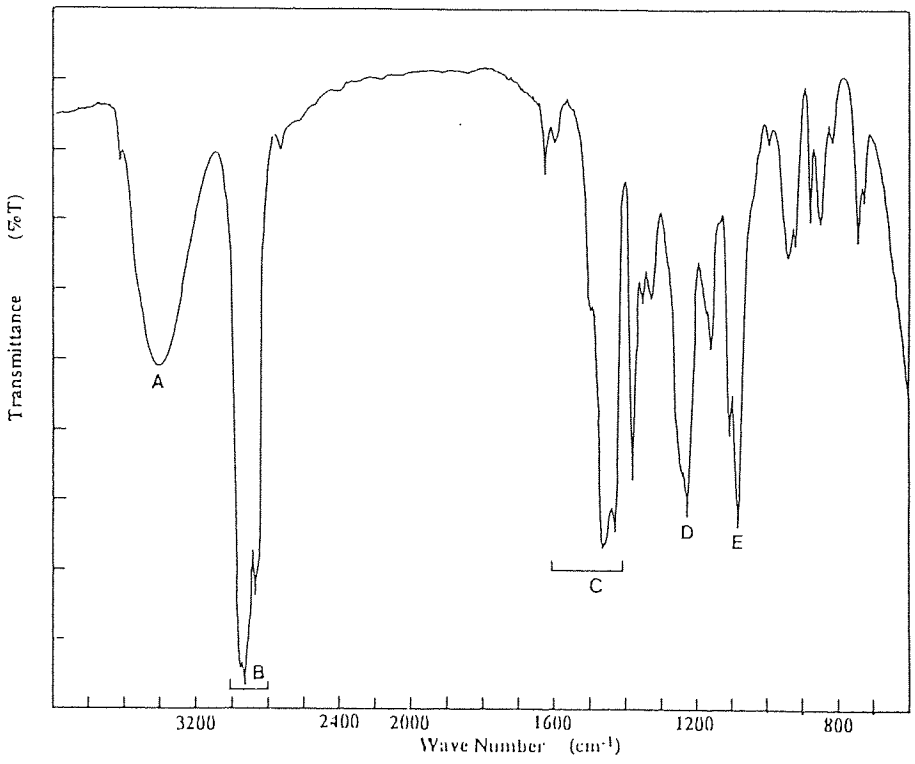

Fig. 2.23 UV spectrum of GM in DCM solution.

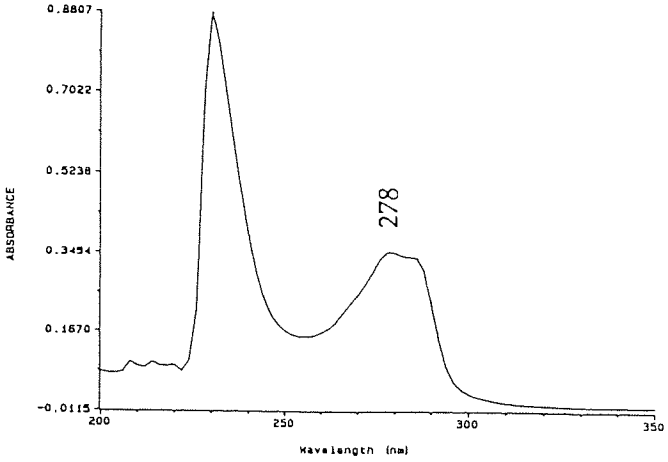

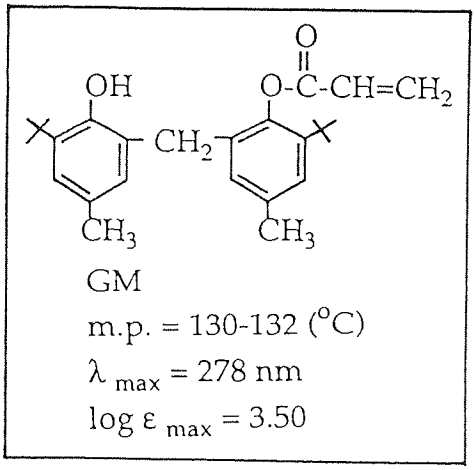

Fig. 2.24 FT-IR spectrum of GM using KBr disk.
A : Str. OH (3493 cm^{-1}), B : Str. CH for Ar. (3106 cm^{-1}), C : Str. =CH (3003 cm^{-1}), D : Str. CH (2956, 2915, 2868 cm^{-1}), E: Str. C=O (1729 cm^{-1}), F : Str. ring (1599, 1479, 1439cm^{-1}).

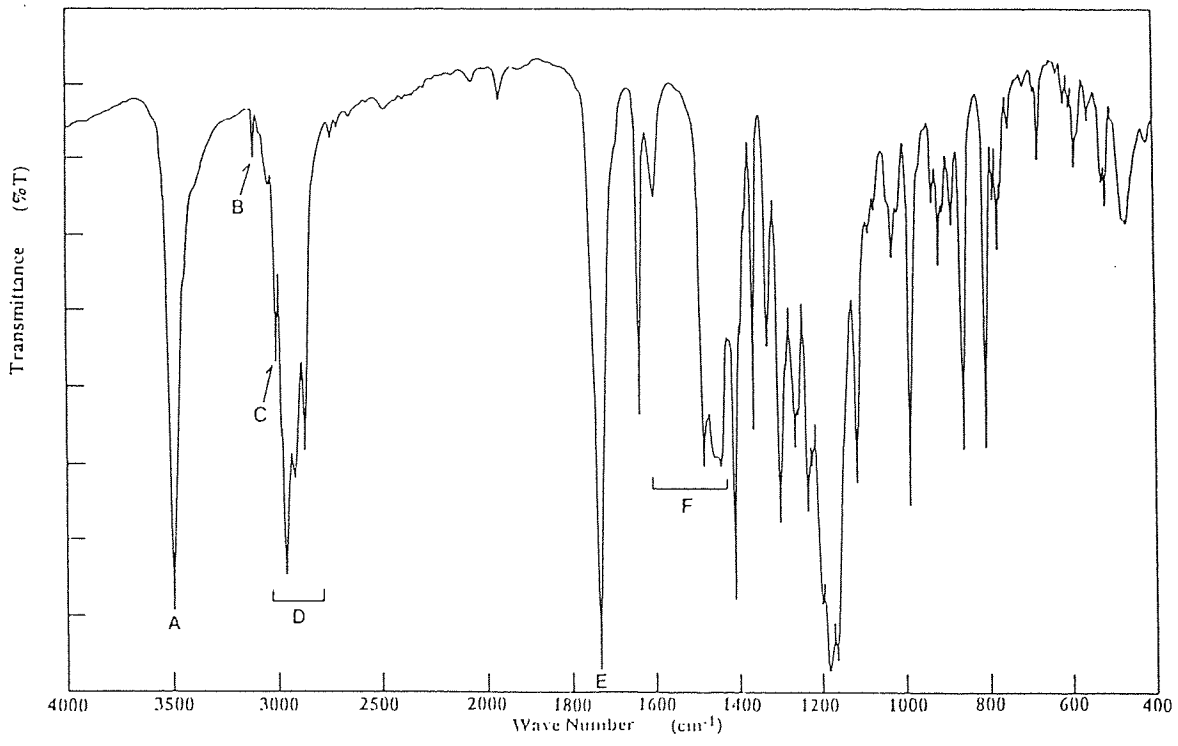

Fig. 2.25 UV spectrum of IPPD in DCM solution.

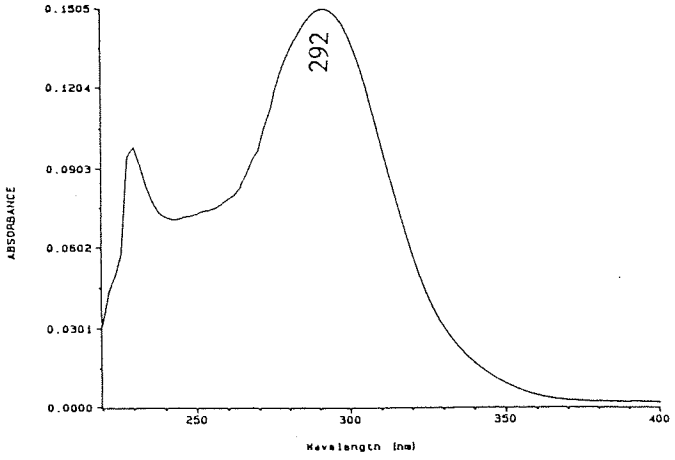

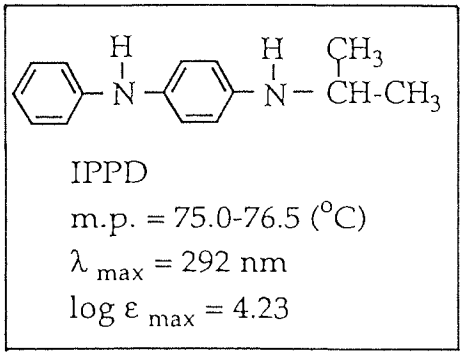

Fig. 2.26 FT-IR spectrum of IPPD using KBr disk.
A : Str. NH (3378 cm^{-1}), B : Str. CH for Ar. (3084, 3026 cm^{-1}), C : Str. CH (2978, 2964, 2931, 2868 cm^{-1}), D : Def. NH (1516 cm^{-1}), E : Str. =CN (1314 cm^{-1}), F : Str. CN (1299 cm^{-1}).

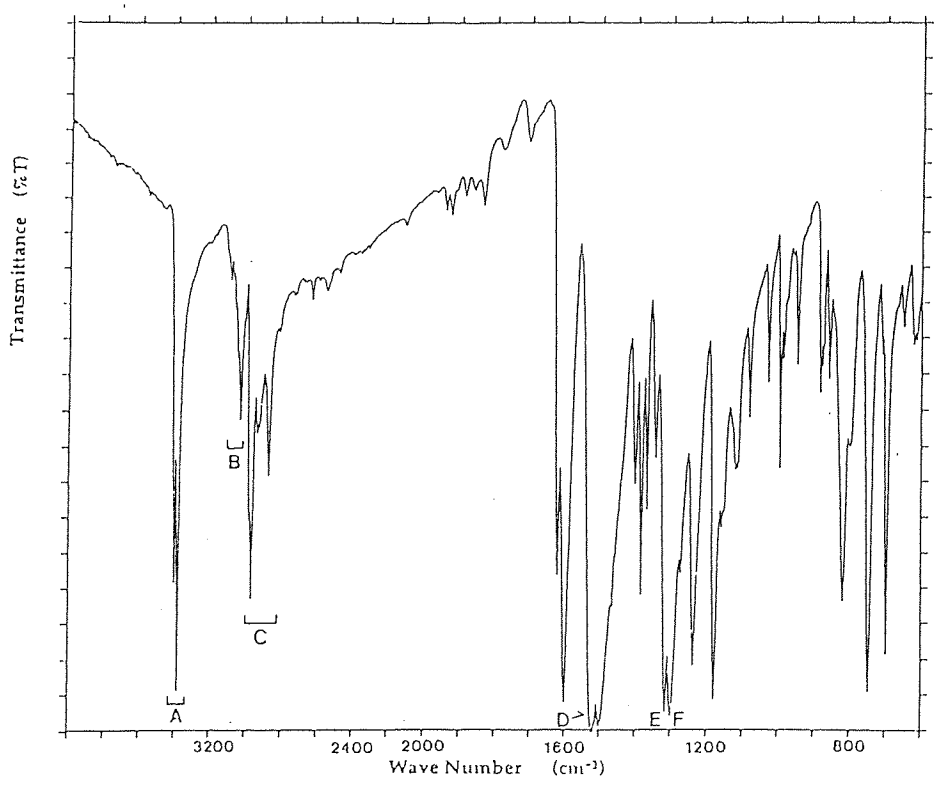

Fig. 2.27 UV spectrum of 6PPD in DCM solution.

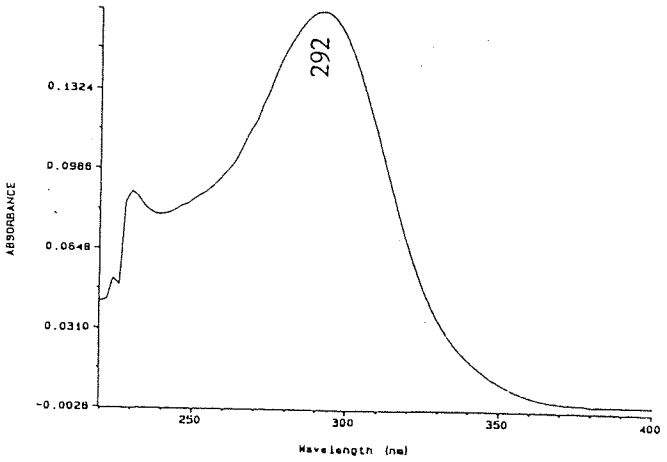

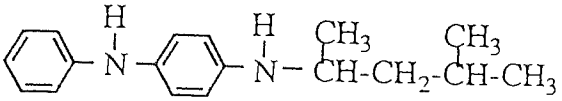

6PPD

m.p. = 48.0-50.0 (°C)

λ_{max} = 292 nm

log ε_{max} = 4.21

Fig. 2.28 FT-IR spectrum of 6PPD using KBr disk.
A : Str. NH (3390, 3378 cm^{-1}), B : Str. CH for Ar. (3043, 3021 cm^{-1}), C : Str. CH (2963, 2951, 2917, 2865 cm^{-1}), D : Def. NH (1516 cm^{-1}), E : Str. =CN (1314 cm^{-1}), F : Str. CN (1264 cm^{-1}).

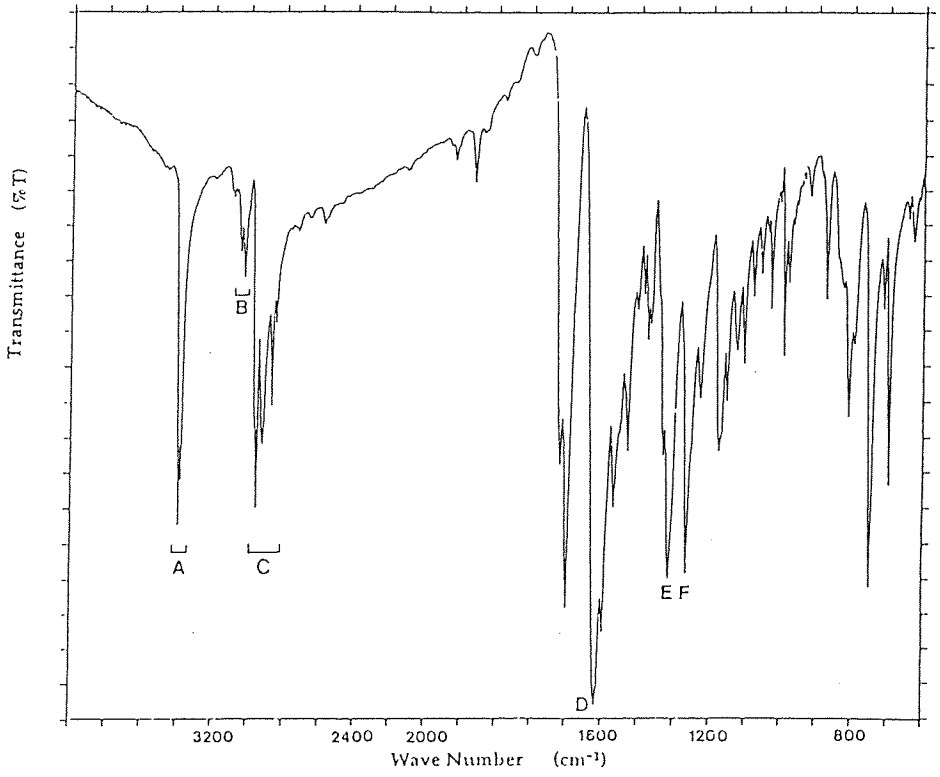

Fig. 2.29 UV spectrum of TMQ in DCM solution.

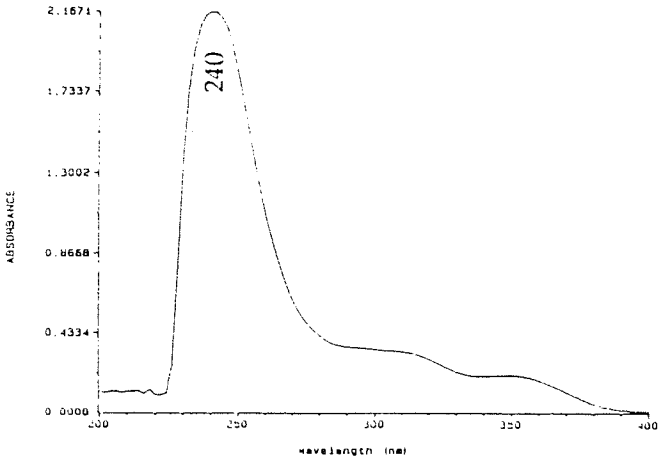

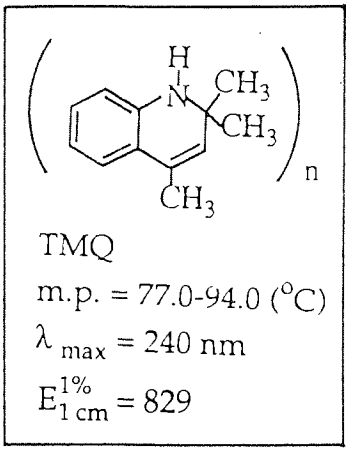

TMQ

m.p. = 77.0-94.0 (°C)

λ_{max} = 240 nm

$E^{1\%}_{1\,cm}$ = 829

Fig. 2.30 FT-IR spectrum of TMQ using KBr disk.

A : Str. NH (3372 cm^{-1}), B : Str. =CH (3017 cm^{-1}), C : Str. CH (2960, 2927, 2866 cm^{-1}), D : Str. C=C (1650 cm^{-1}).

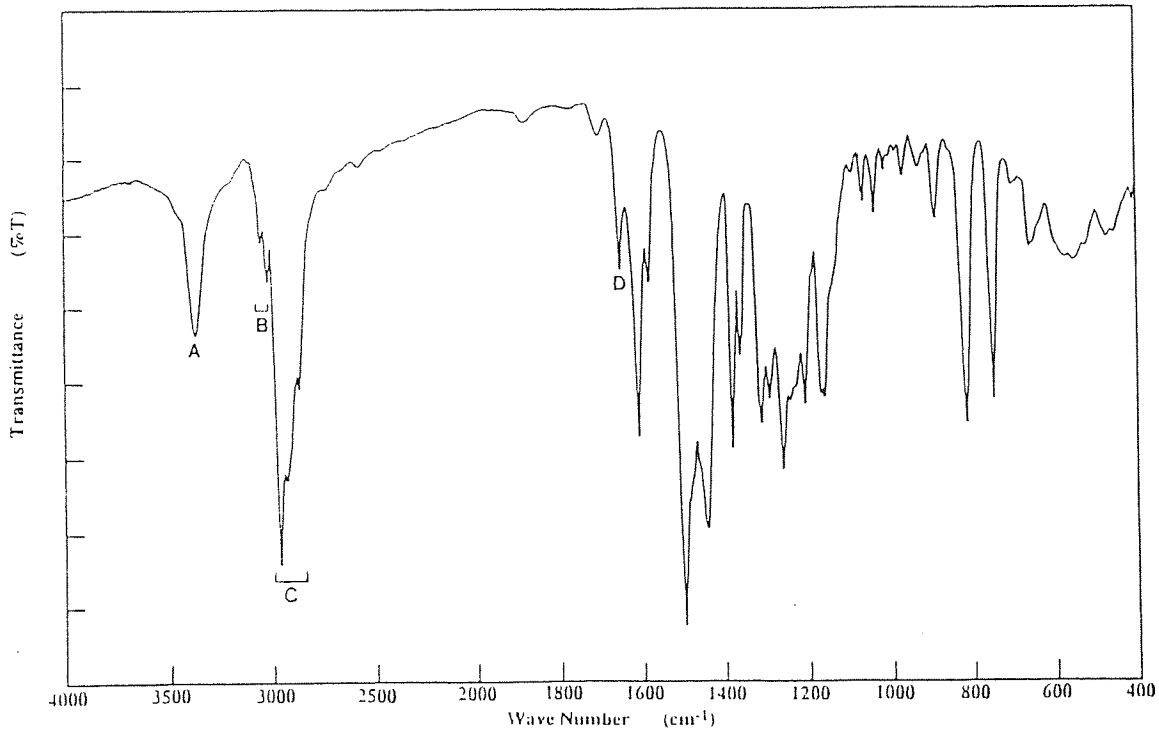

Fig. 2.31 UV spectrum of PM in DCM solution.

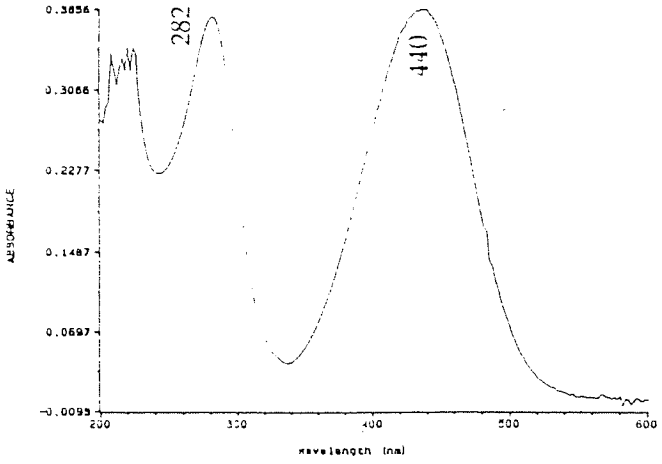

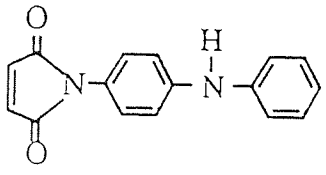

PM

m.p. = 154.0-156.0 (°C)

λ_{max} = 282 nm

log ε_{max} = 4.23

λ_{max} = 440 nm

log ε_{max} = 4.22

Fig. 2.32 FT-IR spectrum of PM using KBr disk.

A : Str. NH (3363 cm^{-1}), B : Str. =CH (3065 cm^{-1}), C : Str. C=O (1757 cm^{-1}).

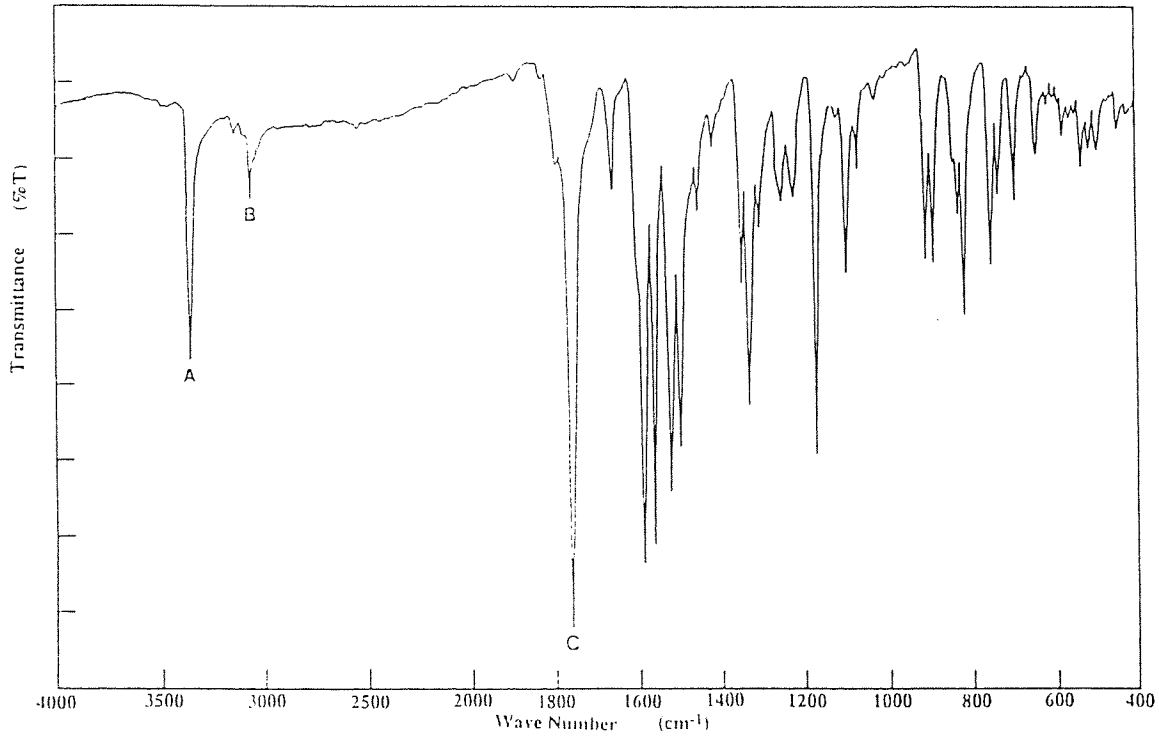

Fig. 2.33 UV spectrum of BTMI in DCM solution.

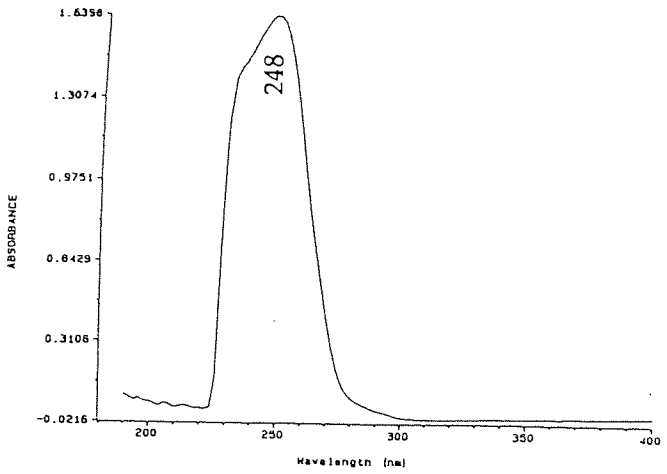

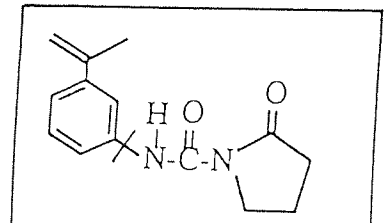

BTMI

m.p. = 54.0-58.0 (°C)

λ_{max} = 248 nm

log ε_{max} = 3.94

Fig. 2.34 FT-IR spectrum of BTMI using KBr disk.

A : Str. NH (3298 cm^{-1}), B : Str. =CH (3090, 3005 cm^{-1}), C : Str. CH (2982, 2963, 2917 cm^{-1}), D : Str. C=O (1712, 1682 cm^{-1}), E : Def. NH (1526 cm^{-1}), F : Str. CN (1244 cm^{-1}).

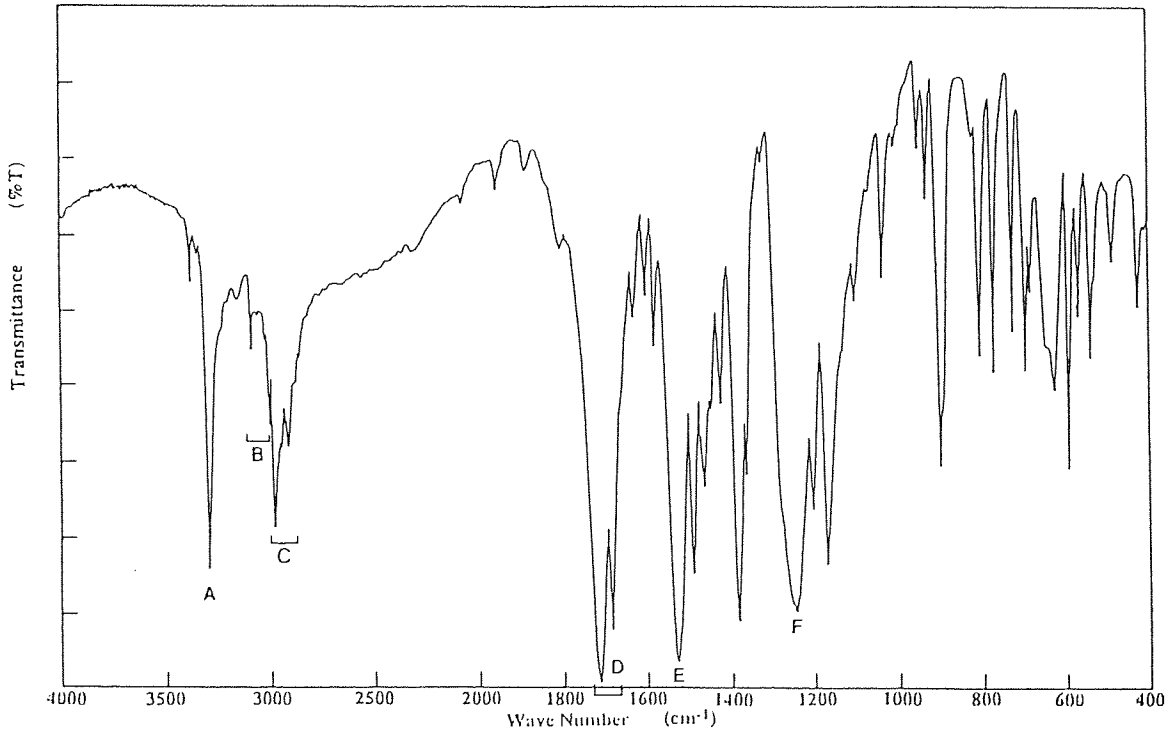

Fig. 2.35 UV spectrum of APMA in DCM solution.

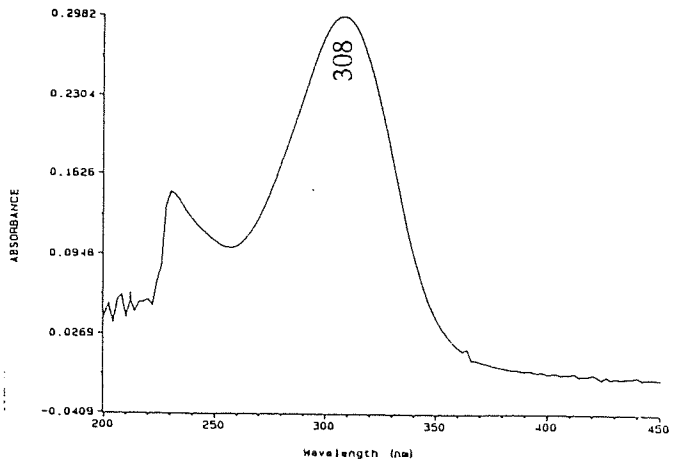

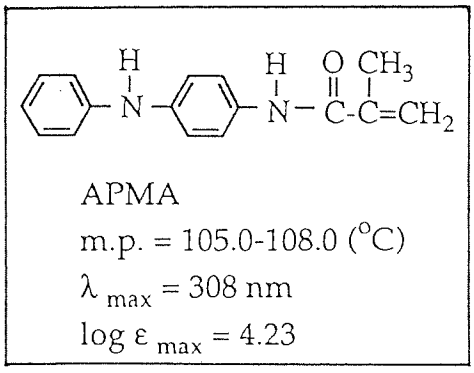

Fig. 2.36 FT-IR spectrum of APMA using KBr disk.
A : Str. NH (3350 cm^{-1}), B : Str. C=O (1653 cm^{-1}), C : Def. NH (1522 cm^{-1}).

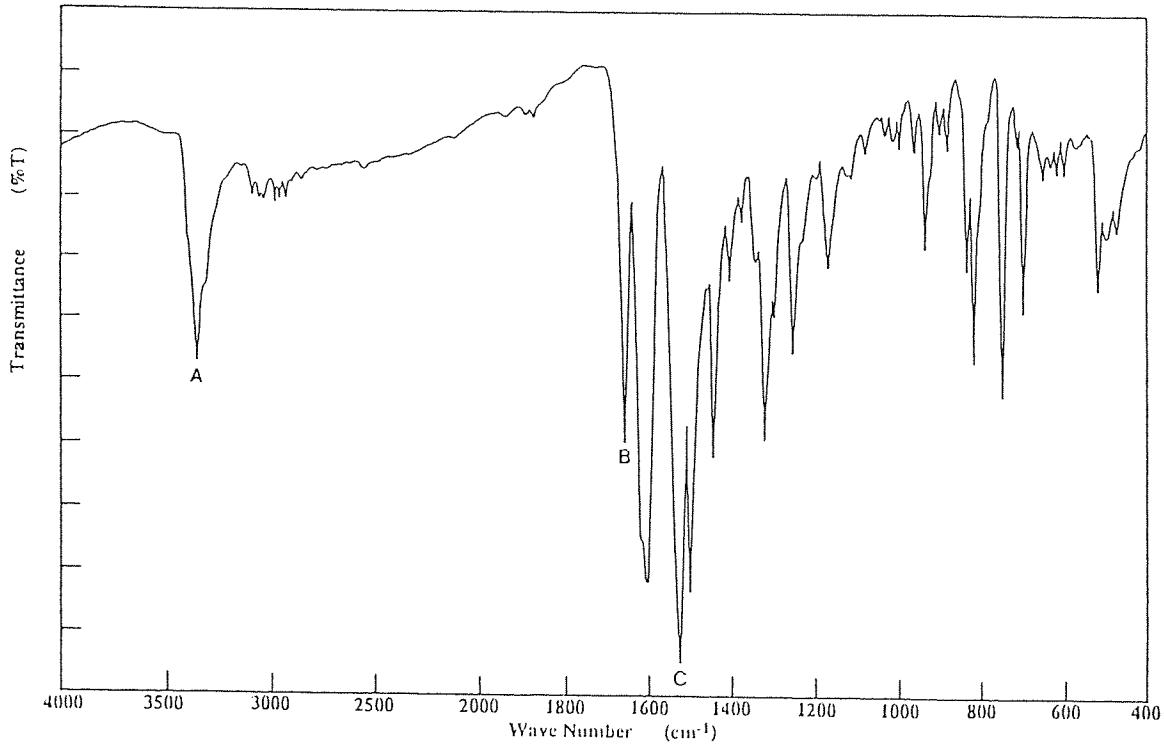

Fig. 2.37 UV spectrum of MADA in DCM solution.

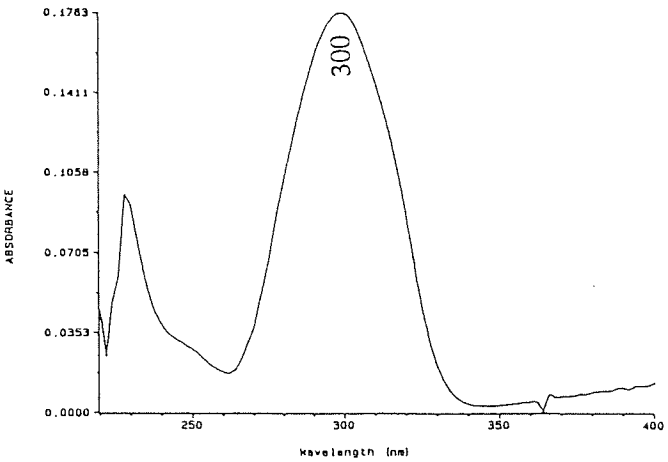

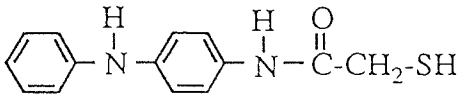

MADA

m.p. = 122.3-147.3 (°C)

λ_{max} = 300 nm

log ε_{max} = 4.37

Fig. 2.38 FT-IR spectrum of MADA using KBr disk.

A : Str. NH (3365 cm^{-1}), B : Str. SH (2525 cm^{-1}), C : Str. C=O (1650 cm^{-1}), D : Def. NH (1539 cm^{-1}).

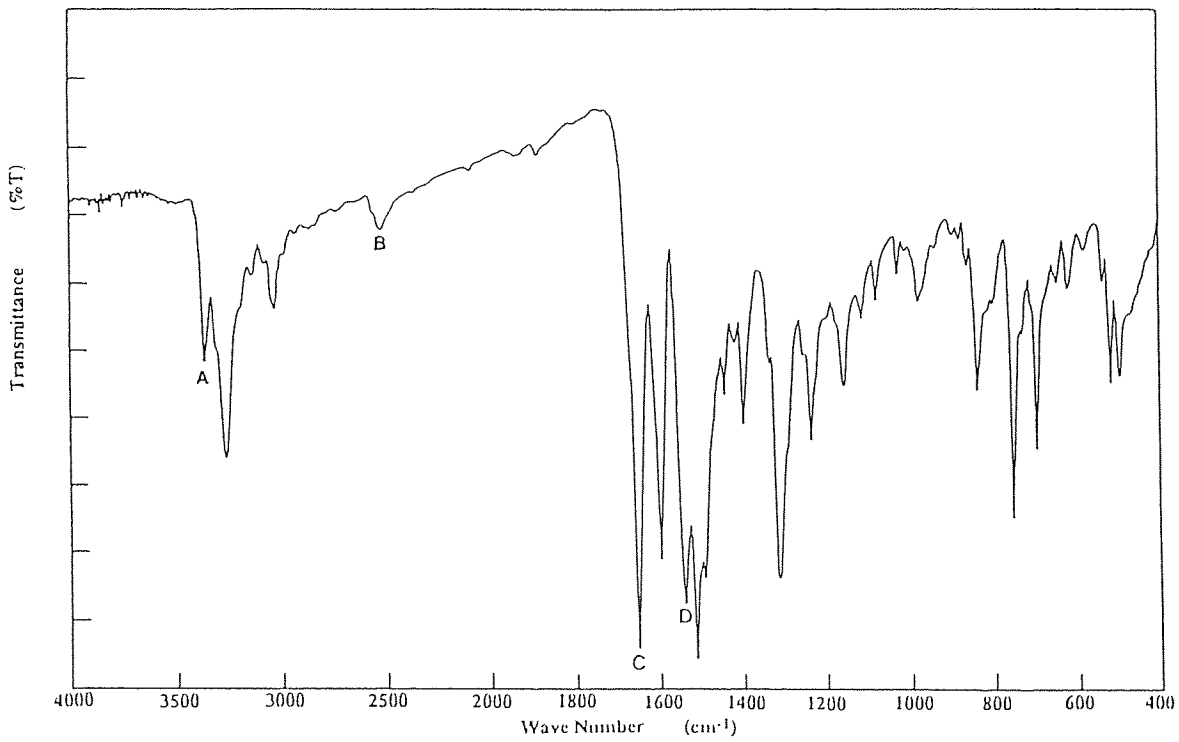

Fig. 2.39 UV spectrum of P168 in DCM solution.

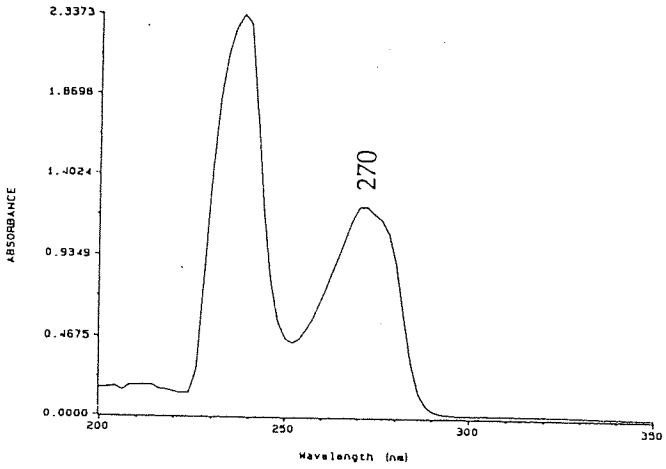

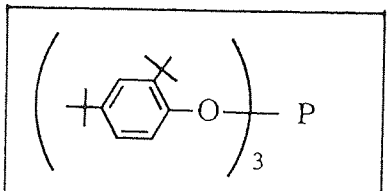

P168

m.p. = 179.0-181.0 (°C)

λ_{max} = 270 nm

log ε_{max} = 3.49

Fig. 2.40 FT-IR spectrum of P168 using KBr disk.

A : Str. CH for Ar. (3031 cm^{-1}), B : Str. CH (2960, 2907, 2868 cm^{-1}), C : Str. ring (1602, 1490 cm^{-1}), D : Str. POC (1213 cm^{-1}), E : Str. POP (906 cm^{-1}).

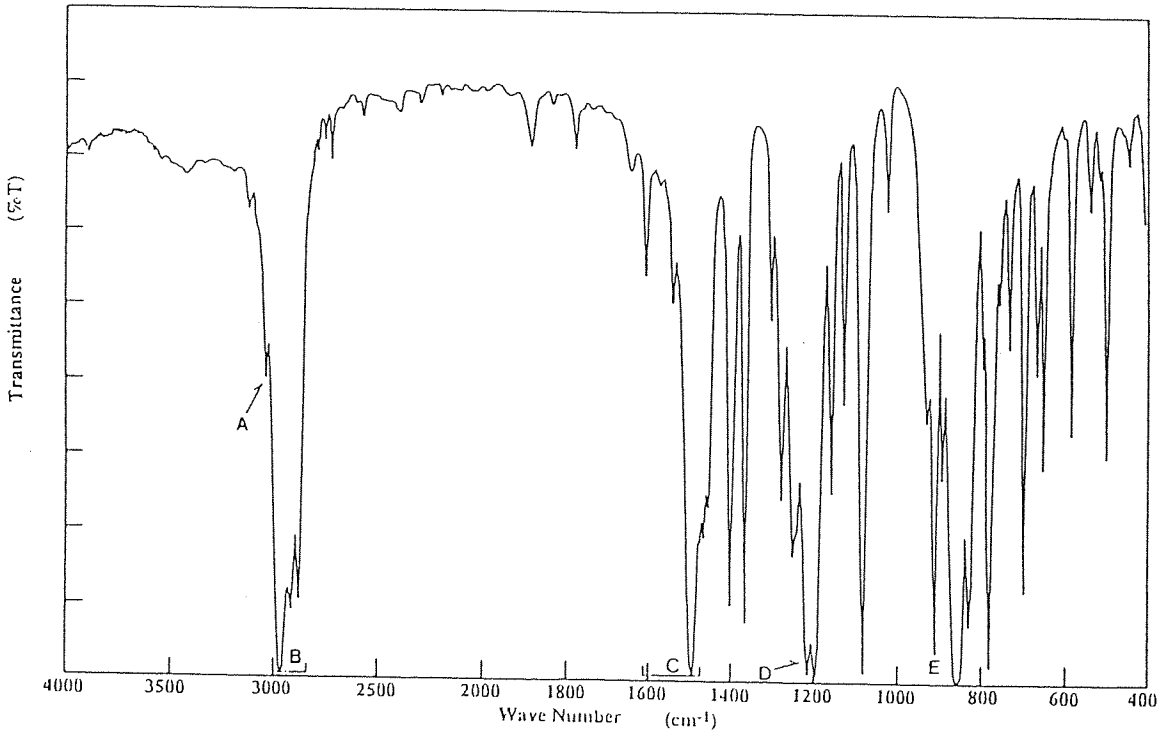

Fig. 2.41 UV spectrum of P626 in DCM solution.

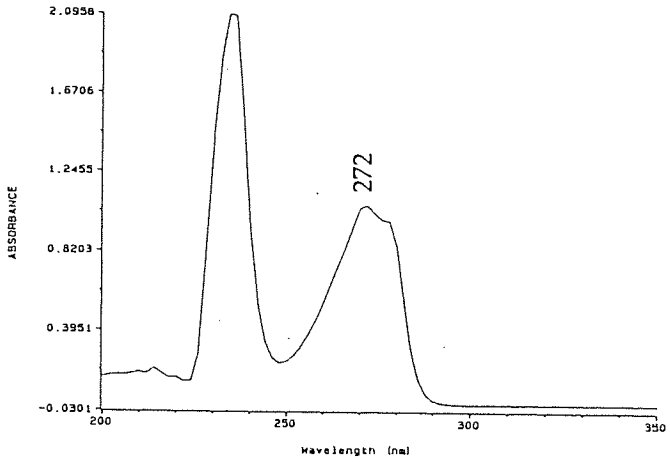

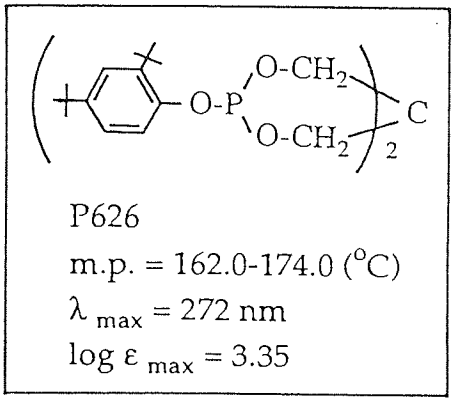

P626
m.p. = 162.0-174.0 (°C)
λ_{max} = 272 nm
log ε_{max} = 3.35

Fig. 2.42 FT-IR spectrum of P626 using KBr disk.
A : Str. CH (2957, 2885, 2868 cm^{-1}), B : Str. ring (1605, 1495 cm^{-1}), C : Str. POC (1227 cm^{-1}).

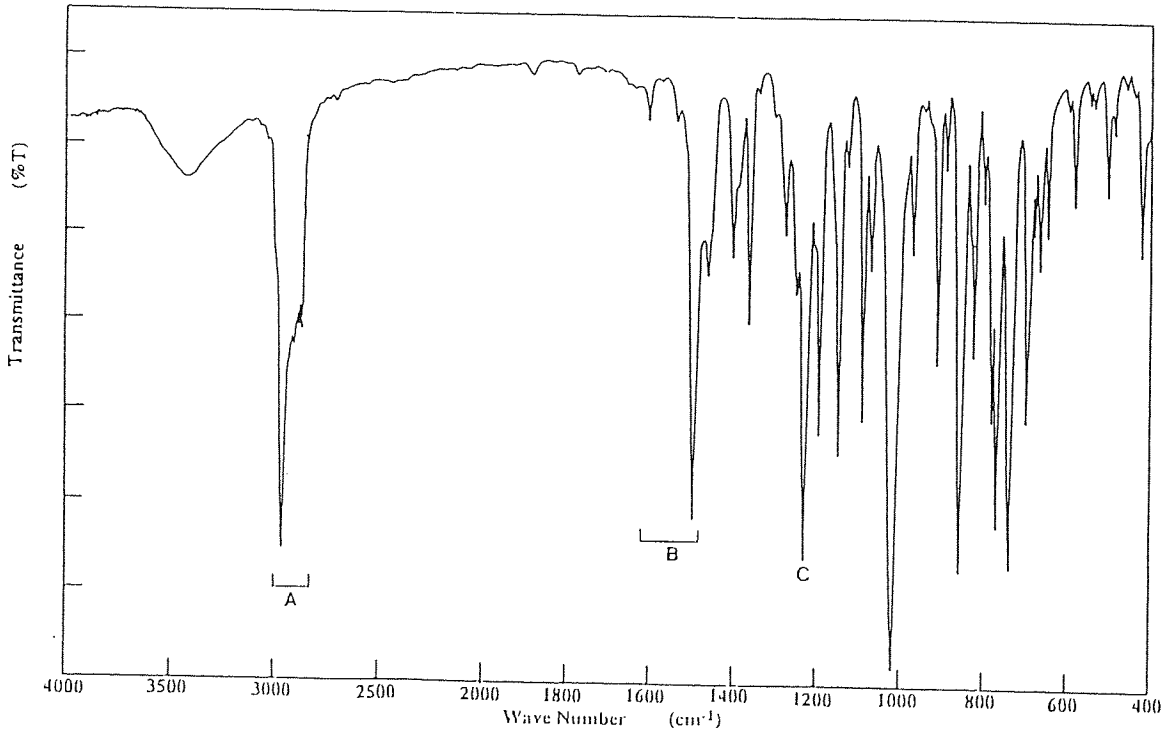

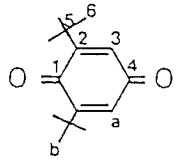

Table 2.8 ^{1}H-NMR summary of BQ.

No. of Atom	δ (ppm)	m	Integral	H
a	6.4639	s	21.929	2H
b	1.2376	s	180.000	18H

Table 2.9 ^{13}C-NMR summary of BQ.

No of Atom	δ (ppm)	(+)/(-)
4	189.0419	(-)
1	187.7323	(-)
2	157.8248	(-)
3	130.1004	(+)
5	35.5231	(-)
6	29.3285	(+)

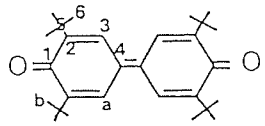

Table 2.10 ^{1}H-NMR summary of DPQ.

No. of Atom	δ (ppm)	m	Integral	H
a	7.6853	s	10.223	4H
impurities	2.147		3.746	-
impurities	1.4601		2.123	-
b	1.3403	s	22.017	36H

Table 2.11 ^{13}C-NMR summary of DPQ.

No of Atom	δ (ppm)	(+)/(-)
1	186.3855	(-)
2	150.3491	(-)
4	136.0547	(-)
3	125.9435	(+)
5	35.9525	(-)
6	29.5147	(+)

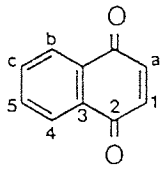

Table 2.12 ^{1}H-NMR summary of NQ.

No. of Atom	δ (ppm)	Integral	H
b	8.0130, 8.0020, 7.9939, 7.9829, 7.9706	197.646	2H
c	7.7047, 7.6937, 7.6856, 7.6746, 7.6629	213.176	2H
impurities	7.2405	-	-
a	6.9147	200.000	2H

Table 2.13 ^{13}C-NMR summary of NQ.

No of Atom	δ (ppm)	(+)/(-)
2	184.8702	(-)
1	138.5215	(+)
5	133.8051	(+)
3	131.7225	(-)
4	126.2549	(+)

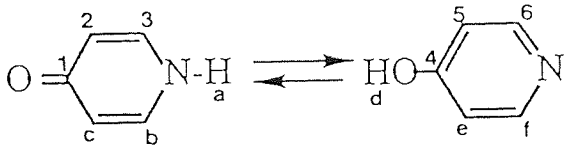

Table 2.14 ^{1}H-NMR summary of PDO.

No. of Atom	δ (ppm)	m	Integral	H
a	11.7242	s	27.809	1H
b	7.6115, 7.5878	d	54.060	2H
c	6.4040, 6.3804	d	52.865	2H

Table 2.15 ^{13}C-NMR summary of PDO.

No of Atom	δ (ppm)	(+)/(-)
1	179.4653	(-)
3	138.5750	(+)
2	116.9851	(+)

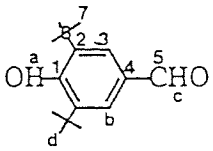

Table 2.16 ^{1}H-NMR summary of HBA.

No. of Atom	δ (ppm)	m	Integral	H
c	9.83232	s	11.368	1H
b	7.7094	s	21.290	2H
a	5.84412	s	11.514	1H
d	1.45754	s	180.025	18H

Table 2.17 ^{13}C-NMR summary of HBA.

No of Atom	δ (ppm)	(+)/(-)
5	191.761	(+)
1	159.592	(-)
2	138.402	(-)
4	128.627	(-)
3	127.584	(+)
6	34.263	(-)
7	29.977	(+)

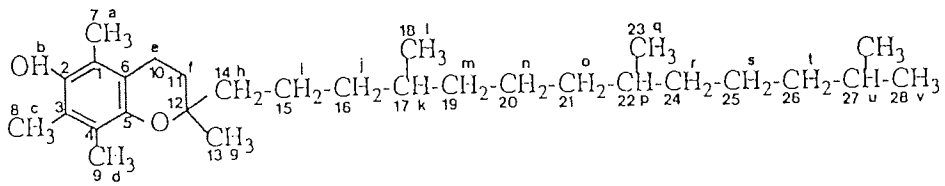

Table 2.18 ^{1}H-NMR summary of αTOC.

No. of Atom	δ (ppm)	m
l, q, v	0.85 - 1.00	
h, i, j, m, n, o	1.05 - 1.40	
g	1.40 - 1.55	
k, p, u	1.55 - 1.70	
f	1.75 - 1.95	
	2.16	
a, c, d	2.17	s
	2.20	s
e	2.60 - 2.70	
b	4.30	

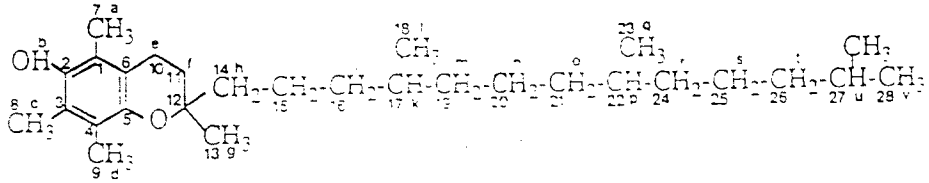

Table 2.19 ^{13}C-NMR summary of αTOC.

No of Atom	δ (ppm)	(+)/(-)
5	145.5098	(-)
2	144.4879	(-)
6	122.5287	(-)
4	121.0851	(-)
3	118.5389	(-)
1	117.2491	(-)
12	74.4375	(-)
11	39.8418	(-)
19	39.7618	(-)
14	39.3540	(-)
26	37.5494	(-)
16	37.4435	(-)
21	37.3753	(-)
24	37.3187	(-)
impurity	37.2729	(-)
22	32.7596	(+)
impurity	32.6640	(+)
impurity	31.5246	(-)
impurity	31.4685	(-)
27	27.9571	(+)
20	24.8012	(-)
25	24.4276	(-)
28	23.7440	(+)
7,8,9	22.7114, 22.6156	(+)
impurity	21.0319	(-)
10	20.7285	(-)
15	19.7260	(+)
13, 18, 23	19.6692, 19.5752	(+)
impurity	12.1628	(+)
impurity	11.7452	(+)
impurity	11.2285	(+)

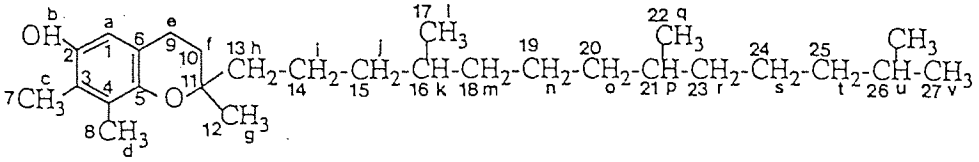

Table 2.20 ^{1}H-NMR summary of γTOC.

No. of Atom	δ (ppm)	m	Integral	H
a	6.3703	s	10.318	1H
b	5.0965	s	9.305	1H
e	2.7064, 2.6852, 2.6637	t	23.870	2H
c,d	2.1853, 2.1726	d	64.925	6H
f	1.8735, 1.8511, 1.8285, 1.8062, 1.7934, 1.7817, 1.7716, 1.7493, 1.7266, 1.7042		24.704	2H
k,p,u	1.6749, 1.6657, 1.6440, 1.6225, 1.6002, 1.5789, 1.5565		34.536	3H
g	1.5344, 1.5122, 1.4624		42.037	
h,i,j,m,n,o, r,s,t	1.4010, 1.3862, 1.3623, 1.3354, 1.3031, 1.2476, 1.2255, 1.2017, 1.1798, 1.1720, 1.1586		187.683	18H
l,q,v	0.9546, 0.9329, 0.9176, 0.9122		129.991	12H

Table 2.21 ^{13}C-NMR summary of γTOC.

No of Atom	δ (ppm)	(+)/(-)
5	146.1211	(-)
2	145.6150	(-)
6	125.6822	(-)
4	121.8507	(-)
3	118.1479	(-)
1	112.3135	(+)
11	75.3965	(-)
10	40.0474	(-)
18	39.9563	(-)
13	39.3389	(-)
25	37.5337	(-)
15	37.4271	(-)
20	37.3715	(-)
23	37.2615	(-)
16	32.7403	(+)
21	32.6356	(+)
impurities	31.3272	(-)
26	27.9469	(+)
19	24.7921	(-)
24	24.4163	(-)
27	24.0008	(+)
7, 8	22.7134, 22.6169	(+)
impurities	22.2500	(-)
9	21.0089	(-)
14	19.7263	(+)
12, 17, 22	19.6630	(+)
impurities	11.8811	(+)

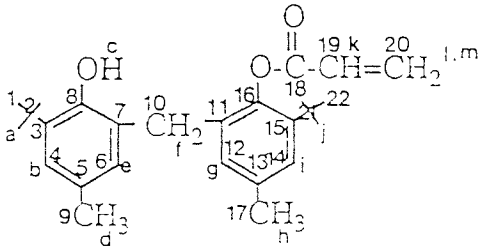

Table 2.22 ^{1}H-NMR summary of GM.

No. of Atom	δ (ppm)	m	Integral	H
b, e, g, i	7.1158, 7.1102, 7.0488, 7.0422		21.504	2H
	6.8317, 6.8256		11.434	1H
	6.6711, 6.6670		16.182	1H
k	6.4702, 6.4356, 6.4126, 6.3780		13.385	1H
impurities	6.1278, 6.1237, 6.0931, 6.0891		13.124	1H
l, m	5.3138	s	19.604	2H
impurities	3.6551, 3.6453	d	26.774	2H
d, h	2.2960	s	30.704	3H
d, h	2.2196	s	28.553	3H
f	2.1739	s	18.194	2H
a , j	1.3871, 1.3549	s*	180.033	18H

(* : expected)

Table 2.23 ^{13}C-NMR summary of GM.

No of Atom	δ (ppm)	(+)/(-)
18	165.5892	(-)
8	151.1310	(-)
16	145.0218	(-)
15	141.1221	(-)
3	136.5790	(-)
13	135.7370	(-)
5	133.7869	(-)
11	131.7431	(-)
19	130.0656	(+)
20	128.2462	(-)
6	127.8213	(+)
12	127.6343	(+)
4	126.8987	(+)
14	126.4758	(+)
7	124.3252	(-)
2, 21	34.6086, 34.5592	(-)
10	31.6831	(-)
impurities	30.8902	(+)
1, 22	30.457, 29.6906	(+)
9, 17	21.2466, 20.7783	(+)

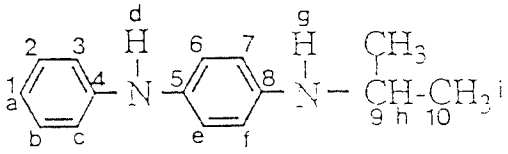

Table 2.24 ^{1}H-NMR summary of IPPD.

No. of Atom	d (ppm)	Integral	H
a, b, c, e, f	7.2387, 7.2145, 7.1898, 7.1866, 7.1618	27.895	2H
	7.0225, 7.0157, 6.9935, 6.9832	27.777	2H
	6.8538, 6.8510, 6.8255	27.348	2H
	6.8042, 6.7799, 6.7556	12.878	1H
	6.5983, 6.5916, 6.5694	26.362	2H
d	5.3843	8.012	1H
h	3.6466, 3.6257, 3.6048, 3.5839, 3.5631	13.581	1H
g	2.1747	9.519	1H
i	1.2349, 1.2141	82.339	6H

Table 2.25 ^{13}C-NMR summary of IPPD.

No of Atom	d (ppm)	(+)/(-)
4	146.2603	(-)
5, 8	143.8065, 132.1810	(-)
2	129.1617	(+)
1	123.9374	(+)
3	118.5826	(+)
6, 7	114.6788, 114.1735	(+)
9	44.6741	(+)
10	23.0270	(+)

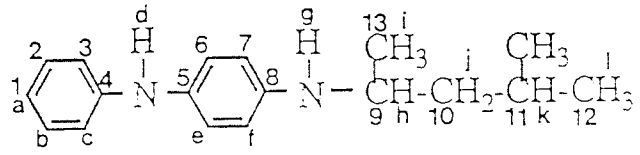

Table 2.26 ^{1}H-NMR summary of 6PPD.

No. of Atom	δ (ppm)	Integral	H
a, b, c, e, f	7.2392, 7.2050, 7.1984, 7.1807, 7.1766, 7.1586, 7.1521, 7.1449	37.417	2H
	7.0228, 7.0123, 7.0051, 6.9902, 6.9830, 6.9723	39.417	2H
	6.8453, 6.8417, 6.8193, 6.8164, 6.8132, 6.8053	39.329	2H
	6.7951, 6.7917, 6.7674, 6.7465, 6.7431	20.833	1H
	6.5916, 6.5812, 6.5740, 6.5590, 6.5521, 6.5412	40.595	2H
d	5.3683	19.148	1H
h	3.5289, 3.5072, 3.4858, 3.4640	24.300	1H
g	3.2067	21.681	1H
impurities	2.1702	5.020	
k	1.8163, 1.7938, 1.7714, 1.7489, 1.7265	22.388	1H
j	1.5291, 1.5058, 1.4836, 1.4606, 1.4369, 1.3096, 1.2865, 1.2639, 1.2414, 1.2183	45.578	2H
i	1.1780, 1.1573	62.186	3H
l	0.9665, 0.9442, 0.9407, 0.9184	124.689	6H

Table 2.27 ^{13}C-NMR summary of 6PPD.

No of Atom	δ (ppm)	(+)/(-)
4	146.3342	(-)
5, 8	144.058, 131.9395	(-)
2	129.1545	(+)
1	124.0833	(+)
3	118.5314	(+)
6, 7	114.6213, 113.9139	(+)
9	46.9340	(+)
10	46.8839	(-)
13	25.0418	(+)
12	22.5278	(+)
11	21.0500	(+)

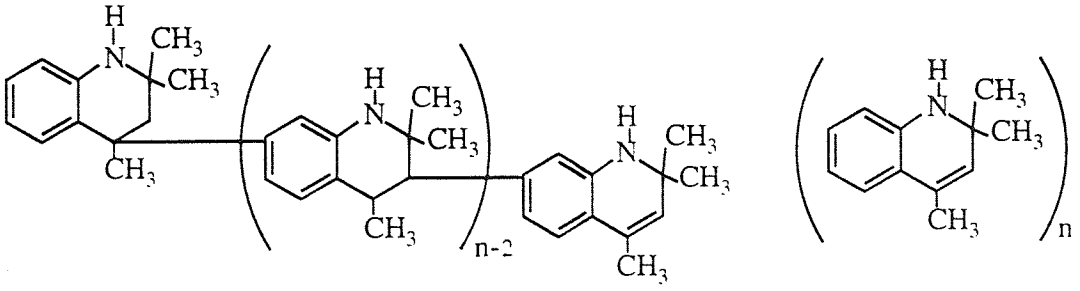

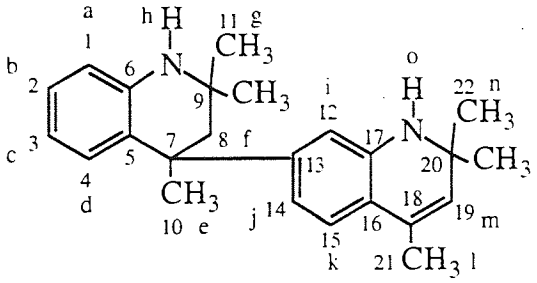

Table 2.28 ^{1}H-NMR summary of TMQ.

No. of Atom	δ (ppm)	Integral	H	
impurities	8.4896 - 7.7346	9.538		
	7.7346 - 7.7243	16.576		
	7.1951 - 7.0630	40.401		
	7.0630 - 6.9400	47.487		
a, b, c, d,	6.9400 - 6.8852	22.549		
i, j, k	6.8852 - 6.7872	31.444		
	6.7872 - 6.5832	63.760		
	6.5832 - 6.4432	36.664		
	6.4432 - 5.9829	70.959		
m	5.5116 - 4.9198	58.355	1H	
h, o	4.3609 - 3.1005	137.978		
impurities	2.7498 - 2.6122	16.718		
impurities	2.6122 - 2.3017	34.269		
f	2.3017 - 2.0716	61.791		2H'
l	2.0716 - 1.7988	165.335	3H	
g	1.7988 - 1.4481	216.838		6H'
n	1.4481 - 0.9878	379.118	6H	
e	0.9878 - 0.5494	120.702		3H'
impurities	0.4946 - 0.1658	0.878		

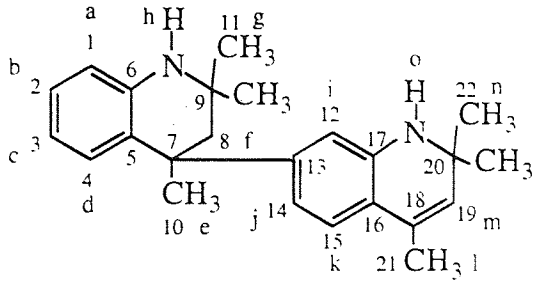

Table 2.29 ^{13}C-NMR summary of TMQ.

No of Atom	δ (ppm)	(+)/(-)
13	143.8530	(-)
6, 17	140.8213	(-)
5	139.2746	(-)
19	129.3077	(+)
18	128.8927	(-)
15	128.2877	(+)
2	126.9528	(+)
4	122.1315	(+)
16	120.9443	(-)
3, 14	116.7446	(+)
1	114.6211	(+)
12	112.3758	(+)
8	100.2725	(-)
20	51.6842	(-)
9	49.6712	(-)
7	40.0565	(-)
11	32.3447	(+)
10	30.7778	(+)
22	30.1747	(+)
21	18.6540	(+)

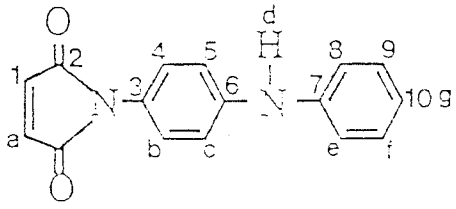

Table 2.30 ^{1}H-NMR summary of PM.

No. of Atom	δ (ppm)	Integral	H
b, c, e, f, g	7.5585, 7.5481, 7.5413, 7.5253, 7.5185, 7.5082	156.576	2H
	7.3563, 7.3381, 7.3282, 7.3217, 7.3029, 7.3002, 7.2814, 7.2754, 7.2687, 7.2456	259.585	2H+α
	7.1455, 7.1417, 7.1349, 7.1167, 7.1058	159.423	2H
	7.0633, 7.0512, 7.0406, 7.0336, 7.0254, 7.0179, 7.0110, 7.0009, 6.9766	247.118	3H
a	6.5794, 6.5612	71.364	1H
d	5.9937	71.704	1H
impurities	2.1600	23.324	
impurities	2.0845	2.245	
impurities	1.6570	49.657	
impurities	1.2412	15.712	

Table 2.31 ^{13}C-NMR summary of PM.

No of Atom	δ (ppm)	(+)/(-)
2	167.8278	(-)
7	147.8115	(-)
impurities	143.6703	(-)
1	143.3998	(+)
6	141.4850	(-)
3	135.7042	(-)
9	129.4207	(+)
impuriyties	128.8312	(+)
4	125.8723	(+)
10	122.2735	(+)
5, 8	119.2691, 116.2823	(+)

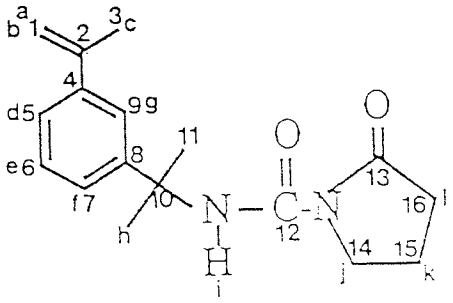

Table 2.32 ^{1}H-NMR summary of BTMI.

No. of Atom	δ (ppm)	m	Integral	H
i	8.9452	s	14.127	1H
d, e, f, g	7.4946, 7.4911, 7.4894, 7.4848, 7.4834, 7.3371, 7.3310, 7.3222, 7.3154, 7.3073, 7.3032, 7.2980, 7.2887, 7.2866, 7.2736, 7.2721		56.151	4H
b	5.3411, 5.3389, 5.3363, 5.3339	s*	15.599	1H
a	5.0635, 5.0585, 5.0535	s*	15.682	1H
j	3.7888, 3.7651, 3.7408	t	29.358	2H
l	2.6229, 2.5963, 2.5687	t	29.437	2H
c	2.1402, 2.1378, 2.1358, 2.1333	s*	41.169	3H
k	1.9929, 1.9687, 1.9669, 1.9426	q	29.634	2H
h	1.7218	s	82.280	6H

(* : expected)

Table 2.33 ^{13}C-NMR summary of BTMI.

No of Atom	δ (ppm)	(+)/(-)
12, 13	177.0890	(-)
2	146.8287	(-)
8	143.4792	(-)
4	141.1543	(-)
6	128.1360	(+)
7	123.9392	(+)
9	123.8510	(+)
5	121.9293	(+)
1	112.3985	(-)
10	55.3373	(-)
14	45.4037	(-)
16	33.5288	(-)
11	29.3013	(+)
3	21.8840	(+)
15	16.7908	(-)

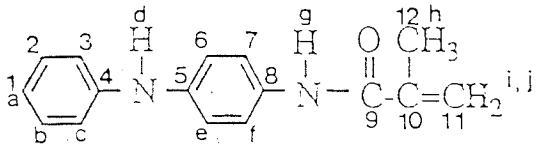

Table 2.34 ^{1}H-NMR summary of APMA.

No. of Atom	δ (ppm)	Integral	H
g	7.6145	8.228	1H
b, c	7.4528, 7.4426, 7.4358, 7.4199, 7.4133, 7.4031	21.235	2H
	7.2589, 7.2525, 7.2422, 7.2338, 7.2309, 7.2119, 7.2062, 7.1992	22.460	2H
e, f	7.0397, 7.0297, 7.0222, 7.0155, 7.0122, 7.0003, 6.9871, 6.9110	43.729	4H
a	6.8868, 6.8619	9.882	1H
i, j	5.7727	20.365	2H
d	5.414	10.025	1H
h	2.1579, 2.1571, 2.0376	33.305	3H

Table 2.35 ^{13}C-NMR summary of APMA.

No of Atom	δ (ppm)	(+)/(-)
9	166.5377	(-)
4	143.3802	(-)
5	140.6944	(-)
10	139.6382	(-)
8	131.2231	(-)
2	129.2710	(+)
7	121.7371	(+)
1	120.5409	(+)
11	119.7031	(-)
3, 6	118.6729, 117.0768	(+)
12	18.7266	(+)

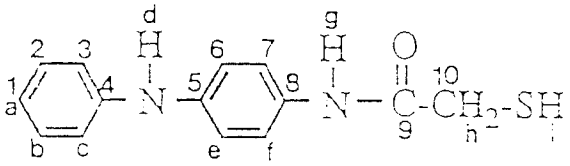

Table 2.36 ^{1}H-NMR summary of MADA.

No. of Atom	δ (ppm)	Integral	H
g	8.4410	63.921	1H*
a, b, c, e, f	7.4378, 7.4278, 7.4210, 7.3984, 7.3885	151.237	2H
	7.2692, 7.2446, 7.2167	192.342	2H+α
	7.0650, 7.0549, 7.0480, 7.0258, 7.0003	320.376	4H
	6.9263, 6.9019, 6.8774	79.927	1H
d	5.6922	48.115	1H*
impurities	3.5886	8.004	
h	3.3909, 3.3601	151.747	2H
impurities	2.3427	4.365	
impurities	2.3011	2.665	
impurities	2.2479	1.146	
impurities	2.1227	55.815	
impurities	2.0362, 2.0054, 1.9748	85.331	
i	1.6663, 1.6271, 1.5899	48.745	1H*
impurities	1.2404, 0.8674	34.752	

(* : expected)

Table 2.37 ^{13}C-NMR summary of MADA.

No of Atom	d (ppm)	(+)/(-)
9	166.9334	(-)
4	143.1760	(-)
5	140.0428	(-)
8	130.6823	(-)
2	129.3302	(+)
7	121.4964	(+)
1	120.8258	(+)
3, 6	118.5897, 117.3120	(+)
10	28.9713	(-)

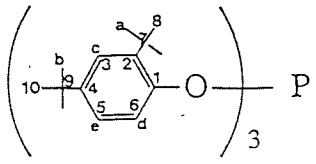

Table 2.38 ^{1}H-NMR summary of P168.

No. of Atom	d (ppm)	m	Integral	H
c	7.3618, 7.3536	s*	4.224	3H
d, e	7.2987, 7.2919, 7.2706, 7.2637	d*	4.404	3H
d, e	7.1078, 7.0995, 7.0796, 7.0713	d*	4.602	3H
a, b	1.3808	s	40.937	27H
a, b	1.2918	s	40.937	27H

(* : expected)

Table 2.39 ^{13}C-NMR summary of P168.

No of Atom	d (ppm)	(+)/(-)
1, 2, 4	149.1950, 149.1407, 145.4387, 138.9238, 138.9002	(-)
3, 5, 6	124.3706, 123.4803, 119.0522, 118.8091	(+)
7, 9	34.9815, 34.4422	(-)
8, 10	31.5122, 30.1315	(+)

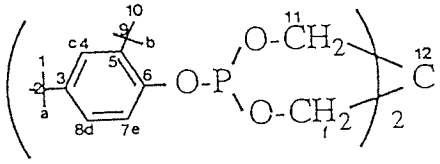

Table 2.40 ^{1}H-NMR summary of P626.

No. of Atom	d (ppm)	m	Integral	H
c	7.3866, 7.3784	s*	4.356	2H
d, e	7.1694, 7.1612, 7.1416		4.666	2H
d, e	6.9890, 6.9611		5.267	2H
f	4.6483, 4.6415, 4.6107, 4.5706, 4.5577, 4.5327, 4.5201		10.022	8H*
impurities	4.1936, 4.1842, 4.1558, 4.1465		5.257	
impurities	3.5166, 3.5092, 3.4795, 3.4444, 3.4378		5.180	
a, b	1.4227	s	42.525	18H
a, b	1.2980	s	42.361	18H

(* : expected)

Table 2.41 ^{13}C-NMR summary of P626.

No of Atom	d (ppm)	(+)/(-)
3,6,10	149.0647, 148.9594, 145.7381, 139.0331	(-)
4, 7, 8	124.3613, 123.6785, 118.5328, 118.3248	(+)
11	62.6277, 62.3643	(-)
12		(-)
2,9	34.8435, 34.4100	(-)
1, 10	31.4334, 30.0827	(+)
impurities	29.5652	(+)

Fig. 2.43 ^{1}H-NMR spectrum of BQ. (300MHz, in $CDCl_3$)

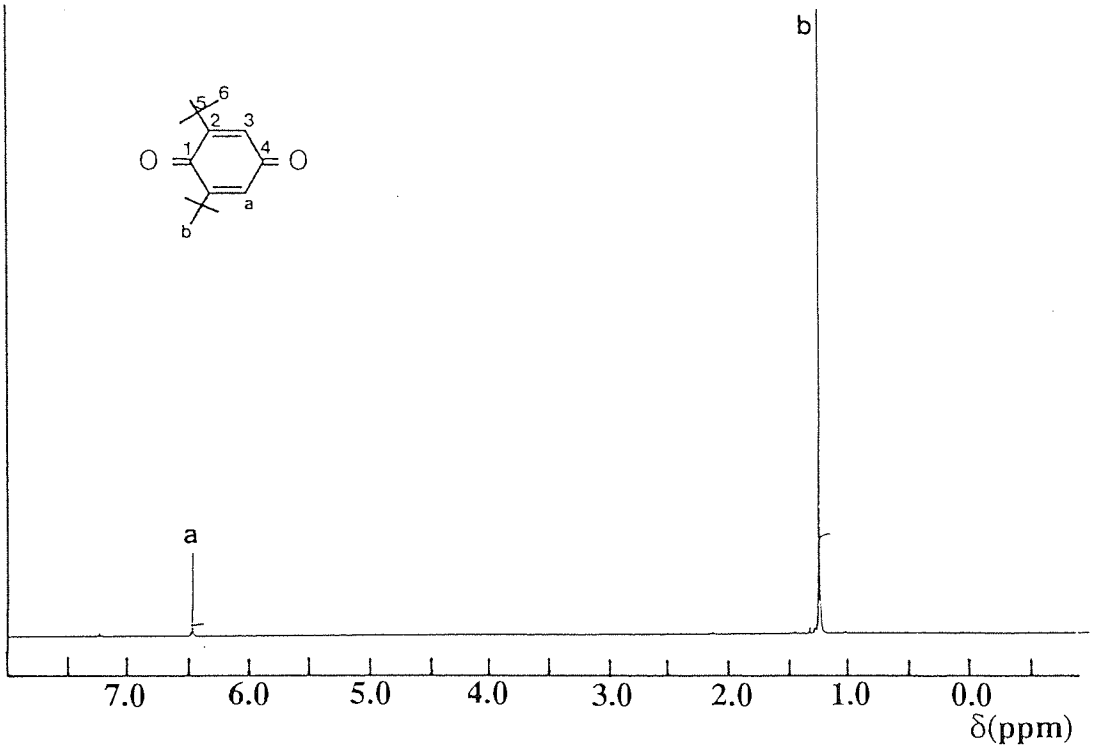

Fig. 2.44 ^{13}C-NMR spectrum of BQ. (75.5MHz, in $CDCl_3$)

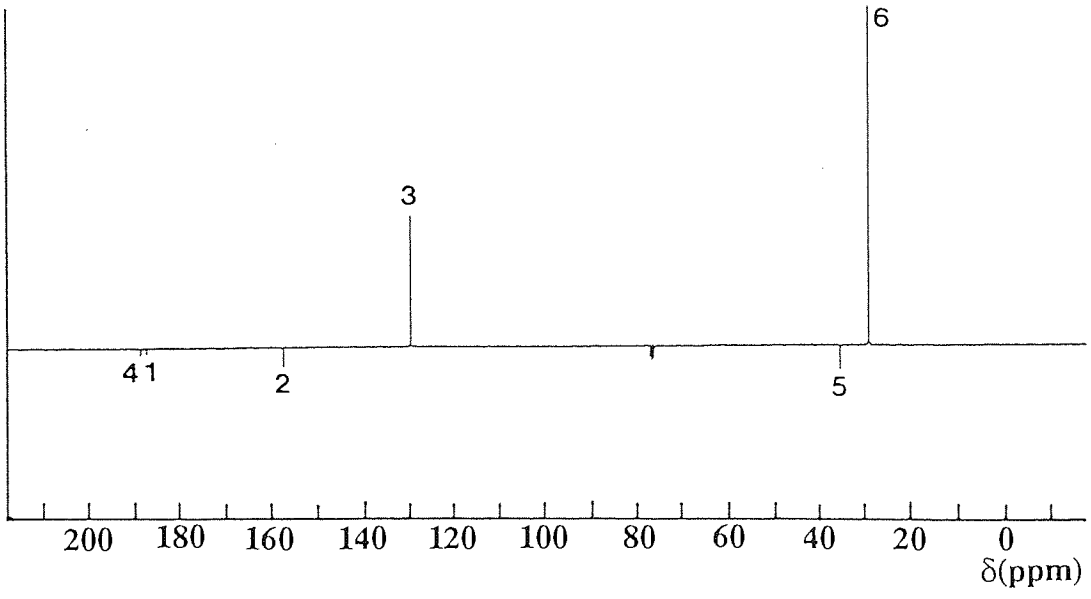

Fig. 2.45 ^{1}H-NMR spectrum of DPQ. (300MHz, in $CDCl_3$)

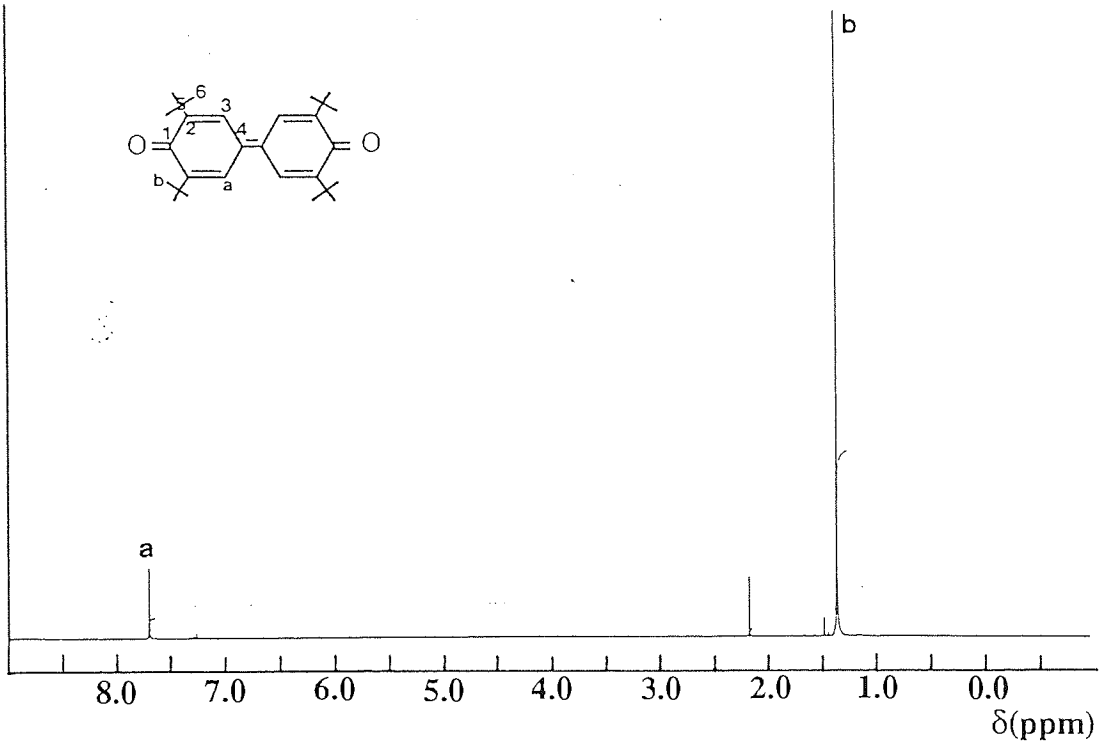

Fig. 2.46 ^{13}C-NMR spectrum of DPQ. (75.5MHz, in $CDCl_3$)

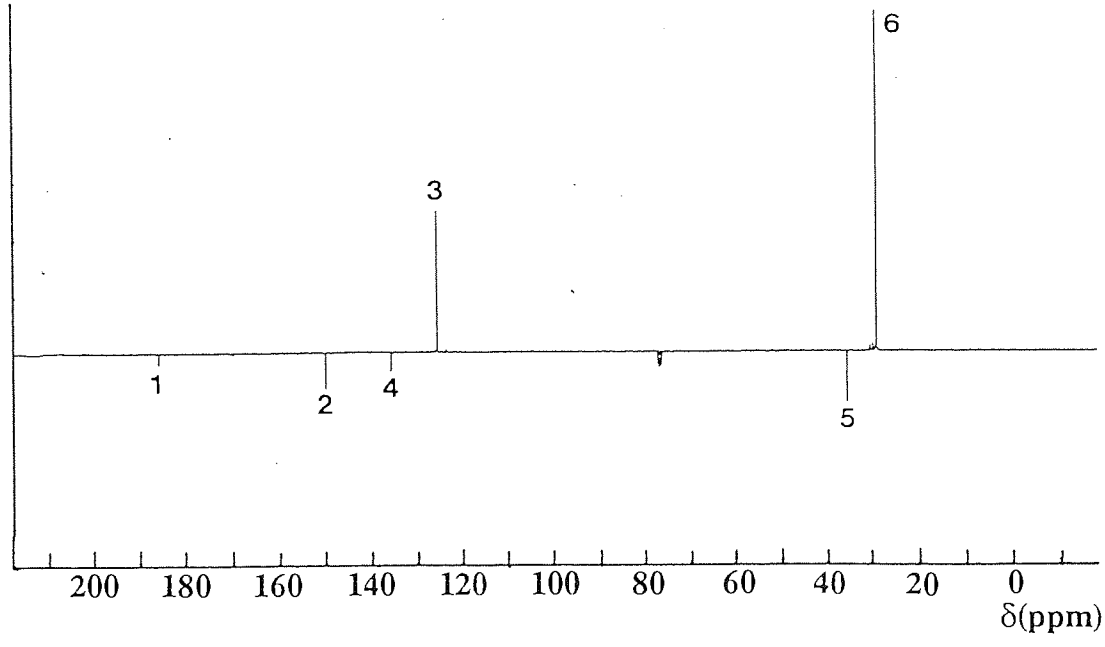

Fig. 2.47 ^{1}H-NMR spectrum of NQ. (300MHz, in $CDCl_3$)

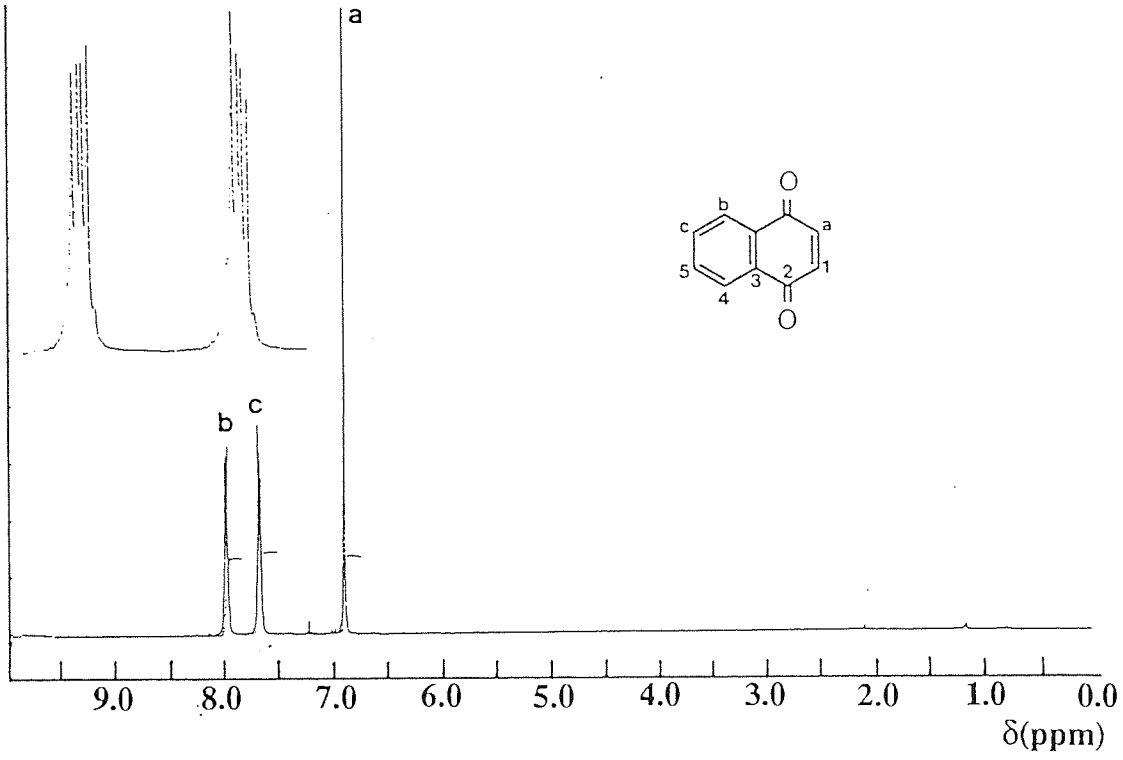

Fig. 2.48 ^{13}C-NMR spectrum of NQ. (75.5MHz, in $CDCl_3$)

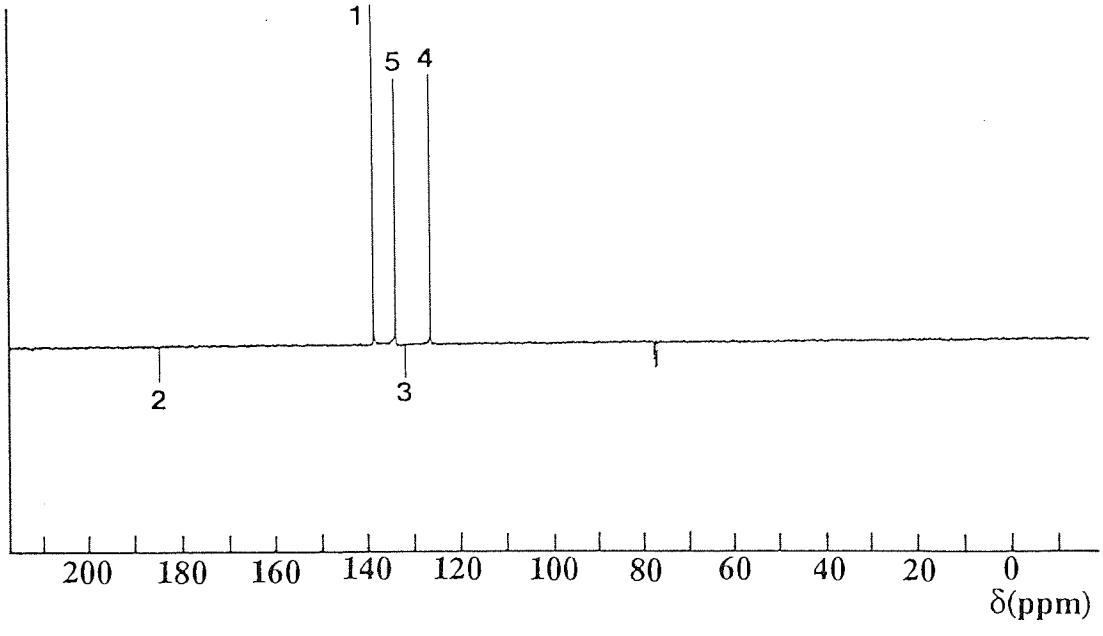

Fig. 2.49 ^{1}H-NMR spectrum of PDO. (300MHz, in $CDCl_3$)

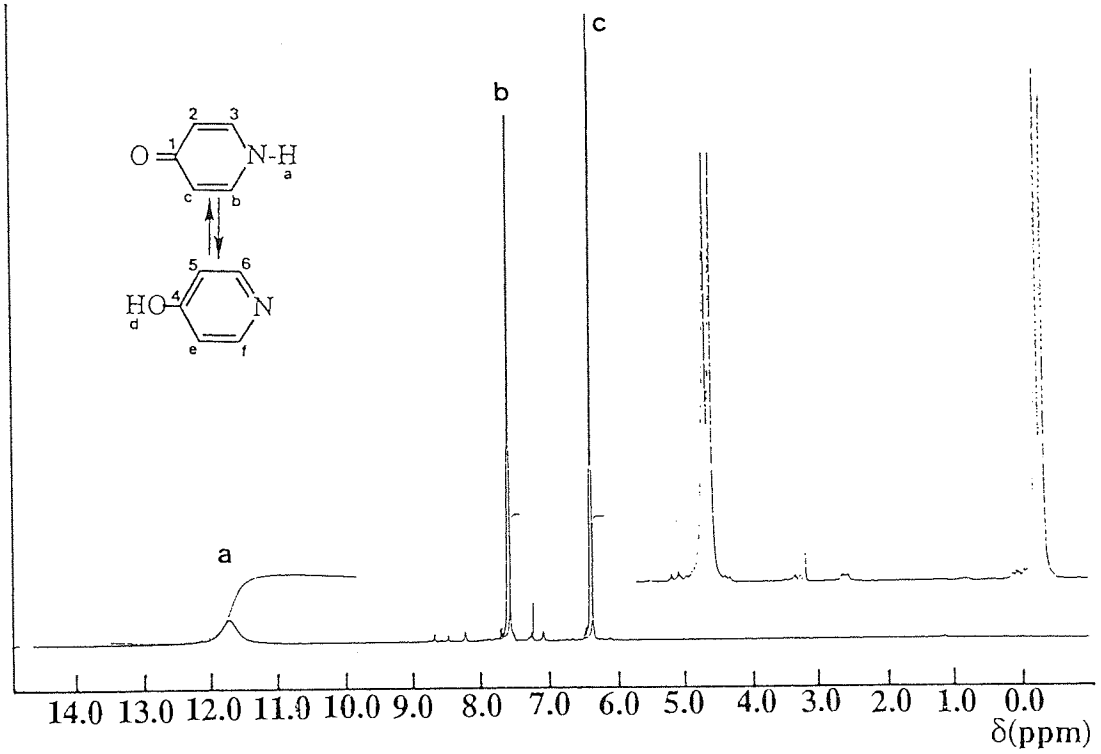

Fig. 2.50 ^{13}C-NMR spectrum of PDO. (75.5MHz, in $CDCl_3$)

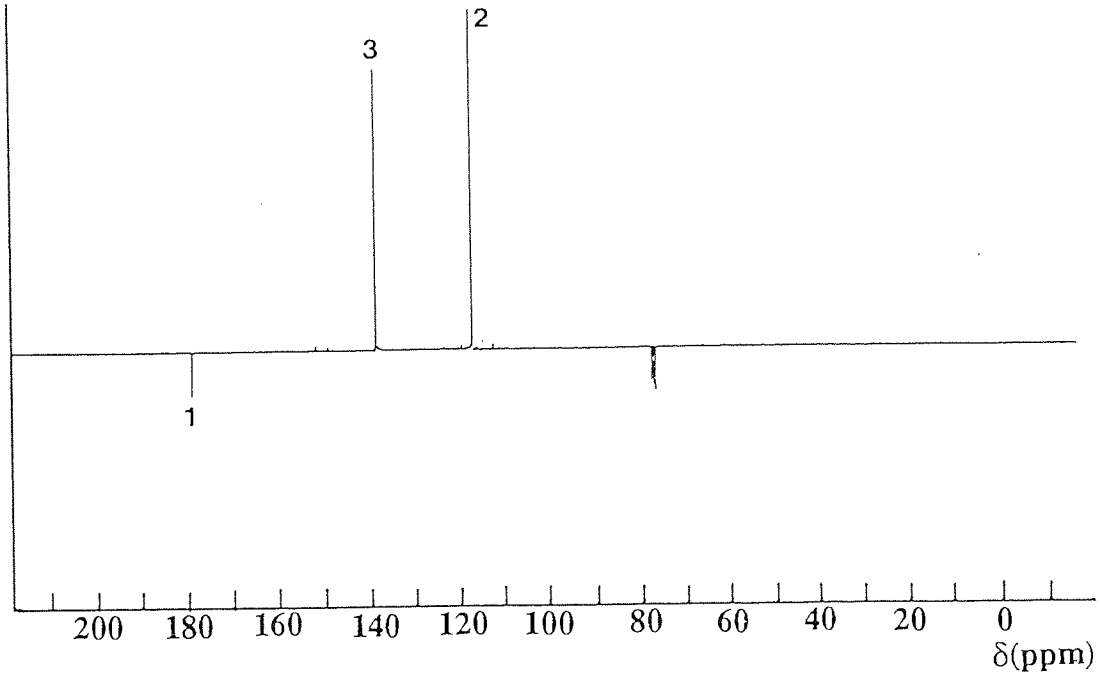

Fig. 2.51 ^{1}H-NMR spectrum of HBA. (300MHz, in $CDCl_3$)

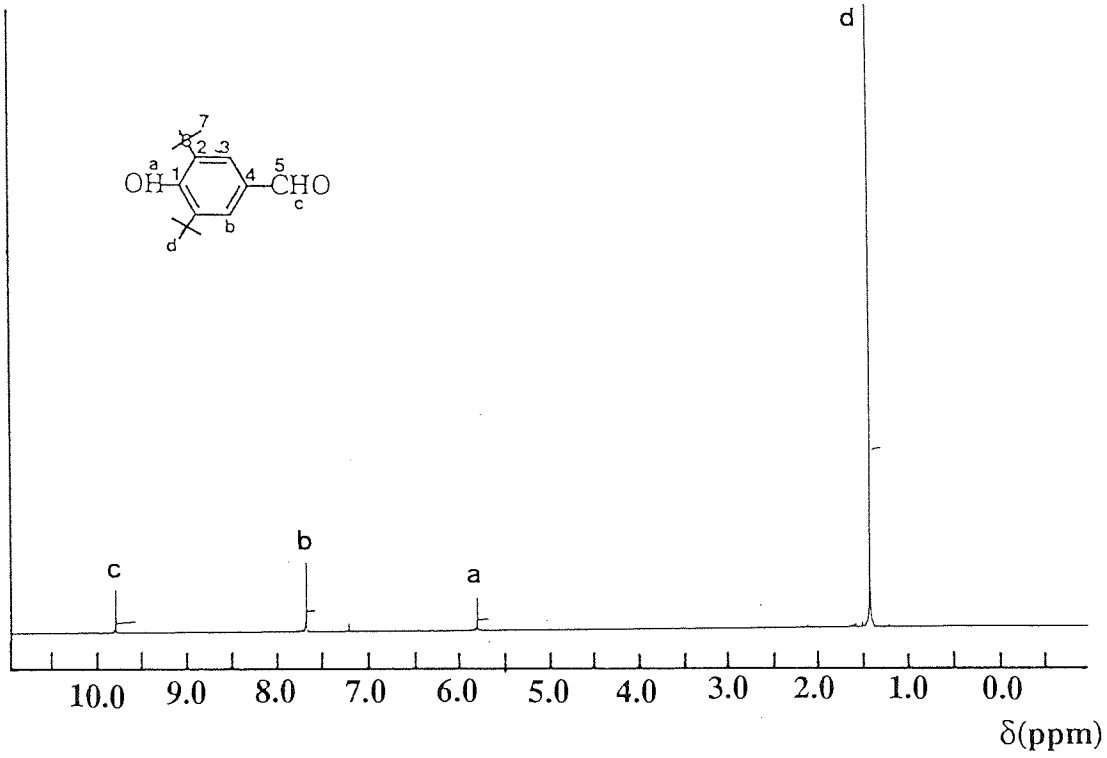

Fig. 2.52 ^{13}C-NMR spectrum of HBA. (75.5MHz, in $CDCl_3$)

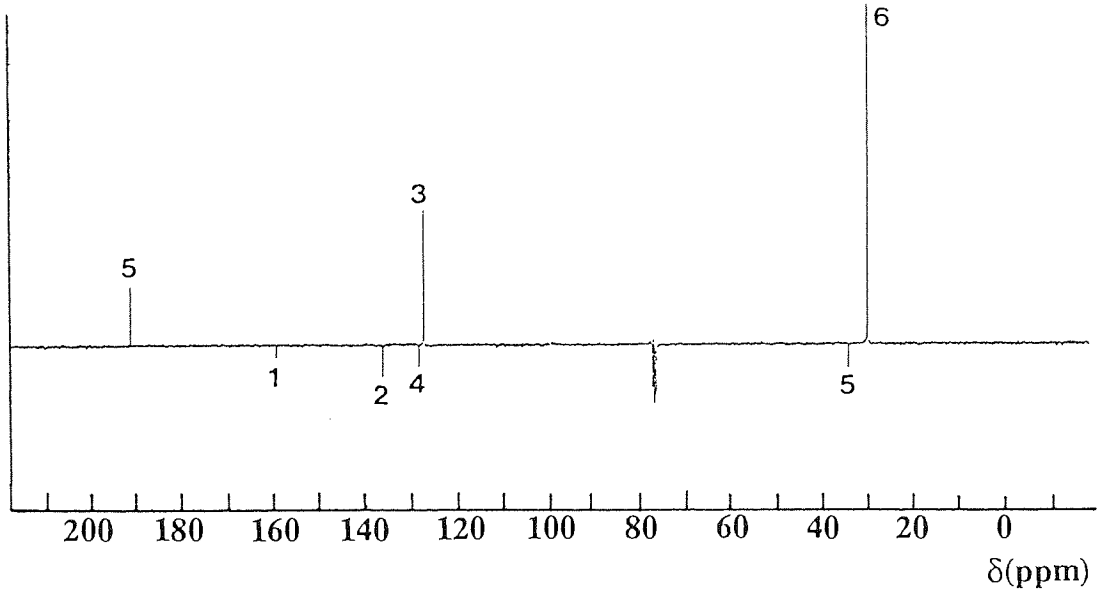

Fig. 2.53 ^{1}H-NMR spectrum of αTOC. (300MHz, in $CDCl_3$)

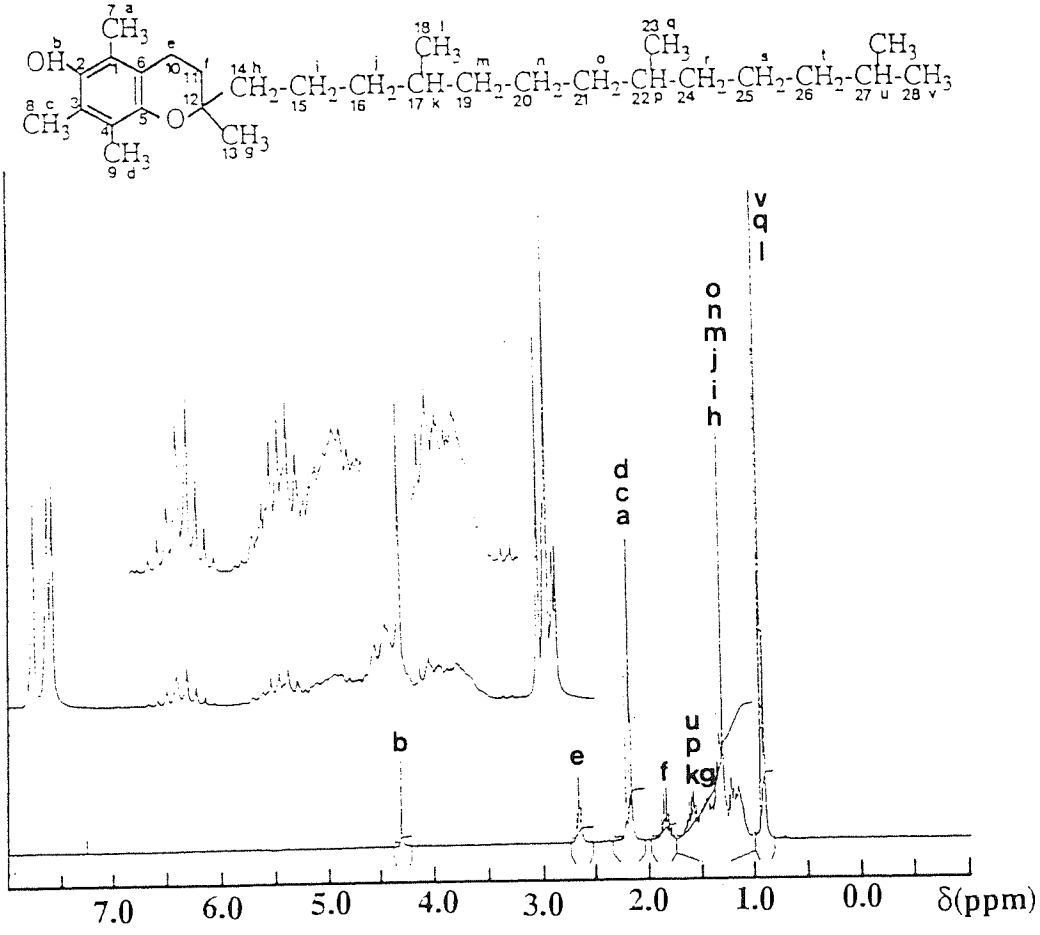

Fig. 2.54 ^{13}C-NMR spectrum of αTOC. (75.5MHz, in $CDCl_3$)

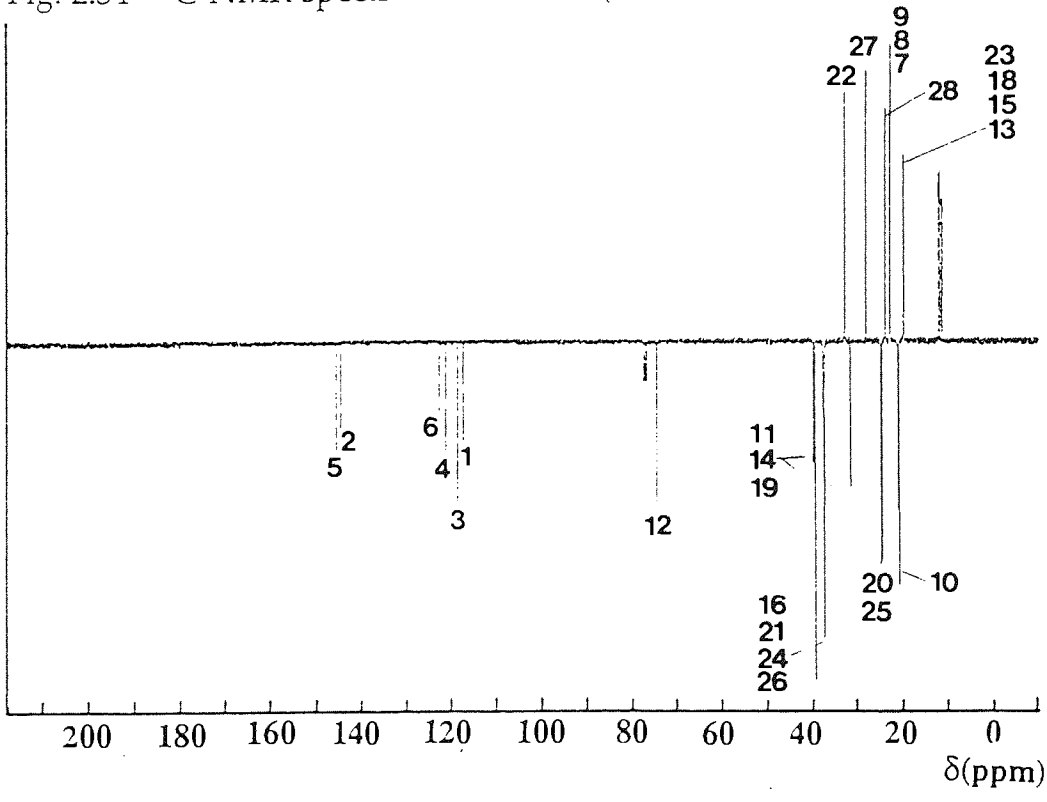

Fig. 2.55 ^{1}H-NMR spectrum of γTOC. (300MHz, in $CDCl_3$)

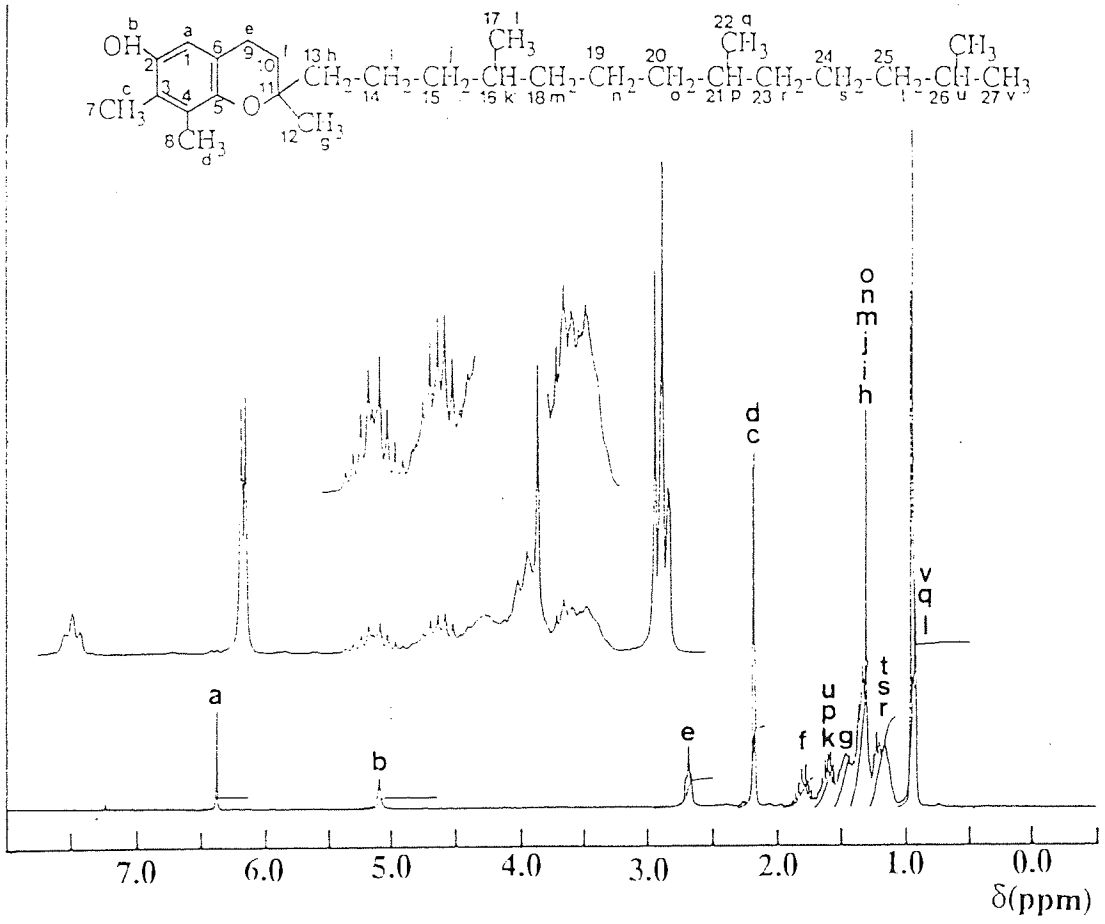

Fig. 2.56 ^{13}C-NMR spectrum of γTOC. (75.5MHz, in $CDCl_3$)

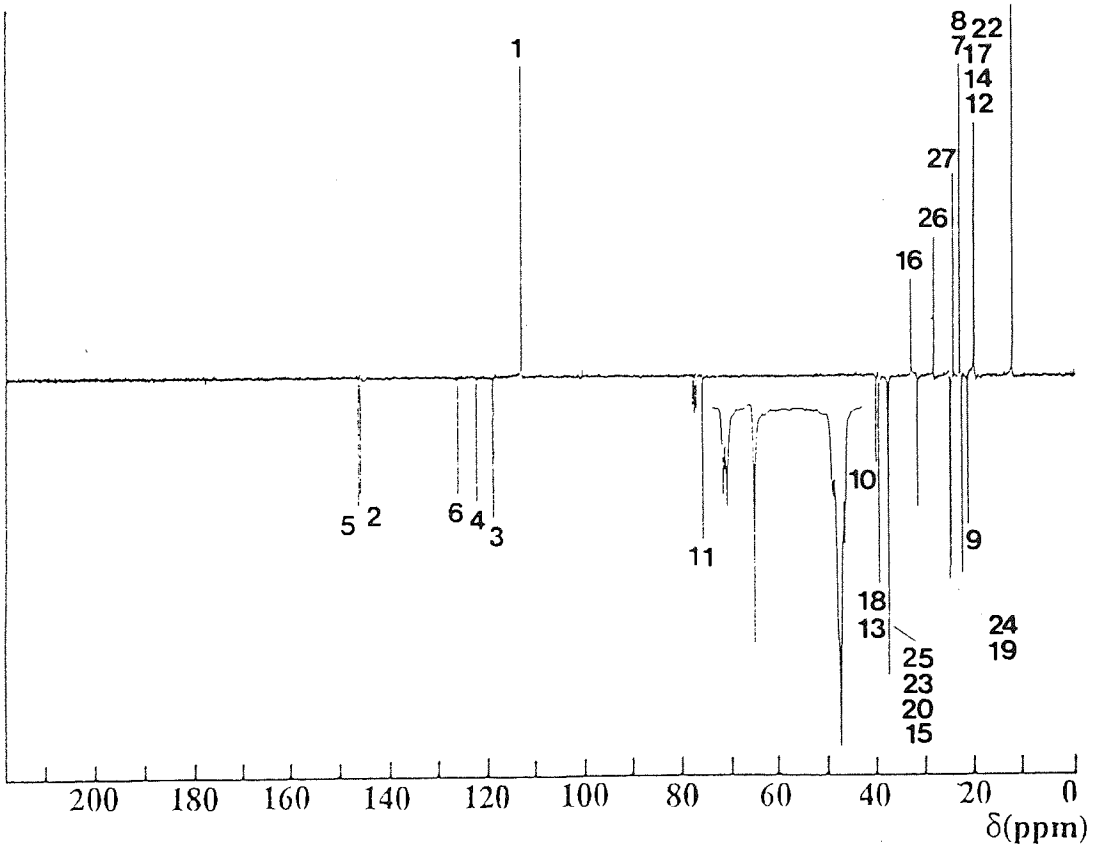

Fig. 2.57 ^{1}H-NMR spectrum of GM. (300MHz, in $CDCl_3$)

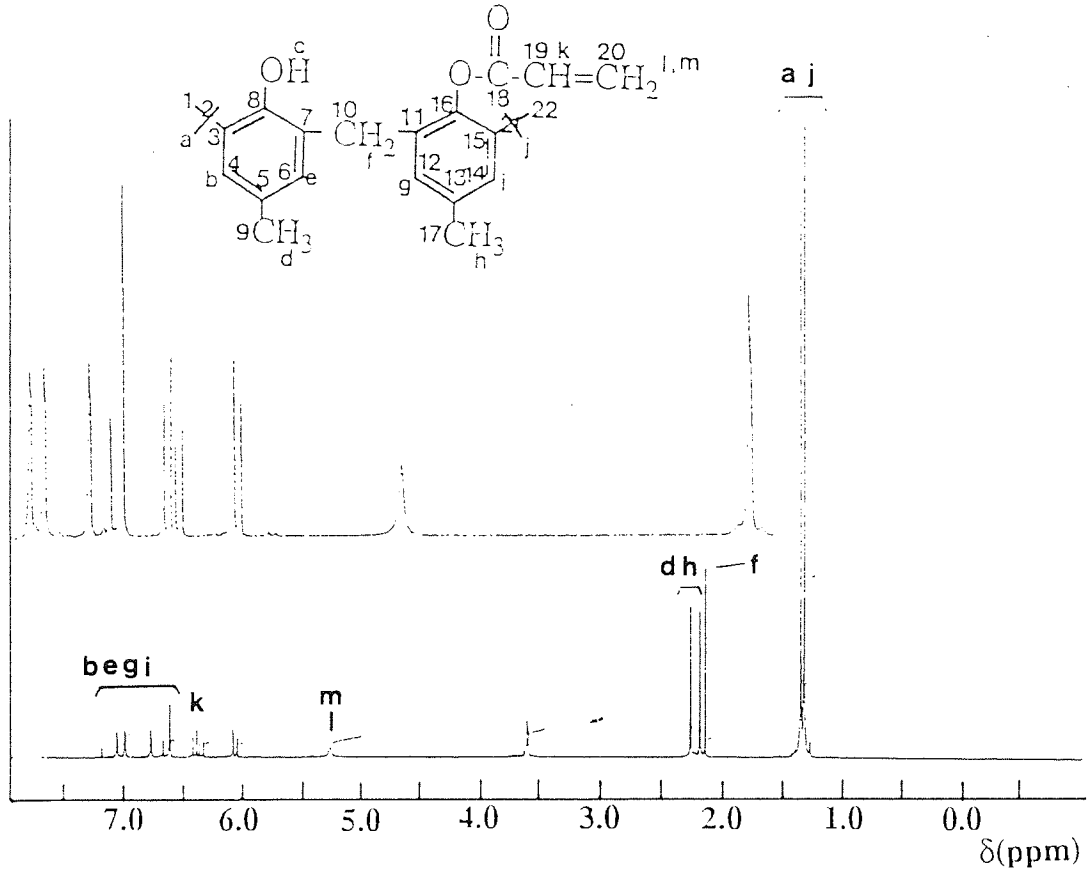

Fig. 2.58 ^{13}C-NMR spectrum of GM. (75.5MHz, in $CDCl_3$)

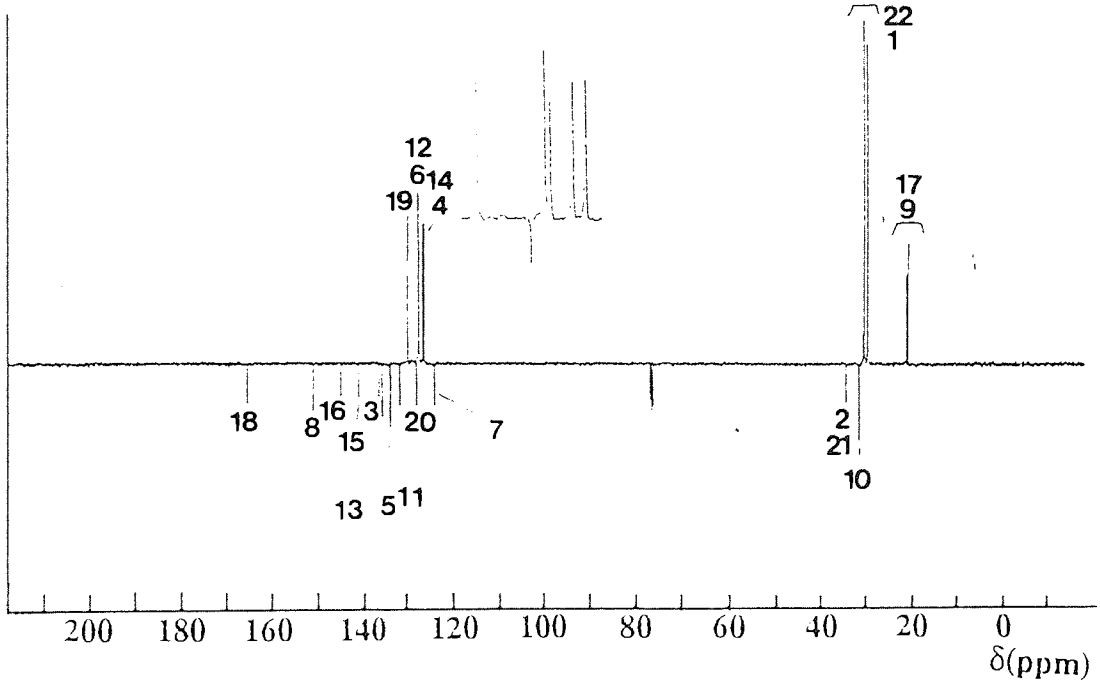

Fig. 2.59 ^{1}H-NMR spectrum of IPPD. (300MHz, in $CDCl_3$)

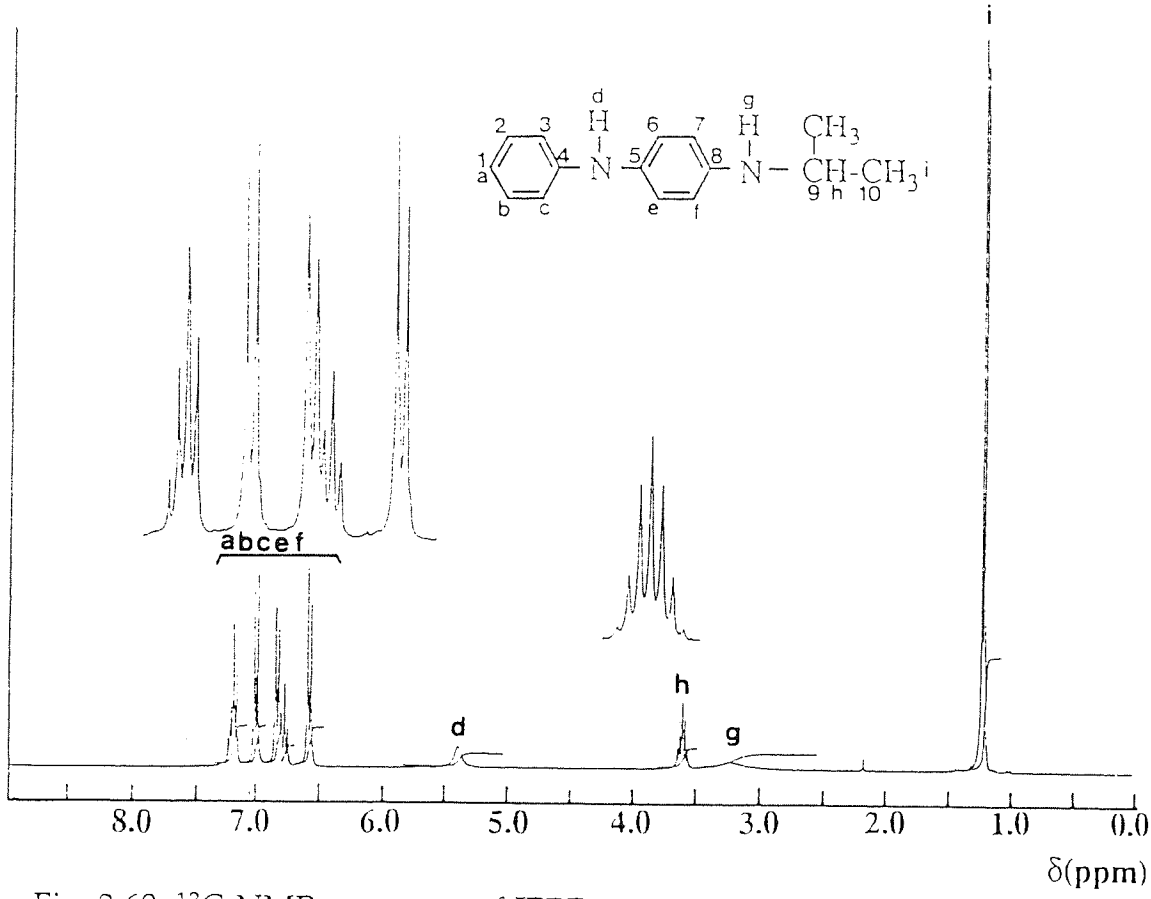

Fig. 2.60 ^{13}C-NMR spectrum of IPPD. (75.5MHz, in $CDCl_3$)

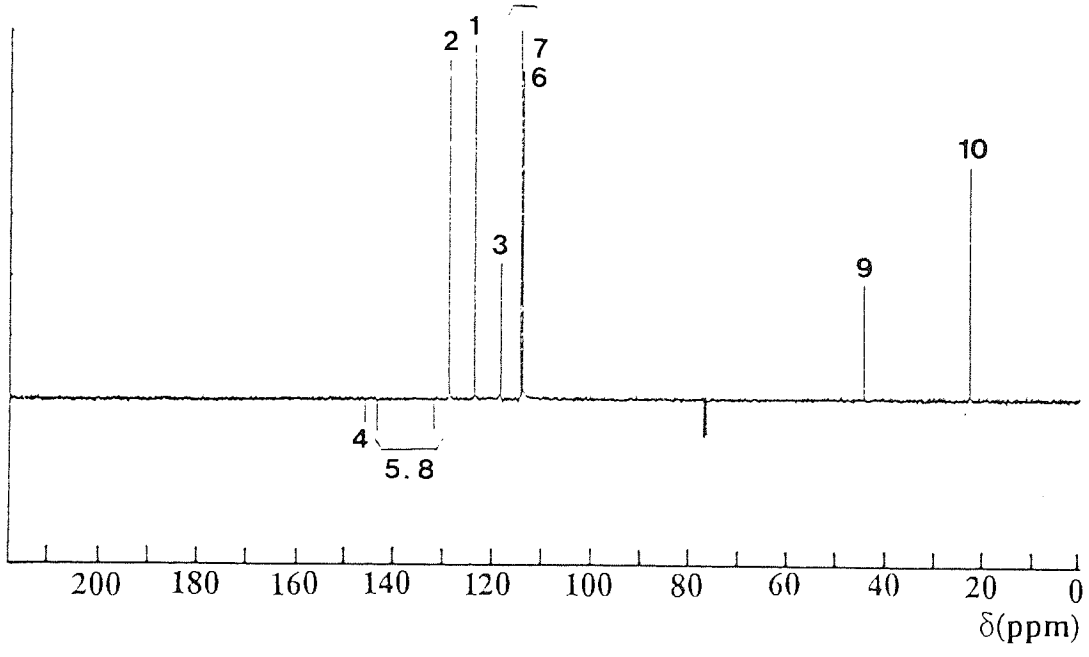

Fig. 2.61 ^{1}H-NMR spectrum of 6PPD. (300MHz, in $CDCl_3$)

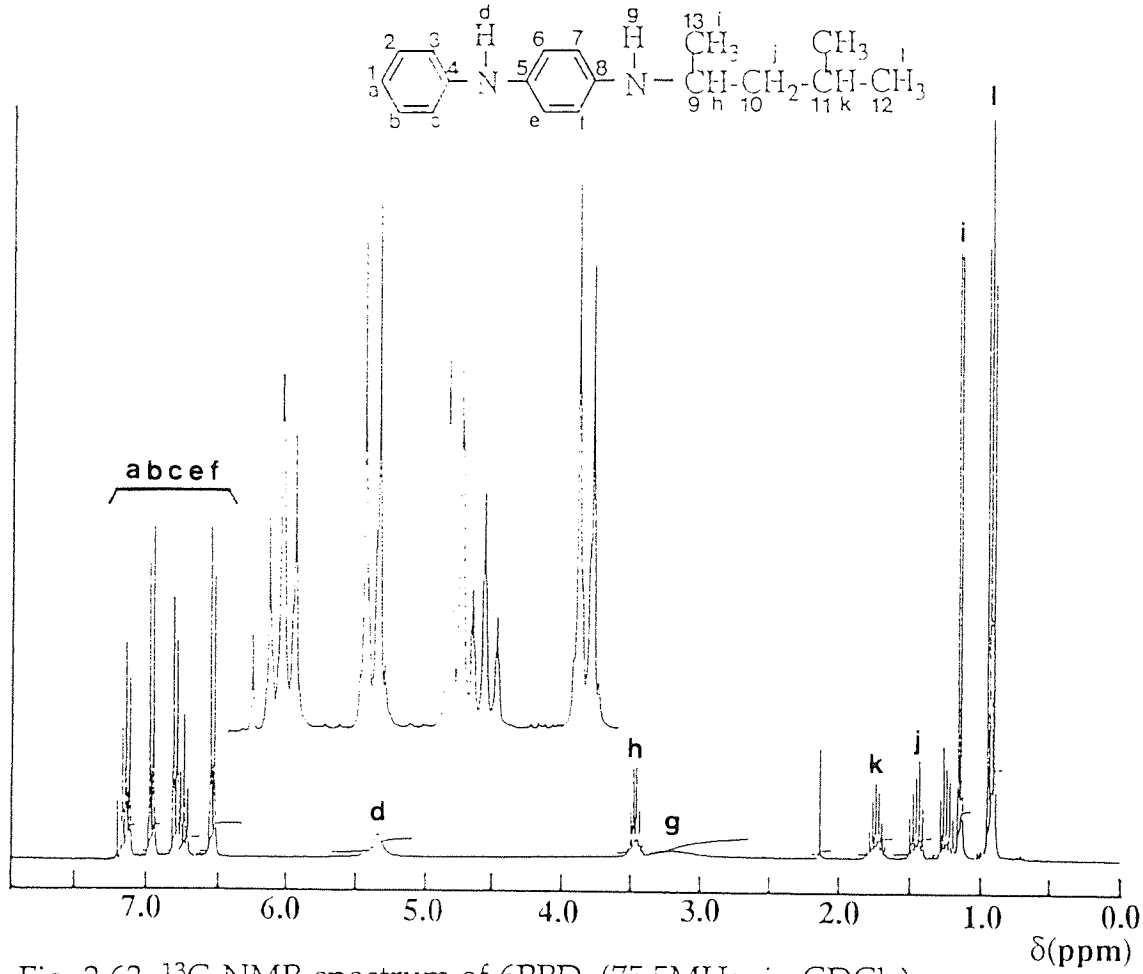

Fig. 2.62 ^{13}C-NMR spectrum of 6PPD. (75.5MHz, in $CDCl_3$)

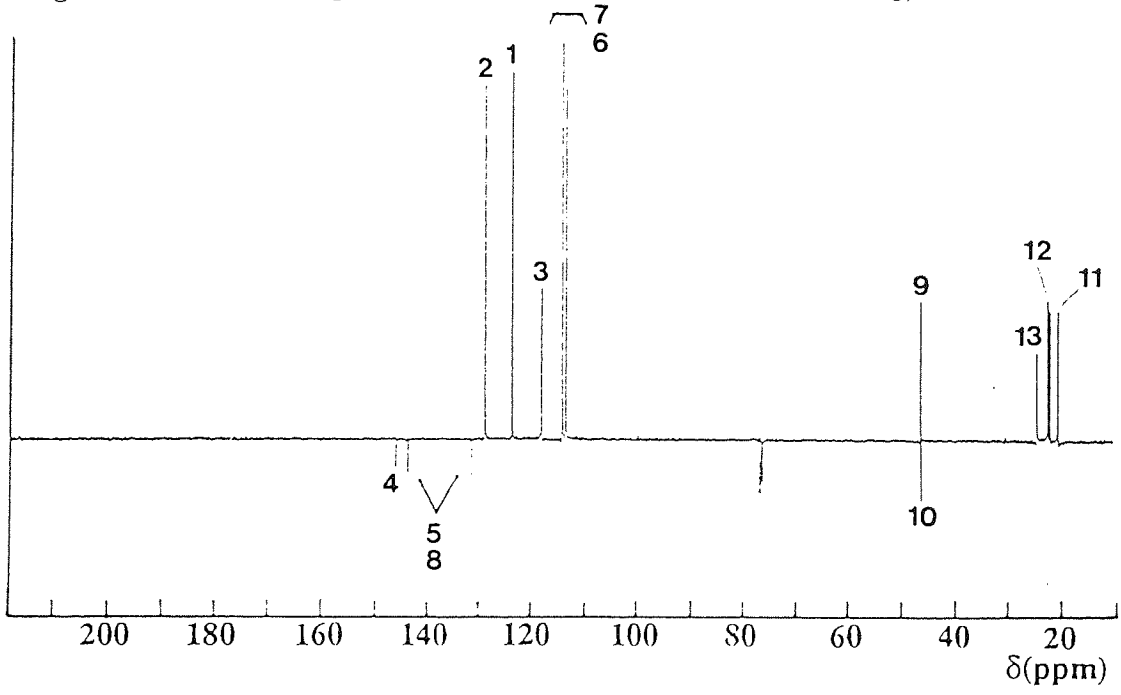

Fig. 2.63 ^{1}H-NMR spectrum of TMQ. (300MHz, in $CDCl_3$)

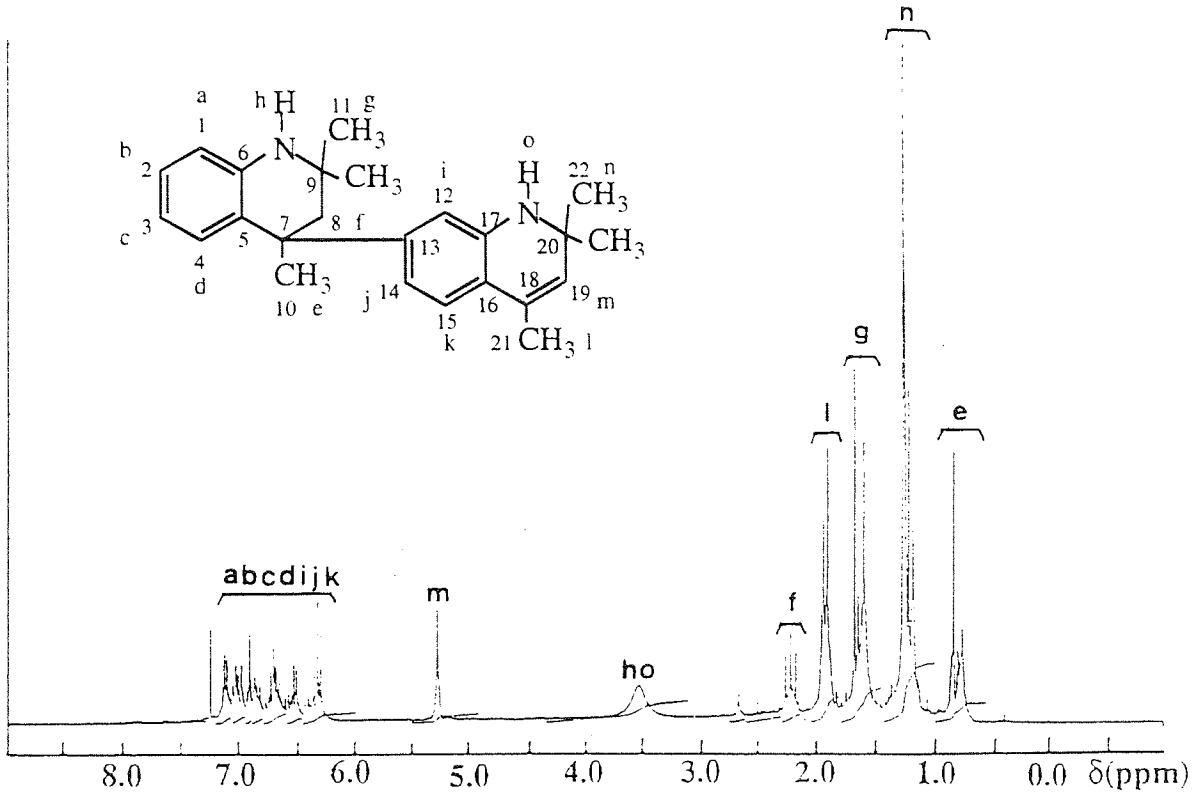

Fig. 2.64 ^{13}C-NMR spectrum of TMQ. (75.5MHz, in $CDCl_3$)

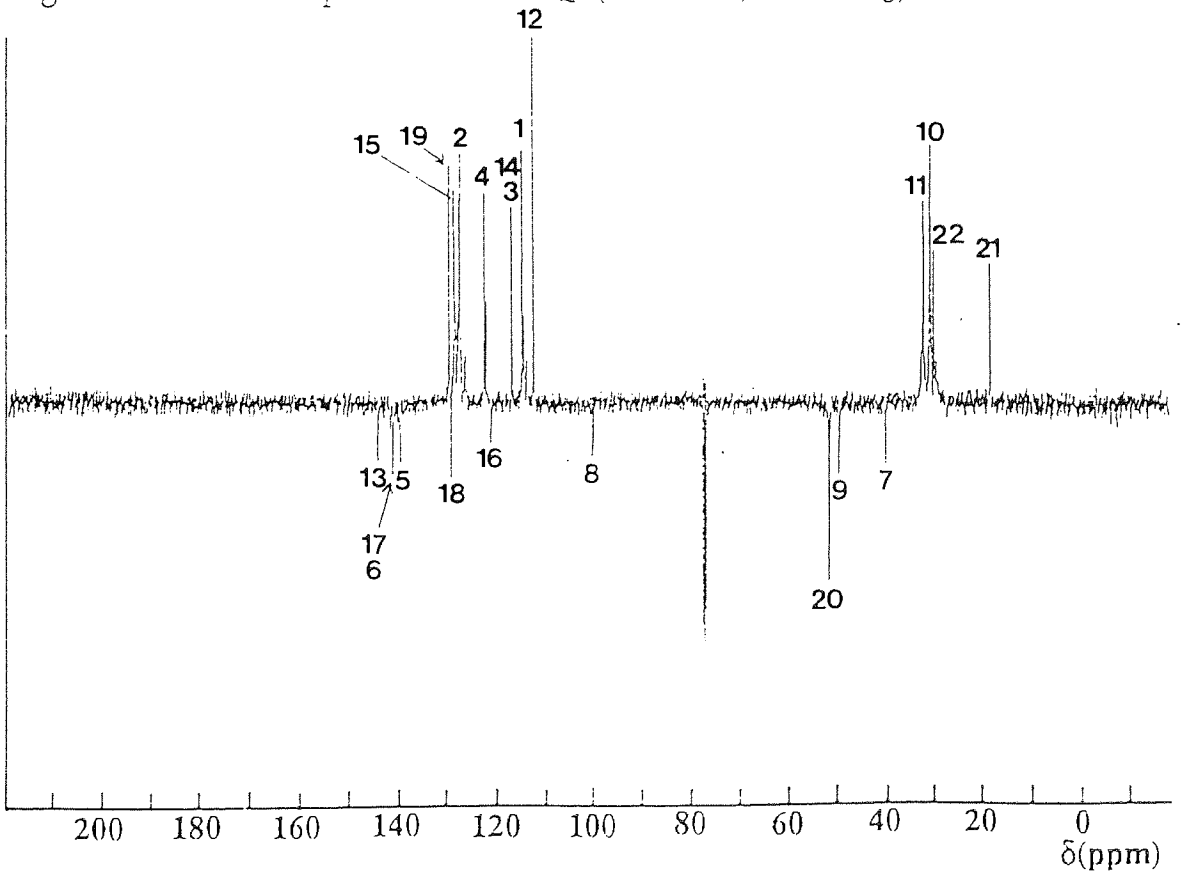

Fig. 2.65 ^{1}H-NMR spectrum of PM. (300MHz, in $CDCl_3$)

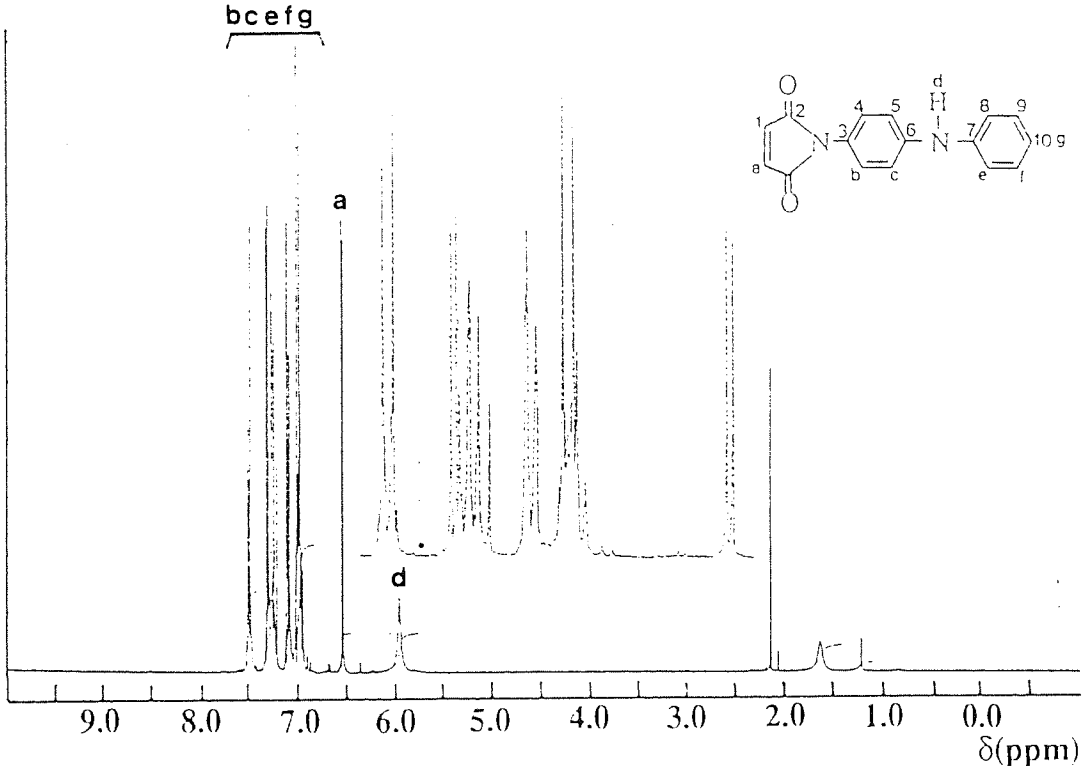

Fig. 2.66 ^{13}C-NMR spectrum of PM. (75.5MHz, in $CDCl_3$)

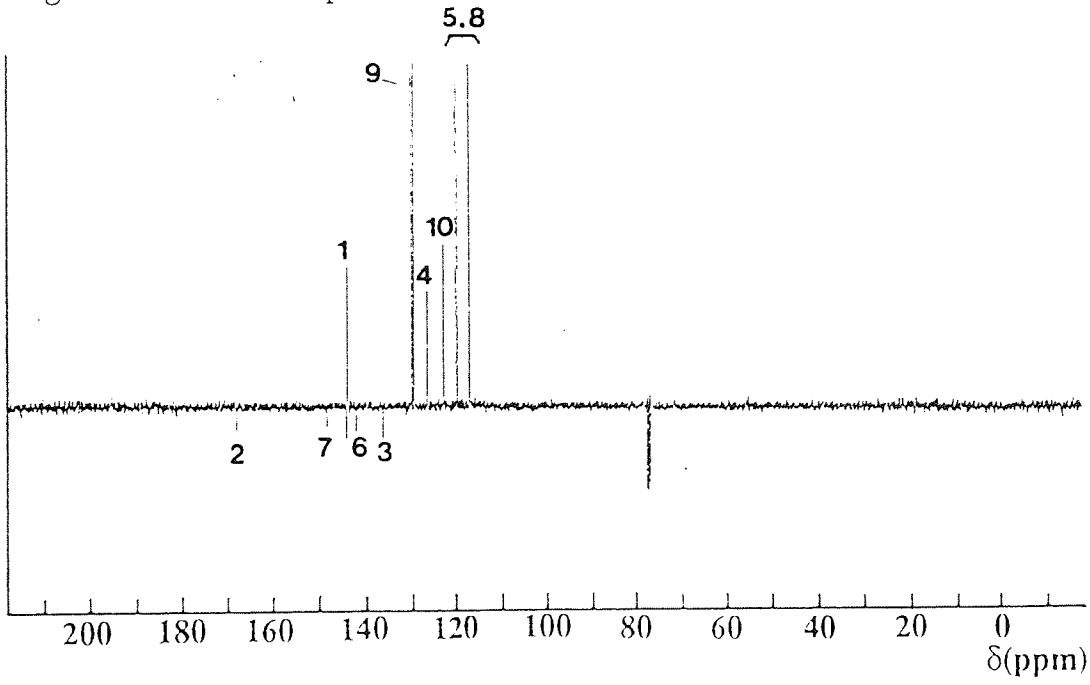

Fig. 2.67 ^{1}H-NMR spectrum of BTMI. (300MHz, in $CDCl_3$)

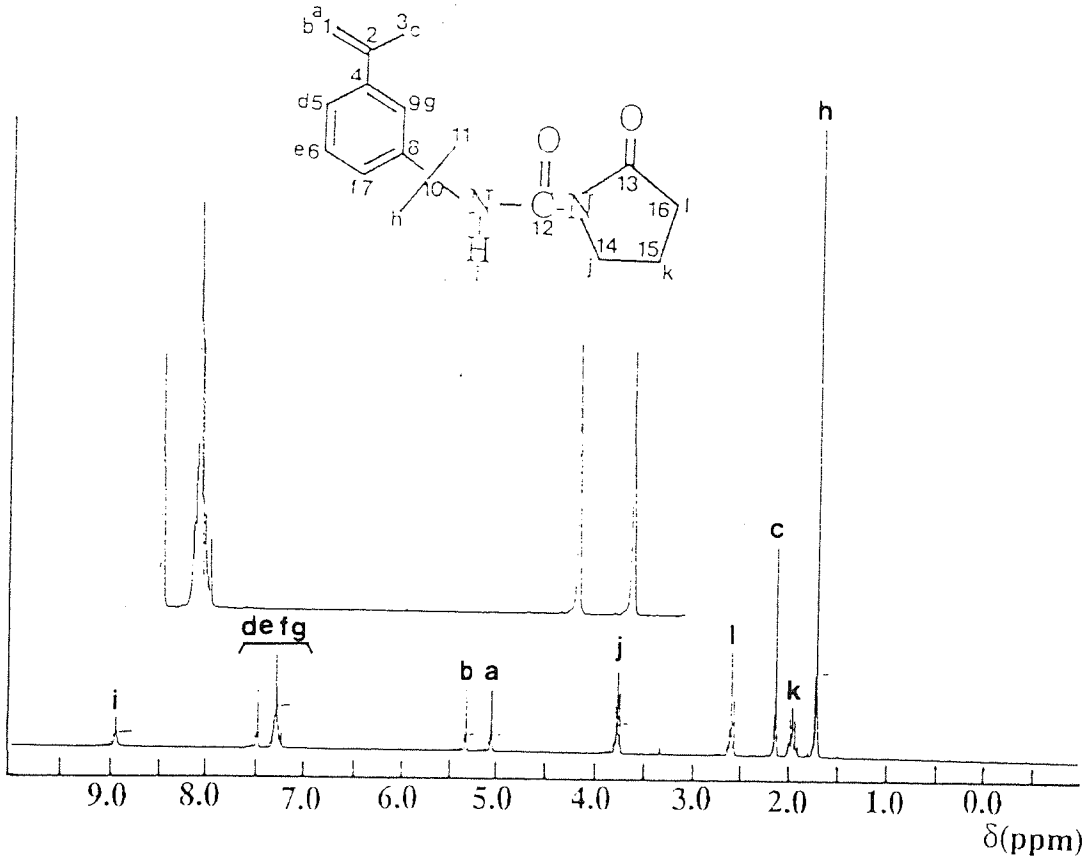

Fig. 2.68 ^{13}C-NMR spectrum of BTMI. (75.5MHz, in $CDCl_3$)

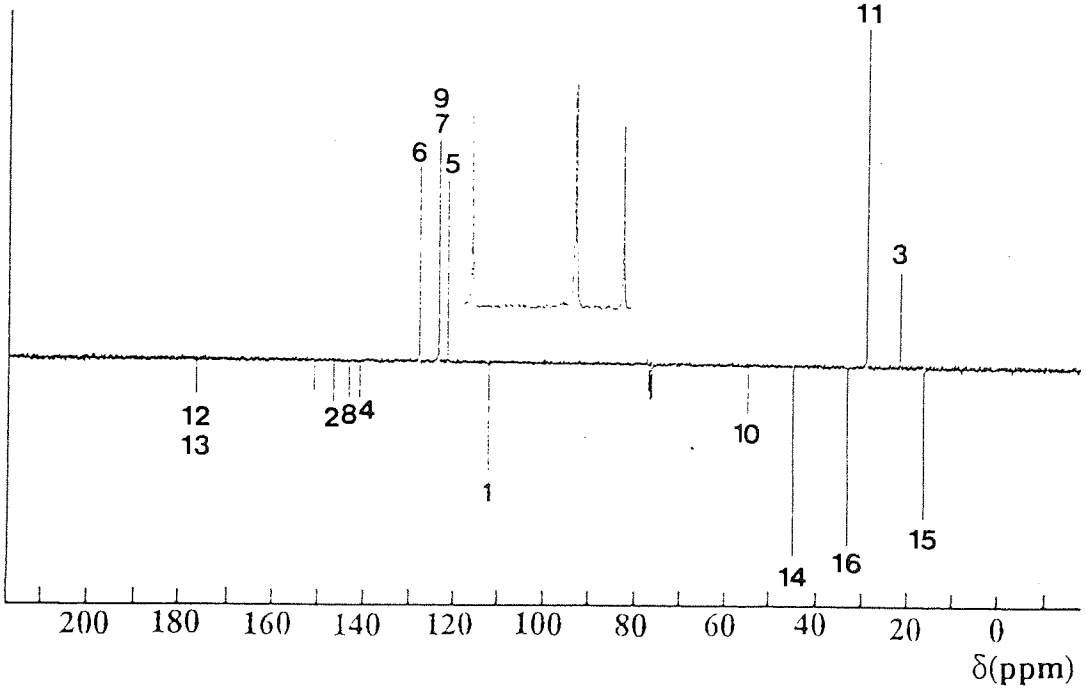

Fig. 2.69 ^{1}H-NMR spectrum of APMA. (300MHz, in $CDCl_3$)

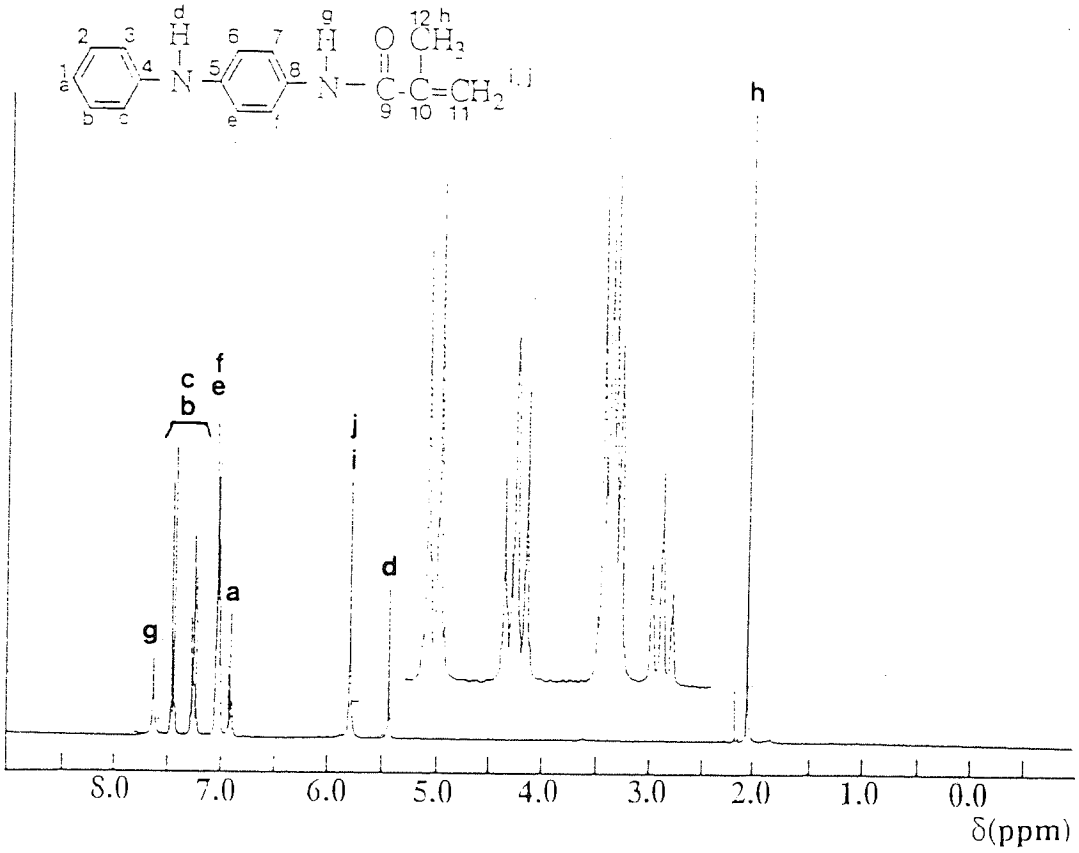

Fig. 2.70 ^{13}C-NMR spectrum of APMA. (75.5MHz, in $CDCl_3$)

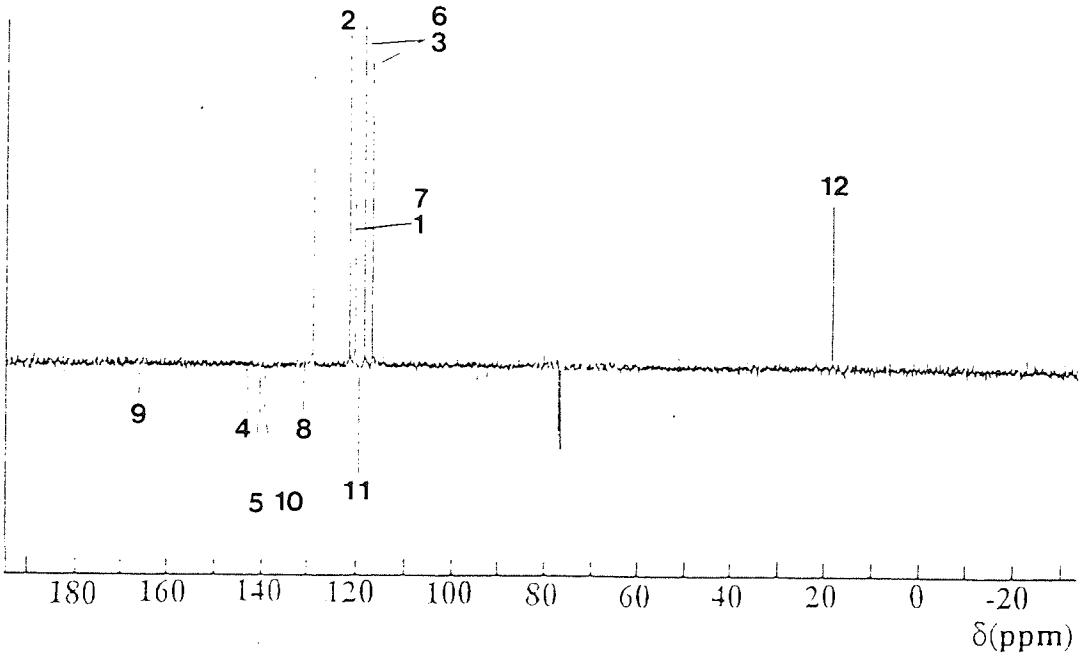

Fig. 2.71 ^{1}H-NMR spectrum of MADA. (300MHz, in $CDCl_3$)

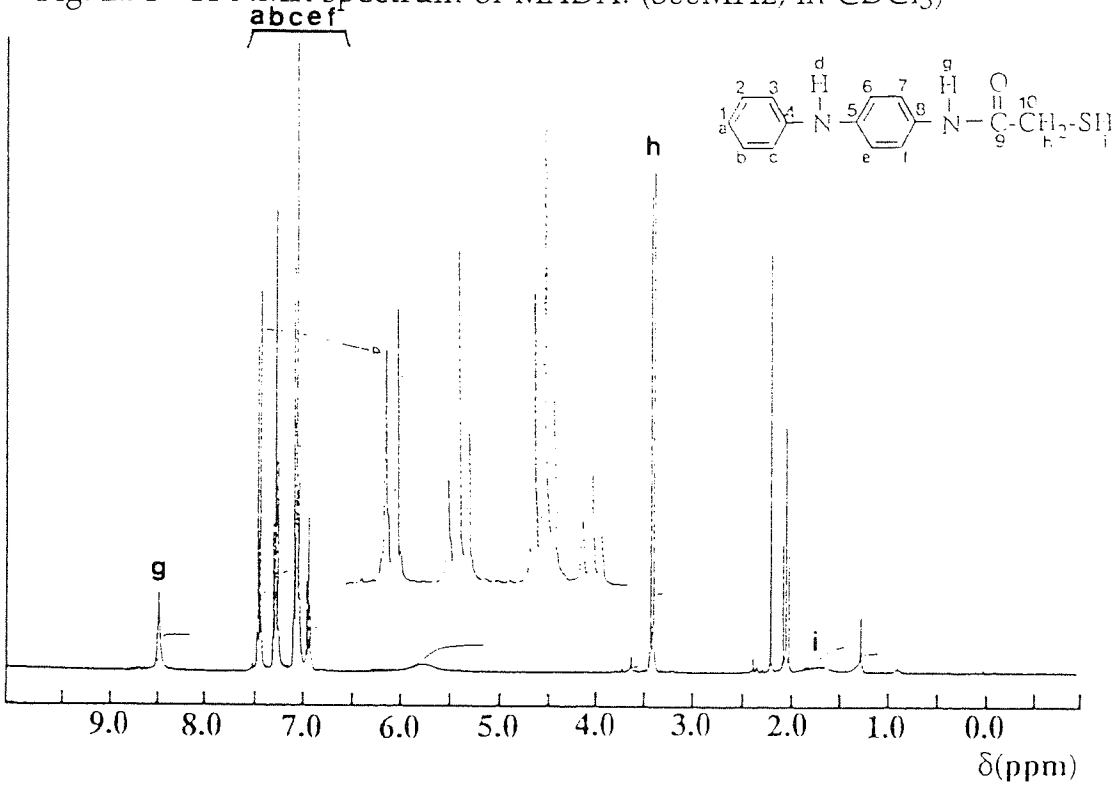

Fig. 2.72 ^{13}C-NMR spectrum of MADA. (75.5MHz, in $CDCl_3$)

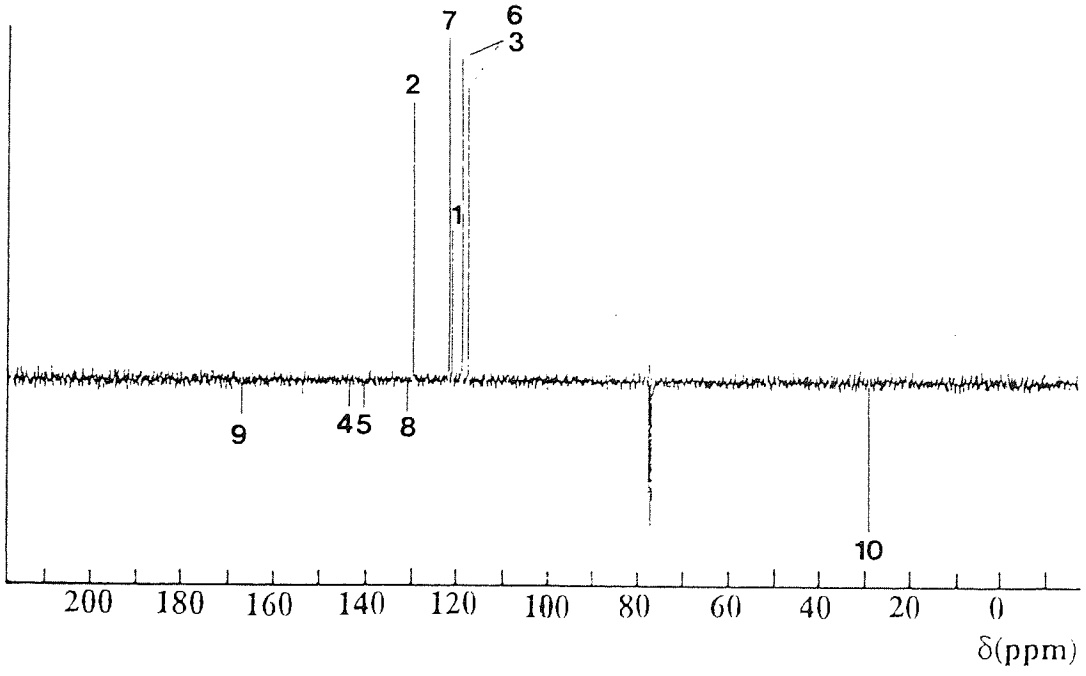

Fig. 2.73 ^{1}H-NMR spectrum of P168. (300MHz, in $CDCl_3$)

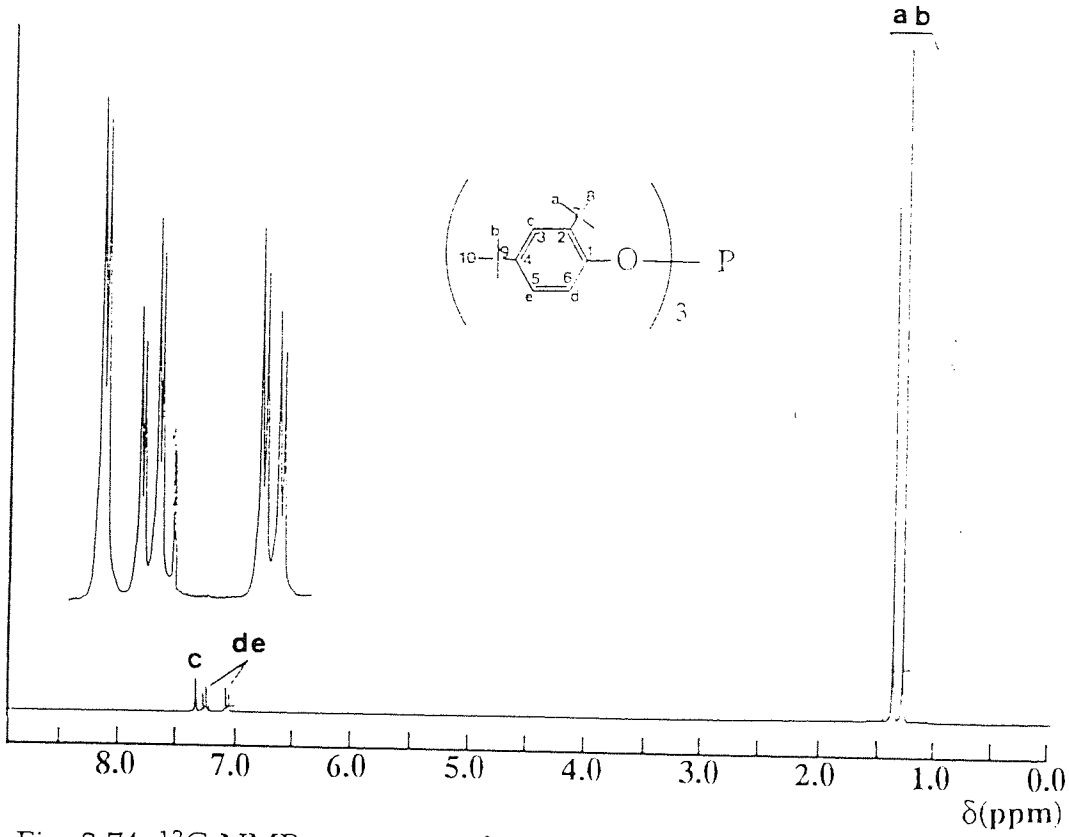

Fig. 2.74 ^{13}C-NMR spectrum of P168. (75.5MHz, in $CDCl_3$)

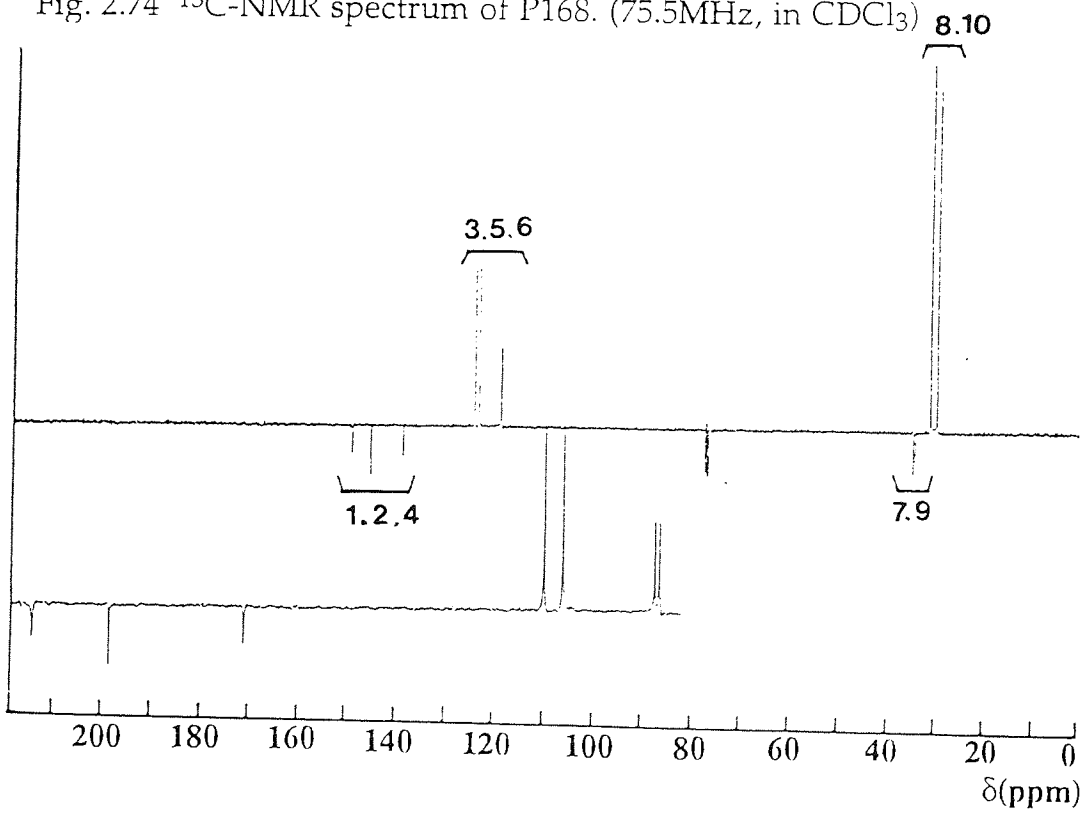

Fig. 2.75 ^{1}H-NMR spectrum of P626. (300MHz, in $CDCl_3$)

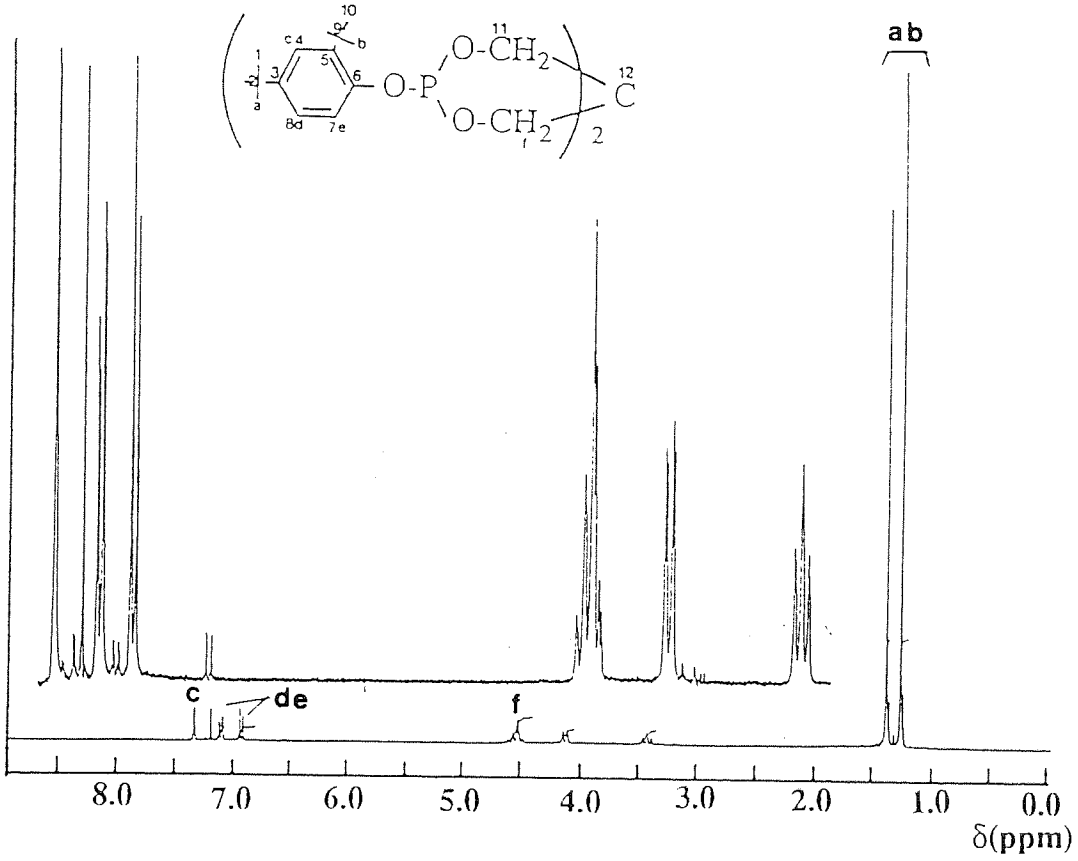

Fig. 2.76 ^{13}C-NMR spectrum of P626. (75.5MHz, in $CDCl_3$)

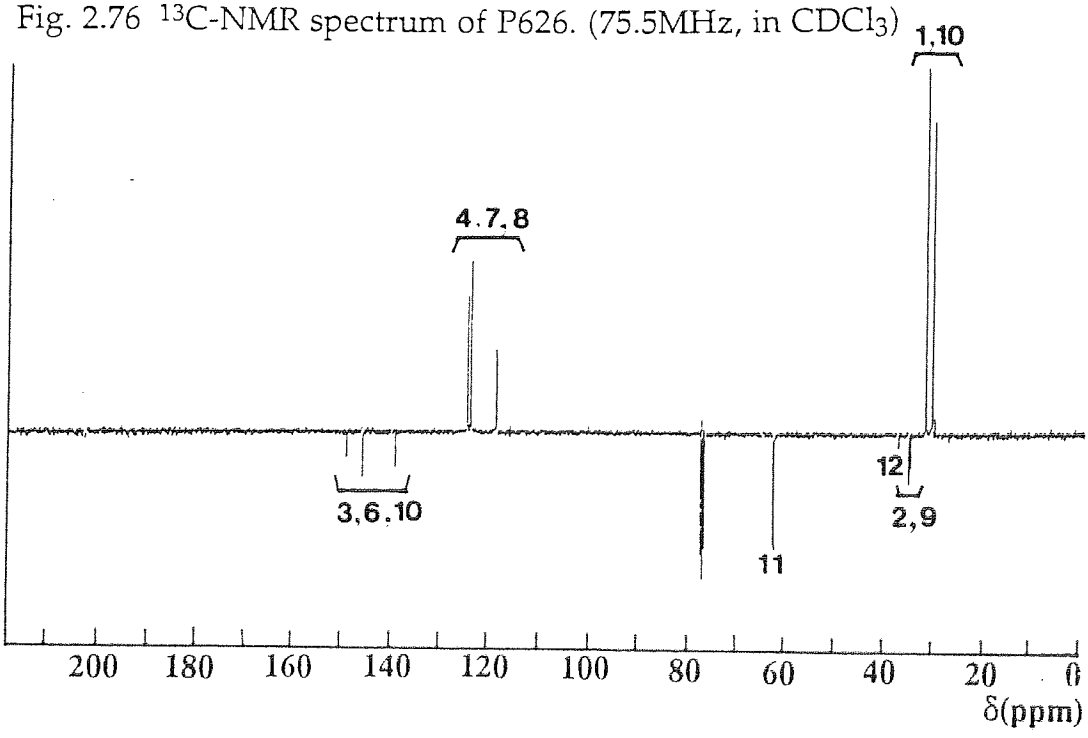

Chapter 3 The Effect of Antifatigue Agents on the Mechanical Properties of Natural Rubber

3.1 Object and Methodology

The effect of various compounds, which act by deactivating macroalkyl radicals, see table 3.1, on the fatigue resistance of sulphur cured NR was evaluated. Generally, rubbers subjected to fatigue are often also subjected to high temperatures, hence the effect of the above compounds on the thermal resistance of NR was also examined. The modification of the rubber mechanical properties caused by addition of these potential antifaigue agents was further investigated.

Quinones have been shown to act as chain breaking acceptor (CB-A) antioxidants[71], hence the compounds investigated as potential antifatigue agents (R· predominate under fatigue conditions) contain either quinonoid function or hindered phenol moiety (see table 3.1) which may lead to the formation of quinones during their antioxidant activity. In addition, diarylamines, such as IPPD and 6PPD, were evaluated for comparison. These amines are widely used as antifatigue agents as well as antioxidants. Their effectiveness has been shown to be due to the formation of nitroxyl radicals during their chain breaking (CB-D) activity [63) - 66)].

The overall methodology used in this work is described in scheme 3.1. It is mainly composed of three parts; (a) sample preparation, (b) physical tests for unvulcanised rubber, and (c) tests for vulcanised rubber. For the sample preparation, initially natural rubber (SMR-L) was masticated and then compounding ingredients (zinc oxide, stearic acid, accelerator and sulphur) and antifatigue agents were added on a roll mill. Finally, unvulcanised rubber sheets from the roll mill were placed on the preheated curing moulds and vulcanised to various type of test samples at 150°C. Before vulcanisation some of the unvulcanised rubber samples were used for physical tests of viscosity and

vulcanisation characteristics measurements. The viscosity was measured on a Mooney viscometer at 100°C (reflects the condition of compounding), while vulcanisation characteristics such as $t_{0.1}$, $t_{0.9}$, f_{min}, and f_{max} were measured on a Monsanto rheometer at 150°C. The vulcanisation speed will be represented by $t_{0.1}$ and $t_{0.9}$, where $t_{0.1}$ was used to examine the possibility of early undesirable vulcanisation (scorch) during processing and $t_{0.9}$ was used to determine the vulcanisation time for sample preparation (vulcanisation time = $1.5 \times t_{0.9}$). The maximum torque, f_{max}, would reflect the modulus of the vulcanised sample and was used to check if the correct extent of crosslinking was achieved. Finally, physical tests for the vulcanised rubber were carried out. These could be divided into two categories; fatigue resistance tests and thermal resistance tests. The tests for fatigue resistance could be subdivided into fatigue failure test and measurement of strain energy. Fatigue failure test was carried out under strain controlling condition (maximum strain was 91.2, 108, 142 and 160 %) at ambient temperature until test samples ruptured completely. Since all samples have slightly different modulus, strain energy was also measured from the stress-strain curve, see section 2.4.1.4, in order to adjust the effect of modulus. On the other hand, the tests for thermal resistance could be subdivided into measurement of crosslink density, chemical stress relaxation, and tensile tests before and after thermal ageing using single cell ovens. The crosslink density was obtained from the intercept of the Mooney-Rivlin plots, see section 2.4.1.3, and was used for the evaluation of chemical stress relaxation results. Even though the same number of chain scission occurs, the rate of chemical stress relaxation will be different for the samples which have different crosslink density. The rate of chain scission reaction was calculated from chemical stress relaxation and crosslink density results. Tensile tests were carried out before and after thermal ageing in Wallace oven and retention of characteristic values for sample strength; elongation at break (Eb) and tensile strength (Tb) were measured. In this way, thermal resistance was evaluated

by two procedures; measurement of chain scission rate, and retention of Eb and Tb during thermal ageing at various temperatures.

Table 3.1 Evaluated compounds as potential antifatigue agents.

	Code	Structure	M.w.	m.p. (°C)
Quinones	BQ	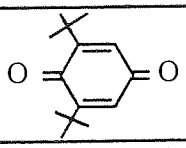	220	66 - 68
	DPQ	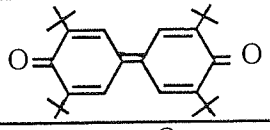	409	246 - 249
	NQ	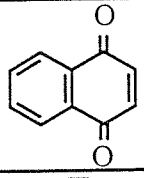	158	118 - 121
	PDO	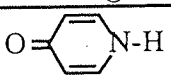	95	136 - 140
Phenols	HBA	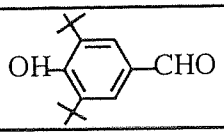	234	189 - 193
	αTOC	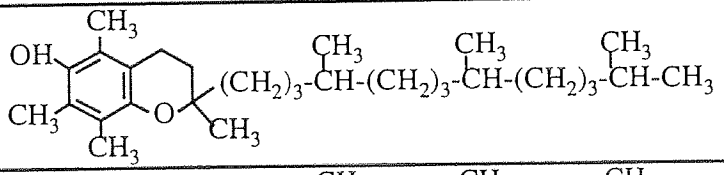	431	oily liquid at room temp.
	γTOC	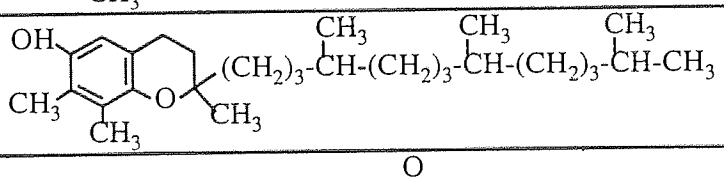	417	oily liquid at room temp.
	GM	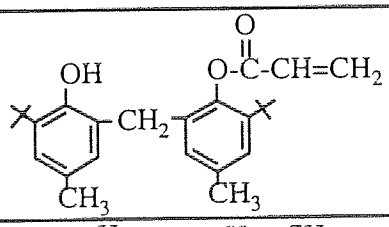	395	130 - 132
Amines	IPPD	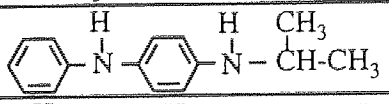	226	75 - 77
	6PPD		268	48 - 50

Scheme 3.1 Experimental flow chart for the preparation of NR samples and physical tests used to assess the performance of compounds used as potential antifatigue agents.

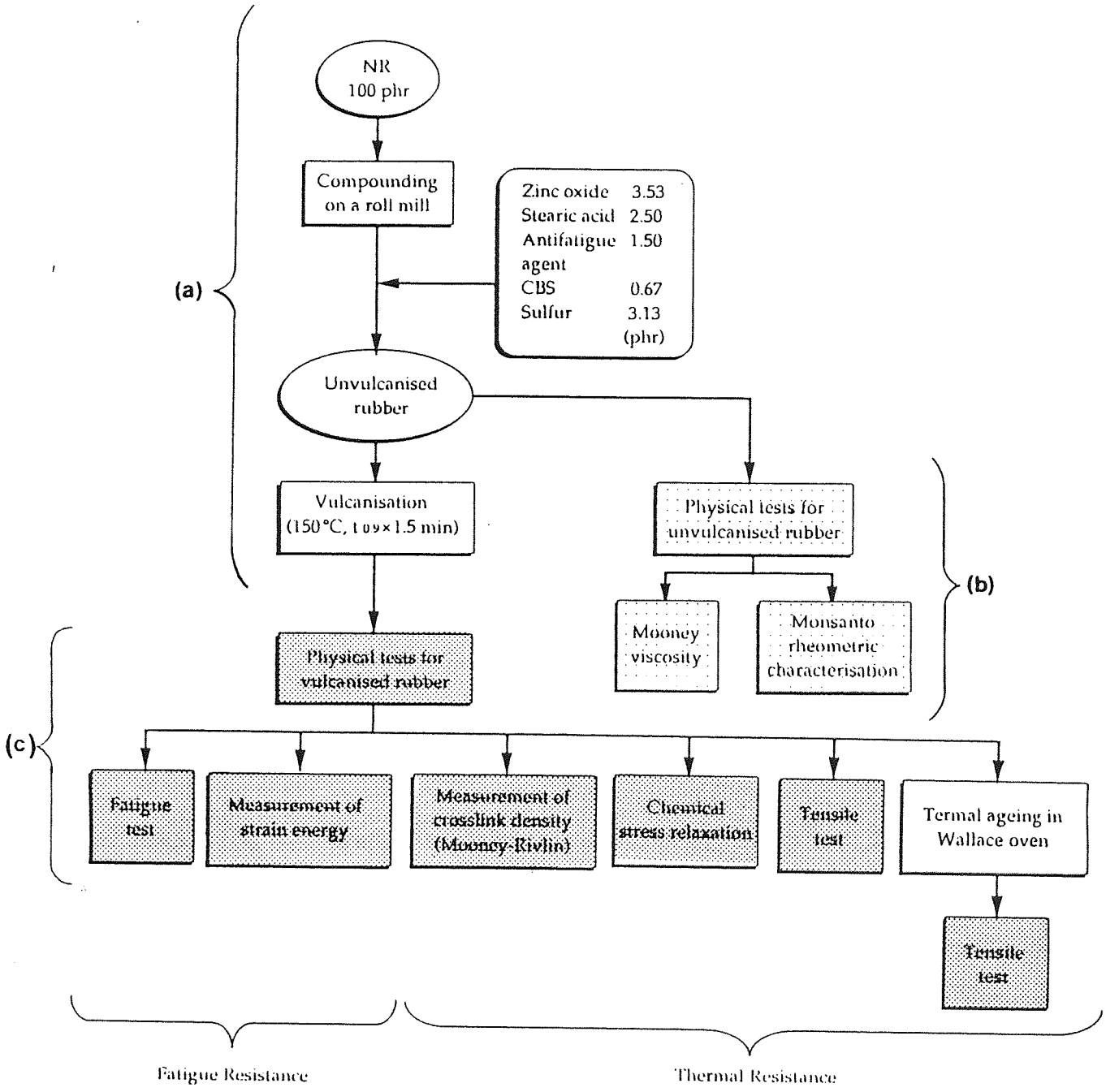

3.2 Results

3.2.1 Unvulcanised Properties

Results of physical tests for unvulcanised rubber are summarised in table 3.2 and rheometer curves are illustrated in fig. 3.1.

Table 3.2 Summary of physical tests for unvulcanised rubber compounded in presence of antifatigue agents. (1.5phr)

Code		Mooney	Monsanto Rheometer Characterisation (150°C)			
		Viscosity ML(1+4),100°C	f_{min} (dN·m)	f_{max} (dN·m)	$t_{0.1}$ (min)	$t_{0.9}$ (min)
Blank		11.4	3.0	41.2	6.1	13.3
Quinones	BQ	17.7	7.0	38.9	5.3	12.8
	DPQ	17.7	6.5	37.2	6.8	14.5
	NQ	18.5	6.4	37.0	4.4	12.2
	PDO	13.8	2.9	30.2	3.9	12.4
Phenols	HBA	14.4	6.1	39.7	7.2	14.4
	αTOC	13.7	7.7	45.6	5.6	12.9
	γTOC	9.2	6.4	40.3	7.3	14.2
	GM	14.8	7.1	43.0	7.4	15.7
Amines	IPPD	20.5	5.2	43.0	5.8	13.6
	6PPD	22.5	6.1	44.2	6.6	14.0

Although none of the antifatigue agents examined, except for PDO, affected the vulcanisation characteristics drastically, quinones showed slight decrease of maximum torque and vulcanisation speed was not affected seriously by these antifatigue agents. Among all evaluated antifatigue agents, amines showed least effect on the vulcanisation characteristics when compared to the blank (containing no antifatigue agent), see fig. 3.1.

Fig. 3.1 Rheometer curves of NR samples containing different antifatigue agents. (at 150°C)

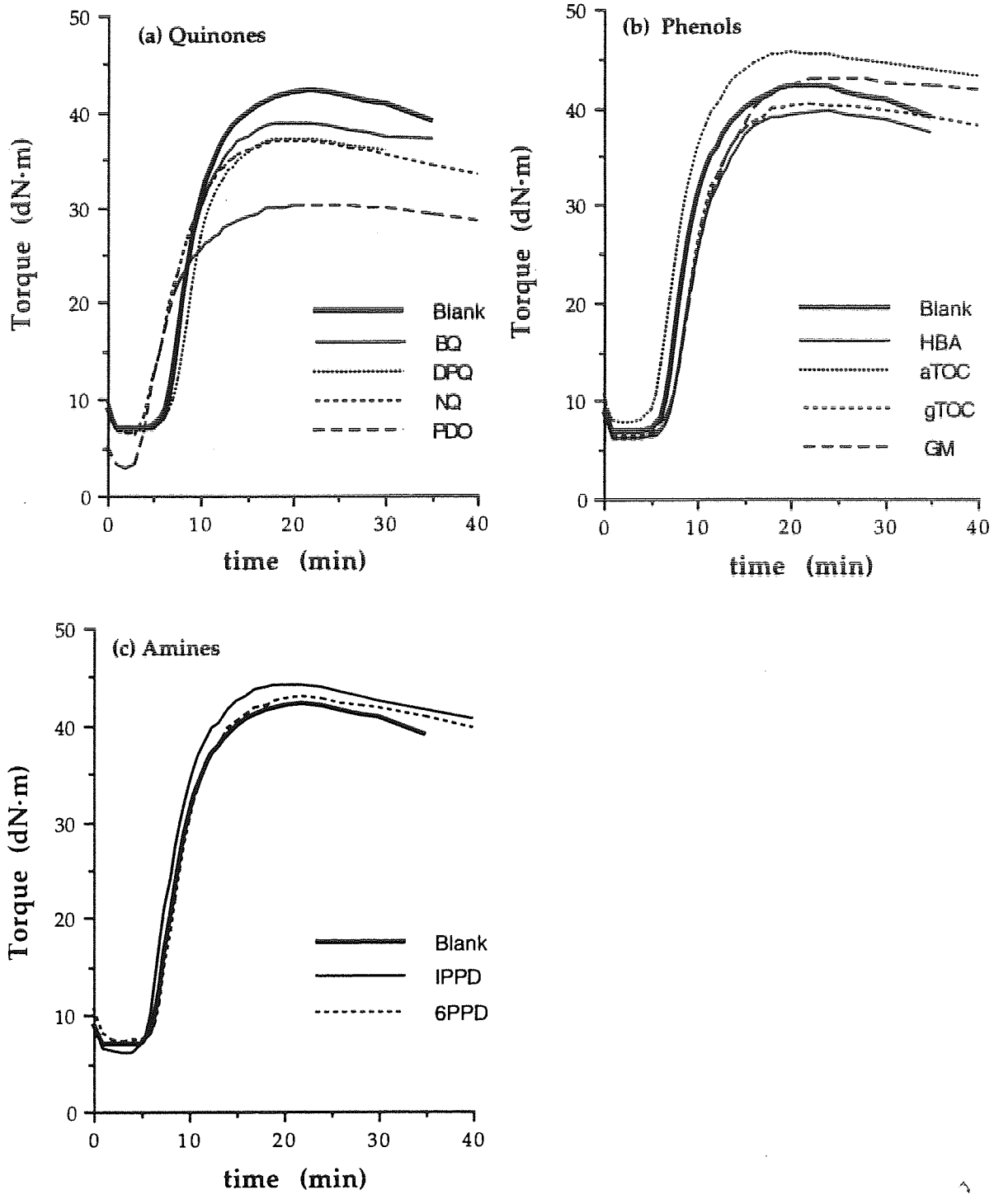

3.2.2 Fatigue Resistance

Fatigue life has generally wide distribution, even though fatigue samples were prepared with special care and testing conditions were precisely controlled; however, it is difficult to have a large number of fatigue tests for every sample. Hence the mean value of fatigue life was calculated based on the hypothesis of binominal distribution. As mentioned in chapter 2, see section 2.4.3, it was calculated in the following way;

$$\textbf{mean fatigue life} = 0.5A + 0.3B + 0.1C + 0.1D \qquad (A > B > C > D) \qquad (1)$$

where A, B, C, and D are fatigue lives. Before using this equation, the real fatigue failure distribution of the Blank, αTOC, and 6PPD samples were confirmed as pre-tests. A number of fatigue test pieces were prepared carefully so as not to have any flaws, dirt particles, and moulding defects and were tested under the same conditions. The results are summarised in table 3.3 - 3.5 (at the end of this chapter) and are illustrated in fig. 3.2.

Figure 3.2 shows that these experimental values fit on the theoretical curve of binominal distribution, hence the procedure for estimating the average fatigue life seems to be acceptable. However, the average fatigue lives calculated by equation (1) showed higher values compared with theoretical fatigue lives, see fig. 3.3 and table 3.6. A sample with longer fatigue life has a wider distribution and larger systematic errors. For these reasons, the small differences in fatigue life (less than 30%) will not be particularly mentioned in this thesis. Besides the ruptured cuts, failed samples had a number of small or medium flaws which appeared from a relatively early stage of fatiguing though those appearing first did not always propagate to failure.

Fig. 3.2 Cumulative probability of fatigue failures of NR.

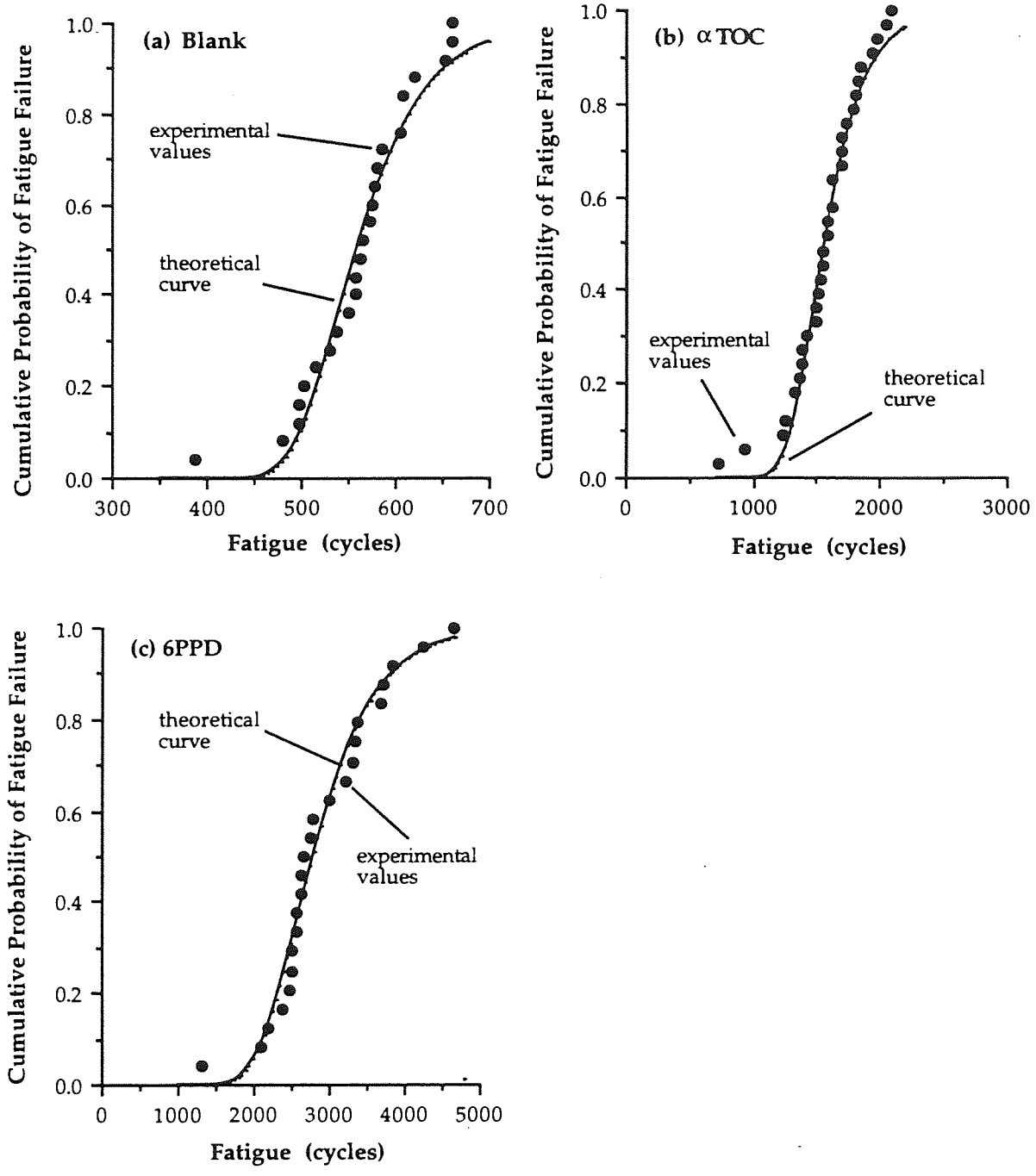

Fig. 3.3 Probability density of fatigue failure of NR in the absence and presence of 1.5 phr of antifatigue agents.

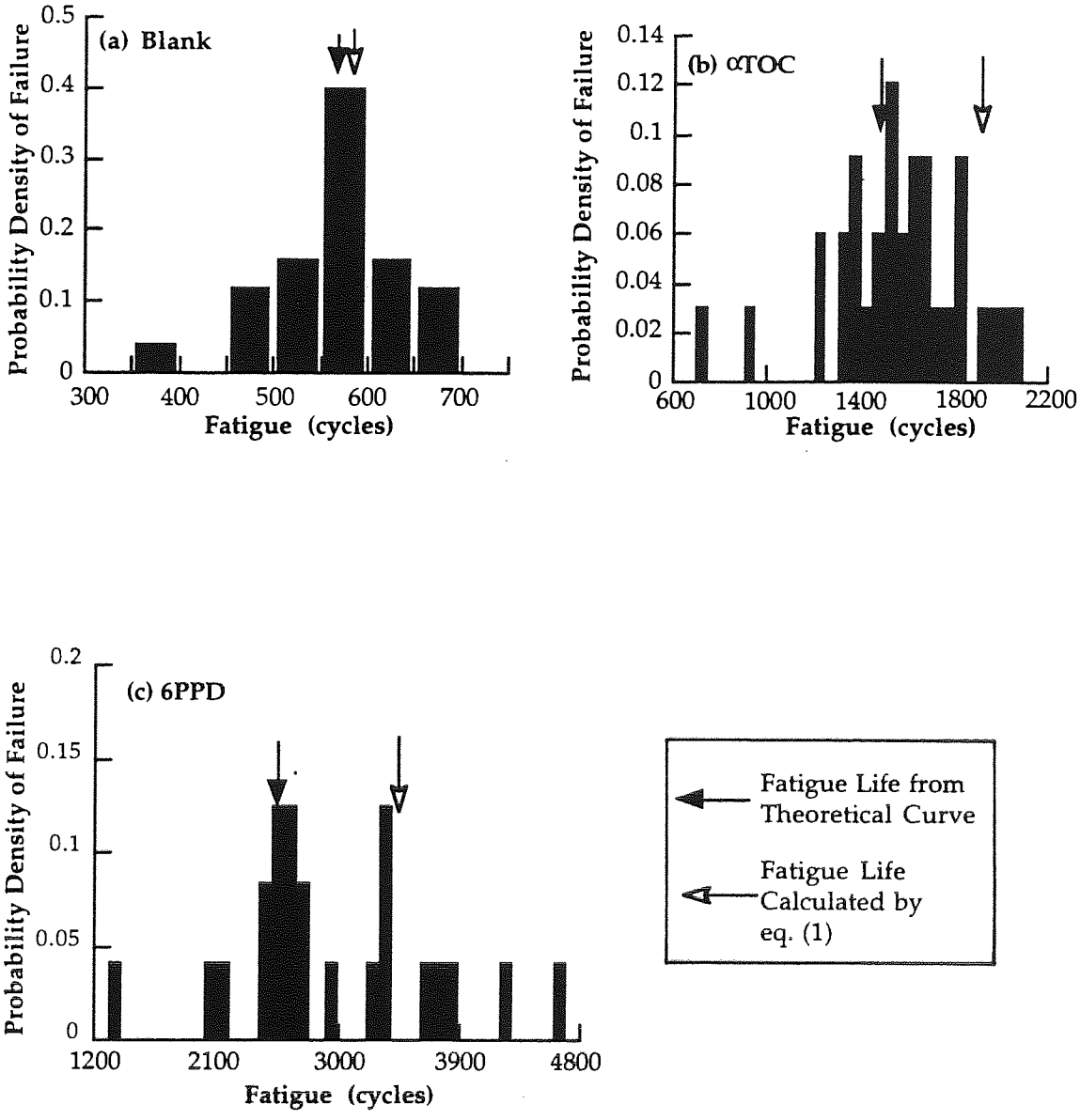

Table 3.6 Systematic errors in fatigue lives.

Sample	Fatigue Life Calculated by Eq. (1) (cycles)	Fatigue Life from Theoretical Curve (cycles)	Error (%)
Blank	58600	54032	+8
αTOC	187600	147080	+22
6PPD	348530	258420	+26

The fatigue lives of NR samples containing the different antifatigue agents are summarised in table 3.7 (at the end of this chapter). Since each sample has a slightly different modulus, the strain energy was measured in order to eliminate the effects of the differences in crosslink density. Fatigue life calculated by eq. (1) and the maximum (A in eq. 1) and minimum (D) are also shown. These results are illustrated in fig. 3.4.

Among all evaluated antifatigue agents, conventional antifatigue agents, amines, showed the best fatigue resistance. In the quinones group, only BQ showed a competitive performance; PDO decreased fatigue resistance rather than increased it. All phenols showed improved fatigue resistance. In this group, αTOC and GM showed a competitive performance. GM is known to trap macroalkyl radicals directly, whereas all other phenols are expected to produce quinonoid compound during processing and in service. The nature of transformation products formed from these phenols will be discussed later.

Fig. 3.4 Fatigue resistance of NR samples containing antifatigue agents. (1.5phr)

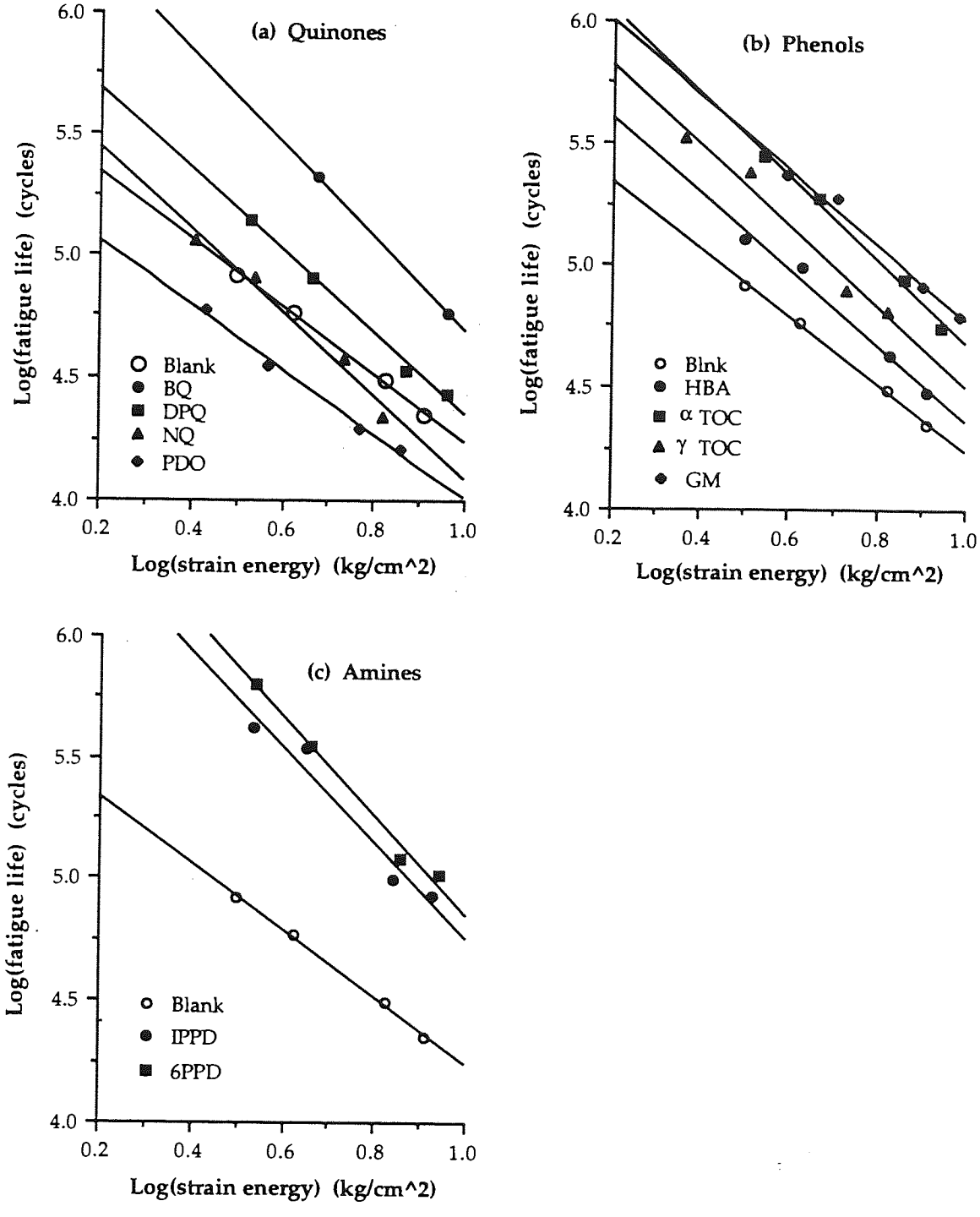

3.2.3 Thermal Resistance

As mentioned before, thermal resistance of NR samples containing antifatigue agents was evaluated in two ways; chemical stress relaxation, and tensile tests before and after thermal ageing of the samples at various temperatures (70, 100, 120°C). Table 3.8 shows the results of chemical stress relaxation and measurement of crosslink density from Mooney-Rivlin plots. Chemical stress relaxation of PDO failed due to rapid sample deterioration.

Table 3.8 Summary of chemical stress relaxation and Mooney-Rivlin curves of NR samples containing antifatigue agents (1.5phr).

Sample		Stress Relaxation (at 100°C)		Mooney-Rivlin Curve		
		$k \times 10^2$ (1/hr)	$q_m \times 10^6$ (mol/ml·hr)	$\upsilon_e \times 10^4$ (mol/ml)	$2C_1$ (N/mm^2)	$2C_2$ (N/mm^2)
	Blank	2.00	2.32	1.15	0.287	0.165
Quinones	BQ	4.76	6.32	1.33	0.329	0.174
	DPQ	0.88	1.27	1.44	0.357	0.130
	NQ	2.49	2.33	0.94	0.232	0.139
	PDO			1.05	0.261	0.147
Phenols	HBA	5.29	5.74	1.08	0.269	0.209
	αTOC	4.02	4.85	1.21	0.299	0.194
	γTOC	2.28	2.56	1.12	0.279	0.100
	GM	1.40	1.35	0.96	0.238	0.327
Amines	IPPD	0.63	0.63	1.01	0.250	0.266
	6PPD	0.59	0.67	1.14	0.282	0.222

Crosslink density was obtained from the stress-strain measurement of the rubber samples with slow extension speed (1 mm/min). When reciprocal strain ($1/\lambda$) vs reduced stress $\{\sigma/(\lambda - \lambda^{-2})\}$ was plotted, its intercept gives the crosslink density, see section 2.4.1.3.

$$\sigma = 2C_1(\lambda - \lambda^{-2}) + 2C_2(1/\lambda) \qquad (2)$$

$$\sigma/(\lambda - \lambda^{-2}) = 2C_1 + 2C_2(1/\lambda) \qquad (3)$$

$$2C_1 = \upsilon_e RT \qquad (4)$$

where σ is stress, λ is strain, R is gas constant, T is absolute temperature, υ_e is crosslink density, and C_1, C_2 are constants. Typical example of Mooney -Rivlin plots is shown in fig. 3.5. From the linear part, the slope ($2C_2$) and intercept ($2C_1$) were calculated. The reduced stress of the rest of the samples were summarised in table 3.9. (at the end of this chapter)

Fig. 3.5 Typical example of Mooney-Rivlin plots.

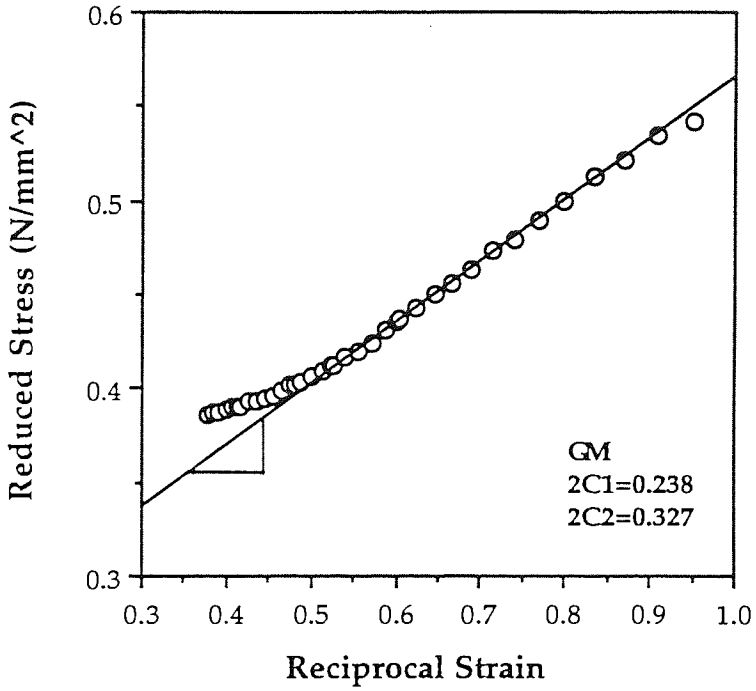

The results of Chemical stress relaxation are summarised in table 3.10 (at the end of this chapter) and are illustrated in fig. 3.6.

Fig. 3.6 Chemical stress relaxation of NR samples containing antifatigue agents. (at 100°C)

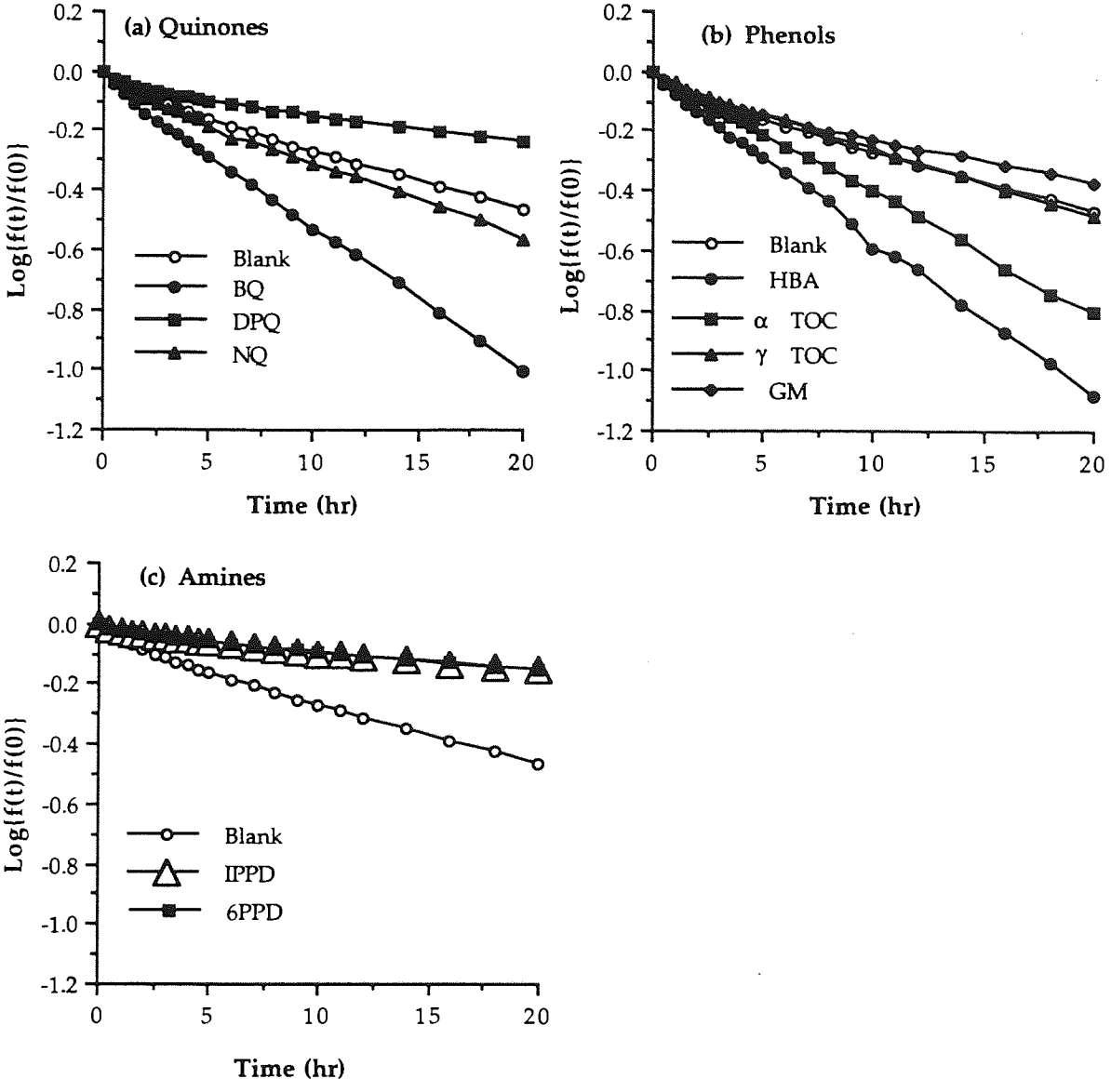

Meanwhile tensile tests results before and after thermal ageing were shown in tables 3.11 and 3.12, and the retention of Eb and Tb were illustrated in figures 3.7 - 3.9.

Fig. 3.7 Eb and Tb retention during thermal ageing of NR samples containing antifatigue agents at 70°C.

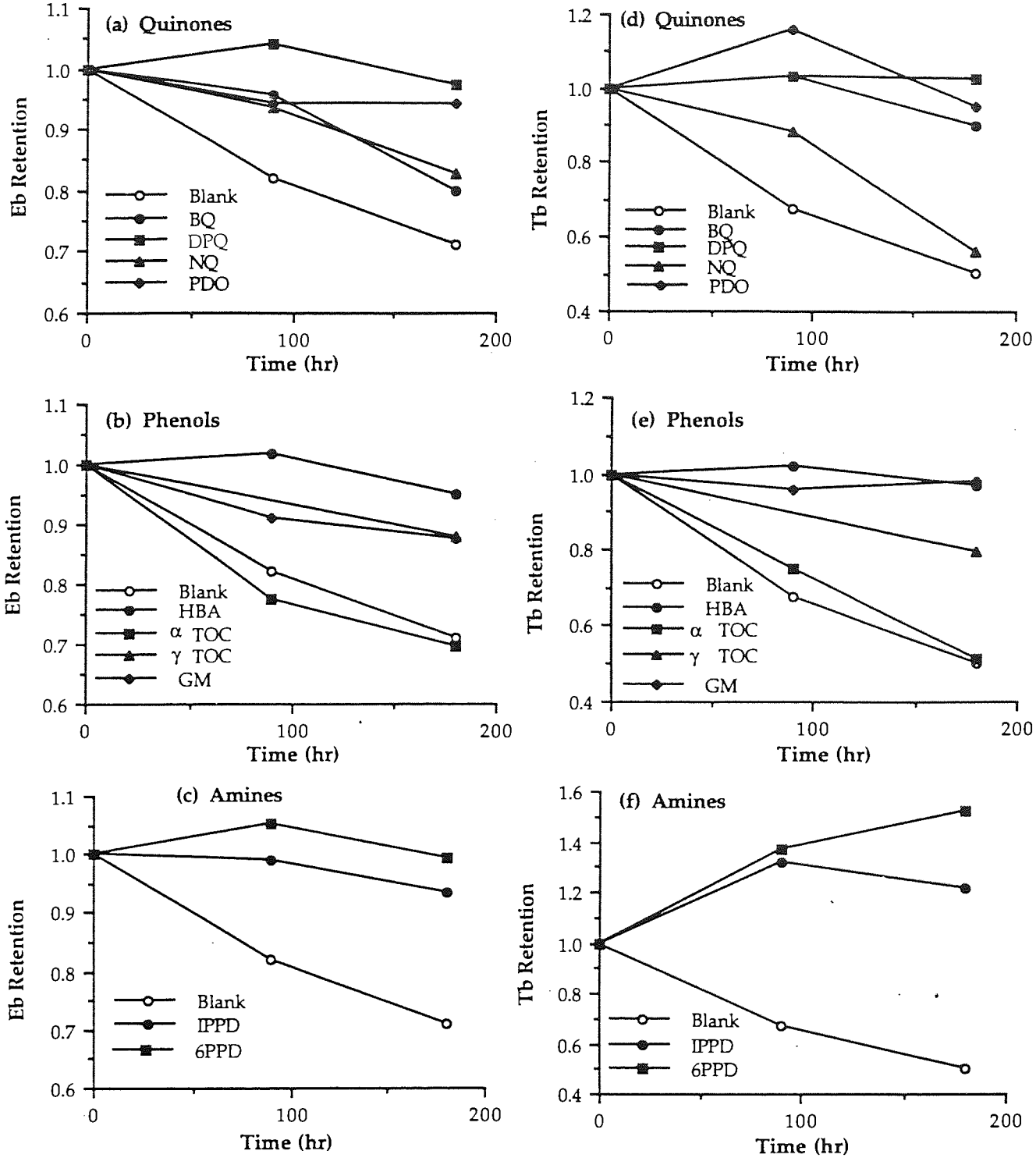

Fig. 3.8 Eb and Tb retention during thermal ageing of NR samples containing antifatigue agents at 100°C.

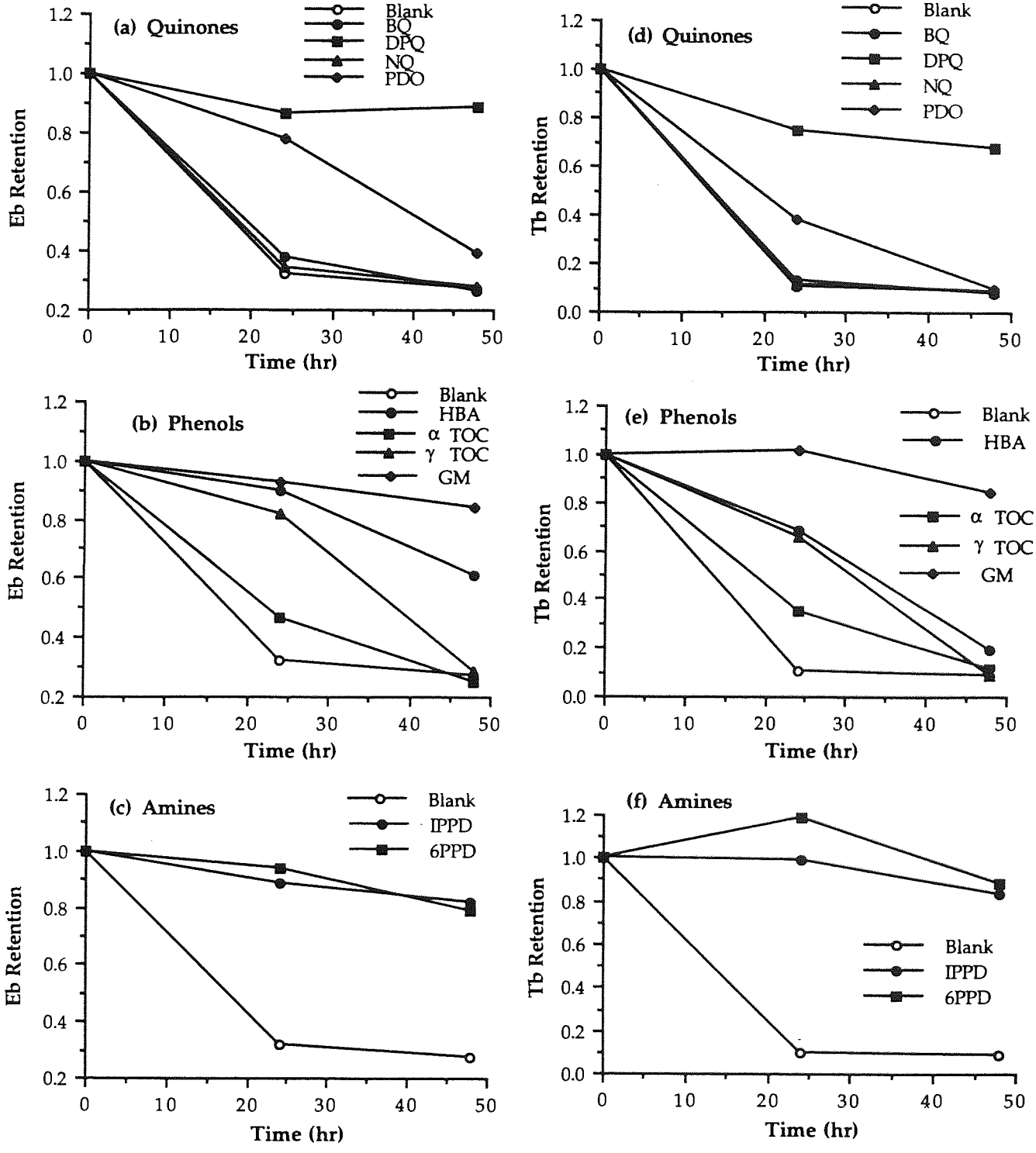

Fig. 3.9 Eb and Tb retention during thermal ageing of NR samples containing antifatigue agents at 120°C.

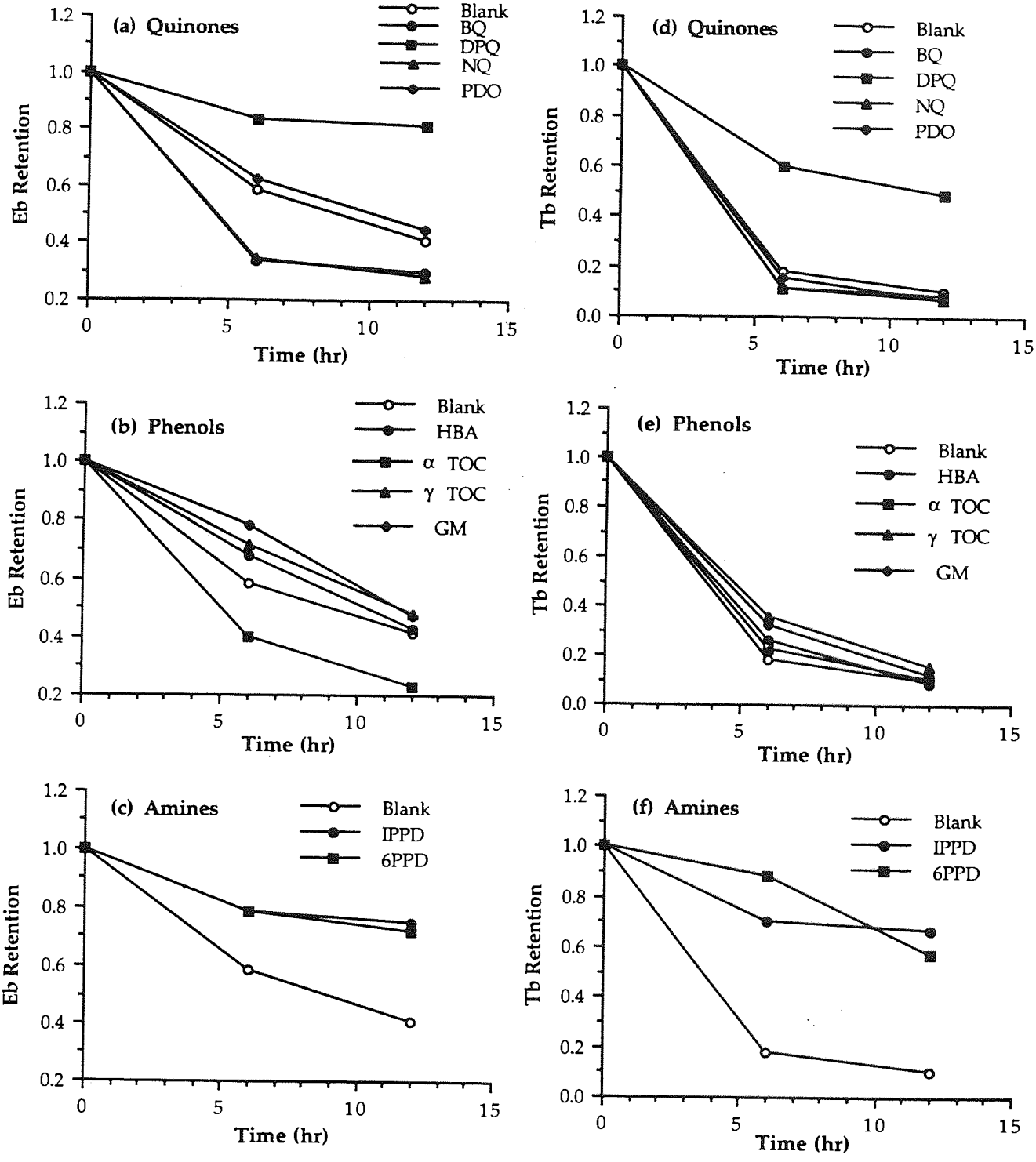

Fig. 3.10 Image illustration of various thermal degradation tests result

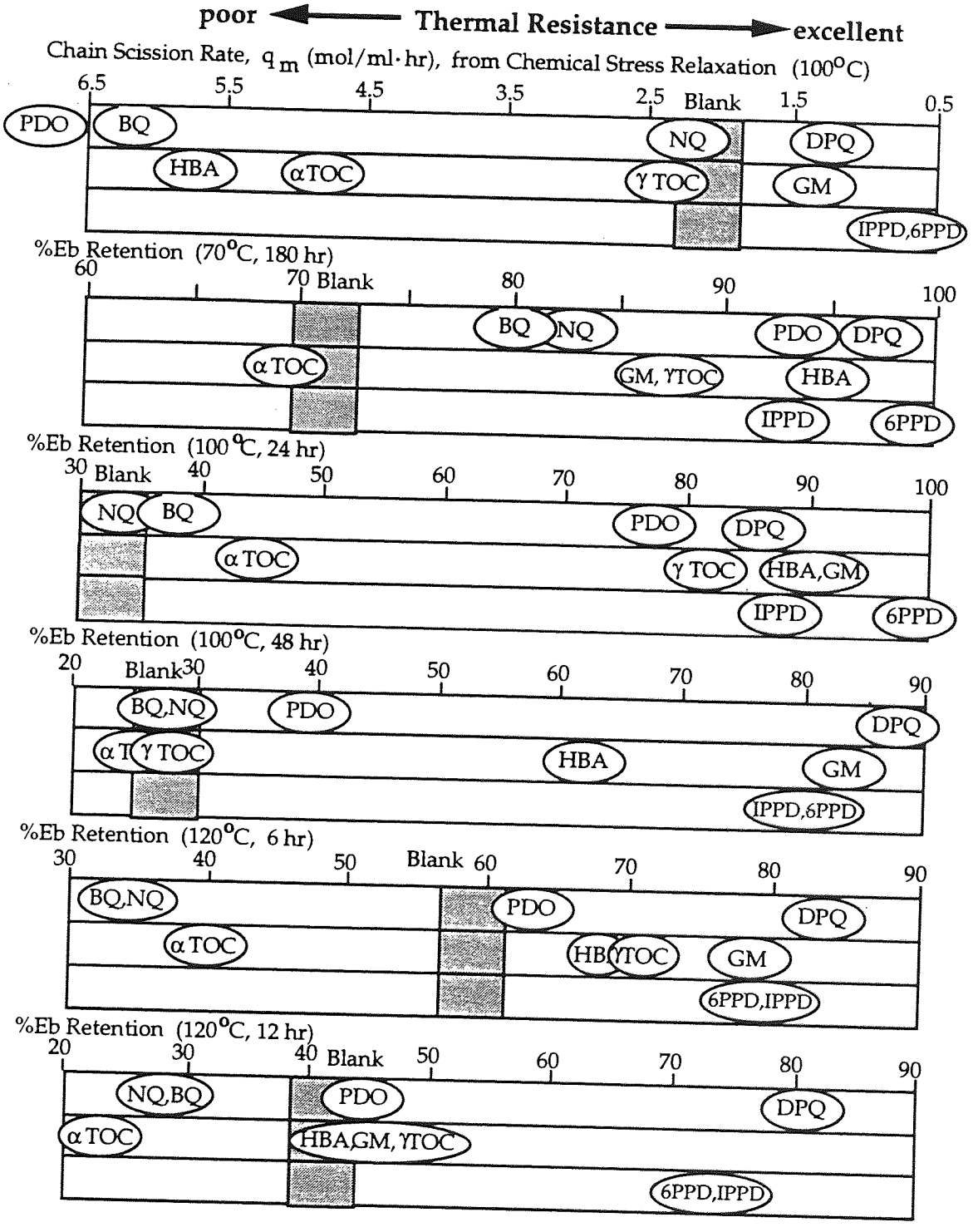

Thermal resistance was evaluated in two different ways, (chemical stress relaxation and tensile tests) and the tensile tests (Eb and Tb) were measured at three different temperatures. Figure 3.10 shows simple image illustration of the thermal resistance so as to compare the effectiveness of the quinones, phenols and amines (separated into three rows in the figure) examined.

The effectiveness of these compounds towards thermoxidative degradation resistance can be categorised into five groups; (1) compounds which showed excellent thermal resistance under all conditions are DPQ, GM, IPPD, 6PPD , (2) compounds which demonstrated worse stress relaxation results compared with tensile tests result are PDO, HBA, (3) compounds which have worse thermal resistance at high temperature compared to low temperature are PDO, HBA, (4) a compound which has lower thermal resistance at longer times ; γTOC, (5) compounds which showed poor thermal resistance under all conditions are BQ, NQ, αTOC.

3.3 Discussion

3.3.1 Fatigue Resistance

3.3.1.1 The Action of Quinones as Antifatigue Agents

The evaluated quinones should act by deactivating macroalkyl radicals which produced mechanically during the fatiguing process, and hence they were expected to act as antifatigue agents. The experimental results however, showed that only BQ and DPQ worked effectively as antifatigue agents, see fig. 3.4.

In order to estimate the reaction scheme of these compounds with radicals, the reactivity index of each compound with isoprene radical (monomer) was calculated using LCAO coefficients obtained from the MOPAC ver. 5.02 calculation with the PM3 method. Normally, in a molecular reaction, electrophilic reaction will occur at the atom which has the highest electron density of the two electrons in the highest occupied molecular orbital (HOMO), while a nucleophilic reaction will occur at the atom which has the highest electron density of the two electrons in the lowest unoccupied molecular orbital (LUMO)[110]. In the case of radical reaction, it will occur at the atom which has the highest sum of the electron density of one electron in HOMO and one electron in LUMO[110], see fig. 3.11. Frontier electron density can be calculated using eq. (5) - (7), see fig. 3.11[110].

$$f_r^{E} = 2(C_{HOMO,r})^2 \qquad (5)$$

$$f_r^{N} = 2(C_{LUMO,r})^2 \qquad (6)$$

$$f_r^{R} = (C_{HOMO,r})^2 + (C_{HOMO,r})^2 \qquad (7)$$

where C is LCAO (linear Combination Atomic Orbital) coefficient and r is an orbital number.

Fig. 3.11 Frontier orbitals for electrophilic, nucleophilic and radical reactions 110).

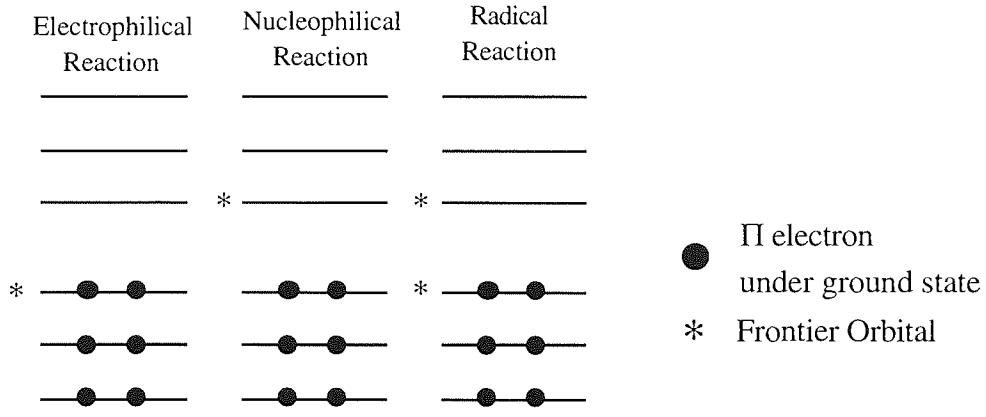

Fujimoto et.al[111] suggested the calculation method of the reactivity index for sizeable molecules. In this theory, not only the extent of HOMO and LUMO, but also their phase changes by interference of orbitals were taken into account in the reactivity index. This method was applied in this work. The details of calculation of reactivity index was as follows;

$$\text{Reactivity Index} = 1/(\lambda_{\mathbf{A}unoc} - \lambda_{\mathbf{B}oc}) + 1/(\lambda_{\mathbf{B}unoc} - \lambda_{\mathbf{A}oc}) \qquad (8)$$

$$\lambda_{oc} = \sum_{i=1}^{HOMO} 2C_{s,i}{}^2\varepsilon_i / q_s \qquad (9)$$

$$\lambda_{unoc} = \sum_{j=LUMO}^{end} 2C_{s,j}{}^2\varepsilon_j / q_s \qquad (10)$$

where A and B were reagent and reactant molecules, λ_{oc} is electron-donating ability, λ_{unoc} is electron-accepting ability, $C_{s,i}$ is LCAO coefficient, ε_i is orbital energy, and q_s is electron density. The LCAO coefficients were calculated by MOPAC ver. 5.02 using PM3 method. Table 3.13 shows the reactivity index of BQ with isoprene monomer radical.

Table 3.13 Reactivity indices of BQ for radical reaction with isoprene monomer radical.

Antifatigue Agent	Orbital	λ_{oc}	λ_{unoc}	Reactivity Index
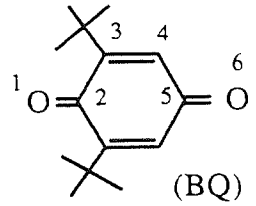 (BQ)	1	-14.5232	-0.0506	0.1494
	2	-15.2653	0.7133	0.1412
	3	-12.4582	0.1022	0.1571
	4	-11.7827	-0.0169	**0.1615**
	5	-14.9148	1.4102	0.1379
	6	-13.9059	0.0499	0.1510

The atom which has the highest reactivity is the carbon No.4; therefore, alkyl radical may be assumed to react mainly on this site and to produce a stable phenoxyl radical (see scheme 3.2 a). This phenoxyl radical will either disproportionate (see scheme 3.2 b) or recombine with other alkyl radicals to produce phenols and olefin (see scheme 3.2 c). According to this, the expected reaction mechanism the antifatigue activity of BQ is shown in scheme 3.2.

Scheme 3.2 Expected reaction mechanism of BQ with alkyl radical.

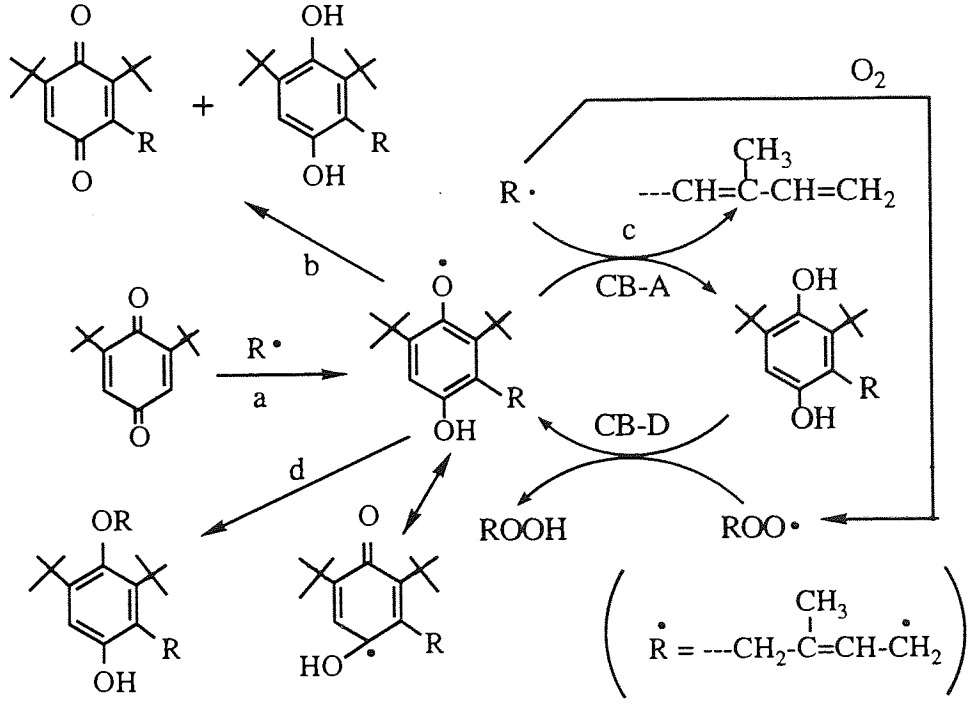

In a similar way, the reactivity indices for other quinones were calculated. Table 3.14 shows the results for DPQ.

Table 3.14 Reactivity indices of DPQ for radical reaction with isoprene monomer radical.

Antifatigue Agent	Orbital	λ_{oc}	λ_{unoc}	Reactivity Index
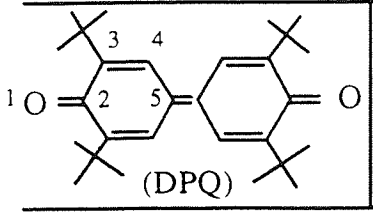 (DPQ)	1	-13.9376	0.1057	0.1505
	2	-14.7449	1.0190	0.1410
	3	-12.0673	0.4452	0.1566
	4	-11.5127	0.2453	**0.1611**
	5	-12.7856	0.5578	0.1522

In the case of DPQ, the carbon No.4 has the highest reactivity index and this seems to be the most reactive site. Alkyl radicals are therefore, likely to react on this site (scheme 3.3 a), then either dispropionate (scheme 3.3 b) or further recombine with other alkyl radicals to produce phenols and olefin (scheme 3.3 d and c). The reaction scheme of DPQ with alkyl radicals is similar to that of BQ.

Scheme 3.3 Expected reaction mechanism of DPQ with alkyl radical.

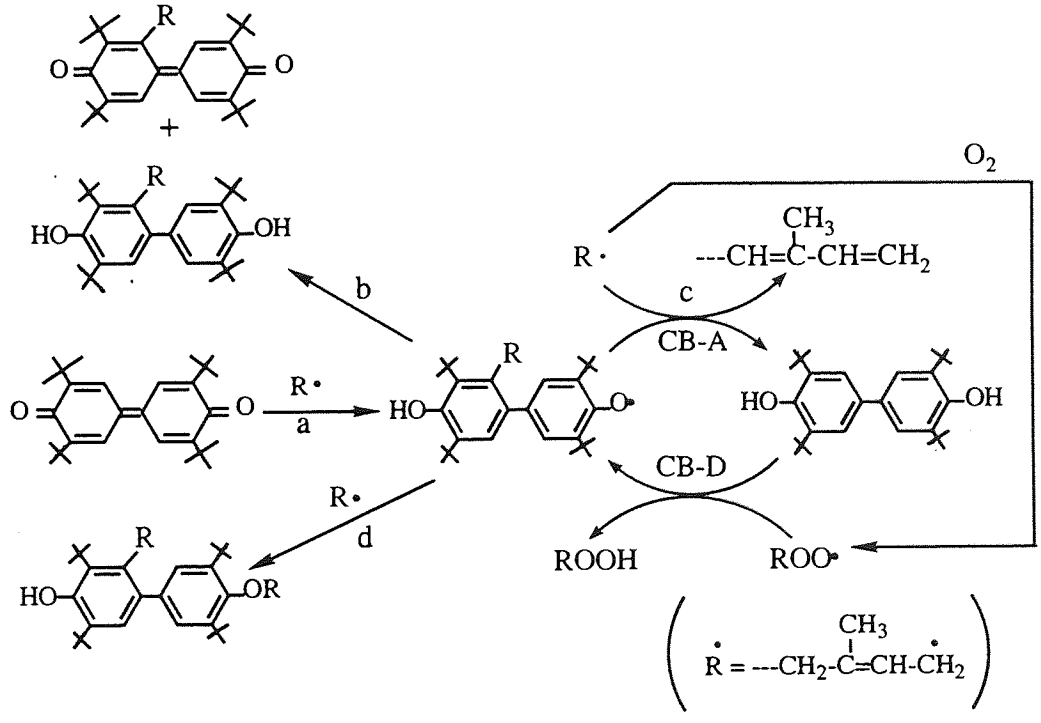

Table 3.15 shows the results of calculation for the NQ for a radical reaction. The carbon atom No.2 seemed to be the most reactive. The expected reaction mechanism for NQ with alkyl radicals is shown in scheme 3.4.

Table 3.15 Reactivity indices of NQ for radical reaction with isoprene monomer radical.

Antifatigue Agent	Orbital	λ_{oc}	λ_{unoc}	Reactivity Index
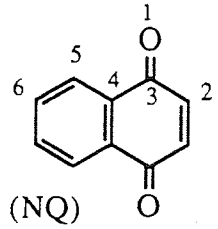 (NQ)	1	-15.7471	-1.0712	0.1538
	2	-11.4280	-0.0367	**0.1637**
	3	-16.4563	2.9448	0.1245
	4	-12.1248	0.9096	0.1531
	5	-11.3152	0.9623	0.1572
	6	-11.8100	1.0972	0.1536

Scheme 3.4 Expected reaction mechanism of NQ with alkyl radical.

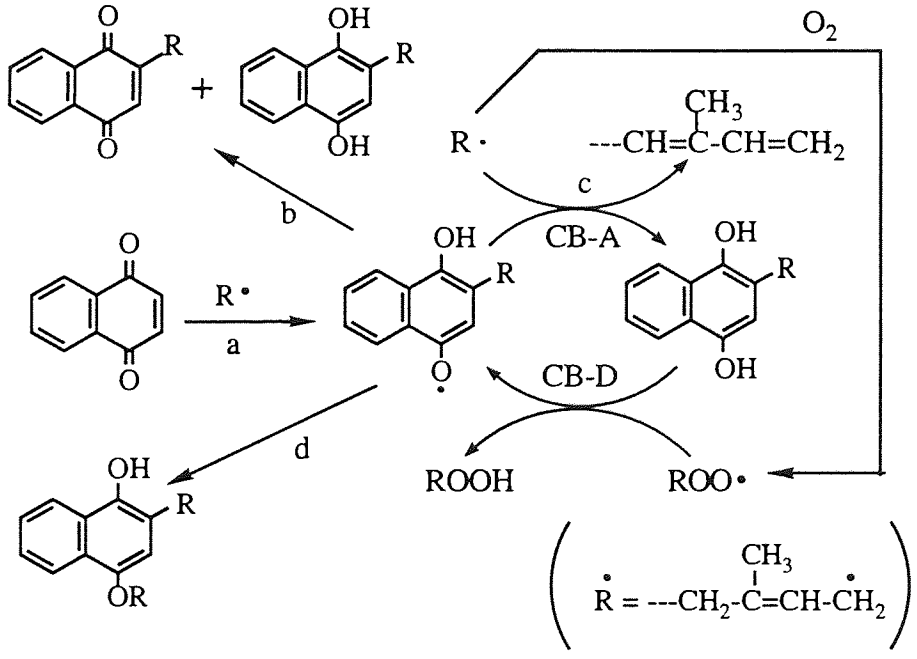

The Fatigue test results of PDO was very poor (worse than Blank), see fig.3.4 (a) which could suggest the possibility of its reaction by a different mechanism compared to the other quinones.

3.3.1.2 The Action of Phenols as Antifatigue Agents.

Although phenols themselves, except for GM, are not able to trap macroalkyl radicals directly, they are known to produce quinones during processing, curing and in service. The formed quinones could then deactivate macroalkyl radicals generated mechanically during fatiguing.

HBA is expected to produce quinonoid compound as shown below;

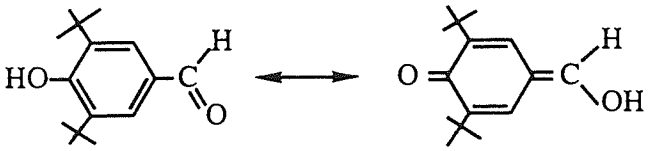

(HBA) (HBA')

and HBA' hence was considered to act by trapping alkyl radicals in a similar way to the action of quinones. The reactivity index of HBA' for a radical reaction was also calculated, see table 3.16, and the expected reaction mechanism is shown in scheme 3.5.

Table 3.16 Reactivity indices of HBA' for radical reaction with isoprene monomer radical.

Antifatigue Agent	Orbital	λ_{oc}	λ_{unoc}	Reactivity Index
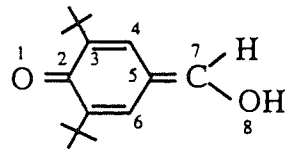	1	-13.4335	0.4174	0.1503
	2	-14.3198	2.451	0.1344
	3	-11.3679	0.9699	0.1569
	4	-11.1992	0.7400	**0.1594**
	5	-11.5118	1.0756	0.1553
	6	-10.9544	0.9399	**0.1595**
	7	-14.0915	0.7488	0.1453
	8	-16.7141	0.7658	0.1362

Scheme 3.5 Expected reaction mechanism of HBA with alkyl radical.

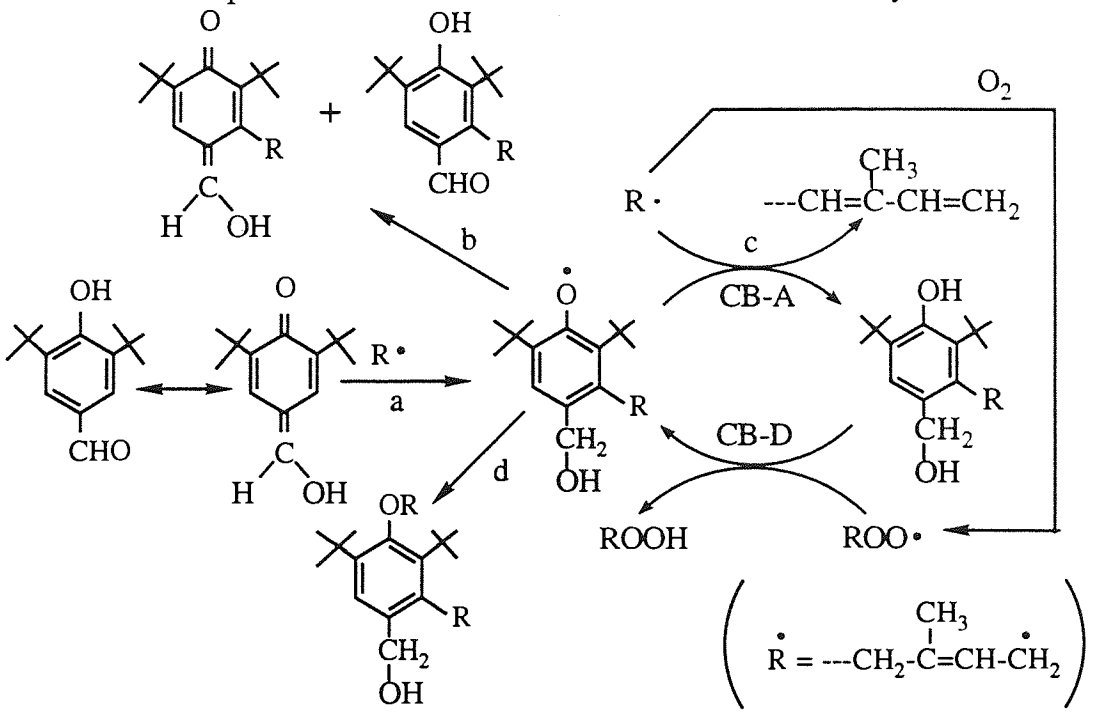

Tocopherols were also expected to produce quinonoid compounds during their oxidation. Many oxidation mechanisms of tocopherols have been reported previously [112)-116)] . Although α- and γ-tocopherols are similar structure, their possible dimers are different and known to be produced via different reaction scheme[112) 117)]. In all the previous publication[112)-116)], the first step of oxidation mechanisms of tocopherols is the removal of phenolic hydrogen with formation of phenoxyl radicals. According to Nilsson[112)], the order of stability of these phenolic radicals depends on the number and orientation of ring substituents, and was observed to be in order, αTOC > γTOC. This differences in reactivity reflects the differences in reaction mechanisms. The phenoxyl radicals will then react in two different ways; (1) phenoxyl radicals rearrange to benzyl radicals followed by coupling (αTOC), (2) two phenoxyl radicals couple through oxygen or ortho position (γTOC), see schemes 3.6 - 3.9 [112) 117)]. Scheme 3.6 shows the oxidation mechanisms of αTOC proposed by Fujimaki (modification of Nilsson' s mechanism). In addition, Winterle

reported the formation of A2 (see table 3.17) and spiro dimer (A5) at higher concentration, and the formation of peroxy ketal (A7) at lower concentration. Schemes 3.7 and 3.8 show the proposed pathways to form A2 and A7 during oxidation of αTOC. Scheme 3.9 shows the oxidation mechanism of γTOC reported by Gottstein [117]. The possible oxidation products from αTOC and γTOC are summarised in table 3.17. (labelled A1 - A7, and G1 - G3) Among these compounds, A2, A3, A5, A7, and G1 are quinonoid compounds and seemed to have the potential of acting as antifatigue agents.

Table 3.17 Expected oxidation products from αTOC and γTOC.

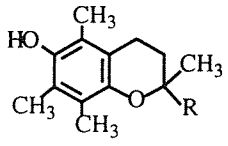 α-Tocopherol (αTOC)	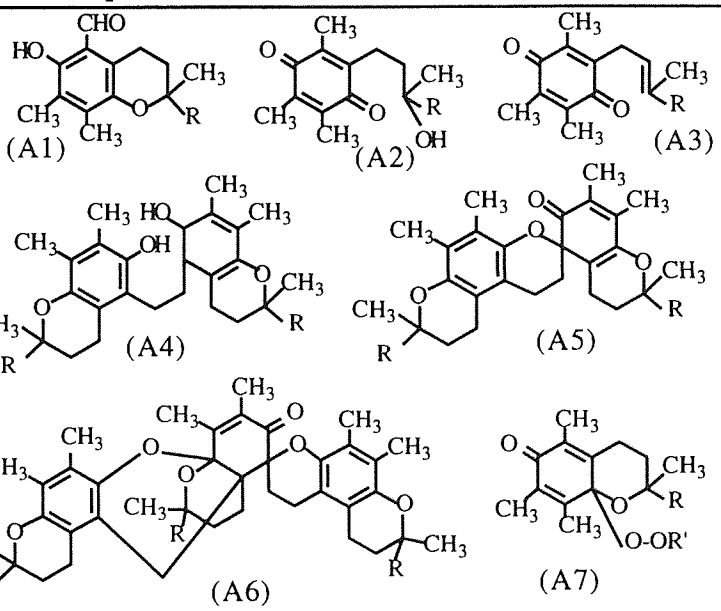 (A1) (A2) (A3) (A4) (A5) (A6) (A7)
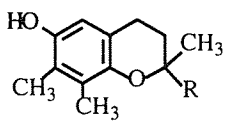 γ-Tocopherol (γTOC)	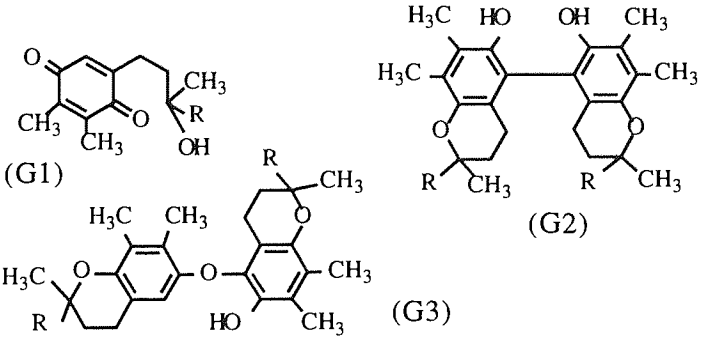 (G1) (G2) (G3)

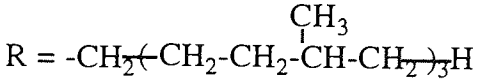

Scheme 3.6 Oxidation mechanisms of αTOC [113].

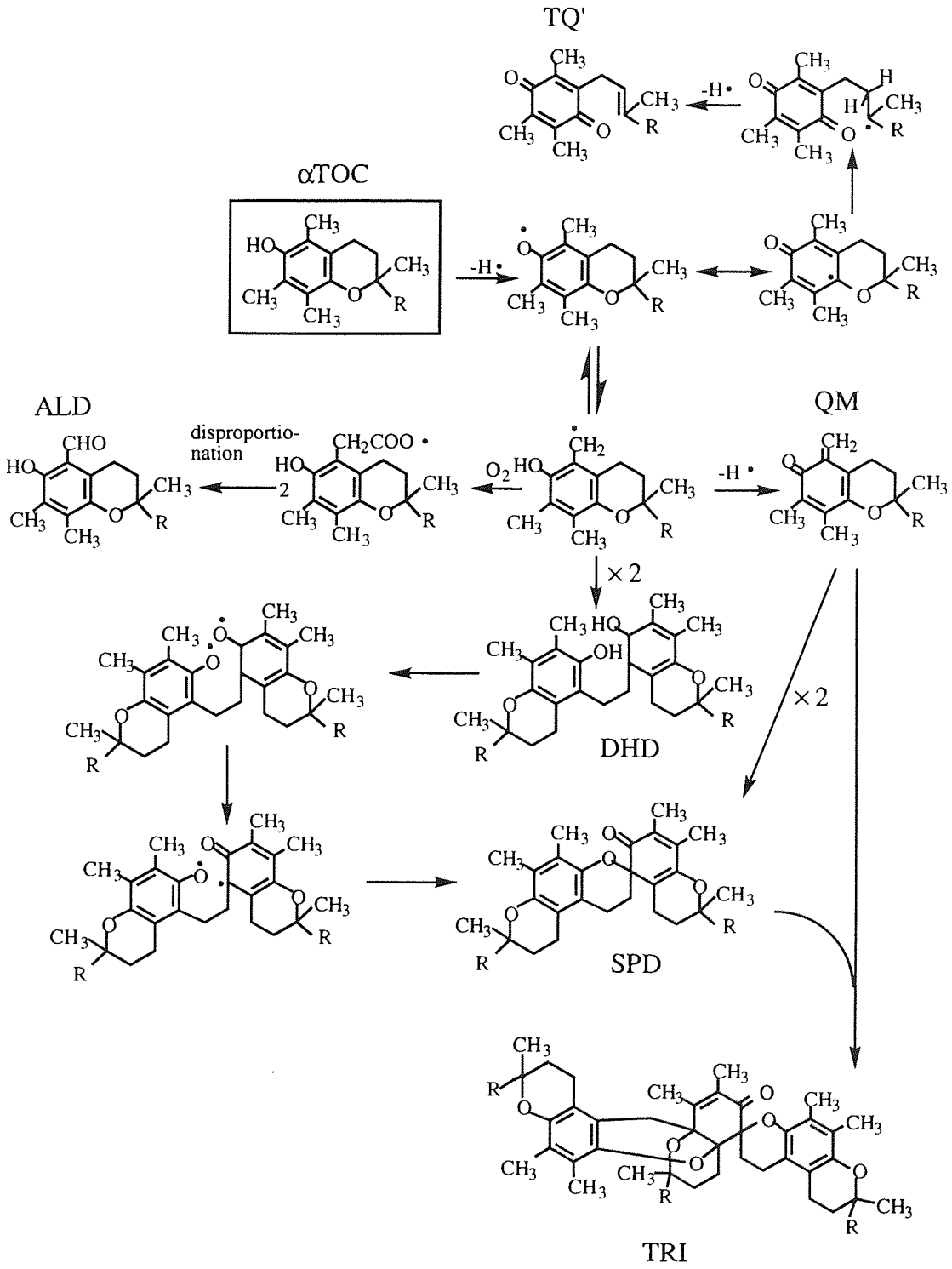

Scheme 3.7 Hypothetical pasway to form quinone (A2) from αTOC [117].

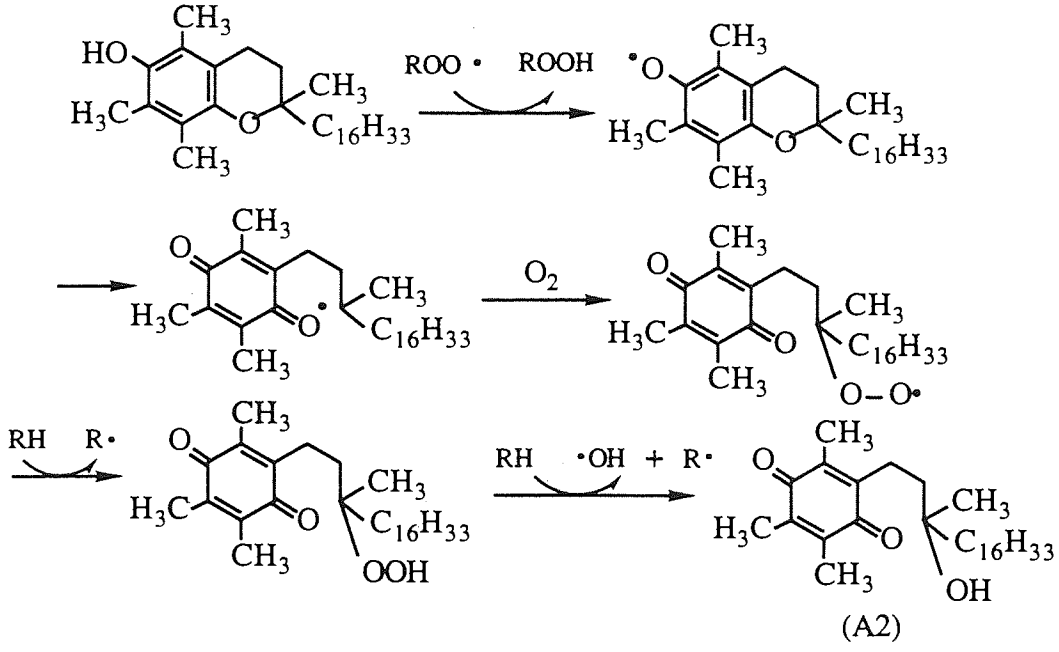

Scheme 3.8 Formation of peroxy ketal from αTOC [114].

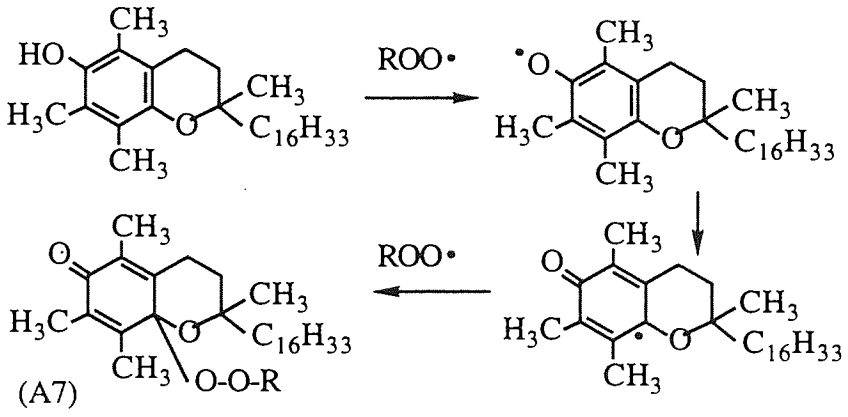

Scheme 3.9 Oxidation mechanism of γTOC [117].

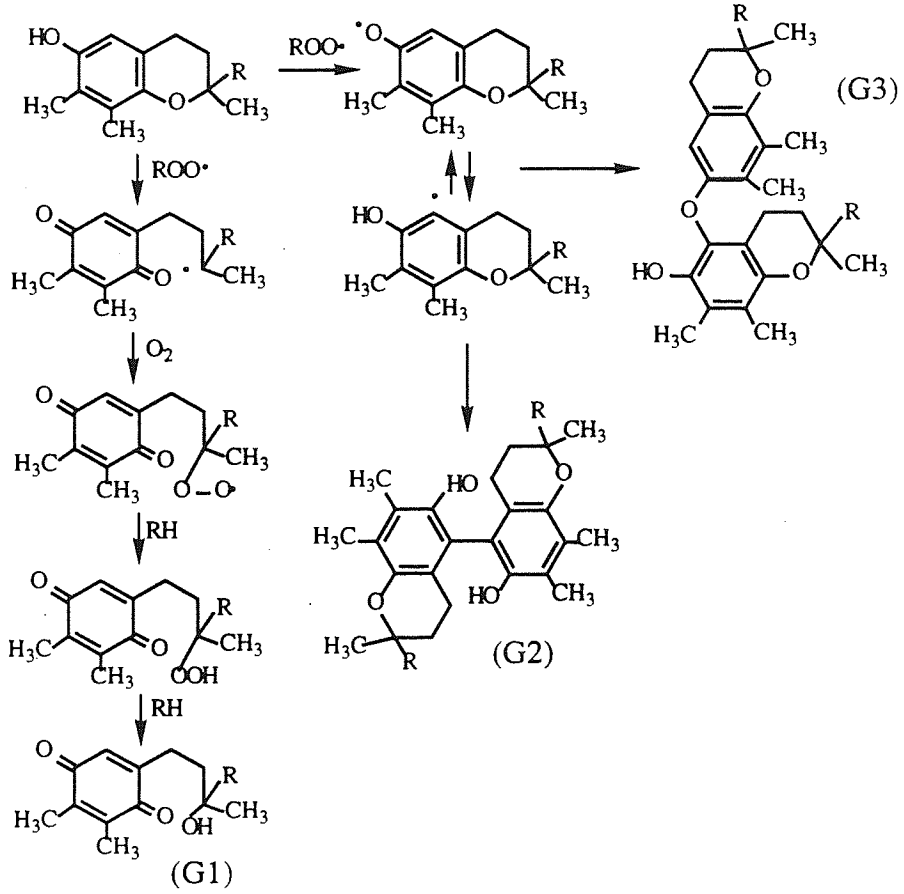

The hindered phenol, GM, is known to deactivate alkyl radical directly [105]. The mechanism of radical trapping of GM proposed by Okita is shown in scheme 3.10 [105]. Alkyl radicals were shown to be added onto the double bond of the acrylate substitutent and a stable radical is produced by a proton transfer.

Scheme 3.10 Alkyl radical trapping mechanism of GM [105].

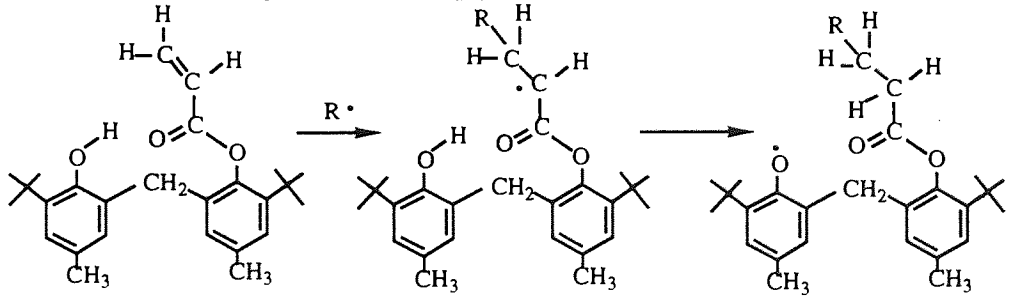

3.3.1.3 Reactivity Indices of Quinones and Phenols

Among the evaluated antifatigue agents, BQ, αTOC, and GM showed good performance as antifatigue agents, see fig. 3.4 though not as good as conventional antifatigue agents such as IPPD and 6PPD. Although the quionones were expected to have high fatigue activity due to their direct alkyl radicals trapping ability, figure 3.4 shows that the overall antifatigue performance was generally lower than that demonstrated by the hindered phenols, e.g. αTOC and GM.

Compounds with higher reactivity with alkyl radicals are expected to lead to higher fatigue resistance. The reactivity scale of antifatigue agents with isoprene monomer radical was calculated with the method mentioned in section 3.3.1.1. The reactivity index which is the highest within each compound is summarised with the fatigue resistance test results in table 3.18.

Table 3.18 Reactivity index of compounds examined in this work as potential antifatigue agents.

Code	Reactivity Index	Log Fatigue Life at 6.3 kg/cm^2	
		DCP Cure	Sulfur Cure
BQ	0.1615	4.946	5.070
DPQ	0.1611	4.729	4.679
NQ	0.1637	4.833	4.422
PDQ	0.1569	3.577	4.267
HBA'	0.1595	4.485	4.672

Fig. 3.12 Relationship between fatigue life (experimental values) and reactivity index (calculated) of compounds examined as antifatigue agents

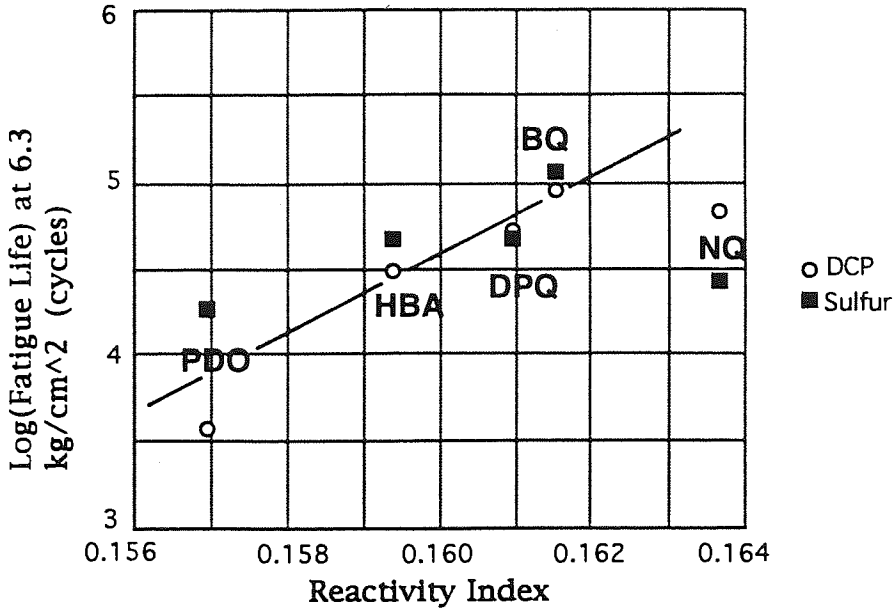

Figure 3.12 shows the relationship between fatigue lives and reactivity index of the potential antifatigue agents with isoprene monomer alkyl radical. It is clear that, with the exception of NQ, the reactivity indices and log fatigue lives showed nearly linear relation. This implies that the predicted radical trapping ability of antifatigue agents can represent relatively acculately the fatigue resistance of rubber samples. Screening of antifatigue agents based on computer aids is therefore, a powerful tool for technological assesment of additives. However, care must be taken when such calculations are performed as the reactivity index calculation, does not take into account the side reaction with other ingredients in the rubber, nor the volatility or compatibility aspects of the additive in the rubber.

In addition to reactivity index calculation, Mooney viscosity which reflects the changes in molecular weight of the rubber may be used for the screening of antifatigue agents. The antifatigue agents may act as processing antioxidants by deactivating mechano radicals produced by milling and hence will be expected to have a direct effect on changes in the rubber molecular weight. Therefore ,

the relationship between Mooney viscosity and fatigue life was examined and is illustrated in fig. 3.13. No clear relationship between Mooney viscosity and fatigue resistance is shown in fig. 3.13. In spite of the fact that under both fatigue and processing conditions, macroalkyl radicals are formed, the differences in the processing and fatigue conditions, for example, differences in the operation temperatures, the oxygen concentration, and the rate of formation of the radicals, can account for the poor relationship between Mooney viscosity and fatigue life observed in fig. 3.13.

Fig. 3.13 Relationship between Mooney-viscosity and Fatigue Resistance of Antifatigue Agents Containing NR.

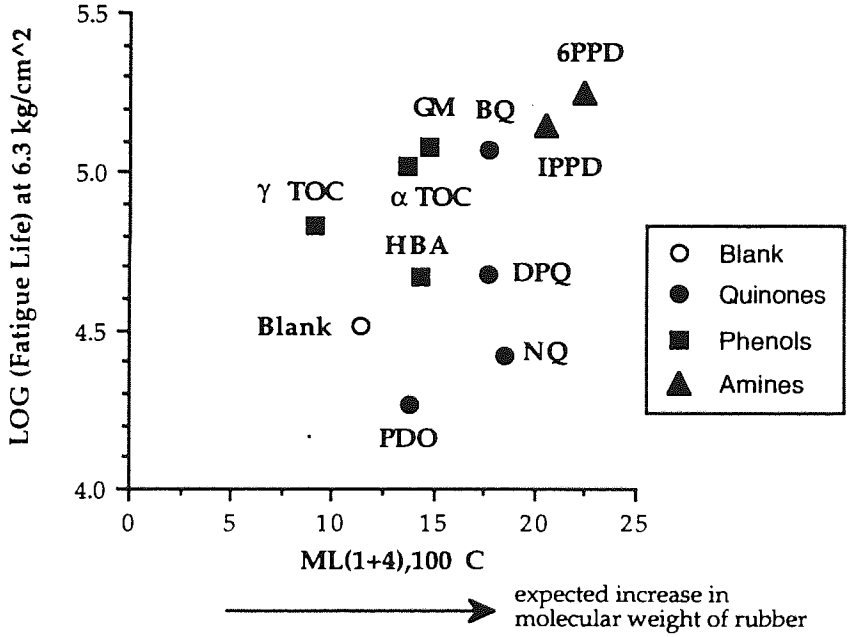

The fact that compounds which have higher reactivity for CB-A action to deactivate alkyl radicals show higher fatigue resistance implies that antifatigue activity can be carried out through the deactivation of alkyl radicals formed during fatiguing. Based on reaction indices, all hypothetical reaction schemes of quinonoid compounds with alkyl radicals are shown in schemes 3.2 - 3.5. Henmann [71] suggested possible mechanisms of the action of quinonoid

compounds as melt stabilisers in polyolefin which deactivate macroalkyl radicals, see scheme 3.11.

Scheme 3.11 Alkyl radical deactivation by quinones [71].

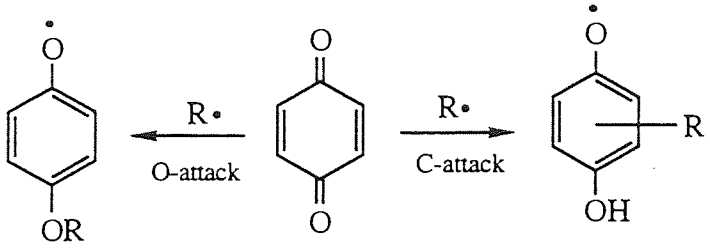

According to his mechanism there are two possibility of reaction pathways. For example, in case of BQ, alkyl radicals seem to have a possibility to react with oxygen No.1 (see table 3.13). Moreover, in case of HBA', alkyl radicals seem to have possibilities to react with oxigen No.1, carbon No.7 and oxygen No.8 (see table 3.16). However, the calculated reactivity indices at these site were lower than the meta position of the ring (carbon No.4 and cabon No. 4 and 6 in tables 3.13 and 3.16, respectively). Similarly in all other compounds where their reactivity index was calculated, the reactivity of C-attack was higher than that of O-attack. For these reasons, the overall antifatigue mechanisms of quinonoid compounds are expected to proceed by the following ways. It starts from the addition of alkyl radicals onto the meta position of the quinone ring with formation of a phenoxyl radicals (C-attack). They either disproportionate or undergo further reaction with other alkyl radicals (the formation of olefin and phenol or the recombination of alkyl radicals to phenoxy radical oxygen). Because of the bulky substitutents at the meta position, the recombination at the para position will be difficult and therefore, this possibility was neglected in the proposed mechanisms of this work. The ratio of further reaction from phenoxyl radicals will depend on the stability and concentration of these phenoxyl radicals and temperature.

3.3.2 Thermoxidative Resistance

Figures 3.7 - 3.10 and tables 3.8 and 3.10 - 3.12 show clearly the poor thermoxidative behaviour of BQ, NQ and αTOC under all conditions tested. The quinones, BQ and NQ, do not act primarily by CB-D process hence their ability to act as thermoxidative antioxidants (by trapping ROO·), is not expected to be high. On the other hand, αTOC is known to act by a CB-D mechanism; however, αTOC did not offer any thermoxidative stabilities to the rubbers and the mode of actions was further investigated (see Chapter 5). Other workers have also shown that the thermoxidative stability of other polymers e.g. polypropylene (PP) and polyethylene (PE), in presence of αTOC is not very high especially at high temperatures [119]. It must be pointed out, however, that lower αTOC concentration (0.5 phr) did lead to much better thermal resistance in the rubber, this is discussed further in chapter 4. This may imply that higher concentrations of αTOC has lead to its dimerisation, producing the spirodimer (A5 in table 3.17) so that the concentration of the original phenol is reduced. Winterle reported the formation of two main oxidation products from αTOC at high concentration; quinon (A2) and spirodimer (A5) [114]. γ-tocopherol also showed similar tendency, i.e, at high concentration, thermal resistance decreased, see fig.4.32 and 33; however the reduction in its effectiveness was less than in the case of αTOC. This may be due to the fact that, in the case of γTOC the expected dimers (G2 and G3 in table 3.17) have hydroxyl groups. The reason why γTOC did not show high thermoxidative stability in longer thermal ageing test can be also explained in the same way, i.e. part of the γTOC was converted to quinonoid compound , G1 (potentially CB-A and not CB-D). At the evaluated temperature of this work γTOC always showed better thermoxidative resistance than αTOC, see figures 3.7 - 3.10 and tables 3.8 and 3.10 - 3.12. Generally, it is known that thermoxidative resistance of phenols which are hindered by methyl, ethyl, tert.-butyl groups is higher

than for phenols without steric hinderence [119]. Although αTOC is hindered from both sides beside hydroxy group, (whereas γTOC is hindered from one side, see table 3.19) the test results of thermoxidative resistance of αTOC were lower than γTOC and this is opposite to the general tendency of hindered phenols. The formation of different types of dimers may explain this contradiction. Nilsson suggested two types of dimerisation schemes of various tocopherols [112], which involve initial formation of phenoxy radical then (1) coupling through oxygen or ortho positions (βTOC, γTOC, δTOC) or (2) rearranging to benzyl radicals followed by coupling (αTOC, βTOC). In case of βTOC the dimerisation through benzyl radical is a major reaction. In this way, γTOC and δTOC produce similar dimers and αTOC and βTOC also produce dimers similarly. It was shown that at high temperatures (≥60°C), the order of thermoxidative resistance of tocopherols is also δTOC > γTOC > βTOC > αTOC, see table 3.19, while at lower temperature it becomes quite different, e.g. αTOC > γ TOC > βTOC > δ TOC [117].

Table 3.19 Structure of various tocopherols.

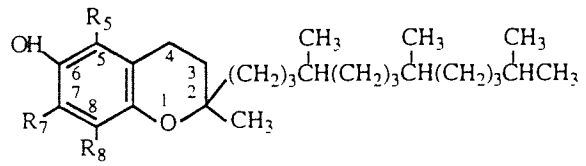

	R_5	R_7	R_8
αTOC	CH_3	CH_3	CH_3
βTOC	CH_3	H	CH_3
γTOC	H	CH_3	CH_3
δTOC	H	H	CH_3

Both PDO and HBA have protons which can be donated to alkyl peroxyl radicals and hence can be expected to act by CB-D process. Although these compounds showed competitive thermal resistance under tensile test at low

(70°C) temperature (see fig. 3.7), their performance decreased drastically at higher temperature (see figures 3.8 and 3.9) and thermoxidative resistance results obtained from chemical stress relaxation (100°C) was poor compared with the tensile test results at the same temperature. The order of thermoxidative resistance under stress relaxation condition was 6PPD ≈ IPPD > DPQ ≈ GM > NQ ≈ γTOC » αTOC > **HBA** > BQ > **PDO**, while that for tensile condition (24 hr) was 6PPD > GM ≈ **HBA** > IPPD ≈ DPQ > γTOC > **PDO** » αTOC >BQ > NQ, see fig. 3.10. Both HBA and PDO are small molecules and are volatile at higher temperatures. Furthermore, the main difference between tensile test and chemical stress relaxation specimen is based on the difference in the thickness of the samples used in each test. Because the relaxation samples are thin films (about 0.3 mm) the relative surface area is much larger than for the tensile samples (about 1.5 mm in thickness) and oxygen concentration in the rubber will be higher in the case of stress relaxation. Therefore, samples which undergo competitive side reactions at high oxygen concentration, or those which volatilise easily, will not be expected to show good performance in a chemical stress relaxation..

Only DPQ, GM, IPPD, 6PPD showed good performance under all thermoxidative conditions, see figures 3.7 - 3.11. The conventional rubber antioxidants, IPPD and 6PPD are expected to offer good thermaoxidative stability. The commercial hindered phenol, GM has an effective CB-D function in addition to its proposed main activity as CB-A, as well as the fact that it could not volatilise easily due to its relatively high molecular weight, hence it can be expected to perform well. However, before testing, all quinones were considered to have poor potential for thermoxidative resistance. Although the details of mechanism of thermoxidative antioxidant activity for DPQ is unclear, the biphenols which are produced through CB-A action (see scheme

3.3 b and c) during processing are considered to perform well. These phenols are relatively high molecular weight and can not volatilise easily.

Except for IPPD, 6PPD and GM, the effective antifatigue agents examined in this work such as BQ and αTOC showed very poor thermal resistance. In order to use these antifatigue agents in industrial products, it will be necessary to compensate for their poor thermal resistance by using them in combination with other antioxidants. The additive effects of reactive antioxidants with these antifatigue agents were investigated for this purpose and the results of the work are discussed in the next chapter.

Table 3.3 Probability density and cumulative probability of fatigue failure of NR samples without any antifatigue agents (Blank). (at 108 maximum strain)

Fatigue (cycles)	Probability density of fatigue failure	Cumulative probability of fatigue failure	Experimental values of fatigue life
300 - 350	0/25	0/25	
350 - 400	1/25	1/25	387
400 -450	0/25	1/25	
450 - 500	3/25	4/25	480, 497, 498
500 - 550	4/25	8/25	503, 514, 530, 537
550 - 600	10/25	18/25	551, 558, 558, 562, 564, 573, 574, 578, 581, 585
600 - 650	4/25	22/25	605, 608, 608, 620
650 - 700	3/25	25/25	653, 659, 660

Table 3.4 Probability density and cumulative probability of fatigue failure of NR samples containing αTOC. (at 108 maximum strain)

Fatigue (cycles)	Probability density of fatigue failure	Cumulative probability of fatigue failure	Experimental values of fatigue life
700 - 750	1/33	1/33	720
900 - 950	1/33	2/33	925
1200 -1250	2/33	4/33	1233, 1244
1250 -1300	0/33	4/33	
1300 -1350	2/33	6/33	1321, 1321
1350 - 1400	3/33	9/33	1366, 1384, 1386
1400 - 1450	1/33	10/33	1422
1450 - 1500	2/33	12/33	1484, 1496
1500 - 1550	4/33	16/33	1514, 1526, 1540, 1548
1550 - 1600	2/33	18/33	1578, 1580
1600 - 1650	3/33	21/33	1614, 1620, 1620
1650 -1700	3/33	24/33	1692, 1694, 1699
1700 - 1750	1/33	25/33	1729
1750 - 1800	1/33	26/33	1789
1800 - 1850	3/33	29/33	1809, 1830, 1848
1850 - 1900	0/33	29/33	
1900 - 1950	1/33	30/33	1930
1950 - 2000	1/33	31/33	1970
2000 - 2050	1/33	32/33	2048
2050 - 2100	1/33	33/33	2801

Table 3.5 Probability density and cumulative probability of fatigue failure of NR containing 6PPD. (at 108 maximum strain)

Fatigue (cycles)	Probability density of fatigue failure	Cumulative probability of fatigue failure	Experimental values of fatigue life
1300 - 1400	1/24	1/24	1320
2000 - 2100	1/24	2/24	2095
2100 - 2200	1/24	3/24	2197
2200 - 2300	0/24	3/24	
2300 - 2400	1/24	4/24	2380
2400 - 2500	2/24	6/24	2470, 2487
2500 - 2600	3/24	9/24	2502, 2553, 2563
2600 - 2700	3/24	12/24	2618, 2632, 2651
2700 - 2800	2/24	14/24	2757, 2780
2800 - 2900	0/24	14/24	
2900 - 3000	1/24	15/24	2987
3000 - 3100	0/24	15/24	
3100 - 3200	0/24	15/24	
3200 - 3300	1/24	16/24	3230
3300 - 3400	3/24	19/24	3301, 3346, 3389
3400 - 3500	0/24	19/24	
3500 - 3600	0/24	19/24	
3600 - 3700	1/24	20/24	3697
3700 - 3800	1/24	21/24	3723
3800 - 3900	1/24	22/24	3858
4200 - 4300	1/24	23/24	4255
4600 - 4700	1/24	24/24	4643

Table 3.7 Fatigue results for NR samples containing antifatigue agents. (1.5phr)

	Sample	Strain (%)	Strain Energy (kg/cm^2)	Fatigue Life × 0.01 (cycles) mean	max	min	Curve Fitting slope:A	intercept:B
	Blank	91.2	3.1	828.2	888	537	-1.3733	5.6115
		108	4.2	586.0	660	492		
		142	6.7	309.2	334	206		
		160	8.1	223.6	243	73		
Quinones	BQ	108	4.7	2078.2	2428	1179	-1.9210	6.6068
		160	9.1	579.5	695	301		
	DPQ	91.2	3.4	1398.2	1550	1025	-1.6797	6.0226
		108	4.6	796.7	827	662		
		142	7.4	337.4	361	232		
		160	9.1	273.9	302	88		
	NQ	91.2	2.6	1129.5	1288	736	-1.6987	5.7812
		108	3.4	813.4	944	306		
		142	5.4	378.1	428	278		
		160	6.6	218.3	242	130		
	PDO	81.2	2.7	595.2	710	462	-1.3186	5.3215
		108	3.7	351.1	361	301		
		142	5.9	197.3	227	99		
		160	7.2	161.0	187	110		
Phenols	HBA	91.2	3.2	1263.5	1413	901	-1.5548	5.9155
		108	4.2	988.2	1051	711		
		142	6.7	429.2	436	374		
		160	8.2	301.7	323	247		
	αTOC	91.2	3.5	2781.4	2924	1730	-1.7138	6.3892
		108	4.6	1876.0	2081	925		
		142	7.2	885.2	946	552		
		160	8.8	551.9	590	257		
	γTOC	91.2	2.3	3312.8	3471	2520	-1.6476	6.1483
		108	3.2	2380.2	2525	1895		
		142	5.4	791.2	861	699		
		160	6.7	643.3	675	380		
	GM	91.2	3.9	2330.1	2724	1781	-1.5401	6.3122
		108	5.1	1882.4	2137	1133		
		142	7.9	821.5	891	696		
		160	9.6	620.7	655	519		
Amines	IPPD	91.2	3.4	4210.4	5721	3278	-1.9731	6.7242
		108	4.5	3443.8	3552	3235		
		142	6.9	997.9	1045	880		
		160	8.4	841.9	914	679		
	6PPD	91.2	3.4	6380.9	7031	3400	-2.0492	6.8929
		108	4.6	3485.3	3858	2095		
		142	7.2	1192.6	1247	1064		
		160	8.7	1036.9	1092	833		

$Y = AX + B$

$Y = \text{Log}\{\text{Fatigue Life}\}$ (cycles)

$X = \text{Log}\{\text{Strain Energy}\}$ (kg/cm^2)

Table 3.9 Reduced stress of NR samples containing antifatigue agents.

Strain (%)	Reciprocal Strain $1/\lambda$	Reduced Stress $\sigma/(\lambda - \lambda^{-2})$ (N/mm^2)				
		Blank	BQ	DPQ	NQ	PDO
5	0.952	0.192	0.182	0.045	0.134	0.082
10	0.909	0.201	0.190	0.048	0.199	0.085
15	0.870	0.287	0.317	0.221	0.218	0.147
20	0.833	0.340	0.374	0.313	0.268	0.235
25	0.800	0.367	0.403	0.359	0.294	0.282
30	0.769	0.380	0.419	0.387	0.308	0.309
35	0.741	0.387	0.429	0.406	0.315	0.326
40	0.714	0.393	0.434	0.418	0.319	0.337
45	0.690	0.393	0.437	0.427	0.321	0.343
50	0.667	0.394	0.437	0.430	0.321	0.346
55	0.645	0.391	0.437	0.432	0.320	0.348
60	0.625	0.391	0.437	0.432	0.318	0.347
65	0.606	0.389	0.433	0.430	0.316	0.356
70	0.588	0.386	0.431	0.431	0.315	0.336
75	0.571	0.383	0.429	0.431	0.313	0.344
80	0.556	0.381	0.427	0.428	0.311	0.342
85	0.541	0.377	0.423	0.429	0.309	0.341
90	0.526	0.373	0.421	0.426	0.307	0.339
95	0.513	0.371	0.419	0.425	0.305	0.337
100	0.500	0.370	0.417	0.423	0.302	0.335
105	0.488	0.369	0.415	0.421	0.300	0.333
110	0.476	0.367	0.412	0.419	0.299	0.331
115	0.465	0.364	0.410	0.417	0.297	0.330
120	0.455	0.363	0.408	0.416	0.295	0.327
125	0.444	0.362	0.406	0.415	0.294	0.326
130	0.435	0.359	0.405	0.412	0.292	0.325
135	0.426	0.358	0.403	0.412	0.291	0.323
140	0.417	0.355	0.401	0.411	0.289	0.322
145	0.408	0.354	0.400	0.409	0.288	0.321
150	0.400	0.353	0.398	0.408	0.287	0.319
155	0.392	0.352	0.398	0.407	0.285	0.319
160	0.385	0.350	0.396	0.405	0.284	0.317
165	0.377				0.284	0.315

(continue)

Table 3.9 Reduced stress of NR samples containing antifatigue agents. (continued)

Strain	Reciprocal Strain	Reduced Stress $\sigma/(\lambda - \lambda^{-2})$ (N/mm^2)					
(%)	$1/\lambda$	HBA	αTOC	γTOC	GM	IPPD	6PPD
5	0.952	0.112	0.175	0.010	0.541	0.427	0.140
10	0.909	0.117	0.351	0.019	0.535	0.446	0.336
15	0.870	0.272	0.399	0.035	0.521	0.439	0.388
20	0.833	0.332	0.417	0.057	0.513	0.455	0.417
25	0.800	0.366	0.428	0.154	0.499	0.446	0.431
30	0.769	0.387	0.435	0.209	0.489	0.439	0.432
35	0.741	0.392	0.437	0.245	0.479	0.433	0.436
40	0.714	0.397	0.434	0.271	0.473	0.427	0.432
45	0.690	0.401	0.432	0.286	0.463	0.421	0.431
50	0.667	0.400	0.430	0.298	0.456	0.415	0.425
55	0.645	0.397	0.423	0.305	0.450	0.409	0.424
60	0.625	0.397	0.422	0.312	0.442	0.404	0.420
65	0.606	0.394	0.419	0.317	0.437	0.399	0.416
70	0.588	0.391	0.415	0.336	0.431	0.411	0.414
75	0.571	0.388	0.412	0.337	0.424	0.405	0.409
80	0.556	0.386	0.409	0.336	0.420	0.400	0.405
85	0.541	0.383	0.406	0.334	0.416	0.395	0.402
90	0.526	0.380	0.401	0.324	0.413	0.382	0.399
95	0.513	0.376	0.398	0.331	0.409	0.386	0.396
100	0.500	0.374	0.397	0.331	0.407	0.384	0.393
105	0.488	0.371	0.393	0.326	0.404	0.376	0.391
110	0.476	0.368	0.391	0.327	0.401	0.376	0.388
115	0.465	0.367	0.389	0.327	0.399	0.374	0.386
120	0.455	0.364	0.387	0.325	0.397	0.371	0.383
125	0.444	0.363	0.384	0.324	0.395	0.369	0.381
130	0.435	0.360	0.382	0.322	0.394	0.366	0.379
135	0.426	0.358	0.380	0.321	0.393	0.364	0.377
140	0.417	0.355	0.379	0.317	0.391	0.358	0.374
145	0.408	0.354	0.377	0.320	0.390	0.360	0.372
150	0.400	0.352	0.376	0.319	0.388	0.359	0.371
155	0.392	0.351	0.374	0.319	0.388	0.357	0.369
160	0.385	0.350	0.372	0.317	0.387	0.356	0.366
165	0.377	0.347			0.386		

Table 3.10 Chemical stress relaxation of NR samples containing antifatigue agents. (at 100°C)

Time	Log { f(t) / f(0) }				
(hr)	Blank	BQ	DPQ	NQ	PDO
0.0	0.000	0.000	0.000	0.000	
0.5	-0.031	-0.043	-0.027	-0.027	
1.0	-0.054	-0.081	-0.040	-0.040	
1.5	-0.071	-0.112	-0.052	-0.052	
2.0	-0.086	-0.142	-0.060	-0.060	
2.5	-0.102	-0.167	-0.068	-0.068	
3.0	-0.112	-0.192	-0.076	-0.076	
3.5	-0.128	-0.217	-0.083	-0.083	
4.0	-0.139	-0.240	-0.090	-0.090	
4.5	-0.153	-0.264	-0.095	-0.095	
5.0	-0.165	-0.289	-0.101	-0.101	
6.0	-0.185	-0.336	-0.114	-0.114	
7.0	-0.209	-0.384	-0.123	-0.123	
8.0	-0.231	-0.429	-0.133	-0.133	
9.0	-0.253	-0.482	-0.140	-0.140	
10.0	-0.273	-0.530	-0.151	-0.151	
11.0	-0.290	-0.574	-0.161	-0.161	
12.0	-0.313	-0.620	-0.168	-0.168	
14.0	-0.346	-0.713	-0.186	-0.186	
16.0	-0.393	-0.812	-0.207	-0.207	
18.0	-0.428	-0.909	-0.221	-0.221	
20.0	-0.467	-1.004	-0.236	-0.236	

(continue)

Table 3.10 Chemical stress relaxation of NR samples containing antifatigue agents. (at 100°C) (continued)

Time	Log { f(t) / f(0) }					
(hr)	HBA	αTOC	γTOC	GM	IPPD	6PPD
0.0	0.000	0.000	0.000	0.000	0.000	0.000
0.5	-0.045	-0.035	-0.026	-0.033	-0.016	-0.015
1.0	-0.081	-0.058	-0.039	-0.053	-0.026	-0.024
1.5	-0.110	-0.079	-0.060	-0.067	-0.034	-0.030
2.0	-0.137	-0.099	-0.074	-0.086	-0.037	-0.035
2.5	-0.164	-0.118	-0.089	-0.098	-0.044	-0.041
3.0	-0.190	-0.135	-0.101	-0.111	-0.045	-0.044
3.5	-0.218	-0.154	-0.113	-0.118	-0.052	-0.049
4.0	-0.242	-0.170	-0.125	-0.132	-0.055	-0.053
4.5	-0.263	-0.191	-0.135	-0.142	-0.059	-0.057
5.0	-0.286	-0.214	-0.149	-0.150	-0.062	-0.063
6.0	-0.342	-0.253	-0.164	-0.169	-0.071	-0.071
7.0	-0.391	-0.289	-0.189	-0.184	-0.079	-0.077
8.0	-0.436	-0.324	-0.218	-0.202	-0.086	-0.083
9.0	-0.510	-0.362	-0.236	-0.216	-0.092	-0.090
10.0	-0.596	-0.401	-0.258	-0.232	-0.100	-0.097
11.0	-0.622	-0.436	-0.286	-0.246	-0.105	-0.103
12.0	-0.664	-0.479	-0.303	-0.261	-0.110	-0.109
14.0	-0.781	-0.562	-0.350	-0.283	-0.123	-0.118
16.0	-0.870	-0.660	-0.398	-0.311	-0.137	-0.131
18.0	-0.976	-0:743	-0.441	-0.340	-0.146	-0.143
20.0	-1.086	-0.806	-0.487	-0.371	-0.157	-0.153

Table 3.11 Eb retention of NR samples containing antifatigue agents during thermal ageing at different temperatures.

Samples		Original Eb (%)	Eb Retention after Thermal Ageing					
			70°C		100°C		120°C	
			90 hr	180 hr	24 hr	48 hr	6 hr	12 hr
	Blank	813.7	0.821	0.711	0.322	0.273	0.585	0.410
Quinones	BQ	810.2	0.956	0.800	0.377	0.261	0.338	0.294
	DPQ	848.3	1.041	0.975	0.865	0.884	0.832	0.811
	NQ	782.2	0.935	0.828	0.340	0.280	0.341	0.282
	PDO	845.7	0.944	0.942	0.781	0.393	0.619	0.450
Phenols	HBA	858.8	1.019	0.950	0.898	0.612	0.680	0.427
	αTOC	853.0	0.774	0.695	0.463	0.251	0.395	0.233
	γTOC	826.5		0.878	0.816	0.284	0.718	0.480
	GM	925.1	0.912	0.875	0.924	0.839	0.781	0.469
Amines	IPPD	855.9	0.990	0.933	0.883	0.821	0.788	0.747
	6PPD	880.8	1.054	0.993	0.939	0.788	0.786	0.719

Table 3.12 Tb retention of NR samples containing antifatigue agents during thermal ageing at different temperatures.

		Original Tb (N/mm2)	Tb Retention after Thermal Ageing					
			70°C		100°C		120°C	
			90 hr	180 hr	24 hr	48 hr	6 hr	12 hr
	Blank	15.828	0.675	0.503	0.102	0.089	0.179	0.099
Quinones	BQ	13.147	1.031	0.898	0.129	0.082	0.112	0.086
	DPQ	18.778	1.033	1.029	0.747	0.677	0.604	0.491
	NQ	12.145	0.886	0.564	0.109	0.090	0.110	0.067
	PDO	14.781	1.162	0.950	0.381	0.099	0.154	0.069
Phenols	HBA	17.724	1.021	0.970	0.686	0.194	0.265	0.085
	αTOC	17.621	0.751	0.511	0.349	0.110	0.225	0.104
	γTOC	15.998		0.794	0.653	0.091	0.353	0.154
	GM	14.327	0.955	0.979	1.019	0.843	0.324	0.120
Amines	IPPD	16.711	1.316	1.220	0.993	0.832	0.701	0.671
	6PPD	17.294	1.372	1.524	1.191	0.885	0.880	0.575

Chapter 4 Grafting of Reactive Antioxidants on Natural Rubber.

4.1 Object and Methodology

The work described in this chapter, deals with reactive processing of antioxidants containing polymer-reactive function (reactive antioxidants, see table 4.1) with NR in an internal mixer in the presence of a free radical initiator, in order to produce polymer containing grafted antioxidant functions. The reactive processing parameters were developed and optimised for APMA which showed the best performance among all other evaluated reactive antioxidants (see table 4.1).

The fatigue and thermoxidative resistance of rubber samples compounded with these reactive antioxidants, when used as additives (i.e. not reactively processed) were first evaluated and compared with their effect when reactively processed in the polymer (evaluation similar to that described in scheme 3.1).

Since the antifatigue agents evaluated in this work (see chapter 3) did not offer high thermoxidative resistance to the rubber samples, combinations of antifatigue agents with the reactive antioxidants and some peroxide decomposers (see table 4.1) were used with the aim of obtaining rubber samples which exhibit good fatigue and thermoxidative resistance.

The work described in this chapter deals with the following:

(1) evaluation of CB-D activity of each reactive antioxidants in the rubber,
(2) determination of the optimum grafting conditions in the case of APMA,
(3) comparison of physical properties of rubber samples containing the reactive antioxidant (APMA) before and after extraction,
(4) determination of the structure of the grafted antioxidant (APMA) in the polymer,
(5) synergestic or additive effects of combinations of antioxidants, e.g. reactive antioxidant with antifatigue agent and a peroxide decomposer.

Table 4.1 Reactive antioxidants, antifatigue agents, peroxide decomposers, and rubber model compound used in work described in chapter 4.

Type	Code	Structure	M.w.	m.p. (°C)
Recative Antioxidants	PM	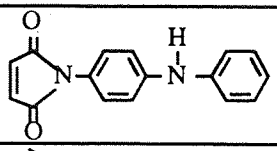	264	154 - 156
	BTMI	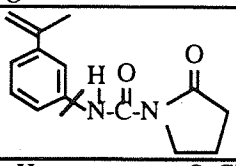	244	54 - 58
	APMA	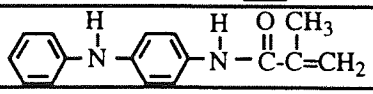	252	105 - 108
	MADA	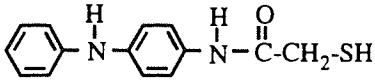	258	122 - 147
Antifatigue Agents	BQ	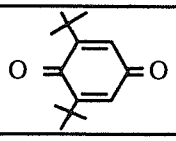	220	66 - 68
	αTOC	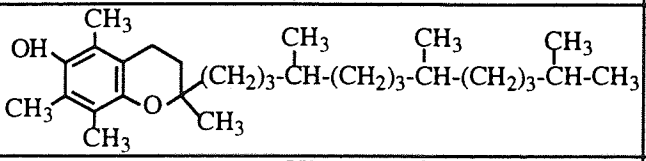	431	oily liquid at room temp.
	γTOC	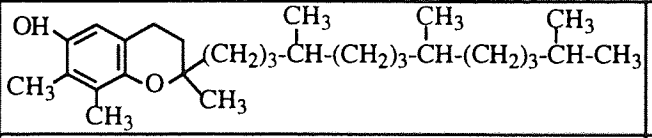	417	oily liquid at room temp.
	TMQ	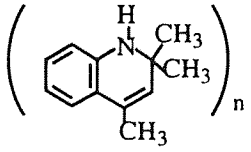		77 - 94
Peroxide Decomposers	P168	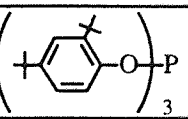	647	179 - 181
	P626	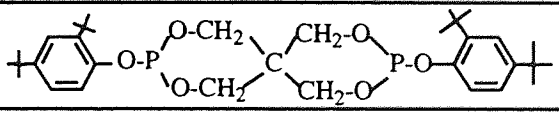	605	162 - 174
Model Compound	squalene	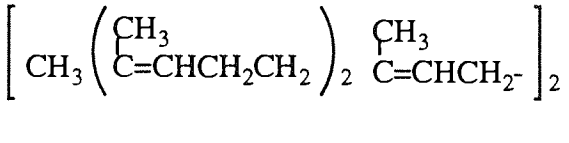	411	transparent liquid at room temp.

Initially, the CB-D activity of the reactive antioxidants was evaluated without grafting on the NR in the same ways as was described in chapter 3, see scheme 3.1. Grafting conditions of the best reactive antioxidant were then optimised. The overall procedure to optimise the grafting conditions of the reactive antioxidants is described in scheme 4.1. As a reactive antioxidant, APMA was investigated further because of its excellent thermoxidative resistance and fatigue resistance when compared to all other evaluated reactive antioxidants. The mechanical grafting reaction was achieved by reactively processing the NR with the reactive antioxidant under an inert atmosphere in a closed chamber of an internal mixer, see fig. 2.86. The processing parameters; temperature, time, rotor speed, and chemical composition; antioxidant's concentration were optimised. The remaining rubber ingredients; zinc oxide, stearic acid, accelerator (CBS), and sulphur were then compounded on a roll mill, with the pre-mixed rubbers containing grafted antioxidant either before or after extraction by acetone, see scheme 4.1. The degree of grafting was evaluated by FT-IR using thin vulcanised rubber films. The compounded rubbers were sheeted out as thin as possible and were vulcanised to make thin films. Films obtained from compounding the pre-mixed rubber without extraction, reffered to as **films A** are expected to include free APMA, grafted APMA during processing and curing. On the other hand, films obtained from compounding the acetone extracted pre-mixed rubber, reffered to as **films B**, are expected to include APMA grafted during reactive processing. **Films C** were obtained from extraction of the **films A** with azeotropic solvents and are expected to contain APMA grafted during reactive processing and curing. The grafting efficiency of the APMA in the rubber during reactive processing and curing was calculated from IR peak area ratio index of the sec.-amide group viz absorption of NH at 3355 cm^{-1} relative to a reference peak at 2727 cm^{-1}, as shown in fig. 2.89 (see section 2.5.2.2, p111).

Scheme 4.1 Procedure to determine the grafting efficiency of APMA on NR chains.

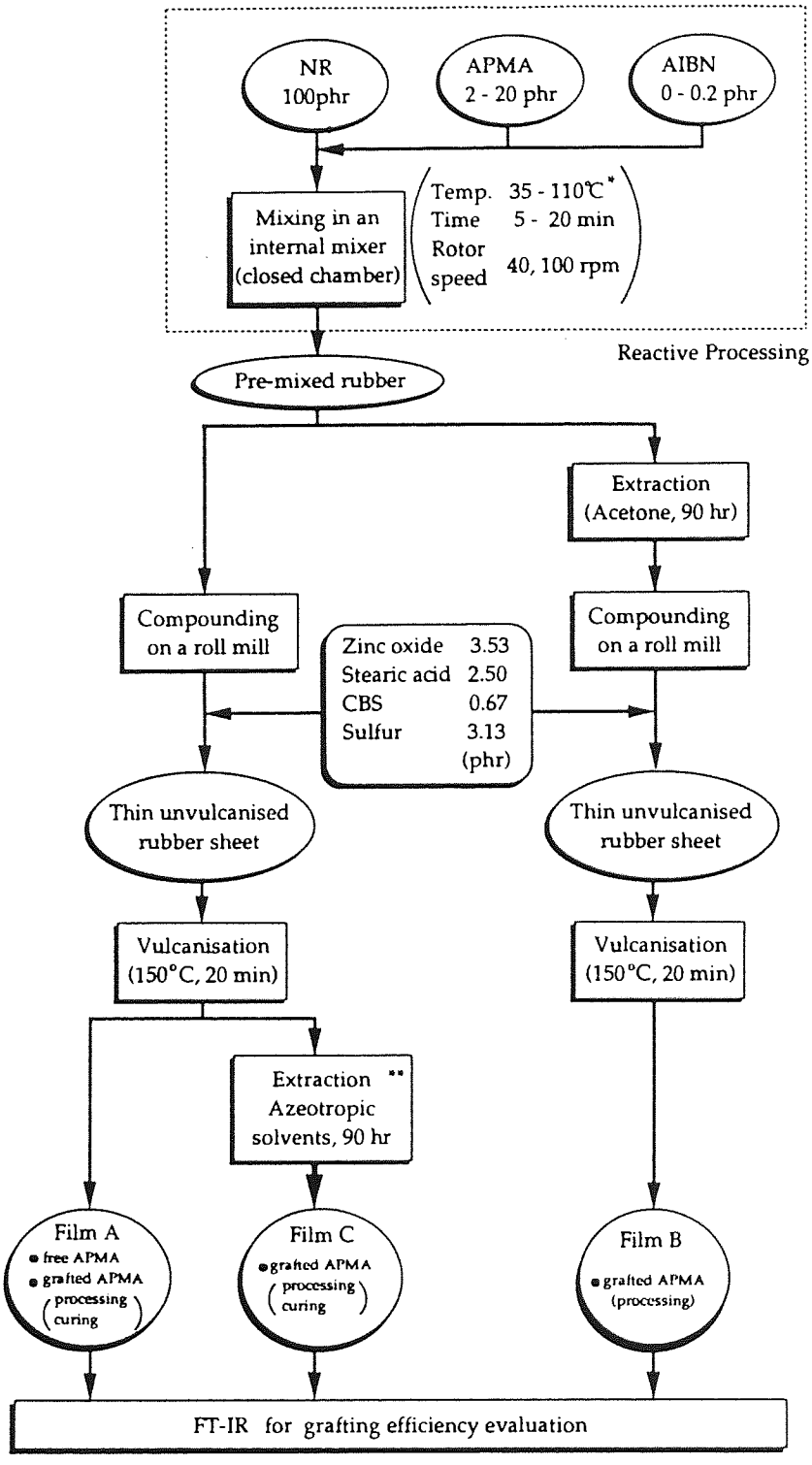

* temperature of heating oil
** methanol 19.8 vol%, acetone 51.9 vol%, 1,1,1-trichroloethane 28.3 vol%

The effect of grafting of the reactive antioxidant onto the polymer was examined by comparison of thermoxidative and fatigue behaviors of the rubber before and after extraction. The experimental procedure used is shown in scheme 4.2 and is similar to that described in scheme 3.1, except for the process of pre-mixing of the reactive antioxidant and extracting the vulcanised rubbers before physical testing.

The additive effect on thermoxidative resistance and fatigue resistance between reactive antioxidants and antifatigue agents and peroxide decomposers were also evaluated in the similar ways, see scheme 4.3.

The structure of grafted reactive antioxidant (APMA) was investigated using squalene as a model compound for NR, see scheme 4.4. The reactive antioxidant, APMA, was dissolved in isopropanol , and the solution was added to the squalene with a radical initiator, AIBN. The grafting reaction was carried out in a two neck round bottom flask. A condenser was placed on the top of the flask and argon gas was bubbled through the other neck. The reaction mixture was heated in a water bath with stirring (magnetic stirrer). The reaction products were separated and analysed in order to determine the structure using FT-IR and NMR spectroscopy.

The polymerisation of APMA itself was also investigated using a similar process, see scheme 4.5. Under argon atmosphere, APMA was polymerised in isopropanol using the radical initiator (AIBN). The reaction products were also separated and analysed in a similar manner.

Scheme 4.2 Experimental flow chart for the conformation of grafting effects of APMA on the physical properties.

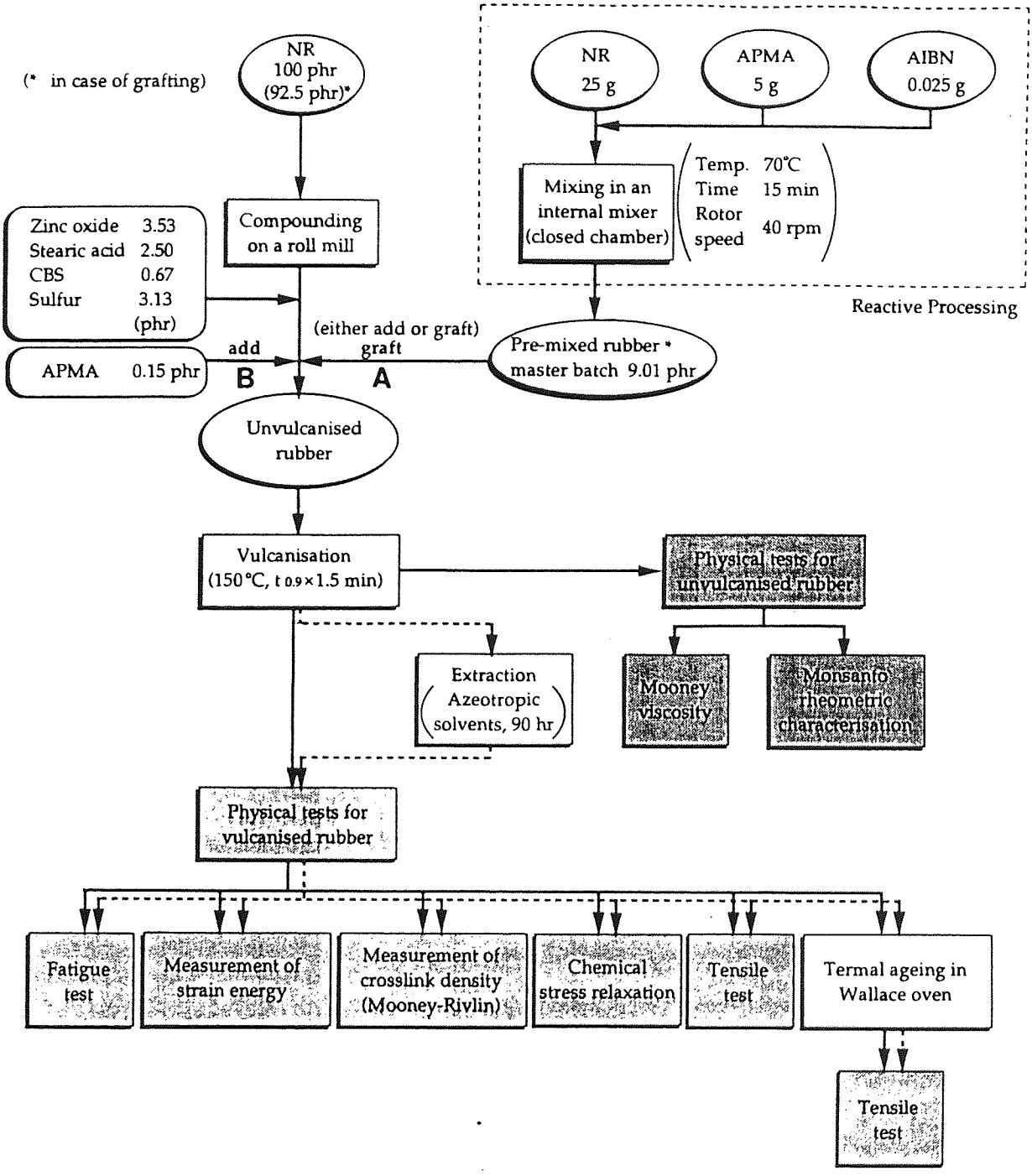

Scheme 4.3 Experimental procedure for the investigation of synergestic or additive effects of APMA with antifatigue agents and with peroxide decomposers on the physical properties.

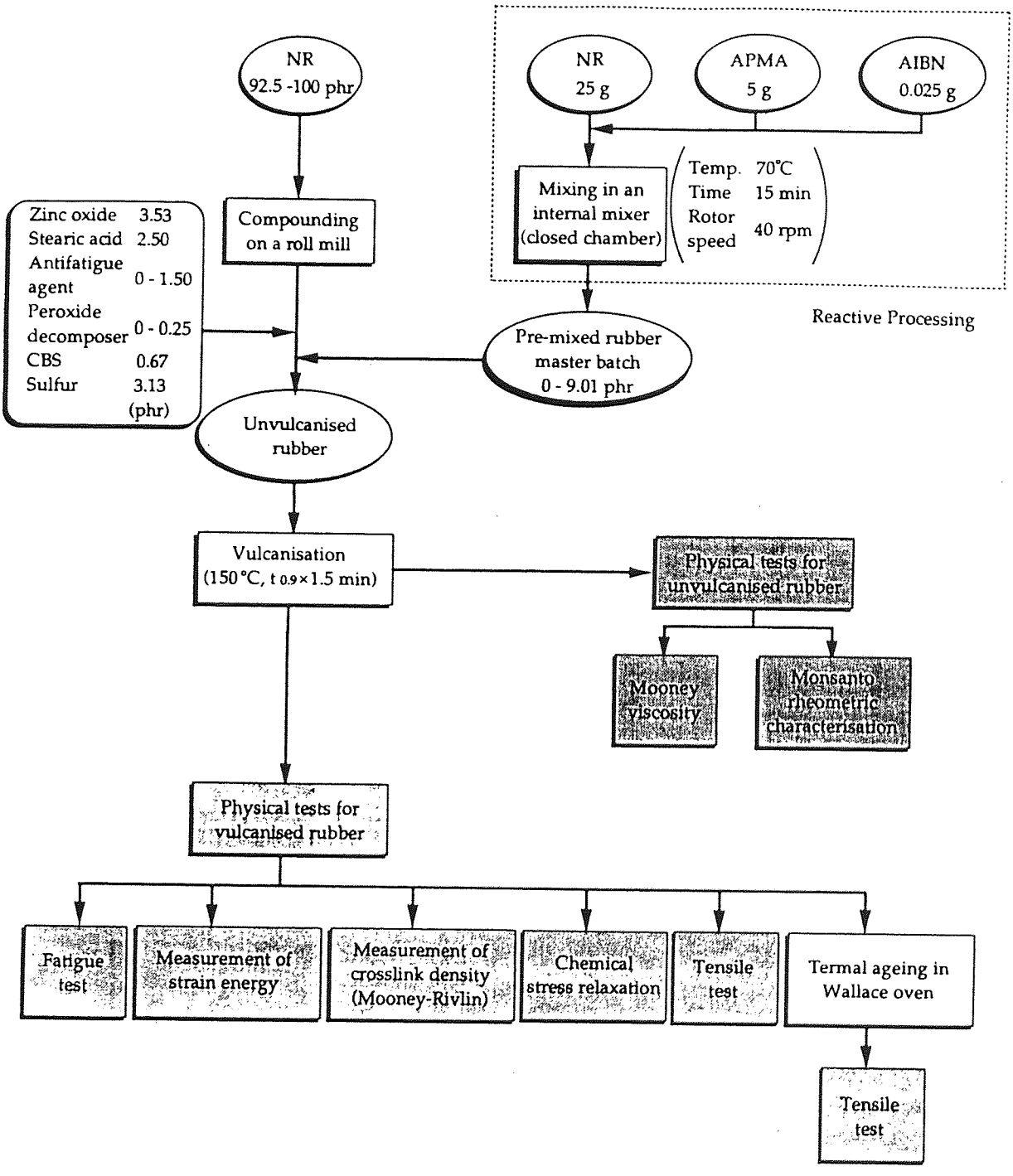

Scheme 4.4 Experimental procedure for the determination of the structures of grafted APMA on squalene.

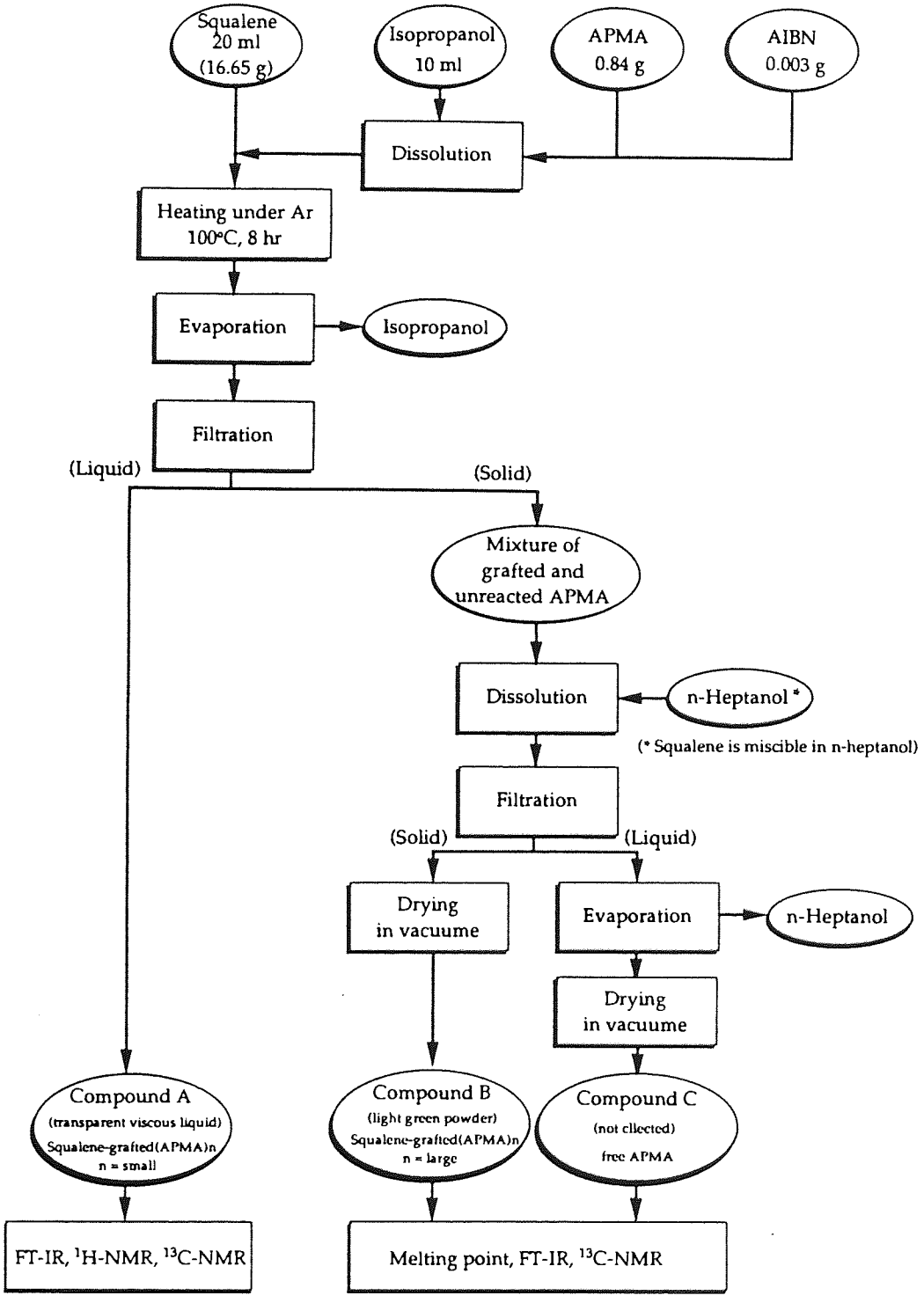

Scheme 4.5 Experimental procedures for determination of the structures of polymerised APMA in isopropanol.

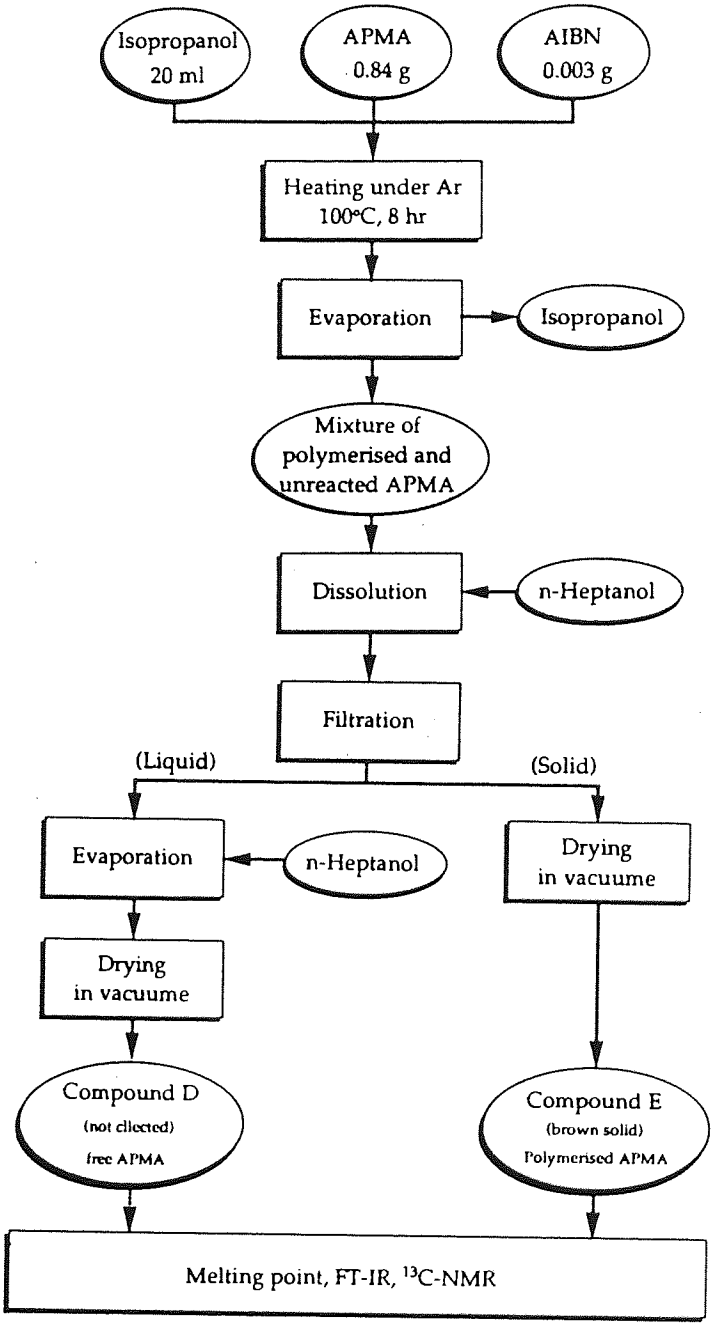

4.2 Results

4.2.1 Screening of Reactive Antioxidants

Four different reactive antioxidants; PM, BTMI, APMA, and MADA, see table 4.1, were evaluated in NR as additives, with respect to their thermoxidative and fatigue resistance. The results of physical tests of the unvulcanised rubber samples containing these antioxidants are summarised in table 4.2.

Table 4.2 Summary of physical tests for reactive antioxidant compounded unvulcanised rubbers.

Code	Mooney	Monsanto Rheometer's Characterisation (at 150°C)			
	ML(1+4),100°C	f_{min} (dN·m)	f_{max} (dN·m)	$t_{0.1}$ (min)	$t_{0.9}$ (min)
Blank	13.3	6.8	42.2	6.5	13.3
PM	15.0	4.8	37.9	10.9	25.3
BTMI	12.8	3.8	40.1	6.2	13.6
APMA	12.7	4.3	41.4	6.4	13.7
MADA	13.6	4.2	?	?	?

Fig. 4.1 Rheometer curves of reactive antioxidants containing rubbers.

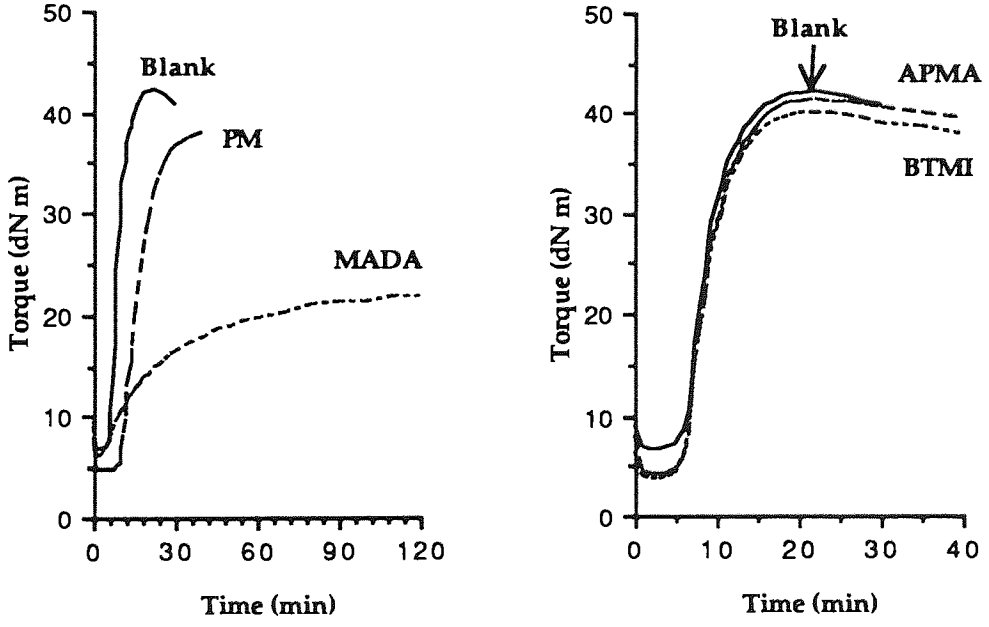

The evaluated reactive antioxidants did not have any significant effect on the Mooney viscosity; however, PM and MADA changed the vulcanisation characteristics drastically, see fig. 4.1. In the case of PM, the maximum torque decreased slightly and the curing rate became slower, while in the case of MADA, both the maximum torque and the curing rate decreased significantly. Furthermore, the curing for MADA was not complete even after 2 hr of measurement. Since the vulcanisation time was decided by $1.5 \times t_{0.9}$, samples of NR containing PM and MADA had to have much longer vulcanisation time, e.g. PM required 38.0 min (= 1.5 × 25.3 min) for vulcanisation. Samples containing MADA were not subjected to physical tests due to very low modulus values even after vulcanisation for 120 min, see fig. 4.1 and table 4.2, hence were eliminated from the evaluation.

Results of the fatigue resistance of reactive antioxidants-containing rubber samples are shown in table 4.3 and fig. 4.2. All the evaluated antioxidants (all are ROO · scavengers) showed some antifatigue activity with APMA showing the highest fatigue resistance. Like other commercial diarylamine antioxidants such as IPPD and 6PPD, these aromatic amines are expected to produce nitroxyl radicals during their antioxidant action, see reaction (1), hence they are likely to act as antifatigue agents as well as antioxidants.

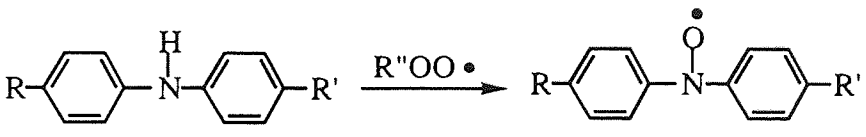

(1)

Table 4.3 Fatigue resistance of reactive antioxidants containing rubbers. (antioxidants used as additives, 1.5phr).

Sample	Strain	Strain Energy	Fatigue Life × 0.01 (cycles)			Curve Fitting *	
	(%)	(kg/cm2)	mean	max	min	slope : A	intercept : B
Blank	91.2	3.1	828.2	888	537	-1.3733	5.6115
	108	4.2	586.0	660	492		
	142	6.7	309.2	334	206		
	160	8.1	223.6	243	73		
PM	91.2	3.8	1914.3	2092	1324	-1.4520	6.1263
	108	5.0	1370.2	1604	879		
	142	7.7	618.9	642	484		
	160	9.3	563.3	613	352		
BTMI	91.2	3.5	1502.7	1746	1212	-1.6848	6.1373
	108	4.5	1307.2	1587	936		
	142	7.0	464.0	480	409		
	160	8.5	377.2	409	269		
APMA	91.2	3.7	2321.8	2512	1552	-1.6010	6.3160
	108	4.9	1842.3	2041	1341		
	142	7.5	827.7	865	710		
	160	9.1	579.5	643	209		
MADA	---	---	---	---	---	---	---

* X : Log (Strain Energy), Y : Log (Fatigue Life), Y = AX + B

Fig. 4.2 Fatigue resistance of reactive antioxidants containing rubbers.

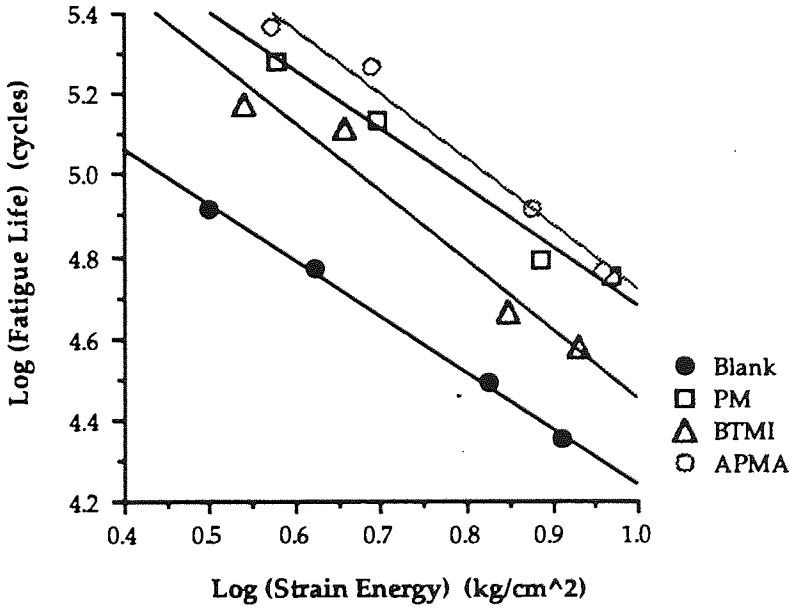

The thermal resistance was evaluated by examining the retention of the elongation at break (Eb) and the tensile strength (Tb) (characteristic parameters obtained from tensile test) after thermal ageing at 70°C, 100°C, and 120°C as well as chemical stress relaxation at 100°C. Resuluts of retention of Eb and Tb at different temperatures are summarised in tables 4.4 and 4.5 (at the end of this chapter) and are illustrated in figures 4.3 to 4.5. PM and APMA showed better retention of properties after thermal ageing with APMA giving higher retention of Eb and Tb than PM, especially at higher temperatures.

The chemical stress relaxation results are summarised in table 4.6 (at the end of this chapter). The rate constants of relaxation by chemical reaction, **k**, and the numbers of chain scissions per unit time, q_m, were calculated from the slope of stress relaxation curves (**Log { f (t) / f (0) } vs time**) and crosslink density, see section 2.4.2.

$$q_m = k / \upsilon_e$$

The crosslink density, υ_e, for q_m calculation was obtained form Mooney-Rivlin plots by calculation from the following equation;

$$2C_1 = \upsilon_e RT$$

where **R** is gas constant, **T** is absolute temperature and $2C_1$ is intercept of curve fitting part of Mooney-Rivlin curve, see section 2.4.1.3. The intercept, $2C_1$, and slope, $2C_2$, of the Mooney-Rivlin curve are also summarised in table 4.6. Although the order of antioxidant activity is different, the relaxation results confirmed the earlier observation that PM and APMA were effective antioxidants.

At the end of this chapter, more detailed chemical stress relaxation and Mooney-Rivlin results are shown in tables 4.7 and 4.8.

Fig. 4.3 Retention of elongation at break (Eb) and tensile strength (Tb) during thermal ageing at 70°C.

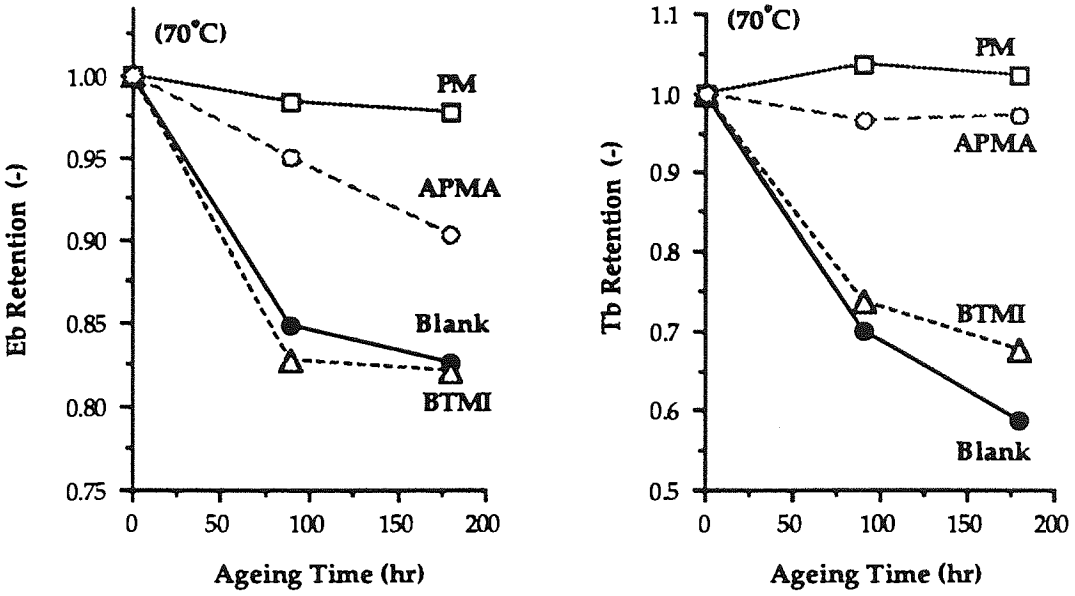

Fig. 4.4 Retention of elongation at break (Eb) and tensile strength (Tb) during thermal ageing at 100°C.

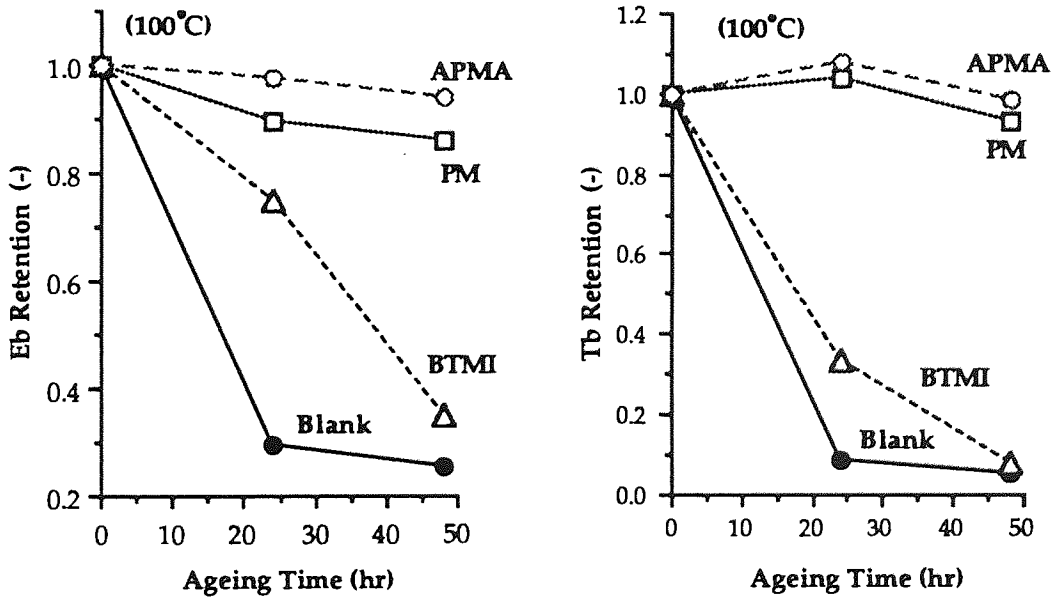

Fig. 4.5 Retention of elongation at break (Eb) and tensile strength (Tb) during thermal ageing at 120°C.

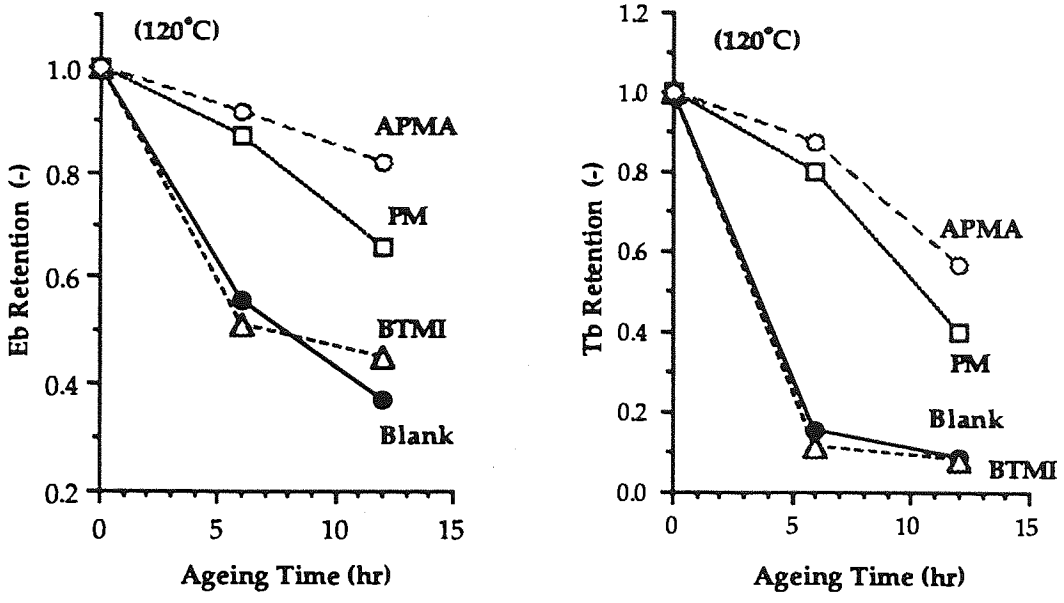

Fig. 4.6 Chemical stress relaxation of reactive antioxidants containing rubbers. (at 100°C)

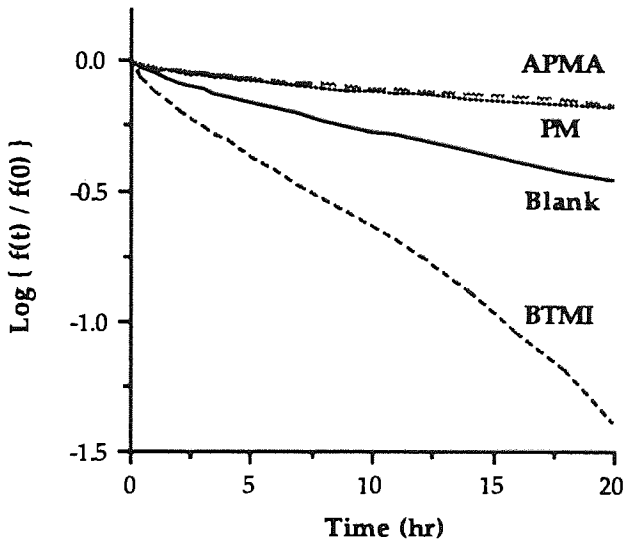

Among the evaluated reactive antioxidants, APMA showed the best ability both in fatigue and thermoxidative resistance and it was competitive even compared with IPPD and 6PPD which are widely used in industry. In addition, although APMA has similar chemical structure (a diarylamine) to the commercial antioxidants, IPPD and 6PPD, the rubber containing it is less coloured, hence it presents less problem especially in applications where staining is a problem. For these reasons, APMA was investigated further and its behaviour when reactively processed in the rubber was examined and is presented in the following section.

4.2.2 Determination of the Optimum Grafting Conditions of APMA on NR.

As a result of the screening tests described in the previous section, APMA was further investigated. Grafting reactions of the antioxidant onto the polymer backbone were conducted by mechanically generating macroalkyl radicals during compounding in an internal mixer. In order to decide on the optimum compounding conditions, the effect of both processing and chemical composition parameters (heating oil temperature, compounding time, rotor speed), (antioxidant concentration, radical initiator concentration) were examined. The details of the compounding conditions, the chamber temperature, and the rotor torque monitored during compounding are summarised in table 4.9.

Table 4.9 Grafting conditions and measured chamber temperature and torque for master batch of APMA in NR.

Variable parameter	Heating Oil Temp. (°C)	Chamber Temp. (°C)	Processing Time (min)	APMA Conc. (phr)	AIBN Conc. (phr)	Rotor Speed (rpm)	Torque arbitry unit
Heating Oil Temperature	35	34.6 → 36.0	10	5	0	40	35 → 24
	50	43.0 → 45.5	↓	↓	↓	↓	33 → 22
	70	57.0 → 58.0	↓	↓	↓	↓	27 → 21
	90	71.5 → 74.0	↓	↓	↓	↓	21 → 18
	110	87.5 → 88.0	↓	↓	↓	↓	15 → 13
Processing Time	70	57.0 → 58.0	5	10	0	40	27 → 23
	↓	57.0 → 59.5	10	↓	↓	↓	27 → 20
	↓	57.5 → 59.0	15	↓	↓	↓	27 → 20
	↓	57.5 → 58.5	20	↓	↓	↓	26 → 19
APMA Conc.	70	56.5 → 58.0	15	2	0	40	27 → 20
	↓	57.0 → 58.0	↓	5	↓	↓	27 → 20
	↓	57.5 → 59.0	↓	10	↓	↓	27 → 20
	↓	56.5 → 58.0	↓	20	↓	↓	28 → 19
AIBN Conc.	80	64.0 → 65.0	15	20	0	40	21 → 18
	↓	64.0 → 66.0	↓	↓	0.05	↓	21 → 18
	↓	63.5 → 65.5	↓	↓	0.1	↓	21 → 18
	↓	64.0 → 66.0	↓	↓	0.2	↓	21 → 18
Rotor Speed	80	64.0 → 65.0	15	20	0	40	21 → 18
	↓	65.0 → 67.0	↓	↓	↓	100	15 → 14

Since the setting temperature was oil temperature of the heater, the chamber temperature was not controlled and increased gradually by the heat generated from NR itself. The starting and final temperature inside the mixer are shown in table 4.9. The temperature increase was no more than 2.5 degrees under all conditions. On the other hand, the torque decreased with processing time in each case; the initial torque and final torque are shown in table 4.9. The torque did not show any increase (due to formation of gels), it decayed during the compounding simply due to chain scission.

The secondary amide index and grafting efficiency measured by FT-IR (see section 2.5.2) are shown in table 4.10. The grafting efficiency during compounding and during both compounding and curing are illustrated in fig. 4.7 for each of the parameters examined.

Table 4.10 Grafting efficiency during processing and curing of NR with APMA.

Variable parameter †		Sec. amide index			Grafting efficiency (%)	
		Films A	Films B	Films C	during * processing	during ** processing and curing
Heating Oil Temperature	35	15.727	10.790	13.199	69	84
	50	16.164	10.849	12.858	67	80
	70	14.582	10.752	12.239	74	84
	90	14.052	10.475	12.084	75	86
	110	14.196	10.124	12.206	71	86
Processing Time	5	16.917	10.087	12.513	60	74
	10	16.496	9.977	11.399	61	69
	15	17.054	10.310	12.658	61	74
	20	19.004	10.566	14.385	56	76
APMA Conc.	2	12.059	10.771	12.950	89	107
	5	14.817	11.095	12.167	75	82
	10	17.054	10.310	12.658	61	74
	20	23.963	11.954	13.760	50	57
AIBN Conc.	0	24.297	9.299	16.254	38	67
	0.05	23.683	9.817	16.508	42	70
	0.1	23.364	9.686	17.147	42	73
	0.2	27.947	10.220	17.103	37	61

* calculated from film A and film B, see scheme 4.1

** calculated from film A and film C, see scheme 4.1

† for other processing conditions and chemical compositions, see table 4.9.

Fig. 4.7 Grafting efficiency of APMA under each compounding condition. Parameters; (a) oil temperature, (b) compounding time, (c) APMA concentration, (d) AIBN concentration. For other processing conditions and chemical compositions, see table 4.9.

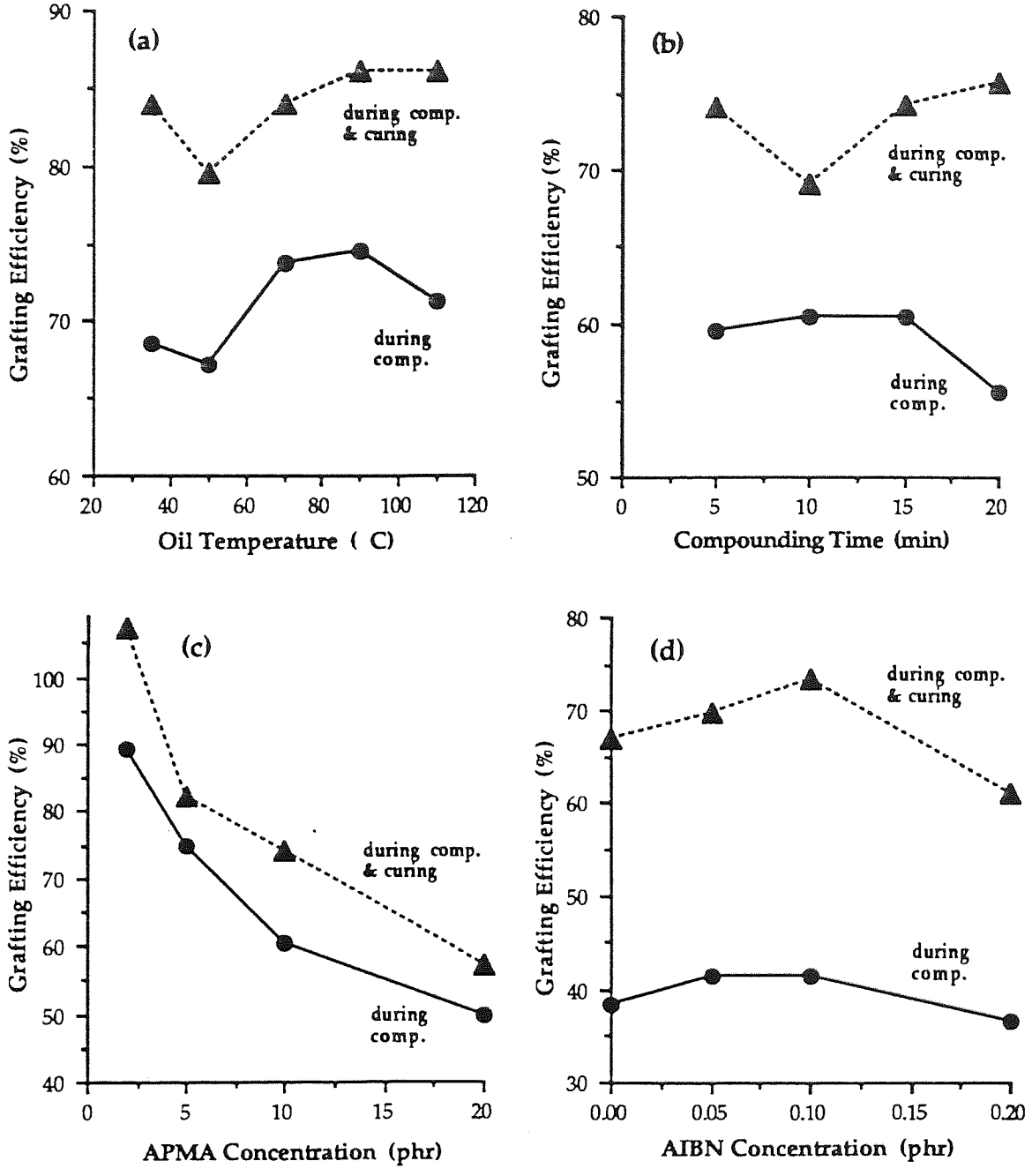

Due to slight variations in thickness of films, the sec. amide area index of APMA in NR (amide; 3355 cm-1, reference; 2727 cm-1), see fig. 2.89, was measured for films A, B and C and used as an identification of the grafting efficiency (instead of absolute value of amide peak area) in order to eliminate

error due to thickness. However, in order to take the experimental error into account a number of samples were measured and the average of these measurements is reported in table 4.10. Some measured sec. amide indices seemed to be erroroneous compared with other data obtained under the same processing conditions. The suspected data were approved by either the Dixon's criterion or Grubbs's criterion, see section 2.5.2.2, and the data outside the critical values were eliminated from the calculation. The Dixon's criterion was applied to sets of data which have only one suspicious value, while the Grubbs's criterion was applied to all other cases.

The solid lines and the dot lines in fig. 4.7 represent the grafting efficiency during processing and during processing and curing, respectively, see scheme 4.1.

$$\text{Grafting Efficiency during Processing} = \frac{\text{sec. Amide Index of Film B}}{\text{sec. Amide Index of Film A}} \times 100$$

$$\text{Grafting Efficiency during Processing \& Curing} = \frac{\text{sec. Amide Index of Film C}}{\text{sec. Amide Index of Film A}} \times 100$$

It is clear that a large amount of APMA becomes grafted during curing as well as during processing. Although the amounts of grafting at the two stages are different, the general trend in both cases is similar. This suggests, therefore, that the amounts of grafting during vulcanisation is nearly constant and the total amount of grafting is dominated by the amount of grafting which occur during processing.

From the testing results, the optimum grafting conditions for APMA is as follows; oil temperature 70 - 90 °C (chamber temperature 57 - 74 °C), compounding time 15 min, APMA concentration (no more than) 2 phr, AIBN concentration 0.10 phr. The rotor speed was optimum at 40 rpm; at faster speed large amount of APMA became stuck on the walls of the chamber and did not mix with NR, hence the rotor speed was fixed to 40 rpm.

4.2.3 Comparison of Physical Properties of APMA Containing Vulcanised Rubbers

Two types of APMA containing rubber samples were compounded for comparison; one was just added APMA in a normal compounding procedure, the second was an APMA grafted by pre-mixing, see scheme 4.2. In the following section, these two sets of samples are reffered to here as **add** and **graft**. Both cases the free APMA was extracted by azeotropic solvents in order to confirm the effect of grafting on the physical properties of NR.

The APMA grafted rubbers (master batches) were mixed before compounding to the other rubber ingredients. Typical changes in torque and chamber temperature during mixing of the master batches are illustrated in fig. 4.8. The conditions for grafting for these master batches were as follows; oil temperature 70°C, compounding time 15 min, APMA concentration 20 phr, AIBN concentration 0.1 phr, and rotor speed 40 rpm.

Fig. 4.8 Changes of torque and chamber temperature during reactive processing APMA with NR in an internal mixer as master batch rubber. (70°C, 15 min, [APMA] = 20 phr, [AIBN] = 0.1 phr, and rotor speed 40 rpm)

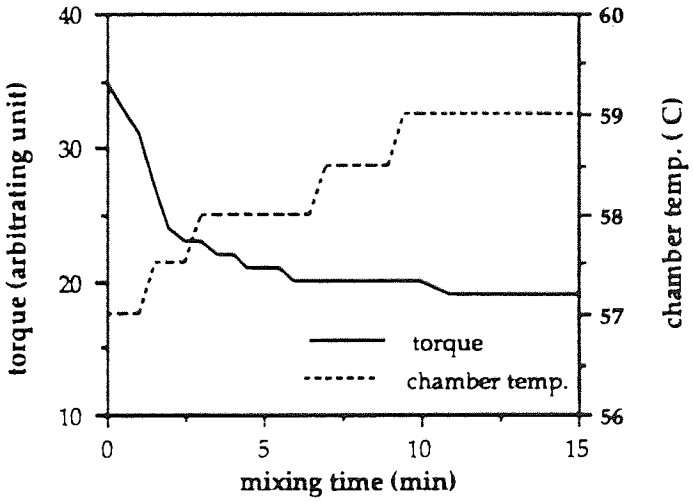

Although compounding lower concentration of APMA gave better grafting efficiency as shown in the previous section, such low concentrations are not practical because of the small size of the chamber of the internal mixer. It was necessary therefore to repeat the mixing operation of the master batches three or four times in order to gain enough rubber for the vulcanisation to obtain large enough samples to satisfy all the physical tests required. The torque decay and the temperature increase shown in fig. 4.8 were one example out of the four times mixed masterbatches.

After compounding the rubber ingredients, these rubber samples were tested for their Mooney viscosity and Monsanto rheometer characterisation. The test results are summarised in table 4.11. The grafting did not show significant effects on the curing characters but the viscosity of rubber decreased slightly because of the break down during the pre-mixing.

Table 4.11 Comparison of unvulcanised physical tests results between added APMA and grafted APMA. (grafting condition; 70°C, 15 min, [APMA] = 20 phr, [AIBN] = 0.1 phr, 40 rpm).

	add	graft
Mooney ML(1+4),100°C	12.7	10.0
Rheometer		
f_{min} (dNm)	4.3	4.5
f_{max} (dNm)	41.4	40.7
$t_{0.1}$ (min)	6.4	6.1
$t_{0.9}$ (min)	13.7	13.1

The grafting efficiency of APMA (measured by FT-IR of thin films) were as follows; during compounding 55 %, during compounding and curing 63 %. After vulcanisation, a fatigue test was carried out for both of add and graft samples before and after extraction of free APMA by azeotropic solvents, see scheme 4.2. The results of fatigue test are summarised in table 4.12 and fig. 4.9.

Table 4.12 Summary of fatigue resistance APMA added and grafted NR.

Sample	Strain (%)	Strain Energy (kg/cm2)	Fatigue Life × 0.01 (cycles)			Curve Fitting	
			mean	max	min	slope : A	intercept : B
APMA	91.2	3.7	2321.8	2512	1552	-1.6009	4.3159
add	108	4.9	1842.3	2041	1341		
before	142	7.5	827.7	865	710		
extraction	160	9.1	579.5	643	209		
APMA	91.2	4.4	2500.7	2797	2119	-1.5725	4.4071
graft	108	5.7	1685.3	2048	1029		
before	142	8.8	788.0	864	619		
extraction	160	10.7	640.9	691	511		
APMA	91.2	3.9	501.2	580	382	-2.3374	4.1728
add	108	5.2	440.1	483	280		
after	142	8.1	98.0	107	55		
extraction	160	9.9					
APMA	91.2	3.9	830.7	906	352	-1.4229	3.7548
graft	108	5.1	568.6	585	504		
after	142	8.0	267.1	294	107		
extraction	160	9.4	253.4	274	187		

X : Log (Strain Energy), Y : Log (Fatigue Life), Y = AX + B

Fig. 4.9 Fatigue resistance of APMA added and grafted (A) NR before and after azeotropic extraction. (see scheme 4.2)
APMA concentration in rubber samples : 1.5 phr, grafting efficiency 63 %
grafting condition 70°C, 15 min, 20 phr (APMA), 0.1 phr (AIBN), 40 rpm

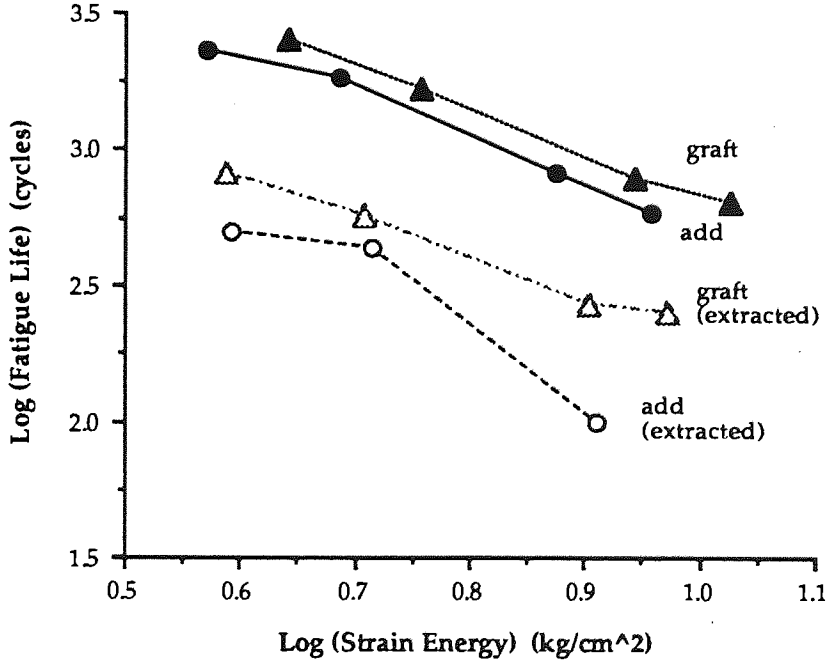

Although the APMA grafting efficiency was not high, **graft** samples showed better fatigue resistance than **add** samples; however, in both samples, the fatigue lives after extraction were much lower, since the extraction removed other components which act as antioxidants such as free sulphur, protein, natural tocopherols. The differences of fatigue resistance between **graft** and **add** implies the presence of grafted APMA on the NR chains.

Thermal resistance is summarised in tables 4.13 and 4.14 (at the end of this chapter) and changes of **Eb** and **Tb** during thermal ageing at different temperatures are illustrated in figures 4.10 - 4.12, and their retentions are shown in figures 4.13 - 4.15 Because pre-mixing and extraction had pushed down the value of the original Eb and Tb, not only the retention, but also the changes of Eb, Tb are illustrated in the figures.

Although in the case of fatigue resistance, there was a clear difference between **add** and **graft** samples, in the case of thermal resistance there appear to be no significant advantages in grafting APMA. The rubber exposed under moderate condition (70°C) showed no advantages in grafting. While the rubber exposed to higher temperatures showed slight differences. Tensile test results of the extracted add samples (after thermal degradation at 120°C) were not reported because of too much deterioration. The rubbers which have higher grafting efficiency should be subjected to further physical tests in order to confirm the effect of grafting.

Because the effects of grafting on thermal resistance were not large enough, the usage of reactive antioxidants should be considered case by case in terms of their service conditions and required properties. Although the grafting of APMA had advantage for fatigue resistance, it did not have clear advantage in thermal resistance and was likely to have disadvantages of slight deterioration of original Eb values in addition to the extra time need for the pre-mixing process required for the preparation of vulcanised rubber samples.

Fig. 4.10 Effect of APMA grafting (A) on thermal resistance (Eb, Tb retentions after thermal ageing at 70°C), see scheme 4.2.
APMA concentration in rubber samples : 1.5 phr, grafting efficiency 63 %
grafting condition 70°C, 15 min, 20 phr (APMA), 0.1 phr (AIBN), 40 rpm

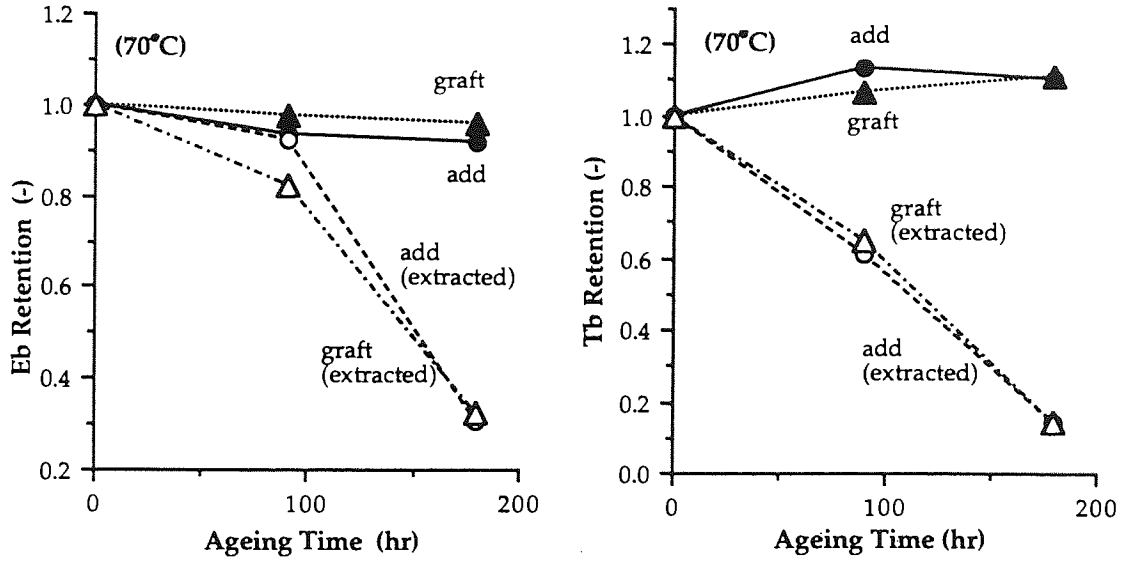

Fig. 4.11 Effect of APMA grafting (A) on thermal resistance (Eb, Tb retentions after thermal ageing at 100°C), see scheme 4.2.
APMA concentration in rubber samples : 1.5 phr, grafting efficiency 63 %
grafting condition 70°C, 15 min, 20 phr (APMA), 0.1 phr (AIBN), 40 rpm

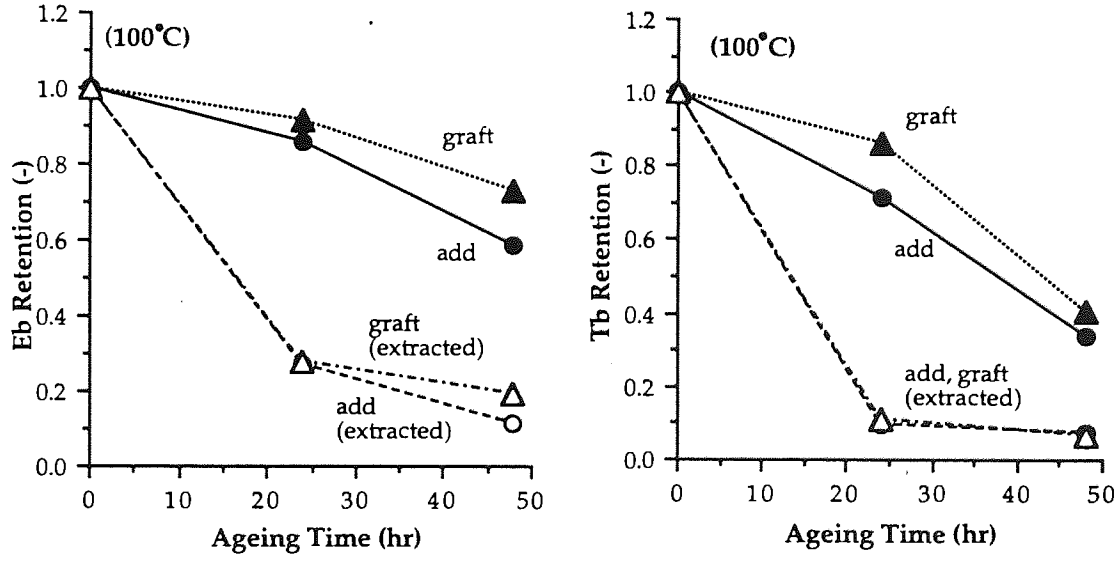

Fig. 4.12 Effect of APMA grafting (A) on thermal resistance (Eb, Tb retentions after thermal ageing at 120°C), see scheme 4.2.
APMA concentration in rubber samples : 1.5 phr, grafting efficiency 63 %
grafting condition 70°C, 15 min, 20 phr (APMA), 0.1 phr (AIBN), 40 rpm

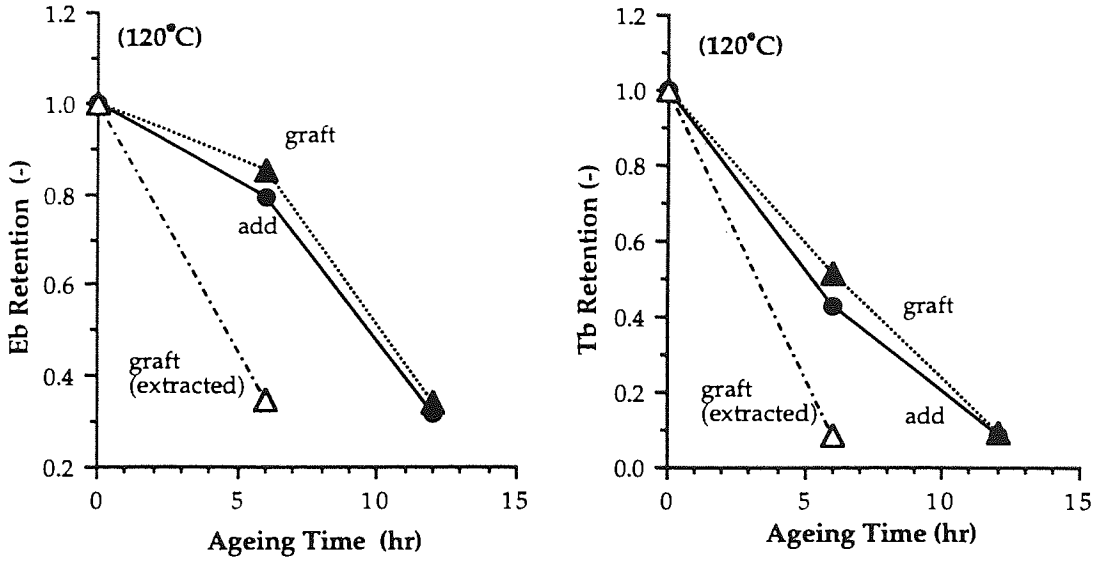

Fig. 4.13 Effect of APMA grafting (A) on thermal resistance (Eb and Tb after thermal ageing at 70°C), see scheme 4.2.
APMA concentration in rubber samples : 1.5 phr, grafting efficiency 63 %
grafting condition 70°C, 15 min, 20 phr (APMA), 0.1 phr (AIBN), 40 rpm

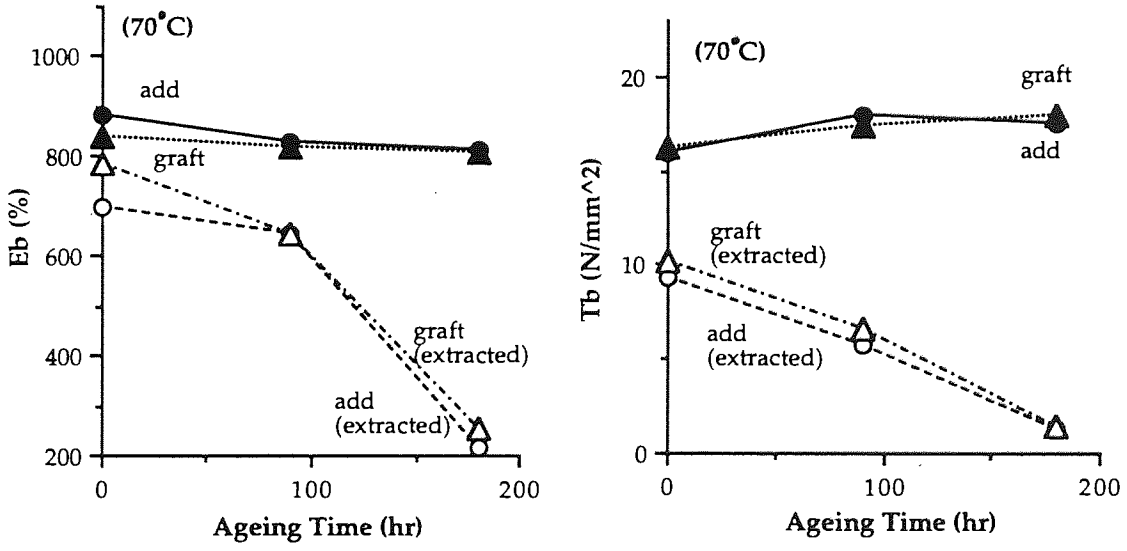

Fig. 4.14 Effect of APMA grafting (A) on thermal resistance (Eb and Tb after thermal ageing at 100°C), see scheme 4.2.
APMA concentration in rubber samples : 1.5 phr, grafting efficiency 63 %
grafting condition 70°C, 15 min, 20 phr (APMA), 0.1 phr (AIBN), 40 rpm

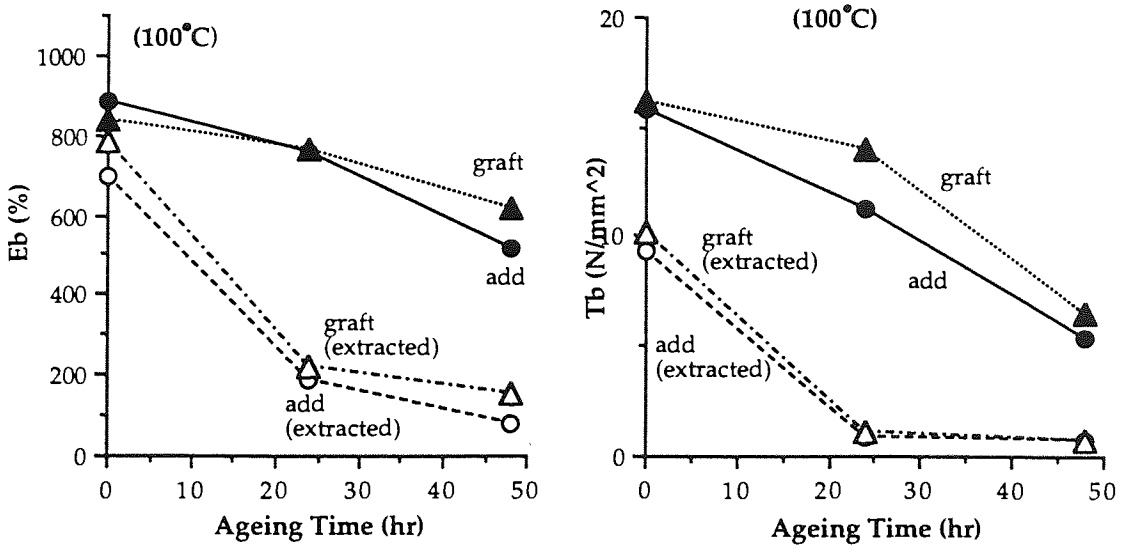

Fig. 4.15 Effect of APMA grafting (A) on thermal resistance (Eb and Tb after thermal ageing at 120°C), see scheme 4.2.
APMA concentration in rubber samples : 1.5 phr, grafting efficiency 63 %
grafting condition 70°C, 15 min, 20 phr (APMA), 0.1 phr (AIBN), 40 rpm

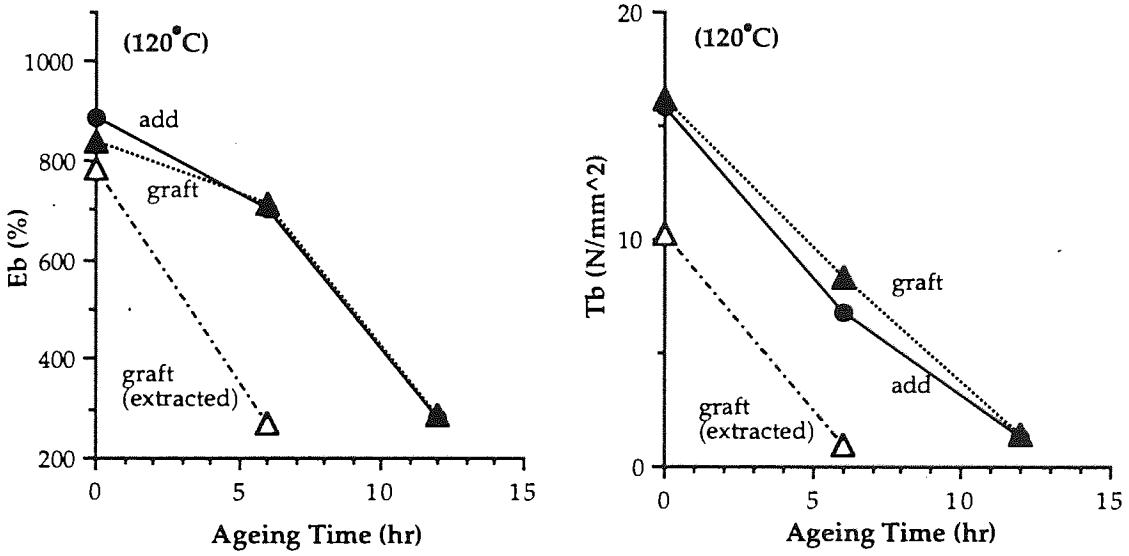

4.2.4 Determination of Structure of Grafted APMA on Polymer Chains.

The structure of grafting APMA on NR was investigated using model compound, squalene, for NR, see scheme 4.4, and structure of polymerised APMA in inert solvent was also analysed for comparison, see scheme 4.5. The concentration of APMA in squalene was decided to be equivalent to 10 phr of APMA in NR calculated on the basis of the number of APMA per isoprene unit. The reaction temperature of 100°C is much higher than the reactive processing chamber temperature of 57 - 58°C, and reaction time of 10 hr is much longer than reactive processing time 15 min, because in the same reaction condition as reactive processing, APMA did not show any grafting on the squalene. Compounds A, B and C in scheme 4.4 are expected to be the APMA grafted squalene (which has shorter APMA chain), the APMA grafted on the squalene (longer APMA chain), and the free APMA, respectively. The compound D and E in scheme 4.5 are also expected to be the free APMA and the polymerised APMA, respectively.

Only small amount of compound C was collected and therefore, further analysis was not carried out. In addition, in the experiment in scheme 4.5, all reaction products were insolube in n-heptanol and compound D was not detected. Compound A was a transparent viscous liquid which had slighty typical amines' colour, violet brown. Compound B was light green powder which had higher and wider melting point than original APMA (105 - 108°C), and although it was measured until about 230°C, compound B did not melt completely at that temperature, it started melting at 135°C. In addition this compound was insoluble in n-hepthanol and chloroform (parent APMA was soluble in both solvents), therefore, heptanol was used for separation of compound B from unreacted APMA (compound C), see scheme 4.4. Compound E was light grown powder which also had higher and wider melting point. Compound E started melting at 150°C and did not melt completely even at 230°C. Compound E dissolved neither n-heptanol nor in chloroform.

4.2.5 Synergistic Effects on Fatigue and Thermoxidative Resistance between Reactive Antioxidants and Antifatigue Agents and Peroxide Decomposers.

The effect of combination of four antifatigue agents with APMA and with peroxide decomposers on the fatigue and thermoxidative resistance of NR was evaluated. From the phenolic containing antioxidants, αTOC and γTOC were chosen, from the quinonoid group, BQ, and from the amine containing group, as a reference TMQ was chosen for testing, see table 4.1. Evaluation was carried out at various concentration of both APMA and the antifatigue agents in the combination in order to examine the indivisual effects on properties. Samples without any APMA nor antifatigue agents and samples containing only peroxide decomposers were also evaluated at the same time. Each additive effect was approved by the Scott's definition of synergism, antagonism, and additive [60) 61)], see sec. 1.6.1 and fig. 1.28.

In these series of testing, all APMA used were grafted master batch samples and the mixing conditions of APMA were the same as described in the previous tests (oil temperature 70°C, compounding time 15 min, APMA concentration 20 phr, AIBN concentration 0.1 phr, and rotor speed 40 rpm). The various concentration of APMA were adjusted by changing the amount of the master batch rubber added to fresh NR.

All samples were evaluated for their unvulcanised physical tests before testing the fatigue and thermoxidative resistance, see tables 4.20 - 4.24 (at the end of this chapter).

APMA grafted sample showed slight increase of Mooney viscosities compared with that of Blank sample, though that of in the previous testing (see table 4.2) showed small decrease due to break down during mixing. This implies the formation of gels during compounding due to APMA. The viscosity became higher, at the high concentration of APMA. Because of large number of

compounding, Mooney test schedule was delayed one or two days than in a normal schedule (usually the next day after compounding). The gel formation seemd to be slow and may be brought about during storing.

All fatigue results for additive effect investigations are summarised in table 4.25 - 4.29 (see the end of this chapter), and their results are illustrated for each series individually in fig. 4.32 (a) - (d).

In case of αTOC and γTOC series using with APMA, fatigue resistance showed that they work just like additive or slightly synergestic. It implies there were no special interaction between tocopherols and APMA.

While in the case of BQ series, they showed obvious antagonistic results, although both APMA and BQ had good antifatigue activity when they were used individually.

In industry, TMQ has been well known as a good antioxidant and antifatigue agent to use with other diarylamine antioxidants because of synergestic effect regenerating the other amine antioxidants during long service life [106]. However, in this work fatigue resistance seemed to be just additive effect or a small synergistic effect.

Althogh there are various types of TMQ which have different forms and different degree of polymerisation, the sample used in this work presented a problem during copmpounding as it stuck onto the roll mill. Therefore, in the case of using TMQ only the fatigue resistance slightly decreased at high concentration. In most cases except for BQ, fatigue resistance did not increase linearly like is the case with literature data, see fig. 1.28 [61]. Fatigue resistance of αTOC and γTOC also did not increase linearly with concentration, probablly due to the formation of dimers, see section 3.3.2.

0.25 phr of peroxide decomposers were added to 0.75 phr of APMA and 0.75 phr of antifatigue agents. In all cases they reduced the fatigue resistance. The samples containing these compounds seemed to be less flexible than others and they showed bad dispersion in NR due to the high melting poin, see table 2.7.

Fig. 4.32 Additive effects of APMA and various antifatigue agents and peroxide decomposers on fatigue resistance.
●: APMA only, ▲: antifatigue agent only, □: APMA + antifatigue agent,
○: APMA + antifatigue agent + P168, △: APMA + antifatigue agent + P626
(a) αTOC series, (b) γTOC series, (c) BQ series, (d) TMQ series

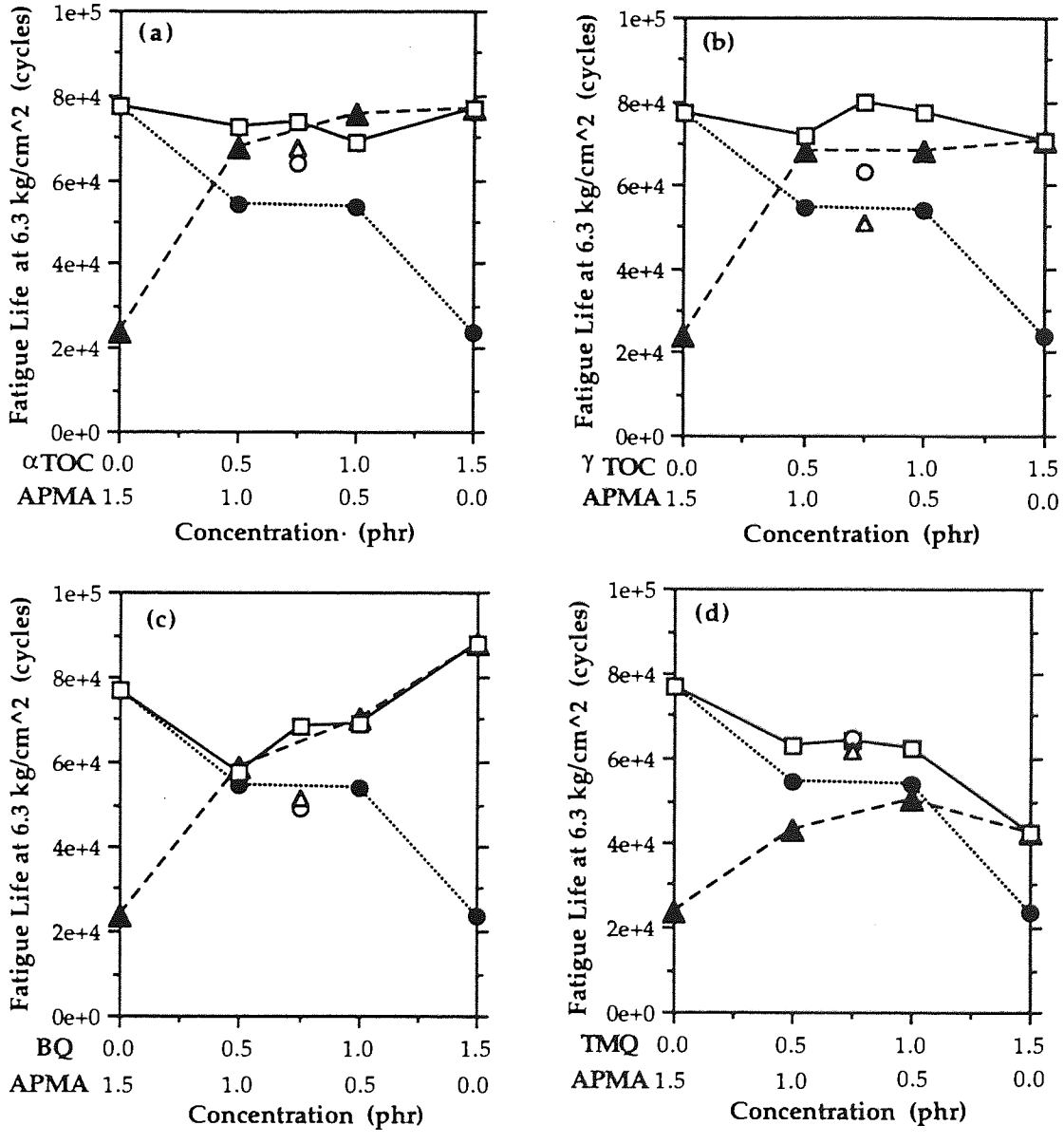

Results of thermoxidative resistance for these investigations are summarised in tables 4.30 - 34 (at the end of this chapter) and they are illustrated in figures 4.33 and 4.34. The retention of Eb and Tb after ageing at 100°C for 24 hr are shown individually in each series.

The thermoxidative resistance of αTOC and BQ series were dominated by the concentration of APMA, see fig. 4.33 (a), (c) and fig. 4.34 (a), (c), since both have poor thermal resistance. When only BQ was used, thermal resistance was nearlly independent on its concentration, while αTOC showed better activity at lower concentration and suddenly dropped down with increasing concentration, see fig. 4.33 (a), (c) and fig. 4.34 (a), (c).

The thermoxidative resistance of γTOC and TMQ when used with APMA and peroxide decomposers seemed to give just an additive effect, see fig. 4.33 (b), (d) and fig. 4.34 (b), (d). Again TMQ was expected to work strongly synegestically, however, it showed just an additive effect or small synegysm. Although γTOC showed analogous profiles of retention curves as those of αTOC, the degree of decrease of thermoxidative resistance at higher concentration was much smaller than that of αTOC.

Peroxide decomposers did not have any significant effects on thermal resistance because vulcanised rubber had already included large amount of sulfur compounds which can decompose peroxides. Further addition of other peroxide decomposers have only contributed to property deterioration.

Fig. 4.33 Additive effects of APMA and various antifatigue agents and peroxide decomposers on thermal resistance (Eb retention after ageing at 100°C for 24 hr).
●: APMA only, ▲ : antifatigue agent only, □ : APMA + antifatigue agent,
○: APMA + antifatigue agent + P168, △: APMA + antifatigue agent + P626
(a) αTOC series, (b) γTOC series, (c) BQ series, (d) TMQ series

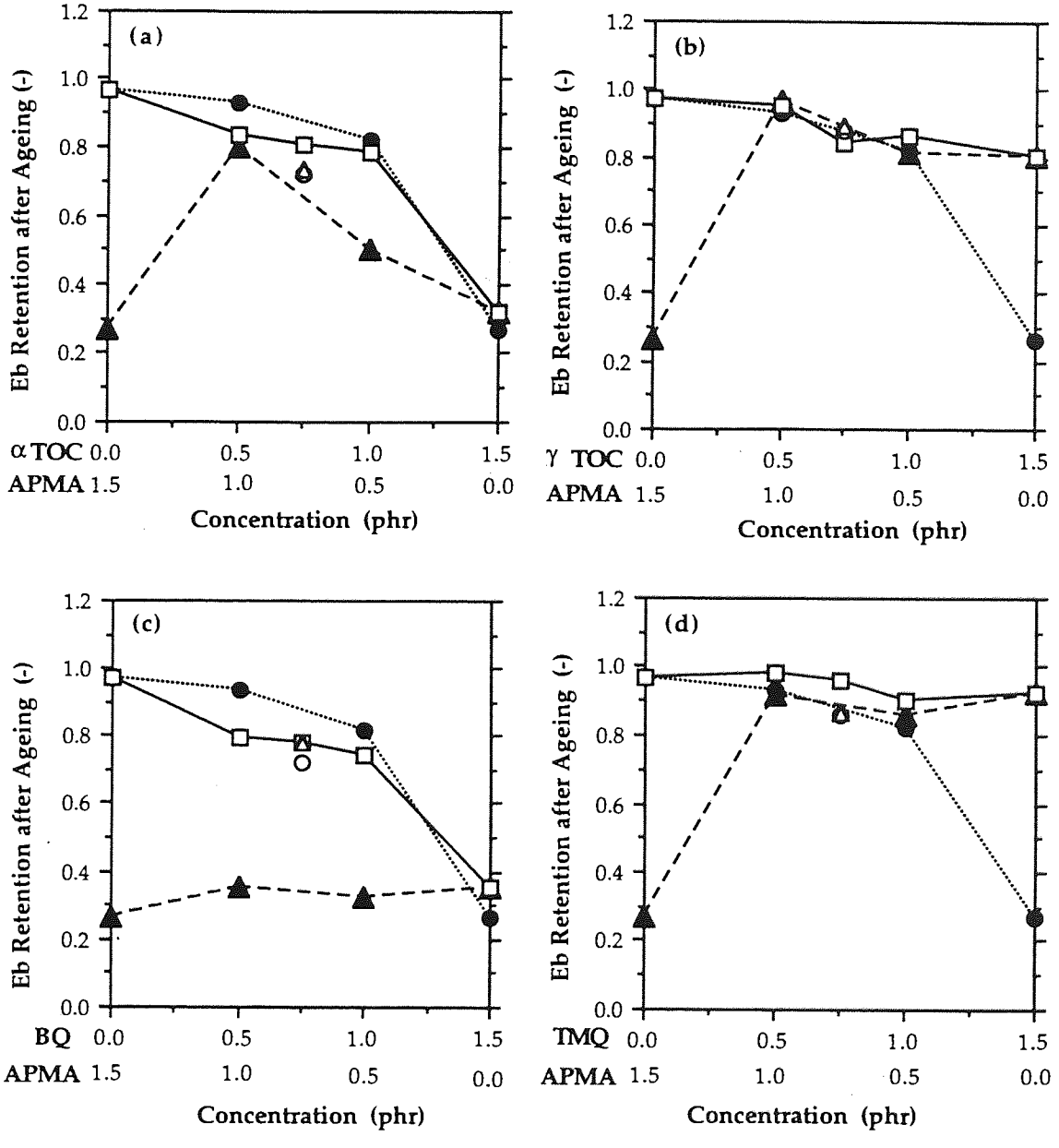

Fig. 4.34 Additive effects of APMA and various antifatigue agents and peroxide decomposers on thermal resistance (Tb retention after ageing at 100°C for 24 hr).
●: APMA only, ▲: antifatigue agent only, □: APMA + antifatigue agent,
○: APMA + antifatigue agent + P168, △: APMA + antifatigue agent + P626
(a) αTOC series, (b) γTOC series, (c) BQ series, (d) TMQ series

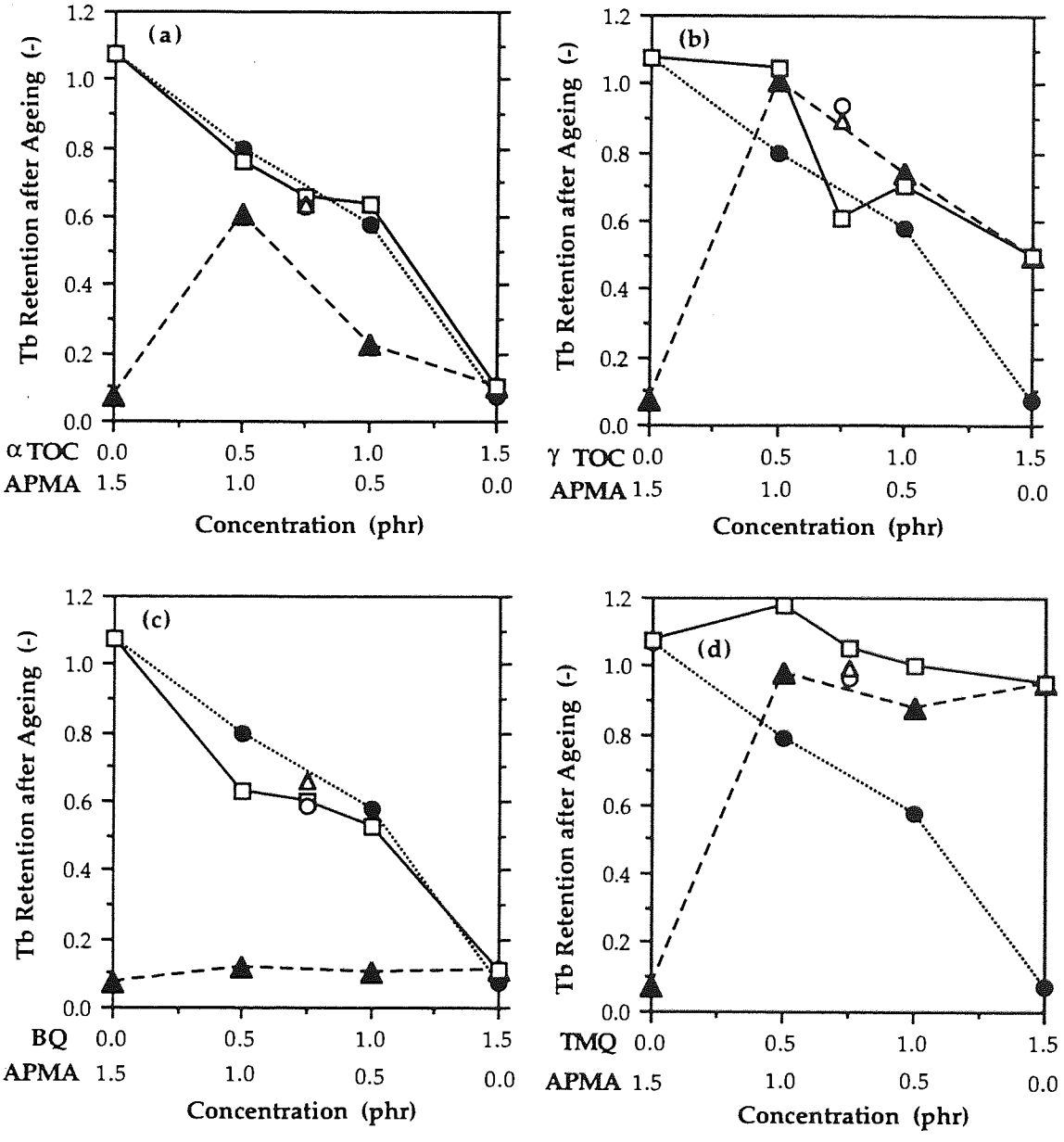

4.3 Discussion

4.3.1 Screening of Reactive Antioxidants

Among the evaluated reactive antioxidants, PM and APMA showed relatively good thermoxidative resistance, see figures 4.3 - 4.6. However, it is not clear whether the testing results for screening experiments represent only the difference in the ability to scavenge alkyl peroxyl radicals or overall effects of some extent of grafting which may have occured during compounding (on the roll mill) and curing. At low temperature, PM showed better thermoxidative resistance than APMA; however, the order was reversed at higher temperature. This difference may be either due to the difference in levels of volatility between APMA and PM or possibly due to the different extent of grafting. The difference in the results obtained from tensile tests and relaxation is likely to be due to the difference of sample thickness; the relaxation samples were around 0.3 mm thick, while the tensile samples were around 1.5 mm thick. The concentration of oxygen and possibilities of volatilisation of antioxidants are, therefore expected to be different. Thermogravimetric analysis may give further information.

Some samples showed the increase of Tb (compared with original Tb) at low temperature (see figures 4.3 and 4.4), and this is most certainly caused by an increase of modulus of these rubber samples. According to the auther's unpublished research [120], the activation energy of chain scission of main chain reaction is larger than that of crosslink formation reaction; therefore, increasing ageing temperature laeds to different extent of increase in the rates of the reactions. The Arrhenius curves of chain scission reaction and crosslink formation reaction normally crossover around 60 - 100 °C, see fig. 4.35[120]. Hence in the low temperature region, crosslink formation reaction is faster than chain scission when there are enough amount of sulfur or

polysulfide crosslinks in the rubber for further crosslink formation, the modulus will become higher and Tb may increase unless higher crosslink density disturb the mobility of the chains, see fig. 1.6.

Fig. 4.35 Typical Arrhenius curves of chain scission reaction and crosslink formation reaction of vulcanised NR [120].

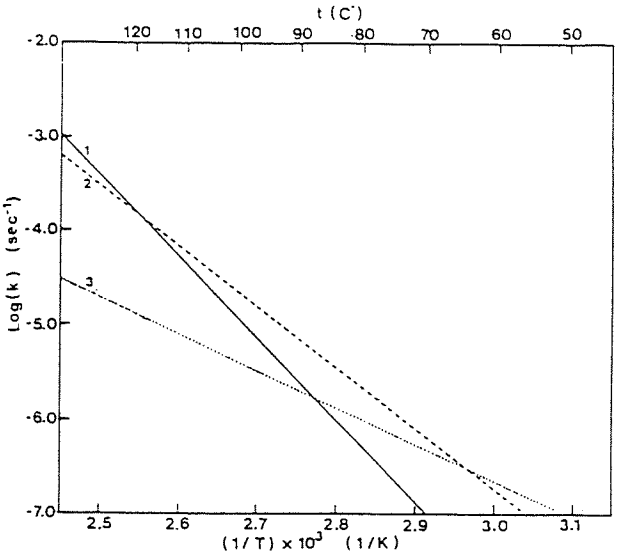

1. Chain scission along mainchain (with antioxidants)
2. Chain scission along mainchain (without antioxidants)
3. Crosslink formation

The reactivity of the different antioxidants with peroxyl radicals was calculated by MOPAC using PM3 method in order to help in these screening experiment. In a previous research by Samukawa and coworkers [121], it was shown that the reactivity index of antioxidants for radical reactions have linear relationship with the activities. Table 4.36 shows the results of calculations of reactivity index of each of the reactive antioxidants evaluated in this work, as well as, that of others based on the commercial amine antioxidants, IPPD, 6PPD, and TMQ. The calculated reactivity indices showed that in the case of IPPD and 6PPD, the reactivity of the NH group positioned between two aromatic rings (position I, see table 4.35) is higher than that in position II, whereas in the case of APMA and MADA, the situation is reversed, see table 4.35. The experimental values of Eb retention (100°C, 24hr) of rubber samples containing these antioxidants are ploted against calculated reaction indices, see fig. 4.36. Calculated reactivity shows that APMA has the highest potential

for alkyl peroxyl radical scavenging ability. In spite of the fact that MADA has also high potential for CB-D antioxidant activity, see table 4.35, its undesired vulcanisation characteristics disturbed further testing, see fig.4.1.

Table 4.35 Reactivity indices of evaluated reactive antioxidants and other normal amine antioxidants and Eb retention of these antioxidants containing rubber samples. (100°C, 24 hr, 1.5phr)

Code	Structure	Reactivity Index	λ oc	λ unoc	Eb retention (-)
PM	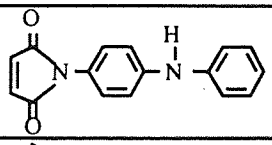	0.0944	-16.6650	5.3465	0.897
BTMI	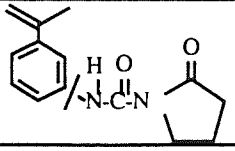	0.1067	-14.2156	2.9160	0.749
APMA	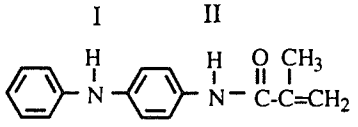	I 0.1159 **II 0.1240**	-12.4306 **-11.3552**	1.7782 **0.6022**	0.976
MADA	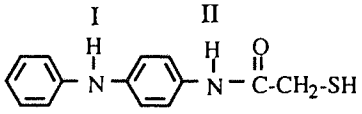	I 0.1070 **II 0.1157**	-13.9661 **-12.7671**	3.0694 **1.4321**	---
IPPD	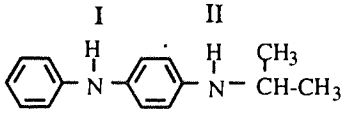	**I 0.1139** II 0.1014	**-12.5623** -14.7280	**2.2757** 4.8358	0.883
6PPD	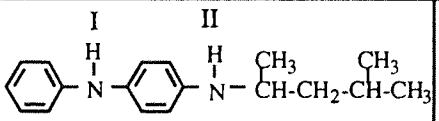	**I 0.1175** II 0.1019	-12.0737 -14.7474	1.7085 4.1903	0.939
TMQ	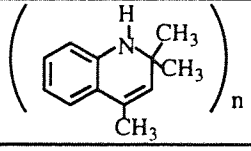	0.1193	-11.8027	1.4451	0.925

Fig. 4.36 Relationship between reactivity indices and thermal resistance.

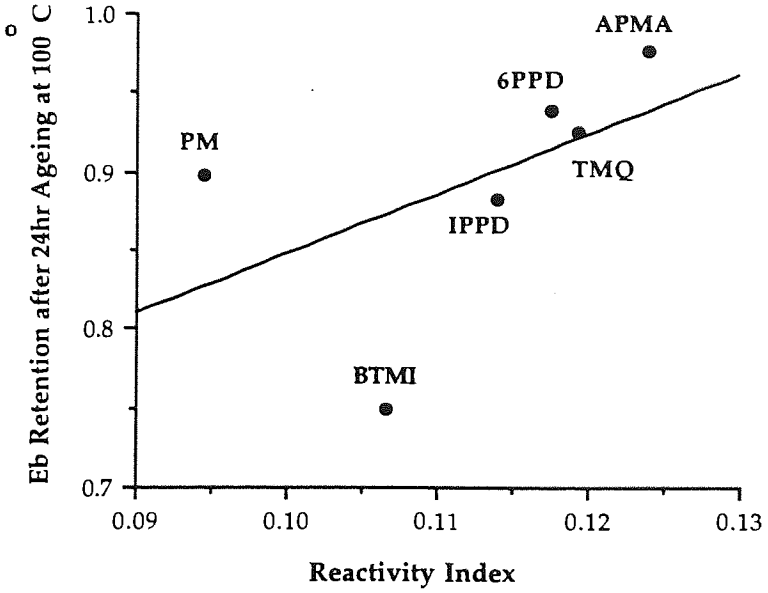

The screening test results showed that APMA is effective under all testing temperatures, see figures 4.3 - 4.6 and this was supported by the calculated results of reactivity index which also illustrated that APMA has the highest potential for trapping alkyl peroxyl radical. Moreover, APMA has also shown the best fatigue resistance among all the evaluated reactive antioxidants, see fig. 4.2. For these reasons, APMA was chosen for further testing as a reactive antioxidants to be grafted onto the NR chain during processing.

4.3.2 Optimum Grafting Conditions of APMA.

The optimum grafting conditions were shown to be as follows; oil temperature 70 - 90 °C (chamber temperature 57 - 74 °C), compounding time 15 min, APMA concentration 2 phr, AIBN concentration 0.1 phr, see fig. 4.7.

At low temperature, mechano radicals will be produced more than in the case with higher temperatures because of the low mobility of molecules by Brownian movement; however, the grafting speed will not be high enough under low temperature condition. At higher temperatures, the reaction speed will increase, while the mechano radical generation will decrease. Moreover side reactions such as oxidation can not be neglected under higher temperatures condition, although the grafting was carried out in a closed chamber of an internal mixer where oxygen access is restricted. For these reasons, the temperature of 57 - 74 °C (this corresponds to 70 - 90°C oil temperature, see table 4.9) seemed to be reasonable to be the optimum temperature for the grafting reaction.

It was initially expected that longer processing time would lead to more effective grafting. The testing results, however, showed a sudden drop of the grafting efficiency at 20 min after gradual increase up to 15 min, see fig. 4.7 (b). This may be due to some experimental error as this was not the case for results obtained after curing (see dot line in fig. 4.7 (b)). Longer processing times is expected to cause excess break down of the NR molecules leading to deterioration of properties. The grafting efficiency seemed to reach a plateau even around 5 - 10 min. In the case of master batch compounding (i.e. 20 phr of APMA) the optimum time was taken to be 15 min.

Lower concentration of APMA showed better grafting efficiency, see fig. 4.7 (c). When large amount of APMA was compounded, the total amount of APMA in the rubber would increase; however, the amount of grafting did not show a parallel increase resulting in lower grafting efficiency. This may be explained on the basis of lower (not enough) overall concentration of alkyl radicals available for such high APMA concentration to achieve high grafting efficiency. Methods available which may contribute to increasing the radical concentration during processing include the use of radical initiator or the increase of the rotor speed. In this work, higher rotor speed did not give good mixing, probably due to the slip on the wall of the mixer chamber. Among the various radical initiators, AIBN was chosen because of its effective temperature (half-life at 60°C = 18.6 hr, at 70°C = 5.0hr, at 80°C = 1.3hr [122]). It works well at relatively lower temperature and produce no deterioud products which can affect rubber deterioration.

In order to compound low concentrations of APMA master batch, a large mixer will be necessary which was not available in this work. If rubber is compounded in a larger internal mixer, it will be possible to compound APMA with all other rubber ingredients and hence further work on the compounding schedule must be investigated in such a case. Moreover, the procedure for determining the grafting efficiency should be reconsidered because the results had wide distribution and was difficult to get very precise data. Analysis of the solvents which extract the free APMA from unvulcanised or vulcanised rubber is required for more accurate results.

4.3.3 Structure Determination of Grafted APMA.

A suggested mechanism for the grafting of APMA on the polymer chains is shown in scheme 4.6. The double bond of the methacryloyl group in APMA is expected to contribute to the grafing on the polymer chains. The model compound for NR, squalene, is liquid and the grafted APMA (see scheme 4.6) may have a small value for **n**, hence this may be a liquid (compound A in scheme 4.4), while if **n** has a large value, the resulting compound can be solid (compound B in scheme 4.4). In both cases, the spectra of grafted APMA are expected to be similar to the combination of APMA and squalene spectra except for the peaks which represent C=C in methacryloyl group in APMA (should disappear in the case of grafted products).

Scheme 4.6 Suggested mechanism of APMA grafting on isoprene unit.

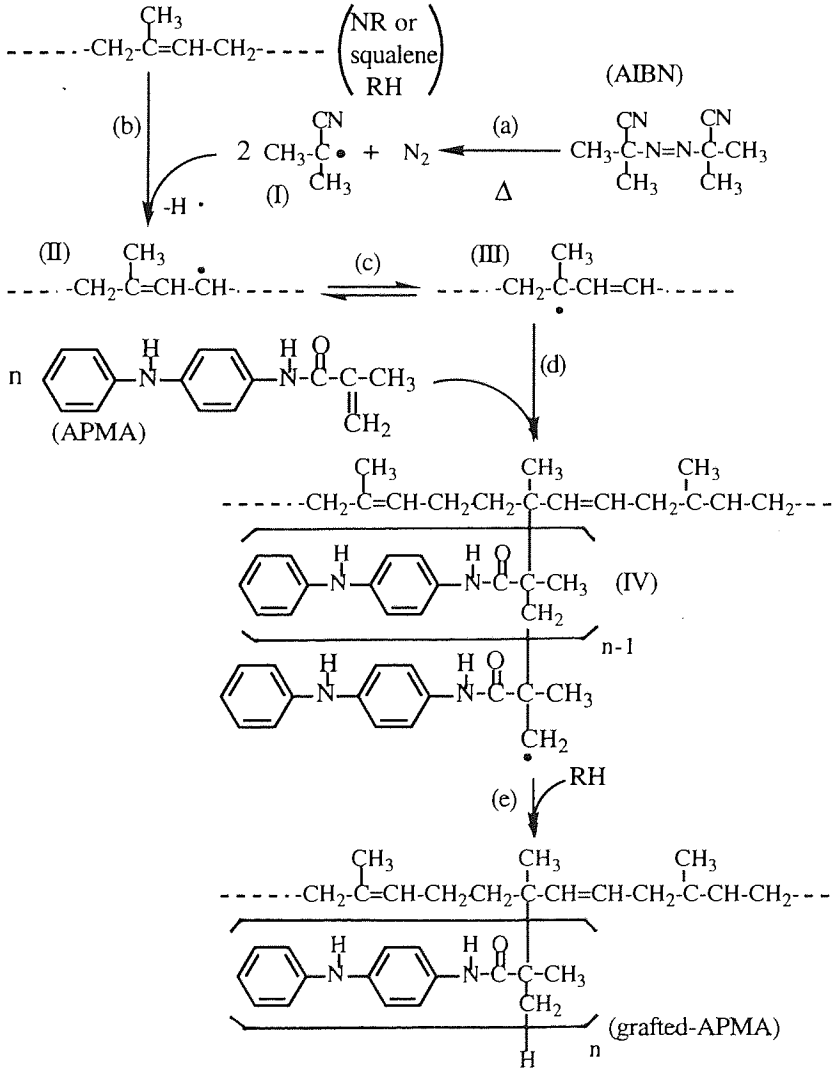

The grafting reaction of APMA on the polymer chain occurs competitively with its own polymerisation reaction, see scheme 4.6, hence even the grafted APMA, is expected to have some extent of polymerisation. If APMA grafts on squalene, compounds A and B should satisfy the following three points :

(I) FT-IR and NMR spectra of compounds A and B should include both APMA and squalene related peaks

(II) FT-IR and NMR peaks which represent C=C in methacryloyl group in APMA should disappear or decrease in the case of compounds A and B (new peaks due to saturated structure should appear in a lower chemical shift region in the case of NMR of compounds A and B)

(III) melting point of compound B should be higher than original APMA and solubility in solvents should become lower.

Compound E which was just polymerised in isopropanol for comparison will show similar results to the grafted product, compound B, except for (I).

Compound A was a transparent liquid which has slightly violet brown colour of amines. Compound A was filtered off from the mixture of the reaction products of APMA and squalene (see scheme 4.4) and microfiltered (>0.2μm) before spectroscopic analysis. The typical colour of amines for compound A suggest the presence of grafted APMA on squalene, however, all spectroscopic results did not show any evidences of grafting, see figures 4.16 - 4.18 and 4.27 - 4.28. The obtained FT-IR and NMR spectra of compound A were all same as original squalene spectra (see figures. 2.5 - 2.7) and no APMA related peaks were confirmed. For example, the peaks for νN-H (3350 cm^{-1}), νC=O (1653 cm^{-1}), and νC=C (1614 cm^{-1}) of APMA did not appear in the spectrum of compound A, although they are strong absorption peaks (see figures 4.17 and 4.18). From these results, compound A has either no grafted-APMA or very low concentration

(lower than the minimum sensitivity of FT-IR, ^{1}H-NMR and ^{13}C-NMR) of grafted-APMA.

On the other hand, FT-IR specra of compound B showed both APMA and squalene origined peaks, see figures 4.19 - 4.22. For example, represent APMA related peaks and represent squalene related peaks, see fig. 4.19. Since squalene and n-heptanol are miscible, all free squalene should be removed from the reaction mixtures of APMA and squalne, and consequently no ungrafted squalene is expected in compound B theoretically, see scheme 4.4 (point (I) is therefore satisfied). Although there must be no free squalene in compound B, there is possibility of the presence of small amount of free squalenen remaining in compound B, therefore, it is neccesarry to prove that compound B is not just a mixture of free APMA and free squalene. Because APMA is expected to graft using the C=C in the methacryloyl group (see scheme 4.6), FT-IR and NMR peaks which represent this group should change in the case of grafting. The IR peaks for CH_2=CRR' of APMA disappeared in the FT-IR spectrum of compound B.

• ν_{as} (=CH_2), ν_s (=CH_2)	3082, 2923 cm-1	(see fig. 4.20)
• ν C=C	1614 cm-1	(see fig. 4.21)
• δ CH (out of plane)	935 cm-1	(see fig. 4.22)

In addition, the IR peak for ν C=O in secandary amide group of APMA which is just adjacent to the methacryloyl group became broad and shifted to higher wave number, due to changes in the bond character of C=O caused by the different substituents on the carbonyl group.

- ν C=O (sec. amide) 1653 cm^{-1} → 1663 cm^{-1} (see fig. 4.21)

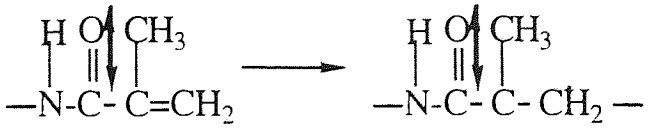

Similar changes in IR spectra were observed in the case of compound E (polymerised APMA), see figures 4.24 - 4.26. Although the peak at 1663 cm^{-1} of compound B (see fig. 4.21) may be the combination of the squalene peak at 1669 cm^{-1} and APMA peak at 1653 cm^{-1}, similar changes of peak width and position occurs in case of compound E as well (see fig. 4.25). It means this peak change in compound B is mainly induced by the changes of C=O character. Because compound B is expected to have a large value of **n** (a long chain of grafted APMA), the similarity of compounds B and E is reasonable. Not only in FT-IR spectra, but also in solid state ^{13}C-NMR spectrum, C=C related peaks showed changes. The peaks for No. 10 and 11 carbon (140.9, 111.6 ppm, respectively) of original APMA (see fig. 4.31 and table 4.19) are expected to shift to lower region for alkanes. New peaks for carbon No. 11, 12, 15, 16, and 14 of compound B (see fig. 4.29 and table 4.17) appeared at 46.5, 25.9, 17.7 and 16.1 ppm and the C=C related peak of APMA at 111.6 ppm disaooeared. (Because the peak at 140.9 ppm is so close to the peaks for the aromatic carbon in APMA, that it could not confirm whether disappear or not.) Similarly, in the case of compound E, the C=C related peaks disappeared and new peaks appeared in the alkanes' region (47.1, 39.9, and 30.9 ppm). Because the new peaks at 17.7 and 16.1 ppm are likely to represent the carbon in squalene which binds to APMA chain, point (II) is therefore satisfied. Finally, the melting point and solubility in solvents are expected to change, because grafted APMA are expected to be polymerised to some extent due to the competing reactions of grafting and polymerisation. Both compounds B and E showed higher and wider melting point than the melting point of the original APMA and they were insoluble (or quite less soluble) in n-heptanol and chloroform in which APMA was soluble (point (III) is satisfied). For these reasons, APMA is considered to graft on squalene in compound B with some extent of polymerisation.

It is expected that grafted APMA represent a long branch on squalene since it appeared in the solid phase (compound B) rather than the liquid phase (compound A), see scheme 4.4. In this work, the grafting efficiency on NR (see section 4.2.2) does not refer to the length of APMA branch. The high grafting efficiencies might be obtained by long branches (large **n** of APMA unit) rather than large number of grafting sites with short APMA branches (small **n** of APMA unit) which is more desirable for polymer stabilisation. Further optimisation of grafting conditions should be investigated.

If the reaction (d) in scheme 4.6 is much faster than termination reaction (e), chain sequence will repeate many times before termination leading to long APMA branch, see scheme 4.6. If radical initiation reaction (a) and (b) is not efficient, the concentration of (III) will be low and this will also cause long APMA branch. Under these conditions, APMA can easily make longer chains and side reaction which is just polymerisation of APMA (not grafting) can occur as well. In order to make short APMA pendants on many sites widely in squalene, reaction (a) and (b) should be high enough for providing high concentration of (III) and at the same time, reaction (e) should be faster than reaction (d), see scheme 4.6. In the work with model compound, reaction temperature of 100°C was too high for AIBN, other radical initiators must be used instead of AIBN, hence APMA branch became long in compound B.

4.3.4 Effects of APMA Grafting on Mechanical Properties of Rubber Samples

The effects of grafting of APMA on mechanical properties of vulacnised rubbers were examined by comparison of APMA grafted and just added rubber samples both before and after extraction of free APMA by azeotropic solvent, see section 4.2.3. The fatigue resistance of APMA grafted rubber showed a clear advantages compared with just additive rubber samples even after extraction, see fig.4.9. On the other hand, in case of thermoxidative resistance, the advantage of grafting was quite small or nothing, see figures 4.10 - 4.15. The reason as to why grafting of APMA has advantage when it acts by CB-A, but not via its CB-D activity is unclear. One possible reason is due to the difference of the effect of antioxidant mobility at different degradation temperature. As mentioned in the previous section, the grafted APMA may form long branches on the NR chains. If the grafted APMA is highly polymerised in NR, they will be maldistributed around the grafting sites and also the mobility of the antioxidant will become lower than in the case with free APMA due to higher molecular weight and binding on the polymer chains. At low temperature, however, the oxidation reaction proceeds much slower, in such case the effects of maldistribution and less mobility of antioxidant will not be significant. At high temperature, on the other hand, peroxyl radicals react rapidly before they migrate to the antioxidants, hence the effects of maldistribution and less mobility of antioxidant will become more significant. Fatigue test was carried out at ambient temperature, while thermoxidative degradation samples were degradated at high temperature (70 - 120°C). For example, the reaction rate of chain scission reaction at 100°C will be nearly two hundred thousand times as fast as that reaction rate at 20°C (this was based on calculation using activation energy of 39.4 kcal/mol for the sulphur vulcanised antioxidant containing rubber, see fig. 4.35 line 1). For these reasons, the advantages of APMA grafting was confirmed only under condition of fatigue resistance. Further optimisation of grafting conditions which lead to shorter APMA branches and better distribution will improve thermoxidative resistance as well fatigue resistance.

4.3.4 Additive Effects between APMA and Antifatigue Agents and Peroxide Decomposers.

As mentioned in the previous chapter, most of the quinonoid type antifatigue agents showed low thermoxidative resistance. Changing the concentration of additive is expected to cause changes in the thermoxidative resistance of rubber. In case of BQ, thermoxidative resistance was low at all BQ concentrations examined (see figures 3.33 c and 3.34 c), however, αTOC and γTOC showed better resistance at low concentrations and decayed with increasing their concentration (see figures 3.33 a, b and 3.34 a, b). This may be due to the formation of certain transformation products which affect the thermoxidative resistance at higher concentrations, most likely the spirodimer. Winterle reported that at high concentration, main oxidation products of αTOC at 50°C in acetonitrile and hexane were α-tocoquinone and spirodimer [114]. Because the spirodimer (see SPD, A5) does not have a phenol group, its thermoxidative resistance is expected to be low. Although the profiles of thermal resistance curves with increasing the tocopherol concentration (see figures 4.33 and 4.34) were of similar shapes, the extent of decrease at the higher concentrations of αTOC was much larger than that of γTOC because γTOC is expected to form other type of dimers (e.g. G2 and G3) which have -OH groups [112) 117]. The antioxidant efficiency decreases with increasing concentrations of tocopherols were also reported by Parkhurt [123] and Wakakura [124]. In the case of former, [123] tocopherols were oxidised in lard at 97°C and the decreases of antioxidant efficiency started above 300 μg/g (0.03%) in case of α-tocopherol and above 500 μg/g (0.05%) in case of γ-tocopherol. Wakakura [124] examined the effect of concentration of δ-tocopherol in squalane at 150°C and suggested that 0.5 - 1 % was the optimum concentration and this value was much higher than Parkhurt's [123] results. In this work, in both cases of αTOC and γTOC, the concentrations of 0.5 phr (0.46%) were the optimum and these values are similar to the Wakakura's optimum concentration.

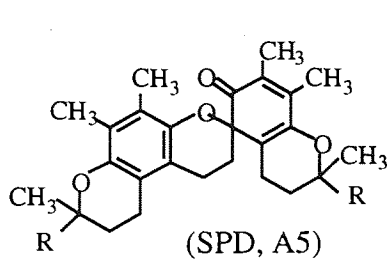

(SPD, A5)

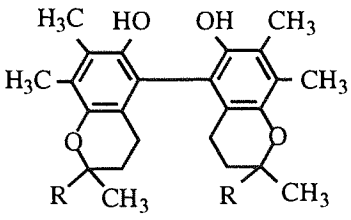

(G2)

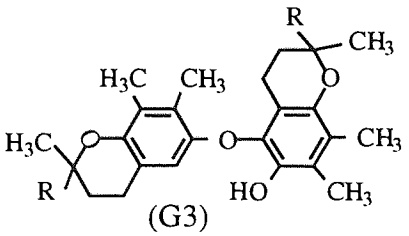

(G3)

Because BQ did not contribute to improving the thermoxidative resistance, the thermoxidative resistance of a BQ-APMA system was dominated by APMA concentration, see figures 4.33 and 4.34. In both systems of αTOC-APMA and γTOC-APMA, thermoxidative resistance was shown to be also dependent on APMA concentration and there was no significant synergestic effect. Although there are several literatures which examined the effect of amines on tocopherols' antioxidant efficiency [124) - 126)], the effect of amines were changeable. For example, Wakakura reported synergistic effect of α- and γ-tocopherols (1%) with naphthyl amine (1%) in squalane at 150°C [124)], and Ishikawa also reported synergestic effect of tocopherol mixture (0.04%) with several aliphatic amines (e.g. tri-n-octylamine) in lard at 60°C [125)], however, Olcott reported antagonistic effect of α-tocopherol with aromatic amines (e.g. diphenyl-p-phenylenediamine and 6-ethoxy-2,2,4-trimethyl-1,2-dihydro-quinoline) [126)].

Although two types of peroxide decomposers were evaluated, they also seemed to work just as additives. Vulcanised rubbers contain various sulphides which act as peroxide decomposers, the addition of a small amount of phosphorous compounds did not have any drastic effects on the overall stabilising activity of the system, see figures 4.33 and 4.34. Moreover, these phosphorous compounds have high melting points and their distribution during compounding was poor leading to the small deterioration observed in the fatigue resistance, see fig. 4.32. Wakakura reported that ZnDDP which is a peroxide decomposer worked just as additive with tocopherols [124)]. However inorganic phosphate is known to regenerate α-tocopherol during oxidation process [127)], see scheme 4.7, hence the

phosphorous compounds used in this work were also expected to have a potential of synergistic effects (althogh they did not show any synegisms in this work), since they produce similar compounds during peroxide decomposition process as shown below;

$$ROOH + (R'O)_3P \longrightarrow ROH + (R'O)_3P{=}O$$

Scheme 4.7 Chemistry of α-tocopherol with phosphorous compound [127].

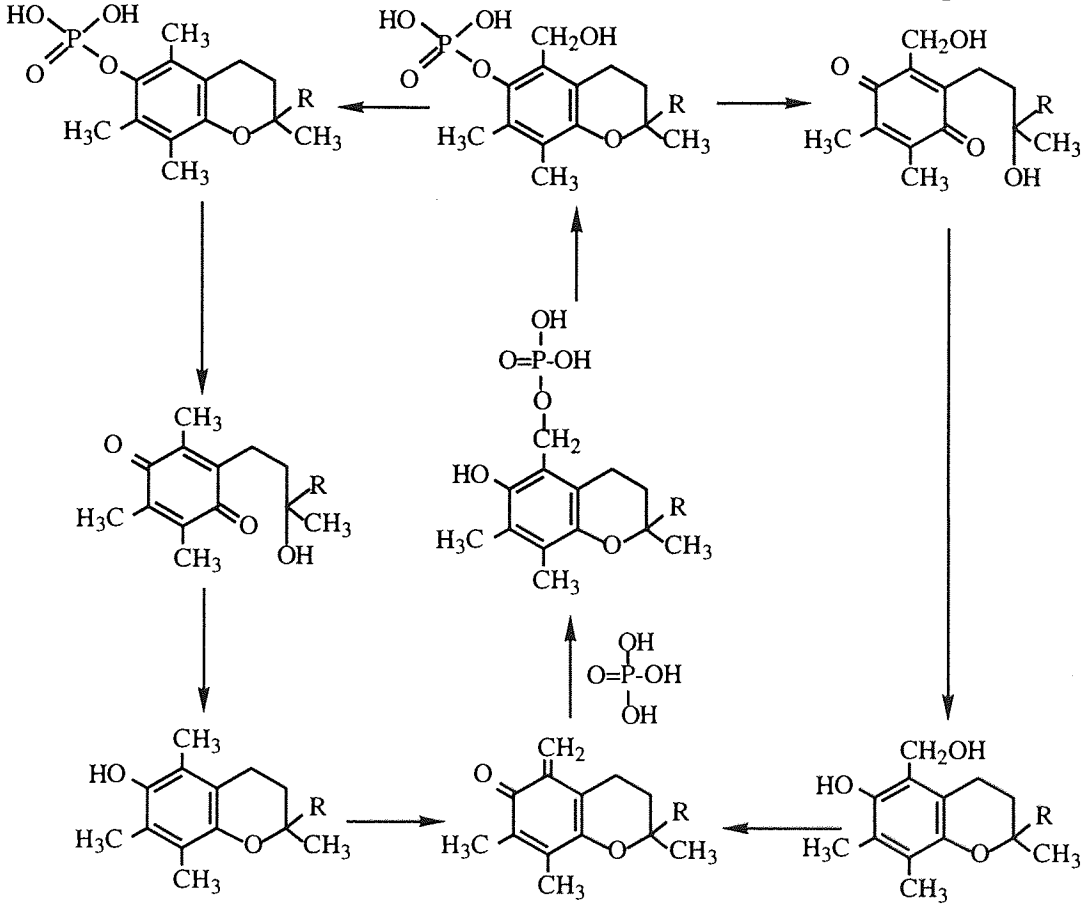

In the case of αTOC-APMA and γTOC-APMA systems, fatigue resistance was also shown to be just as additives and no synergism was observed. However, good overall fatigue resistance is clear from fig. 4..32 and both systems were effective. However BQ showed an obvious antagonism and the reasons for this are not clear from this work.

Table 4.4 Retention of elongation at break (Eb) after thermal ageing of reactive antioxidants containing rubbers.

Sample	Original Eb (%)	Eb Retention (-)					
		70°C		100°C		120°C	
		90 hr	180 hr	24 hr	48 hr	6 hr	12 hr
Blank	820.8	0.849	0.825	0.293	0.255	0.555	0.370
PM	907.8	0.984	0.977	0.897	0.858	0.869	0.657
BTMI	945.0	0.828	0.821	0.749	0.348	0.514	0.452
APMA	881.7	0.949	0.903	0.976	0.939	0.912	0.820
MADA	---	---	---	---	---	---	---

Table 4.5 Retention of tensile strength (Tb) after thermal ageing of reactive antioxidants containing rubbers.

Sample	Original Tb (%)	Tb Retention (-)					
		70°C		100°C		120°C	
		90 hr	180 hr	24 hr	48 hr	6 hr	12 hr
Blank	15.940	0.699	0.587	0.090	0.053	0.152	0.089
PM	16.342	1.036	1.023	1.042	0.930	0.799	0.399
BTMI	16.007	0.736	0.676	0.338	0.083	0.111	0.077
APMA	13.582	0.964	0.972	1.076	0.985	0.876	0.565
MADA	---	---	---	---	---	---	---

Table 4.6 Chemical stress relaxation and Mooney-Rivlin curves of reactive antioxidants containing rubbers.

Sample	Stress Relaxation (at 100 °C)		Mooney-Rivlin Curve		
	$k \times 10^2$ (1/hr)	$q_m \times 10^6$ (mol/ml·hr)	$\upsilon \times 10^4$ (mol/ml)	$2C_1$ (N/mm^2)	$2C_2$ (N/mm^2)
Blank	2.00	2.32	1.15	0.287	0.165
PM	0.63	0.57	0.90	0.222	0.331
BTMI	5.54	4.56	0.82	0.204	0.303
APMA	0.66	0.44	0.66	0.165	0.404
MADA	---	---	---	---	---

Table 4.7 Reduced stress of NR samples containing reactive antioxidants.

Strain (%)	Reciprocal Strain $1/\lambda$	Reduced Stress $\sigma/(\lambda - \lambda^{-2})$ (N/mm^2)		
		PM	BTMI	APMA
5	0.952	0.507	0.451	0.533
10	0.909	0.518	0.466	0.528
15	0.870	0.500	0.463	0.516
20	0.833	0.499	0.453	0.502
25	0.800	0.487	0.447	0.489
30	0.769	0.478	0.437	0.475
35	0.741	0.468	0.429	0.464
40	0.714	0.460	0.421	0.453
45	0.690	0.450	0.414	0.443
50	0.667	0.442	0.402	0.435
55	0.645	0.436	0.400	0.427
60	0.625	0.430	0.394	0.420
65	0.606	0.424	0.387	0.413
70	0.588	0.418	0.383	0.407
75	0.571	0.414	0.379	0.403
80	0.556	0.409	0.373	0.398
85	0.541	0.405	0.370	0.393
90	0.526	0.401	0.367	0.389
95	0.513	0.398	0.363	0.386
100	0.500	0.395	0.361	0.383
105	0.488	0.392	0.358	0.380
110	0.476	0.389	0.356	0.378
115	0.465	0.387	0.354	0.375
120	0.455	0.385	0.352	0.374
125	0.444	0.383	0.351	0.372
130	0.435	0.380	0.349	0.370
135	0.426	0.379	0.348	0.369
140	0.417	0.378	0.347	0.367
145	0.408	0.377	0.346	0.366
150	0.400	0.376	0.345	0.364
155	0.392	0.375	0.344	0.361
160	0.385	0.374	0.343	0.361
165	0.377	0.373	0.343	0.360

Table 4.8 Chemical stress relaxation of NR samples containing reactive antioxidants. (at 100°C)

Time	Log { f(t) / f(0) }		
(hr)	PM	BTMI	APMA
0.0	0.000	0.000	0.000
0.5	-0.024	-0.071	-0.016
1.0	-0.036	-0.118	-0.026
1.5	-0.042	-0.156	-0.034
2.0	-0.051	-0.190	-0.041
2.5	-0.057	-0.223	-0.047
3.0	-0.063	-0.253	-0.053
3.5	-0.068	-0.283	-0.057
4.0	-0.073	-0.311	-0.060
4.5	-0.079	-0.339	-0.065
5.0	-0.083	-0.366	-0.070
6.0	-0.093	-0.419	-0.080
7.0	-0.106	-0.480	-0.086
8.0	-0.112	-0.531	-0.095
9.0	-0.117	-0.591	-0.101
10.0	-0.124	-0.636	-0.108
11.0	-0.130	-0.695	-0.114
12.0	-0.136	-0.754	-0.120
14.0	-0.150	-0.888	-0.134
16.0	-0.160	-1.039	-0.145
18.0	-0.175	-1.189	-0.157
20.0	-0.184	-1.391	-0.171

Table 4.13 The effect of the grafting of APMA on the Eb and Eb retention after thermal ageing.

Sample	Original Eb (%) & (retention)	Eb (%) and Eb Retention (-) after Thermal Ageing					
		70°C		100°C		120°C	
		90 hr	180 hr	24 hr	48 hr	6 hr	12 hr
add	884.8	827.8	812.6	759.6	517.0	701.0	284.1
	(1.000)	(0.936)	(0.918)	(0.858)	(0.584)	(0.792)	(0.321)
graft	839.4	819.4	805.1	767.2	613.8	714.9	285.7
	(1.000)	(0.976)	(0.959)	(0.914)	(0.731)	(0.852)	(0.340)
add-ext.	699.2	646.3	216.2	187.6	81.9	—	—
	(1.000)	(0.924)	(0.309)	(0.268)	(0.117)	—	—
graft-ext.	784.0	645.5	252.2	219.0	151.5	270.5	—
	(1.000)	(0.823)	(0.322)	(0.279)	(0.193)	(0.345)	—

* ext. = extracted

Table 4.14 The effect of the grafting of APMA on the Tb and Tb retention after thermal ageing.

Sample	Original Tb (N/mm^2) & (retention)	Tb (N/mm^2) and Tb Retention (-) after Thermal Ageing					
		70°C		100°C		120°C	
		90 hr	180 hr	24 hr	48 hr	6 hr	12 hr
add	15.886	18.037	17.494	11.328	5.390	6.827	1.356
	(1.000)	(1.135)	(1.101)	(0.713)	(0.339)	(0.430)	(0.085)
graft	16.238	17.363	18.027	13.938	6.562	8.315	1.484
	(1.000)	(1.069)	(1.110)	(0.858)	(0.404)	(0.512)	(0.091)
add-ext.	9.358	5.735	1.335	0.893	0.709	—	—
	(1.000)	(0.613)	(0.143)	(0.095)	(0.076)	—	—
graft-ext.	10.238	6.638	1.495	1.152	0.692	0.908	—
	(1.000)	(0.648)	(0.146)	(0.112)	(0.068)	(0.089)	—

* ext. = extracted

Fig. 4.16 FT-IR spectrum of compound A pasted on KBr crystal. (transparent viscous liquid)

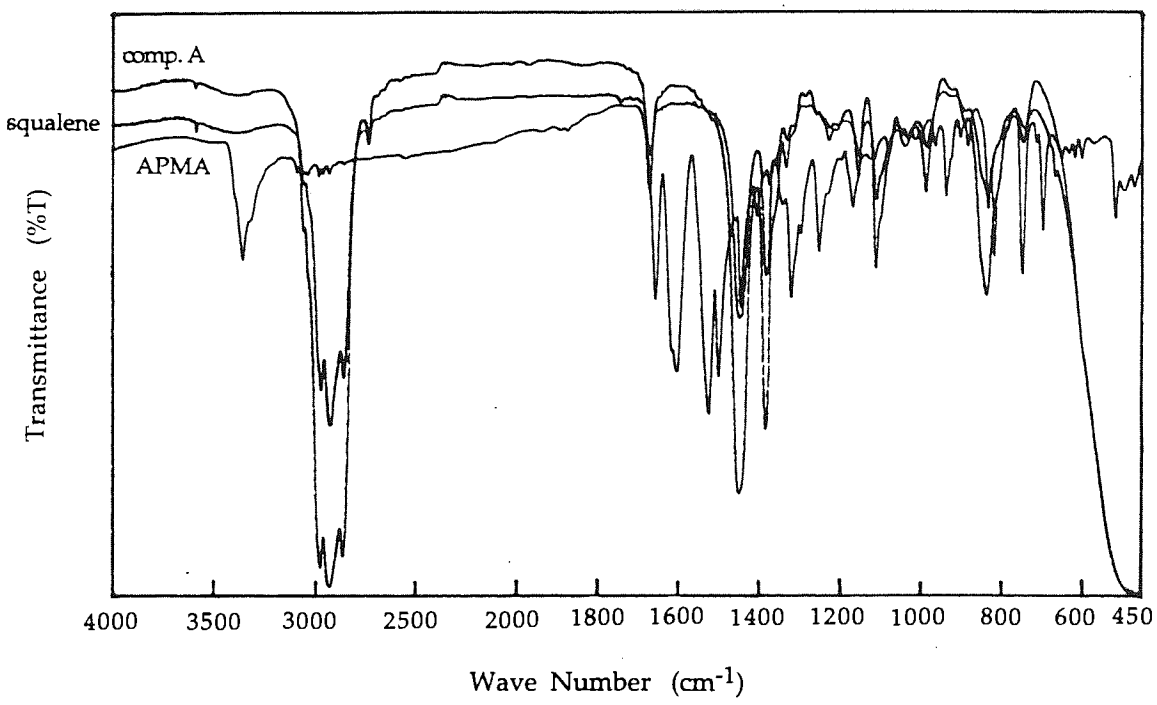

Fig. 4.17 FT-IR spectrum of compound A pasted on KBr crystal in the amide streching region (3800 - 2500 cm-1)

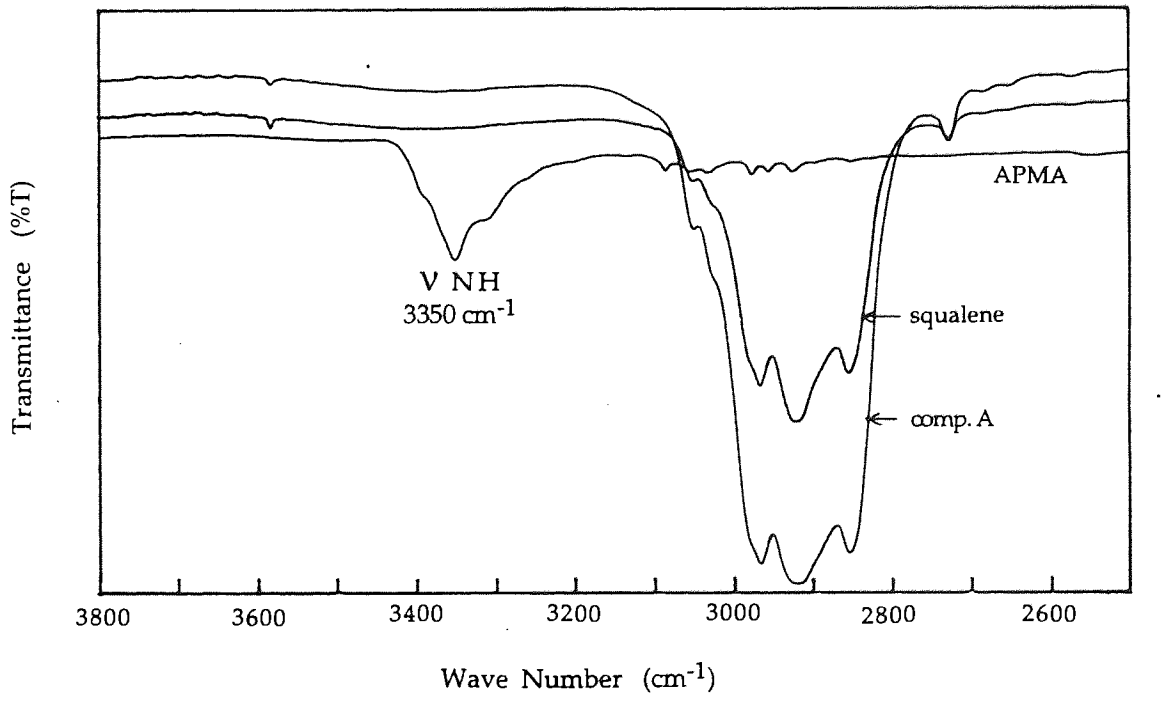

Fig. 4.18 FT-IR spectrum of compound A pasted on KBr crystal in the carbonyl streching region (1800 - 1400 cm-1).

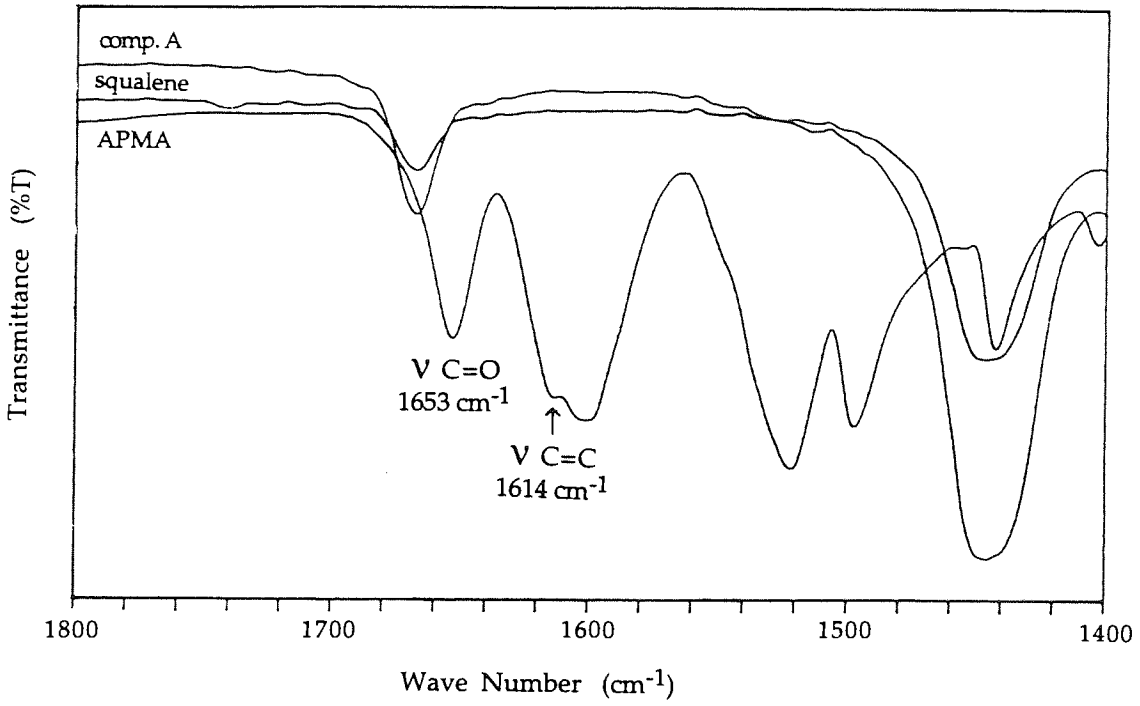

Fig. 4.19 FT-IR spectrum of compound B using KBr disk. (light green powder)
(● : APMA origined peaks, △ : squalene origined peaks)

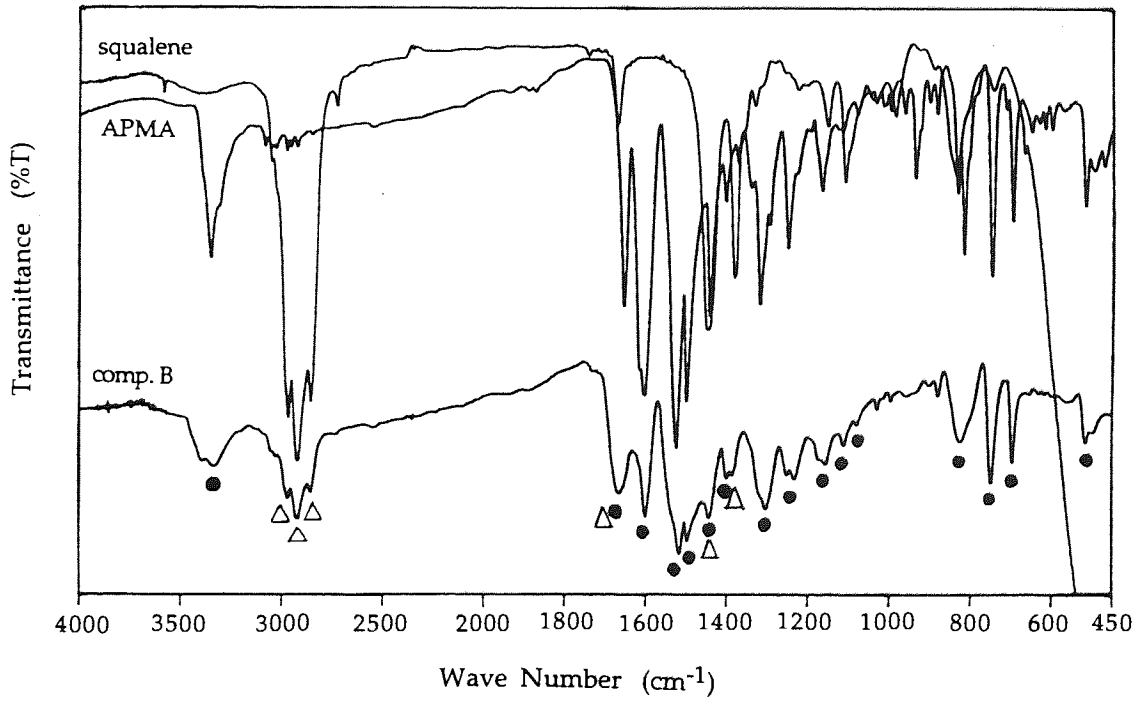

Fig. 4.20 FT-IR spectrum of compound B in KBr disk in the amide streching region (3200 - 2800 cm-1)

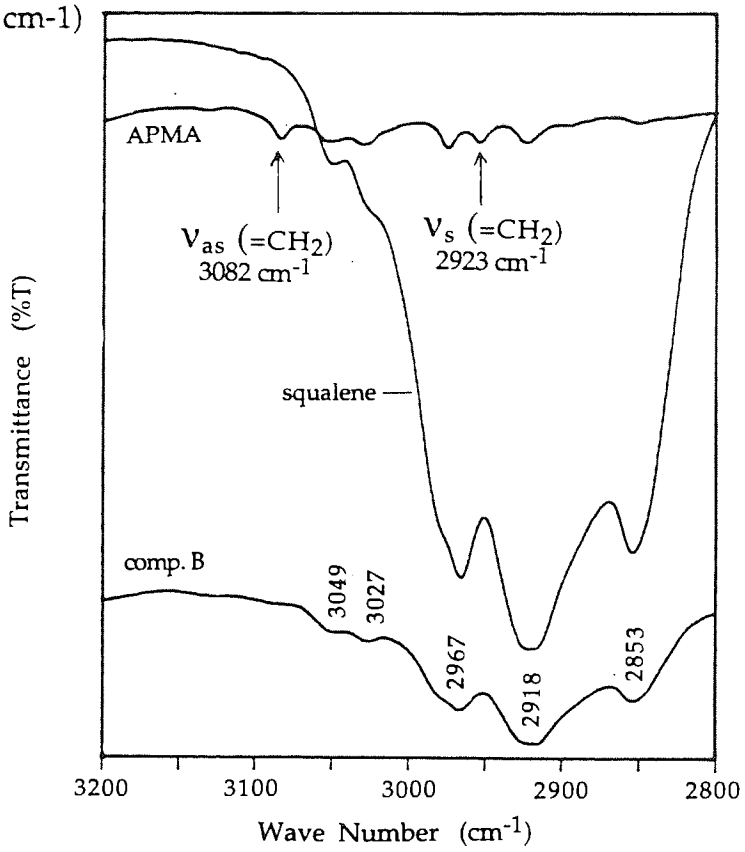

Fig. 4.21 FT-IR spectrum of compound B using KBr disk in the carbonyl streching region (1800 - 1400 cm-1)

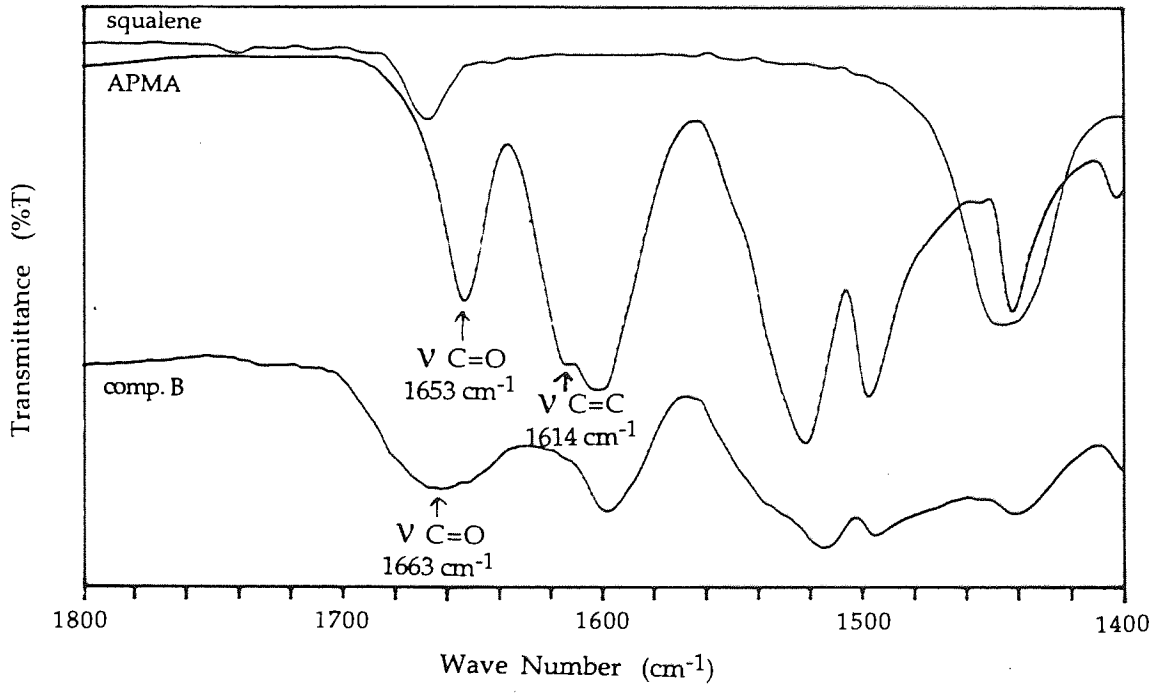

Fig. 4.22 FT-IR spectrum of compound B using KBr disk in the out of plane bending region (1000 - 600 cm-1)

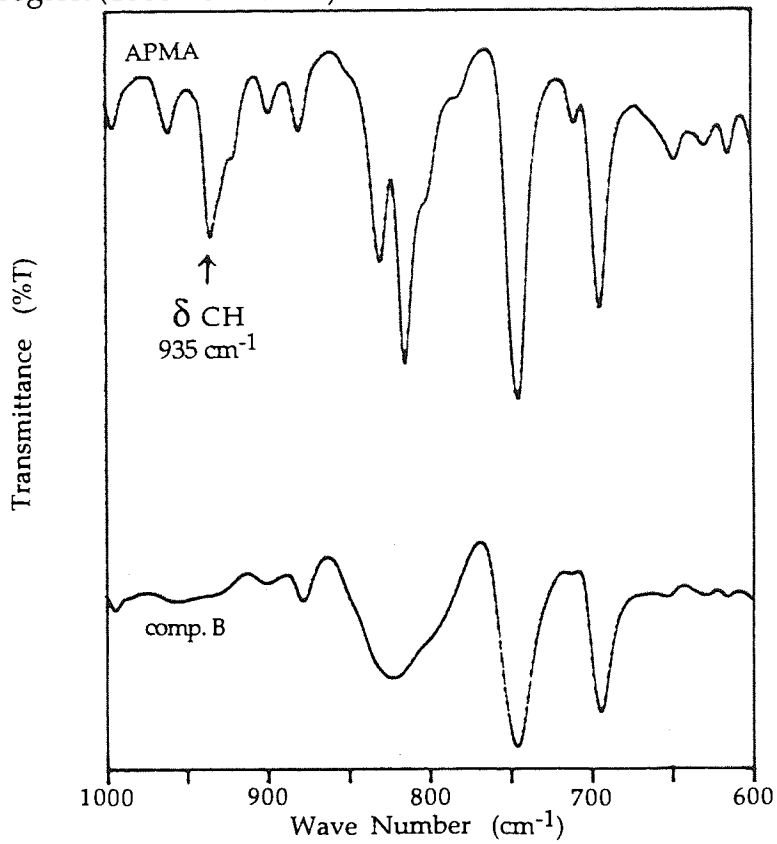

Fig. 4.23 FT-IR spectrum of compound E using KBr disk. (light brown powder)

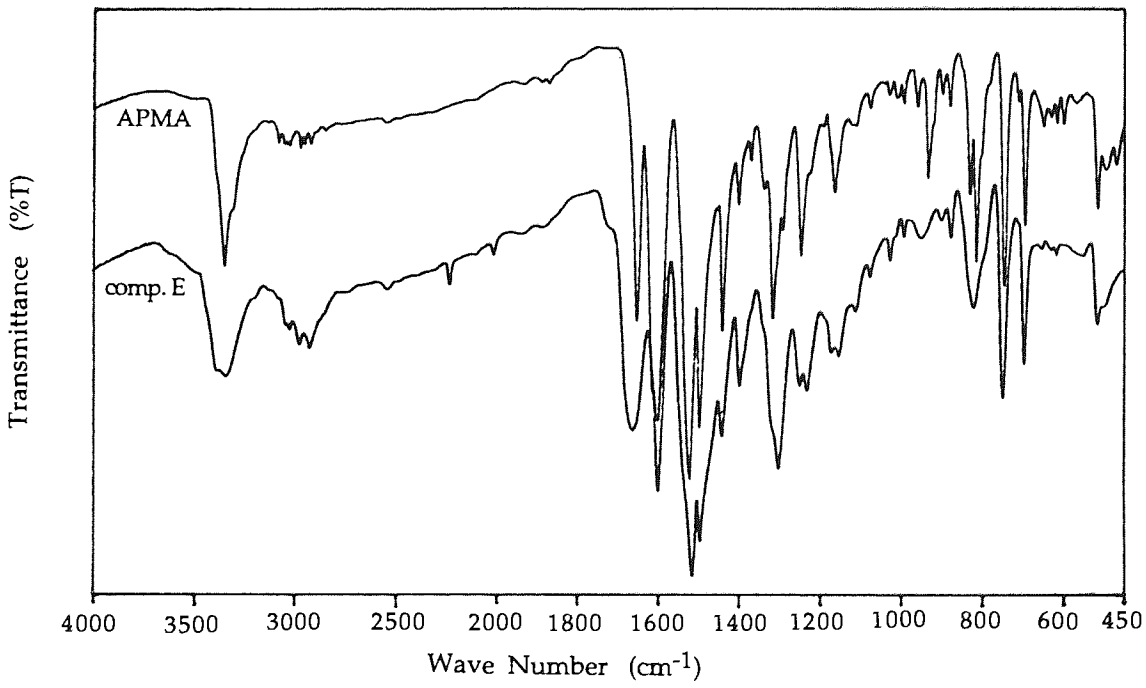

Fig. 4.24 FT-IR spectrum of compound E in KBr disk in the amide streching region (3200 - 2800 cm-1)

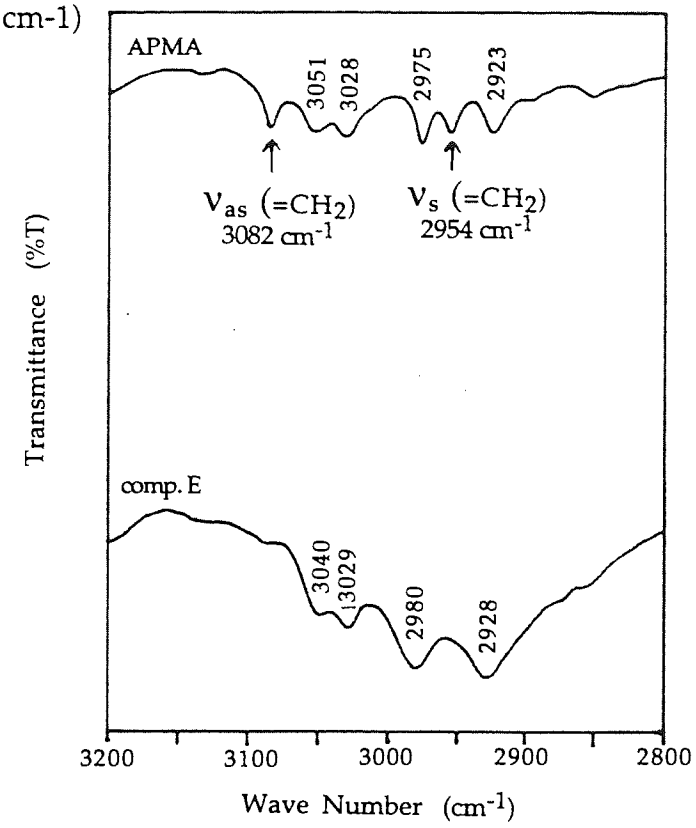

Fig. 4.25 FT-IR spectrum of compound E in KBr disk in the carbonyl streching region. (1800 - 1400 cm-1)

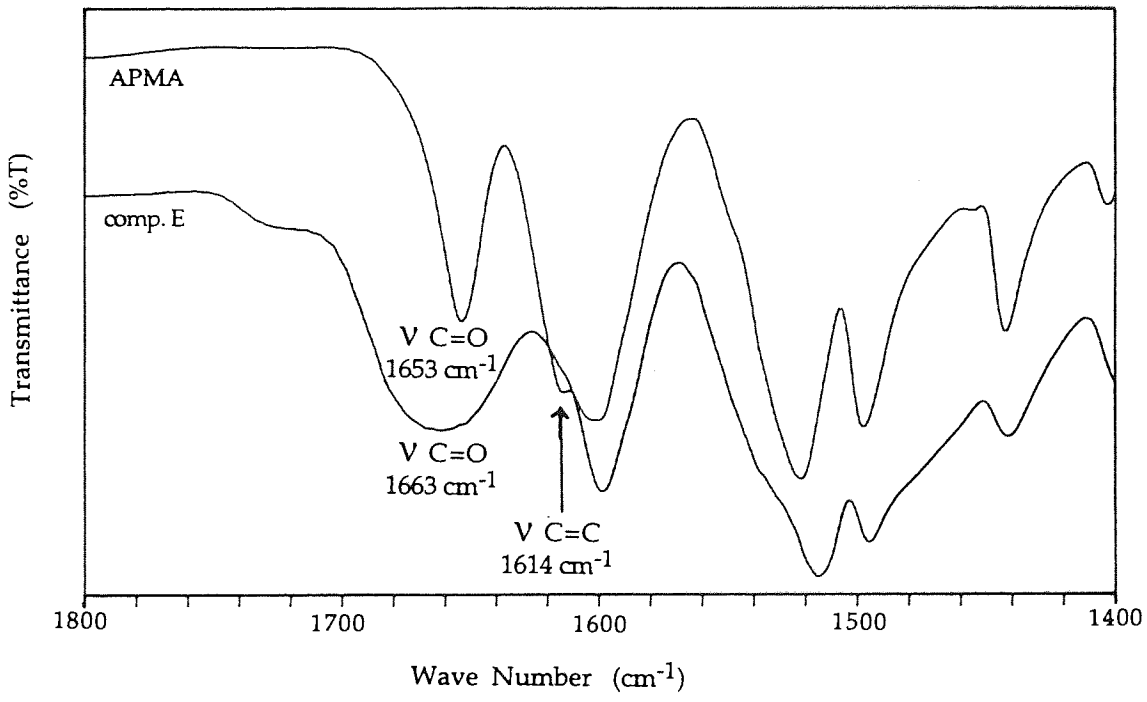

Fig. 4.26 FT-IR spectrum of compound E in KBr disk in the out of plane bending region (1000 - 600 cm-1)

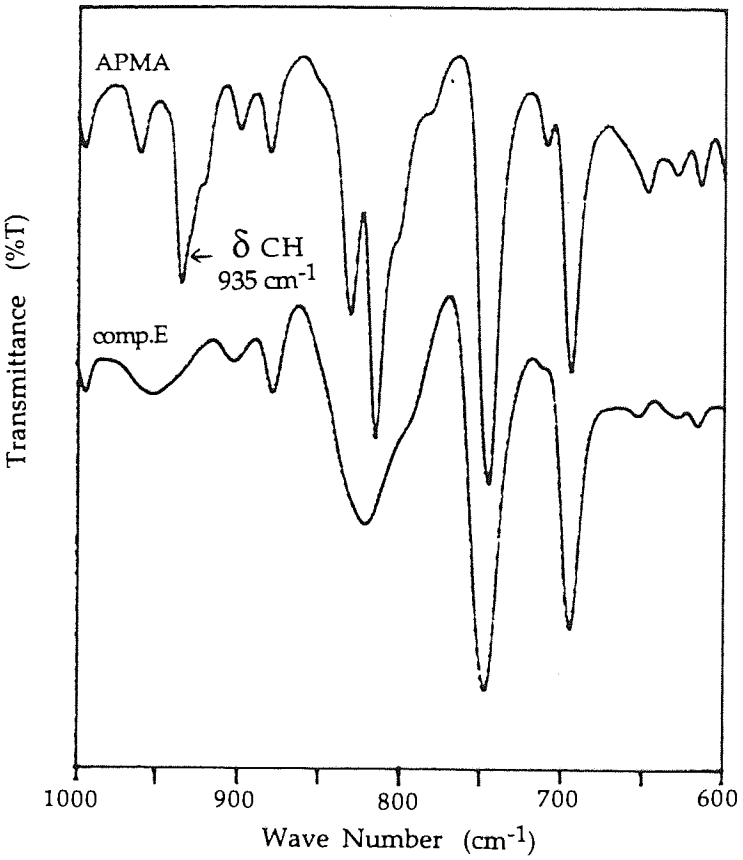

Fig. 4.27 ^{1}H-NMR spectrum of compound A (300MHz)

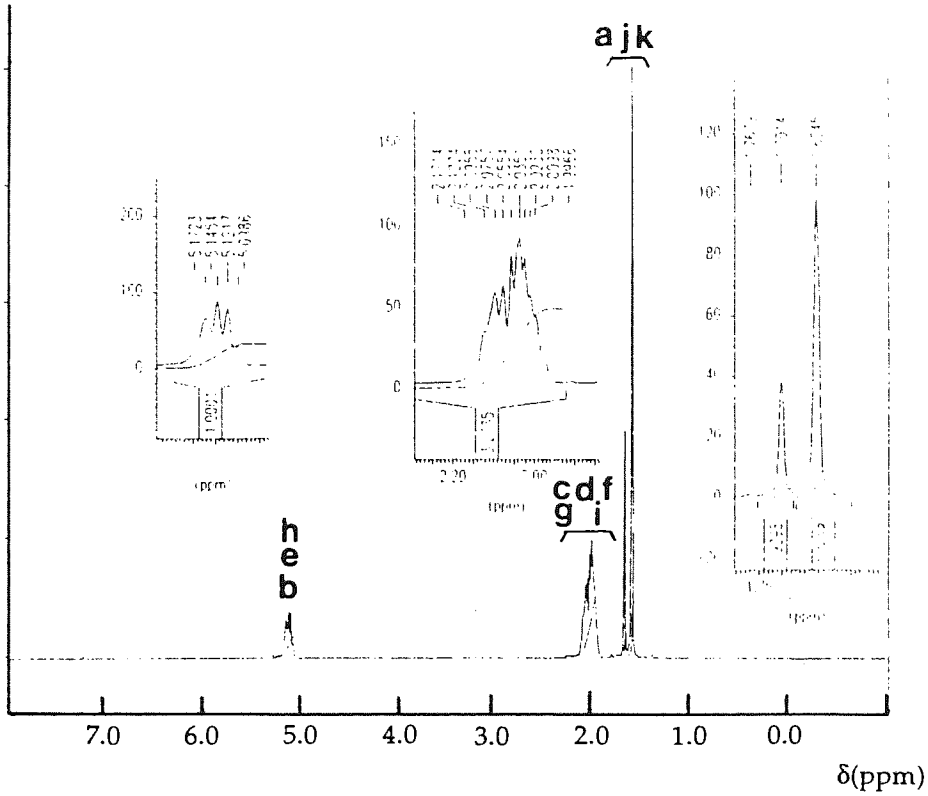

Table 4.15 ^{1}H-NMR summary of compound A

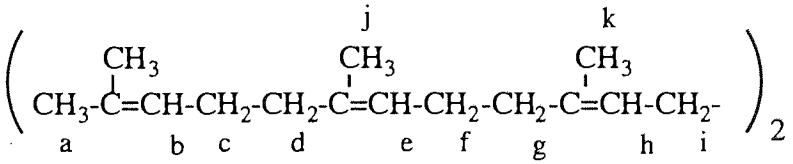

No. of Atom	δ (ppm)	Integral
b, e, h	5.1723, 5.1454,5.1217,5.0986	1.00
c, d, f, g, i	2.1714, 2.1224, 2.0955, 2.0757, 2.0554, 2.0351, 2.0230, 2.0098, 1.9966	3.27
a, j, k	1.7014, 1.6245	3.70

Fig. 4.28 ^{13}C-NMR spectrum of compound A (75.5MHz)

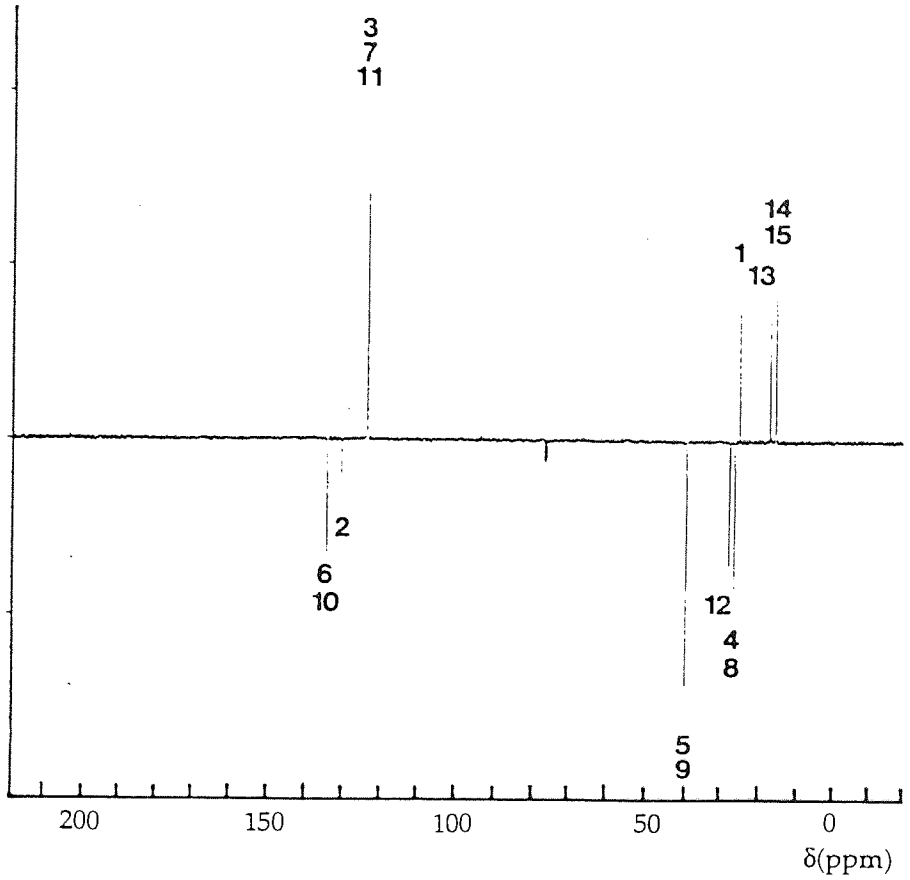

Table 4.16 ^{13}C-NMRspectrum of compound A

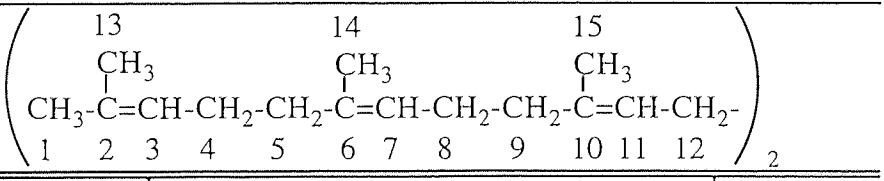

No. of Atom	δ (ppm)	(+) / (-)
6, 10	134.9555, 134.7534	(-)
2	131.0706	(-)
3, 7, 11	124.4129, 124.3118, 124.2685	(+)
5, 9	~ 39.8	(-)
12	28.2729	(-)
4, 8	26.7565, 26.6409	(-)
1	25.6589	(+)
13	17.6147	(+)
14, 15	15.9828, 15.9395	(+)

Fig. 4.29 Solid state ^{13}C-NMR spectrum of compound B (75.5MHz).

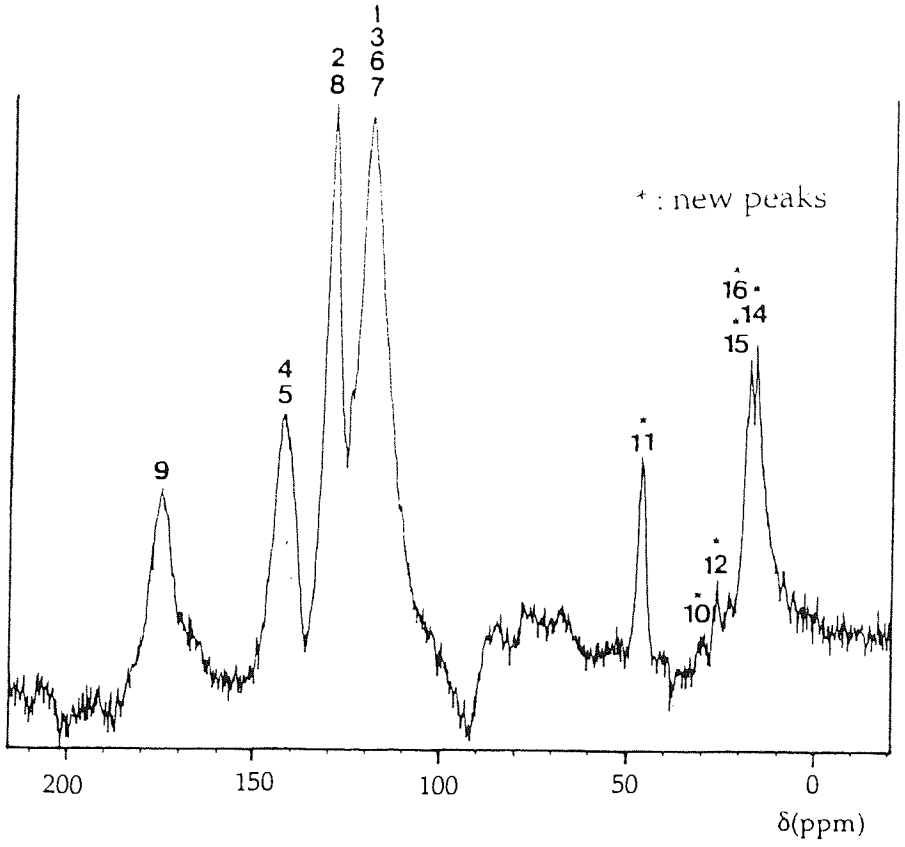

Table 4.17 ^{13}C-NMR summary of compound B

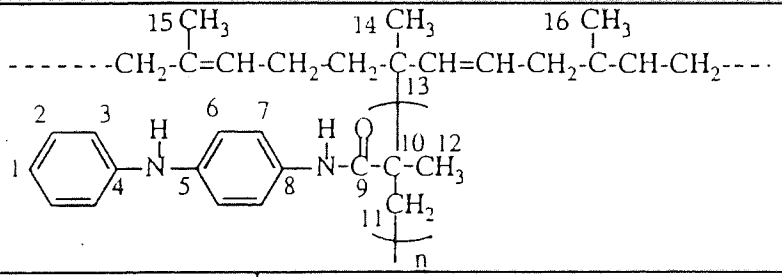

No. of Atom	δ (ppm)
9	175.0998
4, 5	141.9686
2, 8	129.2881
1, 3, 6, 7	119.2649
11*	46.4745
10*	≈ 31
12*	25.9372
15, 16*	17.7338
14*	16.1162

* : new peaks

Fig. 4.30 Solid state ^{13}C-NMR spectrum of compound E (75.5MHz).

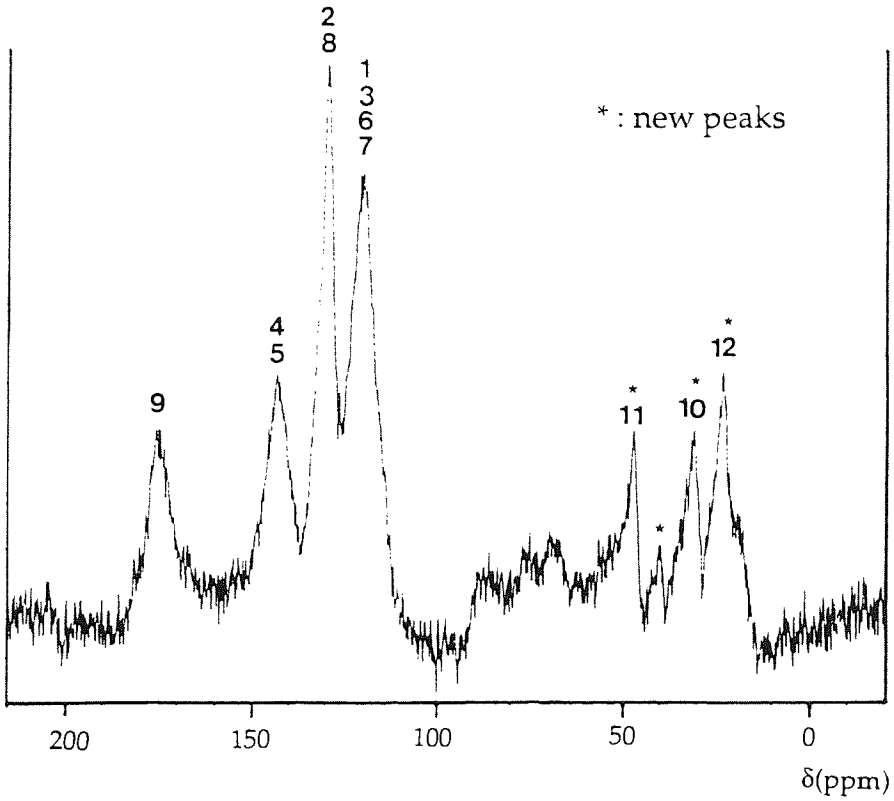

Table 4.18 ^{13}C-NMR summary of compound E

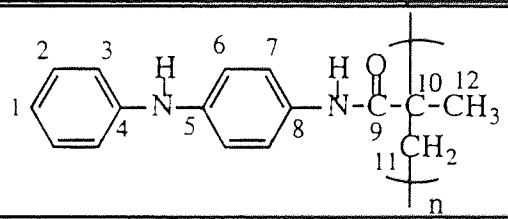

No. of Atom	δ (ppm)
9	175.0132
4, 5	143.2973
2, 8	129.7213
1, 3, 6, 7	120.1604
11 *	47.1099
*	39.8887
10 *	30.9054
12 *	23.3086

* : new peaks

Fig. 4.31 Solid state ^{13}C-NMR spectrum of APMA(75.5MHz).

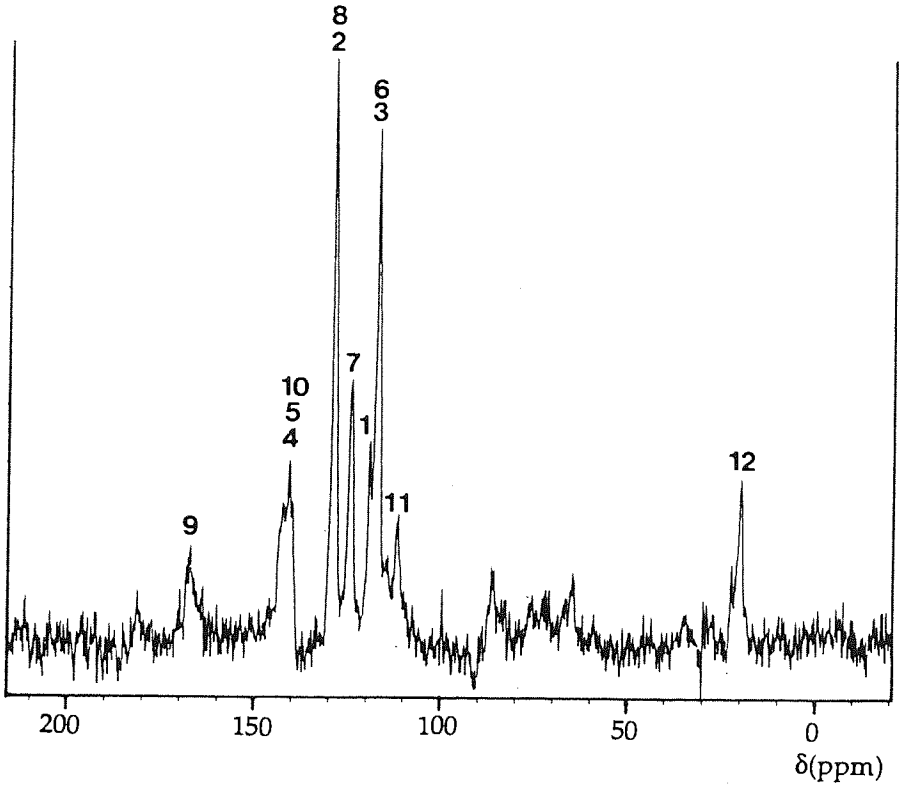

Table 4.19 ^{13}C-NMR summary of APMA

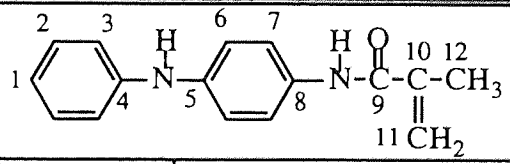

No. of Atom	δ (ppm)
9	167.1564
4, 5, 10	140.8999
2, 8	129.0281
7	124.3198
1	119.3805
3, 6	117.3007
11	111.5815
12	19.8424

Table 4.20 Unvulcanised test results of Blank, APMA, and peroxide decomposer series of samples.

APMA	Antifatigue agent	Peroxide Decomposer		Mooney Viscosity	Rheometer			
		P168	P626		f_{min}	f_{max}	$t_{0.1}$	$t_{0.9}$
(phr)	(phr)	(phr)	(phr)	ML(1+4),100°C	(dNm)	(dNm)	(min)	(min)
0.00	0.00	0.00	0.00	15.6	7.0	47.5	6.7	14.8
0.50	0.00	0.00	0.00	16.1	5.6	46.5	7.5	15.1
1.00	0.00	0.00	0.00	20.9	10.6	51.7	8.1	16.2
1.50	0.00	0.00	0.00	20.6	10.5	50.3	7.3	15.2
0.00	0.00	0.25	0.00	13.6	4.0	44.1	7.7	15.0
0.00	0.00	0.00	0.25	18.7	4.4	45.1	9.4	17.7

Table 4.21 Unvulcanised rubber physical tests in αTOC synergestic system series.

APMA	αTOC	Peroxide Decomposer		Mooney Viscosity	Rheometer			
		P168	P626		f_{min}	f_{max}	$t_{0.1}$	$t_{0.9}$
(phr)	(phr)	(phr)	(phr)	ML(1+4),100°C	(dNm)	(dNm)	(min)	(min)
0.00	0.50	0.00	0.00	17.1	4.1	43.6	7.3	15.5
0.00	1.00	0.00	0.00	17.7	6.7	47.1	7.1	15.5
0.00	1.50	0.00	0.00	16.5	4.0	43.1	6.4	14.7
1.00	0.50	0.00	0.00	19.2	8.1	47.5	7.2	15.1
0.75	0.75	0.00	0.00	14.9	3.9	43.1	7.1	15.1
0.50	1.00	0.00	0.00	15.4	3.9	43.2	7.5	15.7
0.75	0.75	0.25	0.00	10.0	6.0	45.9	6.9	14.7
0.75	0.75	0.00	0.25	11.6	2.9	42.0	8.2	16.2

Table 4.22 Unvulcanised rubber physical tests in γTOC synergestic system series.

APMA	γTOC	Peroxide Decomposer		Mooney Viscosity	Rheometer			
		P168	P626		f_{min}	f_{max}	$t_{0.1}$	$t_{0.9}$
(phr)	(phr)	(phr)	(phr)	ML(1+4),100°C	(dNm)	(dNm)	(min)	(min)
0.00	0.50	0.00	0.00	16.0	9.0	50.8	7.8	16.2
0.00	1.00	0.00	0.00	16.3	9.0	51.2	8.0	16.0
0.00	1.50	0.00	0.00	17.2	6.1	46.1	7.8	16.1
1.00	0.50	0.00	0.00	12.7	5.3	47.3	7.2	15.1
0.75	0.75	0.00	0.00	12.1	4.2	44.1	7.2	15.2
0.50	1.00	0.00	0.00	15.6	8.2	48.8	8.2	16.1
0.75	0.75	0.25	0.00	13.3	5.0	44.0	6.9	14.1
0.75	0.75	0.00	0.25	14.8	3.2	40.9	7.6	15.7

Table 4.23 Unvulcanised rubber physical tests in BQ synergestic system series.

APMA	BQ	Peroxide Decomposer		Mooney Viscosity	Rheometer			
		P168	P626		f_{min}	f_{max}	$t_{0.1}$	$t_{0.9}$
(phr)	(phr)	(phr)	(phr)	ML(1+4),100°C	(dNm)	(dNm)	(min)	(min)
0.00	0.50	0.00	0.00	13.8	5.0	43.1	7.2	15.0
0.00	1.00	0.00	0.00	17.1	5.0	43.5	7.1	14.9
0.00	1.50	0.00	0.00	19.7	5.1	43.2	7.0	14.8
1.00	0.50	0.00	0.00	22.5	5.4	43.1	7.2	15.2
0.75	0.75	0.00	0.00	18.2	8.0	45.0	7.0	14.7
0.50	1.00	0.00	0.00	23.3	5.9	43.3	6.7	14.2
0.75	0.75	0.25	0.00	18.7	4.2	41.9	7.4	15.1
0.75	0.75	0.00	0.25	22.9	5.0	41.2	7.8	15.7

Table 4.24 Unvulcanised rubber physical tests in TMQ synergestic system series.

APMA	TMQ	Peroxide Decomposer		Mooney Viscosity	Rheometer			
		P168	P626		f_{min}	f_{max}	$t_{0.1}$	$t_{0.9}$
(phr)	(phr)	(phr)	(phr)	ML(1+4),100°C	(dNm)	(dNm)	(min)	(min)
0.00	0.50	0.00	0.00	14.6	6.2	45.9	7.7	17.3
0.00	1.00	0.00	0.00	19.0	7.2	47.8	7.5	15.7
0.00	1.50	0.00	0.00	23.6	7.2	46.8	8.7	19.0
1.00	0.50	0.00	0.00	13.8	3.4	42.9	7.3	15.7
0.75	0.75	0.00	0.00	20.4	5.6	45.4	6.8	15.2
0.50	1.00	0.00	0.00	19.0	8.0	46.9	8.4	18.3
0.75	0.75	0.25	0.00	25.9	5.7	44.8	8.2	16.0
0.75	0.75	0.00	0.25	27.0	8.5	46.5	8.1	16.1

Table 4.25 Fatigue resistance in Blank, APMA, and peroxide decomposers series.

APMA	Antifatigue Agent	Peroxide Decomposer		Strain	Strain Energy	Fatigue Life × 0.01 (cycles)			
		P168	P626			mean	max	min	at 6.3 kg/cm^2
(phr)	(phr)	(phr)	(phr)	(%)	(kg/cm^2)				
0.00	0.00	0.00	0.00	108	4.2	509.5	577	403	237.1
				142	6.6	215.9	245	165	
0.50	0.00	0.00	0.00	108	4.4	1049.6	1089	953	536.9
				142	7.0	446.2	450	424	
1.00	0.00	0.00	0.00	108	4.3	1129.1	1173	950	545.3
				142	6.8	478.1	517	415	
1.50	0.00	0.00	0.00	108	4.8	1267.4	1430	1000	771.8
				142	7.5	564.9	594	501	
0.00	0.00	0.25	0.00	108	3.5	1439.9	1548	1130	519.0
				142	5.4	675.3	716	579	
0.00	0.00	0.00	0.25	108	3.8	1254.5	1292	1194	553.4
				142	6.0	609.0	631	504	

Table 4.26 Fatigue resistance of rubbers in αTOC series

APMA	αTOC	Peroxide Decomposer		Strain	Strain Energy	Fatigue Life × 0.01 (cycles)			
		P168	P626			mean	max	min	at 6.3 kg/cm^2
(phr)	(phr)	(phr)	(phr)	(%)	(kg/cm^2)				
0.00	0.50	0.00	0.00	108	4.8	1045.3	1091	732	675.5
				142	7.6	504.9	535	393	
0.00	1.00	0.00	0.00	108	4.5	1397.1	1457	1316	757.1
				142	7.1	610.3	632	562	
0.00	1.50	0.00	0.00	108	4.4	1354.8	1450	993	770.1
				142	6.9	668.8	719	567	
1.00	0.50	0.00	0.00	108	4.4	1588.4	1706	1269	725.7
				142	6.9	590.9	612	541	
0.75	0.75	0.00	0.00	108	4.1	1461.2	1514	1239	736.8
				142	6.6	692.5	759	609	
0.50	1.00	0.00	0.00	108	4.1	1683.0	1740	1540	689.4
				142	6.4	660.3	732	569	
0.75	0.75	0.25	0.00	108	3.3	2119.9	2412	1636	637.5
				142	5.2	913.8	935	811	
0.75	0.75	0.00	0.25	108	3.4	2087.5	2112	1935	678.9
				142	5.3	935.4	872	774	

Table 4.27 Fatigue resistance of rubbers in γTOC series.

APMA	γTOC	Peroxide Decomposer		Strain	Strain	Fatigue Life × 0.01 (cycles)			
		P168	P626		Energy	mean	max	min	at 6.3 kg/cm^2
(phr)	(phr)	(phr)	(phr)	(%)	(kg/cm^2)				
0.00	0.50	0.00	0.00	108	4.1	1317.3	1380	1097	683.2
				142	6.5	657.2	767	474	
0.00	1.00	0.00	0.00	108	4.2	1694.6	1873	1428	679.7
				142	6.3	682.0	708	575	
0.00	1.50	0.00	0.00	108	3.6	2459.0	2566	2018	704.4
				142	5.5	936.0	1104	730	
1.00	0.50	0.00	0.00	108	3.9	1636.2	1674	1412	716.2
				142	6.2	738.2	796	564	
0.75	0.75	0.00	0.00	108	3.8	2054.1	2162	1745	798.2
				142	5.9	910.9	1058	700	
0.50	1.00	0.00	0.00	108	4.0	2086.9	2123	1941	775.9
				142	6.2	801.0	836	567	
0.75	0.75	0.25	0.00	108	3.4	1847.1	1884	1799	634.9
				142	5.2	883.2	981	734	
0.75	0.75	0.00	0.25	108	3.2	1852.6	1976	1514	507.4
				142	4.9	815.5	851	703	

Table 4.28 Fatigue resistance of rubbers in BQ series.

APMA	BQ	Peroxide Decomposer		Strain	Strain	Fatigue Life × 0.01 (cycles)			
		P168	P626		Energy	mean	max	min	at 6.3 kg/cm^2
(phr)	(phr)	(phr)	(phr)	(%)	(kg/cm^2)				
0.00	0.50	0.00	0.00	108	3.8	1371.3	1478	1203	589.6
				142	5.9	657.3	683	540	
0.00	1.00	0.00	0.00	108	3.7	1769.5	2119	1341	701.1
				142	5.8	815.4	894	675	
0.00	1.50	0.00	0.00	108	3.6	2306.6	2473	1799	880.8
				142	5.7	1052.5	1219	734	
1.00	0.50	0.00	0.00	108	3.7	1452.5	1530	1335	576.5
				142	5.9	658.8	752	536	
0.75	0.75	0.00	0.00	108	3.8	1658.2	1753	1505	687.1
				142	5.9	769.9	785	750	
0.50	1.00	0.00	0.00	108	3.8	2042.1	2147	1774	692.7
				142	5.9	804.8	827	717	
0.75	0.75	0.25	0.00	108	3.3	1719.7	1756	1610	492.4
				142	5.1	745.3	759	687	
0.75	0.75	0.00	0.25	108	3.3	1726.5	1798	1456	514.4
				142	5.0	786.3	840	674	

Table 4.29 Fatigue resistance of rubbers in TMQ series.

APMA	TMQ	Peroxide Decomposer		Strain	Strain	Fatigue Life x 0.01 (cycles)			
		P168	P626		Energy	mean	max	min	at 6.3 kg/cm^2
(phr)	(phr)	(phr)	(phr)	(%)	(kg/cm^2)				
0.00	0.50	0.00	0.00	108	4.2	793.5	809	707	429.5
				142	6.6	400.1	414	368	
0.00	1.00	0.00	0.00	108	4.2	827.9	898	720	501.8
				142	6.6	479.6	518	386	
0.00	1.50	0.00	0.00	108	3.9	1028.3	1182	702	425.6
				142	6.2	439.3	478	388	
1.00	0.50	0.00	0.00	108	4.5	1324.4	1415	890	632.9
				142	6.8	537.4	561	503	
0.75	0.75	0.00	0.00	108	4.5	1237.8	1305	996	641.9
				142	6.8	555.0	595	474	
0.50	1.00	0.00	0.00	108	3.9	1365.7	1489	998	626.5
				142	6.1	658.1	732	493	
0.75	0.75	0.25	0.00	108	3.8	1688.0	1810	1354	649.6
				142	5.9	733.8	758	676	
0.75	0.75	0.00	0.25	108	3.5	1531.6	1577	1376	618.4
				142	5.4	786.5	812	715	

Table 4.30 Thermal resistance of rubbers in Blank, APMA and peroxide decomposer series.

APMA	Antifatigue Agent	Peroxide Decomposer		Elongation at Break (Eb)			Tensile Strength (Tb)		
		P168	P626	Orig. Eb	Aged Eb	Retention	Orig. Tb	Aged Tb	Retention
(phr)	(phr)	(phr)	(phr)	(%)	(%)	(-)	(N/mm^2)	(N/mm^2)	(-)
0.00	0.00	0.00	0.00	820.7	218.7	0.266	17.771	1.271	0.072
0.50	0.00	0.00	0.00	826.6	676.7	0.819	20.652	11.888	0.576
1.00	0.00	0.00	0.00	784.5	731.2	0.932	20.458	16.251	0.794
1.50	0.00	0.00	0.00	821.5	797.0	0.970	18.881	20.241	1.072
0.00	0.00	0.25	0.00	824.8	750.8	0.910	18.315	18.816	1.027
0.00	0.00	0.00	0.25	823.3	772.5	0.938	19.190	19.935	1.039

Table 4.31 Thermal resistance of rubbers in αTOC series.

APMA	αTOC	Peroxide Decomposer		Elongation at Break (Eb)			Tensile Strength (Tb)		
		P168	P626	Orig. Eb	Aged Eb	Retention	Orig. Tb	Aged Tb	Retention
(phr)	(phr)	(phr)	(phr)	(%)	(%)	(-)	(N/mm^2)	(N/mm^2)	(-)
0.00	0.50	0.00	0.00	803.9	643.5	0.800	21.025	12.719	0.605
0.00	1.00	0.00	0.00	805.7	402.0	0.499	19.553	4.465	0.228
0.00	1.50	0.00	0.00	821.6	262.4	0.319	20.196	2.138	0.106
1.00	0.50	0.00	0.00	816.0	679.9	0.833	19.888	15.105	0.760
0.75	0.75	0.00	0.00	812.0	654.5	0.806	18.745	12.399	0.661
0.50	1.00	0.00	0.00	816.8	638.7	0.782	19.341	12.345	0.638
0.75	0.75	0.25	0.00	858.5	620.7	0.723	15.746	9.927	0.630
0.75	0.75	0.00	0.25	865.8	635.1	0.734	15.825	10.054	0.635

Table 4.32 Thermal resistance of rubbers in γTOC series.

APMA	γTOC	Peroxide Decomposer		Elongation at Break (Eb)			Tensile Strength (Tb)		
		P168	P626	Orig. Eb	Aged Eb	Retention	Orig. Tb	Aged Tb	Retention
(phr)	(phr)	(phr)	(phr)	(%)	(%)	(-)	(N/mm^2)	(N/mm^2)	(-)
0.00	0.50	0.00	0.00	803.3	774.8	0.965	16.985	17.167	1.011
0.00	1.00	0.00	0.00	842.4	681.2	0.809	16.733	12.369	0.739
0.00	1.50	0.00	0.00	852.1	685.1	0.804	17.861	8.854	0.496
1.00	0.50	0.00	0.00	796.6	756.9	0.950	16.643	17.385	1.045
0.75	0.75	0.00	0.00	825.3	691.4	0.838	18.897	11.491	0.608
0.50	1.00	0.00	0.00	815.0	702.5	0.862	19.013	13.361	0.703
0.75	0.75	0.25	0.00	862.2	758.3	0.879	15.336	14.312	0.933
0.75	0.75	0.00	0.25	866.8	771.9	0.891	16.034	14.266	0.890

Table 4.33 Thermal resistance of rubbers in BQ series.

APMA	BQ	Peroxide Decomposer		Elongation at Break (Eb)			Tensile Strength (Tb)		
		P168	P626	Orig. Eb	Aged Eb	Retention	Orig. Tb	Aged Tb	Retention
(phr)	(phr)	(phr)	(phr)	(%)	(%)	(-)	(N/mm^2)	(N/mm^2)	(-)
0.00	0.50	0.00	0.00	822.6	293.8	0.357	16.423	1.889	0.115
0.00	1.00	0.00	0.00	814.5	262.4	0.322	16.771	1.714	0.102
0.00	1.50	0.00	0.00	813.5	286.6	0.352	16.872	1.898	0.113
1.00	0.50	0.00	0.00	831.4	658.9	0.793	18.927	11.905	0.629
0.75	0.75	0.00	0.00	826.9	647.8	0.783	17.979	10.755	0.598
0.50	1.00	0.00	0.00	823.4	614.1	0.746	16.940	8.886	0.525
0.75	0.75	0.25	0.00	872.7	628.0	0.720	15.901	9.287	0.584
0.75	0.75	0.00	0.25	888.3	694.6	0.782	17.779	11.661	0.656

Table 4.34 Thermal resistance of rubbers in TMQ series.

APMA	TMQ	Peroxide Decomposer		Elongation at Break (Eb)			Tensile Strength (Tb)		
		P168	P626	Orig. Eb	Aged Eb	Retention	Orig. Tb	Aged Tb	Retention
(phr)	(phr)	(phr)	(phr)	(%)	(%)	(-)	(N/mm^2)	(N/mm^2)	(-)
0.00	0.50	0.00	0.00	754.0	691.9	0.918	15.227	15.003	0.985
0.00	1.00	0.00	0.00	770.2	689.5	0.895	17.431	15.306	0.878
0.00	1.50	0.00	0.00	784.1	725.2	0.925	18.152	17.324	0.954
1.00	0.50	0.00	0.00	752.2	741.1	0.985	14.982	17.637	1.177
0.75	0.75	0.00	0.00	777.7	749.1	0.963	16.721	17.637	1.055
0.50	1.00	0.00	0.00	816.8	736.7	0.902	16.911	17.014	1.006
0.75	0.75	0.25	0.00	851.0	729.3	0.857	16.826	16.239	0.965
0.75	0.75	0.00	0.25	871.0	757.1	0.869	17.606	17.539	0.996

Chapter 5 Analysis of Transformation Products from Antifatigue Agents

5.1 Objective and Methodology

In chapter 3, various phenols and quinonoid compounds were evaluated as antifatigue agents. In this chapter, antifatigue mechanism of the biological antioxidant, α-tocopherol, was investigated by examining the nature of its transformation products formed during fatiguing of NR using HPLC and spectroscopic analysis. The role of α-tocopherol as an antifatigue agent (as a macroalkyl radical scavenger) in natural rubber has not been examined previously.

The overall methodology used for the work described in this chapter is shown in scheme 5.1. The vulcanised rubbers were prepared in the same way as described in chapter 3, see scheme 3.1. The rubber samples containing α-tocopherol were exposed to fatigue at 108 % maximum strain. Fatiguing was stopped at various stages; 30,000, 60,000, 90,000, 120,000, 150,000, 180,000, and 210,000 cycles. Samples removed at the given number of cycles were immediately extracted with n-hexane under nitrogen atmosphere at ambient temperature for two days, see section 2.6.1. The extracted solutions were then stored in the dark and cold place prior to HPLC analysis. Before HPLC, the solvent (hexane) was evaporated and the solute was dissolved into methanol. The methanol solutions were filtered using microfilter (0.2μm) and analysed quantitatively by HPLC using octadecyl column (C_{18}), i.e. Zorbax ODS 4.6mm ID × 25 cm, in 0.8ml/min at 290nm. Some components which were insoluble or quite less soluble in methanol were dissolved into dichlolomethane (DCM), the microfilter was also washed by large amount of DCM. Similarly, DCM was evaporated and the solute was dissolved in n-hexane. Finally the filtered hexane solution was analysed quantitatively by HPLC using silica gel column (SiO_2), i.e. Zorbax SIL 4.6mm ID × 25 cm, in 0.8 ml/min, at 290nm.

The vulcanised rubber which contain no α-tocopherol was extracted and analysed as a control. Moreover, authentic samples were prepared and their retention times were examined in order to identify the reaction products. The retention times and UV spectra of α-tocopherol-containing samples were compared with the control and that of the authentic samples.

Scheme 5.1 Flow chart of analysis of α-tocopherol transformation products.

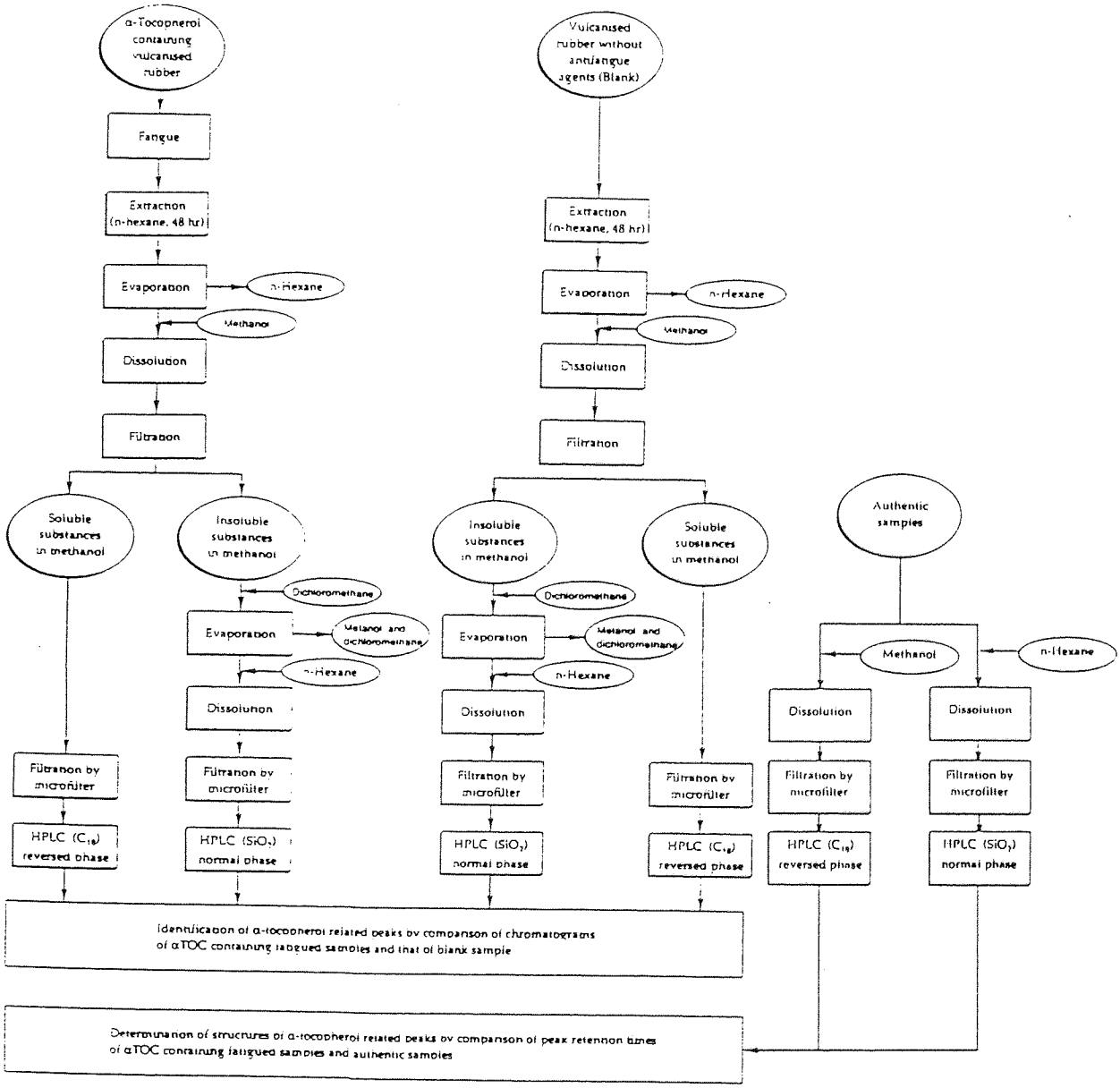

5.2 Results

5.2.1 Extraction of Fatigued Samples

Only the parallel centre part of the dumb-bell samples, see fig 2.82 were used for extraction. These samples were fatigued in a Monsanto Fatigue Failure Tester at a maximum strain of 108 % , at ambient temperature. In order to eliminate the possibility of any unwanted reactions such as oxidation, the fatigued samples were immediately extracted by n-hexane under nitrogen atmosphere at ambient temperature for 48 hr, see fig. 2.91. The samples were not cut down into small pieces in order to avoid the possibility of mechano-radicals formation. The extraction results are summarised in table 5.1.

Table 5.1 Sample weight of fatigue samples.

Fatigue (cycles)	Sample Weight before Extraction (g)	Weight Loss after Extraction	
		(g)	(wt%)
30,000	3.5192	0.0991	2.82
60,000	4.6993	0.1395	2.97
90,000	3.7106	0.1087	2.93
120,000	3.9636	0.1213	3.06
150,000	4.0785	0.1271	3.12
180,000	3.9505	0.1156	2.93
210,000	1.8414	0.0609	3.31

As the fatigue cycles increased, there was an increase in weight loss after extraction. There were no visible blooming of any ingredients from fatigued rubber samples during fatiguing process. This implies that the rubber molecules have undergone chain scission (lower molecular weight) during fatigue, hence was easier to be extracted by solvent..

Fig. 5.1 Weight loss of fatigued samples by extraction.

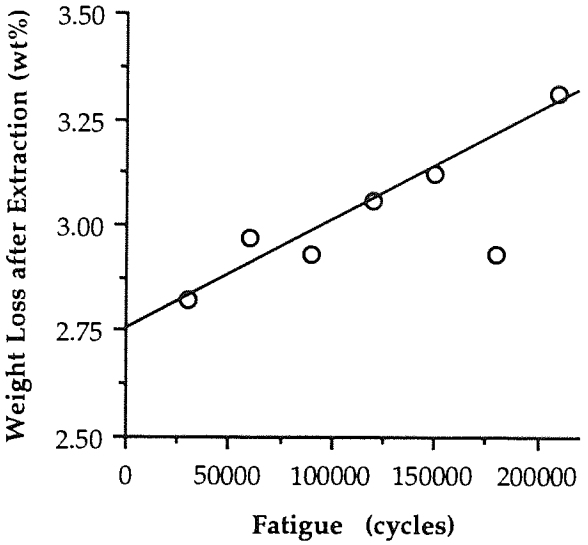

5.2.2 Authentic Samples

Although α-tocopherol was examined in this work as an antifatigue agent for NR, similar transformation products are expected to be produced during processing, curing, and fatiguing to those produced during autoxidation of α-tocopherol. Table 5.2 gives the structures and UV characteristic of some transformation poroducts which have been shown previously to be formed during oxidation of polyolefins containing α-tocopherol [116]. These were obtained from F. Hoffmann La Roche and previous reserchers in our laboratory [116] and were used here as authentic samples by subjecting them to the same conditions of HPLC analysis to those used for the fatigued rubber samples and their retention times and UV-characteristics were compared.

Table 5.2 Some of α-tocopherol expected transformation products used here as authentic samples

Code	Structure (Mw)	Exp. λ max	Literature λ max	Literature ε (cm^2/mol)	Literature Ref.
αTOC α-tocopherol	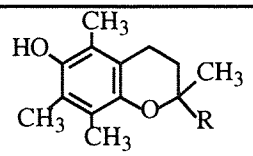 (431)	296 (hexane)	297	3900	128
ALD 5-Formyl-γ-tocopherol	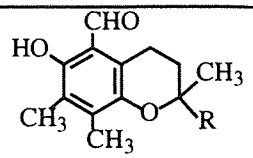 (445)	292 388 (hexane)	239 287 391 (EtOH)	---- 13610 4200	113
TQ α–tocophenoxyl quinone	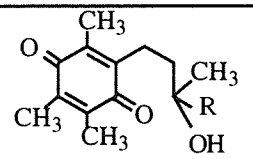 (447)	261 268 (hexane)	260 268	18400 18550	129
DHD Dihydroxy-dimer	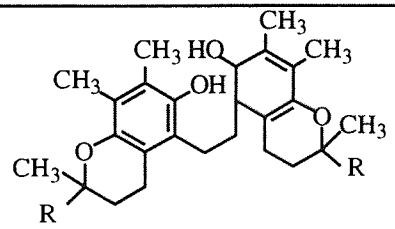 (859)	294 338 (IPA)	295 (EtOH)	6450	130
SPD Spirodimer	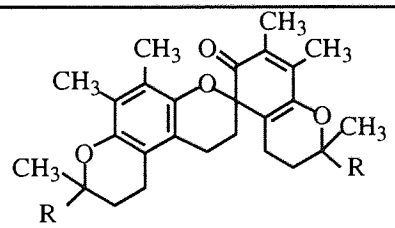 (857)	292 340 (MeOH)	300 345	9350 4300	129
TRI Trimer	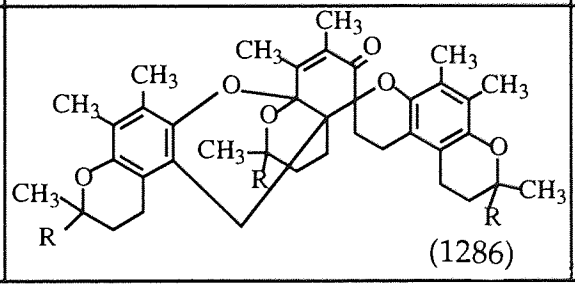 (1286)	292 (IPA)	293 (isooctane)	7600	131

R = -CH_2-(CH_2-CH_2-CH(CH_3)-CH_2)$_3$-H

HPLC detection was used at 290 nm due to the presence of an absorption peak around 290 - 300 in the authentic samples. The molar extinction coefficient of all authentic samples at 290nm are shown in table 5.3 for the quantitative analysis at the end of this chapter. (TQ has a peak at 261 and 268 nm and does not show absorption around 290 nm, however TQ was not detected at all from αTOC containing fatigued rubber samples as a transformation products.)

Table 5.3 Molar extinction coefficient of UV spectra of authentic samples at 290 nm.

Code	ε (cm^2/mol) (in DCM)
αTOC	3487
ALD	9127
TQ	-
DHD	6767
SPD	3664
TRI	6410

5.2.3 Setting the HPLC Analysis Conditions for Reserved Phase

Initially reversed phase, octadecyl column (C_{18}), was chosen as stationary phase for HPLC separation. Since a large number of peaks were detected in the extracts of the NR fatigued samples and these spread across a wide range of polarities, hence gradient elution was thought to be necessary. Isocratic elution was tried before gradient elution. The procedure for the optimisation of the mobile phase is well described in Glajche's publications [132), 133)]. Generally the resolution in LC can be affected by three independent factors:

$$Rs = \underbrace{\frac{\sqrt{N}}{4}}_{\text{efficiency factor}} \underbrace{\left(\frac{k'}{1+k'}\right)}_{\text{capacity factor}} \underbrace{(\alpha-1)}_{\text{selectivity factor}}$$

where **N** is the column plate count, **k'** is the capacity factor, and $\alpha = k'_2/k'_1$ for peak 1 and 2. Therefore optimisation was carried out by the following steps:

(1) the capacity factor was adjusted by changing the solvent strength,

(2) the selectivity factor was adjusted by changing the solvent combinations, (7 combinations of different selectivity solvents were used to elute the samples)

(3) chromatographic optimisation function (COF) map or / and overlapping resolution maps (ORM) were drawn.

5.2.3.1 Solvent Strength

Generally, the capacity factor (**k'**) is desirable to be within the range $1 < k' < 10$ [132]. It is available to calculate from retention time (t_R) and dead time (t_0) or retention volume (V_R) and dead volume (V_0), see shown below:

$$k' = \frac{t_R - t_0}{t_0} = \frac{V_R - V_0}{V_0}$$

It can be adjusted by changing the solvent strength. The solvent strength is often represented by a polarity index **P'** which is a measure of the ability of the solvent to interact with various polar test solutes. The polarity index of a solvent mixture can be calculated by:

$$P' = \Phi_a P'_a + \Phi_b P'_b + \Phi_c P'_c$$

where Φ_a, Φ_b, and Φ_c are volume fractions of solvents A, B, and C in the solvent mixture and P'_a, P'_b, and P'_c are **P'** values of the pure solvents A, B, and C. in this work **P'** values were calculated based on Snyder's data [134], see table 5.4.

Table 5.4 Polarity index for mobile phase in reversed phase.

Solvents	Volume Fraction				Polarity
	Φ IPA	Φ MeOH	Φ ACN	Φ H_2O	P'
Isopropanol	1.00				3.9
Methanol		1.00			5.1
Acetonitrile			1.00		5.8
Water				1.00	10.2
Solvent 1	1.00				3.9
Solvent 2	0.67	0.33			4.3
Solvent 3	**0.33**	**0.67**			**4.7**
Solvent 4	**0.10**	**0.90**			**5.0**
Solvent 5		1.00			5.1
Solvent 6		0.33	0.67		5.3
Solvent 7			1.00		5.8

α-tocopherol eluted at relatively short retention time compared to all other components, see fig 5.8. If the solvent has a lower polarity such as solvent 1, all components will elute together at early stages with poor resolution (see fig.5.8 a). On the other hand, if the solvent has a higher polarity such as solvent 7, the peaks with short retention times will be well separated; however, the longer retention time peaks will become small and broad and will be difficult to detect (see fig.5.8 d). Furthermore, the quite long elution times required will be a major problem for routine analysis. The separation using solvents 3 and 4, P' = 4.7 and 5.0 respectively, showed good resolution and elution time around 60 and 90 minutes (see fig. 5.8 b and c). For quantitative analysis, polarity index of 5.0 was used.

There are two ways to get good resolution. One is a to optimise the solvent selectivity at around **P'** = 4.7 ~ 5.0 in the isocratic elution, another is to start elution from higher **P'** and decrease **P'** during elution using a gradient method. Although the gradient method has higher potential of resolution, generally, the retention time is less precise than in the case of the isocratic method due to the solvent mixture and the more complicated process for setting the analysis parameters. In addition the stationary phase should be equilibrated after each elution before the next analysis, hence not always leading to a reduced the testing time for analysis. Therefore, isocratic method was used initially in this research.

Only the capacity factor of α-tocopherol was calculated, see table 5.5, because the quantity of the authentic samples available was very small and it was not so important to know the precise **k'** values for each various strength of solvent, as far as not to proceed to the gradient elution. The relationship

between k' and Φ_b was shown in fig. 5.9. Generally, the plots of **log k'** versus Φ_b can be represented by the equation;

$$\log k' = A\Phi_b^2 + B\Phi_b + C$$

Table 5.5 Changes of capacity factor of α-tocopherol

Solvents	Φ_{IPA}	Φ_{MeOH}	$k'_{\alpha TOC}$
Solvent 1	1.00		0.07
Solvent 2	0.67		0.40
Solvent 3	0.33		1.15
Solvent 4	0.10		2.57
Solvent 5	0.00	1.00	3.53
Solvent 6		0.33	5.39
Solvent 7		0.00	12.21

Fig. 5.9 Changes of capacity factor of α-tocopherol in reversed phase (C_{18}) using IPA / MeOH and MeOH / ACN system.

(a) Isopropanol / Methanol System

$\log k' = A\Phi_{IPA}^2 + B\Phi_{IPA} + C$

A = -0.58659, B = -1.0091, C = 0.48825

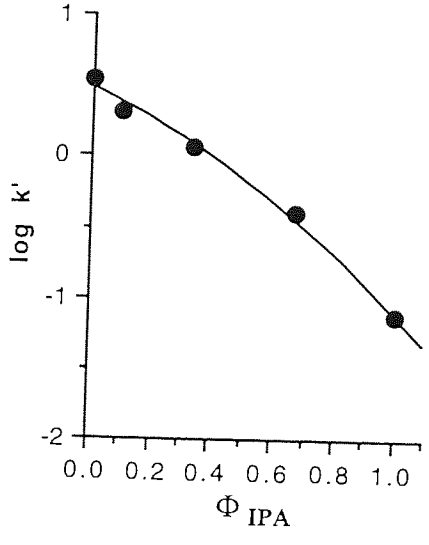

(b) Methanol / Acetonitrile System

$\log k' = A'\Phi_{MeOH}^2 + B'\Phi_{MeOH} + C'$

A' = 0.80335, B' = -1.3421, C' = 1.0869

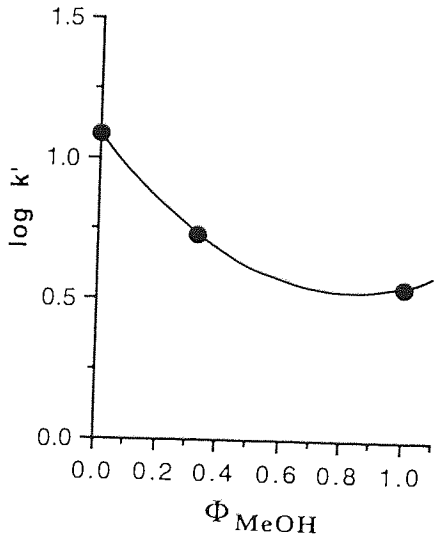

5.2.3.2 Chemical Selectivity Effect

After adjusting the capacity factor by changing the solvent strength, the selectivity factor was adjusted. The most useful variables for the selectivity factor are the mobile phase composition, the stationary phase composition, pH or other ionic effects and secondary chemical equibria[132), 133)]. In this work the mobile phase composition was changed for this purpose.

According to Snyder, [134)] various solvents were classified according to their proton acceptor contribution, proton donor contribution, and strong dipole contribution. In order to find the optimum selectivity, three solvents are selected from various classes to form a triangle, see fig. 5.10. In case of the reversed phase, MeOH, ACN, and tetrahydrofuran (THF) are often chosen with water (H_2O) as carrier solvent[132), 133)]. Since many components are included and their polarities are spread over very widely, relatively longer retention times are required to get enough resolution and hence the solvent strength adjusted in the previous section is relatively weaker than general reversed phase solvents. Therefore, in this work IPA, chloroform ($CHCl_3$), and DCM were used with MeOH as carrier solvent.

Fig. 5.10 Selectivity triangles for preferred solvents in reversed phase and normal phase chromatography [132), 133), 137)].

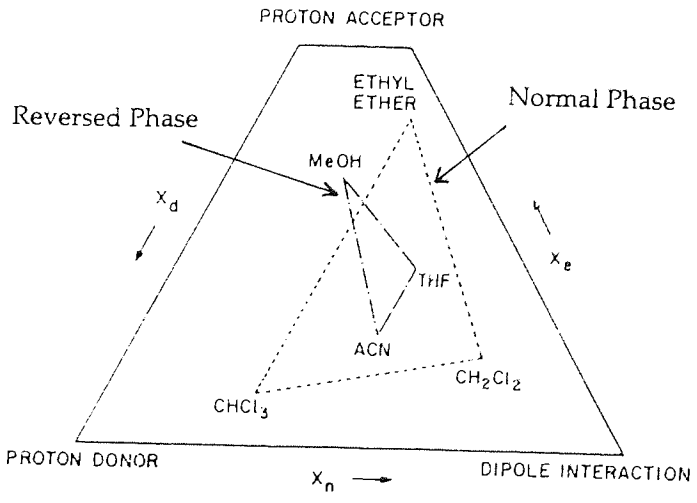

Seven combinations of solvents were designed according to the solvent optimisation strategy [132), 133), 137)], see fig. 5.11. The composition of each mixture solvents is listed in table 5.6 and these chromatogram are shown in figures 5.12 - 18.

Fig. 5.11 Mixture design experiments used in mobile phase optimisation strategy.

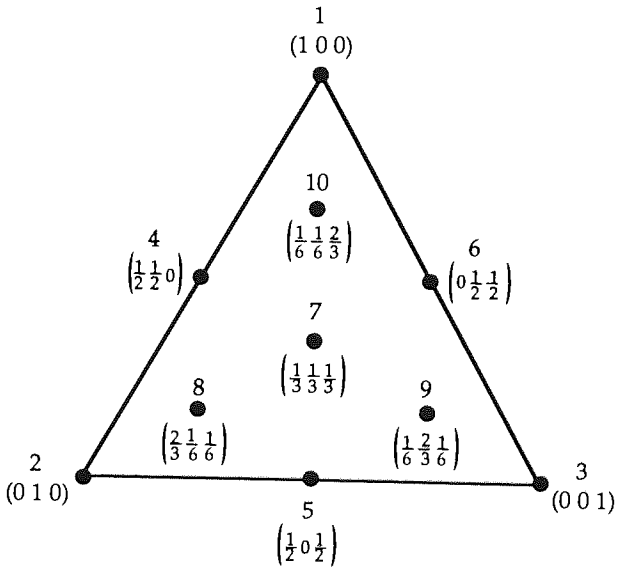

Table 5.6 Solvents used for selectivity optimisation. (P' = 4.7)

	Φ_{IPA}	Φ_{DCM}	Φ_{CHCl3}	Φ_{MeOH}
	P' = 3.9	P' = 3.1	P' = 4.1	P' = 5.1
Run 1	0.33	0.00	0.00	0.67
Run 2	0.00	0.20	0.00	0.80
Run 3	0.00	0.00	0.40	0.60
Run 4	0.17	0.10	0.00	0.73
Run 5	0.17	0.00	0.20	0.63
Run 6	0.00	0.10	0.20	0.70
Run 7	0.11	0.07	0.13	0.69

Elution of "run 1" seemed to give the best resolution obviously, so neither COF map nor ORM maps were drawn practically, although the computer program which drew COF map was programmed based on the Snee's [138] mathematical model, see appendix. In order to examine the deviation of calculated values from COF, three additional runs, No 8, 9, and 10 in fig. 5.11, are recommended to test in the literature; however this was not carried out because COF was not actually calculated. From these test results MeOH / IPA solvent system was chosen for the quantitative analysis used in the results presented later in this chapter using C_{18} column in isocratic method.

5.2.4 Identification of Transformation Products from Reversed Phase Elution.

5.2.4.1 Comparison with Controls

The chromatograms at 268 nm and 290 nm of α-tocopherol containing fatigued samples and a control sample (rubber with no αTOC) were compared with each other in order to identify the α-tocopherol transformation products peaks. The peaks which appeared only in the chromatogram of NR containing α-tocopherol samples were considered to be those of the transformation products. Figure 5.19 (at the end of chapter) shows a typical HPLC elution (at 290 and 268 nm) of extracted substances, which are soluble in methanol, from a vulcanised rubber sample containing α-tocopherol (1.5 phr) after fatigue (12,000 cycles at maximum strain of 108%). Although there are large number of peaks, only those marked A - D, were new compared with the control containing no α-tocopherol, see fig. 5.19 (a). Fig. 5.19 (b), showed that more than thirty components were eluted for the α-tocopherol-NR sample and some of these were eluted after 60 minutes. Although these peaks were very small, they showed good repeatability and reproducibility. Because α-tocophenoxylquinone (TQ) does not have UV absorbance peak around 290 nm, the chromatogram run at 268 nm was also compared, see fig 5.19 (c). From the authentic samples, the measured retention time of TQ was around 7.18 min, however, there was no difference between α-tocopherol containing sample and control sample around this region. For these reasons the retention times and UV spectra for peaks labelled A to D were compared to the retention times and UV spectra of authentic α-tocopherol oxidation products samples.

5.2.4.2 Authentic Samples Analysed by Reversed Phase Condition

The authentic samples shown in table 5.2 were dissolved in methanol (the trimer has low solubility in methanol at room temperature) and eluted by HPLC using the same conditions as those used for NR samples, see figures 5.20 - 24 (at the end of chapter). The retention times measured are listed in table 5.7 and UV spectra are shown in Fig. 5.25 (at the end of chapter). The retention times of peaks A - D were measured more than once at each fatiguing cycles, the average values are listed as a retention time in table 5.7 and the standard deviations of these retention times are also given.

Table 5.7 Retention time and UV absorption of authentic samples and Extracted Materials from Fatigued Rubber. (Reversed Phase C_{18})

	Retention Time (min)	Standard Deviation (min)	λ max (nm)
Peak A	10.3	0.2	292
Peak B	19.2	0.4	288
Peak C	28.9	0.7	293
Peak D	34.4	0.9	295
αTOC	9.6		294
ALD	18.2		288
TQ	7.2		268
DHD	4.2		---
SPD	8.4		292
TRI	---		---

- Stationary Phase: Zorbax ODS 4.6 mm ID × 25 cm
- Mobile Phase: MeOH : IPA = 9 : 1 v / v
- Flow Rate: 0.8 ml/min
- Temp.: ambient
- Detector: 290 nm (UV)

Compound A in a typical NR-αTOC fatigued sample was eluted around the same retention time as that of an authentic αTOC sample and compound B crresponded to the authentic ALD sample; the latter showed the characteristic UV absorbance of ALD around 287, and 390 nm, see fig. 5.25 (at the end of chapter). The retention time of other compounds (C and D) did not match any of the tested authentic samples.

5.2.5 Setting the HPLC Analysis Conditions for Normal Phase.

The components which were insoluble in methanol, see scheme 5.1 were analysed in different way. Since most of these compounds were considered to be relatively polar substances, normal phase analysis was carried out for these samples. From previous work [116), 139)], n-hexane / 1,4-dioxane system with silica gel column gave good separation of α-tocopherol oxidative products. However, if this system was applied to the extracted NR samples directly, large number of peaks would mask the α-tocopherol products' peaks and quantitative analysis will be very difficult to conduct. After removing all the methanol soluble components, the methanol insoluble components (containing for example trimer) were subjected to normal phase HPLC analysis.

The microfilter used for reversed phase solution was washed by very large amount of DCM many times and the remaining methanol insoluble substances were also dissolved in DCM at the same time. DCM and the remaining methanol were completely evaporated and the solute was dissolved in n-hexane then filtered by microfilter (0.2 μm), see scheme 5.1. By changing the volume fraction of n-hexane and 1,4-dioxane, only the solvent strength was adjusted for the analyses conditions, see table 5.8.

Table 5.8 Changes of capacity factor of α-Tocopherol with various polarity index.

	Volume Fraction		Polarity	Capacity Factor
	Φ_{Hex}	Φ_{Dio}	P'	$k'_{\alpha TOC}$
n-Hexane	1.000		0.000	
1,4-Dioxane		1.000	4.800	
Solvent 1	0.971	0.029	0.140	1.99
Solvent 2	0.995	0.005	0.024	10.66
Solvent 3	0.997	0.003	0.014	19.54
Solvent 4	0.999	0.001	0.005	

Fig 5.27 Changes of capacity factor of α-tocopherol in normal phase (Zorbax SIL 4.6 mm ID × 25 cm) using n-hexane and 1,4-dioxane system as mobile phase (0.8 ml/min, at ambient temperature).

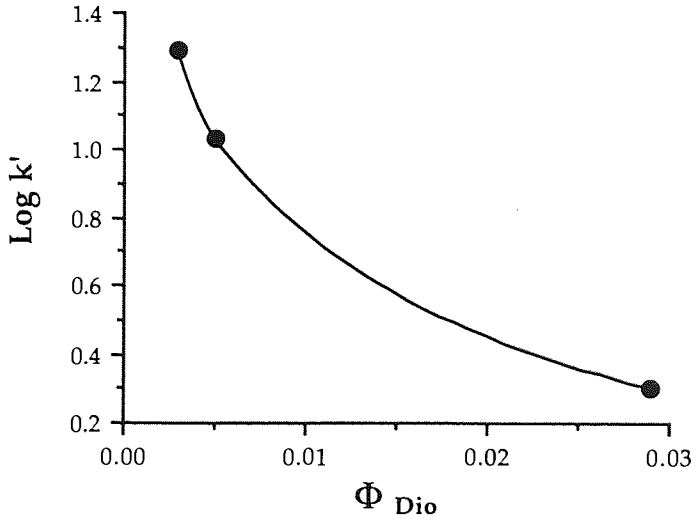

The capacity factor was drastically affected by the volume fraction of dioxane even though the changes were minute, see fig. 5.27. The retention time became slower with increasing dioxane volume fraction. In case of solvent 4, α-tocopherol was not eluted within 120 minutes. For all analysis described in this chapter using normal phase, solvents 2 or 3 were acceptable. Solvent 3, see fig.5.26 (c), had better resolution of peaks; however, it took long time to elute all peaks, whereas solvent 2 seemd to give acceptable resolution and elution time, see fig.5.26 (b); therefore, this was used for the rest of the analysis with normal phase.

5.2.6 Identification of Transformation Products from Normal Phase Elution.

5.2.6.1 Comparison with Control Sample.

In the same way used for the reversed phase, the α-tocopherol (1.5 phr) containing NR samples were compared with control sample prepared by the same procedure as that used for the α-tocopherol samples. Five peaks were identified as specific peaks originating from α-tocopherol containing samples. A typical HPLC chromatogram of α-tocopherol sample is shown in fig. 5.28 (at the end od chapter), and specific peaks are marked as E, F, G, H, and I.

5.2.6.2 Authentic Samples (Normal Phase, SiO_2)

The authentic samples in table 5.2 were solved in n-hexane and eluted by HPLC using the same condition as the case with α-tocopherol containing fatigued rubbers. The retention time and UV absorption of specified peaks (peaks E -I) and authentic samples are shown in table 5.9 and figures 5.28 - 5.34 (at the end of chapter).

Table 5.9 Retention time and UV absorption of authentic samples and extracted materials from fatigued rubber using normal phase condition.

	Retention Time (min)	Standard deviation (min)	λ max (nm)
Peak E	4.3	0.1	
Peak F	5.4	0.1	
Peak G	10.7	0.3	
Peak H	39.1	2.2	
Peak I	59.9	3.6	
αTOC	39.8		297
ALD	14.8		288
TQ	-		
DHD	4.4		296
SPD	5.3		301,343
TRI	55.5		297

- Stationary Phase: Zorbax SIL 4.6 mm ID × 25 cm
- Mobile Phase: Hexane : Dioxane = 100 : 0.3 v / v
- Flow Rate: 0.8 ml/min
- Temp.: ambient
- Detector: 290 nm (UV)

5.2.7 Quantitative Analysis of Transformation Products of α-Tocopherol Formed from αTOC-NR Fatigued Samples.

From the results of the HPLC retention times, the specified peaks (A - I) for α-tocopherol containing fatigued rubber samples were characterised and are summarised in table 5.10. As transformation products, ALD, SPD, DHD, and TRI were detected from all α-tocopherol containing fatigued samples; however, TQ was not detected at all. The parent αTOC was also found in all samples, both using reversed phase and normal phase elutions, (the detected αTOC in normal phase was much smaller than in reversed phase probably due to imperfect dissolution of αTOC in methanol during the preparation of samples for reversed phase analysis, see scheme 5.1). The peaks, C, D, and G (see figures 5.19 and 5.27, at the end of chapter) did not fit to any tested authentic samples and are most likely to be other transformation products of α-tocopherol such as peroxy ketal and chroman-3-ene or due to some contamination during processing, curing, and analysing, e.g. machine oil from roll mill and press machine, contamination from vulcanisation molds, and vacuume grease etc. Further carefull investigation is required to identify these products.

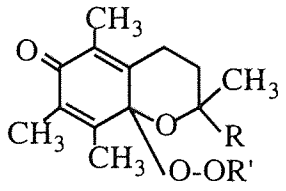

Peroxy ketal

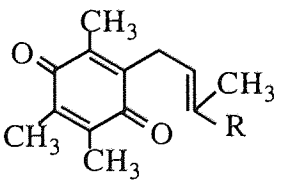

Chroman-3-ene

Table 5.10 Characterisation of specified peaks for αTOC containing samples.

Reversed Phase (C_{18})				Normal Phase (SiO_2)			
Specific Peak	retention time (min)	matched authentic sample	retention time (min)	Specific Peak	retention time (min)	matched authentic sample	retention time (min)
Peak A	10.3	αTOC	9.6	Peak E	4.3	DHD	4.4
Peak B	19.2	ALD	18.2	Peak F	5.4	SPD	5.3
Peak C	28.9	unknown	-	Peak G	10.7	unknown	-
Peak D	34.4	unknown	-	Peak H	39.1	αTOC	39.8
				Peak I	59.9	TRI	55.5

From the peak areas of each specified peak using base line from valley to valley, changes in amount of transformation products formed at various fatigue cycles were calculated using ε values in table 5.3, see table 5.11. Because parent αTOC was detected both in reversed phase elution and normal phase elution, these values were summed up.

Table 5.11 Changes of transformation products from α-tocopherol at various fatigue cycles.

Fatigue (cycles)	Amount of Transformation Products in 1g of Rubber Samples at each Fatigue Level mol/g)				
	αTOC $\times 10^6$	ALD $\times 10^8$	DHD $\times 10^9$	SPD $\times 10^9$	TRI $\times 10^7$
30000	7.44	2.59	2.05	1.29	3.85
60000	4.02	2.12	1.87	0.99	1.46
90000	7.92	3.52	1.06	0.84	2.93
120000	9.62	2.51	1.51	0.95	1.35
150000	7.87	3.12	2.55	1.96	1.54
180000	11.5	2.37	0.76	0	0.32
210000	14.9	2.59	1.41	4.66	1.38

The changes of detected ammount of parent α-tocopherol, transformed products are illustrated in fig. 5.35. This figure shows that only small amount of α-tocopherol was consumed up during its antifatigue action since the peak areas of all other products compared to that of αTOC were much smaller. Although αTOC was expected to decrease during fatiguing, fig. 5.35 shows that it increases. On the other hand, only small amount of dimers (DHD and SPD) were detected during fatiguing, while the TRI and ALD were the main transformation products. Although the ALD concentration did not show a significant change, the TRI decreased and this was accompanied by an observed increase of the concentration of the parent αTOC.

Fig. 5.35 Changes of transformation products during fatiguing.

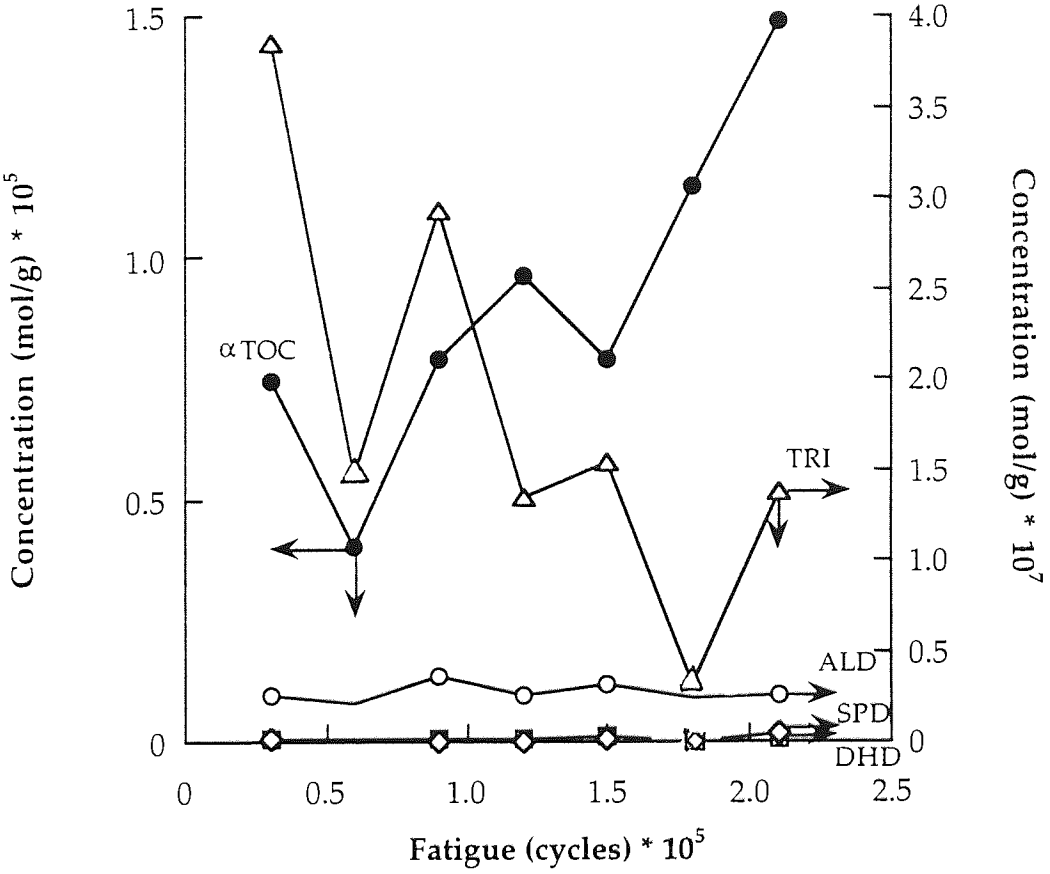

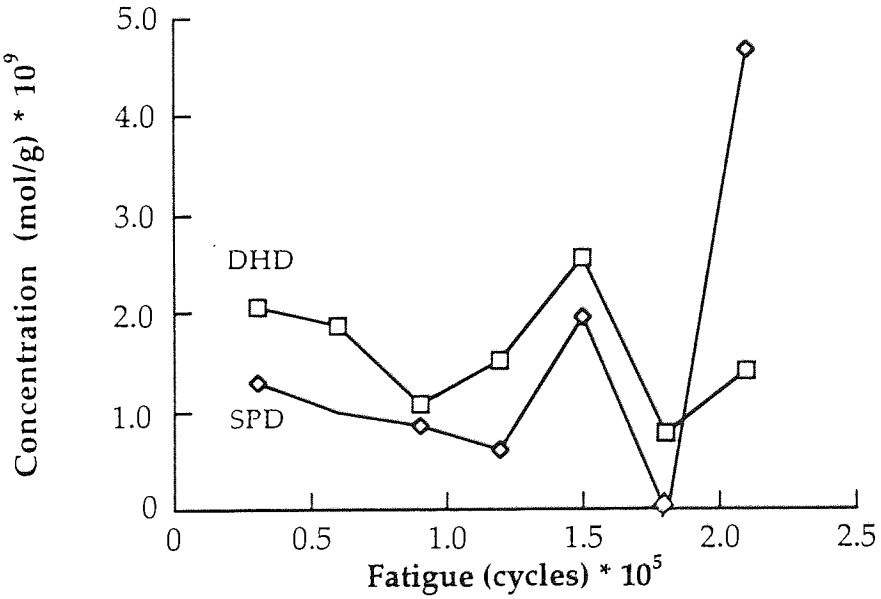

5.3 Discussion

5.3.1 Oxidation of α-Tocopherol during Vulcanisation

Major detected transformation products from α-tocopherol at various fatigue levels were the TRI and the ALD, see fig. 5.35. The oxidation mechanisms of α-tocopherol proposed in the literature [112), 113), 116)] (e.g. scheme 3.6, p203) showed that ALD is an end product in the oxidation sequence. (TRI is also produced at the end of oxidation, however it may be reduced back to SPD and quinone methide.) The oxidation of α-tocopherol starts from abstraction of hydrogen atom to form phenoxyl radical, some of which converts to the benzyl radical. This benzyl radical may either undergo dimerisation (producing DHD), or abstraction of a hydrogen atom leading to the formation of quinone methide. It may also produce the peroxyl radical which disproportionate to the ALD. The reaction of the SPD with the quinone methide leads to formation of the TRI. These products have been shown to be formed during high temperature processing of polyethylene (180°C) [116)]. Unfortunately there is no quantitative analysis of α-tocopherol containing rubber sample without fatiguing, the TRI and the ALD were major transformation products after curing. These compounds are likely to be produced during curing. Probably, at high temperature (150°C) during the rubber curing, the reaction to produce TRI from SPD and quinone methide is much faster than the dimerisation reactions, leading to observed smaller amounts of formation of DHD and SPD, and large amount of formation of TRI.

In addition, some of the transformation products are expected to bind on the rubber main chain. In previous work [116), 140)], the possibility of grafting of α-tocopherol onto polyethylene chain during processing was also reported. This will be discussed in the next section.

5.3.2 Antifatigue Mechanisms of α-Tocopherol during Fatiguing

Although TRI and ALD were detected mainly at all fatigue levels, these compounds are not the products caused by antifatigue activity. During the fatiguing, TRI was mainly consumed and αTOC was mainly produced, while ALD , SPD, and DHD did not change significantly, see fig. 5.35. The tendency of decreasing of TRI and that of increasing of αTOC seemed to fit very well. This implies that αTOC must be, at least in part, reproduced from the TRI during antifatigue activity. The concentration of R· under fatiguing conditions is high and R· is a strongly reducing agent hence these conditions are expected to favour the reversible mechanisms of TRI to SPD and quinone methide and eventually to αTOC as shown in scheme 5.2.

Scheme 5.2 Proposed reactions for regeneration of α-tocopherol in NR containing α-tocopherol during fatiguing.

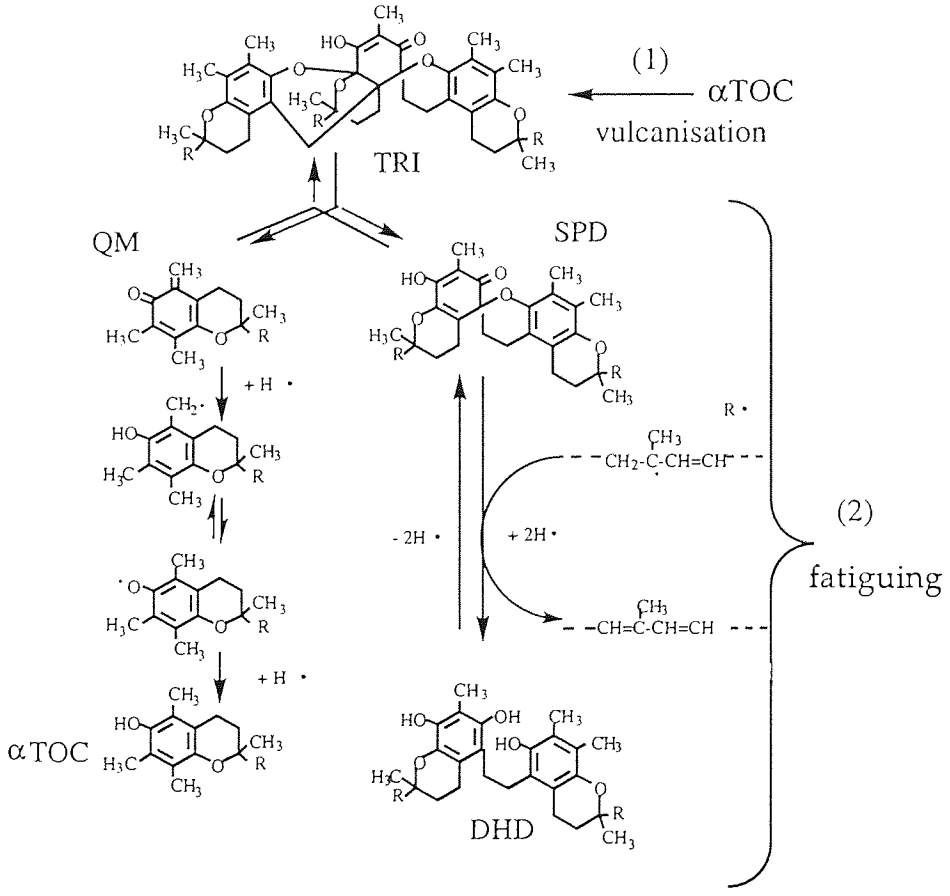

The increase of αTOC was much larger than the decrease of TRI, therefore, other source which is responsible for the formation of the additional αTOC must be necessary. The bound αTOC has the possibility of being this source. The theoretical concentration of α-tocopherol in vulcanised rubber sample is 3.15×10^{-5} mol/g when 1.5 phr of αTOC is compounded. The detected αTOC extracted from fatigued rubber sample using HPLC was much smaller than this value, even though the amounts of αTOC which is converted to other transformation product such as ALD, DHD, SPD and TRI are taken into account, see tables 5.11 and 5.12. For example, in case of the rubber sample after 30000 cycles fatiguing, only 7.44×10^{-6} mol/g αTOCwas detected by HPLC. Even after suming up all other transformation products, detected αTOC in this sample was only 8.62×10^{-6} mol/g, where 1 mol/g of ALD is considered to be equivalent to 1 mol/g of αTOC, similarly 1 mol/g of DHD and SPD are considered to be each equivalent to 2 mol/g of αTOC, and 1mol/g of TRI is considered to be equivalent to 3 mol/g of αTOC. Only 14.3 - 48.8 % of αTOC and its transformation products were detected by HPLC analysis.

Table 5.12 The ratio of detected αTOC concentration compared with theoretical value.

Fatigue (cycles)	Detected Concentration (mol/g)						Detected Ratio †
	αTOC $\times 10^6$	TRI×3 $\times 10^7$	ALD $\times 10^8$	DHD×2 $\times 10^9$	SPD×2 $\times 10^9$	total $\times 10^6$	%
30000	7.44	11.5	2.59	4.09	2.58	8.62	27.4
60000	4.02	4.39	2.12	3.73	1.98	4.49	14.3
90000	7.92	8.78	3.52	2.11	1.69	8.84	28.1
120000	9.62	4.04	2.51	3.03	1.19	1.01	31.9
150000	7.87	4.61	3.12	5.09	3.91	8.37	26.6
180000	11.5	0.96	2.37	1.52	0	11.6	36.9
210000	14.9	4.13	2.59	2.82	9.32	15.4	48.8

† ratio of total detected [αTOC] (including all transformation products) from the extracted fatigue samples to the original (theoretical) [αTOC] added to the sample during compounding.

Although there were three unknown detected compounds, the HPLC peaks of these compounds were not large enough to explain the rest of the undetected amounts, see figures 5.19 (a) and 5.28 (b). Experimental errors such as losses during extraction and analysis are included in the undetected αTOC, however, they still can not explain the rest of the undetected amounts. These facts may suggest the presence of unextracted transformation products due to binding onto the rubber main chains. Bound αTOC based products onto polyethylene and polypropylene were also confirmed in the previous research in polymer processing and performance group at Aston university[140]. The benzyl radical produced during the oxidation of αTOC has the possibility of grafting on the rubber main chains as shown in scheme 5.3.

Scheme 5.3 Possible grafting pathway of αTOC on the NR main chains.

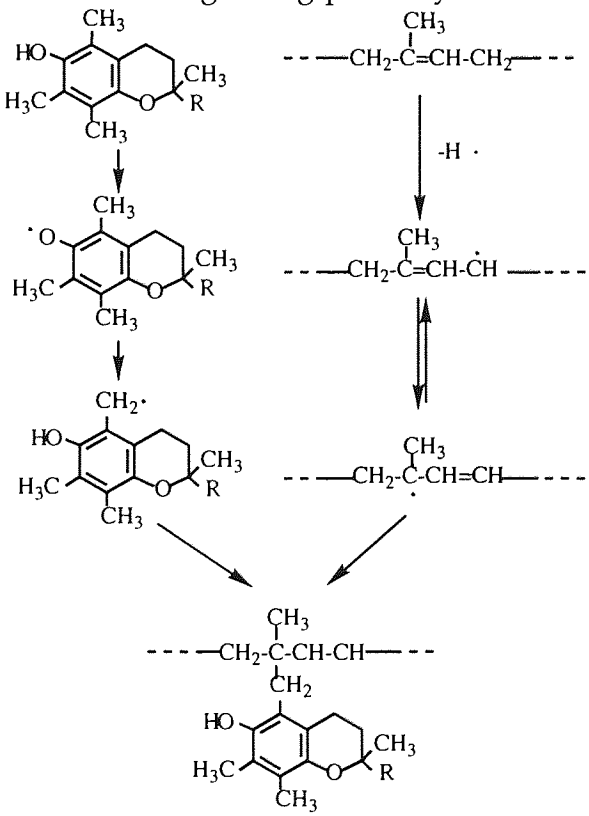

The bound αTOC could also undergo similar mechanism to that of the free αTOC and has the possibility of formation of a TRI-like compound during vulcanisation, see scheme 5.4

Scheme 5.4 Proposed mechanism of formation of grafted-TRI during vulcanisation.

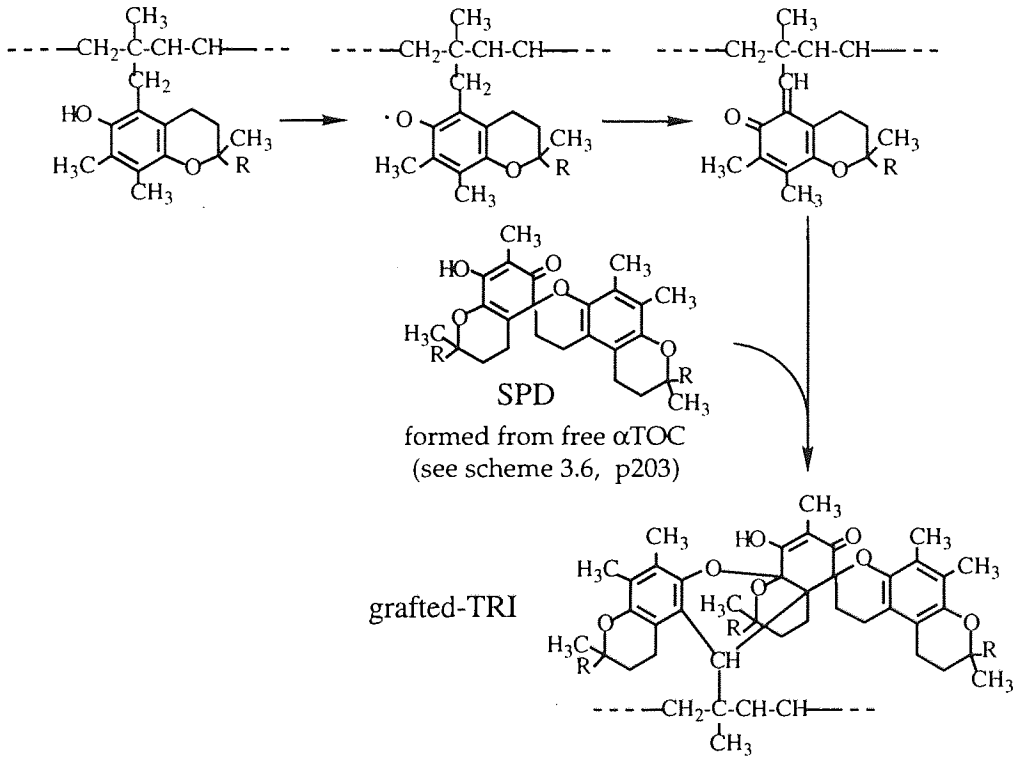

The amounts of undetected αTOC and its products have decreased on fatiguing. Although the DHD seems to be a stable compound, some of the DHD may be cleaved mechanically under high fatiguing conditions leading to the production of benzyl radicals. The formation of αTOC from grafted-TRI via DHD may therefore explain the reason why the increase of αTOC during fatiguing was much lager than the decrease of free TRI.

Fig. 5.2 UV spectrum of α-tocopherol (αTOC) authentic sample (in n-hexane).

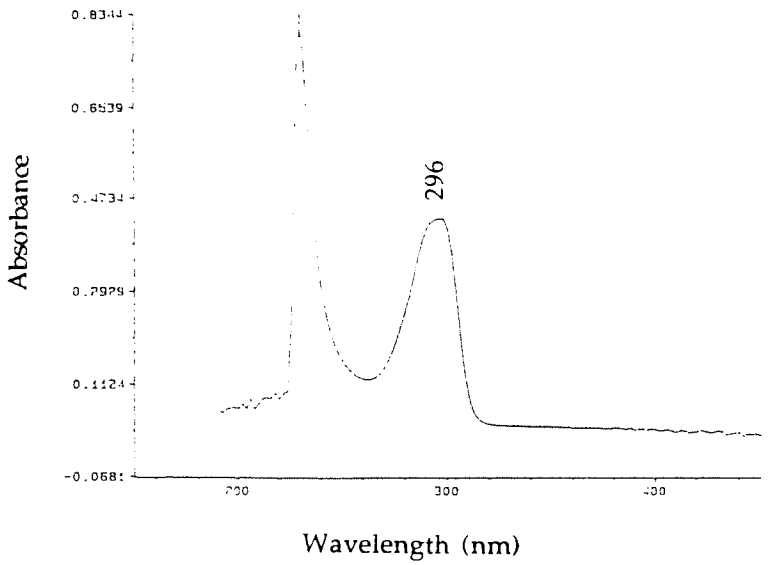

Fig. 5.3 UV spectrum of 5-formyl-γ-tocopherol (ALD) authentic sample (in n-hexane).

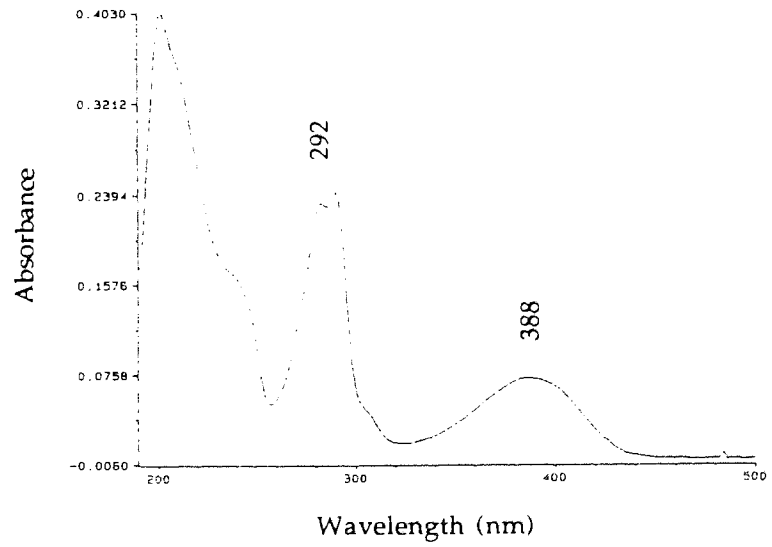

Fig. 5.4 UV spectrum of α-tocophenoxylquinone (TQ) authentic sample (in n-hexane).

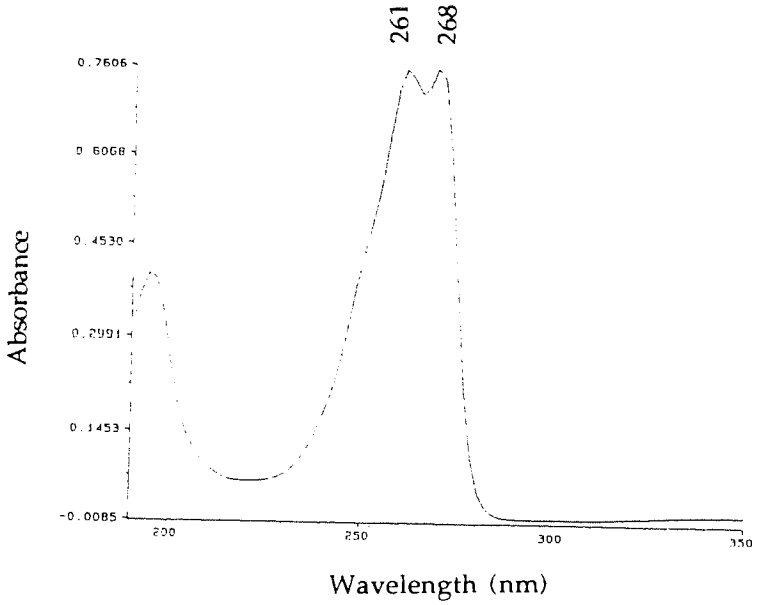

Fig. 5.5 UV spectrum of dihydroxydimer (DHD) authentic sample (in isopropanol).

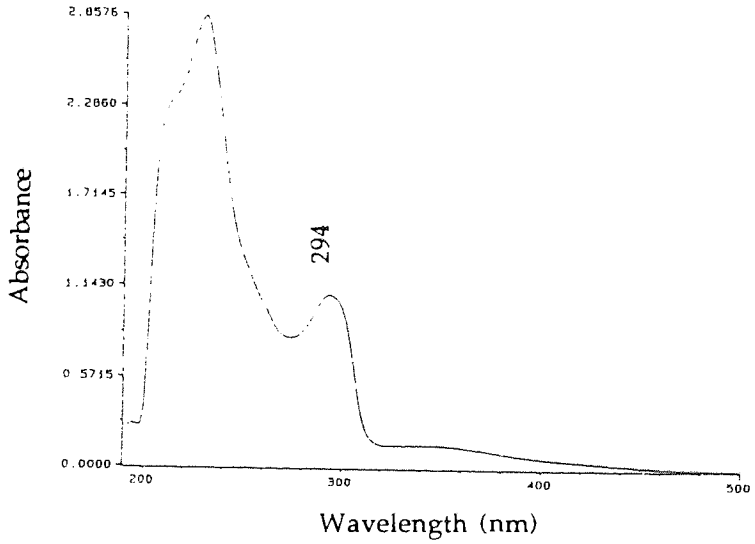

Fig. 5.6 UV spectrum of spirodimer (SPD) authentic sample (in methanol).

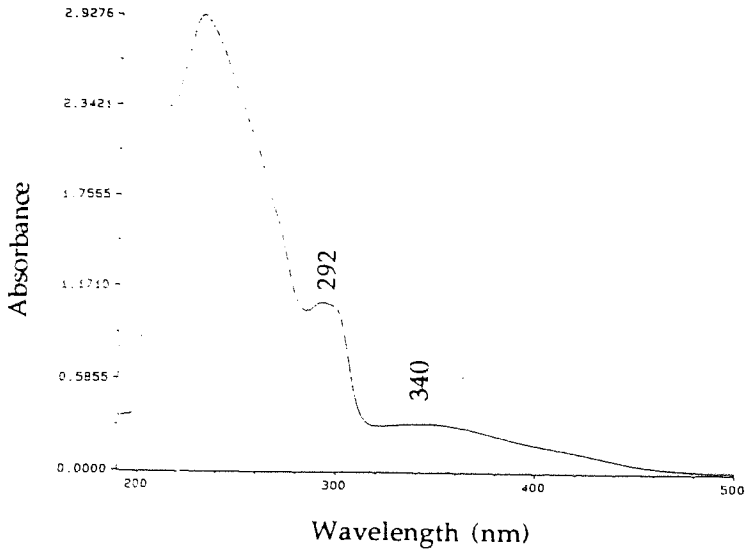

Fig. 5.7 UV spectrum of trimer (TRI) authentic sample (in isopropanol).

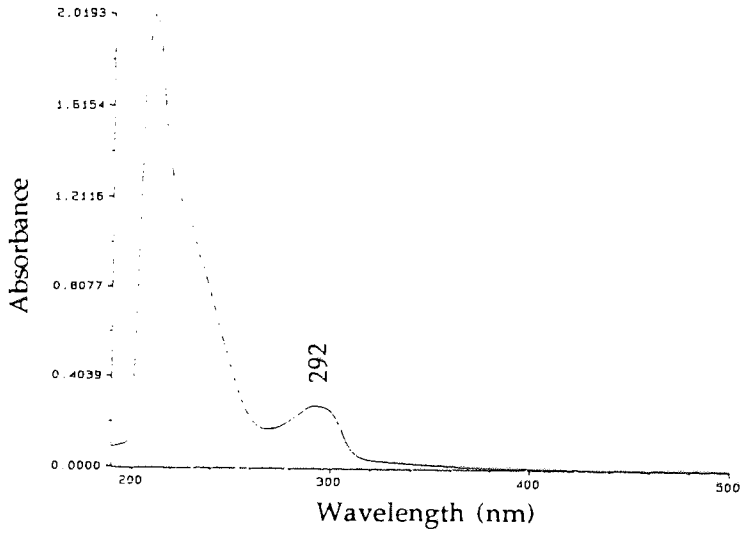

Fig. 5.8 HPLC chromatogram of n-hexane extracted substance from fatigued rubber (10,000 cycles at maximum strain of 108%) using C_{18} column (Zorbax ODS 4.6 mm ID × 25 cm) with various solvents (with 0.8ml/min, at ambient temperature). (a) solvent 1 (pure IPA) (b) solvent 3 (IPA : MeOH = 1 : 2) (c) solvent 4 (IPA : MeOH = 1 : 9) (d) solvent 7 (pure ACN) (marked peaks are α-tocopherol peaks)

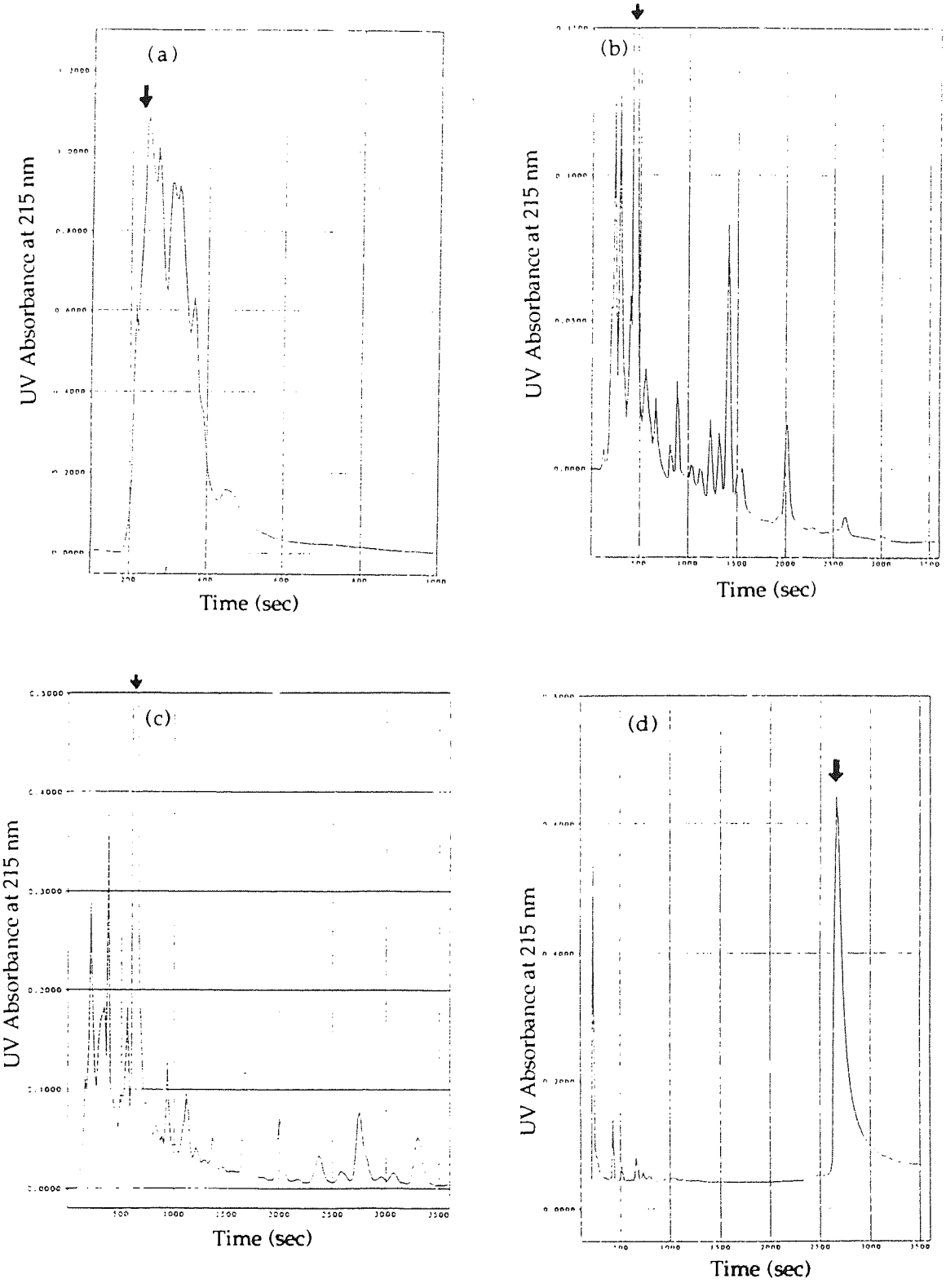

Fig. 5.12 HPLC chromatogram of n-hexane extracted substance from fatigued NR using solvent combination 1. (using Zorbax ODS 4.6 mm ID × 25 cm, with flow rate of 0.8 ml/min, at 290nm for UV detector, at ambient temperature)

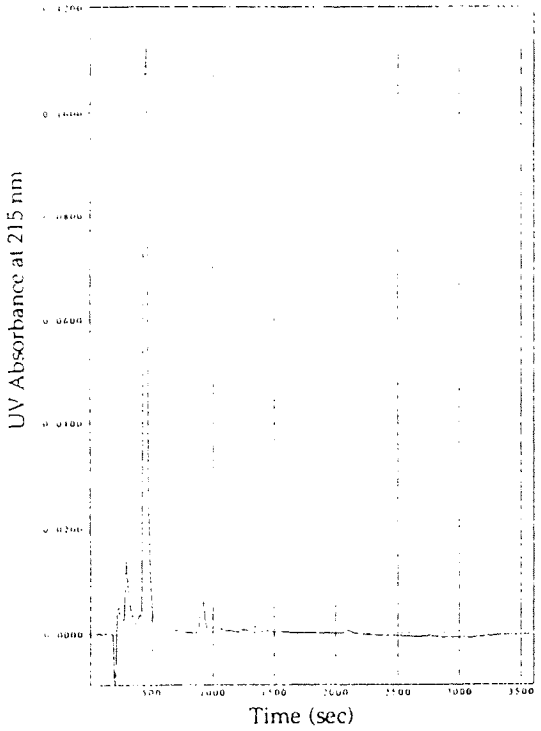

Fig. 5.13 HPLC chromatogram of n-hexane extracted substance from fatigued NR using solvent combination 2. (using Zorbax ODS 4.6 mm ID × 25 cm, with flow rate of 0.8 ml/min, at 290nm for UV detector, at ambient temperature).

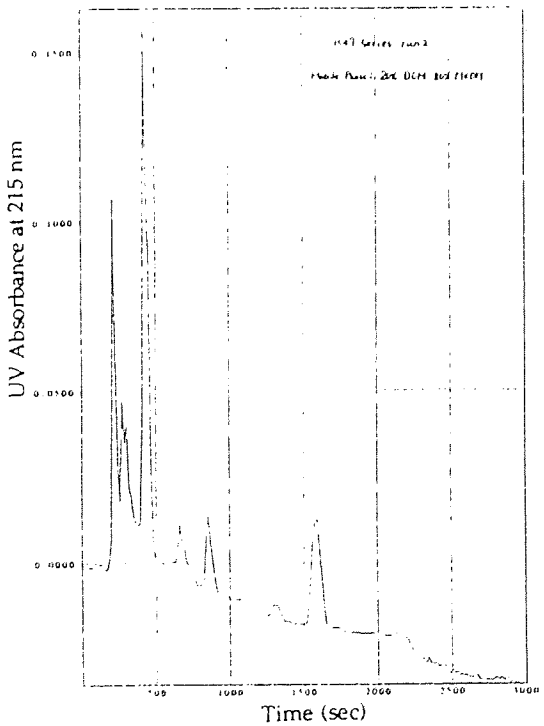

Fig. 5.14 HPLC chromatogram of n-hexane extracted substance from fatigued NR using solvent combination 3. (using Zorbax ODS 4.6 mm ID × 25 cm, with flow rate of 0.8 ml/min, at 290nm for UV detector, at ambient temperature)

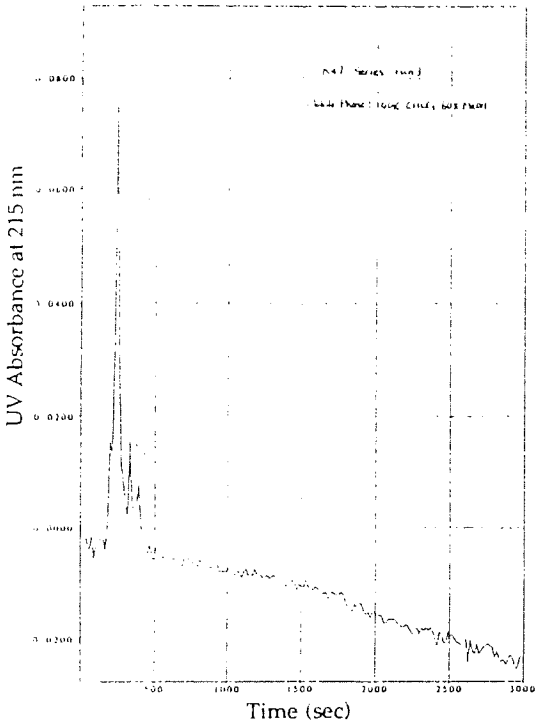

Fig. 5.15 HPLC chromatogram of n-hexane extracted substance from fatigued NR using solvent combination 4. (using Zorbax ODS 4.6 mm ID × 25 cm, with flow rate of 0.8 ml/min, at 290nm for UV detector, at ambient temperature)

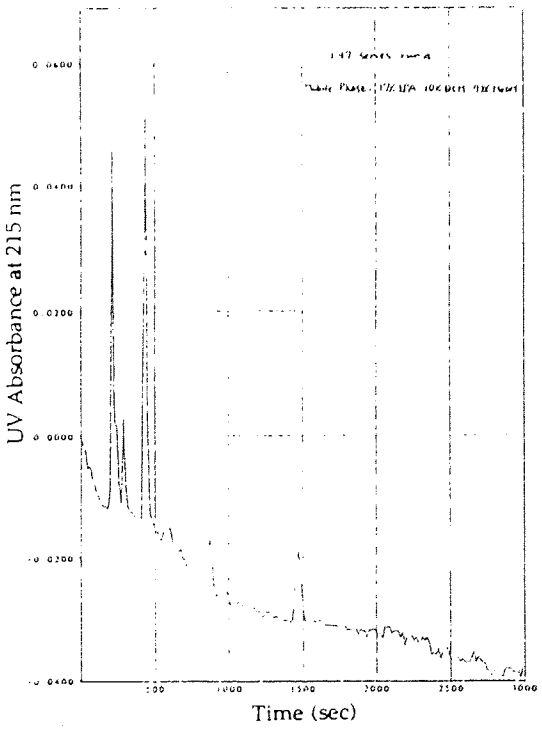

Fig. 5.16 HPLC chromatogram of n-hexane extracted substance from fatigued NR using solvent combination 5. (using Zorbax ODS 4.6 mm ID × 25 cm, with flow rate of 0.8 ml/min, at 290nm for UV detector, at ambient temperature)

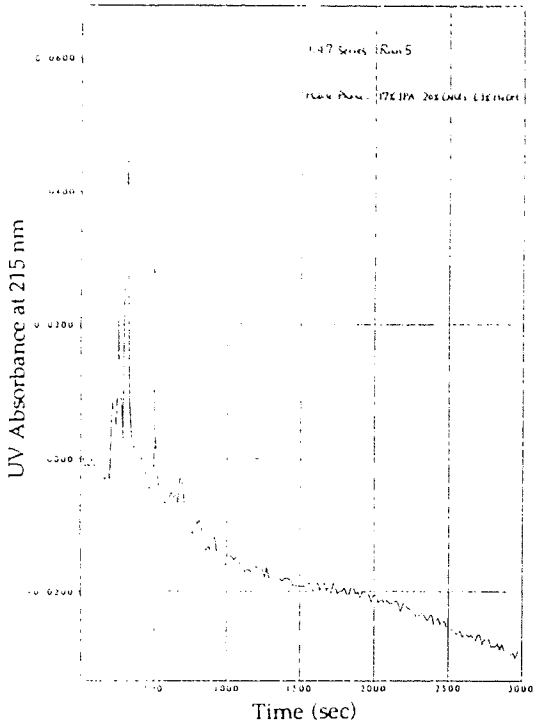

Fig. 5.17 HPLC chromatogram of n-hexane extracted substance from fatigued NR using solvent combination 6. (using Zorbax ODS 4.6 mm ID × 25 cm, with flow rate of 0.8 ml/min, at 290nm for UV detector, at ambient temperature)

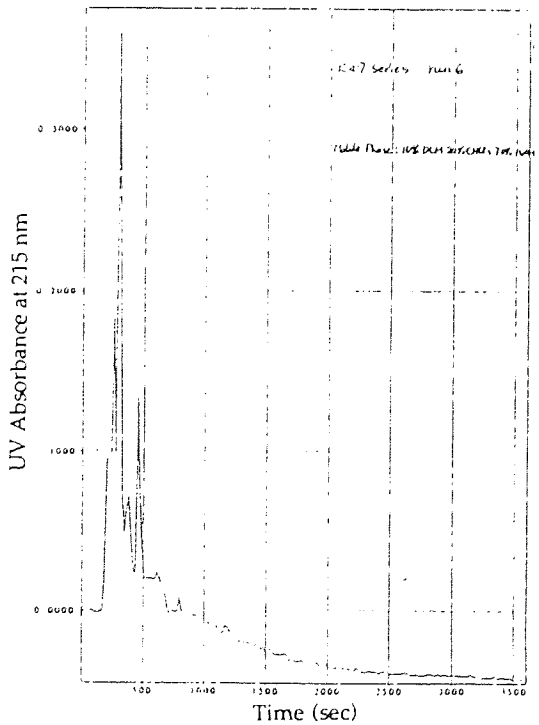

Fig. 5.18 HPLC chromatogram of extracted substance from fatigued NR using solvent combination 7. (using Zorbax ODS 4.6 mm ID × 25 cm, with flow rate of 0.8 ml/min, at 290nm for UV detector, at ambient temperature)

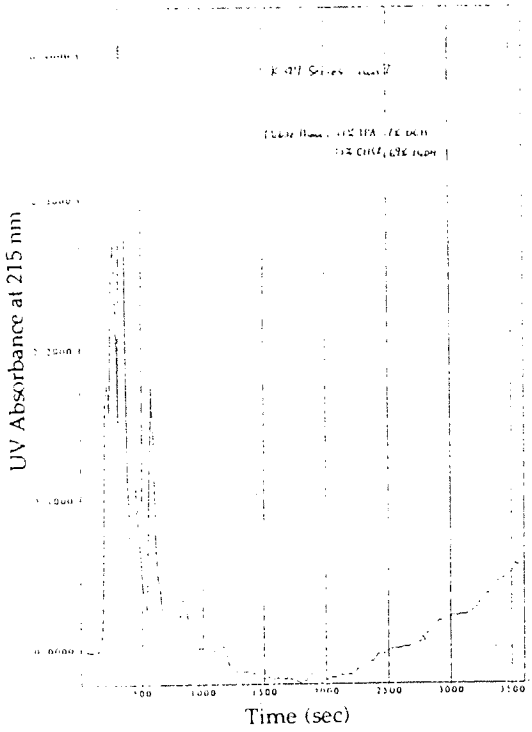

Fig. 5.19 HPLC chromatogram of n-hexane extracted substances from fatigued (120000 cycles at maxmum strain of 108%) α-tocopherol-containing vulcanised rubber samples using reversed phase (Zorbax ODS 4.6 cm ID × 25 cm), eluted by solvent 4 (MeOH : IPA = 9 : 1), with flow rate of 0.8 ml/min, at ambient temperature. (a) blank (no α-tocopherol) detection at 290 nm, (b) fatigued rubber containing α-tocopherol sample, detection at 290 nm, (c) fatigued rubber containing α-tocopherol sample, detection at 268 nm.

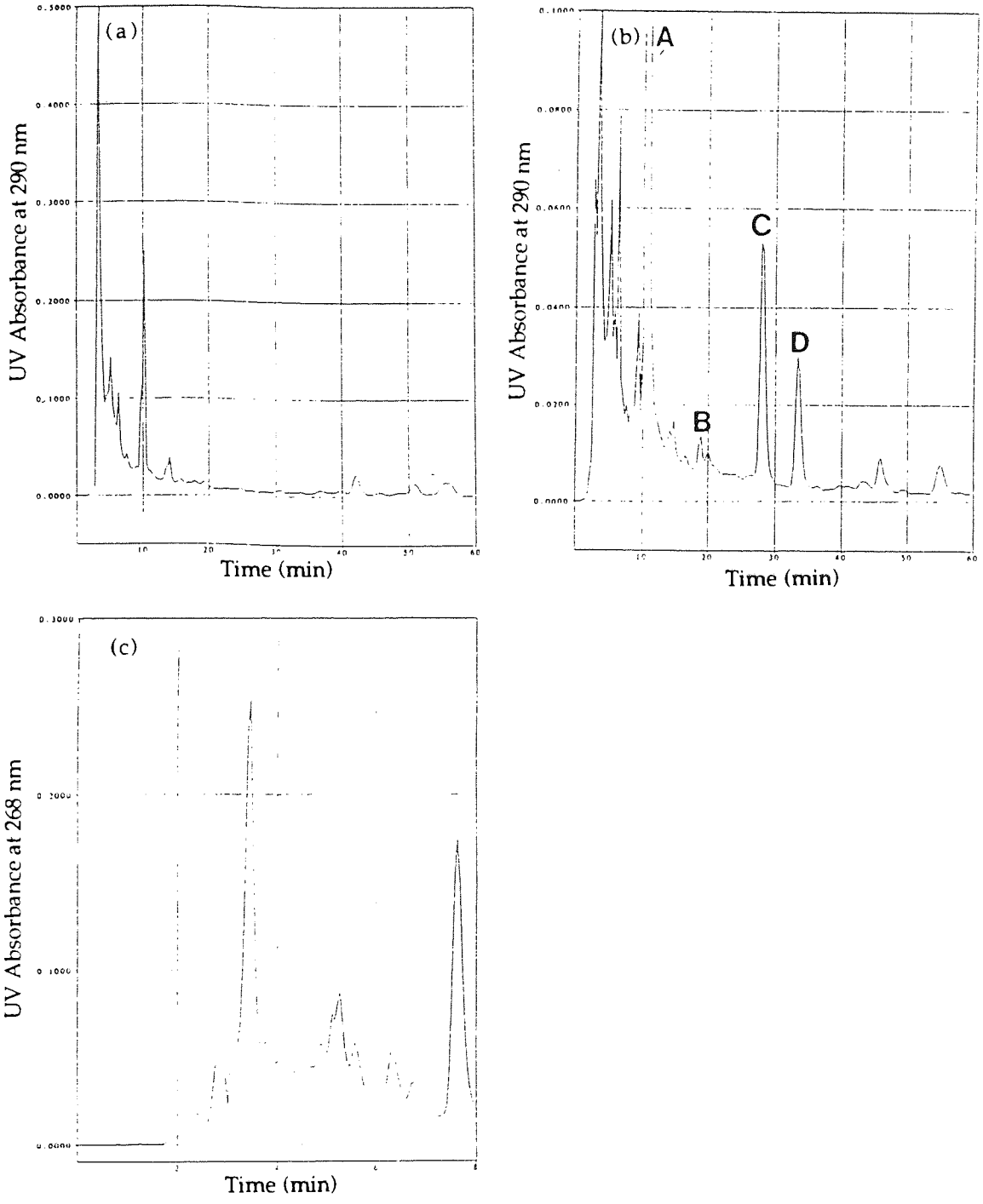

Fig. 5.20 HPLC chromatogram and UV spectrum of α-tocopherol authentic sample using reversed phase condition.

(stationary phase : Zorbax ODS 4.6 mm ID × 25 cm, mobile phase : solvent 4, MeOH : IPA = 9 : 1, flow rate : 0.8 ml/min, temperature : ambient, detector : UV at 290 nm)

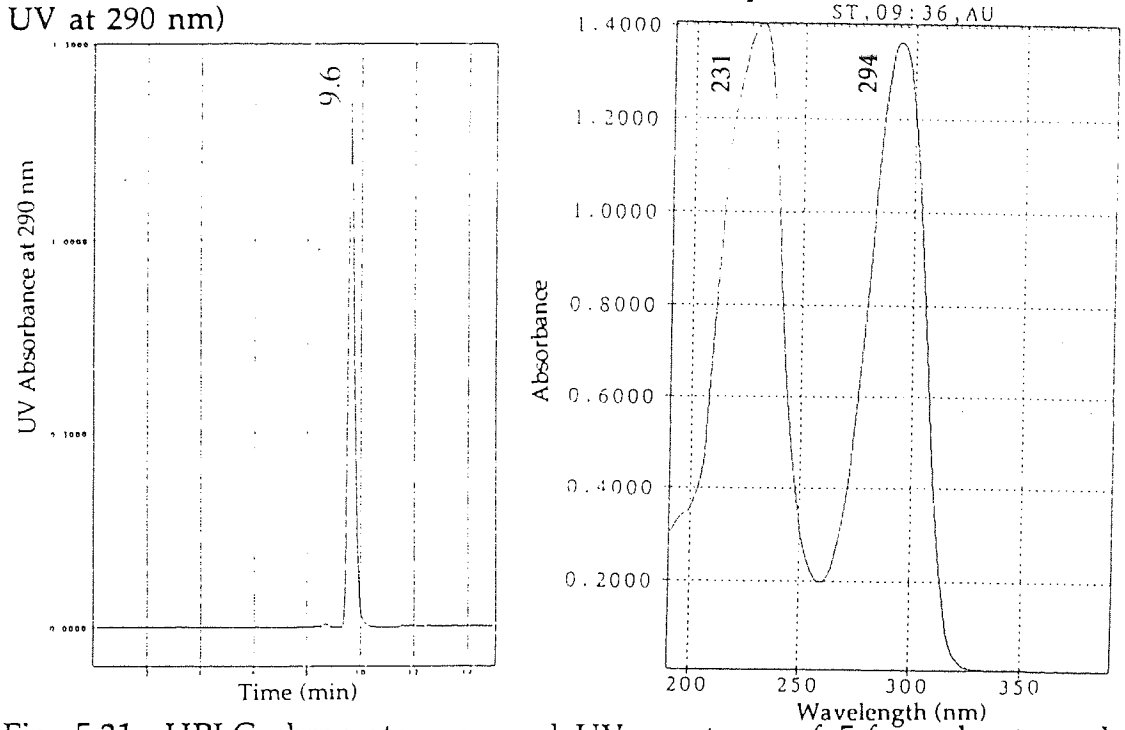

Fig. 5.21 HPLC chromatogram and UV spectrum of 5-formyl-γ–tocopherol authentic sample using reversed phase condition.

(stationary phase : Zorbax ODS 4.6 mm ID × 25 cm, mobile phase : solvent 4, MeOH : IPA = 9 : 1, flow rate : 0.8 ml/min, temperature : ambient, detector : UV at 290 nm)

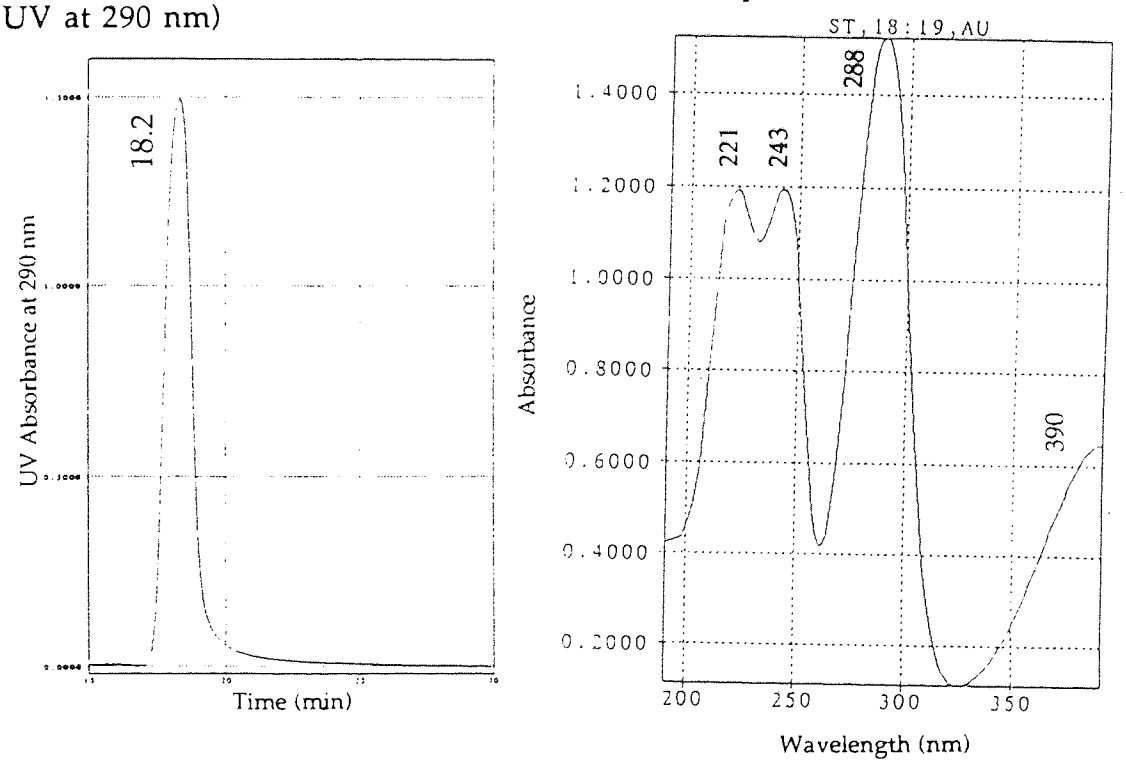

Fig. 5.22 HPLC chromatogram and UV spectrum of α-tocophenoxylquinone authentic sample using reversed phase condition.

(stationary phase : Zorbax ODS 4.6 mm ID × 25 cm, mobile phase : solvent 4, MeOH : IPA = 9 : 1, flow rate : 0.8 ml/min, temperature : ambient, detector : UV at 268 nm)

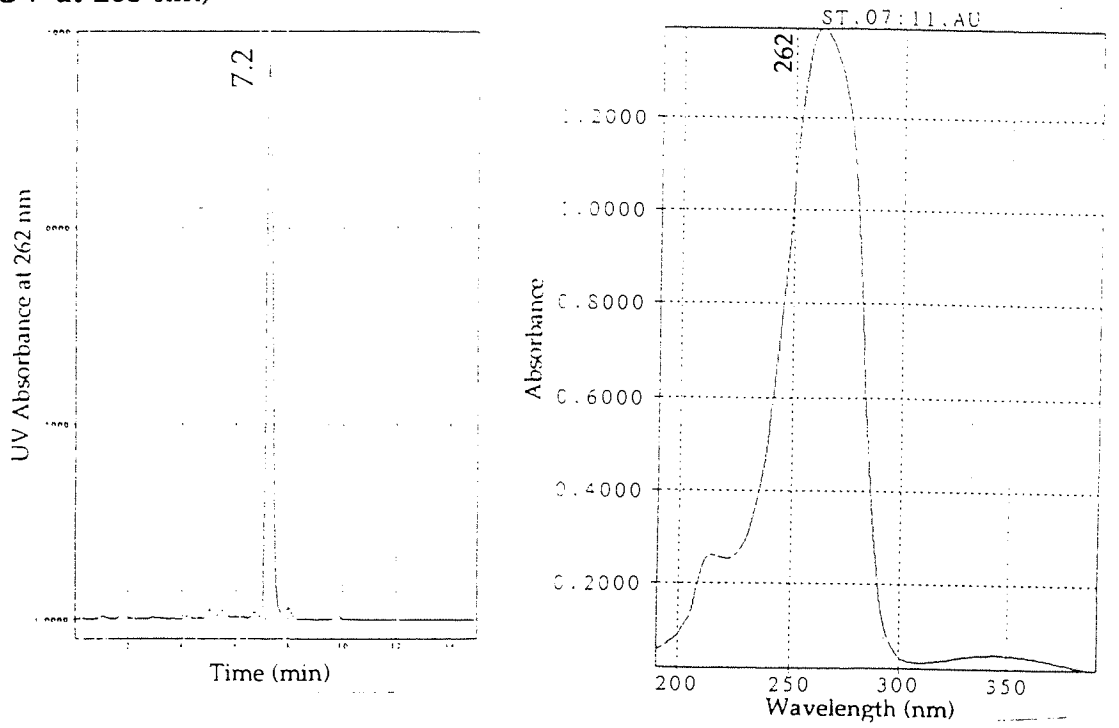

Fig. 5.23 HPLC chromatogram and UV spectrum of dihydroxydimer authentic sample using reversed phase condition.

(stationary phase : Zorbax ODS 4.6 mm ID × 25 cm, mobile phase : solvent 4, MeOH : IPA = 9 : 1, flow rate : 0.8 ml/min, temperature : ambient, detector : UV at 290 nm)

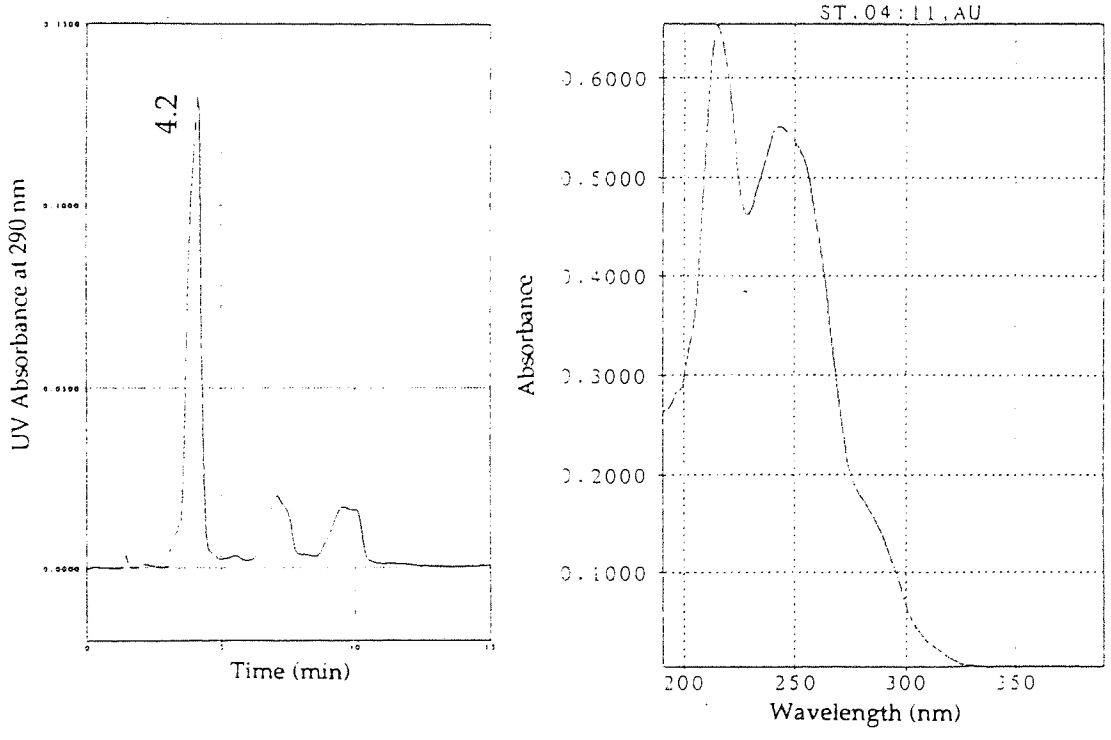

Fig. 5.24 HPLC chromatogram and UV spectrum of spirodimer authentic sample using reversed phase condition.
(stationary phase : Zorbax ODS 4.6 mm ID × 25 cm, mobile phase : solvent 4, MeOH : IPA = 9 : 1, flow rate : 0.8 ml/min, temperature : ambient, detector : UV at 290 nm)

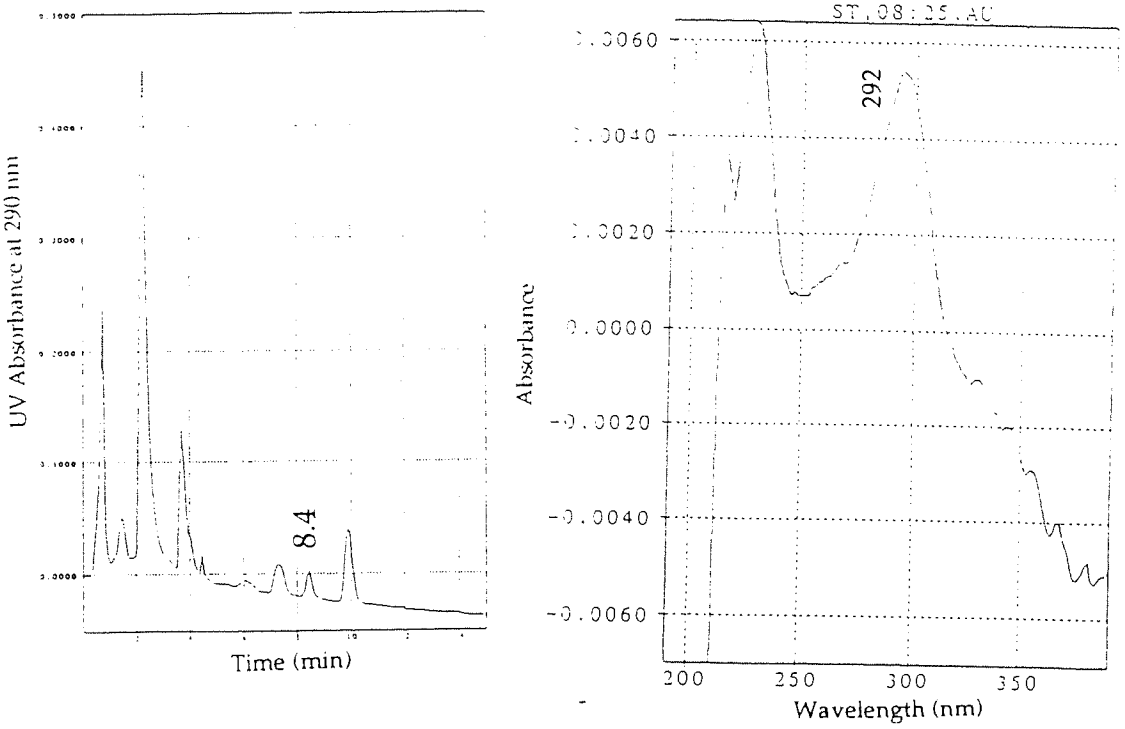

Fig. 5.25 UV spectra of compound A - D from HPLC UV detector.

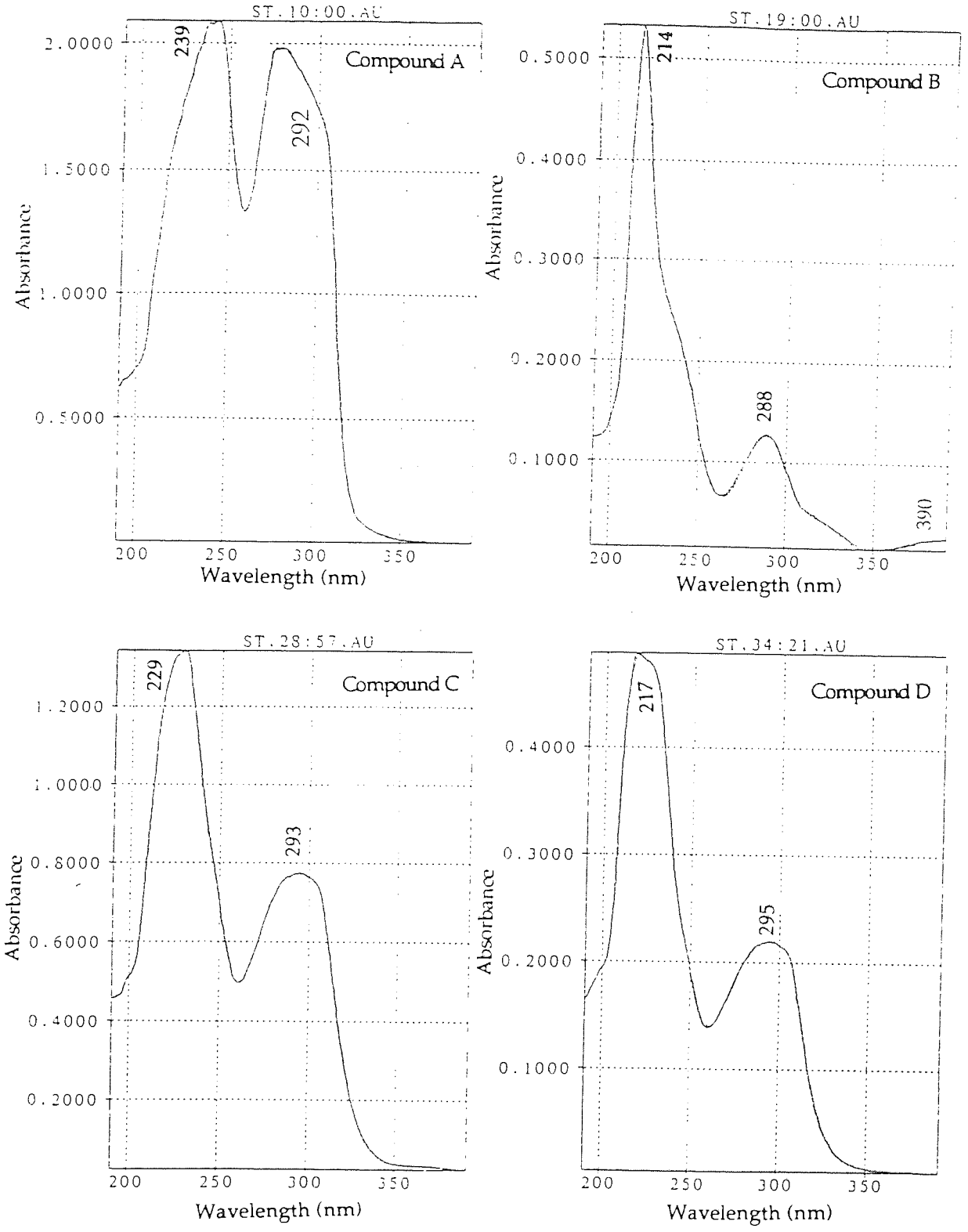

Fig. 5.26 HPLC chromatogram of n-hexane extracted substances from fatigued (10,000 cycles at maximum strain of 108%) NR samples using normal phase (Zorbax SIL 4.6 mm ID × 25 cm) with various solvent strength (various hexane : dioxane volume fraction) (0.8 ml/min, at ambient temperature).
(a) hexane : dioxane = 100 : 3.0 (solvent 1) (b) hexane : dioxane = 100 : 0.5 (solvent 2) (c) hexane : dioxane = 100 : 0.3 (solvent 3) (d) hexane : dioxane = 100 : 0.1(solvent 4)

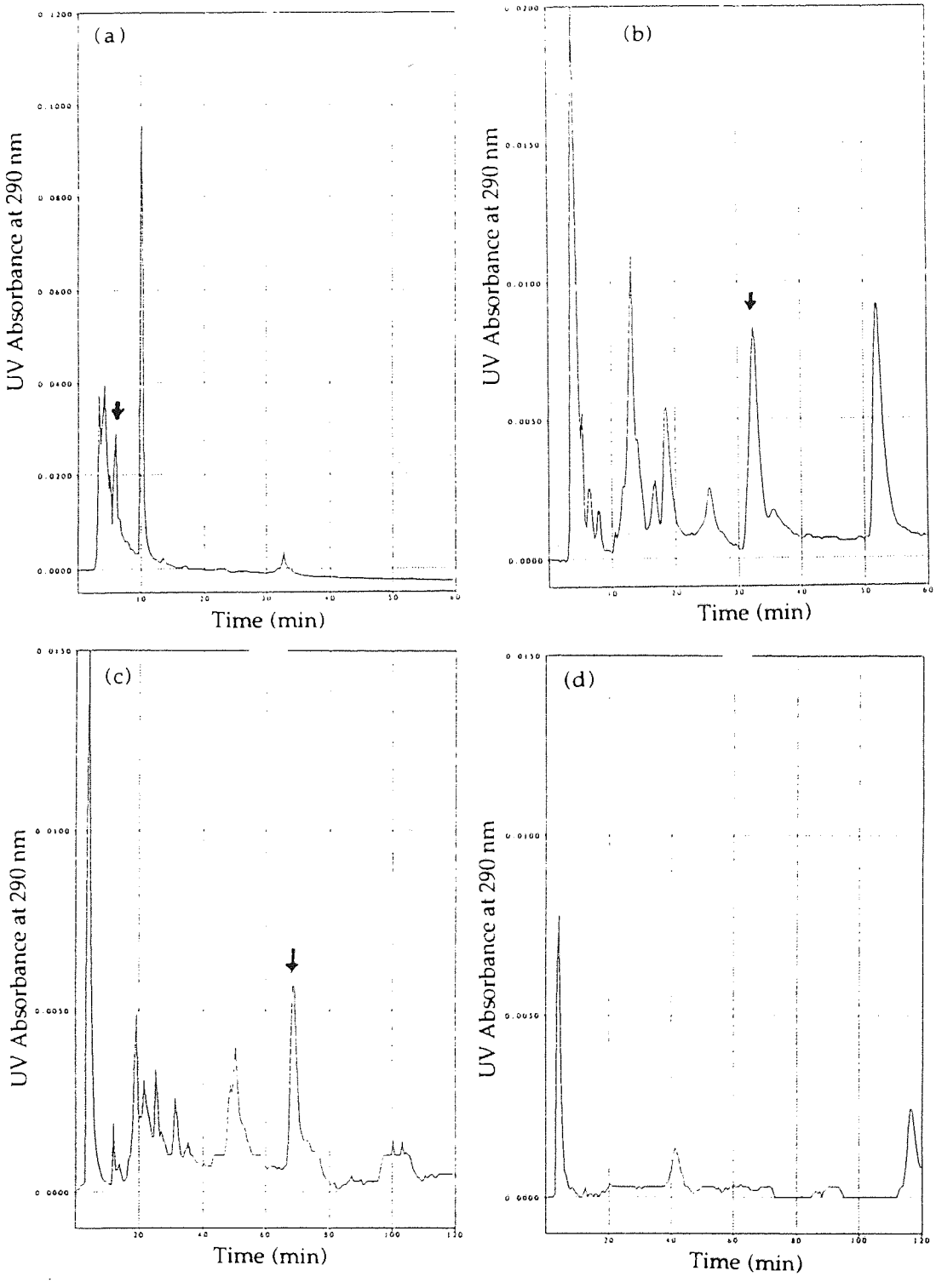

Fig. 5.28 HPLC chromatogram of n-hexane extracted substances from fatigued (15,000 cycles at maximum strain of 108 %) α-tocopherol containing vulcanised rubber samples using normal phase (Zorbax SIL 4.6 ID × 25 cm), eluted by solvent 2 (hexane : dioxane = 100 : 0.3), with flow rate of 0.8 ml/min, at ambient temperature, detected at 290 nm (a) blank (no α-tocopherol) detection at 290 nm (b) fatigued rubber sample containing α-tocopherol detection at 290 nm

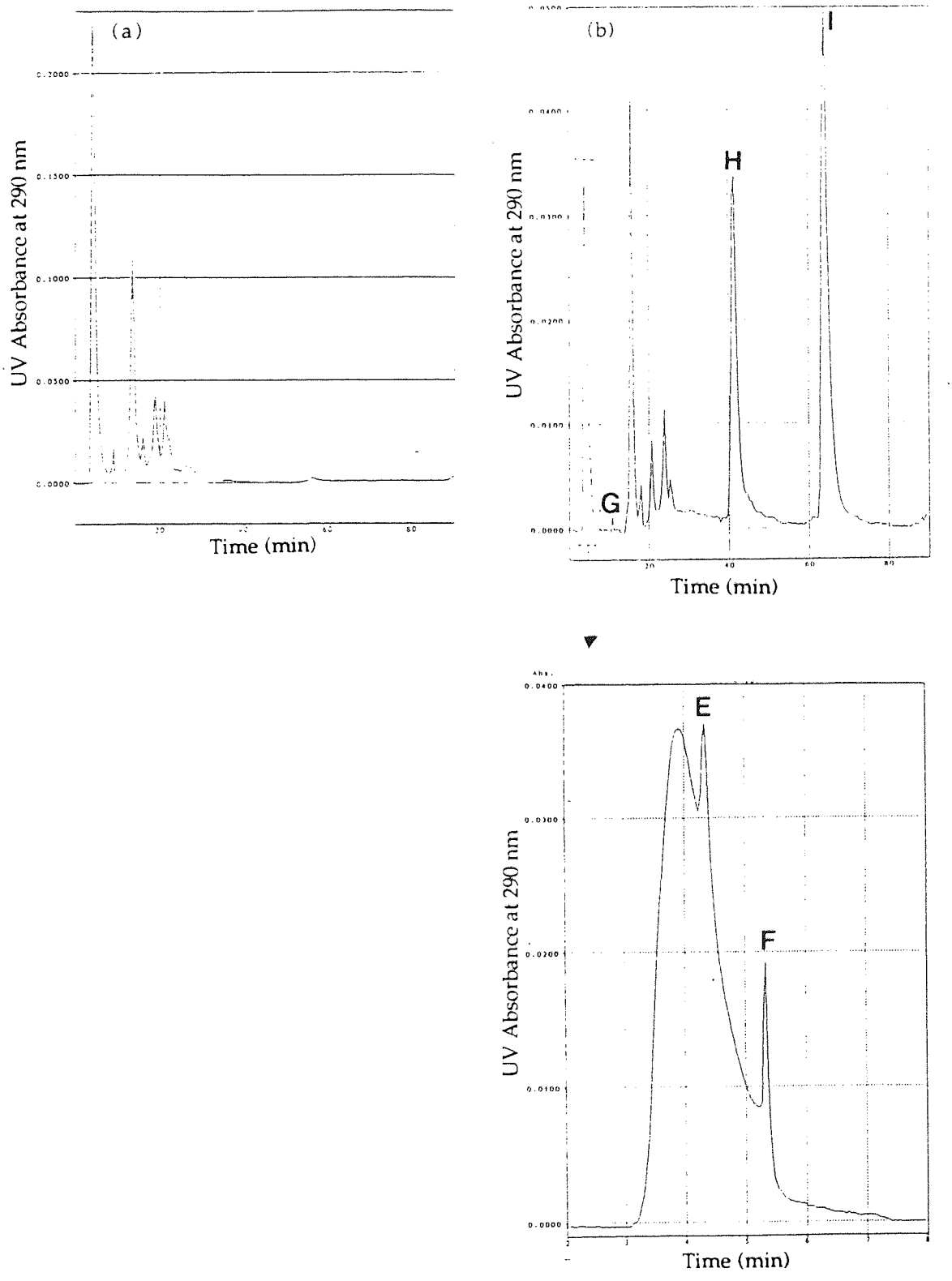

Fig. 5.29 HPLC chromatogram and UV spectrum of α-tocopherol authentic sample (αTOC) using normal phase condition.
(stationary phase : Zorbax SIL 4.6 mm ID × 25 cm, mobile phase : solvent 3, Hexane : Dioxane = 100 : 0.3, flow rate : 0.8 ml/min, temperature : ambient, detector : UV at 290 nm)

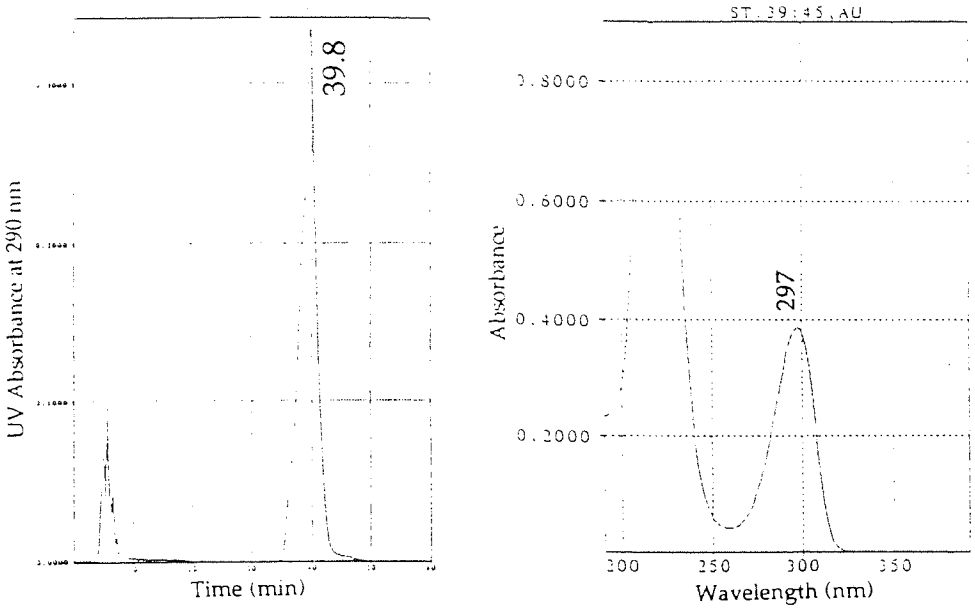

Fig. 5.30 HPLC chromatogram and UV spectrum of 5-formyl-γ–tocopherol authentic sample (ALD) using normal phase condition.
(stationary phase : Zorbax SIL 4.6 mm ID × 25 cm, mobile phase : solvent 3, Hexane : Dioxane = 100 : 0.3, flow rate : 0.8 ml/min, temperature : ambient, detector : UV at 290 nm)

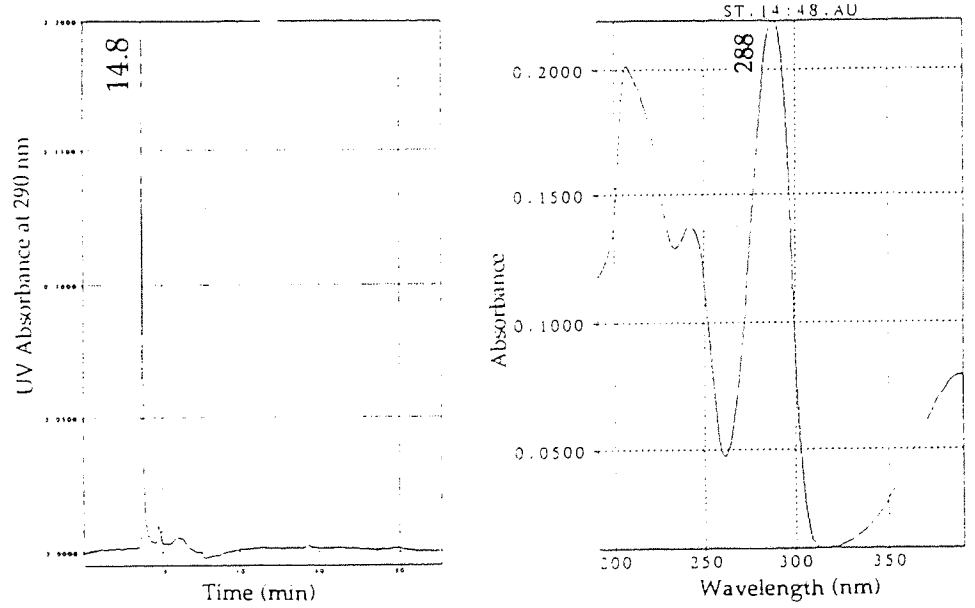

Fig. 5.31 HPLC chromatogram and UV spectrum of Dihydroxydimer authentic sample (DHD) using normal phase condition.

(stationary phase : Zorbax SIL 4.6 mm ID × 25 cm, mobile phase : solvent 3, Hexane : Dioxane = 100 : 0.3, flow rate : 0.8 ml/min, temperature : ambient, detector : UV at 290 nm)

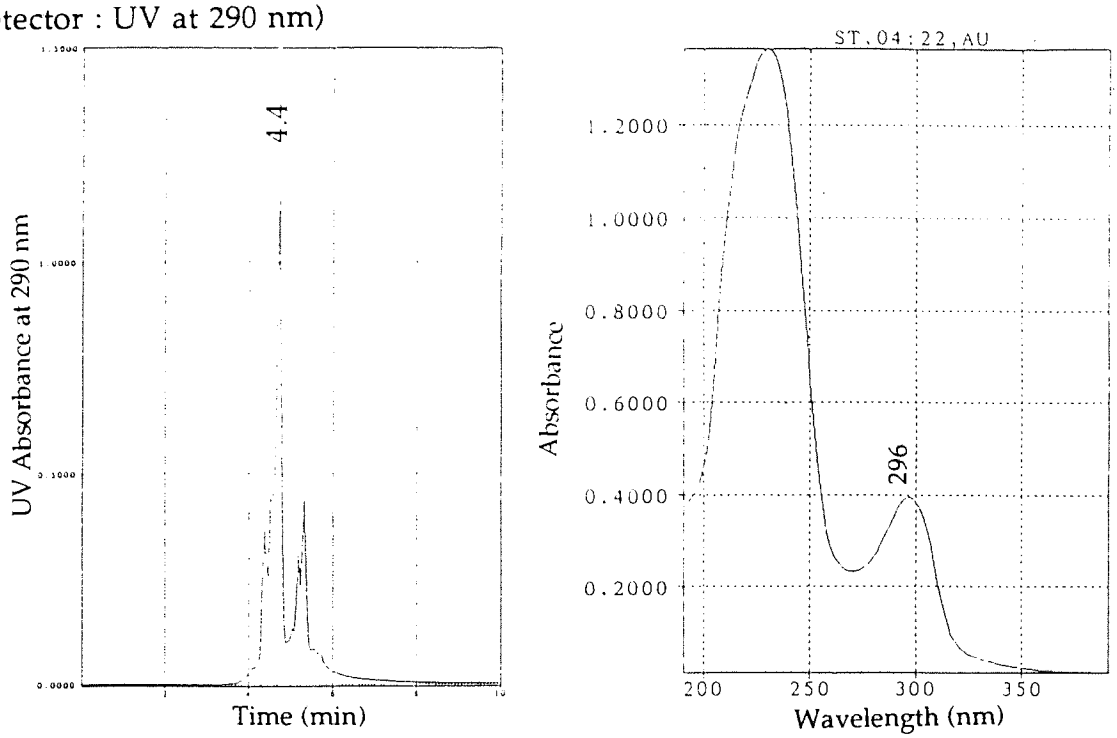

Fig. 5.32 HPLC chromatogram and UV spectrum of Spirodimer authentic sample (SPD) using normal phase condition.

(stationary phase : Zorbax SIL 4.6 mm ID × 25 cm, mobile phase : solvent 3, Hexane : Dioxane = 100 : 0.3, flow rate : 0.8 ml/min, temperature : ambient, detector : UV at 290 nm)

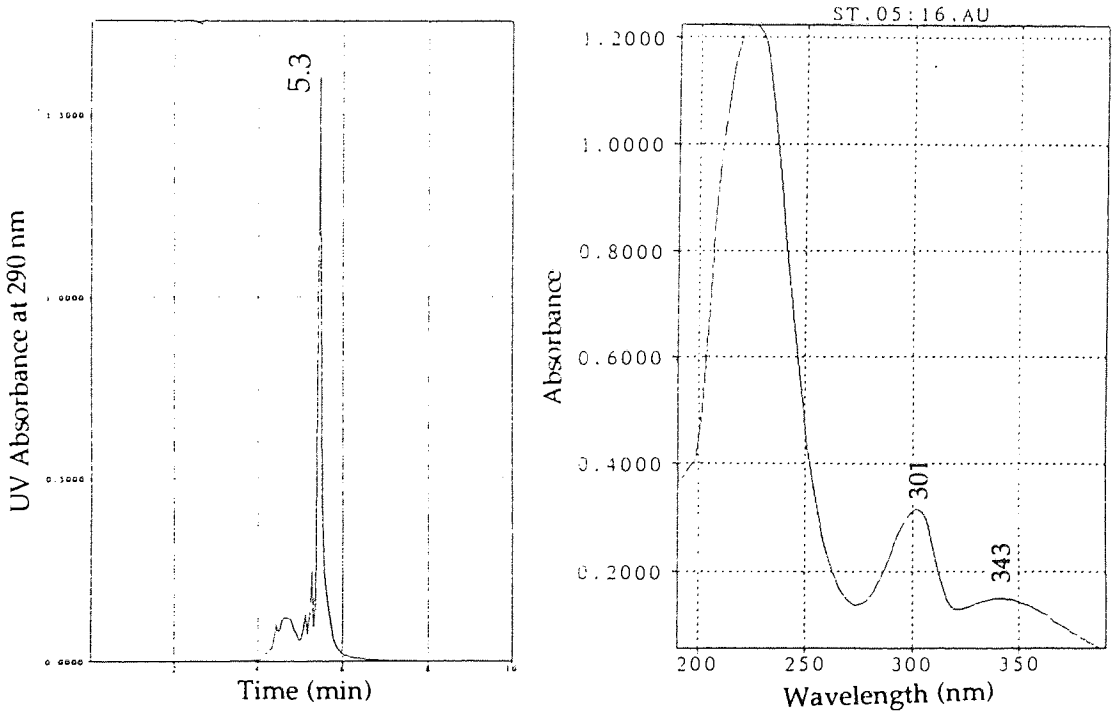

Fig. 5.33 HPLC chromatogram and UV spectrum of Trimer authentic sample (ALD) using normal phase condition.

(stationary phase : Zorbax SIL 4.6 mm ID × 25 cm, mobile phase : solvent 3, Hexane : Dioxane = 100 : 0.3, flow rate : 0.8 ml/min, temperature : ambient, detector : UV at 290 nm)

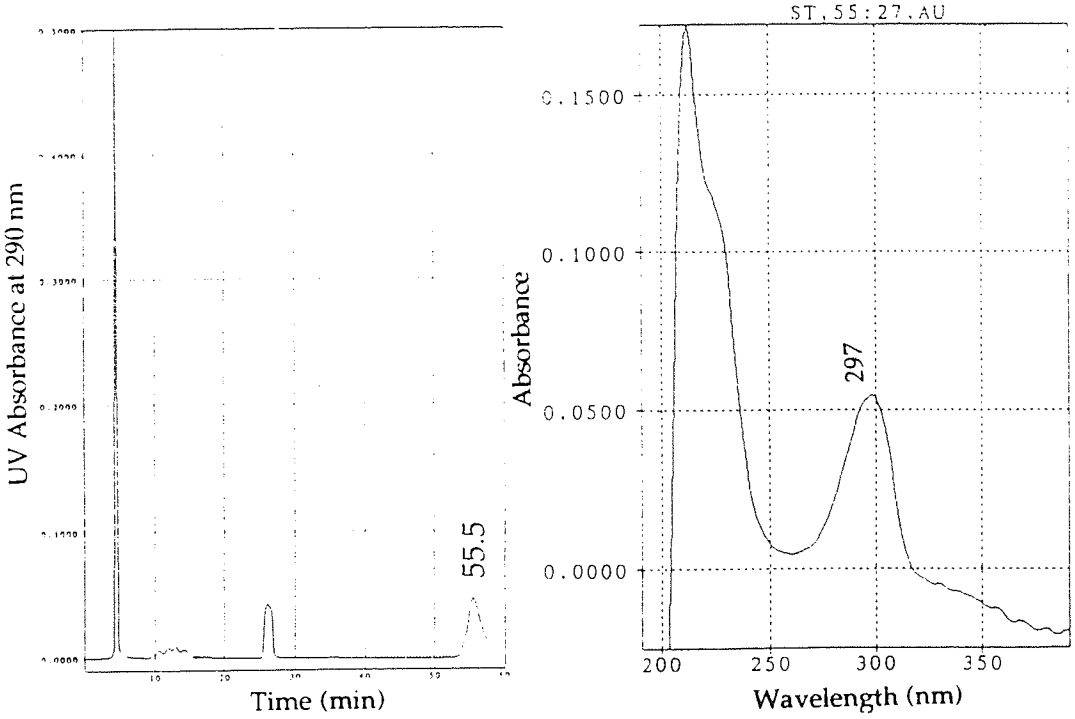

Fig. 5.34 UV spectra of compound E - I from HPLC UV detector.

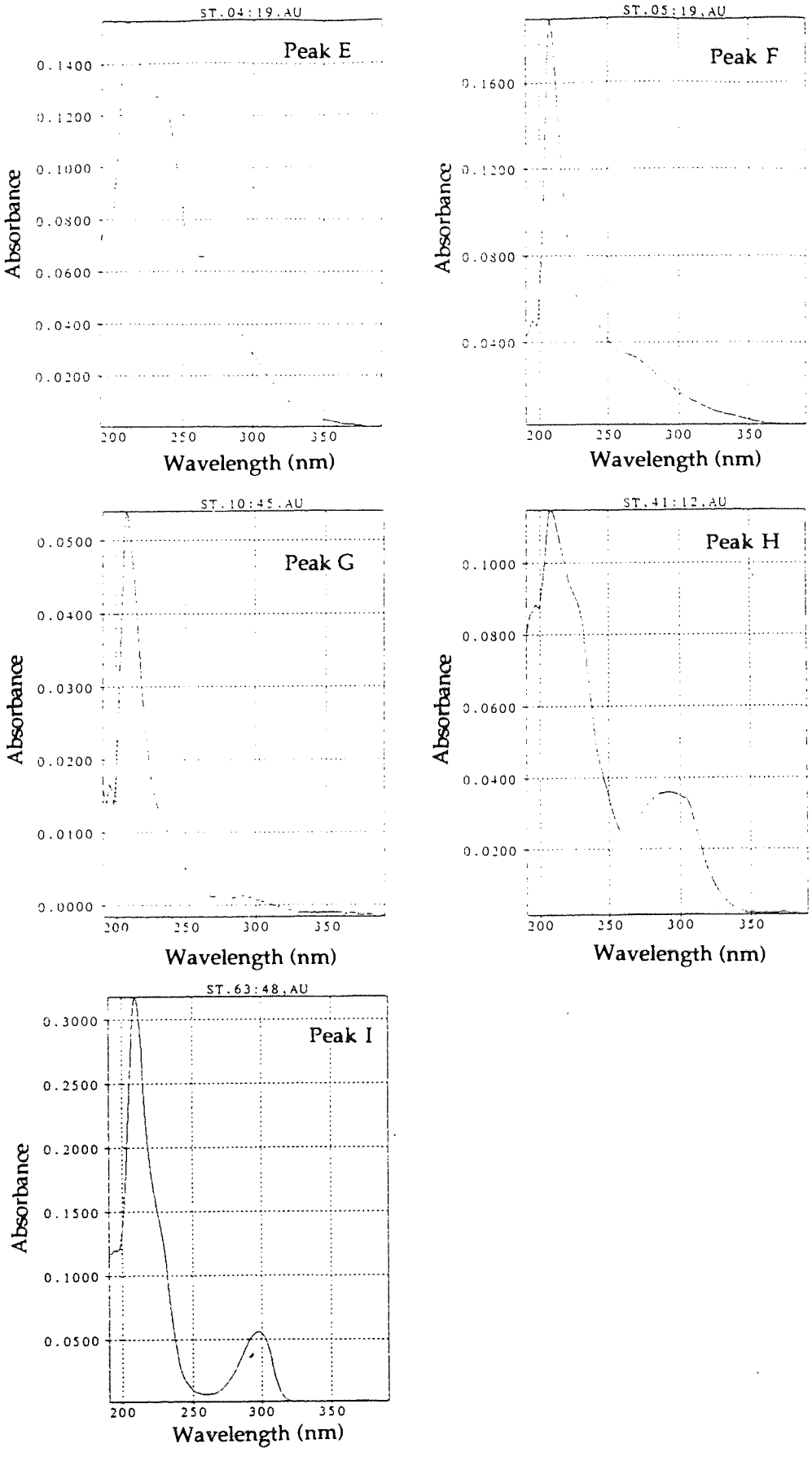

Chapter 6 Conclusions and Suggestions for Further Work

6.1 Conclusions

1. Quinonid compounds and some phenols are expected to deactivate macroalkyl radicals via their action as CB-A antioxidants. Because deterioration of rubber by fatigue is considered to be caused by macroalkyl radicals generated by mechanical chain scission, rather than peroxyl radicals which are well known for the cause of thermoxidation, hence these compounds are expected to have potential as antifatigue agents. Among the evaluated quinones and phenols which are considered to be macroalkyl radical scavengers, BQ, αTOC, γTOC and GM showed relatively good fatigue resistance (see fig. 3.4, p186). Furthermore, fatigue resistance of these compounds showed a linear relationship with the extent of their reactivity with alkyl radical (see fig. 3.12, p207). From these experimental results, compounds examined which have macroalkyl radical scavenging ability were shown to have good antifatigue activity.

2. Quinons (BQ, DPQ, and NQ) are expected to react with alkyl radicals either at the meta position of thier quinone rings (C-attack), producing phenoxyl radicals or at the oxygen of the quinone structure (O-attack). The reactivity calculated showed higher possibility of C-attack rather than O-attack (see tables 3.13 - 3.15, p197 - 199). The produced phenoxyl radicals (by C-attack) are expected either to dispropionate, to recombine with further alkyl radical, or to abstract a hydrogen atom from another alkyl radical producing an olefine, hence regenerating quinones and forming the corresponding phenols (see schemes 3.2 - 3.4, p197 - 199). The hindered phenol, HBA is also expected to have similar antifatigue mechanism, because it can produce quinonoid compound during processing of the rubber sample (see scheme 3.5, p201).

3. Tocopherols are expected to act as antioxidants in the rubber by more complicated reaction mechanisms, therefore, αTOC was further investigated for its role as antifatigue agent and the rubber samples containing α-tocopherol were analysed by HPLC. αTOC was oxidised during vulcanisation (at 150°C) producing TRI and ALD as major transformation products (while DHD and SPD were detected but only as minor transformation products). This TRI performed as a good antifatigue agent and reproduced αTOC during fatiguing (see fig. 5.35, p315). Some of the αTOC became grafted on the NR chain during vulcanisation and a mechanism was suggested for the formation of graft-TRI (see schemes 5.3 and 5.4, p319 and p320). Grafted TRI may be expected to function similarly to the free TRI. In addition, three unknown compounds were detected as oxidation products of αTOC.

4. The effective antifatigue agents, BQ and αTOC showed very poor thermoxidative resistance (see figures 3.6 - 3.9, p189 - 192). Since most rubber products which are required to have long service lives under fatiguing conditions are often exposed to thermoxidative conditions (at various temperature), examination of the thermoxidative resistance is important. In order to compensate for the thermoxidative resistance, the stabilising effect of reactive antioxidants was investigated. Among the evaluated reactive antioxidants, PM, BTMI, APMA, and MADA, APMA showed the best performance (see figures 4.3 - 4.6, p236 - 237). Although high grafting ratio had been achieved, it is suggested that this was a result of large extent of polymerisation producing long APMA pendants on the polymer chains (long grafts). These long branches are expected to decrease the effect of the CB-D activity due to a maldistribution of APMA (a wide distribution of APMA due to short grafting branches is desired). In this work, model compound for NR, squalene, was used for the investigation of the structure of grafted APMA.

5. In general, many antioxidants show synergestic effects when two or more antioxidants with complementary functions are used together. The action of mixtures of APMA with various antifatigue agents (BQ, αTOC, γTOC and TMQ) were investigated but no significant synergism was observed in all cases (just additive effects were obtained), see figures 4.33 and 4.34, p 255 and p256.

6.2 Suggestion for Further Work

1. The antifatigue mechanism suggested for quinonoid compounds was not confirmed by the analysis of transformation products. This mechanism must be investigated using HPLC analysis followed by structure determination using various spectroscopic techiniques.

2. Three unknown products were shown to be formed from α-tocopherol during fatiguing of natural rubber samples should be separated and their structure determined in order to understand their identity role in the overall mechanism.

3. The grafting condition of APMA should be further optimised in order to achieve shorter branch and higher extent of grafting on the rubber chain. This should improve the thermoxidative resistance of APMA containing rubbers.

4. In this work, a model compound for natural rubber, squalene, was used for the investigation of the structure of grafted APMA. Direct analysis of APMA grafted vulcanised rubber is more desiarable. The investigation of solid state NMR of vulcanised rubber (probably swollen by $CDCl_3$) will be worth trying.

References

1. S. Yamashita, "Genneral Properties." in *Gomu Gijutsu no Kiso* , The Society of Rubber Industry Japan,, Tokyo, 1983 pp. 1-50.

2. J. C. Amberg, "Curatives for General-Purpose Elastomers." in *Vulcanization of Elastomers* , G. Alliger and I. J. Sjothum, Eds., Reinhold Publishing, New York, 1963 pp. 126 - 152.

3. A. Y. Coran, "Vulcanization. Part 5. The Formation of Crosslinks in the System: Natural Rubber-Sulfur-MBT-Zinc ion.", *Rubber Chem. Tech.* **37**, 679 - 688 (1964).

4. A. Y. Coran, "Vulcanization. Part 7. Kinetics of Sulfur Vulcanization of Natural Rubber in Presence of Delayed-Action Accelerators.", *Rubber Chem. Tech.* **38**, 1 - 14 (1965).

5. L. Bateman, "Chemistry of Vulcanization." in *The Chemistry and Physics of Rubber-Like Substances* , L. Bateman, Ed. Maclaren & Sons, New York, 1963 pp. 449 - 562.

6. S. Samukawa, "Developments of Accelerators.", *Nihon Gomu Kyokaishi* **48**, 558 - 569 (1975).

7. A. J. Parker and N. Kharasch, "The Scission of The Sulfur-Surfur Bond.", *Chemical Review* **59**, 583 - 628 (1959).

8. S. P. Manik and S. BanerJee, "Studies on Dicumylperoxide Vulcanization of Natural Rubber in Presence of Sulfur and Accelerators.", *Rubber Chem. Tech.* **42**, 744 - 758 (1969).

9. J. I. Cunneen, "Oxdative Ageing of Natural Rubber.", *Rubber Chem. Tech.* **41**, 182 - 208 (1968).

10. D. S. Campbell, "Structural Characterization of Vulcanizates. XI. Network-Bound Accelerator Residues.", *J. Appl. Polym. Sci.* **14**, 1409 - 1419 (1970).

11. M. R. Krejsa and J. L. Koenig, "A Review of Sulfur Crosslinking Fundamentals For Accelerated and Unaccelerated Vulcanization.", *Rubber Chem. Tech.* **66**, 376 - 410 (1993).

12. A. Y. Coran, "Vulcanization." in *Science and Technology of Rubber* , F. R. Eirich, Ed. Academic Press, New York, 1978 pp. 291 - 338.

13. J. L. Bolland, "Kinetics of Olefin Oxdation.", *Quqrt Review* **3**, 1 - 21 (1949).

14. L. Bateman, "Olefin Oxidation.", *Quart Review* **8**, 147 - 167 (1954).

15. S. Al-Malaika, "Effects of Antioxidants and Stabilizers." in *Comprehensive Polymer Science*, G. C. Eastmond, A. Ledwith, S. Russo and P. Sigwalt, Eds., Pargamon Press, Oxford, 1989, vol. 6, pp. 539 - 578.

16. R. B. Mesrobian and A. V. Tobolsky, "Some Structual and Chemical Aspects of Ageing and Degradation of Vinyl and Diene Polymers.", *J. Polym. Sci.* **2 (5)**, 463 - 487 (1947).

17. J. L. Bolland, "Kinetics Studies in the Chemistry of Rubber and Related Materials. 7. Influence of Chemical Structure on the α-Methylenic Reactivity of Olefins.", *Trans. Faraday Soc.* **46**, 358 - 368 (1950).

18. Y. Ohkatsu, "General Statement of Autoxidation.-Chemical Structure and Oxidation Kinetics (2)." in *Jidosanka no Riron to Jissai*, Kagakukogyo-Sha, Tokyo, 1986 pp. 25 - 30.

19. E. M. Bevilacqua, "Oxidation and Antioxidants in Rubber." in *Autoxidation and Antioxidants*, W. O. Lundberg, Ed. John Wiley, New York, 1962, vol. 2, pp. 857 - 918.

20. Z. T. Ossefort, "Influence of Accelerator Residues on Age Resistance of Elastomeric Vulcanizates.", *Rubber World* **140**, 69 - 76 (1959).

21. L. M. Hobbs, R. G. Craig and C. W. Burkhart, "Non-Free Sulfur Curing Systems for Age Resistant Styrene-Butadiene-Rubber.", *Rubber World* **136**, 675 - 686 (1957).

22. H. H. Kausch, "The Role of Chain Scission in Homogeneous Deformation and Fracture." in *Polymer Fracture*, Springler-Verlag, New York, 1978 pp. 173 - 250.

23. G. J. Lake, "Mechanical Fatigue of Rubber.", *Rubber Chem. Tech.* **45**, 309 - 328 (1972).

24. J. Souma, "Mechanodegradation." in *Koubunshi no Rekka*, Shokabou, Tokyo, 1993 pp. 61 - 99.

25. W. D. Potter and G. Scott, "Mechano-Chemical Reactions of Polymers. Formation of Free Radicals in Stressed Rubber.", *Eur. Polym. J.* **7**, 489 - 497 (1971).

26. K. Kanamaru, "Introduction of Mechanochemistry of Macromolecules." in *Koubunshi Hadan no Kagaku*, Kyoritsu Shuppan, Tokyo, 1983 pp. 29 - 39.

27. H. H. Kausch, "Identification of ESR Spectra of Mechanically Forced Free Radicals." in *Polymer Fracture* , Springler-Verlag, New York, 1978 pp. 119 - 139.

28. R. Natarajan and P. E. Read, "Molecular Fracture in Natural Rubber during Testing at Low Temperatures.", *J. Polymer Sci., A2* **10**, 585 - 598 (1972).

29. E. H. Andrews and P. E. Reed, "Deformation of Cross-Linked Polymers Below T_g." in *Deformation and Fracture of High Polymers* , R. I. Jaffee, Ed. Plenum Press, New York, 1972.

30. T. Migita, "Fatigue Resistance.", *Nihon Gomu Kyokaishi* **46**, 626 - 642 (1973).

31. K. Fujimoto, T. Nishi and M. Tanaka, "Heterogenity of Filled Rubber Systems 4. Similarity between Changes in Higher Order Structure of Filled Rubber Vulcanizates due to Thermal Stimuli and Those due to Mechanical Stimuli.", *Nihon Gomu Kyokaishi* **44**, 590 - 605 (1971).

32. T. Yokobori and I. Narusawa, "Fatigue Resistance of Macromolecle Materials." in *Kobunshi Zairyo Kyodogaku* , OHM, Tokyo, 1982 pp. 301 - 344.

33. J. A. Sauer, E. Foden and D. R. Morrow, "Influence of Molecular Weight on Fatigue Behavior of Polyethylene and Polystyrene.", *Polym. Eng. Sci.* **17**, 246 - 250 (1977).

34. N. Urabe, "Formula and Performance of Vulcanised Rubber." in *Gomu Gijutsu no Kiso* , The Society of Rubber Industry Japan,, Tokyo, 1983 pp. 205 - 284.

35. G. J. Lake and P. J. Lindley, Phys. Basis Yield Fracture, Oxford, 1966, pp. 176.

36. G. J. Lake and P. B. Lindley, "Ozone Cracking, Flex Cracking, and Fatigue of Rubber. 1. Cut Growth Mechanisms and How They Result in Fatigue Failure.", *Rubber J. Inst. Plast.* **146 (10)**, 24 - 30 (1964).

37. G. J. Lake and P. B. Lindley, "Ozone Cracking, Flex Cracking, and Fatigue of Rubber. 2. Technological Aspects.", *Rubber J. Inst. Plast.* **146 (11)**, 30 - 36, 39 (1964).

38. J. R. Beatty, "Fatigue of Rubber.", *Rubber Chem. Tech.* **37**, 1341 - 1364 (1964).

39. J. H. Bompas-Smith, "Mortality Curves-Use and Contribution." in *Mechanical Servival-The Use of Reliability Data* , R. H. W. Brook, Ed. McGraw-Hill, London, 1973 pp. 11 - 22.

40. A. D. S. Carter, "Fundamental Aspects of Reliability." in *Mechanical Reliability* , Macmillan Press, London, 1972 pp. 4 - 41.

41. P. D. T. O'Connor, "Introduction to Reliability Engineering." in *Practical Reliability Engineering* , Heyden & Sons, London, 1981 pp. 1 -14.

42. P. D. T. O'Connor, "Analysing Reliability Data." in *Practical Reliability Engineering* , Heyden & Sons, London, 1981 pp. 58 - 87.

43. J. H. Bompas-Smith, "Putting Values to Reliability." in *Brook, R. H. W.* , R. H. W. Brook, Ed. McGraw-Hill, London, 1973 pp. 1 - 10.

44. P. D. T. O'Connor, "Load-Strength Interference." in *Practical Reliability Engineering* , Heyden & Sons, London, 1981 pp. 88 - 108.

45. J. H. Bompas-Smith, "The Theory of Failures." in *Mechanical Servival-The Use of Reliability Data* , R. H. W. Brook, Ed. McGraw-Hill, London, 1973 pp. 27 - 39.

46. A. K. Bhowmick and S. K. De, "Rubber-Science and Technology with Reference to Fractography." in *Fractography of Rubbery Materials* , A. K. Bhowmick and S. K. De, Eds., Elsevier Science, London, 1991 pp. 1 - 31.

47. S. A. Deuri and A. K. Bhowmick, "Effect of Flaw Size on Tensile Rupture and Morphology of Fracture Surface of Synthetic Rubbers with Special Reference to Rocket Insulator Compound.", *J. Appl. Polym. Sci.* **35**, 327 - 343 (1988).

48. T. Kawamura and N. Harashima, "Analysis of Fracture Surface of Rubber.", *Nihon Gomu Kyokaishi* **56**, 275 - 291 (1983).

49. J. Posipisil, "Chain-Breaking Antioxidants in Polymer Stabilisation." in *Developments in Polymer Stabilisation* , G. Scott, Ed. Elsevier Applied Science, London, 1979, vol. 1, pp. 1 - 37.

50. Y. Kamiya, "Inhibitation of Autoxidation by Antioxidants." in *Yuuki Sanka Hannou* , Gihoudou, Tokyo, 1973 pp. 72 - 92.

51. G. R. Browning and R. R. Barnhart, "Leaching of Antiozonants from a Tire Compound.", *Rubber Chem. Tech.* **44**, 1441 - 1442 (1971).

52. T. Watanabe and Y. Yamamoto, "Properties of Organic Rubber Ingredients. Part 2-Volatility of Antioxidants.", *NOC-Shi* **21**, 3 - 55 (1982).

53. A. G. John, Z. George, J. Kurien, R. R. Pandit, P. Sridharan and R. Mukhopadhayay, "Loss of Antioxidants from Truck Tyres. Part 2.2: Loss due to Leaching by Water and Migration.", *Kaustch. Gummi Kunstst.* **37**, 115 - 123 (1984).

54. J. R. Dunn, "Review of Unsolved Problems in the Protection of Rubber against Oxidative Degradation.", *Rubber Chem. Tech.* **47**, 960 - 975 (1974).

55. M. E. Cain, K. F. Gazeley, I. R. Gelling and P. M. Lewis, "The Chemistry and Technology of Rubber-Bound and Related Novel Antioxidants.", *Rubber Chem. Tech.* **45**, 204 - 221 (1972).

56. R. Yamamoto, T. Shichimi, T. Sekine and M. Koukai, "Reactive Antidegradants for Rubber. 1. The Action of Allylphenols for Rubber Antidegradation.", *Nihon Gomu Kyokaishi* **43**, 300 - 306 (1970).

57. G. Scott and A. M. A. Amaraphathy, "Rubber-Bound Antioxidants by Reactions of Natural Rubber in the Latex.", *J. Rubber Research Inst. SriLanka* **54**, 520 - 530 (1977).

58. G. Scott and S. M. Tavakoli, "Mechanisms of Antioxidant Action: Formation of Antioxidant Adducts with Rubbers through Sulphur by Mechanochemical Procedure.", *Polym. Deg. and Stab.* **4**, 343 - 351 (1982).

59. R. H. Kline and J. P. Miller, "Preparation and Activity of Polimerizable Antioxidants for Emulsion Rubbers.", *Rubber Chem. Tech.* **26**, 96 - 105 (1973).

60. G. Scott, "Antioxidants: Preventive Mechanisms." in *Atmospheric Oxidation and Antioxidants*, Elsivier, London, 1965 pp. 170 - 224.

61. G. Scott, "Synergism and Antagonism." in *Atmospheric Oxidation and Antioxidants*, G. Scott, Ed. Elsivier, London, 1993, vol. 2, pp. 431 - 459.

62. M. S. Nordin, "Synergistic Combinations of Antioxidants for Natural Rubber Vulcanizates.", *J. Rubb. Res. Inst. Malaysia* **26**, 76 - 84 (1978).

63. H. S. Dweik and G. Scott, "Mechanisms of Antioxidant Action: Aromatic Nitroxyl Radicals and their Derived Hydroxylamines as Antifatigue Agents for Natural Rubber.", *Rubber Chem. Tech.* **57**, 735 - 743 (1984).

64. H. S. Dweik and G. Scott, "Mechanisms of Antioxidant Action: The Antifatigue Mechanism of Nitrosamines.", *Rubber Chem. Tech.* **57**, 908 - 917 (1984).

65. G. Scott, "A Review of Developments in the Mechanisms of Antifatigue Agents.", *Rubber Chem. Tech.* **58**, 269 - 283 (1985).

66. G. Scott, "Some New Concepts in the Stabilisation of Polymers.", *J. nat. Rubb. Res.* **5 (3)**, 163 - 177 (1990).

67. K. B. Chakraborty and G. Scott, "Mechanisms of Antioxidant Action: Stabilization of Polymers by Spin Traps.", *J. Polym. Sci., Polym. Let. ed.* **22**, 553 - 558 (1984).

68. K. B. Chakraborty, G. Scott and H. Yaghmour, "Mechanisms of Antioxidant Action: C-Nitoso Compounds as UV Stabilizers for Polypropyrene.", *J. Appl. Polym. Sci.* **30**, 189 - 203 (1985).

69. L. P. Nethsinghe and G. Scott, "Mechanisms of Antioxidant Action: The Antioxidant Activity of "Spin-Traps" in Rubber.", *Rubber Chem. Tech.* **57**, 779 - 791 (1984).

70. M. S. S. Coker, G. Scott and H. A. A. Sweis, "Mechanisms of Antioxidant Action: Sulphur Compounds as Inhibitors of Mechanochemical Degradation of Rubber.", *Polym. Deg. and Stab.* **4**, 333 - 341 (1982).

71. T. J. Henman, "Melt Stabilisation of Polypropyrene." in *Developments in Polymer Stabilisation* , G. Scott, Ed. Elsevier Applied Science, London, 1979, vol. 1, pp. 39 - 99.

72. R. M. Russel, "Changes in the Chemical Structure of Natural Rubber Tyre Vulcanisates in Service.", *Br. Polym. J.* **1**, 53 - 58 (1969).

73. A. S. Kuzminsky, "The Mechanisms of Fatigue Resistance and of Antifatigue Agents in Elastomers." in *Developments in Polymer Stabilisation* , G. Scott, Ed. Applied Science, London, 1981, vol. 4, pp. 71 - 109.

74. P. W. Allen, "Natural Rubber Production." in *Natural Rubber and the Synthetics* , Crosby Lockwood, London, 1972 pp. 57 - 88.

75. Rubber Research Institute of Malaysia, "Revisions to Standard Malaysian Rubber Scheme 1979."

76. Chemical Abstract. 60: p14430a, "N-(4-Anilinophenyl)maleimide as a Rubber Antioxidant." (1964).

77. A. H. Weinstein, "Incorporation of Antioxidant Groups into Polydienes. 2. Via Free-Radical Reactions of Phenol- or Amine-Substituted Sulfur Compounds.", *Rubber Chem. Tech.* **50**, 650 - 659 (1977).

78. K. Mizumoto, "Rubber Processing." in *Gomu Gijutsu no Kiso* , The Society of Rubber Industry Japan,, Tokyo, 1983 pp. 135 - 204.

79. BS1674, 1991, "Equipment and General Procedure for Mixing and Vulcanizing Rubber Test Mixes."

80. ASTM D3182-87, "Rubber-Materials, Equipment, and Procedures for Mixing Standard Compounds and Preparing Standard Vulcanized Sheets."

81. BS903, Part A58, 1990, "Methods using the Mooney Viscometer."

82. ASTM D1646-87, "Rubber-Viscosity and Vulcanization Characteristics (Mooney Viscometer)."

83. BS1673, Part 10, 1977, "Measurement of Prevulcanizing and Curing Characteristics by means of Curemeters."

84. ASTM D2084-87, "Rubber Property-Vulcanization using Oscillating Disk Cure Meter."

85. S. H. Morrell, "The Chemistry and Technology of Vulcanisation." in *Rubber Technology and Manufacture* , C. M. Blow and C. Hepburn, Eds., Butterworth Scientific, London, 1982.

86. BS903, Part A2, 1990, "Determination of Tensile Stress-Strain Properties."

87. ASTM D412-87, "Rubber Properties in Tension."

88. H. Kurumiya, "Rubber Testing." in *Gomu Gijutsu no Kiso* , The Society of Rubber Industry Japan,, 1983 pp. 285 - 326.

89. U. Eisele, "Mooney-Rivlin Theory." in *Introduction to Polymer Physics* , Springer-Verlag, London, 1990 pp. 125 - 130.

90. Y. Fukahori and W. Seki, "Molecular Behaviour of Elastomeric Materials under Large Deformation: 1. Re-evaluation of the Mooney-Rivlin Plot.", *Polymer* **33**, 502 - 508 (1992).

91. A. V. Tobolsky, "Stress Relaxation Studies of the Viscoelastic Properties of Polymers.", *J. Appl. Phys.* **27**, 673 - 685 (1956).

92. A. V. Tobolsky, "Chemical Stress Relaxation." in *Properties and Structure of Polymers* , John Wiley & Sons, London, 1960 pp. 223 - 265.

93. K. Murakami, "Recent Chemorheological Studies on Rubber Vulcanizates.", *Rubber Chem. Tech.* **48**, 913 - 943 (1975).

94. K. Murakami and K. Ono, "Chemorheology of Polymers." in , Elsevier Scientific, Oxford, 1979.

95. BS903, Part A51, 1986, "Determination of Resistance to Tension Fatigue."

96. ASTM D4482-85, "Rubber-Property-Extension Cycling Fatigue."

97. Monsanto, "Operation and Service Manual Fatigue to Failure Tester."

98. J. C. Miller and J. N. Miller, "Significance Test." in *Statistics for Analytical Chemistry-3rd edition* , M. Masson, J. Tyson and P. Stockwell, Eds., Ellis Horwood PTR Prentice Hall, London, 1993 pp. 53 - 80.

99. K. Ishikawa, H. Kume and T. Fujimori, "Outliers." in *Toukeiteki Houhou* , Tokyo Kagaku Doujin, Tokyo, 1990 pp. 22 - 24.

100. ASTME178-80, "Dealing with Outlying Observations."

101. S. J. Metro, "2,6-Di-t-butylbenzoquinone.", *J. Am. Chem. Soc.* **77**, 2901 - 2902 (1955).

102. T. J. Barner and W. J. Hickinbottom, "4-Nitro-2,6-di-t-butylphenol and its Thermal Decomposition.", *J. Chem. Soc.* , 953 - 956 (1961).

103. No. 6315, in *The Merck Index-11th ed.* , pp. 1012 (1989).

104. G. M. Coppinger and T. W. Campbell, "Reaction between 2,6-Di-t-butyl-p-cresol and Bromine.", *J. Am. Chem. Soc.* **75**, 734 - 736 (1953).

105. T. Okita, S. Yachigo and Y. Takahashi, "High Performance Processing Stabilizer- Smilizer GM.", *Sumitomokagaku 1985 (II)* , 42 - 55 (1985).

106 "Antidegradants-A Review of Properties and Applications." Published by Monsanto Europe S.A. , Brussels (1989) Publication No.: 15-31 (E) ME-1 (1-89).

107. D. K. Parker and G. O. Schulz, "N-(4-Anilinophenyl)-methacrylamide, A Polymerizable Amine Antioxidant: Synthesis, Copolymerization, Copolymer Properties, and Performance.", *Rubber Chem. Tech.* **62**, 732 - 749 (1989).

108. "Technical Information-IRGANOFOS 168 in Combination with IRGANOX Antioxidants." Published by CIBA-GEIGY (1981) Publication No.: KA 7.52.

109. "Material Safety Data Sheet-ULTRANOX U626." by GE Speciality Chemicals.

110. T. Yonezawa, T. Nagata, H. Kato, A. Imamura and K. Morokuma, "Reactivity of Organic Compounds." in *Ryoshikagaku Nyumon* , Kagaku Doujin, Tokyo, 1983 pp. 203 - 273.

111. H. Fujimoto, K. Hatakeyama, S. Kawasaki and Y. Oishi, "Reactivity Scale for Sizeable Molecules.", *J. Chem. Soc. Perkin. Trans.* **2**, 989 - 993 (1991).

112. J. L. G. Nilsson, G. D. Daves Jr. and K. Folkers, "The Oxidative Dimerization of α-, β-, γ-, and δ-Tocopherols.", *Acta Chem. Scand.* **22**, 207 - 218 (1968).

113. M. Fujimaki, K. Kanamaru, T. Kurata and O. Igarashi, "Studies on the Oxidation Mechanism of Vitamin E. Part I. The Oxidation of 2,2,5,7,8-Pentamethyl-6-Hydroxychroman.", *Agr. Bio. Chem.* **34**, 1781 - 1786 (1970).

114. J. Winterle, D. Dulin and T. Mill, "Products and Stoichiometry of Reaction of Vitamin E with Alkylperoxy Radicals.", *J. Org. Chem.* **49**, 491 - 495 (1984).

115. C. Suarna, D. C. Craig, K. J. Cross and P. T. Southwell-Keely, "Oxidations of Vitamin E (α-Tocopherol) and Its Model Compound 2,2,5,7,8-Pentamethyl-6-hydroxychroman. A New Dimer.", *J. Org. Chem.* **53**, 1281 - 1284 (1988).

116. S. Al-Malaika, H. Ashley and S. Issenhuth, "The Antioxidant Role of α-Tocopherol in Polymers. I. The Nature of Transformation Producuts of α-Tocopherol Formed during Melt Processing of LDPE.", *J. Polym. Sci. Part A , Polymer Chemistry* , **32**, 3099 - 3113 (1994) .

117. T. Gottstein and W. Grosch, "Model Study of Different Antioxidant Properties of α- and γ-Tocopherol in Fats.", *Fat Sci. Technol.* **92**, 139 - 144 (1990).

118. "Evaluation of Alpha-Tocopherol as a Stabilizer in Polyolefine." in Hoffmann-La Roche Report.

119. J. A. Howard and K. U. Ingold, "The Inhibited Autoxidation of Styrene. Part 3. The Relative Inhibiting Efficiences of Ortho-Alkyl Phenols.", *Canadian J. Chem.* **41**, 2800 - 2806 (1963).

120. K. Sugimoto, unpublished work.

121. S. Samukawa, "New Method of Antioxidants Development and Quantum Chemical Study.", *Nihon Gomu Kyokaishi* **42**, 1065 - 1084 (1969).

122. S. R. Sandler and W. Karo, "Poly(vinyl chloride)." in *Polymer Syntheses* , Academic Press, London, 1977, vol. 2, pp. 346 - 369.

123. R. M. Parkhurst, W. A. Skinner and P. A. Sturm, "The effect of Various Concentrations of Tocopherols and Tocopherol Mixtures on the Oxidative Stability of a Sample of Lard.", *J. Am. Oil Chem. Soc.* **45**, 641 - 642 (1968).

124. M. Wakakura, "Antioxidant Effect of Tocopherols on Oxidation of Squalane.", *Kenkyu Houkoku - Kanagawa-ken Kogyo Shikensho* **83 No.53**, 43 - 46 (1983).

125. Y. Ishikawa, E. Yuki and H. Kato, "Synergism of Amines and Their Oxides with Tocopherols in Inhibiting the Oxidation of Lard.", *Yukagaku* **26**, 765 - 767 (1977).

126. H. S. Olcott and E. Einset, "An Antagonistic Effect with Antioxidants for Unsaturated Fats.", *J. Am. Oil Chem. Soc.* **35**, 159 - 160 (1958).

127. J. Green and D. McHale, "Quinones Related to Vitamin E." in *Biochemistry of Quinones* , R. A. Morton, Ed. Academic Press, London, 1965 pp. 261 - 285.

128. J. S. Lowe, R. A. Morton and J. Vernon, " Unsaponfiable Constituents of Kidney in Various Species.", *Biochem. J.* **67**, 228 - 234 (1957).

129. P. Schudel, H. Mayer, R. Ruegg and O. Isler, "The Chemistry of Vitamin E. The Structure of Potassiunferricyanide-Oxidation Products from a-Tocopherol.", *Helv. Chim. Acta* **46**, 636 - 649 (1963).

130. Y. Ishikawa and E. Yuki, "Reaction Products from Various Tocopherols with Trimethylamine Oxide and Their Antioxidative Activities.", *Agr. Biol. Chem.* **39**, 851 - 857 (1975).

131. W. A. Skinner and P. Alaupovic, "Vitamin E Oxidation with Alkaline Ferricyanide.", *Science* **140**, 803 - 805 (1963).

132. J. L. Glajch, J. J. Kirkland and K. Squire, "Optimization of Solvent Strength and Selectivity for Reversed-Phase Liquid Chromatography Using an Interactive Mixture-Design Statistical Technique.", *J. Chromatogr.* **199**, 57 - 79 (1980).

133. J. L. Glajch and J. J. Kirkland, "Optimization of Selectivity in Liquid Chlomatography.", *Anal. Chem.* **55**, 319A - 336A (1983).

134. L. R. Snyder, "Classification of the Solvent Properties of Common Liquids.", *J. Chromatogr. Sci.* **16**, 223 - 234 (1978).

135. L. R. Snyder, J. W. Dolan and J. R. Gant, "Gladient Elution in High-Performance Liquid Chromatography. 1. Theoretical Basis for Reversed-Phase Systems.", *J. Chromatogr.* **165**, 3 - 30 (1979).

136. J. W. Dolan, J. R. Gant and L. R. Snyder, "Gladient Elution in High-Performance Liquid Chromatography. 2. Practical Application to Reversed-Phase Systems.", *J. Chromatogr* , (1979).

137. P. E. Antle, "Solvent Optimization in Normal-Phase Liquid Chromatography of Selected Steroids.", *Chromatographia* **15**, 277 - 281 (1982).

138. R. D. Snee, "Experimenting with Mixtures.", *Chemtech* **9**, 702 - 710 (1979).

139 Y. L. Ha and A. S. Csallany, "Separation of α-Tocopherol and its Oxidation Products by High Performancr Liquid Chromatography.", *Lipids* **23**, 359 - 361 (1988).

140 S. Al-Malaika and S. Issenhuth, unpublished work.

Appendix Computer Program of HPLC Solvent Opimisation

```
1000    CLS 3
1010    '*****************************************
1020    '* HPLC SOLVENT OPTIMIZING PROGRAM       *
1030    '*                    BY KENICI SUGIMOTO *
1040    '*                    16 DEC. 1993       *
1050    '*****************************************
1060    '*******   INPUT   ***********
1070    INPUT "SOLVENT 1=";SOL1$
1080    INPUT "SOLVENT 2=";SOL2$
1090    INPUT "SOLVENT 3=";SOL3$
1100    DIM COF(7),C(8),R(8)
1110    FOR I=1 TO 7
1120    PRINT "RUN";I
1130    INPUT "COF=";COF(I)
1140    NEXT I
1150    B1=COF(1)
1160    B2=COF(2)
1170    B3=COF(3)
1180    B4=4*COF(4)-2*(B1+B2)
1190    B5=4*COF(5)-2*(B1+B3)
1200    B6=4*COF(6)-2*(B2+B3)
1210    B7=27*COF(7)-12*(COF(4)+COF(5)+COF(6))+3*(B1+B2+B3)
1220    FOR I=1 TO 7
1230    PRINT "COF(";I;")=";COF(I)
1240    NEXT I
1250    INPUT "MAX HEIGHT OF CONTOUR LINE=";M1
1260    INPUT "MIN HEIGHT OF CONTOUR LINE=";M2
1270    INPUT "INTERVAL OF CONTOUR LINE=";M3
1280    M4=(M1-M2)/M3+1
1290    IF M4=<8 THEN GOTO 1330
1300    PRINT "TOO MANY CONTOUR LINES"
1310    PRINT "SET BIGGER INTERVAL"
1320    GOTO 1250
1330    '*******   AXES    **********
1340    CLS 3
1350    CONSOLE 0,25,0,1
1360    SCREEN 3
1370    LINE(350,15)-(150,361),7
1380    LINE(350,15)-(550,361),7
1390    LINE(150,361)-(550,361),7
1400    FOR I=1 TO 9
1410    L1=150+40*I
1420    LINE(L1,361)-(L1,365),7
1430    NEXT I
1440    FOR I=1 TO 9
1450    L1=350-20*I
1460    L2=15+34.6*I
1470    L3%=CINT(L2)
1480    L4=L1-3
1490    L5=L3%-2
1500    LINE(L1,L3%)-(L4,L5),7
1510    L6=350+20*I
1520    L7=L6+3
1530    LINE(L6,L3%)-(L7,L5),7
1540    NEXT I
1550    LOCATE 37,2:PRINT "0.1"
1560    LOCATE 32,6:PRINT "0.3"
1570    LOCATE 27,11:PRINT "0.5"
1580    LOCATE 22,15:PRINT "0.7"
1590    LOCATE 18,19:PRINT "0.9"
```

```
1600    LOCATE 23,23:PRINT "0.1"
1610    LOCATE 33,23:PRINT "0.3"
1620    LOCATE 43,23:PRINT "0.5"
1630    LOCATE 53,23:PRINT "0.7"
1640    LOCATE 63,23:PRINT "0.9"
1650    LOCATE 48,2:PRINT "0.9"
1660    LOCATE 52,6:PRINT "0.7"
1670    LOCATE 58,11:PRINT "0.5"
1680    LOCATE 63,15:PRINT "0.3"
1690    LOCATE 68,19:PRINT "0.1"
1700    LOCATE 14,23:PRINT "X1=1.0"
1710    LOCATE 68,23:PRINT "X2=1.0"
1720    LOCATE 40,0:PRINT "X3=1.0"
1730    LOCATE 1,20:PRINT "X1=";SOL1$
1740    LOCATE 1,21:PRINT "X2=";SOL2$
1750    LOCATE 1,22:PRINT "X3=";SOL3$
1760    '*******   COLOR   ********
1770    FOR I=1 TO M4
1780    C(I)=M2+M3*(I-1)
1790    IF I=1 THEN LOCATE 1,1 :PRINT "BLACK      =";C(I)
1800    IF I=2 THEN LOCATE 1,2 :PRINT "RED        =";C(I)
1810    IF I=3 THEN LOCATE 1,3 :PRINT "LIGHT BLUE=";C(I)
1820    IF I=4 THEN LOCATE 1,4 :PRINT "GREEN      =";C(I)
1830    IF I=5 THEN LOCATE 1,5 :PRINT "INDIGO     =";C(I)
1840    IF I=6 THEN LOCATE 1,6 :PRINT "YELLOW     =";C(I)
1850    IF I=7 THEN LOCATE 1,7 :PRINT "VIOLET     =";C(I)
1860    IF I=8 THEN LOCATE 1,8 :PRINT "BLACK      =";C(I)
1870    NEXT I
1880    R(1)=7
1890    R(2)=2
1900    R(3)=5
1910    R(4)=4
1920    R(5)=1
1930    R(6)=6
1940    R(7)=3
1950    R(8)=7
1960    LOCATE 70,1:PRINT "B1="B1
1970    LOCATE 70,2:PRINT "B2="B2
1980    LOCATE 70,3:PRINT "B3="B3
1990    LOCATE 70,4:PRINT "B4="B4
2000    LOCATE 70,5:PRINT "B5="B5
2010    LOCATE 70,6:PRINT "B6="B6
2020    LOCATE 70,7:PRINT "B7="B7
2030    '*********   CONTOUR LINES   **********
2040    FOR X1=0 TO 400
2050    FOR X2=0 TO 400
2060    X3=400-X1-X2
2070    IF X3<0 THEN GOTO 2220
2080    X4=X1/400
2090    X5=X2/400
2100    X6=X3/400
2110    LOCATE 1,11 :PRINT "X1=";X4
2120    LOCATE 1,12 :PRINT "X2=";X5
2130    LOCATE 1,13 :PRINT "X3=";X6
2140    Q=B1*X4+B2*X5+B3*X6+B4*X4*X5+B5*X4*X6+B6*X5*X6+B7*X4*X5*X6
2150    IF QM<Q THEN QM=Q:XAM=X4:XBM=X5:XCM=X6
2160    LOCATE 1,14:PRINT "COF=";Q
2170    V=.03
2180    FOR J=1 TO M4
2190    W=R(J)
```

```
2200    IF Q=>M2+(J-1)*M3 AND Q<M2+((J-1)+V)*M3 THEN GOTO 2380
2210    NEXT J
2220    NEXT X2
2230    NEXT X1
2240    LOCATE 1,10:PRINT "OPTIMUM COMP."
2250    LOCATE 1,11:PRINT "                "
2260    LOCATE 1,11:PRINT "X1=";XAM
2270    LOCATE 1,12:PRINT "                "
2280    LOCATE 1,12:PRINT "X2=";XBM
2290    LOCATE 1,13:PRINT "                "
2300    LOCATE 1,13:PRINT "X3=";XCM
2310    LOCATE 1,14:PRINT "COF=";QM
2320    P1=361-400*(.5*1.73205*XCM)
2330    Z1=150+400*(XBM+.5*XCM)
2340    P2%=CINT(P1)
2350    Z2%=CINT(Z1)
2360    CIRCLE(Z2%,P2%),2,7
2370    END
2380    '******   DRAWING CONTOUR LINES    *********
2390    S1=361-400*(.5*1.73205*X6)
2400    T1=150+400*(X5+.5*X6)
2410    S2%=CINT(S1)
2420    T2%=CINT(T1)
2430    PSET(T2%,S2%),W
2440    GOTO 2220
```